Recent Advances in
Composite Materials for Wind Turbine Blades

Edited by **Dr. Brahim Attaf**
Expert-Researcher in the field of
Composite Materials & Structures

World Academic Publishing - Advances in Materials Science and Applications

www.academicpub.org/amsa/

Recent Advances in Composite Materials for Wind Turbine Blades
Edited by Dr. Brahim Attaf

Published by Word Academic Publishing
Editorial Office: Unit 1105, 11/F., Tower 1, Lippo Centre, No. 89 Queensway, Admiralty, Hong Kong

Notice
The views, opinions, findings, conclusions and recommendations expressed in this book are solely those of the individual contributors and do not necessarily reflect the views of the editors or the publisher. The publisher and the editorial staff assume no responsibility or liability for the accuracy of data contained in the published articles, and disclaim any damage or injury to persons or property arising out of the use of such material.

Editorial Board Member: Wei-Ting Lin
Cover Designer: AMSA Design Office

First published December, 2013
Published in China

A free online edition of this book is available at: www.academicpub.org/amsa/callforbookchapters.aspx

Hard copies can be obtained from amsa@academicpub.org

ISBN 978-0-9889190-0-6

World Academic Publishing

Free on line Books and Journals can be found at: www.academicpub.org/amsa/

Preface

In today's modern society, global efforts have been made to fight against climate change issues through new and concrete actions that target the reduction and limitation of greenhouse gas emissions. Among these actions are the development and implementation of new and renewable energy sources, such as wind energy. This low-carbon solution, taken as an alternative over other less environmentally friendly energies, will open up great perspectives for the development of clean electricity production and assurance of new security of energy supply. However, the management of this process cannot be achieved without taking into account the societal, economic and environmental key pillars that are characterizing the sustainable development concept in which the wind energy system is embedded.

It is in this context that the idea of the book project was launched, aiming to learn about the latest scientific achievements and provide readers worldwide access to research developments in the field of composite materials that will shape the future evolution of wind turbine blades. In line with these research and innovation strategies, chapters proposed by contributors involve R&D and address new solutions in response to the major challenges that the wind turbine blade industry is facing today and those to which it will be encountering in the future. In fact, these issues will be carried out with the promotion of technological innovation for the development of large scale blades for onshore and offshore applications using future fibre-reinforced composite materials made from carbon nanotubes, for instance. In this perspective, it is expected that in the coming years blade designers will reach a nominal output power of 10-20 MW for the next generation of offshore wind turbines. Further to this technological progress, it is planned for the year 2020 to develop and test 15-20 MW turbine prototypes!

To support this sustainable energy policy, several scientific and technological research contributions have been proposed from both spaces of academia and industry. Nevertheless, only chapters that are fully in line with the objectives of the book were selected. To this end, the book provides recent research results obtained by numerical approaches and/or experimental investigations, namely in the field of structural design, manufacturing processes, testing techniques, finite element modelling, characterization of new materials, fluid-structure interaction, stress analysis, modal analysis, fatigue prediction and so forth. These innovative topics will undoubtedly strengthen the capacity of wind energy systems and will respond effectively to the new challenges of technology for designing multi-megawatt wind turbines. In addition, open access book chapters will provide readers with wide-reaching studies on the subject matter and therefore can help designers, manufacturers and suppliers to increase their competitiveness and productivity, which will consolidate the energy efficiency strategy for 2020 and the longer term.

At the same time, I hope that the variety of selected chapters will stimulate future research activities, enhance technology transfer, promote the dissemination of results and respond effectively to the challenges of energy efficiency by giving much more attention to: (i) the chemical substances used, (ii) the search for clean manufacturing processes, (iii) the creation of repair and recycling techniques, (iv) the establishment of qualification/certification procedures, (v) the implementation of new eco-standards, and so forth.

It is in collaboration with active authors in their best research work that this book has been edited. So, I am very pleased to have this opportunity to thank all the authors for their remarkable contributions in their areas of expertise. I also appreciate the resulting synergy between theory and practice coming from different countries of the world. Without this rich variety of relevant contributions, the existence of the book titled "*Recent Advances in Composite Materials for Wind Turbine Blades*" would not have been possible.

Finally, I would like to acknowledge the help given by the staff of Advances in Materials Science & Applications (AMSA), especially Ms. Ariel Huang for her assistance and support during the period of preparation of this book.

December 2013

Dr. Brahim Attaf
Marseille
France

Contents

	Preface	**IV**
	Contents	**V**
Chapter 1	**Designing Composite Wind Turbine Blades from Cradle to Cradle** ..... Brahim Attaf	**1**
Chapter 2	**Natural Fibre-Reinforced Polymer Composites for Wind Turbine Blades: Challenges and Opportunities**..... Kishore Debnath, Inderdeep Singh, Akshay Dvivedi, Pradeep Kumar	**25**
Chapter 3	**Process Simulations for Predicting Quality of Composite Wind Turbine Blades** ..... Konstantine A. Fetfatsidis, James A. Sherwood	**41**
Chapter 4	**General Assessment of Fıber-Reınforced Composıtes Selectıon in Wınd Turbıne Blades**..... Ayşegül Akdoğan Eker, Bülent Eker	**61**
Chapter 5	**On the Fluid-Structure Interaction of a Composite Wind Turbine Blade** ..... Roham Rafiee	**79**
Chapter 6	**Spar Shape Optimization of a Multi Megawatt Composite Wind Turbine Blade: Modal Analysis**..... Mostapha Tarfaoui, Owaisur Rahman Shah	**93**
Chapter 7	**Finite Element Modeling of Composite Wind Turbine Blades**..... Ajaya K. Nayak	**105**
Chapter 8	**Multidisciplinary Optimization of Wind Turbine Blades With Respect to Minimize Vibrations**..... Mariola Jureczko	**129**
Chapter 9	**Testing and Condition Monitoring of Composite Wind Turbine Blades** ..... Wenxian Yang	**147**

Chapter 10 **Mechanical Characterization of Rigid PUR Foams Used for Wind Turbine Blades Construction** **171**
Emanoil Linul, Liviu Marsavina

Chapter 11 **Investigation of Polymer Composites for Wind Turbines Blades** **195**
N. Chikhradze, G. Abashidze

Chapter 12 **Study of Composite and Sandwich Plates Extracted from Wind Turbine Blade Structures under Harsh Environmental Conditions** **207**
Bong Taek Oh

Chapter 13 **Fatigue Life Prediction for Adhesively Bonded Root Joint of Composite Wind Turbine Blade Using Cohesive Zone Approach** **221**
Vahid Azimzadeh Kalkhoran, Davood Salimi-majd, Bijan Mohammadi

Chapter 1

Designing Composite Wind Turbine Blades from Cradle to Cradle

Brahim Attaf

Expert/Researcher in Composite Materials & Structures
39 Blvd. Charles Moretti, 13014 Marseille - France
b.attaf@wanadoo.fr

I. INTRODUCTION

There is no doubt that the use of renewable energies is a positive answer in response to environmental and societal challenges that are facing our society nowadays. It is in this context that wind power is considered to be an alternative source of clean, green, eco-friendly and sustainable energy. To better identify the environmental issues, mitigate the adverse consequences of the greenhouse effect (GHE), minimize their impacts and understand the importance of the use of wind energy as a key feature to fight against global warming, it is worthwhile to address, in the introduction of this chapter, some preliminary points making the reader familiar with the GHE and the associated disequilibrium mechanism. On the other hand, the survey will concentrate on the design process of three-bladed horizontal-axis wind turbines (HAWTs).

A. Greenhouse Phenomenon and Radiative Balance

It is well known that the Earth receives energy from the Sun in the form of visible light called "solar rays" and about 30% of this energy is reflected by white clouds, ice, snow and lower atmosphere. On the other hand, 70% of the remaining energy is absorbed at the Earth's surface by oceans, land and various components of the upper atmosphere. As a result, the absorbed energy heats the surface of the earth, and when the Earth's surface becomes warm it radiates its own rays of heat called "infrared rays" (IR). The energy emitted is equivalent to the energy absorbed according to the principle of energy conservation.

As a matter of fact, climate scientists have revealed that in the absence of GHE, the average temperature of Earth's surface would be -18 ℃ (Fig. 1a); and under such temperature conditions, life would be virtually impossible. However, in the presence of GHE, the temperature is about +15 ℃ (Fig. 1b). It is this temperature condition which enables human beings to live on the Earth's surface. Furthermore, it was claimed that deregulation of Earth's surface average temperature may be avoided if the value of 33 ℃ which corresponds to the temperature difference between absence and presence of greenhouse gases (i.e., +15 ℃ - (-18 ℃) = 33 ℃) is kept constant.

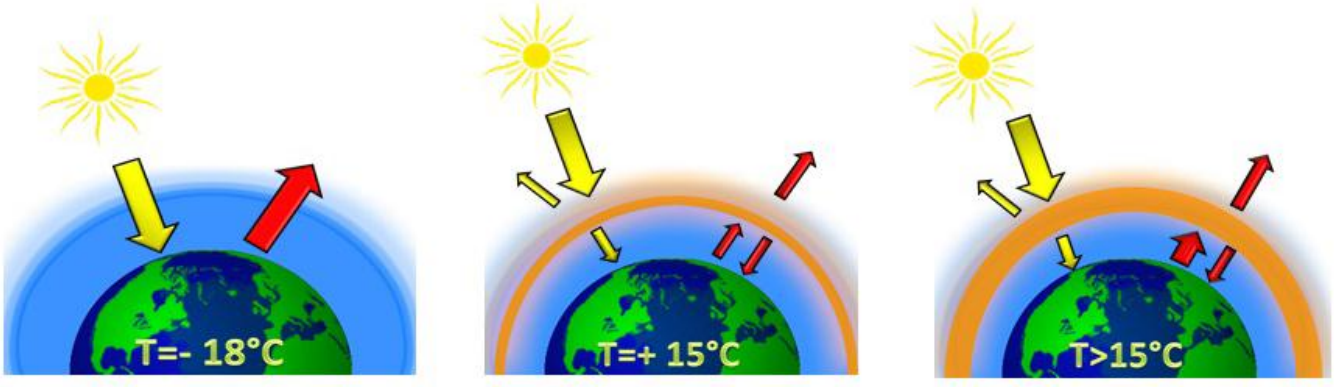

(a) (b) (c)

Fig. 1 Greenhouse effect (GHE): (a) in absence of GHE; (b) in presence of GHE; (c) disequilibrium of the greenhouse mechanism

However, human activities which are classified as industrial, agricultural and domestic have induced an increase in concentration of greenhouse gas (GHG) emissions in the atmosphere [1], where carbon dioxide (CO_2) is the main GHG produced by the human activity; it occupies 74% of the total GHGs. Fig. 2a illustrates the evolution of CO_2 concentration in the atmosphere over the last hundred and thirty years. This increase in temperature may lead to disequilibrium of the

greenhouse mechanism, which can cause global warming, because the Earth's surface temperature will be above +15°C. This increase in temperature can lead to a subsequent climate crisis for future generations (Fig. 2b).

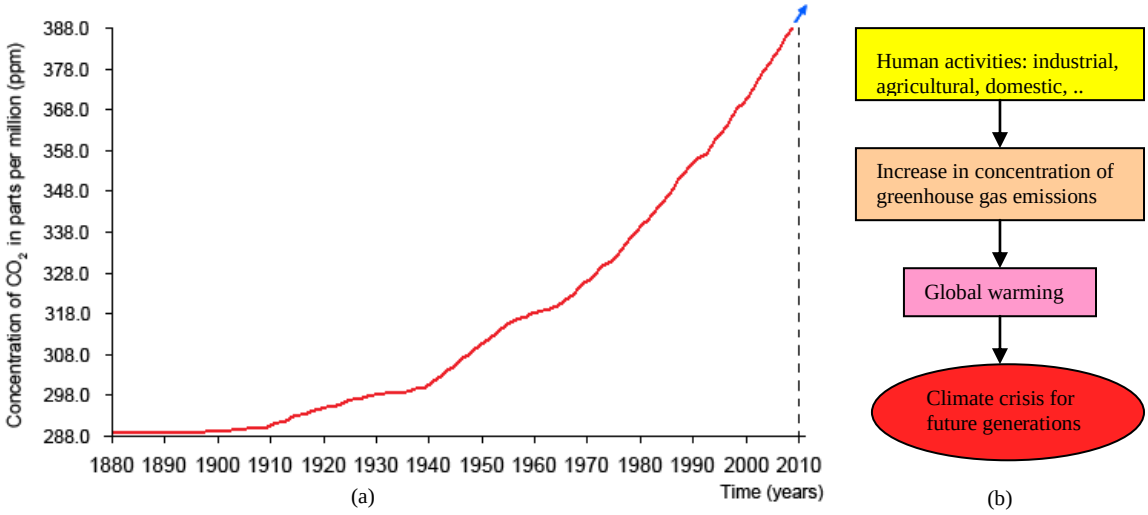

Fig. 2 Global warming: (a) concentration of CO_2 in the atmosphere *vs* time in years, (b) climate change and its consequences

Thus, the consequences of global warming can pose a catastrophic threat to human health and the environment. For instance, by 2100 the temperature across the globe could rise by 1.8 to 6 ℃ according to the agreements of experts and IPCC (Intergovernmental Panel on Climate Change) assessment reports [2, 3]. This increase in temperature will have dramatic impacts with notably:

- an increase in the sea level (15 to 95 cm);
- an effect on both drought and water resources;
- changes in rainfall and wind patterns (heavy rains, cyclones, hurricanes, tornadoes ...);
- an increase in tropical diseases such as malaria in some countries;
- ...

To address this problem and prevent global warming to rise, the only way is to reduce GHG emissions through the use of renewable energies: an important feature of the sustainable development concept.

B. Onshore and Offshore Wind Energy as an Alternative

As revealed by concrete studies that wind energy is a key solution responding to the sustainable development challenges through tackling air pollution, GHG emissions and various industrial wastes, the technological interest to develop larger and more powerful machines is becoming nowadays a major concern for worldwide wind turbine manufacturers [4, 5]. Depending on the statistical distribution of wind speed on the site, two classes of three-bladed HAWTs are considered today to be the most widely used turbines; these are the ones installed on land (i.e., onshore) and the ones installed at sea (i.e., offshore). For the latter class and according to the seawater depth, offshore wind turbines foundations are varying from floating to resting on a reinforced concrete placed into the bottom side of the sea (see Fig. 3). In addition, it was estimated that an offshore production site, situated a few kilometres away from the coast, could produce 50% more energy than onshore site. Furthermore, offshore wind turbines can provide in average 5 to 10 MW, while onshore wind turbine energy production is limited to 3 MW.

Thereby obtaining a high power output depends mainly on the swept area of the rotating blades. Theoretically, the maximum recoverable power of a HWT is given by Betz's formula [6]:

$$P_{max} = \frac{16}{27}\frac{1}{2}\rho S v^3 \quad (1a)$$

where, P_{max} is the maximum power (W); ρ is the air density (kg.m^{-3}); v is the wind speed (m.s^{-1}) and S is the swept area (m^2).

Under normal atmospheric conditions of pressure (P=1.01325 bar) and temperature (T=15 ℃), the density of dry air at sea level is approximately equal to 1.225 kg.m^{-3}. With this approximation, Eq. (1a) becomes:

$$P_{max} = 0.3629 S v^3 \quad (1b)$$

It can be discerned from Eq. (1b) that, for a minimum revolution per minute (RPM) and a given blade number, the power is a function of the swept area S if the wind speed v and the tip speed ratio (TSR=$v_{tip\ speed}$ / $v_{wind\ speed}$) are kept constant. In other words, the power depends on the radius of the area swept by the blades, wherein the radius is no other than the length l of the

blade as shown in Fig. 4.

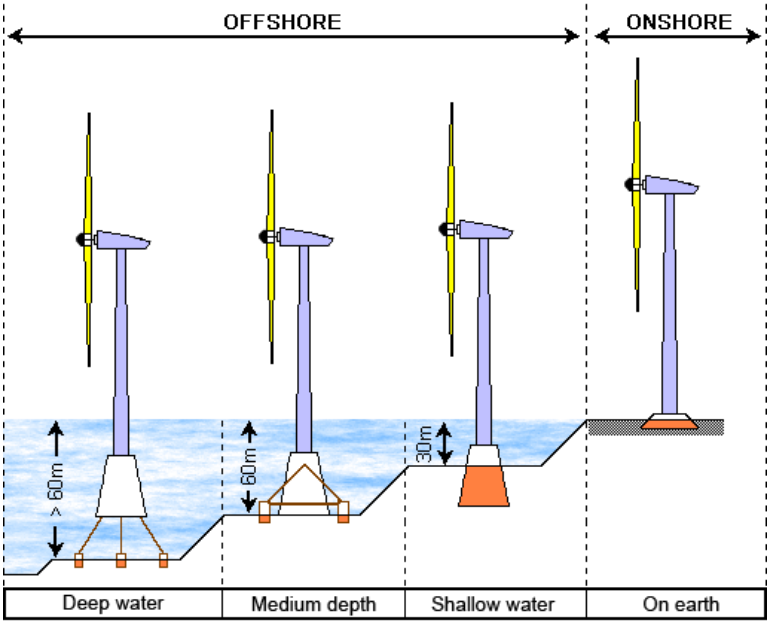

Fig. 3 Onshore and offshore horizontal-axis wind turbines

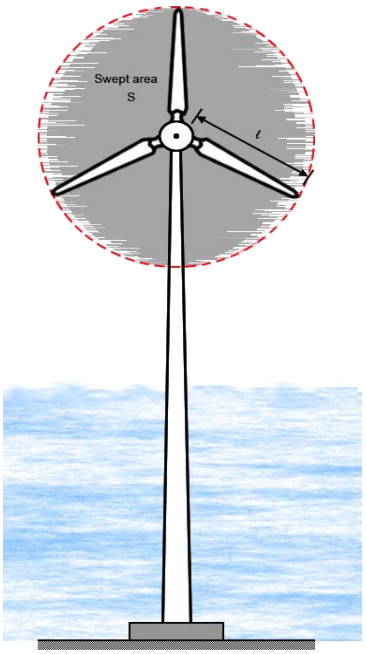

Fig. 4 Power output as a function of the blade length

In practice, this maximum power is multiplied by a coefficient of performance $C_p \in [0.2; 0.7]$, which depends on the type/model of the wind turbine and its installation site (offshore or onshore).

Further to that and under the conditions of constant v and TSR, it can be demonstrated from Eq. (1b) that the maximum power of a HAWT varies parabolically as function of the blade length: the larger the size of the blades, the more energy is captured.

Although the turbine blades rotate with a low speed, so they are less stressed, but this does not prevent them from exposure during their service life to static and dynamic loads, which may have negative effects on their structural behaviour and this may lead to risks of failure. Consequently, to overcome this problem and drastically reduce these risks, fibre-reinforced composite materials are widely used in the design and manufacture of these blades.

It is in this context that this chapter has been elaborated to present the different steps involved in the design process of wind turbine blades using composites based on long fibres and taking into account their optimisation in the manufacturing technology. The results and conclusions presented throughout this chapter can help wind industry designers to manufacture reliable blades capable to withstand, without any adverse effect, harsh environmental conditions and different types of possible shocks.

II. AIRFOIL GEOMETRY, BLADE DIMENSIONS, MATERIALS AND CHARACTERISATION

Although single- and two-bladed HAWTs offer a great saving in cost and weight, three-bladed HAWTs are the most widely used in the world because they offer a good visual impact, generate less noise and provide a better lifetime due to the rotor stability and the low rotation speed of blades. As the three blades are perfectly identical to each other, the analysis will focus only on a typical blade. This latter will be isolated from the whole system according to the substructure method with an accurate modelling of the boundary conditions.

A. Airfoil

The airfoil, or aerofoil, section is a slide of a wind turbine blade seen in cross-section; it is defined mainly by its leading edge, trailing edge, chord, maximum thickness and its associated location point. The important terms used to describe an airfoil are shown in Fig. 5. The airfoil shape is generally characterized by using the four-digit series developed by the National Advisory Committee for Aeronautics (NACA).

In collaboration with the specialized agencies in fluid mechanics and aerodynamics, the standardized profile of the blade can be designed and validated. On the other hand, to further increase the longitudinal blade stiffness, either a spar (box beam) or stiffeners (shear web) are incorporated into the internal structure; thus making the blade structure more stiff and resistant to wind loads and induced vibrations [7, 8]. The stiffeners can be located at 25% C and 55% C with regard to the blade leading edge, where the letter C denotes the chord of the considered airfoil. The upper and lower surfaces (i.e., skin of the blade) are both manufactured from fibre-reinforced laminates. Stiffeners are generally made of the same material that is used for upper

and lower laminated surfaces, but with different thickness.

The evolution of the twist angle (rotation of the profile with respect to the blade twist axis) from the blade inboard section to the blade tip can be improved by the competent bodies in the relevant research area. This twist angle is considered to be the reference for the setting angle for each section. However, the techno-scientific terminology between the position of the elastic centre and the centre of gravity must be the subject of a clear and precise distinction. Then comes the determination of the blade size that must meet a given specification, followed by the determination of different thicknesses, appropriate fibre orientations, and appropriate stacking sequences for each section. This step involves checking the blade mechanical strength using numerical methods.

B. Geometry and Dimensions

The number of zones for which the blade is divided is defined as a function of the blade length. Taking for instance the case of a blade of 8 m length, the structure thereof will be divided into four zones with variables thicknesses, thus four material zones are to be considered, and each material is affected to the corresponding zone. In addition and according to stress distributions along the blade length, a decrease in thickness ranging from blade root to blade tip has to be considered for each zone. In addition, a fifth material zone has to be considered for the two internal stiffeners; each stiffener has a thickness of 3 mm. The different material zones and their positions with regard to the blade structure are illustrated in Fig. 6; these are defined as follows:

- Zone A: upper or lower surface thickness = 12 mm
- Zone B: upper or lower surface thickness = 9 mm
- Zone C: upper or lower surface thickness = 6 mm
- Zone D: upper or lower surface thickness = 3 mm

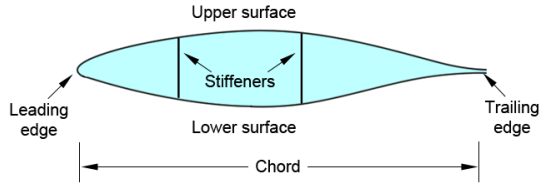

Fig. 5 Airfoil-shaped cross section

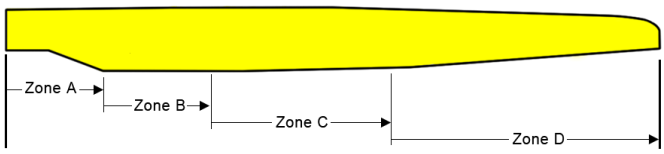

Fig. 6 Different thicknesses associated to different zones along the blade structure

C. Materials

1) Composite materials

Selected materials for the manufacture of wind turbine blades must meet, in one hand, the quality assurance requirements and, on the other hand, the new regulations related to environmental issues. To this end, it is very important to choose carefully: (i) the class of fibres, (ii) the class of matrix, (iii) the foam constituting the core of the sandwich (inserted into the section of the profile for small blades).

As the blade is an essential structural component within the wind turbine machine, it must therefore be designed structurally strong enough to support the various loads to which it may be exposed. In order to meet this requirement, glass-fibre composites such as glass-reinforced plastics (GRP) and carbon-fibre-reinforced plastics (CFRP) are suitable materials for use in such structural applications [9, 10] because of their excellent formability, their mass-saving advantage coupled with high stiffness and strength, and the greater freedom to tailor these high properties in the desired orientation and position. In addition, these lightweight materials have exceptional structural properties with precise objectives that cannot be achieved when using original or conventional materials. These attractive benefits have effectively opened up great opportunities in the design and manufacture of future wind turbine blades. In fact, many structural components of these blades, previously made from conventional materials, are now manufactured from composite materials and are operating successfully in their implantation sites.

2) Nanocomposites (carbon nanotubes)

According to recent advances in nanotechnology, it is expected that carbon nanotubes (CNTs) in the form of continuous fibres can be used in various structural applications and that in order to improve the material properties [11]. These nano-materials are based on graphite which is no other than the stable form of carbon at ordinary temperature and pressure (e.g., pencil tip, as shown in Fig. 7). Its molecular structure consists of an intercalated stacking of noncompact hexagonal honeycomb sheets; each sheet is separated by about 0.336 nm along its normal direction (see Fig. 8).

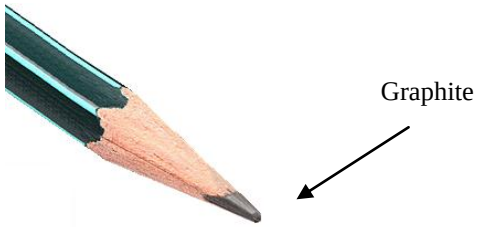

Fig. 7 Stable form of carbon (pencil tip)

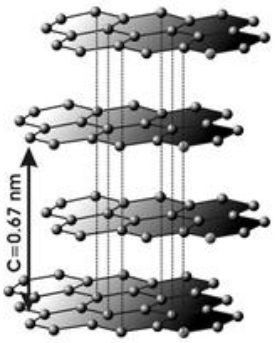

Fig. 8 Graphite molecular structure

Fig. 8 shows the molecular structure of graphene, i.e., a single flat layer of carbon atoms isolated from the crystal structure of graphite. The carbon nanotubes (CNTs) are obtained by rolling graphene sheets on themselves as shown in Fig. 9. Depending on the winding geometry, there are generally three types of CNTs, which are called: armchair, zigzag and chiral.

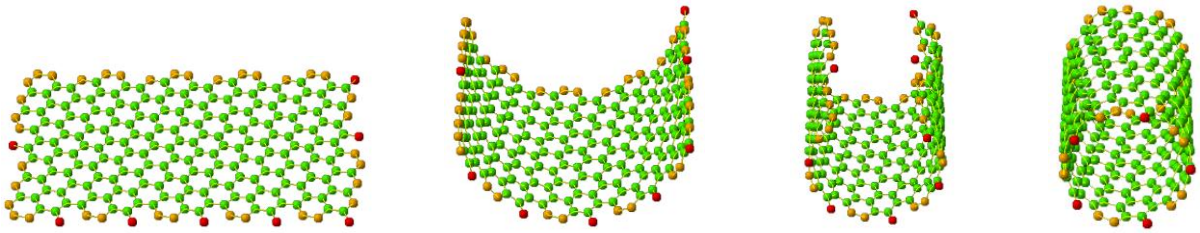

(a) Graphene (b) Rolled up at 50% (c) Rolled up at 75% (d) CNT

Fig. 9 Rolling up a graphene sheet into a carbon nanotube

In general, CNTs can be a single-walled carbon nanotube (SWNTs) as shown in Fig. 10a, or multi-walled carbon nanotubes (MWNTs) as shown in Fig. 10b. The diameter of CNTs is ranging from 1-80nm; whereas the length can reach several micrometres. With these nanometric dimensions, a very high aspect ratio (i.e., length-to-diameter) can be provided, however. Such unique characteristics contribute significantly to the improvement of the durability of structures and structural components.

For the production of CNTs, there are several processes, including the CVD (Chemical Vapour Deposition) process which has been achieved thanks to the recent development in the field of nanotechnology, where CNTs can be aligned in the same direction to form continuous fibres. The growth mechanism of CNTs using CVD process is shown in Fig. 11.

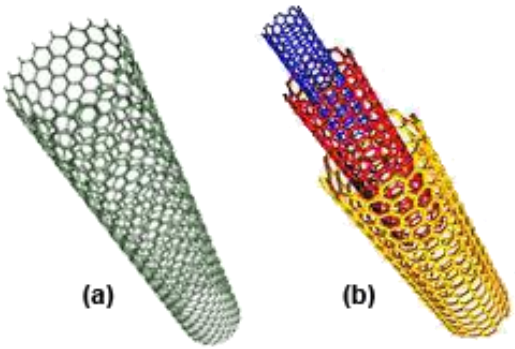

Fig. 10 Carbon nanotubes: (a) Single walled, (b) Multi-walled

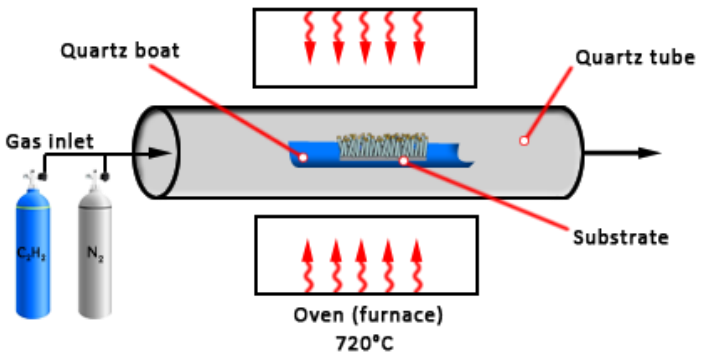

Fig. 11 CVD process for the production of CNTs

The main choice criteria of these nano-materials are believed to be related to the ultra-high-performance indices in terms of specific stiffness and specific strength and other physicochemical properties such as thermal and electrical conductivity. These advantages make CNTs attractive candidate for the reinforcement of composite materials that will play an important role in the design and manufacture of future structural blade parts.

In this fast-growing sector of research and innovation, several research activities are in progress with the object to build a new set of wind turbine blades. Significant improvements and challenges can be reached within the next generation of wind turbine blades made with carbon nanotube-based continuous fibres (see Fig. 12). For instance, the strength of these fibres can be several times higher than standard carbon fibres and weighs much less for an equivalent cross-section: an advantage that will provide a good solution to improve the overall mechanical behaviour of the blade.

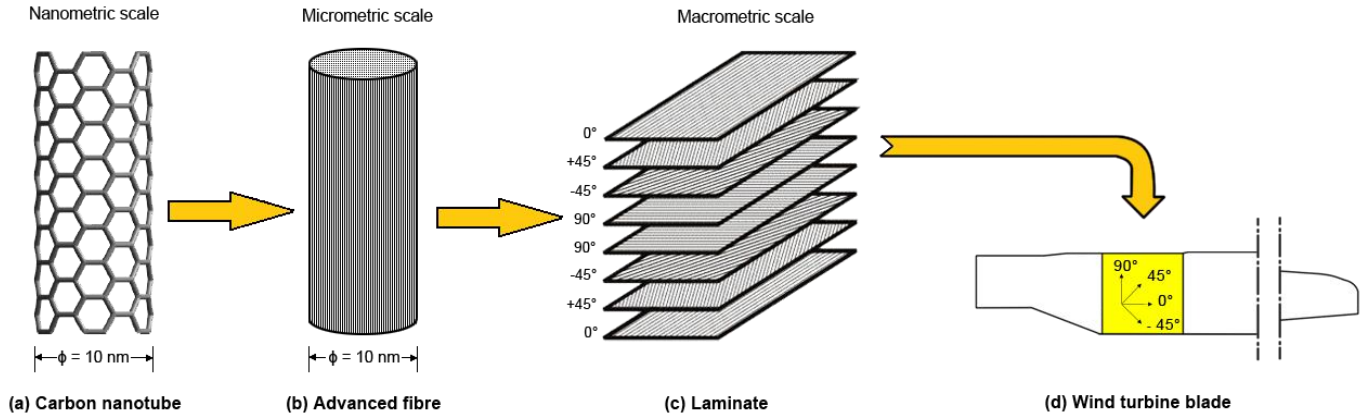

Fig. 12 Application of CNT-based continuous fibres for future design of ultra-mega wind turbine blades

With this great innovation, CNTs are likely to be exploited in the design and manufacture of wind turbine blades with ultra-length up to several hundred meters. This progress reflects the idea of building offshore wind turbines that are capable to produce ultra-mega sources of energy. In addition, CNTs have the potential to be used as sensors for monitoring the structural health of large wind turbine blades. However, from an ecological point of view, these materials are likely to have adverse impacts on the environment and human health throughout the entire cycle life [12].

D. Characterisation of Materials

In materials science, the properties necessary to describe the linear-elastic behaviour of selected fibre-reinforced composite plies can be predicted using the rule-of-mixture formulae, based on theoretical and semi-theoretical formulae. On the other hand, stress-strain curves are made to provide experimentally some of these properties according to standards that are available, such as ISO (International Standards Organization) and ASTM (American Society for Testing and Materials). Further to that, a correlation "calculation-test" is performed to improve the approach of the theoretical models. The necessary characteristics to carry out research activities can be physical, mechanical or hygrothermal.

1) Physical characterization: it involves determining the following constants:

- the fibre volume fraction, V_f (composites used in wind industry have a V_f varying between 40% and 60%);
- the fibre mass fraction, M_f (this terminology is less used than V_f);
- the ply thickness, t (it depends on the ply type and can be unidirectional, bidirectional or mat);
- the density, ρ (in other terms, the mass per unit volume).

2) Mechanical characterization: it involves determining the following engineering constants:

- Young's moduli in i-direction, E_i (i=1, 2, 3): a measure of material stiffness;
- Shear moduli in the i-j plane, G_{ij} (i-j=2-3, 3-1 and 1-2): a measure of material stiffness;
- Poisson's ratio for transverse strain in the j-direction when stressed in the i-direction, ν_{ij} (vice versa ν_{ji});
- Tensile or compressive strength failure in i-direction, $\sigma_{i,f}$ (i=1, 2, 3): a measure of material strength;
- Shear strength failure in the i-j plane, $\tau_{ij,f}$ (i-j=2-3, 3-1 and 1-2): a measure of material strength.

3) Hygrothermal characterization: it involves determining the following hygrothermal expansion coefficients:

- the thermal expansion coefficients, α_i (i=1, 2, 3);
- the moisture expansion coefficients, β_i (i=1, 2, 3).

In structural design, one of the key features that characterise the choice of materials are believed to be related to specific strength and specific stiffness; they are defined as the stiffness-to-weight ratio (E/ρ) and strength-to-weight ratio (σ_f/ρ), respectively. These two technical terms are distinct and their use in engineering design process must not be confused; they are both dependent on material type and its density. The advantage of composite materials is that they offer highest values of these ratios which, from mechanical and economic point of view, are very important because they meet specific needs required in vibration and stability analyses of wind turbine blades. The optimization of natural frequencies and critical buckling loads can be achieved through the selection of optimum ratios. Fig. 13 shows a comparison of specific strength and specific stiffness for some conventional, composite and nanocomposite materials [13, 14]. Within the composite family, it is easy to discern the position of glass-fibre reinforced polymer (GFRP), carbon-fibre reinforced polymer (CFRP) and carbon nanotubes (CNTs).

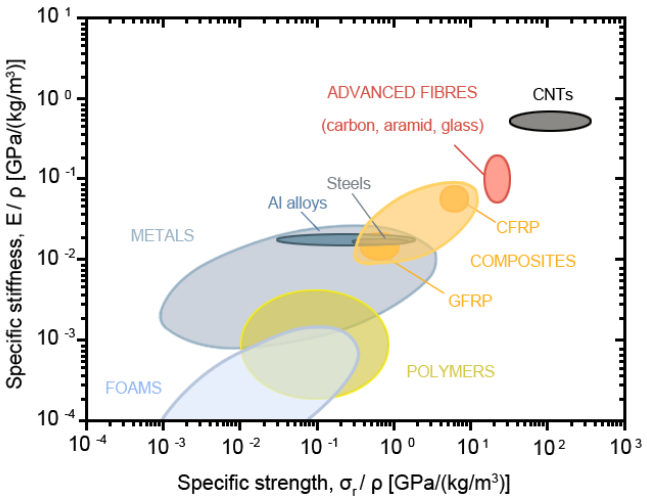

Fig. 13 Specific stiffness *versus* specific strength for some composite materials [13, 14]

III. FINITE ELEMENT ANALYSIS AND EXPERIMENTAL TESTING

The design of composite wind turbine blades must fulfil the normative requirements requested by the standards ISO 2394 and IEC 61400-1 in terms of structural analysis (stress, strength, vibration, fatigue, safety...) and static/dynamic tests of qualification. For the section relative to experimental analysis, it is assumed that the blade is already manufactured by the pre-selected process.

A. State of the Problem and Constitutive Equations

The state of the structural problem is illustrated in Fig. 14, where the blade structure (onshore or offshore) is assumed to be subjected to three main types of loading; these are: (i) mechanical loading (high wind forces, weight, ..), (ii) thermal loading (temperature variation) and (iii) hygrometric loading (moisture and seawater explosure) [15, 16].

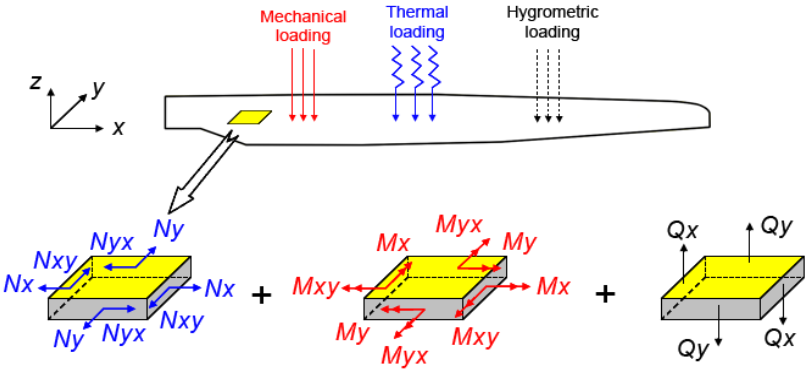

Fig. 14 Resultant forces and moments for a typical blade element subjected to hygrothermomechanical loading

When thermal and moisture effects besides mechanical loading are taken into consideration in the structural analysis, the constitutive relations for an unsymmetrically *n*-layered composite plate, assumed to be extracted from the blade structure, with transverse shear deformations (transverse hygrothermal effect is neglected) can be written in compact matrix form as [17, 18]:

$$\begin{Bmatrix} N \\ \cdots \\ M \end{Bmatrix}_{xyz} = \begin{bmatrix} A_{ij} \vdots B_{ij} \\ \cdots \cdots \\ B_{ij} \vdots D_{ij} \end{bmatrix} \begin{Bmatrix} \varepsilon_0 \\ \cdots \\ \kappa \end{Bmatrix}_{xyz} - \begin{Bmatrix} N^{\Delta T} \\ \cdots \\ M^{\Delta T} \end{Bmatrix}_{xyz} - \begin{Bmatrix} N^{\Delta m} \\ \cdots \\ M^{\Delta m} \end{Bmatrix}_{xyz} \tag{2a}$$

$$\{Q\}_{xyz} = \{F_{ij}\}\{\gamma\}_{xyz} \tag{2b}$$

$$(A_{ij}, B_{ij}, D_{ij}) = \sum_{k=1}^{n} \int_{z_{k-1}}^{z_k} (\bar{Q}_{ij})_k (1, z, z^2)\, dz \qquad (i,j=1,2,6)$$

$$F_{ij} = \delta_{ij} \sum_{k=1}^{n} \int_{z_{k-1}}^{z_k} (\bar{Q}_{ij})_k dz, \qquad (i,j=4,5)$$

where, N is the in-plane forces vector; M is the bending/torsional moments vector; Q is the out-of-plane forces vector; ε^0 is the mid-plane strains vector; κ is the curvatures vector; γ is the transverse shear strain vector; A_{ij} is the extensional stiffness matrix; B_{ij} is the coupling stiffness matrix; D_{ij} is the bending stiffness matrix; F_{ij} is the transverse shear stiffness matrix; ΔT and Δm represent the variations of temperature and moisture, respectively. Whereas $(\overline{Q}_{ij})_k$ is the k-th ply stiffness matrix and δ_{ij} is the transverse shear correction factor.

Difficulties inherent to transverse shear deformation, anisotropy of material, blade geometry and boundary conditions constitute a complex and tedious analysis, which makes it impossible to provide a mathematical solution. To overcome these difficulties, numerical solutions using finite element method (FEM) and experimental investigations are the only approaches that can be employed.

B. Finite Element Analysis

A rigorous calculation of a wind turbine blade structure is generally complex. It may be interesting to obtain rapidly some estimated results for a simplified blade model using analytical formulations. However, for better approach the analysis becomes complicated and the analytical formulations may not provide acceptable results for use in practice. In such situation, the finite element method (FEM) is one of the numerical methods that can provide approximate solutions making then the process of optimum design easily achieved. The derivation of the FE formulations is out of scope for this analysis. However, theories and fundamentals related to the FEM can be found in [19, 20]. It should be pointed out, however, that due to the complex shape of the blade, the anisotropy of the material, the type of applied loads and the degree of accuracy, the elaboration of a numerical model of the blade-structure becomes a complex task, where the solution by the FEM turns into a difficult undertaking work.

For this purpose, a validated commercial finite element computer program can be used to perform analyses of the blade structural behaviour when subjected to static and dynamic loading conditions. To this end, the physical model can be divided longitudinally, transversely and vertically (for stiffeners) into a large number of elements.

Since the elements type choice, used for the discretisation of the different components constituting the whole blade-structure, has a significant influence on the output results, the selected element must be representative and consistent with the real case. For instance, the four-node 12-DOF (degrees of freedom) rectangular plate bending element (see Fig. 15) can be used to create a mesh for the upper and lower blade surfaces; each node possesses six independent degrees of freedom: three displacements u, v, w and three rotations θ_x, θ_y, θ_z. However in most cases of analysis, the rotation around the z-axis θ_z is neglected. On the other hand, the points of attachment of the blade root to the turbine rotor are modelled as fully clamped boundary conditions.

Once the numerical results are obtained, their analysis reveals that further means of strengthening the blade structure still needed to be applied. This requirement is achieved through a reinforcement of the internal section of the blade (i.e., airfoil) with longitudinal stiffeners or box beam structures. Under these conditions, a preliminary study should be undertaken to determine the appropriate number of stiffeners and their position with respect to leading edge. In this context, [21, 22] have developed some interesting results that may be exploited by the wind turbine industry, showing the possibility to reduce the maximum displacement of a composite plate without introducing weight penalty by the incorporation of one, two or three stiffeners as a structural reinforcing elements.

Further numerical results on the blade structural behaviour show that areas with irregular geometrical changes, characterised generally by the shift from a circular shape to airfoil shape, reveals the presence of stress concentration at the transition zone. Therefore, a particular study must be undertaken on the highly stressed areas, and this in order to check the condition of non-failure of individual plies. For this purpose, several criteria of ply failure have been developed and are available in composite materials literature, namely: Tsai-Hill, Tsai-Wu and Hoffman criteria.

For instance, the Tsai-Hill failure criterion function in the state of plane stress (i.e., $\sigma_3^{(k)} = \tau_{13}^{(k)} = \tau_{23}^{(k)} = 0$) is given for each ply constituting the laminate by the following Eqs. [17, 18]:

$$\left(\frac{\sigma_1}{X}\right)^2_{(k)} + \left(\frac{\sigma_2}{Y}\right)^2_{(k)} - \left(\frac{\sigma_1 \sigma_2}{X^2}\right)_{(k)} + \left(\frac{\tau_{12}}{S}\right)^2_{(k)} < 1 \tag{3}$$

where, X is the maximum tensile (compressive) failure stress in the *1*-direction, Y is the maximum tensile (compressive) failure stress in the *2*-direction and S is the maximum shear failure stress in the *1-2* plane.

Fig. 16 illustrates an example of stress concentration for static analysis of a typical ply composing the laminate blade within the transition zone. Failure plies are those for which the failure criterion function, described by Eq. (3), is greater than the limit value of 1 (i.e., 100%).

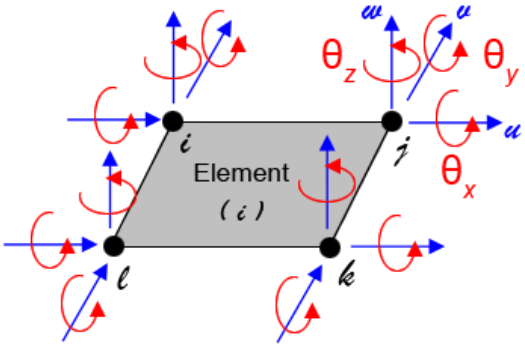

Fig. 15 Four-node 12-DOF rectangular plate bending element

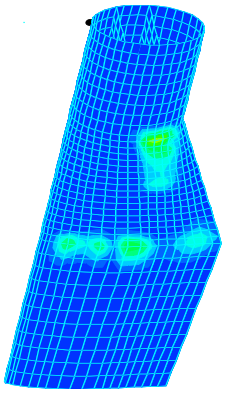

Fig. 16 Stress concentration in the transition zone for the *k*-th ply

By applying the Tsai-Hill criterion for the case of 8 m blade length when this latter is subjected to mechanical loading, it was found that the highly stressed ply is located within the transition zone, and the maximum value of the failure criterion function was found to be approximately equal to 85%. Whereas for the case of 24 m blade length, calculations show that the value corresponding to the highly stresses ply exceeds 100% (the concerned area is generally highlighted in red). In order to remedy this situation and avoid such failure prediction from happening, the ply initially made of glass fibre was replaced by another ply made of carbon fibre. In such case, the problem of structural analysis becomes complex because it deals now with the case of hybrid composite wind turbine blade made of two types of fibre reinforcements: glass and carbon.

In order to get a comprehensive understanding on the structural behaviour of the 8 m composite blade structure under free vibration, the modal analysis was performed using FEM computer programme and the numerical results of natural frequencies and mode shapes are plotted and presented in Fig. 17.

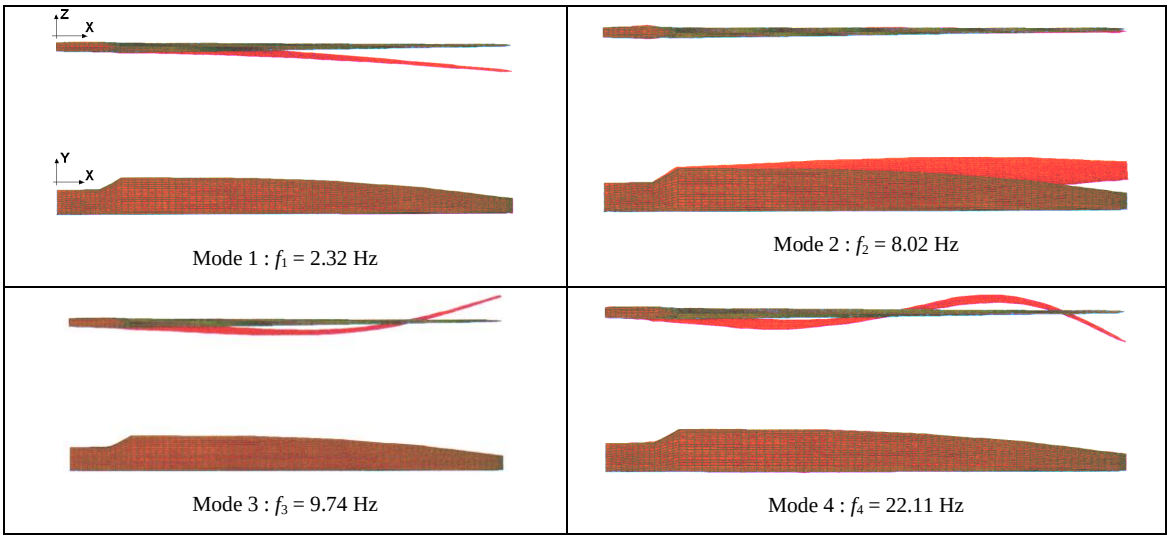

Fig. 17 First four numerical natural frequencies and associated mode shapes of a composite wind turbine blade (8 m length)

The natural frequencies which lie within the frequency range of application must be shifted beyond the forcing frequencies and this in order to avoid resonance phenomenon. The mode shapes give an idea about the deflected shape of the blade structure under each natural frequency and this information can help designers to locate the areas of high amplitudes, where fibre type and orientation could be tailored to reduce these amplitudes. For instance, incorporating fibres with high stiffness-to-weight ratio (E/ρ) can reduce the large amplitudes of vibration and lead to an increase of the natural frequencies.

C. Experimental Analysis

In compliance with the strict condition of the sub-structuring method, the boundary conditions that are representative of the real turbine blade fixture (i.e. attachment of the border blade root to the rotor system) were performed by a mechanical fastening system. It consists of fixing the turbine blade root between two circular steel frames with forty HR bolts (high strength friction grid bolts). The whole system was then mounted on a strong and stiff steel frame.

1) Static testing

For the static test, the prediction of the ultimate load that the blade is expected to withstand is performed using an inextensible cable placed at a specific location (i.e., center of aerodynamic loads in the case of small blades). The tensile force

applied to the cable represents a simulation of the resultant wind forces, the weight of the blade and eventually other loads resulting from environmental conditions. In order to avoid stress concentration and allow the applied load to be uniformly distributed over the defined location without risk of damaging the gel coat layer, a wooden system, known as a saddle, is mounted on that location; it is perfectly cut to matche the geometric shape of the blade profile at the considered section. For large blades, the system remains the same but this time is performed with several saddles positioned on different locations along the blade. It should be noted, however, that old methods and contemporary techniques can be used to predict the blade maximum bearing load, namely: sandbags, hydraulic actuators, electrical winches, ...

2) Dynamic testing

For the free vibration analysis (modal analysis), the blade is subjected to a series of base load excitation. However, the vibration data analysis of the input (impulse force) and the output (acceleration response) in the time history does not give much information for engineering purposes. Therefore, a transformation from the time domain to the frequency domain is necessary and provides the results of spectral analysis of the original time history in the form of an amplitude-frequency spectrum via the Fast Fourier Transform (FFT) technique [21]. For this purpose, an impact hammer can be utilised to obtain the blade natural frequencies, whereas a shaker can be used to demonstrate the mode shapes of vibration.

(a) For **the impact testing**, a hammer (B&K) is used to excite the blade structure via a force transducer mounted on its head. To enable the impact to be reduced but more energy to be produced to excite the whole blade structure without damage or without introducing non-linear responses, an interchangeable resilient material (rubber or plastic) can be attached to the hammer tip. The time histories of the impulse force and acceleration in the form of signals are digitally sampled and stored in a multi-channel digital recorder and controlled by a digital signal processing software which is mounted on a computer. The lower modes of resonance can be detected using a piezoelectric accelerometer stragically placed on the blade structure.

(b) For **the shaker testing**, the measurement is based on the swept frequency method. The electromagnetic shaker is suspended using elastic system and connected to the load cell through a slender rod called stringer, to allow the blade structure to move freely in the other directions (see Fig. 18). The slender rod has a strong axial stiffness, but weak bending and shear stiffness. Consequently, it carries only axial loads but negligible moments or shear loads. To excite the resonant frequencies of a large blade, the size of the shaker is proportional to the size of the blade.

(c) For the **no-contact testing**, modal testing and vibration measurements have evolved over time. For the prediction of the blade natural frequencies and associated mode shapes, the no-contact measuring devices such as the technique of laser Doppler vibrometry (LDV) are highly used because they offer several advantages over the contact measuring systems, namely in terms of high measurement resolution, no calibration of accelerometers, low hysteresis loop, no risk of damaging the blade skin, …

(d) For the **mode shape demonstration**, it is necessary to measure at each resonant frequency of the blade (i) the displacement amplitude at a sufficient number of points and (ii) the corresponding phase relationship between these points. The number of accelerometers and their location on the blade depend on the mode shape to be measured. A vibration pick-up for several points on the blade can be made and the motion of each accelerometer is recorded. Another pick-up (shaker), held at fixed point on the blade, provides a signal used as phase reference, to determine whether the blade motion at various points is in phase or out of phase with the input. And by connecting the points of different amplitudes at the same resonant frequency, the corresponding mode shape can be traced out (Fig. 19). For the higher modes, this method tends to be too complex to distinguish the mode shapes. Consequently, a large number of accelerometers are required.

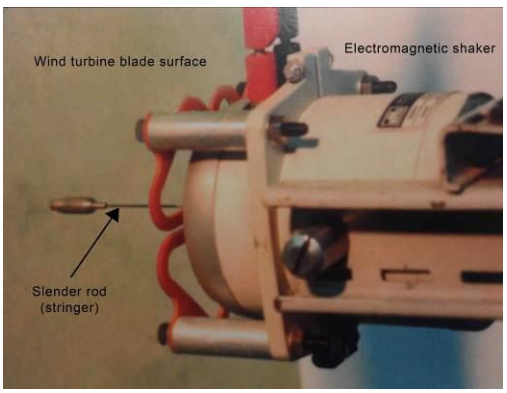

Fig. 18 Electromagnetic shaker load cell and slender rod (stringer)

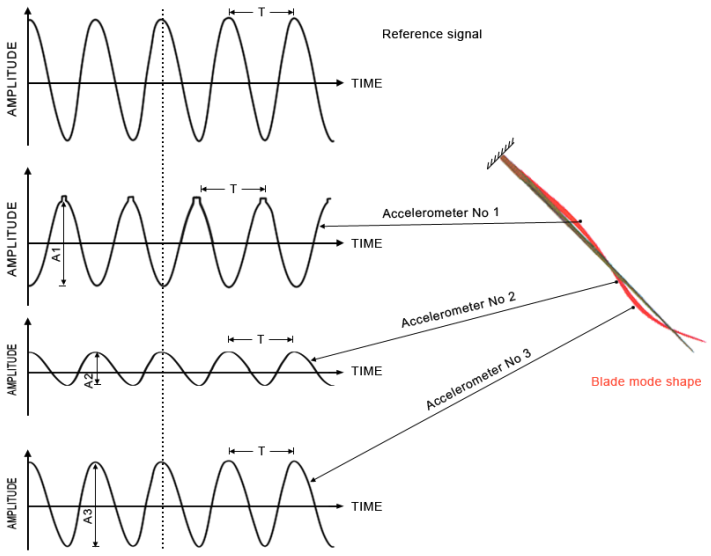

Fig. 19 Demonstration of mode shapes by the method of accelerometers

A typical magnitude against frequency relationship for the 8m composite blade is shown in Fig. 20. Each resonant frequency has a peak value corresponding to the natural frequency of that mode. As can be seen from Fig. 20, strong frequency components are noted at 2.5Hz, 10.5Hz, 23.50Hz and 40.13Hz, which are the fundamental and the three bending modes, respectively.

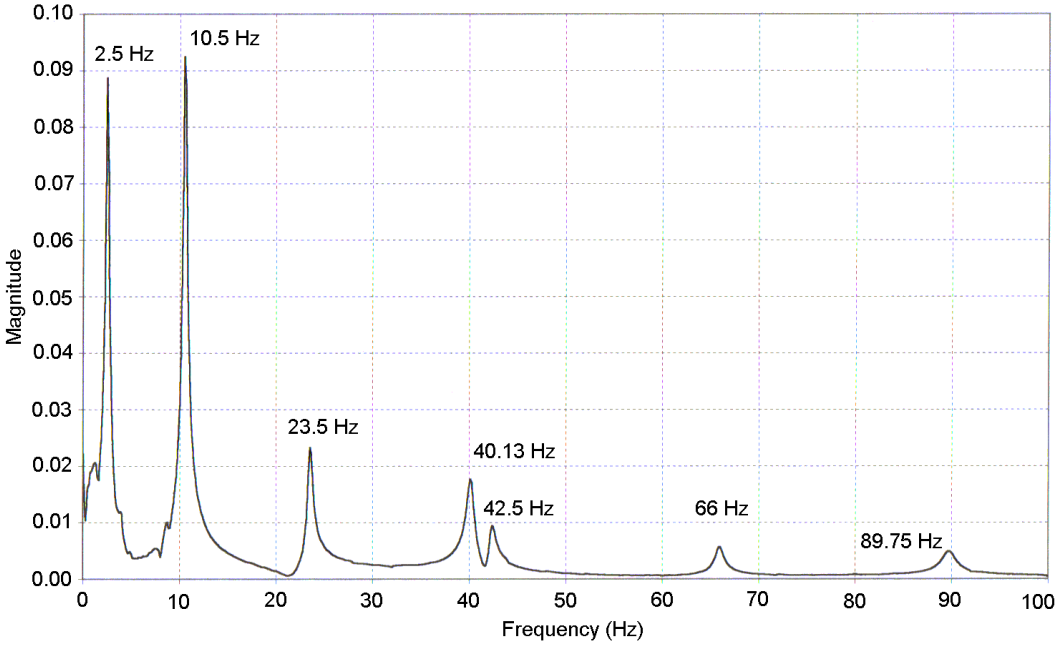

Fig. 20 FFT spectrum of clamped composite wind turbine blade (8 m)

Once the experimental and numerical structural analyses of the wind turbine blade are performed, a comparative study should be undertaken between experimental and numerical results. This correlation "test-calculation" is carried out in order to correct the numerical finite element model and determine whether the basic assumptions made on the material properties, the type of loading and boundary conditions have been properly modelled. When the correlation is good, the numerical model is accepted and validated. Then, an optimisation procedure can be initiated on the basis of the numerical model. This will save considerable time and money during the design process.

For instance, numerical and experimental natural frequency results for the 8 m composite blade are recapitulated in Table 1. It can be observed that there is a non-monotonic frequency sequence between both techniques (i.e., experimental and numerical); for some modes the natural frequencies are higher and for other modes are lower than the finite element values. The source of these variations is believed to be associated to (i) the variation in thickness of the lower/upper surfaces and internal stiffeners of the blade; and/or to (ii) the variation of the material properties. This source of discrepancies can be related to the process of manufacturing. However, a correlation between the two results shows that the percentage error between the two analyses is less than 10%: a value that is generally accepted in practice.

Further to that, it should be noted from Table 1 that the drag mode (i.e., mode 2) does not appear in the experimental results illustrated by the FFT spectrum shown in Fig. 20; this is due to the position of the accelerometer and the direction of the excitation force. For that mode, the accelerometer behaves in the same way as if placed on a nodal point (i.e., zero amplitude). In such situation, the considered mode is not detected at that position.

TABLE 1 NUMERICAL AND EXPERIMENTAL NATURAL FREQUENCIES OF 8 M COMPOSITE WIND TURBINE BLADE

Mode number	Natural frequency (Hz)	Mode description
1	2.62 (2.50)	Bending mode
2	9.53 (-----)	Drag mode
3	11.17 (10.50)	Bending mode
4	24.26 (23.50)	Bending mode
5	39.36 (40.13)	Bending mode
6	43.06 (42.50)	Bending mode
7	68.24 (66.00)	Torsional mode

(---) Parenthesized values denote experimental frequencies

D. Concluding Remarks

The use of finite element method constitutes an appropriate technique providing better approach for examination of the blade behaviour under static and dynamic conditions. The output results are obtained at low computational cost, which provides a significant advantage for optimal design analysis. In applying this technique, the significant factors influencing the static and dynamic structural behaviour are analysed and optimisation studies can be made to arrive at an adequate blade structure that fulfils an efficient structural performance coupled with an economic design. Static and dynamic analyses will provide a better understanding of the structural behaviour of the composite wind turbine blade and will determine the high stressed plies and areas with high structural deflection which are likely to yield a risk of damage.

To avoid stress concentration, resonance phenomenon as well as fatigue problems, one or a combination of the following solutions may be involved during early design development:

- minimization of the maximum structural deflections by incorporating longitudinal stiffeners without introducing significant weight penalty;
- reduction of high amplitudes by placing fibres in the most effective direction;
- minimization of high amplitudes by selecting the appropriate laminate stacking sequence;
- optimisation of the natural frequencies via composite materials that exhibit high stiffness-to-weight ratio;
- reduction of the vibration amplitudes by choosing resin matrix exhibiting high viscoelastic damping.

A comprehensive modelling of a finite element solution from an experimental procedure should be undertaken before parameter studies are made. This will ensure a reliable design, allowing the blade structure to operate safely under severe static and dynamic conditions within the application range of loading and forcing frequencies.

IV. MANUFACTURING PROCESSES AND FORMULATION OF THE PERMEABILITY

A. Manufacturing Processes

In the wind turbine industry, commonly three-bladed turbine, each composite blade can be manufactured using either open mould (e.g., hand lay-up, spray-up) or closed mould (e.g., infusion, resin transfer moulding = RTM for short). However, to respond positively to the new regulations put into force on manufacturing processes and control of VOC (volatile organic compound) emissions such as styrene vapours, it is imperative to use the technology of closed mould. This will indeed ensure the sustainability of the manufacturing process.

With this argument as an objective, two processes currently used for the production of composite wind turbine blades will be discussed in the next section of this chapter; these are: (i) the vacuum infusion process and (ii) the RTM process. However, particular attention and a significant interest will be given to the RTM process. The reason for this is that, in addition to the participation in the reduction of VOC emissions, the RTM process has an industrial solution for the production of wind turbine blades coupled with high quality finishing, good mechanical properties, lower cost, and a total absence of bonding operation of half shells.

1) Vacuum infusion process

The principle of this moulding process consists of applying firstly a release film on the inner face of the mould, followed by a thin layer of gel coat. Next, comes the application of dry fibre reinforcements over the coated area, followed by (i) a peel ply, (ii) a separator film and (iii) a breather. Finally, the whole system is enveloped in bagging film (air tight plastic film) as shown in Fig. 21. Thus, the plastic film will play the role of the top part of a standard mould and acts as a flexible support. Under these conditions, the vacuum created in the closed chamber allows the resin to spread and gradually impregnate the fibre reinforcements until saturation. Once the resin is cured, the plastic film, the peel ply, the separator film and the breather are removed and the upper or lower blade parts are easily demoulded using compressed air and plastic wedges acting as spacers. Before operating, specific locations are carefully defined to prevent any kind of scratches that may occur to the coated blade surface while using plastic wedges.

When applying this process, the composite blade structure is made from two half-shells (upper and lower skins) and a longitudinal spar reinforcement; where each structural part is moulded separately. Then, all the parts are bonded together with a bi-component adhesive (resin and hardener) for producing the full blade. Fig. 22 illustrates an airfoil cross-section of a wind turbine blade internally reinforced by either a box beam configuration or shear web (stiffeners) as shown in Figs. 22a and 22b, respectively. Areas where the adhesive is applied are highlighted in red. At these bonded areas, the transfer of loads from one structural component to another must be performed without any adverse effect that could damage the mechanical strength of the adhesive joint. In the design procedures, the adhesive joint must be designed strong enough to perform safely in operating conditions and hold up the maximum load bearing capacity, fatigue resistance and climate conditions. With these reactions in mind, the author has undertaken some research and development studies on the evolution of the shear stress through the adhesive joint length and the output results are presented and discussed elsewhere [23].

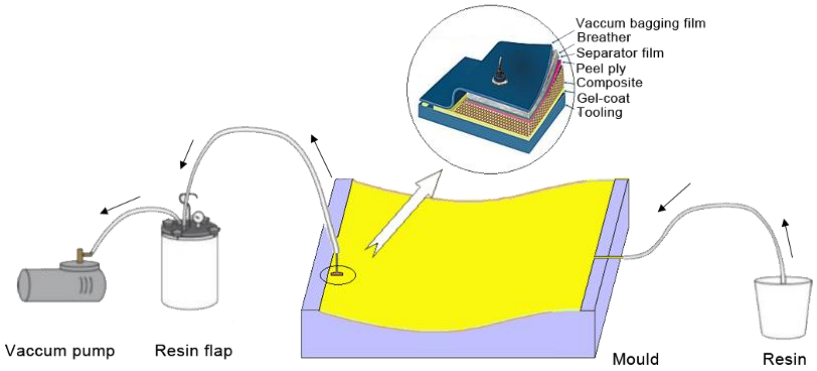

Fig. 21Vacuum moulding process

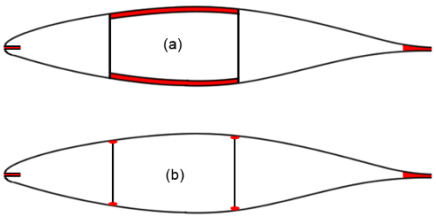

Fig. 22 Blade airfoil bonded areas:
(a) box beam, (b) shear web

In order to avoid the bonding operation of different blade parts and consequently the adhesive joint design and the analysis of its risk of failure, the RTM process is seen to be an alternative and key solution to overcome these issues with a total absence of bonding operations.

2) RTM moulding process

The principle of the RTM process is the same as the infusion, except that the plastic film used in the infusion process is now replaced by the rigid part which in fact represents the upper component constituting a standard mould. The process involves injecting the resin in liquid form into a closed mould cavity, in which the dry fibre reinforcement (glass-fibre preform) was previously placed, relies primarily on the use of pressure difference that occurs inside the closed cavity, allowing the resin to flow and therefore impregnate the preformed dry reinforcement [24, 25]. Fig. 23 illustrates the different stages of the RTM process, which are summarized by [26]:

- *Stage 1*: selection of fibre reinforcement recommended by the design office;
- *Stage 2*: preparation of the fibre preform (orientation of fibres and stacking sequence);
- *Stage 3*: closing the mould and venting operation after placing the fibre preform;
- *Stage 4*: injection of the resin and progressive impregnation of the reinforcement until filling;
- *Stage 5*: polymerisation, drying and hardening of the resin (curing);
- *Stage 6*: opening the mould and demoulding the whole part of the composite blade.

Stage 4 appears to be an important phase in the RTM production process of composite wind turbine blades. In fact, this phase of injection and flow of a resin through the fibrous medium is based on the use of Darcy's law [27] which is mainly governed by the permeability value of the resin *k*, a physical characteristic representing the capacity of resin transfer through the fibrous material that has been selected by the design office. Given the importance of this physical characteristic, a particular study is dedicated to the formulation and measure of the permeability.

As a matter of fact, this permeability depends on several factors such as the nature of the reinforcement, the direction and arrangement of fibres, the stacking sequence of plies, the temperature of the resin, the position of injection-vent ports, and so forth. Therefore, the simulation of flow behaviour in an anisotropic fibrous medium [28] must be studied carefully and the permeability values have to be correctly defined, because a minor error in the calculation of these values can lead to considerable variations that cannot be accepted in practice.

In such RTM process, the injection ports are located on the trailing edge, whereas the vent ports are located on the leading edge. The resin flow behaviour through the fibrous preform during mould-filling stage is simulated using a commercial finite element software developed specifically for this purpose.

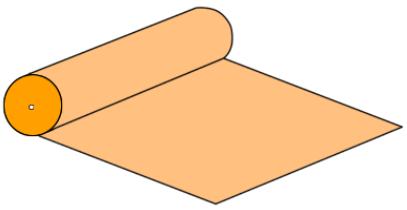

(1) Dry reinforcement

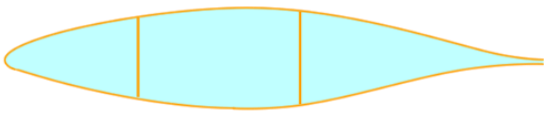

(2) Stage Preform

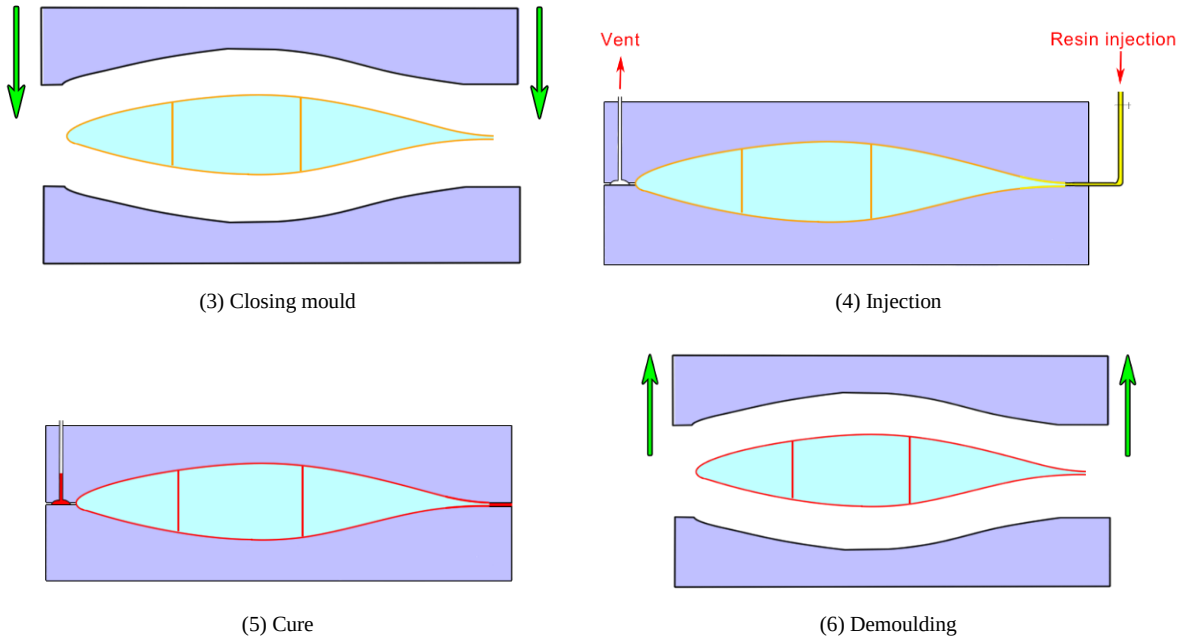

(3) Closing mould (4) Injection

(5) Cure (6) Demoulding

Fig. 23 Different stages for manufacturing a composite wind turbine blade by the RTM process

B. Formulation of the Permeability (Darcy's law)

1) Method of measuring one dimensional permeability

In 1856, Henry Darcy [27] has shown that for a Newtonian incompressible fluid in laminar flow, the speed at which the fluid behaves in a homogeneous isotropic medium is proportional to the pressure gradient and inversely proportional to its dynamic viscosity.

To facilitate the comprehension of the relationship existing between the injection parameters, the analysis will first focus on the case of one-dimensional (1-D) permeability measurement for a simplified model of a wind turbine blade section, as illustrated in Fig. 24. However, it should be noted that the inner part reinforcing the blade structure (i.e., box beam or shear web) takes the form of the letter H, and thus, in order to avoid the risk of air entrapment.

From Darcy's law considerations, the flow of resin Q through a cross-sectional area S can be expressed by:

$$Q = \frac{k}{\mu} \times S \times \frac{\Delta P}{\Delta L} \tag{4a}$$

Using the pressure gradient notation (i.e., $\nabla P = \Delta P / \Delta L$) leads to

$$Q = \frac{k}{\mu} \times S \times \nabla P \tag{4b}$$

where, Q is the flow rate ($m^3 \cdot s^{-1}$); S is the cross-sectional area to be impregnated (m^2); μ is the fluid viscosity (Pa·s); ∇P is the pressure gradient ($Pa \cdot m^{-1}$) and k is the permeability (m^2).

The permeability k can be deduced from Eq. (4a), it is theoretically expressed by:

$$k = \frac{Q}{S} \times \frac{\Delta L}{\Delta P} \times \mu \tag{5a}$$

Furthermore, Darcy's experience is based on the variation of the flow rate Q as a function of the pressure drop ΔP, as shown in Fig. 25. Thus, the permeability is defined experimentally by:

$$k = \frac{\mu \times \Delta L}{S} \times (slope) \tag{5b}$$

And after replacing in Eq. (5b) the slope by its value, deduced graphically from Fig. 25, the permeability k can easily be calculated for fixed values of μ, ΔL and S.

To get an estimate of the permeability magnitude k, let us consider the following values as an example: ΔL=0.2 m; S=0.001 m^2; $\mu = 50 \times 10^6$ Pa·s; $\Delta P = 0.2 \times 10^6$ Pa and $Q = 2 \times 10^{-6}$ $m^3 \cdot s^{-1}$. Consequently, the application of Eq. (5) yields a value of permeability $\boldsymbol{k = 100 \times 10^{-12}\ m^2}$.

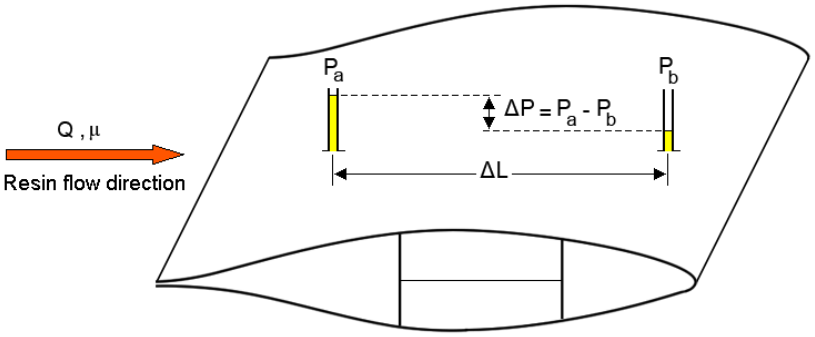

Fig. 24 Measurement of permeability by injection

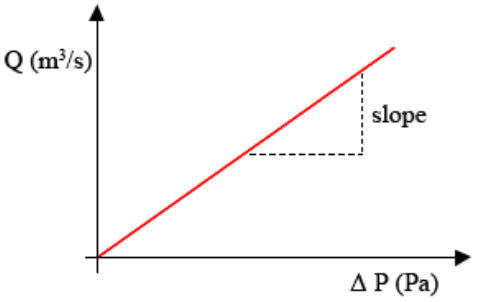

Fig. 25 Flow-pressure relationship

Dimensional study shows that in materials science, the permeability k is expressed in m^2; whereas in hydrogeology and oil/petroleum industries, this latter is expressed in Darcy (1 Darcy = 0.97×10^{-12} m^2).

Furthermore, it should be noted that in some documentation there is sometimes confusion in terminology between *permeability* and *coefficient of permeability*. It is convenient to note these two parameters by the letters k and K, respectively. In this regard, the coefficient of permeability, K, is expressed in ($m\cdot s^{-1}$) and simply defined by the following ratio:

$$K = \frac{k}{\mu} \tag{6}$$

2) Longitudinal and transverse permeabilities

Eq. (4b) can be generalized in a three-dimensional (3-D) system, as illustrated in Fig. 26, where Darcy's law can be written in the following compact matrix form [29, 30]:

$$\{\bar{v}\} = -\frac{1}{\mu}[k]\{\nabla P\} \tag{7a}$$

or in the following developed matrix form:

$$\begin{Bmatrix} v_x \\ v_y \\ v_z \end{Bmatrix} = -\frac{1}{\mu}\begin{bmatrix} k_{xx} & k_{xy} & k_{xz} \\ k_{yx} & k_{yy} & k_{yz} \\ k_{zx} & k_{zy} & k_{zz} \end{bmatrix}\begin{Bmatrix} \partial P/\partial x \\ \partial P/\partial y \\ \partial P/\partial z \end{Bmatrix} \tag{7b}$$

where $\{\bar{v}\}$ is the velocity vector ($m\cdot s^{-1}$); $[k]$ is the permeability tensor (m^2); $\{\nabla P\}$ is the pressure-gradient vector ($Pa\cdot m^{-1}$).

Generally, the thicknesses of the laminate constituting the blade structure are thin in comparison with its other lateral dimensions (length and width). To this end, the transverse permeability through the preform thickness (along the z-axis) is very small in comparison to the other lateral permeabilities and may therefore be neglected ($k_{zx}=k_{zy}=k_{zz}=0$). Based on this assumption, Eq. (7b) can be written in the two-dimensional flow system (2-D) as:

$$\begin{Bmatrix} v_x \\ v_y \end{Bmatrix} = -\frac{1}{\mu}\begin{bmatrix} k_{xx} & k_{xy} \\ k_{xy} & k_{yy} \end{bmatrix}\begin{Bmatrix} \partial P/\partial x \\ \partial P/\partial y \end{Bmatrix} \tag{7c}$$

As the permeability tensor $[k]$ depends on the angle of fibre orientation, θ; it can therefore be written as [30]:

(i) in the (1, 2) principal coordinate system: $\begin{bmatrix} k_{xx} & k_{xy} \\ k_{xy} & k_{yy} \end{bmatrix} = \begin{bmatrix} k_{11} & 0 \\ 0 & k_{22} \end{bmatrix}$

(ii) in (x,y) general coordinate system: $\begin{bmatrix} k_{xx} & k_{xy} \\ k_{xy} & k_{yy} \end{bmatrix} = \begin{bmatrix} k_{11}C^2+k_{22}S^2 & (-k_{11}+k_{22})CS \\ (-k_{11}+K_{22})CS & k_{11}S^2+k_{22}C^2 \end{bmatrix}$

where, $C = cos\theta$, $S = sin\theta$

Also, the permeability in (1, 2) system can be evaluated from Carman-Kozeny Eq. [31] as follows:

$$k_{ij} = \frac{1}{c_{ij}}\frac{R_f^2}{4}\frac{(1-V_f)^3}{V_f^2} \quad (i, j=1, 2)$$

where c_{ij} is Kozeny constant, R_f is the fibre radius and V_f is the fibre volume fraction.

In the case of 3-D system flow, the average transverse permeability $\bar{k}_{ij}$ for a preform composed of n plies can be calculated according to the rule of superposition:

$$\bar{k}_{ij} = \frac{1}{H}\sum_{k=1}^{n} h^{(k)} k_{ij}^{(k)} \tag{8}$$

where H is the total thickness of the preform and $h^{(k)}$ is the thickness of each ply k (k= 1, 2, .., n).

Using a combination of Darcy's law and continuity equations yields the equation governing the pressure distribution, which can be written in compact matrix form as:

$$\nabla \cdot \left(\frac{[k]}{\mu} \{\nabla P\} \right) = 0 \tag{9a}$$

Or in fullydeveloped form, Eq. (9a) can be written as:

$$\frac{\partial}{\partial x}\left(\frac{k_{xx}\,\partial P}{\mu\,\partial x} \right) + \frac{\partial}{\partial x}\left(\frac{k_{xy}\,\partial P}{\mu\,\partial y} \right) + \frac{\partial}{\partial y}\left(\frac{k_{yx}\,\partial P}{\mu\,\partial x} \right) + \frac{\partial}{\partial y}\left(\frac{k_{yy}\,\partial P}{\mu\,\partial y} \right) = 0 \tag{9b}$$

This system of equations can be solved by numerical approaches for which the associated boundary conditions are appropriately defined [31].

For large-scale composite wind turbine blades, designed mainly for offshore applications, the resin injection is carried out in a sequential manner. In application of this technique, Fig. 27 shows the position of the injection and vent ports and illustrates how the injection process is performed. This latter starts from the blade root, defined by the section S_1 (transition zone), and once the fibrous preform corresponding to section S_1 is saturated with resin, the operation of injection is then moved progressively to the next section S_2 and so on, until the last section S_n is reached. This latter case corresponds here to the section covering the blade tip.

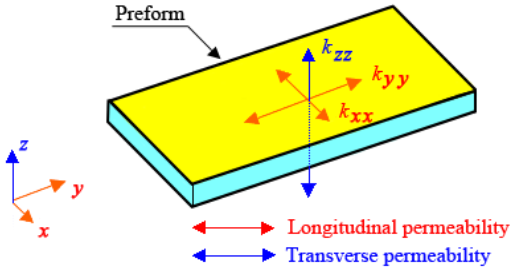

Fig. 26 Permeabilities in a 3-dimensional flow system

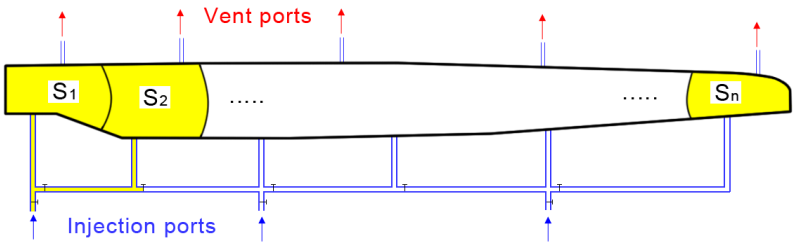

Fig. 27 Sequential injection for RTM process

C. Simulation of Flow Resin Behaviour for Composite Wind Turbine Blade Section

1) Case of orthotropic preforms

Three cases of lay-up constituting the orthotropic preforms were achieved by superposing several unidirectional plies, all orientated in the same angle θ; these are: (i) lay-up at [0 °], (ii) lay-up at [90 °] and (iii) lay-up at [45 °]. Positions of injection and vent ports are illustrated in Fig. 28a-c. The angle θ=90 ° is the reference angle which corresponds to fibres orientated along the length of the blade.

From Fig. 28a, it can be seen that the flow of the resin along the fibre direction θ=0 ° is more important than the other directions (Figs. 28b and c). The reason for this is due to the presence of important volume fraction of pores in the longitudinal direction of fibres that are parallel to the direction of resin flow. Obviously, the presence of these pores will provide the preferential path of resin flow through the porous medium and will accelerate the process of impregnation. However, this case of fibre orientation does not reflect the real stacking sequence for wind turbine blades.

For the case shown in Fig. 28b, it has been found that when the fibres are orientated at θ=90 ° (close to the practical case of design), the flow rate is slow compared with the previous case. This difference can be explained by the fact that when fibres are perpendicular to the direction of resin flow, the fibre arrangement will create a sort of barrier that prevents the resin from spreading easily in the fibrous medium because of the low presence of volume fraction of pores in such direction. Therefore, the idea of a concentric flow of resin with regard to the position of single-point injection is not truly representative for orthotropic fibre preforms.

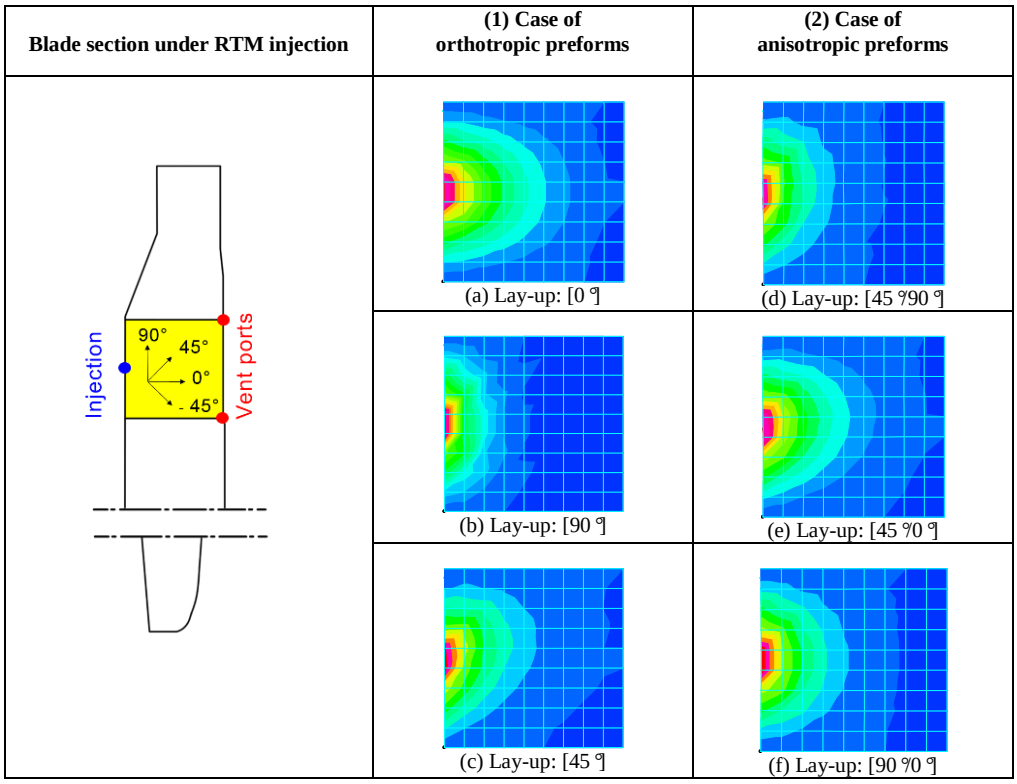

Fig. 28 Numerical simulation of resin flow behaviour during mould filling stage for one and double-layer fibrous preforms

2) Case of anisotropic preforms

For this case study, the positions of injection and vent ports are the same as those of the previous analysis. However, the three lay-up cases constituting the anisotropic preforms were achieved by superposing alternatively several unidirectional plies with two specific angles of fibre orientations. To this end, three different case studies were considered in this analysis; these are symbolised by the following staking sequences: [45 °/90 °], [45 °/0 °] and [90 °/0 °]. The output results of this investigation are presented in Fig. 28d-f.

It can be discerned that the resultant flow is dominant in the case where stacking arrangement presents a significant distribution of volume fraction pores through the fibrous preform. This provides a better flow of resin as shown in Fig. 28f. On the contrary, the drainage of resin is slower and less important for the case shown in Fig. 28d. In addition to the fibre direction effects, it should be pointed out that permeabilities depend also on the order of stacking sequence of layers (mainly for the transverse permeability). However, these factors were not considered in this analysis.

But, it should be noted that the choice of an appropriate stacking sequence is usually determined by a finite element structural analysis. The output results must meet the criteria required by the technical specifications and at the same time the applied standards for certification. Therefore, any change in the fibre orientation of layers constituting the preform may, in one hand, promote the process of drainage of the resin, but can, however, affect the mechanical properties of the material and consequently the stiffness and strength of the resulting composite wind turbine blade. The final choice of stacking sequence must respond favourably and simultaneously to the conditions defined by the numerical calculations and those imposed by the principles governing the RTM process. This particular issue should be carefully considered before the implementation of the RTM process.

V. REPAIR METHODS AND MAINTENANCE PROCEDURES

A. Different Types of Defects and Damage

1) Manufacturing defects or anomalies

Defects associated to composite wind turbine blades are usually due to the type of production process used and/or to the non-qualification of operators. In the ISO quality system, these defects are defined as “anomalies” that can be classified as either minor or major. Some of the anomalies that can appear during blade manufacturing are the following [32, 33]: improper fibre volume fraction, gel-coat/skin debonding, porosity; matrix cracking, misalignment of fibres, improper matrix distribution and so forth.

Poor impregnation between the plies and/or porosity defects may be the main factors that could cause the delamination

phenomenon. Its presence results in a separation between plies, and this can easily cause the risk of local buckling which could substantially alter the overall stiffness of the blade and its critical buckling load, and this can lead to premature failure of the blade. Therefore, a comprehensive study on the delamination growth must be performed on the most stressed upper and lower blade laminates, where the effects of the critical load on the length of delamination will be identified and analysed.

2) Damage mechanisms

Types of damage that may arise during service life can be classified as: bird strikes, harsh sun, lightning strikes, leading edge erosion (e.g., sand and sea-salt), surface erosion (e.g., heavy rain, ice, hail and insects), adhesive joint failure, gel-coat cracking, damage at the attachment points and material fatigue [33, 34].

According to the climatology of the region, offshore and onshore wind turbines are exposed to climatic conditions such as variations in temperature, moisture, sand and salt laden air. These natural events can easily damage the skin of the blade, especially the gel-coat layer. However, a composite wind turbine blade is highly durable if the layer that protects the blade skin from external environment exhibits good physico-chemical characteristics (e.g., high modulus of elasticity, good elongation after rupture, higher resistance to erosion, adequate thickness, absence of porosity, ..).

The inappropriate choice of these characteristics can result in risk of formation of blisters, creation of small cavities and appearance of cracks; resulting in a laminate exposure to external environment and facilitating contact with natural phenomena (e.g., ice, temperature variation, contact with sea/rain water, ..). These risks can be regarded as the main factors that accelerate degradation, aging and reduction of a wind turbine blade lifetime. Consequently, during the design process, a particular study on the behaviour of the gel-coat to weather events and to hygrothermomechanical loading must be undertaken to predict the adverse effects.

B. Reference Documents for Repair

Certifying bodies and associated documents for certification do not provide sufficient repair procedures specific for wind turbine blades. However, it is important that instructions for repair and maintenance must be clearly defined and standardized in order to be equitably exploited by the various wind energy companies. The availability of approved guidelines will regulate all activities related to the repair techniques and maintenance procedures for each type of composite wind turbine blade. Associated procedures should have the same level of requirements as the existing set of rules established by the FAA (Federal Aviation Administration) and DGCA (Directorate-General for Civil Aviation), namely the joint aviation requirements (i.e., JAR Part 145) and the federal aviation regulation (i.e., FAR Part 145).

C. Repair Process

Damages in service or manufacturing defects can be detected through periodic inspection or quality control, usually carried out by qualified operators. For manufacturing defects, the techniques that can be used for detecting the non-conformities include: visual inspection, tapping test or NDT (Non-Destructive Test). Moreover, for detecting damages in service, the most widely used techniques are mainly: thermography, shearography, binoculars, ultrasonic testing and sometimes X-Ray. However, it is recommended not to use the latter technology because of the potential risk of X-ray to human health.

According to the assessment of defects and damages (minor or major), the composite blade structure may be repaired or fully replaced using typical procedures, usually inspired from international aviation standards, for example the Aircraft Structural Repair Manual (SRM). For on-site repairs, operators must be qualified in repair of composite structures and in the same time have the climbing skills.

D. Scarf Repair Technique

The most common repair method used is the scarf repair method which is performed by the following steps (Fig. 29):

- localisation of the damaged area;
- removal of material at the damaged area;
- definition of the geometry of the area to be repaired;
- definition of the appropriate stacking sequence;
- cutting fibre plies with fitting sizes;
- application of an adhesive film;
- stacking up plies in accordance with the order and orientation assigned to each ply;
- adding extra plies (if this does not affect the aerodynamic efficiency of the blade);
- utilisation of hot bond repair unit for the curing phase (Fig. 30).

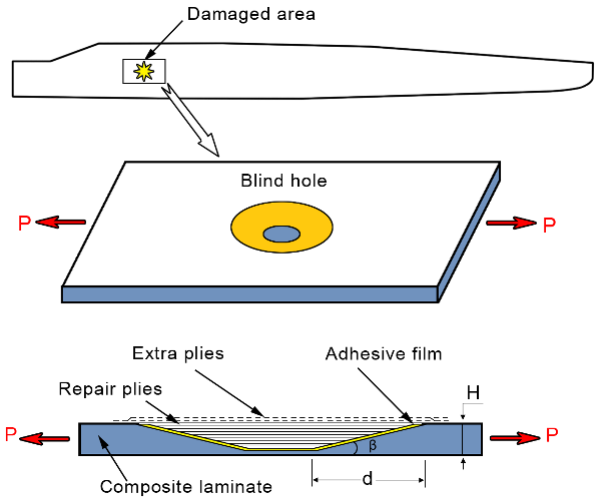

Fig. 29 Schematic showing the repair patchhnique technique

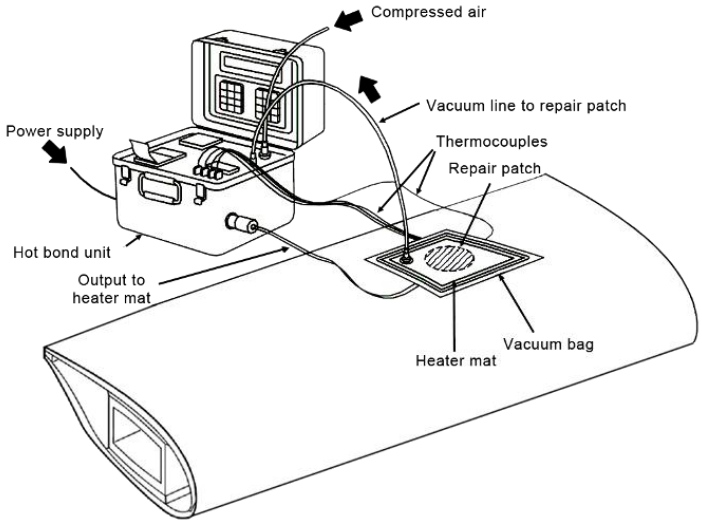

Fig. 30 On-site repair using a hot bond repair unit (Anita)

For instance, Fig. 29 shows the pattern of damage located near the transition zone. The damage is assumed to be a blind hole (30 to 80% of the thickness). The repair patch edges are tapered and the corresponding bevelled angle β is variable from 2 to 3. The filling operation is performed using the technique of deposition ply-by-ply or layer-by-layer. The necessary equipment for curing may be performed using a mobile hot bond repair unit, as shown in Fig. 30.

As the repaired structure will not have the same mechanical characteristics as the original one (undamaged structure), it is therefore important, but not indispensable, to add extra plies in order to compensate the loss in strength and stiffness. However, it should be noted that the added extra plies can create extra weight, and thus a residual unbalance (since the mass will not be uniformly distributed). On the other hand, extra plies may also cause stress concentration problem due to the slight modification in the blade aerodynamic profile at the repaired zone which may lead to a loss of skin smoothness and thereby reducing the aerodynamic efficiency of the blade.

VI. LIFE CYCLE ANALYSIS, ECODESIGN AND RECYCLING METHODS FOR COMPOSITE WIND TURBINE BLADES

A. Life Cycle Analysis of Composite Wind Turbine Blades

The life cycle analysis (LCA), or life cycle assessment, is an environmental evaluation method for quantifying the impacts of wind turbine blades throughout their entire life cycle, ranging from the extraction of raw materials, manufacturing, transportation, use and maintenance to the end of life, taking into account the sustainability requirements, REACH regulations and the ecodesign notion. Although the average lifespan of a composite wind turbine blade is between 20 to 25 years, it is predicted that by 2034, around 225000 tonnes of composite materials originated from wind turbine blades will be recycled each year all over the world.

International Standard ISO 14040 specifies and explains the different phases of the implementation of LCA before, during

and after the design process of composite wind turbine blades. From an environmental point of view, LCA plays a crucial role in developing effective ways to reduce ecological risks and help promote green production. With this in mind, environmentally conscious designers of blades have to factor in the impacts of their products on the environment and find new alternatives to make the bade-product more competitive in the worldwide composite market, by means of clear regulations, specific safety standards and legal predictability [12].

B. Ecodesign of Composite Wind Turbine Blades

In addition to the classical design criteria applied for the production of blades, the ecodesign notion is a new approach which takes into account new criteria for innovative blades, ranging from waste management, reduction in VOC emissions, optimisation of energy consumption, waste recovery system, to ways of recycling specific to blades retired from service. In order to achieve these requirements, an ecodesign key performance indicator (KPI) can be developed on the basis of probability theory rules. This KPI will provide blade designers the ability to control via green rules the performance level of assessment for each design step. For further details on this subject area, the reader is invited to refer to previous works conducted by the author and published elsewhere [36-38].

C. Recycling Methods for Composite Wind Turbine Blades

Composite materials used in the manufacture of wind turbine blades are a combination of fibres and a polymer matrix. The fibres chosen are usually glass fibres, carbon fibres, natural fibres or a hybrid (i.e., composed of two or more fibres of different natures). The polymer matrix selected may be thermosetting or thermoplastic. However, due to the existence of cross-linking phenomenon within the molecular chain of thermosetting polymer matrices, they are hard to recycle. Thus, there are actually two major recycling methods employed in the wind industry; these are: (i) the mechanical method and (ii) the thermal method.

For both recycling methods, the first step is to cut in-situ the retired wind turbine blades into small pieces in order to facilitate their transportation to the recycling plant. For the mechanical method, the following step is to crush with a mechanical hammer the blade pieces and transforming them into grains with variable diameters: e.g., 50 μm for fine grains and 10 mm for coarse grains. The recycled materials can then be used in other applications such as civil engineering. For the thermal method, the next step is to put (after the cutting operation) the different cut parts into a rotary kiln incinerator and then burn them at a temperature of 500 ℃ using the pyrolysis process. Consequently, the polymer matrix is fully burned and transformed into a gas which may be recovered and used for the production of electrical energy. Residues of the fibres can be used in other structural applications such as ingredients of concrete in the construction of buildings and roads. They can also be used as a structural component within other less stressed composite structures.

In fact, studies show that glass fibres are the most commonly used in the manufacture of wind turbine blades because they are less expensive. Whereas, thermosetting polymer matrices (polyester and epoxy) do not attract much the attention of blade manufacturers, as their use will face the problem of recyclability. In contrast, thermoplastic polymer matrix is one of the most attractive ones and is intended to be used in the manufacture of future wind turbine blades; it provides the possibility to be easily recycled after use and therefore sustainable. For instance, an innovative anionic polyamide PA-6 thermoplastic matrix has been developed and intended to be incorporated in the wind blade industry [39].

VII. PROCEDURES OF QUALIFICATION AND CERTIFICATION

A. Qualification of Wind Turbine Blades

This part includes static and dynamic testing of a composite wind blade manufactured by a special process. The qualification process is characterized by a verification of the compatibility between the blade design and the aerodynamic and/or environmental loads (temperature and moisture) that the blade may be subjected to during its lifetime. These tests consist in imposing a static and dynamic environment more severe than the real case [8].

The experimental testing methods consist in manufacturing a blade prototype and making it undergo static and dynamic testing in laboratory for the identification of critical areas that can cause failure. These experimental methods are described and detailed in Section III.

Working in this context, a test bench and strain gauges are needed to perform the fatigue testing. The experimental results will quantify the lifetime of the blade with a degree of confidence. On average, the lifespan is estimated at 23 years old.

B. Certification of Wind Turbine Blades

In accordance with ISO standards and IEC procedures relative to the blade design, Fig. 31 shows the main steps for the certification process [15]. Certification of wind blades may be issued by a competent body such as Germanischer Lloyd (GL).

The certification for a specific wind turbine blade is carried out on the basis of IEC 61400 standards and external audits which focus mainly on the following points:

- the evaluation of design reports and associated documents;

- the evaluation of the site and its manufacturing processes;
- the evaluation of testing equipment for static, dynamic and fatigue analyses;
- the control of the qualification of operators and workers involved in the design process;
- the evaluation of experimental/numerical results and validation of blade prototypes;
- the assessment of the quality management systems;
- the declaration of commitment regarding the periodic monitoring.

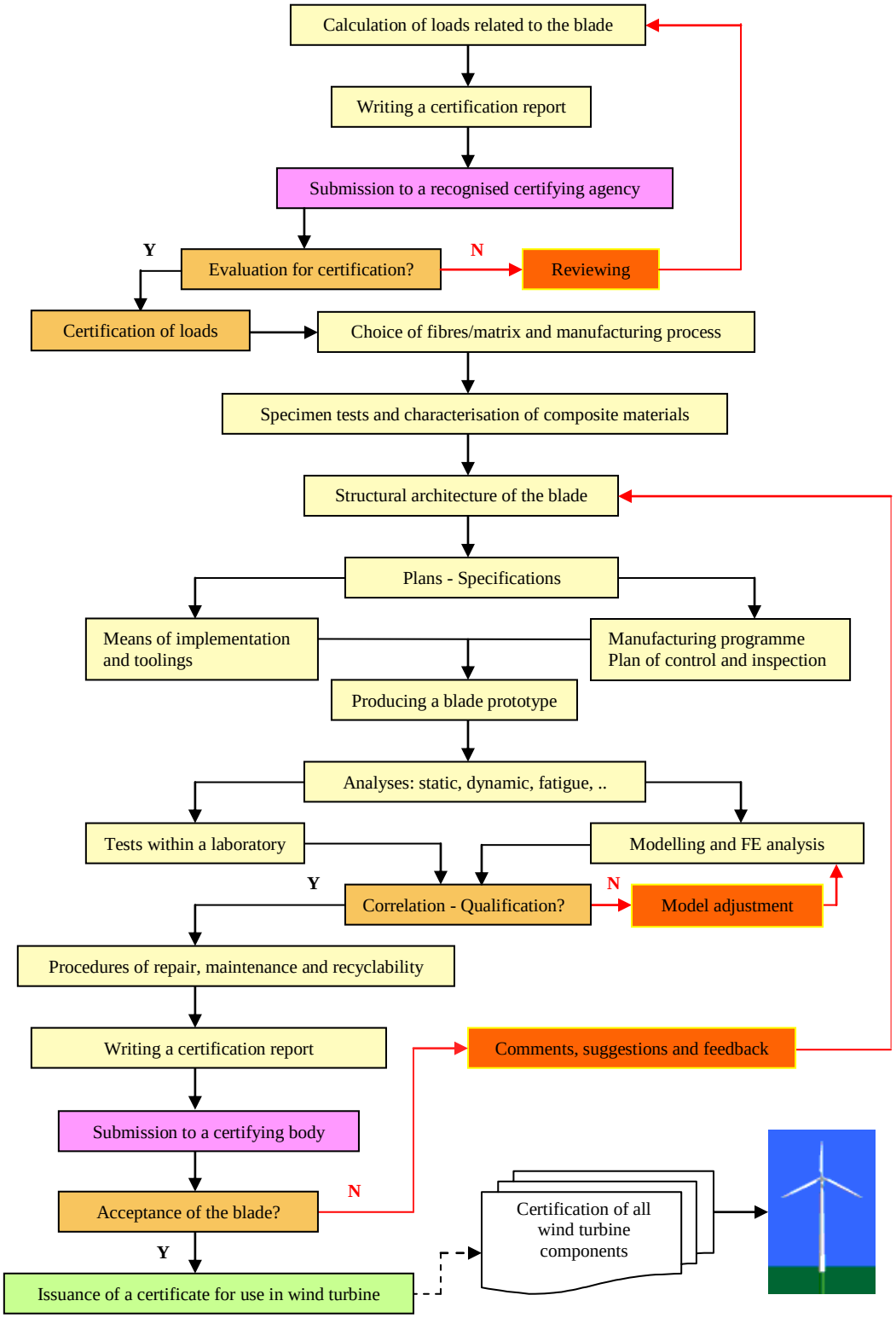

Fig. 31 Flowchart summarising the process of qualification/certification of a wind turbine blade

VIII. CONCLUSIONS

To minimise the effect of global warming and leave a more stable environment for future generations, each country with windy areas is encouraged to play a crucial role in boosting research, innovation and creativity in the field of wind energy, particularly in the technology of composite wind turbine blades. This eco-action can help energy consumers and stakeholders to be less dependent on the fossil fuels as the rate of GHG emissions is increasing and continue to accelerate the global warming phenomenon.

Moreover, this survey is in line with the European Union roadmap on wind energy and responds to the 3×20 objectives that must be achieved on 2020, namely:

- 20% reduction in GHG emissions;
- 20% increase in the share of renewable energies;
- 20% reduction in energy consumption.

For wind energy, composite materials based on glass fibres and/or carbon fibres occupy a predominant place in the modern industry of wind turbine blades. Indeed, these materials offer attractive advantages in terms of specific stiffness and specific strength. However, besides these advantages, the notion of ecodesign has to be taken into account in all design stages for the production of green, clean and eco-friendly wind turbine blades. As a matter of fact, the ecodesign approach has become one of the most efficient tools aiming to preserve the environment and protect human health during the design process and this, alongside traditional criteria such as cost effective, quality, feasibility and market expectations.

In fact, to meet the ecodesign requirements within the manufacturing processes of composite wind turbine blades, companies that are engaged towards the implementation of environmental management system (EMS) are encouraged to boost and develop the following main points:

- the development of clean manufacturing processes by reducing emissions of VOCs;
- the development of new high-performance materials with cost effective and environment friendly;
- the creation of specific standards for qualification, repair and recycling of composite blades at the end of their life-cycle;
- the implementation of cooperative activities between the university, research centres and the industry;
- the encouragement of innovative technology transfer;
- the development of university-entreprise training partnerships (UETPs) to form more technical engineers for production, repair and maintenance activities in the wind energy technology.

It is in the context of global efforts to fight against climate change for which this chapter has been developed enabling the improvement of design process, qualification and certification of future wind turbine blades. This will providentially offer great potential for the development of clean energy and the guarantee of a new security of energy supply. In addition, were also taken into account the environmental impacts and requirements regarding health, hygiene & safety, while remaining consistent with a logic cost-efficiency ratio.

ACKNOWLEDGMENT

The author would like to thank Mr. Cherif Attaf for his help and kind assistance in improving the quality of figures and illustrations which appear in this chapter.

REFERENCES

[1] W. C, Wang, Y. L. Yung, A. A Lacis, T. Mo, and J. E. Hansen, “Greenhouse effects due to man-made perturbations of trace gases,” *Science*, vol. 194, iss. 4266, pp. 685-690, Nov. 1976.

[2] W. D Nordhaus, “To slow or not to slow: the economics of the greenhouse effect,” *The Economic Journal*, vol. 101, pp. 920-937, Jul. 1991.

[3] “IPCC 1991: Report of the fifth session of the WMO/UNEP,” Intergovernmental Panel on Climate Change (IPCC) 13-15 Mar. 1991, Geneva.

[4] L. M. Kamp, R. E. H. M. Smits, C. D. Andreisse, “Notion on learning applied to wind turbine development in the Netherlands and Denmark,” *Energy Policy*, vol. 32, iss. 14, pp. 1625-1637, Sept. 2004.

[5] T. Justin, “New record: Word’s largest wind turbine (7+ Megawatts),” in News, Renewable Power, available on line at: http://www.metaefficient.com/news/new-record-worlds-largest-wind-turbine-7-megawatts.html, 2008.

[6] A. Sarkar, D. K. Behera, “Wind turbine blade efficiency and power calculation with electrical analogy,” *Int. Journal of Scientific and Research Publications*, vol. 2, iss. 2, Feb. 2012.

[7] B. Attaf, and L. Hollaway, “Vibrational analyses of glass reinforced polyester composite plates reinforced by a minimum mass central stiffener,” *Composites*, vol. 21, N 5, 1990, p. 425-430.

[8] B. Attaf, “Vibrational analyses of fibre-reinforced composite wind turbine blades: theory and experiment,” *Europe’s Premier Wind*

Energy Event (EWEA 2013), paper ID 71, Vienna, 4-7 Feb. 2013.

[9] J. Xu, and Z. Lu, "Application of fiber-reinforced composites in wind turbine blades," *World Non-Grid-Connected Wind Power and Energy Conference (WNWEC 2010)*, Nanjing, 5-7 Nov. 2010.

[10] L. Hollaway, and B. Attaf, "On the vibration of glass/polyester composite stiffened and unstiffened rectangular plates," *Chinese Society of Aeronautics, in: Seventh International Conference on Composite Materials*, Beijing, 1989, p. 435-444.

[11] J. Gou, F. Liang, Y. Tang, and J. Kapat, "Multifunctional nanocomposites for offshore wind energy," *Proc. of the 20th Int. Offshore & Polar Eng. Conf.*, Beijing, China, 20-25 Jun., 2010.

[12] B. Attaf, "European eco-factor," *Pan European Networks: Science & Technology*, iss. 07, Jun. 2013, p. 128-129.

[13] A. J. Hart, "Nanocomposites and fibers," Lectures/Tutorials - *University of Michigan*, ME599-002, Michigan, 15 Apr. 2009.

[14] National Academy of Sciences report (2005), http://www.nap.edu/catalog/11268.

[15] B. Attaf, "Eco-conception et développement des pales d'éoliennes en matériaux composites," *Revue des Energies Renouvelables - 1er Séminaire Méditerranéen sur l'Energie Eolienne*, Tipasa, Algeria, 11-12 Apr., 2010, pp. 37-48.

[16] B. Attaf, "Structural ecodesign of onshore and offshore composite wind turbine blades," *1ère Conférence Franco-Syrienne sur les Energies Renouvelables*, 24-28 Oct., 2010, Damascus, Syria.

[17] R. M. Jones, *Mechanics of composite materials*, Scripta Book Company, Washington, D.C., 1975.

[18] O. Saarela, "Computer programs for mechanical analysis and design of polymer matrix composites," *Prog. Polym. Sci.*, vol. 19, pp. 171-201, 1994

[19] T. Y. Yang, *Finite element structural analysis*, Prentice-Hall, Inc., New Jersey, 1986.

[20] O. C. Zienkiewicz, R. L. Taylor, and J. Z. Zhu, *The finite element method: its bases and fundamentals*, Elsevier Butterworth-Heinemann, Oxford, 2005.

[21] B. Attaf, "Vibration and stability analyses of unstiffened and stiffened composite plates," PhD thesis, University of Surrey, England, UK, Jun. 1990.

[22] B. Attaf, and L. Hollaway, "Vibrational analyses of glass reinforced polyester composite plates reinforced by a minimum mass central stiffener," *Composites*, vol. 21, n 5, pp. 425-430, Sep. 1990.

[23] B. Attaf, "Ecobonding of composite wind turbine blade structural parts using eco-friendly adhesives," *Advances in Materials Science & Applications (AMSA)*, vol. 3, iss. 2, pp. 31-37, Jun. 2013.

[24] K. M. Pillai, "Governing equations for unsaturated flow through woven fiber mats. Part 1. Isothermal flows," *Composites A*, vol. 33, no. 7, pp. 1007-1019, 2002.

[25] C. Nardari, B. Ferret, and D. Gay, "Simultaneous engineering in design and manufacture using the RTM process," *Composites A*, vol. 33, no. 2, pp. 191-196, 2002.

[26] B. Attaf, "Ecomoulding of composite wind turbine blades using green manufacturing RTM process," *ISRN Materials Science*, vol. 2012, Article ID 734328, 9 pages, 2012.

[27] H. Darcy, *Les fontaines publiques de la ville de Dijon*, V. Dalmont, 1856, Paris.

[28] A. Shojaei, S. R. Ghaffarian, and S. M. H Karimian, "Three-dimensional process cycle simulation of composite parts manufactured by resin transfer molding," *Compos Struct* 65, pp. 381-390, 2004.

[29] H. Kris et *al*., "New set-up for measurement of permeability properties of fibrous reinforcements for RTM," *Composites*: Part A 33, pp. 959-969, 2002.

[30] H. P. Chung, I. L. Woo, S. H. Woo, and A. Vautrin, "Weight minimization of composite laminated plates with multiple constraints," *Compos Sci Technol* (63), pp. 1015-1026, 2003.

[31] H. Jinlian, L. Yi, and S. Xueming, "Study on void formation in multi-layer woven fabrics," *Composites*: Part A 35, pp. 595-603, 2004.

[32] M. Gower, G. Sims, R. Lee, S. Frost, and M. Wall, "Assessment and criticality of defects and damage in Material systems," Measurement Good Practice Guide No. 78, National Physical Laboratory, Teddington, Middlesex, UK, Jun. 2005.

[33] E. Greene, Marine Composites NDE: Wind Energy, SSC Project SR-1464, pp. 54-59.

[34] G. Marsh, "Meeting the challenge of wind turbine repair," *Reinforced Plastics*, pp. 32-36, Jul. /Aug. 2011.

[35] K. Larsen, "Recycling wind turbine blades," *Renewable Energy Focus*, 2009.

[36] B. Attaf, "Generation of new eco-friendly composite materials via the integration of ecodesign coefficients," In Brahim Attaf (ed.), *Advances in composite materials-Ecodesign and analysis*. Intech Open Access Publisher, 2011, p. 1-20.

[37] B. Attaf, "Probability approach in ecodesign of fibre-reinforced composite structures," *in Proc. CAM'09*, Algeria, 2009.

[38] B. Attaf, "Eco-characterisation of composite materials," *JEC Composites* 42, 2008, p. 58-60.

[39] K. V. Rijswijk, "Thermoplastic Composite Wind Turbine Blades – Vacuum Infusion Technology for Anionic Polyamide-6 Composites," PhD dissertation, Delft University of Technology, Delft, 2007.

Brahim Attaf works as an independent Expert/Researcher in the field of composite materials and structures. He obtained his Engineering degree from the Ecole Nationale Polytechnique of Algiers (ENPA), Algiers, Algeria, in 1985, and then his Ph.D. degree from the University of Surrey, Guildford, UK, in 1990.

He has previously worked as a Lecturer/Researcher (Maitre de Conferences) within the Departments of Aeronautics, Mechanics and Civil Engineering at the University of Blida in Algeria (1990–2000), and he was responsible for design office and quality assurance with composite firms in France (2000–2003). Since 2003 he has been independently involved in sustainability research actions leading to ecodesign of composite materials and structures through the integration of environmental and health aspects into product lifecycle. His main

research and teaching interests focus on vibration and stability analyses of composite structures subjected to hygrothermomechanical loading using finite-element approach and experimental investigations.

Dr. Attaf has published many scientific papers, edited two books, and successfully trained/supervised many engineers and postgraduate students (Master's and Ph.D.'s).

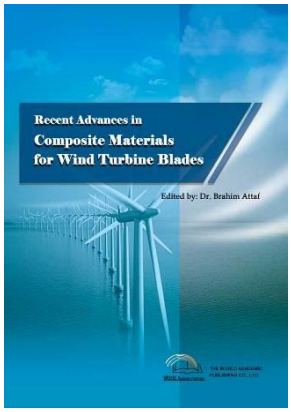

Recent Advances in Composite Materials for Wind Turbine Blades
Edited by Dr. Brahim Attaf

ISBN 978-0-9889190-0-6

Hard cover, 232 pages

Publisher: The World Academic Publishing Co. Ltd.

Published in printed edition: 20, December 2013

Published online: 20, December 2013

This book of science and technology provides an overview of recent research activities on the application of fibre-reinforced composite materials used in wind turbine blades. Great emphasis was given to the work of scientists, researchers and industrialists who are active in the field and to the latest developments achieved in new materials, manufacturing processes, architectures, aerodynamics, optimum design, testing techniques, etc.. These innovative topics will open up great perspectives for the development of large scale blades for on- and off-shore applications. In addition, the variety of the presented chapters will offer readers access to global studies of research & innovation, technology transfer and dissemination of results and will respond effectively to issues related to improving the energy efficiency strategy for 2020 and the longer term.

How to cite this book chapter

Attaf, B. (2013). Designing Composite Wind Turbine Blades from Cradle to Cradle, *Recent Advances in Composite Materials for Wind Turbines Blades*, Dr. Brahim Attaf (Ed.), ISBN 978-0-9889190-0-6, WAP-AMSA, Available from: http://www.academicpub.org/amsa/chapterInfo.aspx

World Academic Publishing - Advances in Materials Science and Applications

Chapter 2

Natural Fibre-Reinforced Polymer Composites for Wind Turbine Blades: Challenges and Opportunities

Kishore Debnath[*1], Inderdeep Singh[2], Akshay Dvivedi[3], Pradeep Kumar[4]

Department of Mechanical and Industrial Engineering, Indian Institute of Technology Roorkee
Roorkee – 247 667, India

[*1]debnath.iitr@gmail.com; [2]dr.inderdeep@gmail.com; [3]akshaydvivedi@gmail.com; [4]kumarfme@gmail.com

I. INTRODUCTION

A wide variety of sources including wood, coal, coke, oil, natural gas and nuclear materials have been used to generate energy. Over the years, the consumption of energy has increased due to the increasing population and civilization. At the same time, the ecological awareness has become the major environmental issue in the global marketplace. In today's scenario the major threat for the environment is the imbalance in the ecological system which is increasing due to the disposal of toxic waste. This issue has led to the increased interest on renewable and sustainable energy sources. The only concern for the sustainable development is minimum pollution and reduction in energy consumption. The increasing interest in the direction of using renewable energy has led to the development of the concept of wind energy. The wind energy is a prominent renewable energy source and is a solution of global energy problem. To convert the kinetic energy of the wind into mechanical or electrical energy, wind turbines or mills have been established. Most of the wind turbines basically consist of three rotor blades that rotate around a horizontal hub and convert the wind energy into the mechanical energy. The development of wind turbines for the generation of power is an emerging area. The rotor blades of wind turbines are considered as one of the key component of the wind turbine. The efficiency of the wind turbine majorly depends on the aerodynamic shape and length/angle of the blades as well as the materials used to manufacture the blades. Further, the wind turbines generate power according to the speed of the wind, not according to the demand. The basic criterion for the selection of materials for the wind turbine blades is that the material should possess high strength and stiffness, low density and adequate fatigue strength. The strength of the blade should be satisfactory so that the blade can withstand the load acting upon it without fracturing and stiff enough that it will not strike the tower during extreme loading conditions. The high fatigue strength of the blade means that it can withstand time-varying loads throughout its intended period of life. The wind turbine industries are constantly focussing on the development of light weight, cost-effective and environmental friendly materials for the production of wind turbine blades. The selection of suitable blade materials plays a significant role which determines the ultimate efficiency of the wind turbine.

Glass, carbon or aramid fibre-reinforced polymer (FRP) composites have replaced many metallic components in the various manufacturing sectors. But, the use of these materials is not considered as suitable for the environment, because these materials are highly dependent on petroleum based resources which are depleting rapidly. Due to the several environmental issues, the attention of the researchers and technologist has shifted on the utilization of natural biodegradable materials. Owing to this fact, the use of natural fibre-reinforced polymer (NFRP) composites is multiplying at a very fast pace. Recently, NFRP composites have been used as automotive parts because of their excellent combination of mechanical properties and lightweight characteristics. In addition, NFRP composites exhibit certain advantages those cannot be obtained with synthetic fibre-reinforced composites which include low density, low cost, non-abrasive properties, biodegradability and renewable nature. Natural fibres such as sisal, flax, hemp, kenaf, bagasse, banana, jute, abaca and bamboo are easily available and require low processing cost.

Mostly glass and carbon fibre-reinforced plastics (i.e., GFRP and CFRP, respectively) have been used for the production of large scale wind turbine rotor blades. The use of glass and carbon fibre is no more attractive to the rotor blade manufacturers, because the cost of these materials is high and the use of these materials causes environmental hazards. These attributes of synthetic fibres stimulate researchers to develop alternative materials for wind turbine rotor blades. Natural fibre-reinforced composites can be an alternative material for the manufacturing of wind turbine rotor blades. These materials can be used as a potential core material for the production of wind turbine rotor blades. Natural fibre-reinforced composites can be used as a viable alternative material in order to meet the demands of renewability and recyclability. Further, the uses of such materials minimize the total cost of the wind turbine. The increasing number of publication in terms of research articles in the area of development, processing and characterization of natural fibre-reinforced composites also emphasize the importance of these materials in the future wind turbine technology.

II. CONCEPT OF DEVELOPMENT OF NATURAL FIBRE REINFORCED COMPOSITES

Petroleum-based fibres (e.g., glass, carbon and aramid) are extensively used as reinforcement in polymer matrix composites. On the other hand, petroleum-based matrices such as epoxy, polyester and polypropylene are the major resin system reinforced with fibres to form fibre reinforced polymer composites. The composite materials consisting of petroleum-based fibres and matrix are mostly used in high-end structural applications where high strength and stiffness are required. However, the emerging global environmental awareness in the direction of recycling or reuse of the product at the end of their service poses a significant problem when petroleum-based fibre and matrix are used for the development of new products. This is due to the fact that both the fibre and matrix are non-biodegradable in nature which is a threat for the environment when ecological balance is the prime concerned. Due to the growing environmental awareness in the public, the utilization of petroleum-based composites is diminishing in the recent period. To avoid the depletion of limited fossil resources, increasing release of toxic fumes and volume of non-biodegradable composite waste, the development of natural biodegradable materials become significant to the users of composites. This fact leads to the development of natural fibre-reinforced composites or bio-composites. The use of natural fibre was found in ancient age of Egypt where mud and chopped straw have been used to made bricks. The mud and straw have been mixed together and then placed in the sun to bake into hard bricks. Mud bricks are excellent building materials because it can resist both squeezing and tearing. Another example of natural fibre composite is the Mongols bows which have been made by combining cattle tendons, horn, bamboo and silk where natural pine resin has been used for binding [1]. The development of bio-composites has intensified in late 1980s [2]. In 1990s, wood plastic composites were first introduced in the market for manufacturing of decks [3]. Over the time, variety of bio-composites has been developed with fairly good mechanical properties using different natural fibres and biodegradable/non-biodegradable polymers. The ultimate load carrying capacity of the developed natural fibre-reinforced composites is highly influenced by the properties of the natural fibres and the interfacial bonding strength between the fibre and matrix. In spite of having some disadvantages such a low modulus of elasticity, high moisture absorption and poor interfacial bonding between the fibre and matrix, the most important attribute of the natural fibre-reinforced composites is their biodegradable nature. Due to the biodegradability characteristic of the natural fibre-reinforced composites, they decompose in the environment and subsequently get transformed into water and carbon dioxide [4-6]. From this discussion, it is clear that the natural fibre-reinforced composites have the potential to replace the traditional petroleum-based non-biodegradable polymer composites. Recently, seeking for technologies for developing fire-proof natural fibre reinforced composites is also one of key issues to apply them for aircraft interior components [7].

III. NATURAL FIBRE REINFORCED COMPOSITES: TYPES AND CONSTITUENTS

Natural fibres can be classified based on their origin, derivations of plant, animal and mineral types [7]. Depending upon the source, natural fibres can be broadly divided into three categories: (i) plant fibres, (ii) animal fibres and (iii) mineral fibres. Fig. 1 shows the various types of natural fibres that are commonly used to develop natural fibre reinforced composites. The fact is that the natural fibre itself is a composite material where hollow cellulose fibrils are held together by lignin and pectin in hemicellulose matrix. The properties of natural fibres are mostly dependent on the cellulose content in the fibres, the degree of polymerisation of the cellulose and the angle of the microfibrils. Cellulose is an important constituent of the natural fibres. The type of cellulose present within the fibre defines the mechanical properties of the fibre, because each type of cellulose has its own cell geometry. Based upon the type of matrix, natural fibre reinforced polymer composites may be broadly classified into two categories: partially biodegradable and fully biodegradable composites. Reinforcing of biodegradable polymer with natural fibre results in fully biodegradable composites, whereas, reinforcing of traditional petroleum based non-biodegradable polymer with natural fibre results in partially biodegradable composites. According to Fig. 1, it should be noted that asbestos fibres are harmful to human health. Fig. 2 shows the various biodegradable and non-biodegradable polymers and the types of composites derived from these two types of polymers.

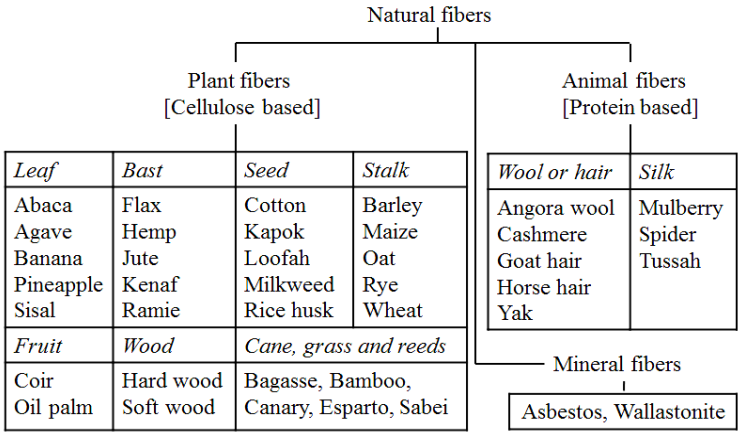

Fig. 1 Classification of natural fibres

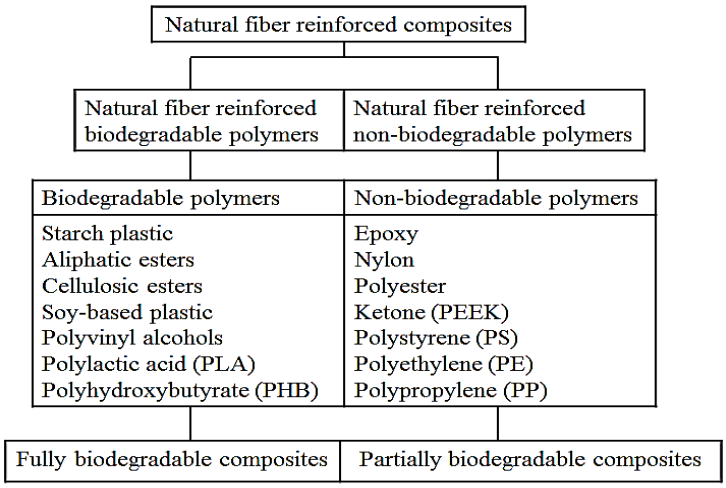

Fig. 2 Types of polymers and their composites

The two main constituents or phases of the natural fibre reinforced composites are reinforcement/fibres and matrix/polymer. Both the constituents are physically and chemically different from each other. There are a variety of natural fibres that can be used as reinforcement for the synthesis of polymer composites. The main function of the reinforcement is to carry the load and to provide the adequate strength and stiffness in the resulting composites. The natural reinforcements are the main load carrying member in natural fibre reinforced composites. The reinforcements are added in the matrix in order to enhance the mechanical properties of the neat resin system. The matrix also plays a significant role in determining the overall properties of the resulting composites. The matrix acts as a bridge to binds the fibres together, transfer the loads to the reinforcement, provide good surface finish and prevent the reinforcements from the environmental attack. The matrix materials should have the ability to deform easily under applied load, transfer the load onto the fibres and evenly distribute stress concentration. The presence of different constituents in composites results in a contiguous region between the reinforcement and matrix that is interphase. Interface has the characteristics that are not depicted by any of the constituent in isolation [4]. The interface of reinforcement and matrix plays a significant role during the service of the resulting composites in response to its load bearing capacity. The wettability characteristic of the reinforcement and matrix defines the adhesion efficiency of the constituents. The adequate adhesion means that the resulting composite has superior mechanical properties. The adhesion between reinforcement and matrix can be improved by treating the natural fibres. The treatment of natural fibres results in enhanced interfacial bonding strength between the fibre and matrix which means an enhanced mechanical strength and dimensional stability in the resultant composites. Chemical treatments of natural reinforcements based on the chemical source include: alkali, silane, acetylation, benzoylation, acrylation and acrylonitrile grafting, maleated coupling agents, permanganate, peroxide, isocyanate, stearic acid, sodium chlorite, triazine, fatty acid derivate (oleoyl chloride) and fungal [8].

IV. MAJOR PROBLEMS ASSOCIATED WITH THE USE OF NATURAL FIBRES

Despite several advantages, the use of NFRP composites has been restricted due to certain characteristics of the natural fibres such as moisture absorption tendency, poor wettability, poor adhesion with the synthetic counterparts and low thermal stability during processing. However, the major problem associated with the thermoplastic composite systems is the poor interfacial adhesion of the non-polar hydrophobic matrix material with polar hydrophilic fibre which results in poor mechanical properties in the final composites [9, 10]. When a material is intended for a prolonged period of usage, its durability becomes a critical issue. The physical and mechanical properties of polymer matrix composites are significantly influenced by hygro-thermo-mechanical loads. The mechanical properties of natural fibre reinforced composites deteriorate over a period of time as fibres, fibre-matrix interface region and matrix is typically affected by the moisture. The degree of deterioration and reversibility of the properties of the natural fibre composites is largely dependent on the extent of moisture absorption [11, 12]. Natural fibre encompasses abundant polar hydroxide groups which readily absorb moisture. The high moisture absorption level of natural fibre composites is a major obstacle in preventing their extensive engineering applications. Another disadvantage of natural fibres, to be used as reinforcement for the polymer matrix, is that they are thermally unstable at elevated temperature. Generally, most natural fibres are thermally weakened at about 160 ℃. Pre-treatment of natural fibres using chemical methods (for instance, use of coupling agent such as silane compound) enhances the adhesion at the fibre-matrix interface and reduces moisture sorption of natural fibres. The chemical treatment of fibres also helps in improving mechanical properties under both controlled and environmental aging conditions. In addition, the amount of moisture sorption can be reduced significantly by replacing natural fibres with a small amount of synthetic fibre such as glass or carbon [13-21]. Thermoplastic polymer composites are becoming popular and showing potential in many structural applications due to the advancement and improvements in the polymer industry. Recently, natural fibre reinforced bio-composites have been used as automotive parts because of their good mechanical properties and light weight. At present, many components of automobiles are fabricated by using natural fibre reinforced composite materials [22-24].

V. COMPOSITE MATERIALS FOR WIND TURBINE BLADES

In the early stage of development of wind turbine blades, wood has been widely used. Plain wood and laminated wood have been used extensively for the construction of blades. The manufacturing of plain wood blade is typically based on the concept of wooden boat-building technique. The turbine blades made out of plain wood performed well but the high moisture absorption tendency of the wood poses a critical problem for long term service. Laminated wood-epoxy based blades have also been used in wind turbine industry because these are lightweight and acquire adequate strength for the whole blade structure. For the time being bamboo has been used in the aeroshells and for sandwich structure within the rotor blade. The mechanical properties and biodegradable nature of bamboo makes it an attractive material for wind turbine rotor blades. Bamboo-poplar epoxy laminate has also been developed for rotor blades. The mechanical properties such as tensile and compressive stress-strain behaviour, tension-tension fatigue life and fracture resistance of the bamboo-poplar laminate panes formed by hot pressing have been studied in order to ascertain their feasible use in wind turbine blades [25].

Fibre reinforced composites have been introduced in the wind industry decades ago for the production of wind turbine blades. Fibre reinforced composites are largely used for production of small to large size wind turbine blades. In 1959, the first fibre reinforced wind turbine blade has been built by Ulrich Hutter's. The use of fibre reinforced composite for production of blades has intensified in the mid-1970s with the development of small scale Danish turbines. The concept of Danish turbines is similar to the Hutter's one, but the only difference is that in Danish turbine polyurethane foam has been used in blades for better stability of the skins. In the later stage of development of blades, the single shear web concept has been exaggerated, where the unidirectional fibres have been placed below and above the shear web. The main reason of conceptualizing this technique lies in the fact that the stability of the skins has been improved and tip deflection has been reduced. After that, sandwich panel has been introduced at the leading and trailing edges of the blade. The final change in blade structure has been observed when second shear web has been introduced due to the increasing gravity load with the increase in length of blades [26]. The shells which define the aerodynamic profile of the blade are mostly manufactured using glass fibre reinforced polyester and sandwich panel comprising of polymer composite sheets and light weight polymer foam or balsa wood cores. For the production of large scale blades, E-glass laminates are extensively used. CFRP composites are now used by some wind turbine blade manufacturers. CFRP composites are well suited for turbine blades because of their high strength, high elastic modulus and increased fatigue life. CFRP composites can be potentially used as reinforcement for aeroshell of blades as these possess adequate properties but the only drawback is their high cost. Sometimes, both glass and carbon fibre laminates as hybrid composites are used in order to take the advantage of properties of both fibres. As a large section of the blades is made up of the synthetic fibre based composites, for a certain section such as aeroshell and internal sandwich structures, natural materials such as wood and natural fibre composites can be used. It has been established that the natural fibre with surface modification can have superior mechanical properties and can be used in high-end structural applications (e.g., wind turbine blades).

It is true that, the wind turbine becomes the central part of the energy generation, but the problem comes when all those wind turbines need to be replaced. The currently used materials like glass or carbon fibres in wind industry need to be replaced because these are not biodegradable in nature. It has been predicted that US alone will install 170,000 wind turbines by 2030 and each year 34,000 blades has to be trashed away. Each blade weighing 18 tons and can stretch the length of a standard football field need to be trashed which means a large amount of unplanned waste. The disposal of such large structure that is reflected as hidden pollution is going to be a big threat for the environment in future. For the prevention of this large waste, research effort has been made for developing the biodegradable blade materials. Today most of the used blades are ground up for incineration and burial in landfills. For the manufacturing of wind turbine components, the next generation best materials is the lingo-cellulose based natural fibre reinforced composites. National Science Foundation (NSF) has already granted 1.9 million dollars to investigate how the natural fibre based composites can be introduced in wind industry to replace the oil-based materials [27].

VI. NATURAL FIBRE REINFORCED COMPOSITES: ISSUES AND CHALLENGES

It is clear from the discussion that natural fibre reinforced composites have the potential to be introduced for the manufacturing of turbine rotor blades. These materials satisfy almost all the criteria to use as basic material for wind turbine rotor blades. But, there are some challenges with respect to their processing. The analysis of the challenges encountered during processing of natural fibre reinforced composites may expand their utilization in wind turbine industry or in other application fields. Therefore, in the following sections, the various pros and cons in light of the potential utilization of natural fibre reinforced composites for the manufacturing of wind turbine rotor blades have been discussed. The various issues and challenges encountered during adhesive bonding and machining of natural fibre reinforced composites has also been discussed. Adhesive bonding and machining of the composite parts are the two main secondary operations that have been performed in wind industry in order to get the complete structural integrity of the rotor blades. The various components of the blade are assembled together by means of adhesive bonding only. In addition, a large segment of the wind turbine blades necessitates machining operation to cut off excess material from the root end, milling of root face, drilling of axial and radial holes. Therefore, the machining behaviour of natural fibre reinforced composites has also been included in the present chapter.

A. Primary Manufacturing of Natural Fibre Reinforced Composites

The major design aspect that is considered during the manufacturing of wind turbine blade is the aerodynamic shape of the blade. The efficiency and durability of the blade mostly depend on its aerodynamic shape. The prerequisite shape of the blade can be achieved during its primary manufacturing. The most common techniques used for the manufacturing of wind turbine blades are wet hand-lay-up, filament winding, prepreg technology and resin infusion technology. These techniques have been developed mostly for the processing of glass, carbon or other synthetic fibre reinforced composites. The processing industry for natural fibre reinforced composites uses the same techniques without much modification. However, there are some challenges encountered during the primary manufacturing of natural fibre reinforced composites; those are discussed in the subsequent section.

Challenges with Primary Manufacturing:

The primary processing or manufacturing of natural fibre reinforced plastics is typically challenging because certain number of variables are involved during processing. In spite of having several good properties, it is important to understand the challenges associated with primary manufacturing of natural fibre reinforced composites in order to further expand their utilization. Fundamentally, the challenges encountered during the manufacturing of natural fibre reinforced plastics are different from those of synthetic fibre reinforced plastics. The following points give an inkling of some of the challenges arising during the manufacturing of natural fibre reinforced composite parts.

a) The variety of natural fibres and matrix and their combination and the number of manufacturing process and associated controlling parameters makes it very difficult to choose the best processing technique for the primary manufacturing of natural fibre reinforced composites. The selection of appropriate manufacturing process is a key consideration in order to ascertain good properties in the final composite product.

b) The physical and mechanical properties of the natural fibres vary according to the geographical location and environmental condition in which plants grow. The distinct physical, chemical and mechanical properties of the natural fibres and polymers make it difficult to blend them during primary processing. The proper blending of fibre and matrix substantially enhances the mechanical properties of the resulting composites.

c) It is well known that the natural fibres have poor adhesion property as compared to the traditional glass/carbon fibres. The poor adhesion between the fibre and matrix results in internal defects and low performance of the final composite parts. For that, several techniques have been developed in order to improve the interfacial adhesion between the natural fibre and matrix. Chemical treatment and coating of the natural fibres are the prominent methods used for the modification of fibre surface. Sometimes, additives, fillers and catalysts are added during the processing of natural fibre reinforced composites.

d) Various combinations of fibres and matrix make it difficult to control or optimise the processing parameters during primary manufacturing. This may be attributed to the fact that the different fibre and matrix present in composites demands different conditions for processing.

B. Joining Behaviour of Natural Fibre Reinforced Composites

The construction of wind turbine blade may be a one-piece or two-piece construction. In one-piece construction, a spar is fixed to the inner shell and then to the outer shell through adhesive joining. Whereas, in two-piece construction, the shear webs are adhesively joined with the shells. In addition to adhesive bonding of spar or shear webs, the shells of the blade are also bonded together by means of adhesive joining. In wind industry, two component metering and mixing equipment have been used to apply the adhesive to the blade. Two-component adhesive containing resin and hardener are mechanically pumped through a delivery pipe from their respective containers to the mixer head. In the mixer head, the resin and hardener are mixed together and then discharged. The adhesive bonding of various components in turbine blade typically consists of five steps. In the very first step, the adhesive is applied to the first shell. In the second step, spar or shear webs are installed in the desired position. The third step involves the application of adhesive to the top of the spar or shear webs for the bonding of the second shell. In the fourth stage, the second shell is placed over the spar or shear webs which define the complete construction of the blade components. In the final stage (fifth stage), the mould is closed and left for a required period of time till the adhesive is cured [28]. In Fig. 3, the adhesive joining of various sections of the blade has been represented for both one-piece and two-piece construction of blades.

In adhesive bonding or joining, two substrate materials are joined together by means of applying an adhesive. It is usually known that, to join the thermosetting polymer based composite parts, thermosetting polymers as adhesive is usually used, whereas for the joining of thermoplastic polymer based composite parts, thermoplastic adhesives are mostly used. Thermoplastic adhesives have some advantages over thermosetting adhesives. The major advantage of using thermoplastic adhesive is the processing time of joining is very short as compared to the thermosetting adhesive. Further, the high thermal stability, high chemical resistance, low moisture absorption tendency, and retention of bond strength at elevated temperature can be achieved while using thermoplastic adhesives. The most common types of thermoplastic adhesives are polyvinyl acetate, polyvinyl acetals, polyvinyl alcohols, polyamides, acrylics and phenoxies. The selection of an appropriate adhesive is an important joining consideration which depends on the several factors such as type of substrate material to be adhesively joined,

required joint strength, impact resistance, resistance to chemical attack, electric current and humidity, service temperature and cost requirements. The efficiency of the adhesive bonding depends upon various factors, such as surface preparation of the substrates, type and amount of adhesive to be used for bonding, fitting of substrates to be joined and the curing procedure. Depending upon the requirements of the bond strength, an adhesive is generally chosen on the basis of its ability to wet the substrate surface, resistance to heat, resistance to moisture and chemicals, shear, peel strength and toughness of the resulting joint. The adhesive joining of natural fibre reinforced composites usually follow the same steps as the joining of typical synthetic fibre reinforced plastics. The steps involved for adhesive joining of natural fibre reinforced composites are shown in Fig. 4.

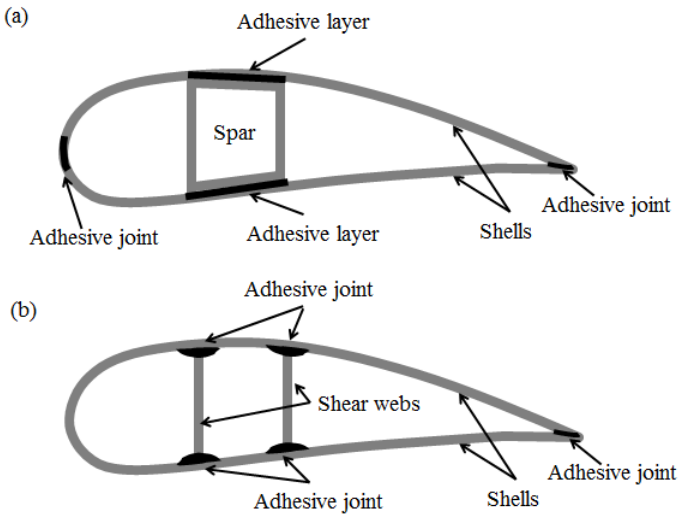

Fig. 3 Adhesive joints at the various sections of the blade: (a) one-piece construction, (b) two-piece construction

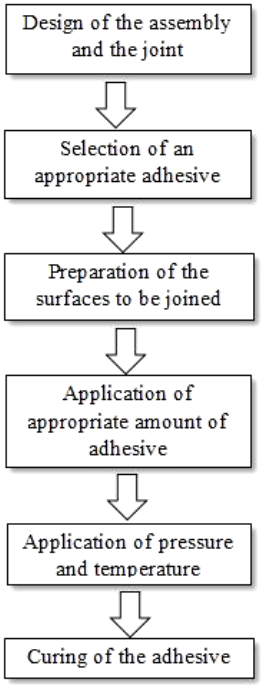

Fig. 4 Steps involved in adhesive joining of natural fibre reinforced composites

1) Challenges with Adhesive Joining:

In spite of having various positive characteristics, there are few drawbacks in adhesive joining. The major problem encountered during adhesive bonding is that the surface preparation of the substrates, that cannot be avoided. During the preparation of surfaces of the substrates, surfaces are pre-treated in order to enhance the wettability which in turn improves the joint strength by improving the contact between the adhesive and substrate. Surface preparation is important because the surface has to be free from contaminants (e.g., dust, dirt, foreign particles, greases, oil etc.) to avoid poor bonding. For example, thermosetting polymer based composite parts are often found to be contaminated with mould release agents, additives, waxes

etc. These contaminants can be removed by abrading the surface with emery paper. But, in case of thermoplastic based parts, oxidation by flame treatment, plasma and corona treatment, ionised inert gas treatment, or application of primers or adhesion promoters are usually adopted to clean the surface [29]. Another disadvantage of the adhesive joining is the nature of adhesive bonding, which may be permanent or semi-permanent type; this means the components which have been joined together cannot be disassembled or may be disassembled by compromising with the surface damage. While considering the type of failure of adhesive joining, two different types of failure mode namely adhesive and cohesive failure have been observed. The adhesive failure basically occurs at the interface between the adhesive and the substrates. Adhesive failure may be due to inadequate surface preparation, selection of wrong adhesive and high peeling stress. But, in case of cohesive failure, the failure occurs only in the adhesive or in the substrate material. The main reason of cohesive failure is believed to be related to the stronger bonding strength between the adhesive and the substrate than the individual mechanical strength of the adhesive or the substrate material. If, the applied load exceeds the individual strength of the adhesive or the substrates, then the cohesive failure appears. The quality of the joint can be considered as poor if the failure occurs adhesively at the interface between the adhesive and substrate. It confirms that the bond strength is weaker than the individual strength of the adhesive or the substrate material.

The main criteria for selection of materials for wind turbine blades are that the materials should possess high-strength to weight ratio, high-stiffness to weight ratio, adequate fatigue strength, damage tolerance and corrosion resistance. Nowadays, wind industry is continuously trying to replace the current thermosetting based composites materials with the thermoplastic based composite materials in order to take the advantages of sustainability like recyclability and benefits of joining methods such as resistance welding and repair methods. In the subsequent section, an alternative method for joining natural fibre reinforced thermoplastic composite parts has been proposed. This method has shown superior joint strength as compared to the joint made by means of applying adhesive for the same natural fibre reinforced composites.

2) An Alternative Technique for Joining Natural Fibre Reinforced Composite Parts:

The issues and challenges associated with adhesive bonding of natural or synthetic fibre reinforced composite have been discussed. It can be inferred from the discussion that the adhesive bonding is not a perfect joining method. The adhesive joining can be replaced by established microwave joining technique. This promising joining technique is suitable for joining natural fibre reinforced composite structural parts. Microwave joining has been established to minimize all the defects detected in adhesive joining. The main benefit of using microwave energy for joining is that it does not change the microstructure and property of the substrates to be joined together. Microwave joining basically involves the use of high frequency electromagnetic radiation to heat a susceptor material located at the joint interface. The generated heat melts the thermoplastic materials and joins the materials upon cooling. Basically, a susceptor has a high dielectric constant material which can absorb electromagnetic energy and then convert it to heat energy. This dielectric property of a material determines its ability to absorb microwave radiation. A susceptor may be of ceramic or metallic materials. The important process parameters that can affect the joint strength are exposure time, power level, applied pressure and percentage of susceptor to be used. Microwave joining comprises several advantages over traditional joining methods, such as:

a) Rapid processing,
b) Saving of energy and no generation of polluting gases,
c) Joining of complex geometries,
d) Volumetric heating and uniform temperature distribution,
e) High strength and homogenous microstructure of the joint.

3) Microwave Heating Mechanism:

The wavelength and frequency of microwaves can vary from 1 mm to 1 m and 300 GHz to 300 MHz, respectively. For general heating purpose, frequencies of 0.915 GHz and 2.45 GHz have been commonly used. The household microwave oven works at a frequency of 2.45 GHz corresponding to a wavelength of 12.2 cm; whereas, industrial microwave oven works at 0.915 GHz. The microwave heating process is fundamentally different from the conventional heating process. In conventional heating, the external surface of the material is heated first and then heat is transferred to the inside of the material by thermal conduction; whereas, in microwave heating material is heated all the way through at the same time. Because of this volumetric nature of the heating, microwave heating consumes 10 to 100 times less energy. It is well understood that in microwave heating, electromagnetic energy is converted into thermal energy. The energy is transfered to the material through molecular interaction with the electromagnetic field. Since microwaves can penetrate the material and supply energy, heat can be generated throughout the volume of the material resulting in volumetric heating. In the case of conventional heating, a slow heating rate is always preferred to reduce thermally induced stress.

A typical microwave furnace consists of three major components, such as source, transmission line and applicators. Fig. 5 represents a typical microwave processing setup. The main purpose of source is to generate electromagnetic radiation, where transmission lines carry away the electromagnetic energy from the source to the applicator. In the applicator the energy is either absorbed or reflected by the material. The design of these three basic elements and their combination into an efficient

system require an understanding of the electromagnetic theory. The theoretical analysis of each component is governed by the appropriate boundary conditions and Maxwell's equations [30].

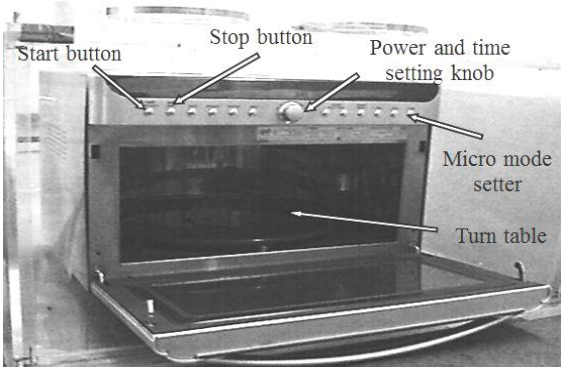

Fig. 5 Microwave processing setup

4) Microwave Joining of Plastic Materials: Research Initiatives:

Microwaves have been used for many years for kitchen and industrial heating applications as it significantly saves the processing time as well as energy. Now-a-days primary and secondary processing of various materials is readily done by using microwave energy. This is because the microwaves heat the materials volumetrically. In addition to material processing applications, microwave heating can also be used for joining advanced materials [31]. For joining metallic materials, it has been applied successfully [32]. Microwave welding of thermoplastic materials is an electromagnetic bonding technique which is relatively a new polymer welding technique [33]. Microwave processing of conventional materials is an emerging field, which is progressing very rapidly during the last several years. Sintering of various materials by means of microwave heating is a very innovative method and can be applied to traditional ceramics, advanced ceramics, specialty ceramics and ceramic composites. Development of functionally graded materials: joining, melting, fibre drawing, reaction synthesis of ceramics, synthesis of ceramic powder, phosphor materials, whiskers, microtubes and nanotubes, sintering of zinc oxide varistors, glazing of coating surface and coating development have been performed using microwave heating. In addition, microwave energy is being explored for the sintering of metal powders also [34]. The welding characteristics of engineering thermoplastics (ultra-high molecular weight polyethylene, polycarbonate and acrylonitrile-butadiene-styrene) using focused microwave energy have been studied [35].

The joining process is carried out in two different stages. In the first stage microwave energy is directly focused onto the specimen joint interface, whilst in the second stage, epoxy based primer is used to promote the joining by means of microwave energy. Finally, the bond strength is determined to see the quality of the bond at the interface by performing tensile test on the specimen. The work underlines the various aspects such as time required, bond strength, and quality of the joint. The study concluded that at a higher input power (1000 W), the time taken was three times less, where, bond strength was 2.5 to 3 fold greater for both the thermoplastic materials namely polycarbonate and acrylonitrile-butadiene-styrene.

A state-of-the-art review of microwave technologies, processing methods and industrial applications, using variable frequency microwave (VFM) facility has also been presented [36]. It has been reported that the welding of thermoplastic materials through microwave irradiation took place in 2–120 s with lap shear strength of 19.0 $\pm$ 2.0 N/mm^2 [37]. Inevitable limitations of mechanical and adhesive bonding can be minimized using microwave joining of composite materials as it provides several advantages through energy saving, rapid heating, reduction in manufacturing cost and unique micro structure [38]. The load carrying capacity of the natural fibre reinforced composite parts bonded through microwave radiation has been experimentally investigated [5].

Four different natural fibre based composites (nettle- PP, grewia optiva- PP, nettle- PLA and grewia optiva- PLA) have been developed in order to study their microwave joining behaviour. The joint strength has been determined for all the developed composites as per standard procedures. The results show that microwave joining offers higher joint strength as compared to adhesive bonding. Fixed frequency of 2.45 GHz and a maximum power output of 900W have been employed for microwave joining. Two different input parameters, power and exposure time have been considered for microwave joining. It has been found that the bonding strength of natural fibre reinforced PLA composites improved when specimen were exposed for 200 s. The microwave heating process has been accelerated by using a susceptor material. Charcoal has been used as susceptor material because it quickly couples with the microwave energy and produce rapid heating effect.

For proper joining of the specimens, an initial holding pressure has been applied to the joint by using a teflon tape. The top surfaces of the composite specimen to be joined get heated through conventional modes of heat transfer from the heated charcoal. As the process continues, there is eventually sufficient rise in temperature which causes fusion of the interfaces. From the experimentation of such technique, it has been observed that the grewia optiva fibre reinforced PLA adherends recorded maximum joint strength, whereas nettle fibre reinforced PP adherends showed minimum joint strength. Microwave

joining of natural fibre reinforced composites has a potential of being a viable and sustainable alternative as it is a green processing technology. The steps involved for microwave joining of natural fibre reinforced composites are shown in Fig. 6.

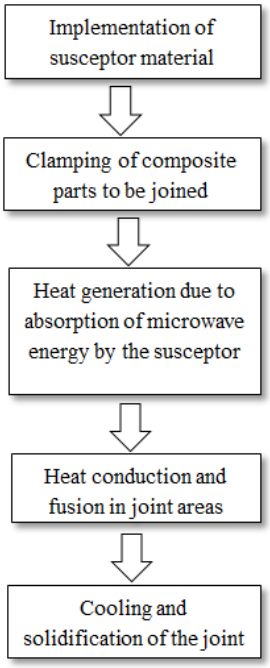

Fig. 6 Steps involved in microwave joining of natural fibre reinforced composites

C. Machining Behaviour of Natural Fibre Reinforced Composites

Most of the composite parts are made to a near-net shape through primary manufacturing. But, the complexity in the product makes the machining process necessary in order to ascertain the structural integrity. Machining operation such as drilling, milling, grinding, and boring are the most common machining operations frequently performed on composite parts. Among all the machining operations, drilling is the most frequently and widely used machining operation. Drilling is performed in polymer composites in order to fulfill the purpose of joining through bolting or riveting. Drilling is almost an unavoidable machining operation for any material, because several components need to be assembled together to make a complete assembly. While considering the machining of wind turbine blades, number of machining operations need to be performed in order to achieve the complete blade structure and to install the blade in the turbine hub. The specific machining operations, such as cutting off excess material from the root end, milling of root face, drilling of axial and radial holes are frequently performed by wind turbine industry. Facing of the root end and drilling of both the axial and radial holes within the required tolerances is important in order to precisely position the blade [39]. The turbine rotor blade contains both an axial hole drilled span wise and a radial hole drilled from the root that intersects the axial hole. Round metallic steel nut is inserted into the radial hole and the threaded root bolt is inserted into the axial hole and screwed into the barrel nut. This forms a very robust and strong mechanical joint rather than a bond joint [40].

The joining through adhesive bonding is not always possible for obtaining the ultimate structural integrity. Mechanical fastening such as riveting and bolting are the important methods of joining of natural fibre reinforced composite parts. The mechanical fastening demands the making of good quality holes of the desired size in composite parts. The making of holes is mostly done through conventional drilling. Various novel techniques have been developed for making of holes in polymer composites, but the conventional drilling is one of the most common methods of drilling. The fundamental concept of drilling of natural fibre reinforced composites is similar when compared with the drilling of traditional polymer matrix composites. But, the fact is that, the drilling behaviour of natural fibre reinforced composites is different from the drilling of traditional polymer matrix composites. Drilling of natural fibre reinforced composites is a tedious task, because several factors are involved that control the quality of the drilled hole. The optimization of the operating variables such as cutting speed and feed rate, selection of compatible tool material, designing of optimum tool point geometry and the evaluation and characterization of machining induced damage are some of the research areas that need substantial attention in order to enlarge the applications of the natural fibre reinforced composites.

1) Drilling Behaviour of Natural Fibre Reinforce Composites: Research Initiatives

The application spectrum of natural fibre reinforced composites has increased in past few years. Now, these materials are used for both structural and non-structural applications. The simple shaped of natural fibre composite parts has been created through primary manufacturing processes. But, the fabrication of complex parts necessitates joining of many components to

ascertain final shape. Mostly, composite parts are joined together by means of mechanical fastening. The mechanical fastening of natural fibre composite parts necessitates desired size of hole in the components to be joined together. Conventional drilling is often used to generate holes in the composite components. Extensive work has been performed in light of drilling of polymer matrix composites, but the studies on drilling behaviour of natural fibre reinforced composite are scanty. It is interesting to note that, recently, the drilling behaviour of sisal fibre reinforced PP composite has been investigated [41].

The effect of cutting speed, feed rate and tool geometry on the thrust force and torque has been studied. It has been found from the investigation that drill point geometry has substantial influence on the drilling forces during drilling of sisal- PP laminated composites. It has also been observed that trepanning tool which is hollow in nature performed well in terms of quality of drilled hole as compared to twist drill (solid in nature) for the drilling of sisal fibre reinforced PP composites. This is because the fundamental mechanism of cutting of fibre and matrix is different for both drill point geometries.

In twist drilling, the drilling operation starts from the center of the drill i.e., the chisel edge of the twist drill first creates an indentation on the composite part and then the complete engagement of the drill starts with the composite laminate. But, in the case of trepanning tool, there are two cutting edges on the periphery of a hollow cylindrical shank, and cutting action takes place from the outer periphery of the trepanning tool. Further, the twist drill removed the material from the composite in the form of continuous chips but the trepanning tool removed material in the form of round circular plate. The drilling of coir fibre reinforced polyester composites has been studied in light of the effect of drill diameter, spindle speed and feed rate on the thrust force, torque and tool wear. From the experimental study, it has been observed that drill bit of 6 mm diameter is most suitable for minimum drilling forces and tool wear [42]. A comparative study on drilling behaviour of glass and natural fibre (hemp, jute and banana) reinforced polyester composites has been performed in order to compare the drilling induced delamination. The study reveals that the quality of the hole produced in the natural fibre reinforced composites is comparable with the corresponding quality of hole produced in GFRP. According to the results, it has been established that hemp fibre reinforced composites performed better in terms of minimum hole damage out of all the composites. Whereas, jute fibre reinforced composites experienced maximum damage in all drilling conditions [43].

The evaluation of delamination during drilling of rice husk reinforced polyester composites has been studied. It has been experimentally found that the delamination value is lower in rice husk reinforced polyester composites as compared to the GFRP [44]. An investigation on influence of alkali treated fibres on the mechanical and machinability of Roselle and sisal fibre hybrid polyester composites has been performed. It has been concluded form the study, that after alkali treatment the mechanical properties and machinability of the Roselle and the sisal fibre hybrid polyester composites has improved [45].

From the above research initiatives, it can be emphasized that natural fibre reinforced composites have the potential to replace GFRP in many applications where machining is needed. There are only few studies reported on the drilling of NFRP composites, which means a significant research scope is available in the field of machining behaviour of natural fibre reinforced composites.

2) Challenges Encountered During Drilling of Natural Fibre Reinforced Composites:

The importance of the drilling operation has already been discussed in the previous section. The researchers and technologists are continuously focusing their research activities on the development of cost-effective high quality drilling methods. Machinability study of anisotropic materials like natural fibre reinforced composites is an emerging area. But, there are many challenges associated with drilling of natural fibre reinforced composites. The major challenges encountered during drilling of natural fibre reinforced composites are highlighted as follows:

a) The drilling response of natural fibre reinforced composites is completely different as compared to the drilling of metals. The fundamental difference between drilling behaviour of natural fibre reinforced composite and metals lies in the fact that in natural fibre reinforced composite, tool has to cut two distinct phases (natural fibre and matrix) simultaneously, whereas, in case of drilling of metals the tool experiences only the cutting of a single phase. Drilling of natural fibre reinforced composites is a very complex process. The drilling response fluctuates according to the interaction of the tool with the distinct phase of material being machined.

b) The drilling behaviour of natural fibre reinforced composites is influenced by several factors related to the specification of composites, such as properties of the natural fibre and the matrix, volume fraction of natural fibre, and the orientation of the natural fibre in the resulting composite. The optimum drilling conditions for a particular composite may not be applied to the composite of same material but having different fibre volume fraction and fibre orientation. Further, the optimum drilling condition for a particular combination of fibre and matrix may not be the same for other types of composites with different constituents.

c) Drilling of NFRP composites results in exposure of fibres to the environment. The exposed natural fibres have the tendency of absorbing moisture which may adversely affect the overall load bearing capacity of the natural fibre composite structure.

d) Drilling parameters such as cutting speed, feed rate, tool material, and tool geometry are some of the key variables which determine the amount of surface damage. The most common types of damage observed in drilling of natural fibre reinforced composites are matrix burning and deformation, delamination, fibre pull-out, splintering etc. These types of damage

adversely affect the structural integrity of the natural fibre reinforced composite. The optimization of all the drilling parameters can minimize the drilling induced surface damage.

3) Damage Analysis During Drilling of Natural Fibre Reinforced Composites:

The difficulties encountered during the drilling of natural fibre reinforced composites have already been discussed. From the discussion, it is clear that the major problem encountered during the drilling is the damage phenomenon that appears in the form of surface delamination. The characterization of the drilling induced delamination is an important issue, because the delamination during drilling is responsible for the failure of the complete composite structure. It is well known that the main reason of delamination is the generation of thrust force during drilling. Further, the generation of thrust force has been affected by drill point geometry. Fig. 7 represents the two different types of drill point geometry commonly used for drilling of natural fibre reinforced composite laminates. The thrust force signal during the drilling of nettle fibre reinforced PP composites has been presented in Fig. 8. As the drilling progresses, thrust force start to increase and then the magnitude of the thrust force is almost constant in a specific domain. In this domain, the drill bit is fully engaged with the composite laminate. Finally, drill bit comes out of composite laminate and shows a continuous decrease in thrust force. The drilling behaviour of natural fibre-reinforced composites can be critically analysed in respect of the thrust force signal and correlated with the drilling induced delamination.

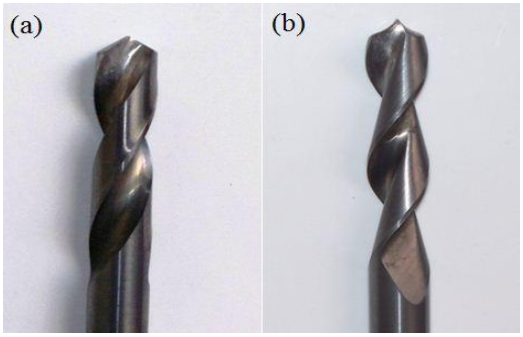

Fig. 7 Drill point geometry: (a) twist drill, (b) parabolic drill

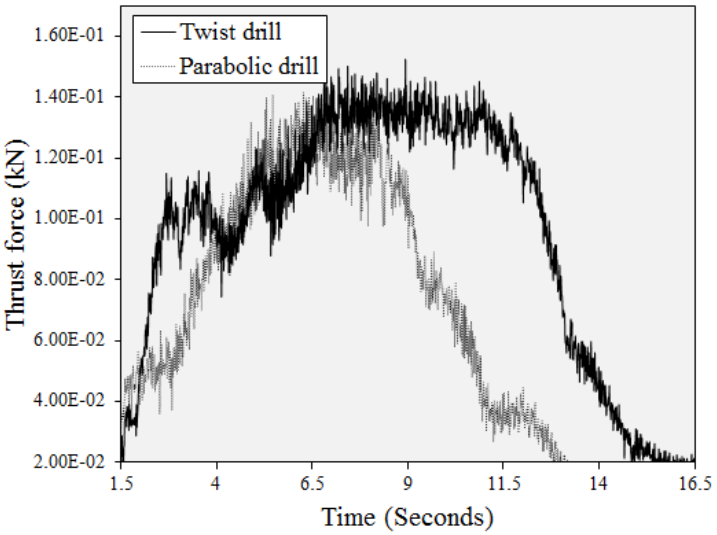

Fig. 8 Thrust force signals (cutting speed of 900 rpm and feed rate of 0.05 mm/rev)

Two different types of delamination has been observed during drilling of natural fibre reinforced composites, these are peel-up and push-down delamination. Peel-up delamination occurs during the entry of the drill bit. As the cutting edge of the drill bit comes in contact with the composite, a peeling force through the slope of the drill bit flutes separates the composite laminate and causes formation of delamination around the entry side of the drilled hole. Push-down delamination occurs during the exit of the drill bit. As the drill bit approaches to the hole exit side, thrust force plays a critical role, which defines the quality of the drilled hole. If the generated thrust force exceeds the inter-ply bonding strength, then there is formation of delamination around the drilled hole [46]. It has also been established that push-down delamination is much dangerous as compared to the peel-up delamination. Maximum products fail because of the push-down delamination. It is estimated that in the aircraft industry, 60% composite parts are rejected due to the drilling induced delamination around the drilled hole [47]. Many methodologies have been experimented upon in order to prevent the push-down delamination. These are the use of a backing plate during drilling, use of dedicated drill point geometry, use of non-conventional machining methods etc. Further, there are many techniques which have been developed in order to quantify the delamination; some of these are digital image

analysis of the drilled hole, non-destructive dye penetrant test, X-ray non-destructive inspection test and ultrasonic C-scan. Fig. 9 typically represents the delamination area that can be obtained using digital image analysis technique. A digital image of the drilled hole has been magnified so that the damage around the hole can be clearly distinguished. The pixel aspect ratio has been maintained as unity so as to avoid any distortion of image that may result in invalid results. A factor known as delamination factor has been defined in order to measure the damage area. The delamination factor is the ratio of the maximum diameter of the delaminated area (D_{max}) to the diameter of the drilled hole (D). Fig. 10 represents the actual damage zone at the hole exit side during the drilling of natural fibre reinforced composites. The other types of damage observed during the drilling of natural fibre reinforced composites are matrix burning especially in case of drilling of thermoplastic composites, cracks in the resinous region, hole geometry error, fibre pull-out, uncut fibres etc.

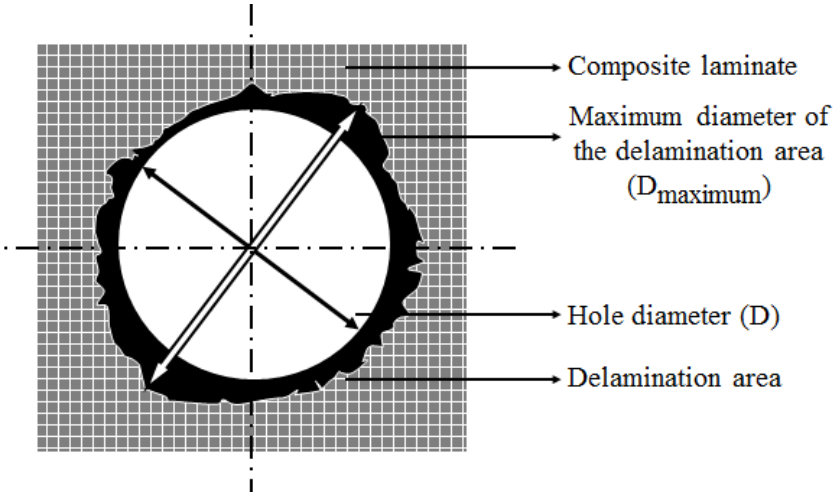

Fig. 9 Representation of delamination around the drilled hole

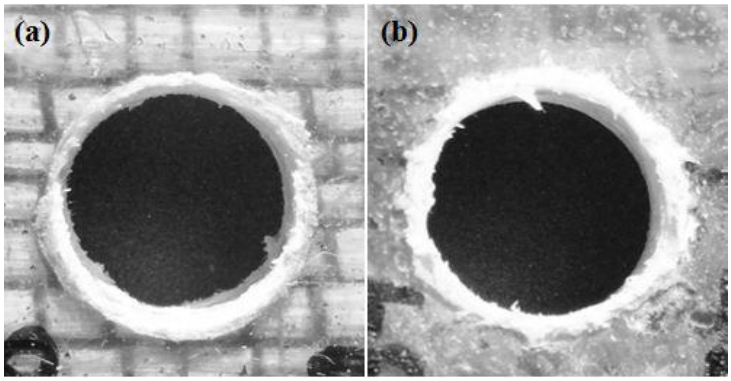

Fig. 10 Damage during drilling of (a) sisal-PLA composites and (b) grewia optiva-PLA composites

VII. CONCLUSIONS

The generation of energy is very essential for human survival and social development, but the generation of energy without polluting the environment is the biggest challenge of the twenty-first century. This problem can be solved by utilizing sustainable energy sources. Wind energy is the greatest example of sustainable energy source. Wind energy is clean, environmentally friendly and inexhaustible and can act as an alternative to fossil fuels. The fundamental concept of using sustainable energy lies in the fact that it can reduce greenhouse gases and pollution. It is true that wind power is the fastest-growing alternative energy system, but the materials used for wind turbine components are not environmentally attractive.

As the modern wind turbines are designed for estimated life span of 20 years, a large structure need to be disposed to the environment in future after the end of service life. The materials used for wind turbines are still non-biodegradable in nature. For this reason, scientists and engineers are constantly focussing on replacing the existing material system of wind turbines with bio-degradable materials. Natural fibre reinforced composites form one such class of materials which not only possess superior mechanical properties but are also bio-degradable in nature. Natural fibre reinforced composites can be a potential candidate where they can replace the conventional material systems of wind industry. These materials can be introduced for the manufacturing of various sections of a wind turbine. However, in order to expand the application spectrum of natural fibre reinforced composites, there is an imminent need to develop high-quality and cost-effective processing techniques.

In the present chapter, the viability of potential utilization of natural fibre reinforced composites for wind turbine blades has

been discussed. The various issues and challenges in light of their primary manufacturing have also been addressed. Further, the chapter highlights the two important secondary processing techniques; adhesive joining and machining which are performed frequently in wind industry. As in wind industry, a large section of the blade requires joining in the form of adhesive bonding, it is necessary to find an alternative method of joining, as adhesive joining has its own limitations. For joining of plastic materials, an alternative joining technique namely microwave joining has been discussed in this chapter which can be implemented in the wind industry. It has been found that microwave joining of plastic materials produces superior joint strength as compared to the adhesive joint. Finally, the machining behaviour of natural fibre reinforced composites has been discussed. The machining in terms of drilling of fibre reinforced composites is a challenging task. Therefore, the various issues and challenges encountered during the drilling of natural fibre reinforced composites have been highlighted in order to get a comprehensive understanding in the area of processing of natural fibre reinforced composites.

REFERENCES

[1] http://www.acmanet.org/composites/history-of-composites.

[2] F. Vilaseca, J. A. Mendez, A. Pelach, M. Llop, N. Canigueral, J. Girones, X. Turon, and P. Mutje, "Composite materials derived from biodegradable starch polymer and jute strands," *Process Biochemistry*, vol. 42, no. 3, pp. 329-334, 2007.

[3] http://en.wikipedia.org/wiki/Wood-plastic_composite.

[4] P. K. Bajpai, I. Singh, and J. Madaan, "Development and characterization of PLA based 'green' composites: A review," *Journal of Thermoplastic Composite Materials*, DOI: 10.1177/0892705712439571, 2012.

[5] P. K. Bajpai, I. Singh, and J. Madaan, "Joining of natural fibre reinforced composites using microwave energy: Experimental and finite element study," *Materials and Design*, vol. 35, pp. 596-602, 2012.

[6] I. Singh, P. K. Bajpai, D. Malik, A. K. Sharma, and P. Kumar, "Feasibility study on microwave joining of 'green composites'," *Academeia*, vol. 1, no. 1, pp. 1-6, 2011.

[7] M. P. Ho, H. Wang, J. H. Lee, C. Ho, K. Lau, J. Leng, and D. Hui, "Critical factors on manufacturing processes of natural fibre composites," *Composites Part B: Engineering*, vol. 43, no. 8, pp. 3549-3562, 2012.

[8] M. M. Kabir, H. Wang, K. T. Lau, and F. Cardona, "Chemical treatments on plant-based natural fibre reinforced polymer composites: An overview," *Composites Part B: Engineering*, vol. 43, no. 7, pp. 2883-2892, 2012.

[9] H. Demir, U. Atikler, D. Balköse, and F. Tıhmınlıoğlu, "The effect of fibre surface treatments on the tensile and water sorption properties of polypropylene-luffa fibre composites," *Composites Part A: Applied Science and Manufacturing*, vol. 37, no. 3, pp. 447-456, 2006.

[10] J. Son, H. J. Kim, and P. W. Lee, "Role of paper sludge particle size and extrusion temperature on performance of paper sludge-thermoplastic polymer composites," *Journal of Applied Polymer Science*, vol. 82, no. 11, pp. 2709-2718, 2001.

[11] N. P. Cheremisinoff (Ed.), *Handbook of Engineering Polymeric Materials*, Marcel Dekker, New York, 1997.

[12] S. K. De and J. R. White (Eds.), *Short Fibre-Polymer Composites*, Woodhead, Cambridge, 1996.

[13] A. Valadez-Gonzalez, J. M. Cervantes-Uc, R. Olayo, and P. J. Herrera-Franco, "Chemical modification of henequen fibres with an organosilane coupling agent," *Composites Part B: Engineering*, vol. 30, no. 3, pp. 321-331, 1999.

[14] X. Yuan, Y. Zhang, and X. Zhang, "Maleated polypropylene as a coupling agent for polypropylene-waste newspaper flour composites," *Journal of Applied Polymer Science*, vol. 71, no. 2, pp. 333-337, 1999.

[15] A. Valadez-Gonzalez, J. M. Cervantes-Uc, R. Olayo, and P. J. Herrera-Franco, "Effect of fibre surface treatment on the fibre-matrix bond strength of natural fibre reinforced composites," *Composites Part B: Engineering*, vol. 30, no. 3, pp. 309-320, 1999.

[16] S. Kumar, "Chemical modification of wood," *Wood and Fibre Science*, vol. 26, pp. 270-280, 1994.

[17] S. Sreenivasan, P. B. Iyer, and K. K. Iyer, "Influence of delignification and alkali treatment on the fine structure of coir fibres (Cocos nucifera)," *Journal of Materials Science*, vol. 31, no. 3, pp. 721-726, 1996.

[18] A. K. Bledzki, S. Reihmane, and J. Gassan, "Properties and modification methods for vegetable fibres for natural fibre composites," *Journal of Applied Polymer Science*, vol. 59, no. 8, pp. 1329-1336, 1996.

[19] R. Mohan and Kishore, "Jute-glass sandwich composites," *Journal of Reinforced Plastics and Composites*, vol. 4, no. 2, pp. 186-194, 1985.

[20] N. Chand, P. K. Rohatgi, "Toughness of sun hemp-carbon fibre polymer hybrid composites," *Polymer Communications*, vol. 28, no. 5, pp. 146-147, 1987.

[21] C. Pavithran, P. S. Mukherjee, and M. Brahmakumar, "Coir-glass intermingled fibre hybrid composites," *Journal of Reinforced Plastics and Composites*, vol. 10, no. 1, pp. 91-101, 1991.

[22] J. Holbery, and D. Houston, "Natural-fibre-reinforced polymer composites in automotive applications," *The Journal of The Minerals, Metals and Materials Society*, vol. 58, no. 11, pp. 80-86, 2006.

[23] N. A. Ibrahim, W. M. Z. W. Yunus, M. Othman, and K. Abdan, "Effect of chemical surface treatment on the mechanical properties of reinforced plasticized poly (lactic acid) biodegradable composites, *Journal of Reinforced Plastics and Composites*, vol. 30, no. 5, pp. 381-388, 2011.

[24] A. Baltazar-y-Jimenez, I. Seviaryna, M. Sain, and E. Y. Maeva, "Acoustic, tomographic, and morphological properties of bismaleimide-modified PLA green composites," *Journal of Reinforced Plastics and Composites*, vol. 30, no. 16, pp. 1329-1340, 2011.

[25] J. W. Holmes, P. Brøndsted, B. F. Sørensen, Z. Jiang, Z. Sun, and X. Chen, "Development of a bamboo-based composite as a sustainable green material for wind turbine blades," *Wind Engineering*, vol. 33, pp. 197-210, 2009.

[26] K. V. Rijswijk, "Thermoplastic composite wind turbine blades," Ph.D. thesis, Aerospace Engineering, Delft University of Technology, Delft, 2007.

[27] http://www.fastcoexist.com/1680889/turbine-blades-made-out-of-vegetables-to-solve-winds-hidden-pollution-problem.

[28] K. P. Subrahmanian and F. Dubouloz, "Adhesives for bonding wind turbine blades," *Reinforced Plastics*, vol. 53, no. 1, pp. 26-29, 2009.

[29] S. K. Mazumder, *Composites Manufacturing: Materials, Product, and Process Engineering*, CRC Press, New York, USA, 2001.

[30] E. T. Thostenson and T. W. Chou, "Microwave processing: Fundamentals and applications," *Composites Part A: Applied Science and Manufacturing*, vol. 30, no. 9, pp. 1055-1071, 1999.

[31] P. K. Bajpai, I. Singh, and J. Madaan, "Finite element model for microwave heating of thermoplastic composites," *International Journal of Materials Engineering Innovation*, vol. 3, no. 3, pp. 247-258, 2012.

[32] M. S. Srinath, A. K. Sharma, and P. Kumar, "A new approach to joining of bulk copper using microwave energy," *Materials and Design*, vol. 32, no. 5, pp. 2685-2694, 2011.

[33] N. Amanat, N. L. James, and D. R. McKenzie, "Welding methods for joining thermoplastic polymers for the hermetic enclosure of medical devices," *Medical Engineering and Physics*, vol. 32, no. 7, pp. 690-699, 2010.

[34] S. Das, A. K. Mukhopadhyay, S. Datta, and D. Basu, "Prospects of microwave processing: An overview," *Bulletin of Materials Science*, vol. 31, no. 7, pp. 943-956, 2008.

[35] P. K. D. V. Yarlagadda, and T. C. Chai, "An investigation into welding of engineering thermoplastics using focused microwave energy," *Journal of Materials Processing Technology*, vol. 74, no. 1, pp. 199-212, 1998.

[36] H. S. Ku, F. Siu, E. Siores, J. A. R. Ball, and A. S. Blicblau, "Applications of fixed and variable frequency microwave (VFM) facilities in polymeric materials processing and joining," *Journal of Materials Processing Technology*, vol. 113, no. 1, pp. 184-188, 2001.

[37] P. Kathirgamanathan, "Microwave welding of thermoplastics using inherently conducting polymers," *Polymer*, vol. 34, no. 14, pp. 3105-3106, 1993.

[38] P. K. Bajpai, D. Malik, I. Singh, J. Madaan, and A. K. Sharma, "Investigation for microwave joining of green composites using finite element approach," in *Proc. ICCMM 2011*, 2011.

[39] http://windsystemsmag.com/article/detail/76/an-automated-approach-to-blade-manufacturing.

[40] http://compositestutorial.com/forum/node/285.

[41] P. K. Bajpai, and I. Singh, "Drilling behaviour of sisal fibre-reinforced polypropylene composite laminates," *Journal of Reinforced Plastics and Composites*, DOI: 10.1177/0731684413492866, 2013.

[42] S. Jayabal, and U. Natarajan, "Drilling analysis of coir-fibre-reinforced polyester composites," *Bulletin of Materials Science*, vol. 34, no. 7, pp. 1563-1567, 2011.

[43] D. Babu, K. S. Babu, and B. U. M. Gowd, "Drilling uni-directional fibre-reinforced plastics manufactured by hand lay-up: Influence of Fibres," *American Journal of Materials Science and Technology*, vol. 1, pp. 1-10, 2012.

[44] S. A. Azuan, J. M. Juraidi, and W. M. Muhamad, "Evaluation of delamination in drilling rice husk reinforced polyester composites," *Applied Mechanics and Materials*, vol. 232, pp. 106-110, 2012.

[45] A. Athijayamani, M. Thiruchitrambalam, U. Natarajan, and B. Pazhanivel, "Influence of alkali - treated fibres on the mechanical properties and machinability of roselle and sisal fibre hybrid polyester composite," *Polymer Composites*, vol. 31, no. 4, pp. 723-731, 2010.

[46] H. Hocheng, and C. K. H. Dharan, "Delamination during drilling in composite laminates," *Transactions of the ASME, Journal of Engineering for Industry*, vol. 112, pp. 236-239, 1990.

[47] D. F. Liu, Y. J. Tang, and W. L. Cong, "A review of mechanical drilling for composite laminates," *Composite Structures*, vol. 94, no. 4, pp. 1265-1279, 2012.

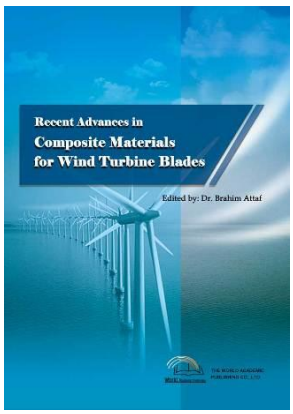

Recent Advances in Composite Materials for Wind Turbine Blades
Edited by Dr. Brahim Attaf

ISBN 978-0-9889190-0-6

Hard cover, 232 pages

Publisher: The World Academic Publishing Co. Ltd.

Published in printed edition: 20, December 2013

Published online: 20, December 2013

This book of science and technology provides an overview of recent research activities on the application of fibre-reinforced composite materials used in wind turbine blades. Great emphasis was given to the work of scientists, researchers and industrialists who are active in the field and to the latest developments achieved in new materials, manufacturing processes, architectures, a

erodynamics, optimum design, testing techniques, etc.. These innovative topics will open up great perspectives for the development of large scale blades for on- and off-shore applications. In addition, the variety of the presented chapters will offer readers access to global studies of research & innovation, technology transfer and dissemination of results and will respond effectively to issues related to improving the energy efficiency strategy for 2020 and the longer term.

How to cite this book chapter

Debnath K., Singh I., Dvivedi A. and Kumar P. (2013). Natural Fibre Reinforced-Polymer Composites for Wind Turbine Blades: Challenges and Opportunities, *Recent Advances in Composite Materials for Wind Turbines Blades*, Dr. Brahim Attaf (Ed.), ISBN 978-0-9889190-0-6, WAP-AMSA, Available from: http://www.academicpub.org/amsa/chapterInfo.aspx

World Academic Publishing - Advances in Materials Science and Applications

Chapter 3

Process Simulations for Predicting Quality of Composite Wind Turbine Blades

Konstantine A. Fetfatsidis[*1], James A. Sherwood[2]

Department of Mechanical Engineering, University of Massachusetts Lowell
One University Ave, Lowell, MA 01854, USA

[*1]Konstantine_Fetfatsidis@uml.edu; [2]James_Sherwood@uml.edu

I. INTRODUCTION

Wind turbines are often installed in high-altitude and off-shore locations, where wind energy can be converted into electrical power most efficiently. Furthermore, because the power output of a wind turbine is proportional to the area swept by the rotor, there is strong motivation to make the wind turbine blades as long as is physically reasonable from manufacturing, shipping, installation and field-service perspectives. Subsequently, as blade lengths increase, weight, stiffness and strength considerations become more important. The blades must be designed such that they are a good compromise between being aerodynamically efficient and structurally sound.

Continuous-fiber reinforced composite materials are the material of choice to manufacture wind turbine blades. Despite the advantages these materials exhibit over metals, such as high stiffness-to-weight and strength-to-weight ratios and corrosion resistance, blades continue to be overdesigned due to uncertainties in material behaviour and potential defects formed during manufacturing, and thereby the weight and the costs of the blades increase unnecessarily. Prototypes are often built and tested to understand how the materials behave and what effect the defects have on blade reliability and performance. However, this trial-and-error approach is time consuming and expensive. Additionally, the issue of scalability arises when studying the effect of defects in one blade and attempting to predict how the same defect would affect a much larger blade. The cost of blade testing is prohibitive to testing a large number of blades, and therefore, does not provide a sufficient sampling size when quantifying the effect of defects. As wind turbine blades increase in size to capture more wind, there is likewise potentially going to be increases in operating and maintenance costs. A credible design tool capable of simulating the manufacturing process and predicting the structural quality and performance of composite blades would be valuable to evaluate blade designs for weight, performance and cost.

In an effort to keep the cost of wind energy competitive, blade manufacturers often turn to relatively inexpensive fabrication processes such as hand layup and resin transfer moulding. More recently, a vacuum assisted resin transfer moulding process known as the Seemann Composites Resin Infusion Moulding Process (SCRIMP®) is used in which a vacuum compacts several layers of continuous-fiber reinforced composite fabrics and a core material, e.g. balsa, in a mold, and then pulls liquid resin into the dry layup (Fig. 1).

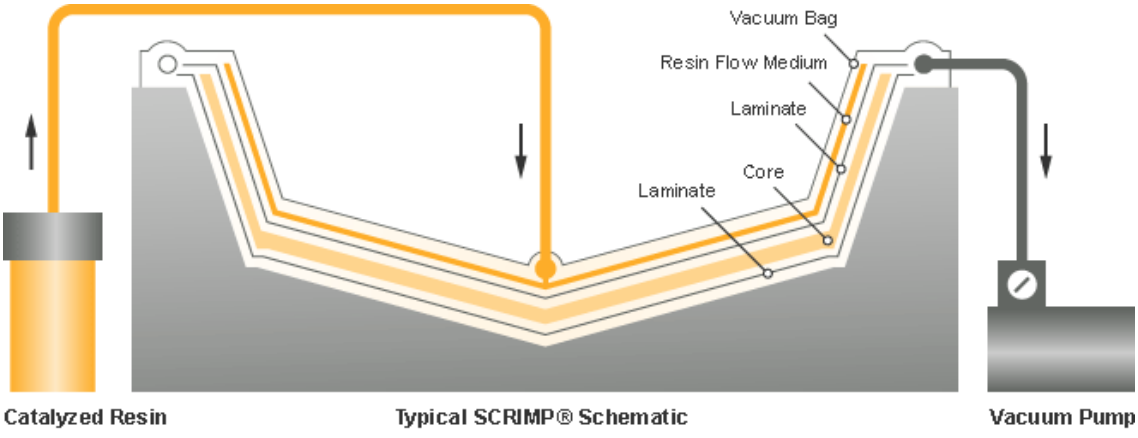

Fig. 1 Typical SCRIMP® Schematic [1]

While several types of continuous fiber reinforcements exist, Non-Crimp Fabrics (NCFs) are particularly attractive due to

the lack of yarn undulations that exist in woven fabrics. The absence of undulations, i.e. crimp, provides better in-plane mechanical properties than the woven fabrics, and the use of through-thickness stitching in NCFs allows for handling stability and delamination toughness [2]. The yarns of NCFs can be aligned in prescribed directions, and the layers held together by a through stitching. Because the stitching is a multi-axial warp knitted stitch, the in-plane shear stiffness in the direction parallel to the stitch can be significantly higher than the stiffness in the direction perpendicular to the stitch [3, 4].

The manufacturing of strength-driven designs with low-cost processes often leads to defects that compromise the overall structural behavior of the blades. These defects are typically in the form of in-plane yarn waviness, and/or out-of-plane waves due to layers of fabric bunching together during the vacuum compaction of the fabric plies. Subsequently, these waves may either fold onto adjacent layers to create wrinkles that can lead to delaminations (Fig. 2a), or the area beneath the waves can be resin rich, creating a weak spot at that location along the blade (Fig. 2b). These defects reduce the fatigue life of the blades and increase costs associated with repairs and replacements. It is estimated that blade failures contribute to 20% of wind turbine downtime [5]. While there are several ongoing efforts dedicated to improving blade reliability, it is believed that improved manufacturing of wind turbine blades offers the best return on investment [6].

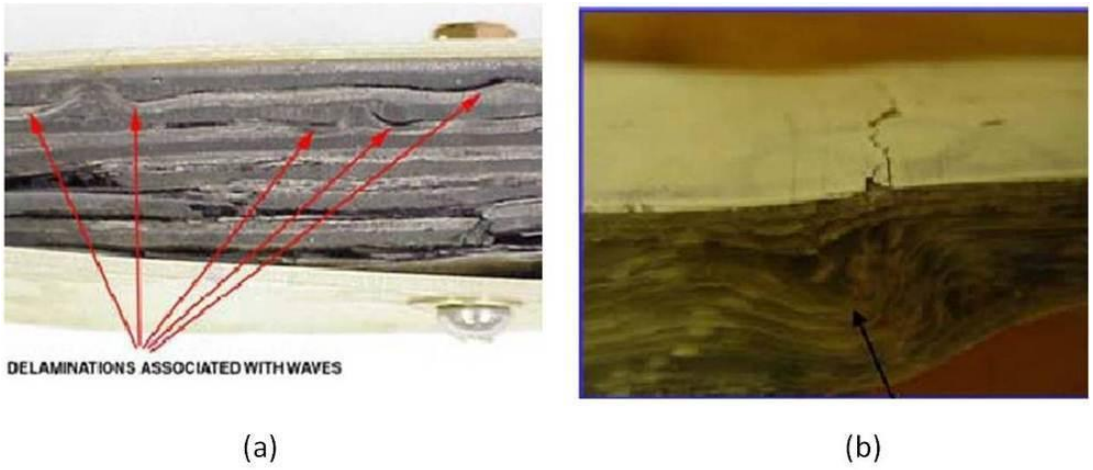

Fig. 2 Typical manufacturing-induced defects in composite wind turbine blades [6]: (a) delaminations, (b) out-of-plane wave defect

High-fidelity forming simulations offer a relatively quick and inexpensive method for studying what manufacturing parameters lead to the formation of defects, and what consequences those defects may have on the blade's structural properties. Many of the currently available design tools that account for fabric deformation use simplified kinematic algorithms to predict how the yarns in a fabric will deform to conform to the blade mold geometry. Areas of high in-plane shear are used to determine where a fabric may buckle out-of-plane. However, these kinematic models do not consider the mechanical behaviour of the fabric, and thus, cannot predict if the fabric may actually buckle out-of-plane or develop in-plane waviness during vacuum compaction, thus changing the yarn orientations. The mechanical behaviour of the fabric includes the in-plane shearing and tensile behaviours, bending stiffness and friction between contacting surfaces. By experimentally characterizing the mechanical behaviour of the fabric and resin materials used in a blade design and incorporating the respective material behaviours in user-supplied material models, a finite element simulation can provide insight into the formability of a given fabric to a given geometry. The simulation is also able to capture fabric stresses, and changes in yarn orientations, including in-plane and out-of-plane yarn waviness, as the fabric layers conform to the shape of the mold during layup (by hand or automated layup) as well as during the vacuum compaction (debulking) stage of the manufacturing process.

II. MODELING FABRIC REINFORCEMENTS

A discrete approach utilizing standard beam and shell elements in conjunction with a user-defined material subroutine with a hypoelastic description can be used to model composite fabric blanks. The use of these common element types allows the approach to be extended to popular finite element packages with user material subroutine capabilities such as Abaqus, LS-DYNA and ANSYS, without the need for any special-purpose element types or special software. Such an approach is attractive to industry because the method uses commercially available finite element codes.

This discrete approach captures the deformation and reorientation of the individual yarns and therefore can be referred to as a discrete mesoscopic approach (as opposed to microscopic, i.e. the scale of the individual fibers, which would be too CPU-intensive). In a biaxial NCF model, a unit cell is defined as the distance between adjacent yarns and is represented by the size of a 2-D shell element, as illustrated in Fig. 3 [7]. This shell element defines the fabric shear stiffness. For many fabrics, the in-plane shearing is the main mode of deformation, resulting in a change of the angle between the initially orthogonal yarns. Four 1-D beam elements simulating the yarns of the fabric are merged to the perimeter of the 2-D shell, and these beam elements capture the tensile and bending stiffnesses of the fabric. This discrete unit-cell approach can similarly be extended to a variety of fabric architectures including a balanced plain-weave fabric (Fig. 4a) and a balanced twill-weave fabric (Fig. 4b).

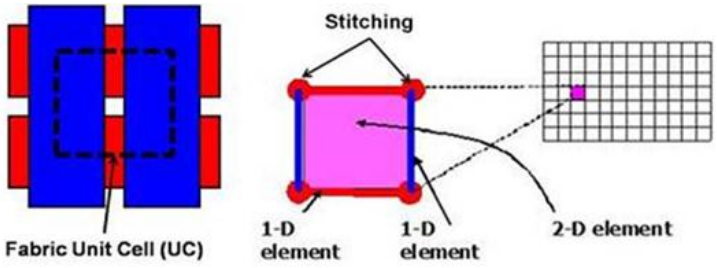

Fig. 3 Principle of the discrete mesoscopic modeling approach using a combination of 1-D and 2-D elements [7]

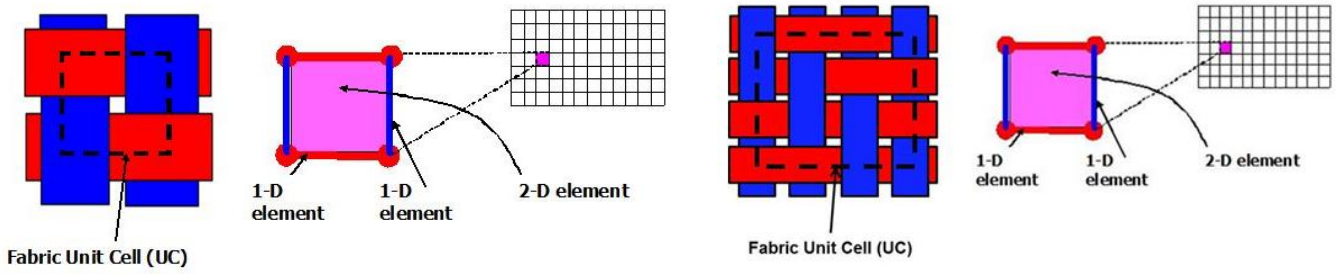

(a) (b)

Fig. 4 Principle of the discrete mesoscopic modeling approach for (a) a balanced plain-weave fabric and (b) a balanced twill-weave fabric

In the biaxial NCF unit cell shown in Fig. 3, the effect of the through stitching is captured by the pin-jointed connections at the nodes. However, in other types of NCFs, it may be necessary to incorporate additional 1-D beam or truss elements to explicitly model the stitching (Fig. 5) and to capture the effect(s) that the stitching may have on the fabric behaviour. For example, in a unidirectional or biaxial NCF, out-of-plane deformation is likely due to a combination of in-plane shear, tension, and bending stiffness. However, in many double-bias NCFs, the stitch pattern can causes out-of-plane buckling earlier than it would if the same yarns were simply woven together.

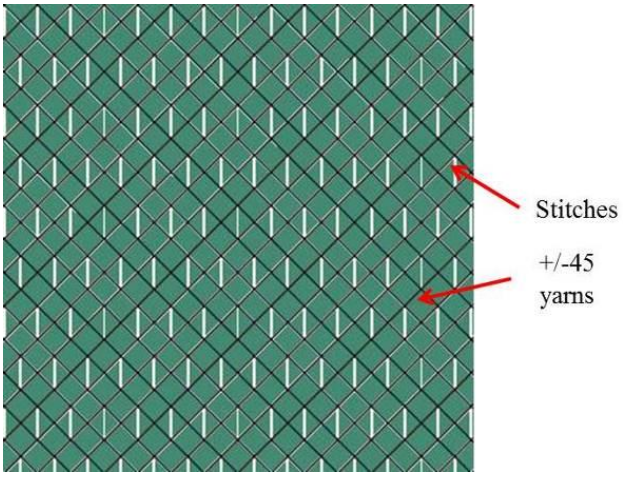

Fig. 5 FE model of a double-bias NCF with cross-stitch pattern

Furthermore, the pin-jointed unit-cell approach fails to capture the slipping of yarns in many NCFs. The so-called NCFs are given their name due to the absence of the crimp that exists in woven fabrics. The lack of crimp improves the drapability over complex curvatures because the yarns are not interlocked and are able to move more freely via sliding to conform to the geometry. However, depending on the geometry, the amount of sliding can negatively impact the design of the part by introducing large voids between yarns and thereby compromising local stiffnesses. Currently, hand layup of the fabric reinforcements in many wind turbine blades is like “patch-work”, where the fabrics are cut and oriented such that the yarns run mostly in their intended directions with little sliding. However, as manufacturers strive to automate the process, yarn sliding could become more of a concern, and it is therefore important to be able to capture this behavior in the model to provide valuable feedback into the design process. The discrete mesoscopic modeling approach could be modified to allow for yarn slipping by placing the yarn crossovers at the centre points of the shells rather than at a node, as demonstrated in Fig. 6. This layout of the unit cells is such that no yarn is “pinned” to any other yarn, thereby allowing sliding of the yarns relative to one another.

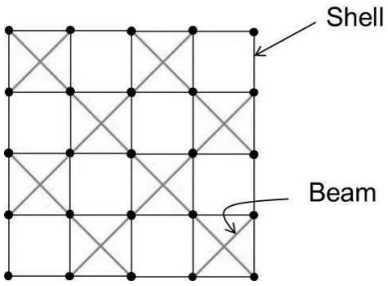

Fig. 6 Discrete model that allows for NCF yarns to slide/separate [8]

Regressions of experimental data are used to conclude empirical models that are then implemented as user-defined material subroutines to capture the mechanical behaviour of the fabric material in the finite element solver [9]. Finite element models of the various tests are completed to validate that the fabric model behaviour can be properly simulated using the finite element method. Additionally, the finite element method allows for contact to be defined between layers of fabric and therefore friction is experimentally measured using a friction-test apparatus [10].

A. Unit-Cell Scaling

The unit cell of each fabric is determined by measuring the number of individual yarns per meter of fabric. These unit-cell measurements assist in concluding the size of the shell elements used in the finite element fabric model. However, relative to the size of a wind turbine blade, if the unit-cell size of the fabric was used, it would lead to a relatively fine mesh of the fabric finite element model and would make the model computationally expensive. Therefore, the unit cell size of each fabric layer can be scaled by some factor in an effort to coarsen the mesh associated with each fabric layer to reduce computation time. It is important to conduct parametric studies to confirm that the credibility of a forming analysis will not be compromised by the "coarse" mesh and thereby reduce the applicability of the model. An example of such a parametric study is illustrated by the forming of a fabric into a hemisphere in Fig. 7. A path is drawn from the center of the hemisphere (apex) to the region of maximum in-plane shear, indicated by the red contours. The shear angles along this path are compared between the measured unit-cell size and the scaled unit-cell size. Fig. 8 shows that if scaled too much, the accuracy of the analysis is compromised.

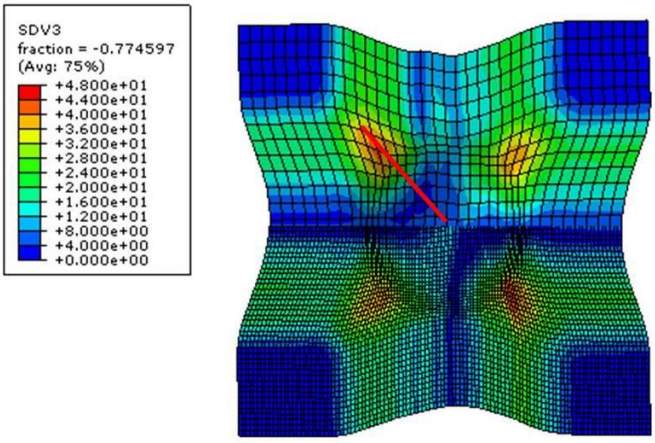

Fig. 7 Forming simulation showing in-plane shear angle contours with the original unit-cell size mesh (bottom) and a scaled (x3) mesh (top)

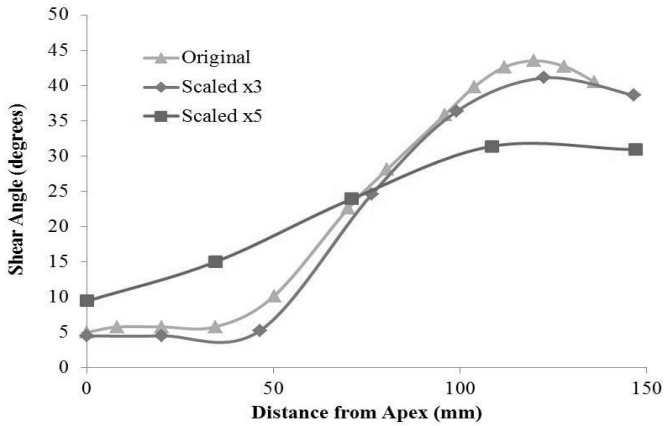

Fig. 8 Comparison of shear angles between refined, coarse (x3), and excessively coarse (x5) meshes in formed hemisphere model

Consider the root section of a 9-meter wind turbine blade. When forming a layer of fabric into this root section, the amount by which the unit-cell is scaled can limit how well the fabric conforms to the mold geometry. Fig. 9a shows the shear angle contours of a layer of biaxial NCF pressed into the root using the fabric's actual unit-cell size. However, this unit-cell size must be scaled to make a simulation of the entire blade model practical, considering the number of layers included in the 9-meter blade. Fig. 9b scales the unit-cell of the same fabric by a factor of 3 and the resulting shear angle contours correlate well to the original unit-cell model. However, if scaled by a factor of 5 (Fig. 9c) the fabric is not able to conform to curvatures in the mold geometry and causes element surfaces to unrealistically penetrate each other during contact, as indicated by the circled area.

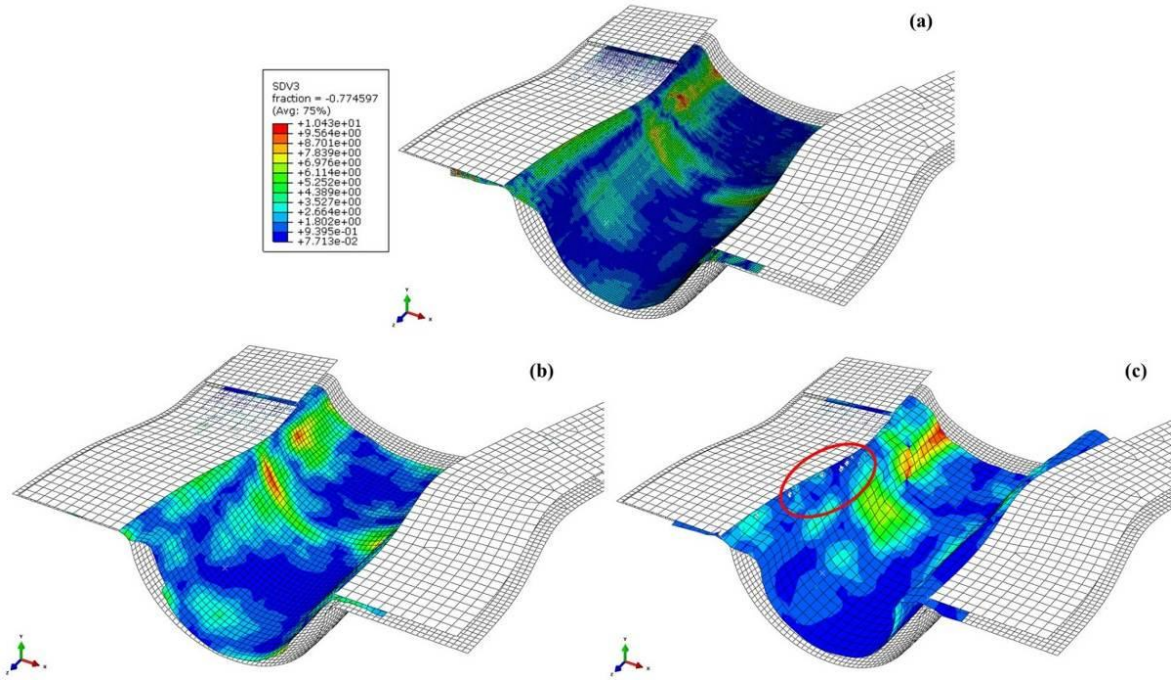

Fig. 9 Forming of a fabric layer in the root section of a 9-meter wind turbine blade using the unit-cell size of a biaxial NCF (a) actual, (b) scaled (x3) and (c) excessively scaled (x5)

B. Simulating the Manufacturing Process

Generally, the manufacture of a composite wind turbine blade consists of hand-laying several layers of fabric and core material into a low-pressure (LP) and high-pressure (HP) mould, followed by a vacuum pressure to first compact (debulk) the layers and then to infuse each mold with resin. The fully cured LP and HP sides are then bonded with a spar to create the full wind turbine blade. In the finite element model for the manufacture of a blade, the hand layup of fabric layers is simulated by using a rigid core (punch) to press the fabric into a fixed, rigid mould (Fig. 10). The punch is allowed to move only in the vertical direction. Additionally, rigid binders which can translate vertically, provide in-plane tension in the fabric to prevent folding and sliding of the fabric layers as they are pressed into the mold by the punch.

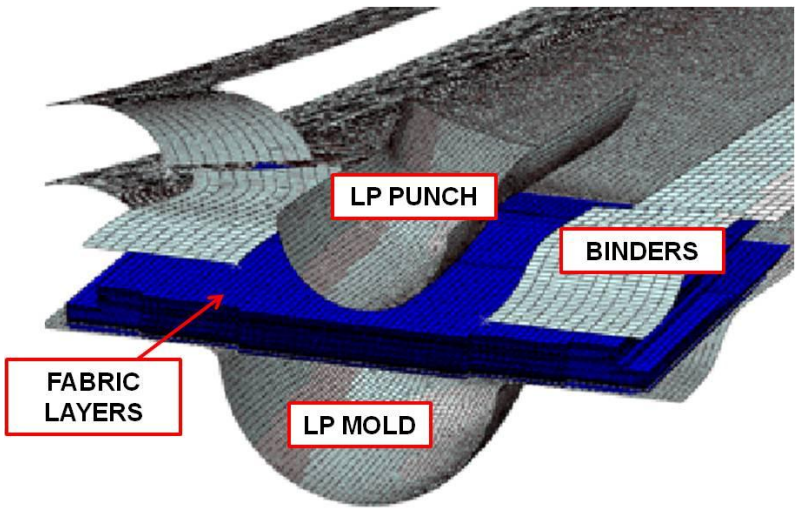

Fig. 10 Punch pressing fabric layers into the LP mould (binders are used to provide in-plane tension in the fabric)

Typically, an explicit formulation (Abaqus/Explicit) is used to perform this type of forming simulation due to its computing time efficiency, its relatively robust contact algorithms and its option to account for the mechanical behavior of the fabrics via user-defined material models. To save computation time, layers are pressed into each mould in groups. After initially being pressed into the mold using the rigid punch, additional pressures are subsequently applied to press the layers tightly into each mold. After all of the layers of fabric have been pressed into the molds, the compaction of the fabric layers is simulated by applying a pressure equivalent to atmospheric pressure directly onto the surface of the top layers. It is believed that during this stage in the manufacturing process, fabric layers may bunch together to form out-of-plane wave defects that eventually compromise the performance and reliability of wind turbine blades [11]. Because the formation of wave defects most likely occurs during the hand layup and vacuum compaction stages of the manufacturing process, the resin infusion process is not simulated. Instead, it is assumed that once the layers of fabric have deformed, the resin is evenly distributed across each mold with a fiber volume fraction of 55%, which is typical for the blades manufactured using the SCRIMP® process [11]. After the LP and HP molds are individually modeled, they are bonded together with tie constraints, resulting in the full blade model.

III. EXPERIMENTAL CHARACTERIZATION TECHNIQUES

When required to deform over double-curvature geometry, the yarns of a non-crimp fabric may be pulled in a certain direction to conform to the features of the geometry. However, the absence of yarn undulations such as those in woven fabrics allows for very little stretching of the fibres at the mesoscopic scale during deformation. Thus, the in-plane shearing of the fabric yarns becomes the principal mode of deformation. This in-plane shearing results in a change of the angle between the initially-orthogonal yarns of a biaxial non-crimp fabric. In addition, the fabric bending stiffness and the friction between fabric layers can result in unwanted in-plane and out-of-plane waviness and/or folds in the fabric. To capture these modes of deformation using the beam and shell elements in the fabric model, the mechanical behaviour of the fabric must be characterized.

C. Shear-Frame Testing

The standard test for measuring the shear behaviour of fabrics is the shear-frame test [12], also known as the trellis-frame test, or the picture frame test, as shown in Fig. 11. In this test, a fabric specimen is clamped with the yarns typically directed perpendicular and parallel to the four clamping bars. Shear deformation is developed by fixing one corner and applying a tensile load on the opposing corner. The shear-frame test assumes that the shear angle is uniform over the entire sample and equal to the frame angle. These two assumptions have been verified for woven fabrics via Digital Image Correlation (DIC) [13, 14]. The deformation of the fabric in the shear-frame test is shown in Fig. 12.

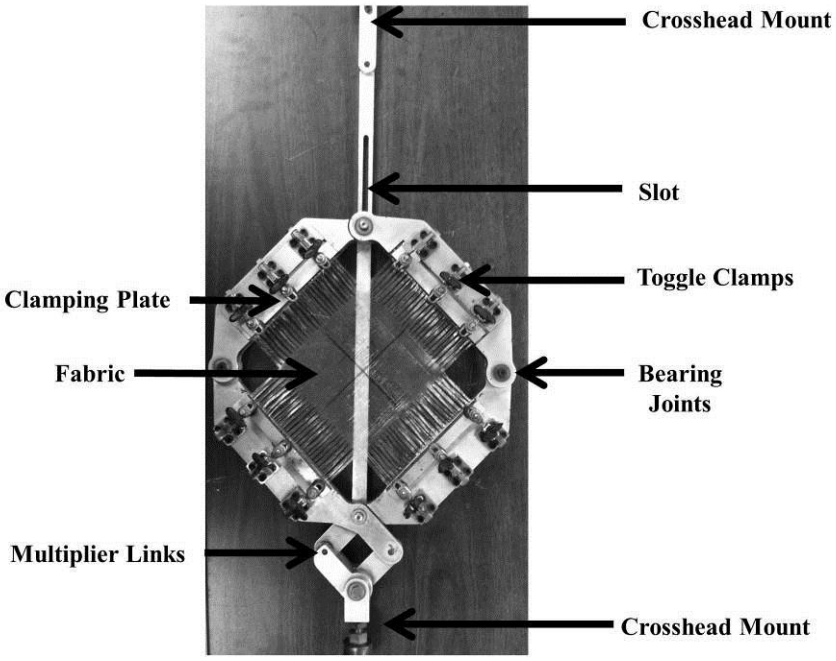

Fig. 11 Shear-frame test

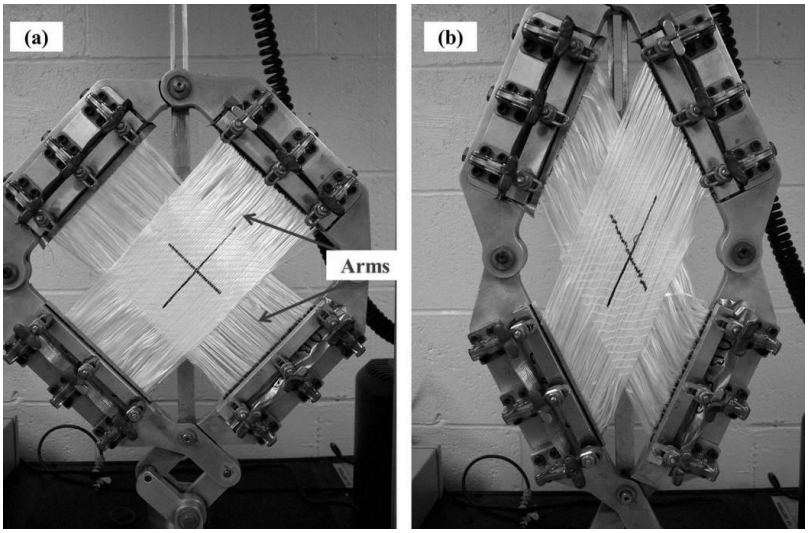

Fig. 12 Deformation of shear-frame test (a) before deformation and (b) after deformation

The cross yarns are removed in the arms of each sample to minimize edge effects and allow the yarns to rotate freely relative to each other. Consider a unidirectional NCF shown in Fig. 13. This fabric is mounted in the shear frame in only one direction, because there are no perpendicular yarns. Without the presence of "arms" in the sample, an out-of-plane wave pattern is observed across the width of the test sample and extending along its whole length when pulled in the frame (Fig. 13a). The out-of-plane deformations are caused by the clamped fabric edges, which do not allow individual fibers to slide relative to each other. The stitching between the yarns can be partially cut to create 50-mm arms at each end of the sample (Fig. 13b). The addition of arms allows for in-plane sliding of the yarns in the middle of the sample, as shown in Fig. 13c, and significantly reduces out-of-plane deformation [15].

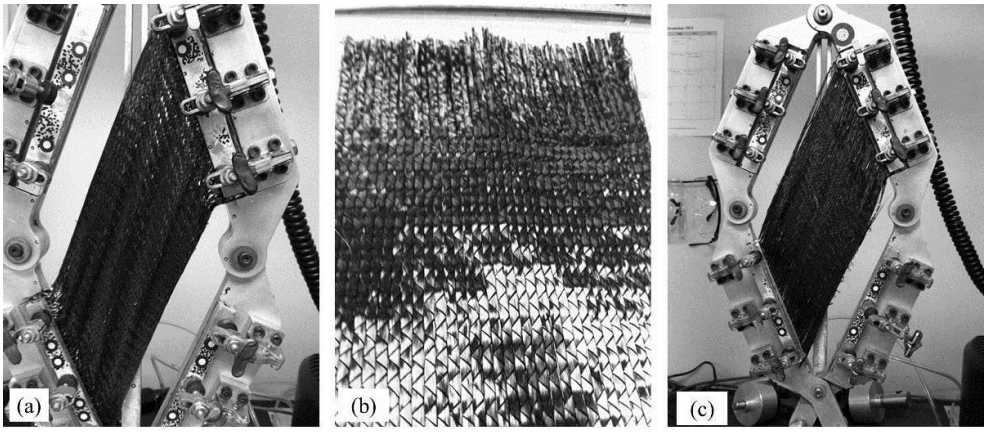

Fig. 13 Unidirectional NCF loaded in the shear frame (a) without arms. The absence of arms causes out-of-plane deformation due to edge effects, which necessitates the (b) addition of arms in the sample. The arms (c) significantly reduce the out-of-plane deformation

Woven fabric samples are typically loaded and unloaded several times in the shear frame before measuring the shear stiffness. The intent of this mechanical conditioning is to reduce the effect of undesired tension in the yarns that could arise from a misalignment of the yarns [12, 16]. The mechanical conditioning also allows for increased repeatability from sample to sample even though in reality, a fabric will be taken off of a roll and laid into a mold without any mechanical conditioning. Typically for a given sample, the measured loads during the first shear-frame test run will be higher than those of the subsequent runs, in which the load curves appear to be very similar. Non-crimp fabrics, however, are more sensitive to mechanical conditioning because of the through-thickness stitching which can tear after repeated loading and unloading of the same sample. This stitching plays a very important role in the shear stiffness and in the wrinkling characteristics of a NCF and cannot be neglected. Therefore, NCFs should not mechanically condition, and the first load-displacement curve should be taken as the representative shear deformation curve.

The measured load is converted to a force that is normalized by the length of the frame. This normalization accounts for various shear-frame sizes that may be used. The normalized force can then be divided by the thickness of the fabric sample to obtain the shear stress. Similarly, the shear angle can be determined by knowing the length of the frame, length of the fabric sample, and the measured displacement data. This angle can then be converted to a logarithmic shear strain, which is consistent with the shear strain definition used by the finite element code. After testing a minimum of three samples, the average shear stress and logarithmic strain are calculated and plotted with error bars of one standard deviation.

A typical load-shear angle curve from a biaxial NCF is shown in Fig. 14. The yarns are initially orthogonal to one another. Upon initiation of intra-ply shear deformation, the yarns begin to rotate and possibly to slip relative to one another. The shear stiffness steadily increases as the yarns continue to rotate and compress against each other, thus increasing the friction between adjacent yarns. As the yarns continue to rotate, an angle referred to as the locking angle is reached where the yarns are no longer able to compact easily and the shear stiffness increases rapidly. In addition to a significant increase in stiffness, deformation beyond the locking angle can also cause the fabric to buckle out-of-plane, as the deformation mode becomes a combination of shear, yarn compaction and tension. The locking angle is determined from the intersection of two lines tangent to the load-shear angle curve.

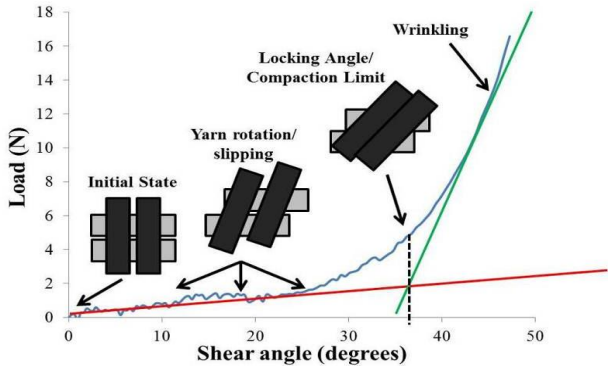

Fig. 14 Load-shear angle curve with schematics of shear behaviour for a biaxial NCF

After all of the stress-logarithmic strain plots have been generated, polynomial fits are made to these curves. These functions are implemented into the finite element code via its user-defined material subroutine, which for Abaqus/Explicit is VUMAT, to capture the shear behaviour of each fabric. Abaqus/Explicit uses rate-independent constitutive equations, also called hypoelastic laws, to model large deformation and strains. Stresses are updated using the following equations:

$$\sigma_{ij}^{t+1} = \sigma_{ij}^{t} + \Delta\sigma_{ij}^{t+1} \tag{1}$$

$$\Delta\sigma_{ij}^{t+1} = C_{ijkl}\ \Delta\varepsilon_{kl}^{t+1/2} \tag{2}$$

where $\Delta\sigma_{ij}^{t+1}$ is the stress increment at time step t+1, C_{ijkl} is the constitutive matrix and $\Delta\varepsilon_{kl}^{t+½}$ is the midpoint strain increment obtained from the integration of the strain rate tensor. The custom constitutive models obtained through regressions of experimental data and implemented into the VUMAT subroutine are linked with the overall solver to update the stress (Eq. 2). The strain increment, $\Delta\varepsilon_{kl}^{t+½}$, is given by the solver to VUMAT that subsequently returns the corresponding stress increment to the solver. The stress update is made in the local reference frame for the element, i.e. a co-rotational frame that rotates with the element. The summation of the strain increments gives a logarithmic (or true) strain in the principal-stretch directions. Details associated with the constitutive equations as they pertain to the 1-D and 2-D elements of the current unit-cell model are provided in [9].

A finite element model of the fabric shear-frame test, including the "arms" of the specimens, is generated to ensure that the 2-D shell elements are accurately capturing the shear stiffness of each fabric (Fig. 15a). The arms are modeled using 1-D beam elements, and the frame is modeled using four aluminum trusses. The constants that define the tangent shear modulus are obtained by deriving the polynomial fits of the experimental stress-logarithmic strain curves and are defined in the Abaqus input file material card. The model correlates with the assumption of pure shear in the fabric sample (Fig. 15b).

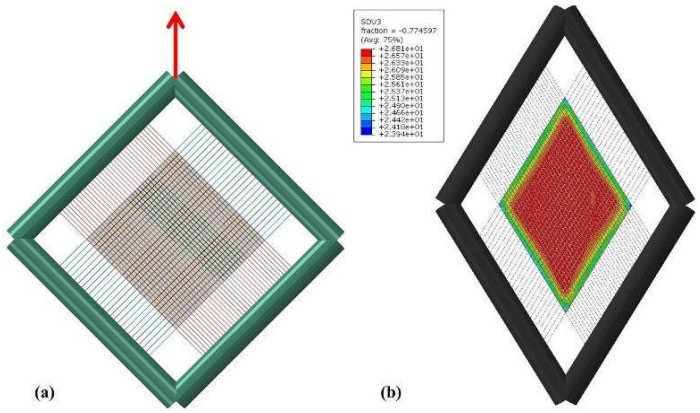

Fig. 15 Finite element model of (a) the shear-frame test and (b) the resulting uniform shear angle contours

D. Tensile Testing

As fabric is pressed into a mould, certain yarns may exhibit high tensile stresses as they bridge undulated regions of the geometry, i.e. peaks and valleys. These high tensile stresses can ultimately cause the yarns to break, leading to a poor-quality part. High stresses can be used to indicate local areas where fiber breakage could be a problem. Furthermore, failure criteria could be implemented into the beam elements of the fabric model to cause them to visually break. Therefore, to characterize the tensile mechanical behaviour of the yarns, uniaxial tensile tests are performed on individual yarns extracted from each fabric. To prevent slipping at the pneumatic grips (Fig. 16a), tabs are created by consolidating small pieces of Twintex® commingled glass/polypropylene woven-fabric (Fig. 16b).

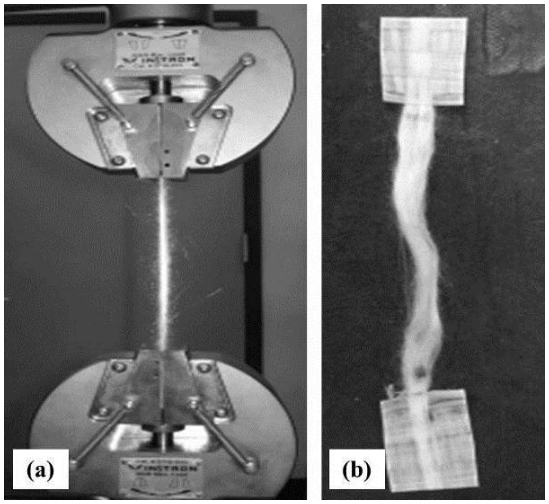

Fig. 16 Tensile test setup with (a) pneumatic grips and (b) Twintex® tabs to prevent yarn slippage

The tensile tests quantify the fracture load (Fig. 17a) and modulus of the yarn. The modulus of each yarn is obtained from the slope of the associated stress/true-strain curve (Fig. 17b), where the stress is determined by dividing the measured load by the effective cross section of the yarn, A_{eff}. This effective cross section of the yarn is determined based on the linear density of the yarn ρ_{linear} and the fiber material density ρ_{mat}:

$$A_{eff} = \frac{\rho_{linear}}{\rho_{mat}} \tag{3}$$

The true strain is used to again be consistent with the finite element code:

$$\varepsilon = \ln\left(1+\frac{l}{l_o}\right) \tag{4}$$

where l is the measured length of the sample and l_0 is the initial length.

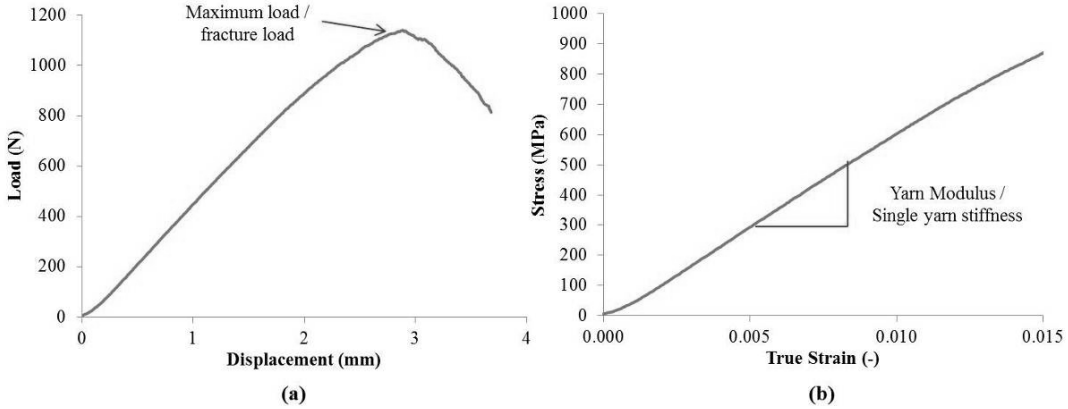

Fig. 17 Yarn tensile testing resulting in (a) a typical load-displacement curve and (b) the determination of the fabric tensile behaviour from the yarn modulus for a typical yarn

Abaqus/Explicit applies Eq. (2) to the definition of the 1-D beam element material behaviour, where C_{ijkl} is the tangent tensile modulus, or yarn modulus. A single yarn is modeled using a set of beam elements and pulled uniaxially. The slope of the stress-true strain curve is determined from the model and is compared to the yarn modulus obtained experimentally to ensure that the tensile stiffness is being accurately captured in the finite element fabric model.

E. Bending Stiffness Test

To use the finite element method for predicting the formation of in-plane and/or out-of-plane waviness during the manufacture of composite wind turbine blades, the overall mechanical behaviour of the composite fabric reinforcements must be thoroughly defined. The in-plane shearing behaviour is often used as an indicator via the "locking angle" as to when wrinkles may develop in the form of in-plane and/or out-of-plane waves. As yarns rotate relative to one another, they eventually reach a point where they can no longer rotate in-plane and must buckle out-of-plane. However, it has been shown that simply relating wrinkling to the shear angle is not sufficient. The formation of wrinkles and/or waves depends on the combination of in-plane shear, tension and bending behaviours of the fabric [17]. Thus, it is important to characterize the bending stiffness of the fabrics.

When characterizing the dry fabric bending stiffness, a cantilever "beam" method is often used [18], where the fabric is allowed to bend due to its own weight (Fig. 18). However, depending on the length of the sample, the effective direction of the distributed load on the sample changes due to the large deformations, and thus, a single value for the fabric bending stiffness cannot be concluded for all lengths despite efforts to compensate for the effect of gravity. An alternative method for characterizing the bending stiffness is to align the length of the beam with gravity and thereby reduce the nonlinear loading effects [19]. Fabric samples are clamped at one end and hung vertically. A horizontal load is applied to displace the tip of the fabric a known amount. This load is applied by attaching masses to a string tied to the tip of the fabric sample (see Fig. 18).

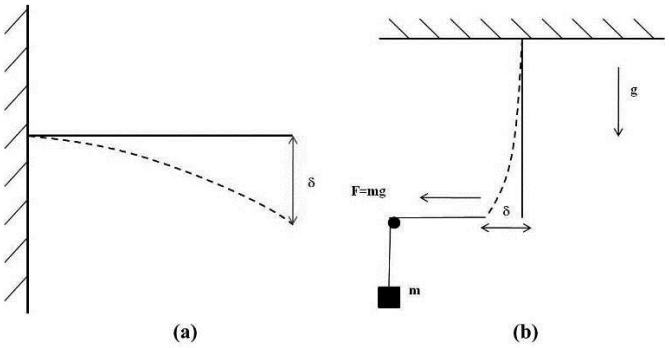

Fig. 18 Schematic of (a) cantilever experimental setup and (b) hanging-fabric bending stiffness setup

With the effective fabric length positioned in the clamp, various tip displacements are applied using an appropriate load, and a digital image of the fabric is captured. Individual data points are generated along the fabric length (Fig. 19a) and plotted (Fig. 19b).

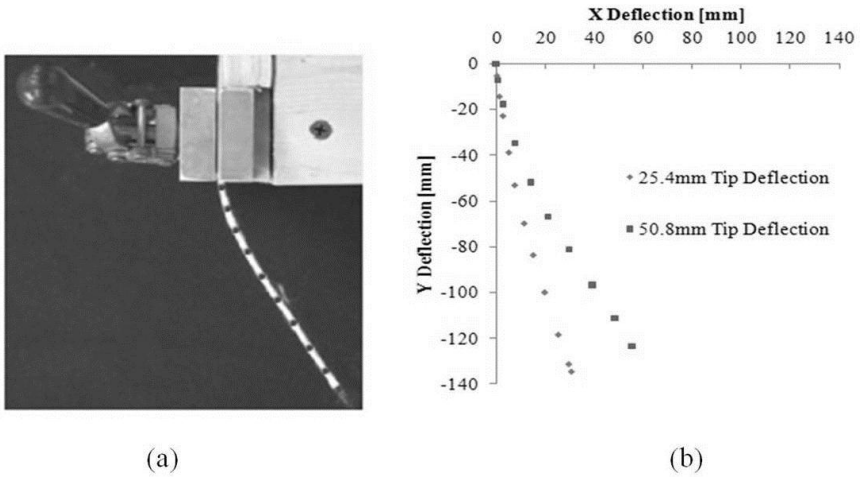

Fig. 19 Postprocessing of experimental data including (a) generation of x and y data points and (b) plotting of data points

Finite element models similar to the experimental fabric samples are used to calibrate the fabric bending stiffness. The bending stiffness is defined per yarn and is therefore assigned to each of the 1-D beam elements in the fabric. Equivalent tip displacements are prescribed in the models, and a range of bending-stiffness values are used to replicate the experimental profile shape of the sample. While several values of bending stiffness may lead to a similar profile shape, the force required to displace the tip a known amount is compared to the experimental force to ensure that the correct bending stiffness is being used in the model. Note that for the effective bending stiffness as used here the unit for moment, M, is N-mm and for curvature, κ, is mm^{-1}. Thus, the bending stiffness M/κ defined in the finite element model is given as $N\text{-}mm^2$. As a means of verifying that the bending stiffness is valid, the bending stiffness is applied to models with different tip displacements and different fabric sample lengths (Fig. 20).

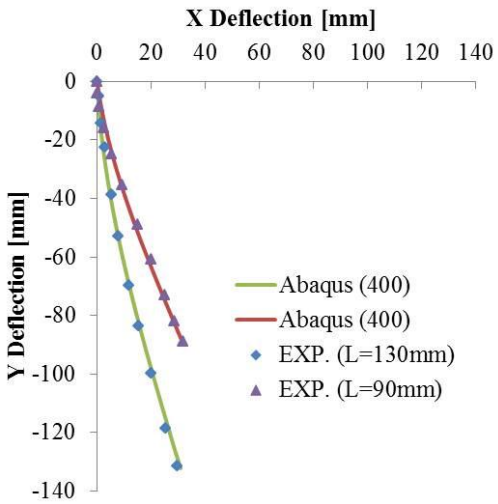

Fig. 20 Comparison of experimental data to FE model of a biaxial NCF for varying tip displacements and fabric lengths

As mentioned previously, the formation of wrinkles and/or waves depends on the combination of in-plane shear, tension and bending behaviours of the fabric. It is certainly possible to predict defects based on the in-plane shear and tension behaviours alone. However, the bending stiffness is needed to describe the wrinkle/wave shape. For example, compressing a fabric sample model from two sides will yield a different number of out-of-plane waves with different amplitudes depending on the magnitude of the bending stiffness. A much stiffer fabric will result in fewer waves with greater amplitude (Fig. 21a) than a fabric with a low bending stiffness (Fig. 21b).

Fig. 21 FE model of a fabric sample compressed from each side with (a) high bending stiffness and (b) low bending stiffness

In the unit-cell discrete modeling approach, the 1-D beam elements carry the bending stiffness of the fabric yarns. The bending stiffness is assigned to the beam elements' section properties. Without explicitly defining the bending stiffness as part of the beam section properties, finite element codes will by default consider the product of the elastic modulus, E, and the area moment of inertia, I, of the elements to define the bending stiffness. This default definition is typically much higher than the measured bending stiffness.

F. Friction Testing

As layers of fabric are laid into the LP and HP moulds of a wind turbine blade, on top of other layers of fabric and the core material, their ability to deform and develop in-plane and out-of-plane waviness depends highly on the friction between adjacent surfaces. Often, a tackifying spray is used to increase the friction between layers of fabric during hand layup. Therefore, it is important to capture the effect of this increased friction in the simulation of the manufacturing process.

Friction between contacting surfaces can be measured using an apparatus similar to that developed in [10]. This apparatus consists of a fabric holder that is sandwiched between two platens. The bottom platen is fixed while the top platen provides a normal force, *N*, onto the fabric clamped inside the holder. The holder then pulls the clamped fabric from between the two platens and the tensile force, *T*, is measured. The effective coefficient of friction, μ_{eff}, can be obtained by:

$$\mu_{eff} = \frac{T}{2N} \tag{5}$$

where the normal force *N* is multiplied by a factor of two to account for the two contacting surfaces. When plotting the effective coefficient of friction versus the pull-out distance (as shown in Fig. 22), a sharp peak is initially observed, representing the static coefficient of friction or the frictional force needed to be overcome to initiate motion. This peak then decays exponentially to a somewhat steady-state value of the friction coefficient referred to as the dynamic coefficient of friction. The value of the normal force is chosen such that the pressure on the fabric sample in the holder is equivalent to the atmospheric pressure applied by the vacuum during the compaction stage of the manufacturing process.

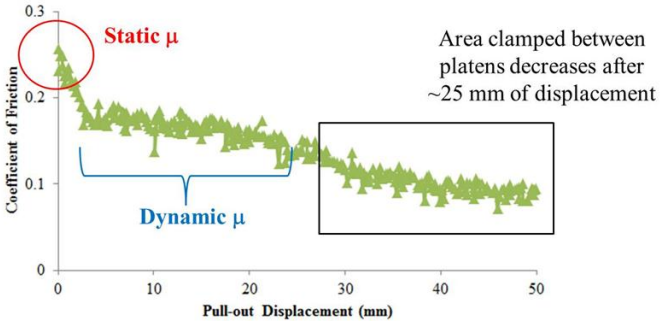

Fig. 22 Typical friction-test curve for determining the static and dynamic coefficient of friction

While the pressure from the vacuum will be constant during the manufacturing process, the interlaminar slip velocity can vary as a function of position and the degree of forming. To explore whether or not the dry Coulomb friction varies with velocity, the fabric samples can be pulled at different rates. Fig. 23 shows the resulting static and dynamic coefficients of friction between two dry fabrics at two pull-out velocities (i.e., 2 mm/s and 25 mm/s). The error bars denote one standard deviation. In this particular case, the friction was shown not to be rate dependent.

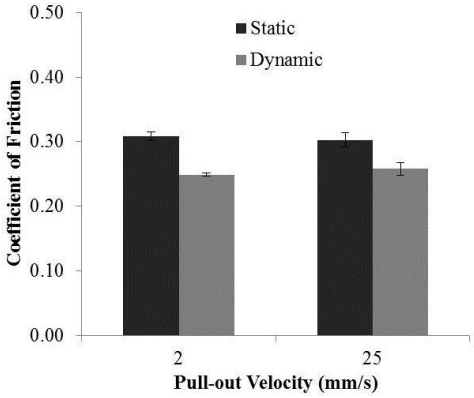

Fig. 23 Coulomb friction between carbon unidirectional and glass biaxial NCF as a function of pull-out velocity

Exponential decay model:

The static coefficient of friction defines the force necessary to initiate slipping between contacting surfaces. Once motion is initiated, the coefficient of friction generally drops to a lower value known as the dynamic coefficient of friction. Most commercially available finite element codes have a built-in static-dynamic exponential decay function (Eq. 6) that can be used to define this transition from the static to the dynamic coefficient friction,

$$\mu_{eff} = \mu_d + (\mu_s - \mu_d)\, e^{-\beta\dot{\gamma}} \tag{6}$$

where μ_s is the static friction coefficient, μ_d is the dynamic friction coefficient, β is the decay constant and $\dot{\gamma}$ is the slip rate. The decay constant defines the transition rate from zero velocity to final velocity (static to dynamic friction coefficient), as shown in Fig. 24. This relationship can thus be used in forming simulations to define the frictional behaviour between the various contacting fabric layers.

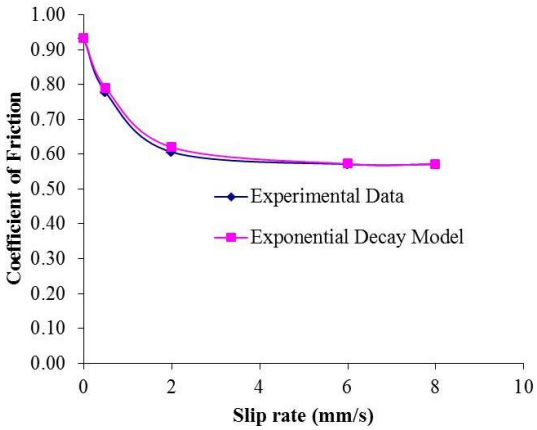

Fig. 24 Determination of the decay constant for static-dynamic exponential decay model

IV. PROCESS SIMULATION RESULTS

With the mechanical behaviour of the NCF reinforcements defined, forming simulations are conducted to explore the deformation of the fabrics, specifically the reorientation of the fabric yarns, and the fabric stresses during the hand layup stage of the manufacturing process. These simulations serve as a design tool to determine the number of layers and fabric orientations for drapability as well as for structural stiffness. While the fabric layers of most blades are currently placed by hand, the hand layup process can be loosely simulated by using a rigid mould paired with a matched core. These rigid tools are generated by dividing a solid CAD model of the blade into two parts to represent the LP and HP moulds (Fig. 25).

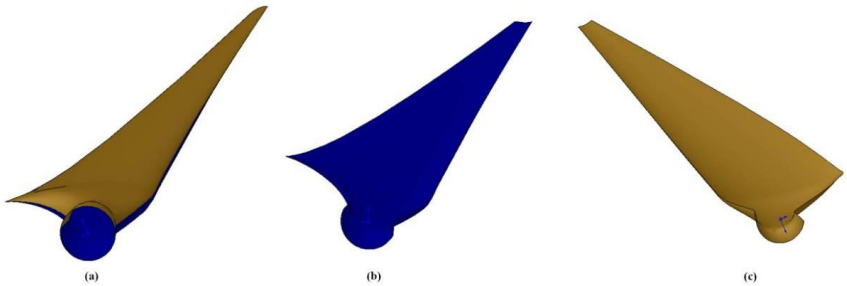

Fig. 25 CAD model of (a) 9-meter blade split into (b) LP mould and (c) HP mould

The rigid mould geometries are scaled down based on the radius of the root sections to create cores that could accommodate the thickness of the layers that would be pressed into each mould (Fig. 26). The moulds and cores are meshed with enough resolution of rigid shell elements to maintain smooth curvatures. Fig. 27 shows that without sufficient resolution, the mold surfaces would be jagged and the fabric layers would subsequently conform to those jagged surfaces.

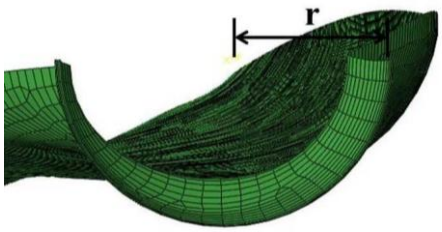

Fig. 26 Scaling of rigid cores for forming simulations

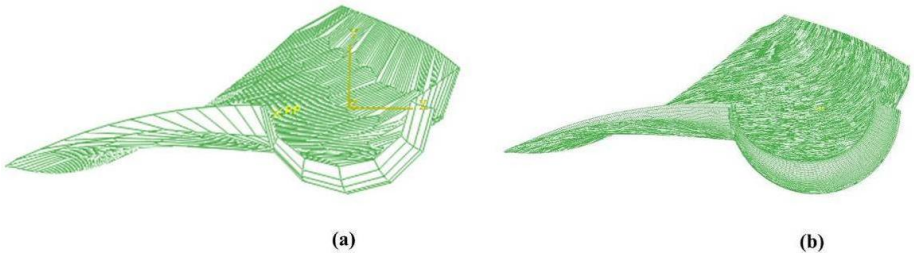

Fig. 27 Blade tooling meshed using rigid shell elements with (a) insufficient resolution and (b) sufficient resolution

To provide a smooth surface finish, a gelcoat typically covers the entire inner mould surfaces. This gelcoat is then covered by a mat of random chopped fibers, followed by a few additional NCFs. The deformation of these initial fabric layers is insignificant and defects are not likely to form in these layers [11]. However, the thickness of these layers is considered in the finite element model by using the built-in Composite Ply feature in Abaqus. The ply-stack plot shown in Fig. 28 shows the thickness and the fiber orientations of each of the first four layers.

With the thickness of the first few layers accounted for, the placing of the root layers is simulated next. During the manufacturing process, fabric layers are laid into a mould individually by hand. However, to simulate the placing of layers individually, the core would need to be changed each time to account for the changing thickness due to additional plies. Therefore, to save time, all of the fabrics are pressed into the root section of each mould simultaneously, and the core is scaled accordingly to account for the thickness of all of the root layers. To prevent folding and sliding of the fabric layers as they are pressed into the mould, flanges are added to the molds with matching rigid binders to provide in-plane tension in the fabric layers. This in-plane tension is analogous to the hand stretching of the fabric layers as they are manually positioned in the mold during the layup process. Because of ply drops in the root section, the effective overall thickness tapers down as viewed from the base of the blade looking to the tip, and thus the binders are segmented (Fig. 29b) to maintain binder contact along the tapered plane, as shown in Fig. 29a. Otherwise, a continuous binder would provide in-plane tension in the thickest section but would not induce such tension in areas where the thickness had decreased.

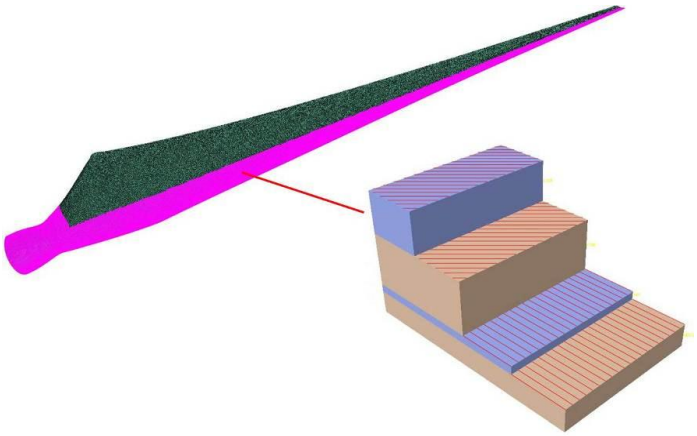

Fig. 28 Ply-stack plot of first four layers laid over the initial gelcoat

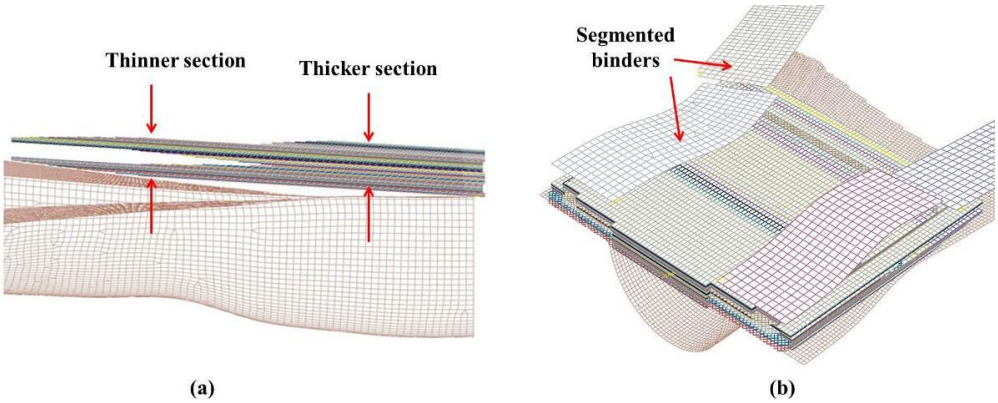

Fig. 29 Forming simulation with (a) varying root-layer sizes requiring (b) segmented binders

In addition to the flanges and binders added to the molds to accommodate the "automated" manufacturing process, the intersection area between (Fig. 30a) the trough of the moulds and flanges is rounded (Fig. 30b) to prevent convergence issues that could arise as elements attempt to wrap around what would otherwise have been sharp edges as shown in Fig. 30a. To keep the curvature of the rounded edges smooth, the mesh of the mold in Fig. 30b is also refined.

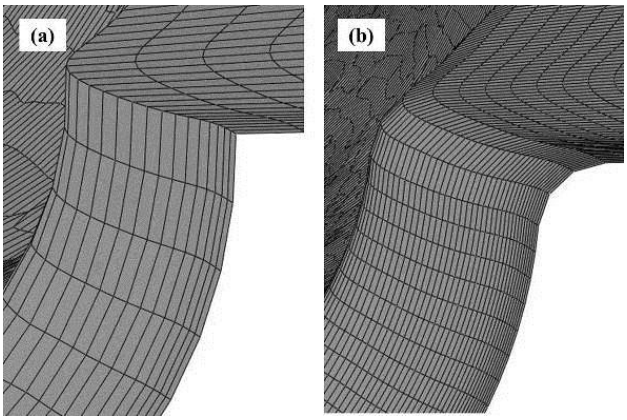

Fig. 30 Flanges added to rigid mould with (a) sharp edges changed to (b) rounded edges to allow fabrics to drape more easily

After the simultaneous forming of the root layers, the moulds with the flanges and binders are replaced by the moulds without the flanges. Pressures are applied to the surfaces of the root layers preceding the first spar cap layers to press them tightly into the molds. Once sitting firmly in the mold, the nodes of those root layers are fixed into place, as shown in Fig. 31a, and the spar-cap layers are formed using a combination of rigid cores (Fig. 31b) and additional pressure (Fig. 31c). Note that a multi-piece core is used because the thickness at the skin of the blade is much less than that at the root section and a single-piece core would not be able to press the spar-cap layers fully into the mould in the skin section. Pressure could be applied uniformly over the entire spar-cap surface or over different regions such as the root section shown in Fig. 31c, depending on how well the layers were pressed into the mold by the rigid cores.

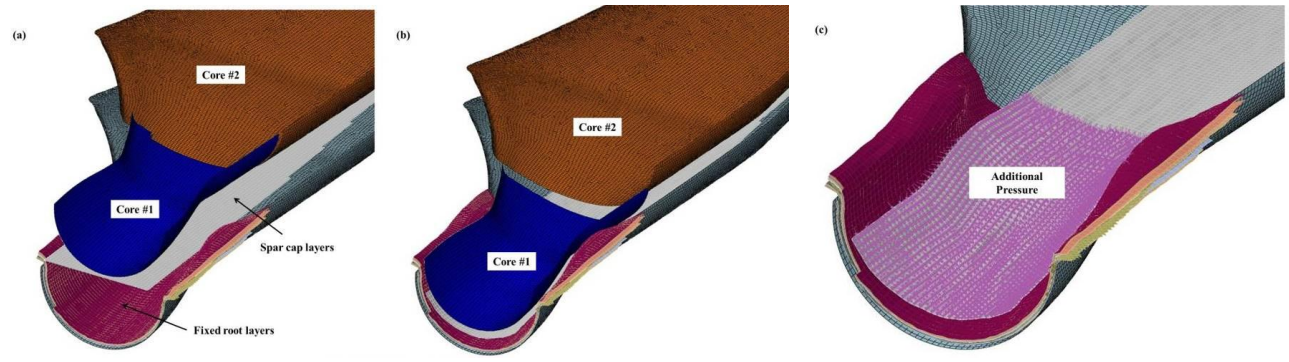

Fig. 31 (a) Forming of spar cap layers using (b) rigid cores and (c) additional pressure

In cases where the low shear stiffness of a fabric leads to the distortion of some shell elements (Fig. 32a), tensile forces can be applied to the edges of the fabric in an effort to straighten the elements (Fig. 32b). Subsequent pressures can then be reapplied to press the fabric down into the mould. This combined step of in-plane tension and downward pressure is analogous to the manipulation of the fabric done by hand by operators on the manufacturing floor and to what would need to be done if the process were to be automated.

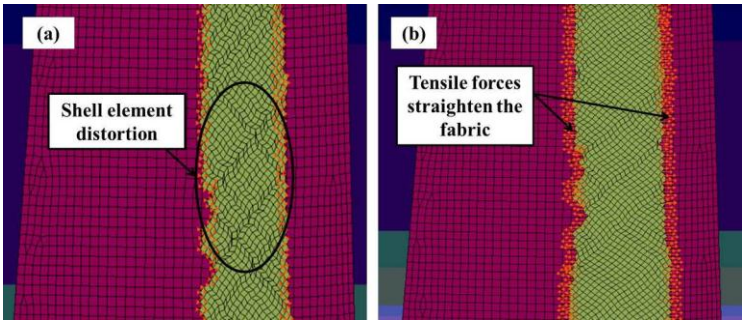

Fig. 32 (a) Forming of a double-bias spar-cap layer leading to element distortion; (b) In-plane tension is applied to straighten the fabric

For this particular 9-meter blade model, additional root layers follow the first few spar cap layers. In a similar approach, those root layers are pressed into each mould until the next group of spar-cap layers. Those spar-cap layers are then formed using the same approach presented for the first few spar-cap layers. The resulting LP and HP molds are shown in Fig. 33.

Fig. 33 Formed layers in (a) LP mould and (b) HP mould

During the forming simulations, the fabric stresses of each individual layer are examined to determine if any problematic areas exist as a result of the fiber reorientations and stretching. In particular, in-plane shear angle contours are observed to see if any yarns have trellised beyond the locking angle that might lead to out-of-plane buckling. Also, the tensile forces in the yarns are examined to indicate if any yarns are in danger of breaking. The limits of the shear angle contours are based on the locking angles determined from shear-frame tests, and the limits of the tensile force contours are based on the yarn fracture loads determined via tensile tests on individual yarns.

Fig. 34a shows the shear angle contours in a biaxial HP root layer with the maximum shear angle set to the locking angle of 36^{o}. For the most part, the yarns remain oriented in their intended directions, as indicated by the blue regions and the annotations. However, despite little in-plane shearing, the contours still indicate that the shearing is not uniform throughout the part. Structurally, a zone-based or ply-based modeling approach could not account for the nonuniform shearing without the use of knockdown factors or by breaking the zone into many smaller zones, thereby making the defining of the property variations a very tedious task.

Note in Fig. 34b that the yarns of a double-bias fabric also did not shear significantly in the root section. While the double-bias fabrics do not necessarily have a locking angle, as defined for the biaxial fabrics, the contours in Fig. 34b show that the yarns did not deviate much from their intended $\pm 45^{o}$ orientations. However, some slight in-plane waviness is observed, as shown in the zoomed-in view of the double-bias fabric in Fig. 35.

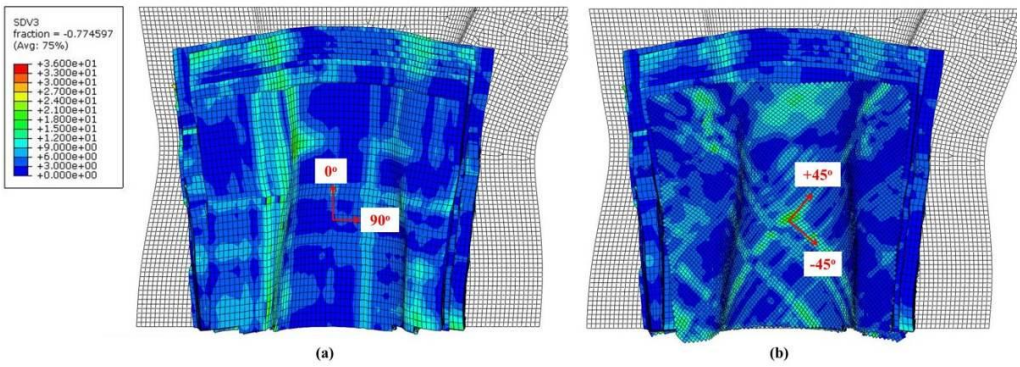

Fig. 34 In-plane shear angle contours in a (a) 0/90 biaxial NCF and (b) +/-45 double-bias NCF

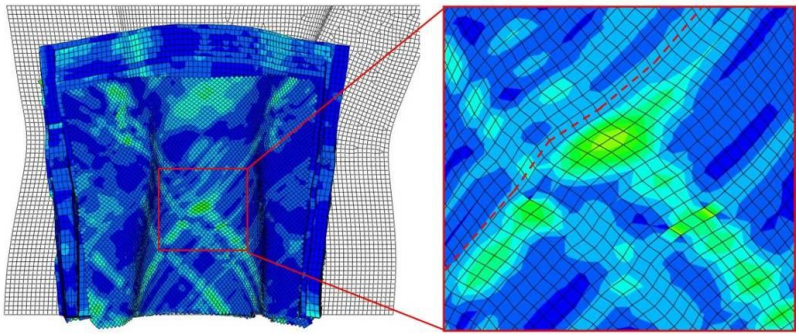

Fig. 35 Zoomed-in view of double-bias NCF showing slight in-plane waviness of yarns

Similarly, typical tensile-load contours from a biaxial root layer (Fig. 36a) and a double-bias root layer (Fig. 36b) indicate that none of the yarns have experienced tensile forces beyond their respective fracture loads. The areas annotated in Fig. 36b that show high tensile forces are in the excess fabric flange regions which are later cut from the fabric.

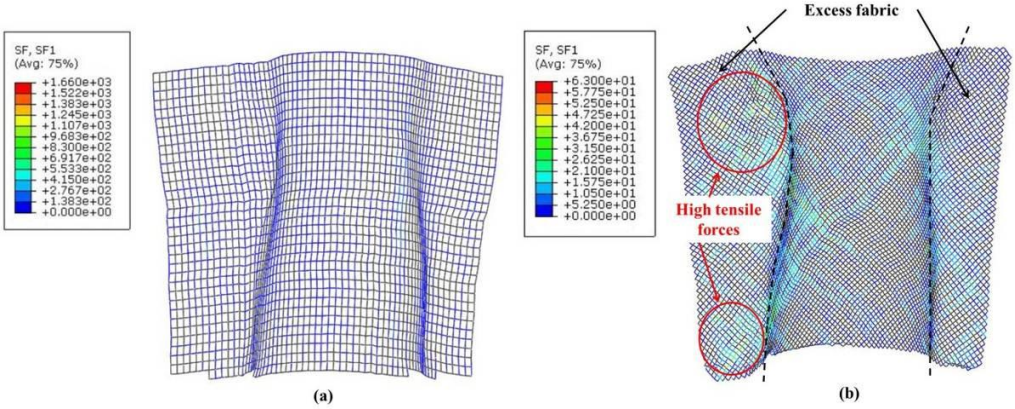

Fig. 36 Yarn tensile force contours in a (a) 0/90 biaxial NCF and (b) +/-45 double-bias NCF

Fig. 37 shows the workers cutting away the excess material after the fabric has been placed in the mold. Using the forming simulation methodology of the current research, the initial fabric blank sizes, or flat patterns, can be optimized to reduce the amount of excess fabric that must be cut prior to placement in the mold in either a manual or automated composite manufacturing process. Flat pattern optimization could help reduce material costs and the time needed to cut away excess material. After first running a forming simulation with an oversized blank, the "ideal" blank geometry is extracted, as indicated by the path of nodes in Fig. 38a. A second forming simulation, shown in Fig. 38b, is done to validate the "ideal" blank size such that no excess fabric will exist after pressing the layer into the mold.

Fig. 37 Manual cutting of excess fabric during the manufacturing process

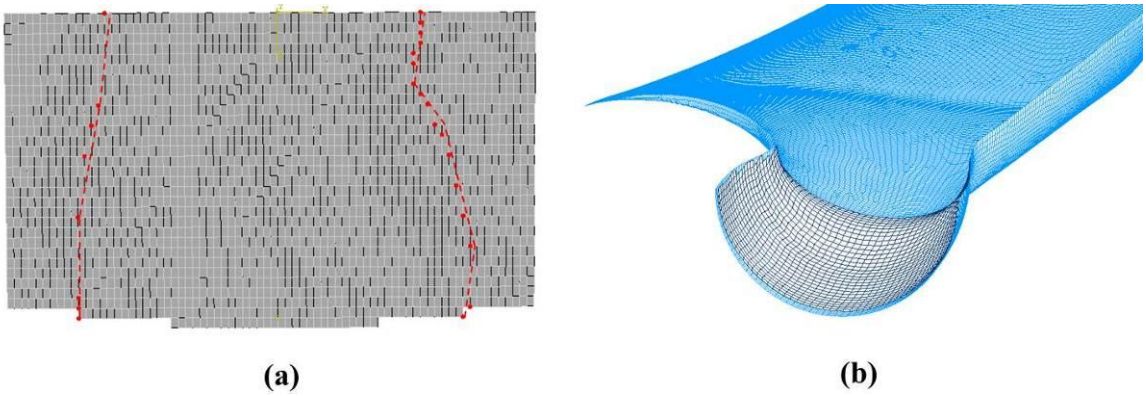

Fig. 38 Flat pattern with (a) node path from deformed fabric to determine where to cut the fabric for (b) minimal excess material after forming

Out-of-plane wave defects:

After the forming simulations and draping analyses are complete, a pressure equivalent to atmospheric (101 kPa) is applied to the top-fabric surfaces to simulate the compaction of the layers during the manufacturing process via a vacuum bag. It is during this stage that layers of fabric can potentially bunch together to form out-of-plane waves that are later filled with resin to form resin-rich pockets. Composite wind turbine blade manufacturers have been challenged as to avoid the formation of wave-defects. Manufacturers have expressed the desire for a high-fidelity simulation such as the discrete mesoscopic approach presented in this chapter that can provide insight into where defects may form and what mechanisms are responsible for their formation. To demonstrate the usefulness of such a process simulation for predicting wave defects, variations in the bending stiffness and interlaminar friction were made in the spar-cap layers of the 9-m blade LP mould. The simulations are summarized in Table 1. Note that EI represents the bending stiffness of the fabric and μ_s, μ_d and β represent the static coefficient of friction, dynamic coefficient of friction and exponential decay constant, respectively.

TABLE 1 PARAMETRIC STUDY ON WAVE DEFECT FORMATION IN 9-M BLADE SPAR CAP

Simulation No.	EI (N-mm^2)	μ_s	μ_d	β
1	300	0.93	0.57	1.0
2	3	0.93	0.57	1.0
3	300	0.30	0.25	0.7
4	3	0.30	0.25	0.7

Simulations no. 1 and 2 varied the fabric bending stiffness while maintaining the static and dynamic friction coefficients equal to those measured between fabrics with a tackifier sprayed between them. Simulation no. 1 used the actual bending stiffness of a carbon NCF (300 N-mm^2) while Simulation no. 2 used the lowest measured bending stiffness value of 3 N-mm^2 (double-bias NCF). After the application of atmospheric pressure, the spar-cap layers remained undeformed using these combinations of bending stiffness and friction. The contours in Fig. 39 represent out-of-plane displacement in units of mm. The upper contour limit of displacement (4 mm) was based on the amplitude of typical defects found in wind turbine blades [11]. Note the lack of any significant out-of-plane displacements when using the 4 mm max as a reference.

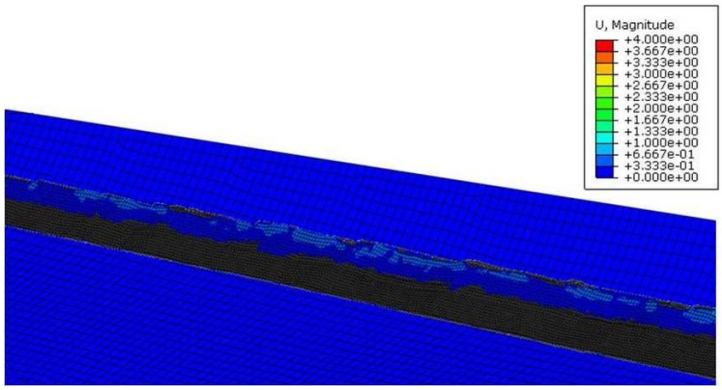

Fig. 39 CX-100 spar cap without out-of-plane deformation (Simulation no.1)

Simulations no. 3 and 4 used the same bending stiffness values as were used in the first two simulations, but used lower coefficients of friction representing the Coulomb friction measured without the tackifying spray between the carbon and E-Glass spar-cap fabrics. When defining lower friction coefficients with the stiffer fabric in Simulation no. 3, no out-of-plane deformation was observed, but the combination of low bending stiffness and low friction coefficients in Simulation no. 4 led to the formation of a wave at the 6.7 m spanwise location. The wave did not propagate across the entire width of the spar cap (as illustrated in Fig. 40).

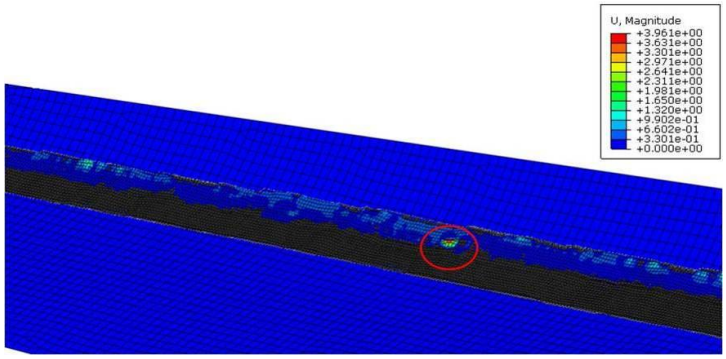

Fig. 40 Blade spar cap with out-of-plane deformation (Simulation no.4)

According to the contour plot in Fig. 40, the height of the wave defect was 3.96 mm, which falls within the range of typical defect heights found in wind turbine blades. However, because the mesh density of the fabric layers in the blade model are chosen to allow for reasonable computational times, too course a mesh can compromise the resolution and thereby compromise the ability of the model to predict accurately the size, location and severity of a defect. Fig. 41 shows the out-of-plane displacement contours in the spar cap in units of mm. These contours are the result of applying a vacuum pressure using the same parameters as that in Simulation no. 4, but with a coarser mesh. Although some out-of-plane deformation is still observed at the 6.7 m location, the contours indicate that the wave height is over two times the height (7.983 mm) cited in Fig. 40. Furthermore, out-of-plane deformations that are most likely singularities as a result of poor mesh resolution are shown in multiple areas along the spar-cap length. Fig. 41 shows the importance of having a sufficient mesh either prior to performing simulations of the manufacturing process.

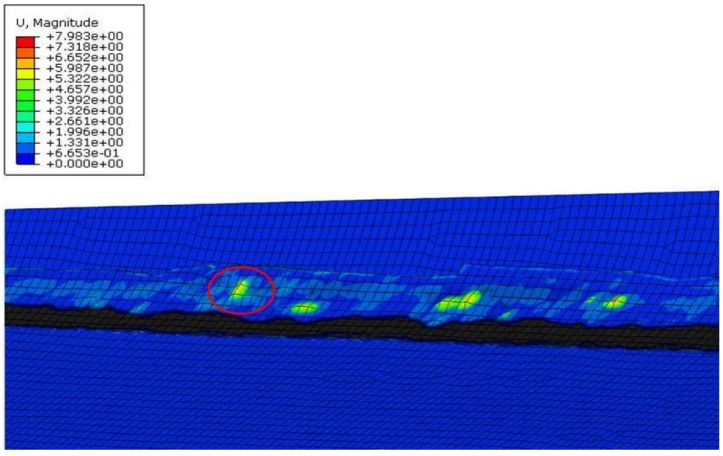

Fig. 41 Coarse spar-cap mesh showing out-of-plane deformation with insufficient mesh refinement

V. CONCLUSIONS

A discrete mesoscopic approach using 1-D beam and 2-D shell elements was used in the commercially available finite element software, Abaqus, to model the mechanical behaviour of non-crimp fabrics (NCFs) used in a 9-m long wind turbine blade. The mechanical behaviour of the NCFs was defined in terms of the in-plane shear stiffness, yarn tensile stiffness and bending stiffness, as well as the friction between contacting layers. A shear-frame test was used to characterize the in-plane shear behaviour of each fabric, and uniaxial tensile tests were performed on individual yarns to quantify the tensile stiffness of the fabric yarns. The bending stiffness was characterized by hanging fabric samples vertically and applying a horizontal load to displace the tip of the samples. The deformed profile was plotted digitally and the moment-curvature relation was determined.

The static and dynamic coefficients of friction between contacting layers of fabric were characterized using a load-control friction-test apparatus. The friction was studied between dry layers of fabric and with an adhesive, called a tackifier, sprayed onto the fabric surfaces. This tackifier simulated the conditions during the manufacturing process. The results of the various mechanical experiments were implemented into finite element models of the fabrics using the Abaqus/Explicit user-supplied material subroutine, VUMAT, to capture the mechanical behaviour of the non-crimp fabrics.

With the mechanical behaviour of each NCF defined, simulations were performed to mimic the hand-layup of the several plies during the manufacturing process. Contours of in-plane shear and tensile loads were observed to analyze the deformation of the fabric layers while conforming to the moulds of the blade. A parametric study was conducted to show that the bending stiffness of the material as well as the friction between layers were some parameters that could influence the formation of out-of-plane wave defects. The modeling approach presented in this chapter allows for the reorientation of the fabric yarns to be tracked during the manufacturing process.

ACKNOWLEDGMENTS

The authors would like to acknowledge the U.S. Department of Energy for supporting this research through Award No. DE-EE0001374. In addition, TPI Composites (Warren, RI) the National Renewable Energy Laboratory, and Sandia National Laboratories must also be recognized for their support with the fabrication and testing of composite coupon specimens and multiple 9-meter wind turbine blades.

REFERENCES

[1] TPI Composites, SCRIMP® in detail: http://www.tpicomposites.com/innovation/patents.aspx (last checked Feb. 10, 2011)

[2] G. Creech, A. K. Pickett, and L. Greve. “Finite element modelling of non-crimp fabrics for draping simulation.” Proceedings of the 6th ESAFORM conference, Salerno, Italy, 2003.

[3] W. Yu, P. Harrison, and A. Long. “Finite element forming simulation for non-crimp fabrics using a non-orthogonal constitutive equation.” Composites: Part A-Appl S, 36, pp. 1079-1093, (2005).

[4] J. Hu, and Y. Jiang. “Modeling formability of multiaxial warp knitted fabrics on a hemisphere” Composites: Part A-Appl S, 33, pp. 725-734, (2002).

[5] Snelson, J., Harris, T., and Hendricks, S. (GL Garrad Hassan): “Wind Turbine Failure Rates,” AWEA WINDPOWER 2011, Anaheim, CA, May 2011.

[6] Cairns, D., Palmer, N., Ehresman, J. (Montana State University): “Improved Wind Turbine Blade Reliability,” 2010 Wind Turbine Blade Workshop, Albuquerque, NM, Jul. 2010.

[7] Li, Xiang. “Material Characterization of Woven-Fabric Composites and Finite Element Analysis of the Thermostamping Process,” D.Eng. Dissertation, Dept. of Mechanical Engineering, University of Massachusetts Lowell, 2005.

[8] Sidhu, R. M. J. S., Averill, R. C., Riaz, M. and Pourboghrat, F.: “Finite element analysis of textile composite preform stamping,” Composite Structures 52, pp. 483-497, 2001.

[9] Jauffrès, D., Sherwood, J.A., Morris, C. D., and Chen, J.: “Discrete mesoscopic modelling for the simulation of woven-fabric reinforcement forming,” International Journal of Material Forming, 2009.

[10] Fetfatsidis, K. A., Sherwood, J. A., Chen J., Jauffres, D, Gamache, L., and Gorczyca, J. “Design of an apparatus for measuring tool/fabric and fabric/fabric friction of woven-fabric composites during the thermostamping process,” International Journal of Material Forming, vol. 6, iss. 1, pp. 1-11 (2013).

[11] Nolet, S. 2010, TPI Composites, Inc., Personal communication, February.

[12] Cao J., Akkerman R., Boisse P., Chen J., Cheng H. S., DeGraaf E. F., Gorczyca J., Harrison P., Hivet G., Launay J., Lee W., Liu L., Lomov S., Long A., Deluycker E., Morestin F., Padvoiskis J., Peng X. Q., Sherwood J., Stoilova T., Tao X. M., Verpoest I., Willems A., Wiggers J., Yu T. X., Zhu B.: Characterization of mechanical behavior of woven fabrics: experimental methods and benchmark results. Composites: Part A, 39:1037-1053, 2008.

[13] Jauffres D., Morris C. D., Sherwood J., Chen J. Simulation of the thermo stamping of woven composites: determination of the tensile and in-plane shearing behaviors. 12th ESAFORM Conference. Twente, Nederlands, 2009.

[14] Lomov S., Boisse P., Deluycker E., Morestin F., Vanclooster K., Vandepitte D., Verpoest I., Willems A.: Full-field strain measurements in textile deformability studies. Composites: Part A, 39:1232-1244, 2008.

[15] Petrov, A.S., Sherwood, J.A., Fetfatsidis, K.A.: “Characterization and Finite Element Modeling of Unidirectional Non-Crimp Fabric for Composite Manufacturing,” Proceedings of the 15th ESAFORM Conference, Erlangen, Germany, 2012.

[16] Lomov S., Willems A., Verpoest I., Zhu Y., Barburski M., Stoilova T.: Picture frame test of woven composite reinforcements with full-field strain registration. Textile Research Journal, 76:243-252, 2006.

[17] Boisse, P., Hamila, N., Vidal- Sallé, E., Dumont, F.: "Simulation of wrinkling during textile composite reinforcement forming. Influence of tensile, in-plane shear and bending stiffnesses," Composites Sci. and Tech., 10.1016/j.compscitech.2011.01.011 (2010).

[18] de Bilbao, E., Soulat, D., Hivet, G., and Gasser, A.: Experimental Study of Bending Behaviour of Reinforcements. Experimental Mechanics, Mar. 2009.

[19] Soteropoulos, D., Fetfatsidis, K., Sherwood, J., and Langworthy, J.: "Digital Method of Analyzing the Bending Stiffness of Non-Crimp Fabrics," Proceedings of the 14th ESAFORM Conference, Belfast, United Kingdom, 2011.

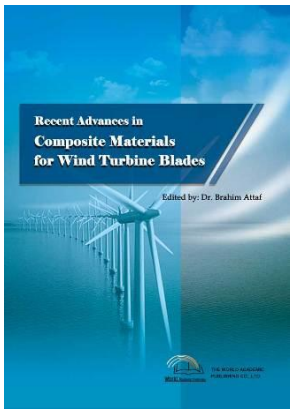

Recent Advances in Composite Materials for Wind Turbine Blades
Edited by Dr. Brahim Attaf

ISBN 978-0-9889190-0-6

Hard cover, 232 pages

Publisher: The World Academic Publishing Co. Ltd.

Published in printed edition: 20, December 2013

Published online: 20, December 2013

This book of science and technology provides an overview of recent research activities on the application of fibre-reinforced composite materials used in wind turbine blades. Great emphasis was given to the work of scientists, researchers and industrialists who are active in the field and to the latest developments achieved in new materials, manufacturing processes, architectures, aerodynamics, optimum design, testing techniques, etc.. These innovative topics will open up great perspectives for the development of large scale blades for on- and off-shore applications. In addition, the variety of the presented chapters will offer readers access to global studies of research & innovation, technology transfer and dissemination of results and will respond effectively to issues related to improving the energy efficiency strategy for 2020 and the longer term.

How to cite this book chapter

Fetfatsidis K. A. and Sherwood J. A. (2013). Process Simulations for Predicting Quality of Composite Wind Turbine Blades, *Recent Advances in Composite Materials for Wind Turbines Blades*, Dr. Brahim Attaf (Ed.), ISBN 978-0-9889190-0-6, WAP-AMSA, Available from: http://www.academicpub.org/amsa/chapterInfo.aspx

World Academic Publishing - Advances in Materials Science and Applications

Chapter 4

General Assessment of Fiber-Reinforced Composites Selection in Wind Turbine Blades

Ayşegül Akdoğan Eker[*1], Bülent Eker[2]

[1]Mechanical Engineering Department, Yıldız Technical University, İstanbul, Turkey
[2]Biosystem Department, Namık Kemal University, Tekirdağ, Turkey
[*1]akdogan@yıldız.edu.tr; [2]beker@nku.edu.tr

I. INTRODUCTION

The reduction of fossil fuel dependency is an important goal for both developed and developing countries. All these energy sources are limited and at the same time these energy sources create pollution problems. This has led to the focus on a sustainable energy supply, which implies optimized use of energy, minimized pollution. To achieve this goal, the renewable energy production in particular world energy generation must be drastically increased.

That is why wind energy is prominent and it is one of the solutions to the global energy problem. The wind energy is generated by using wind turbines. Wind speed is considered to be increased with the help of continuity principle [1]. This can be realized by installation and expansion of many off-shore and on-shore wind parks built with large and extra-large wind turbines.

Wind turbines come in many sizes and configurations and are built from wide range of materials. In simple terms, a wind turbine consists of a rotor that has wing shaped blades attached to a hub; a nacelle that houses a drivetrain consisting of a gearbox, connecting shafts, support bearings, the generator, plus other machinery; a tower; and ground-mounted electrical equipment [2].

The turbine blades play very important role in the wind turbines. Blades are required to preserve an optimum cross-section for aerodynamic efficiency to generate the maximum torque to drive the generators. The efficiency of the wind turbine depends on the material of the blade, shape of the blade and angle of the blade. Therefore, the material of the turbine blade plays a vital role in the wind turbines. The material of the blade should possess high stiffness, low density and long fatigue life features (Fig. 1) [3].

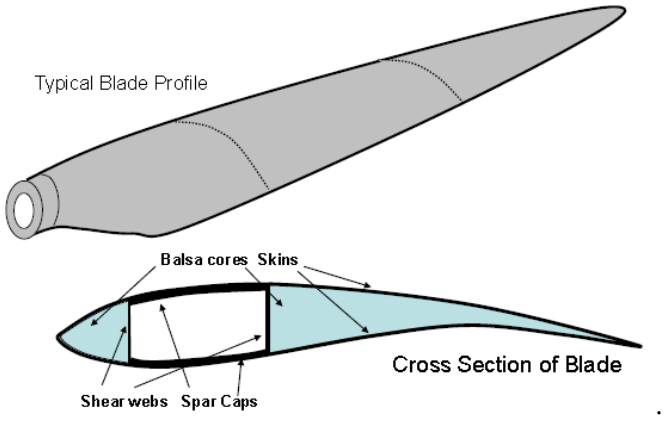

Fig. 1 Typical Blade profile and its cross-section [3]

The wing shaped blades on the rotor actually harvest the energy in the wind stream. The rotor converts the kinetic energy in the wind to rotational energy transmitted through the drivetrain to the generator. Generated electricity can be connected directly to the load or feed to the utility grid [4].

The weight and cost of the turbine are the key points for making wind energy competitive with other power sources, because research programs have significantly improved the efficiency of the rotor and maximized the energy capture of the machine. The real opportunity today is through better, low cost materials and though high volume production, while ensuring the reliability is maintained [2].

The components of turbines are changing as the technology improves and evolves. There is a trend toward lighter weight systems. Light weight, low cost materials are especially important in blades and towers for several reasons. First, the weight of the blades and rotor is multiplied throughout the machine. The tower weight is a key feature because it is typically 60% of the weight of the turbine above the foundation, due to the fact that sophisticated lightweight, high-strength materials are often too costly to justify their use.

A wide range of materials are used in wind turbines. There are substantial differences between small and large machines and there are projected changes in designs that will accommodate the introduction of new material technologies and manufacturing methods. Components and materials for wind turbines are major and expanding business opportunities for at least the next 10 years.

There are new component developments underway now that will significantly change the materials usage patterns. Generally there are trends toward lighter weight materials, as long as the life-cycle cost is low.

Most composites are made up of just two materials. One material (the matrix or binder) binds together a cluster of fibers or the fragments of a much stronger material and the second material (the reinforcement) surrounds these fibers or fragment. Nowadays, many wind turbine manufacturers are taking a big interest in composite materials which many researcher of wind technology see as the materials of the future. The main concern is to get the cost down, so that composites can be used in products and applications which at the present time do not justify the cost. At the same time they want to improve the performance of the composite, such as making them more resistant to impact [5].

Mechanical and physical properties of fibrous composite materials are beneficial compared to other constructional materials of wind turbine blades. The major advantages of this type of materials are low weight and high strength [6, 7]. Therefore, wind turbine blades built up with composite materials have much less weight than traditional constructions. Composite materials reinforced with fiberglass (Fig. 2a), carbon (Fig. 2b) and Kevlar (Fig. 2c) fibers are considered [8].

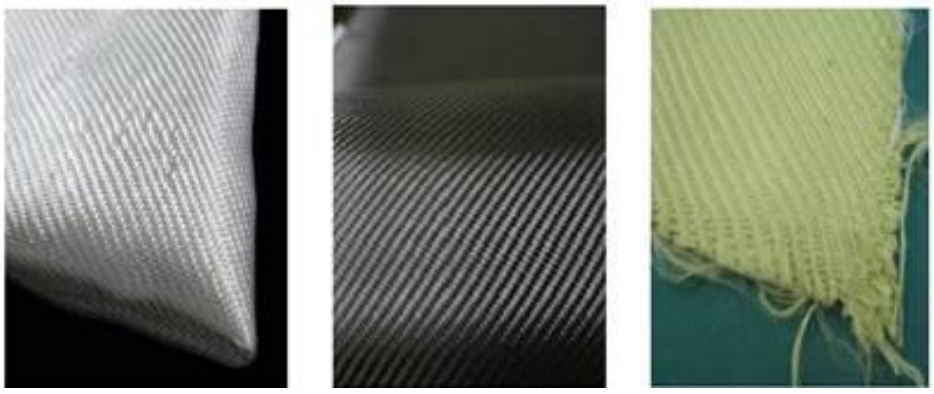

(a) (b) (c)

Fig. 2 Composite materials: (a) Fiberglass, (b) Carbon, (c) Kevlar [8]

Most rotor blades in use today are built from glass fiber-reinforced-plastic (GRP). Other materials that have been tried include steel, various composites and carbon filament-reinforced-plastic (CFRP). As the rotor size increases on larger machines, the trend will be toward high strength, fatigue resistant materials. As the turbine designs continually evolve, composites involving steel, GRP, CFRP and possibly other materials will likely come into use. For purposes of example, Gurit blades materials portfolio is shown in Fig. 3 [9].

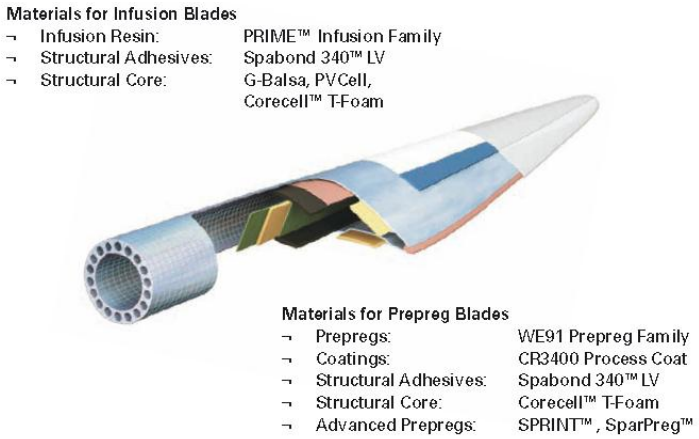

Fig. 3 Gurit blades material portfolio [9]

Blades are primarily made of GRP, which is expected to continue, while use of CFRP may help to reduce weight and cost to some extent. Low cost and reliability are the primary drivers for material selection. Increasing the use of offshore applications may partially offset this trend in favor of the use of composites. New trend of advanced composites used in wind turbines blades should be developed, improved and utilized.

In the longer term, there is scope for improving the materials used in wind turbine blades. As indicated previously, wind turbine blades need to be strong, stiff and light. Two particular weaknesses of laminated fiber-reinforced composites are their low tensile and shear strength in the out-of-plane direction and the fact that developments that increase their stiffness and tensile strength in the fiber direction do not generally provide the same beneficial effect on the compressive strength. A further consideration is recyclability. The thermosetting resins currently used cannot be recycled, and the only disposal method for fiber-reinforced composites containing these resins is to break the composite up into small pieces and incinerate them, feeding the heat into a district heating system. This is not necessarily a major disadvantage, but to allow greater flexibility in recycling and disposal is desirable. Carbon fiber reinforcements are being introduced into blades. These can be used to improve the stiffness and tensile strength in the fiber direction, as compared to materials containing glass, but the gains in compressive strength are generally significantly lower [10].

Thus, it is often most economical to use a mixture of glass and carbon, with carbon being used mainly to increase the global blade stiffness. The same is likely to apply to any new high-strength and high-stiffness reinforcement fibers that may be introduced. At present, moderately priced polymer resins and adhesives tend to be either strong, stiff, and brittle or weak, compliant, and tough. The development of products that provide a better combination of strength (including good adhesion), stiffness and toughness than those available at present would be a great step forward. However, such materials must not degrade in service and should, if possible, be recyclable [10].

In this chapter, the application of advanced composites in wind turbine blades technology, requirements for such composites, their properties and constituent, manufacturing technologies and defects are reviewed.

II. COMMONLY USED MATERIALS IN WIND BLADES

Nowadays, modern wind turbine engineers avoid building large machines with an even number of rotor blades. The most important reason is the stability of the turbine. A rotor with an odd number of rotor blades (and at least three blades) can be considered to be similar to a disc when calculating the dynamic properties of the machine. A rotor with an even number of blades will give stability problems for a machine with a stiff structure. The reason is that at the very moment when the uppermost blade bends backwards, because it gets the maximum power from the wind, the lower most blade passes into the wind shade in front of the tower.

So, most of the modern wind turbines are three-bladed designs with the rotor position maintained upwind (on the windy side of the tower) using electrical motors in their yaw mechanism. The design life time of modern wind turbines is normally thought to be 20 years. The basic design aspects for a rotor blade are the selection of material and shape. The material should be stiff, strong and light [11].

The development of wind turbines has made a significant contribution to human achievement and technological advancement throughout history. Recent advances in technology and performance have resulted in current wind turbine designs being increasingly efficient, cost effective and reliable. The material selection of the wind turbine blades plays an important role in the wind turbine designs. An ever-increasing variety of materials is available today, with each having its own characteristics, applications, advantages and limitations. When selecting materials for engineering designs, we must have a clear understanding of the functional requirements for each individual component. In selecting materials for an application, technological considerations of material properties and characteristics are important. The economic aspects of material selection, such as availability, cost of raw materials and cost of manufacturing, are equally important [11, 12].

There are number of factors which effect the material selection. They are properties of materials, performance requirements, material's reliability, safety, physical attributes, environmental conditions, availability, disposability and recyclability, and finally economic factors [12]. In these properties,

- One of the most important factors affecting selection of materials for engineering design is the properties of the materials. The important properties of the materials are mechanical, thermal, chemical properties, etc.
- The material of which a part is composed must be capable of performing a part's function (always it must be possible or not) without failure.
- A material in a given application must also be reliable.
- A material must safely perform its function.
- Physical attributes such as configuration, size, weight, and appearance sometimes also serve functional requirements can be used.
- The environment in which a product operates strongly influences service performance.

- A material must be readily available, and available in large enough quantity, for the intended application.
- The cost of the materials and the cost of processing the materials into the product or part. The development and manufacture of satisfactory products at minimum cost is to make a sound, economic choice of materials [11, 12].

The material selection process involves the following major operations:

- Analysis of the materials application problem.
- Translation of the materials application requirements to materials property values.
- Selection of candidate materials.
- Evaluation of the candidate materials.

In any material selection, the following requirements should be focused; they are:

- High material stiffness is needed to maintain optimal shape of performance.
- Low density is needed to reduce gravity forces.
- Long-fatigue life is needed to reduce material degradation [11, 13].

The optimal design of the rotor blades is today a complex and multifaceted task and requires optimization of properties, performance and economy [11]. The exact shape of the internal structure will determine the stiffness and strength of the blade under each loading mode for any given materials (Fig. 4) [3]. In general terms, however, we need a material that is as light as possible for a given stiffness in order to satisfy the blade design criteria and to minimize the weight induced fatigue loads [14, 15].

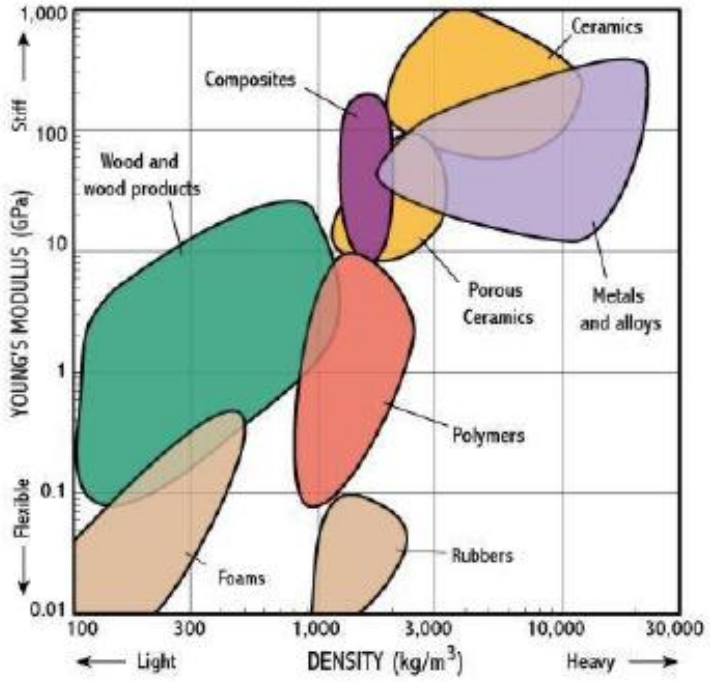

Fig. 4 Ashby material selection diagram [3], [15], [24]

Wind energy is harvested by the rotation of the wind turbine's rotor blades. Rotor blades have historically been made of wood; but because of its sensitivity to moisture and processing costs, modern materials such as glass fiber-reinforced-plastic (GFRP), carbon fiber-reinforced-plastic (CFRP), steel and aluminium are replacing the traditional wooden units.

During the 19th century blades used to be made by wood and canvas. Wood shows good fatigue characteristics and it is relatively cheap; therefore, could be used for small wind turbine applications. However, wood is not strong enough for larger wind turbines. To improve its resistance against environmental degradation, wood was coated with weather resistance finish [16].

Wood is a composite of cellulose and lignin; it finds many engineering applications and has long been a common construction material. Woods are potentially interesting because of their low density, but their rather low stiffness makes them difficult to limit the (elastic) deflections for very large rotor blades. Even wood materials with cellulosic fibers, all aligned in the major load-bearing directions, are close to the maximum performance possible for wood. Furthermore, wood is a natural material and thus environmentally attractive, but at the same time difficult to obtain in reproducible and high quality, which is a requirement for stable and economical manufacturing of rotor blades and thus economically attractive wind energy.

In the late 19th century, wood was replaced with thin sheets of galvanized steel and it became thoroughly popular. This initiated extensive research and understanding of metal behaviour for wind turbine applications. Alloy steel was once thought to be an optimum choice for blade fabrication, but was soon abandoned because of its high weight and low fatigue level. However, steel brought a range of problems like excessive weight, therefore, aluminium was introduced but it also faced problems like low fatigue resistance and high cost.

Then the most popular and widely used material for wind turbine blades was introduced called composites, more specifically polymer matrix composite (PMC) also called as fiber reinforced plastic (FRP). These composites were composed of 2 parts; matrix and fiber. These two combined parts form a useful material for blade application. The most commonly used fiber and its matrix is E-glass fiber and polyester resin for structural applications. A fiber is the primary load carrying element of the composite material. Its orientation in alternating directions gives the material strength and stiffness. The composite material is only strong and stiff in the direction of the fibers. Unidirectional composites have predominant mechanical properties in one direction and are said to be anisotropic, having mechanical and/or physical properties that vary with direction relative to natural reference axes inherent in the material. The amount of fiber (FVF- Fiber volume fraction) in the resin determines the strength of the composites. The volume fraction of fiber is highly dependent on the manufacturing method. However, fiber can only be added up to a certain extent, after which composite's mechanical properties begin to deteriorate. The reason behind is related with the lack of resin to transfer the exerted load to reinforced fibers. Normal hand layup technique achieves FVF of around 30-35%, while sophisticated techniques like SCRIMP and vacuum infusion using prepregs can achieve up to 70%. The manufacturing technique also determines the extent of air inclusion and voids which reduce strength directly [17, 3, 12, 18].

Composite materials are becoming more important in the construction of wind turbine blade structures. New generation of large wind turbine blades are designed with all composite fuselage and wing structures, and the repair of these advanced composite materials requires an in-depth knowledge of composite structures, materials and tooling. These materials have a significant part to play in maintaining and developing the wind turbine industry.

Composites are classified according to their matrix phase. There are polymer matrix composites (PMCs), ceramic matrix composites (CMCs) and metal matrix composites (MMCs). Materials within these categories are often called "advanced" if they combine the properties of high strength and high stiffness, low weight, corrosion resistance, and in some cases special electrical properties. This combination of properties makes advanced composites very attractive for aircraft, aerospace structural parts and wind turbine blades [17].

The primary advantages of composite materials are their high strength, relatively low weight and corrosion resistance. It was recognized that structures are hybrids of different engineering materials and that to achieve true benefits from advanced composites, developments in this area must include the integrated structural system as well. It is important to create critical mass for this technology if it is to be successful in a commercial exploitation.

A matrix supports the fibers and bonds them together in the composite material. The matrix transfers any applied loads to the fibers, keeps the fibers in their position and chosen orientation, gives the composite environmental resistance and determines the maximum service temperature of a composite.

III. MECHANICAL PROPERTIES OF ADVANCED COMPOSITES

If composites combine the properties of high strength values and high stiffness values, with low weight and corrosion resistance, these materials are often called as advanced composite materials (ACMs). Advanced composite materials are also known as advanced polymer matrix composites [19]. These are generally characterized or determined by unusually high strength fibers with unusually high stiffness, or modulus of elasticity characteristics, compared to other materials, while bound together by weaker matrices (Fig. 5). These are termed advanced composite materials (ACM) in comparison to the composite materials commonly in use such as reinforced concrete, or even concrete itself. The high strength fibers are also low density while occupying a large fraction of the volume [20].

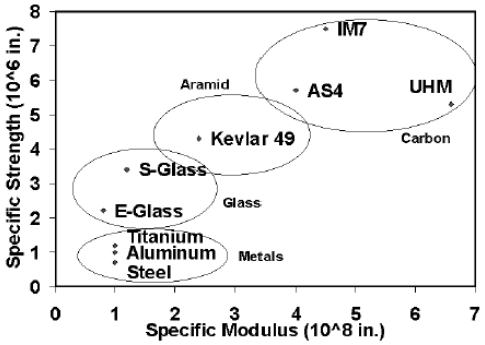

Fig. 5 Advanced composites general characteristics [20]

Structural properties, such as stiffness, dimensional stability and strength of a composite laminate, depend on the stacking sequence of the plies. The stacking sequence describes the distribution of ply orientations through the laminate thickness. As the number of plies with chosen orientations increases, more stacking sequences are possible. For example, a symmetric eight-ply laminate with four different ply orientations has 24 different stacking sequences. The strength and stiffness of a composite build-up depends on the orientation sequence of the plies. The practical range of strength and stiffness of carbon fiber extends from values as low as those provided by fiberglass to as high as those provided by titanium [18]. Advanced composites can be classified according to their fiber orientation and the used types of fiber and resin [19]. These classifications are detailed in the following sub sections.

A. Fiber Orientation

This range of values is determined by the orientation of the plies to the applied load. Proper selection of ply orientation in advanced composite materials is necessary to provide a structurally efficient design. The part might require 0 °plies to react to axial loads, ±45 °plies to react to shear loads and 90 °plies to react to side loads. Because the strength design requirements are a function of the applied load direction, ply orientation and ply sequence have to be correct. It is critical during a repair to replace each damaged ply with a ply of the same material and ply orientation. The fibers in a unidirectional material run in one direction and the strength and stiffness is only in the direction of the fiber. Pre-impregnated (prepreg) tape is an example of a unidirectional ply orientation. The fibers in a bidirectional material run in two directions, typically 90 °apart. A plain weave fabric is an example of a bidirectional ply orientation. These ply orientations have strength in both directions but not necessarily the same strength (Fig. 6) [18].

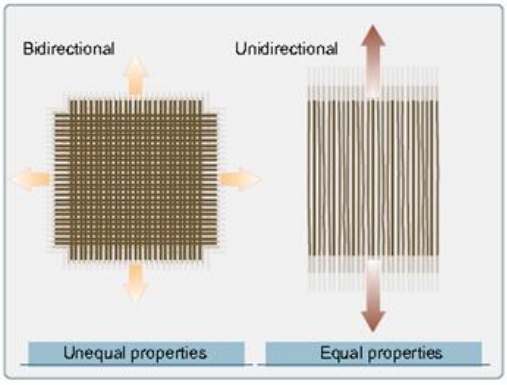

Fig. 6 Bidirectional and undirectional material properties [18]

The plies of a quasi-isotropic layup are stacked in a 0 °, –45 °, 45 °and 90 °sequence or in a 0 °, –60 °and 60 °sequence. (Fig. 7) These types of ply orientation simulate the properties of an isotropic material. Many wind turbine blades composite structures are made of quasi-isotropic materials.

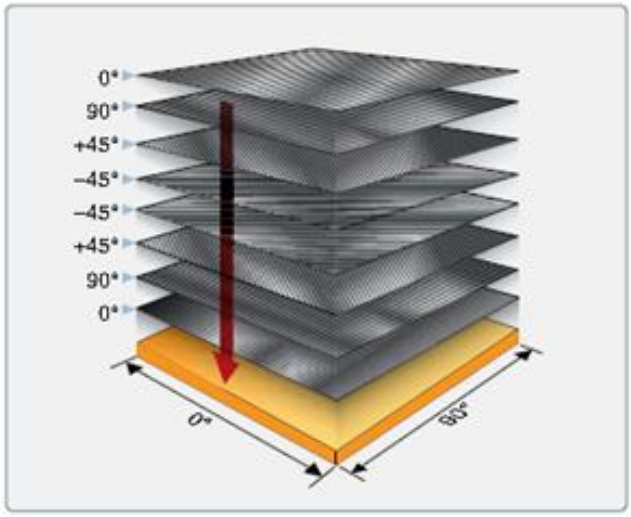

Fig. 7 Quasi-isotropic material lay-up [18]

Warp indicates the longitudinal fibers of a fabric. The warp is the high strength direction due to the straightness of the fibers. A warp clock is used to describe direction of fibers on a diagram, spec sheet, or manufacturer's sheets. If the warp clock is not available on the fabric, the orientation is defaulted to zero as the fabric comes off the roll. Therefore, 90 °to zero is the

width of the fabric across (Fig. 8).

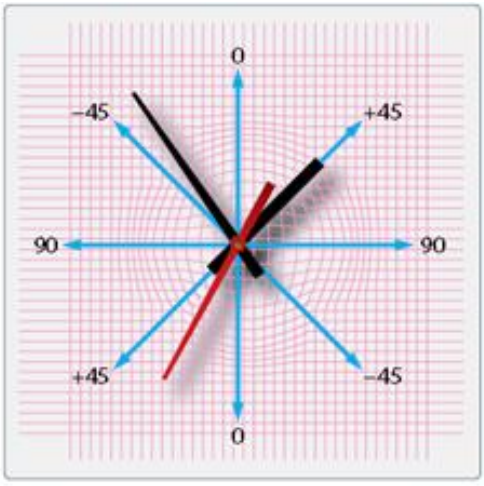

Fig. 8 A warp clock [18]

All product forms generally begin with spooled unidirectional raw fibers packaged as continuous strands. An individual fiber is called a filament. The word strand is also used to identify an individual glass fiber. Bundles of filaments are identified as tows, yarns, or rovings. Fiberglass yarns are twisted, while Kevlar® yarns are not. Tows and rovings do not have any twist. Most fibers are available as dry fiber that needs to be impregnated (impreg) with a resin before use or prepreg materials where the resin is already applied to the fiber [18].

A roving is a single grouping of filament or fiber ends, such as 20-end or 60-end glass rovings. All filaments are in the same direction and they are not twisted. Carbon rovings are usually identified as 3K, 6K, or 12K rovings, where K refers to 1,000 filaments. Most applications for roving products utilize mandrels for filament winding and then resin cure to final configuration. Unidirectional prepreg tapes have been the standard within the wind turbine blades industry for many years, and the fiber is typically impregnated with thermosetting resins. The most common method of manufacture is to draw collimated raw (dry) strands into the impregnation machine where hot melted resins are combined with the strands using heat and pressure. Tape products have high strength in the fiber direction and virtually no strength across the fibers. The fibers are held in place by the resin. Tapes have a higher strength than woven fabrics (Fig. 9) [18].

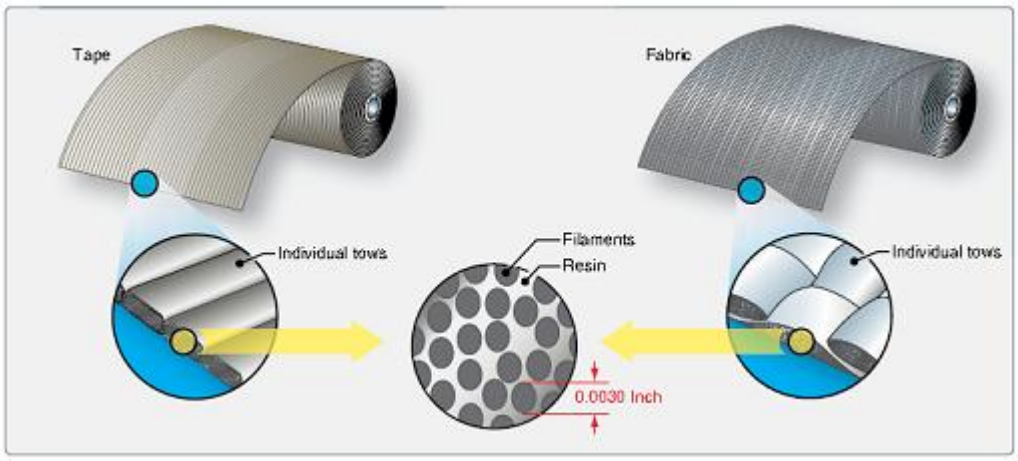

Fig. 9 Tape and fabric products [18]

Most fabric constructions offer more flexibility for layup of complex shapes than straight unidirectional tapes offer. Fabrics offer the option for resin impregnation either by solution or the hot melt process. Generally, fabrics used for structural applications use like fibers or strands of the same weight or yield in both the warp (longitudinal) and fill (transverse) directions. For aerospace structures, tightly woven fabrics are usually the choice to save weight, minimizing resin void size and maintaining fiber orientation during the fabrication process. Woven structural fabrics are usually constructed with reinforcement tows, strands, or yarns interlocking upon themselves with over/under placement during the weaving process. The more common fabric styles are plain or satin weaves. The plain weave construction results from each fiber alternating over and then under each intersecting strand (tow, bundle, or yarn). With the common satin weaves, such as 5 harness or 8 harness, the fiber bundles traverse both in warp and fill directions changing over/under position less frequently. These satin weaves have less crimp and are easier to distort than a plain weave. With plain weave fabrics and most 5 or 8 harness woven fabrics,

the fiber strand count is equal in both warp and fill directions. Example: 3K plain weave often has an additional designation, such as 12 x 12, meaning there are twelve tows per inch in each direction. This count designation can be varied to increase or decrease fabric weight or to accommodate different fibers of varying weight (Fig. 10) [18].

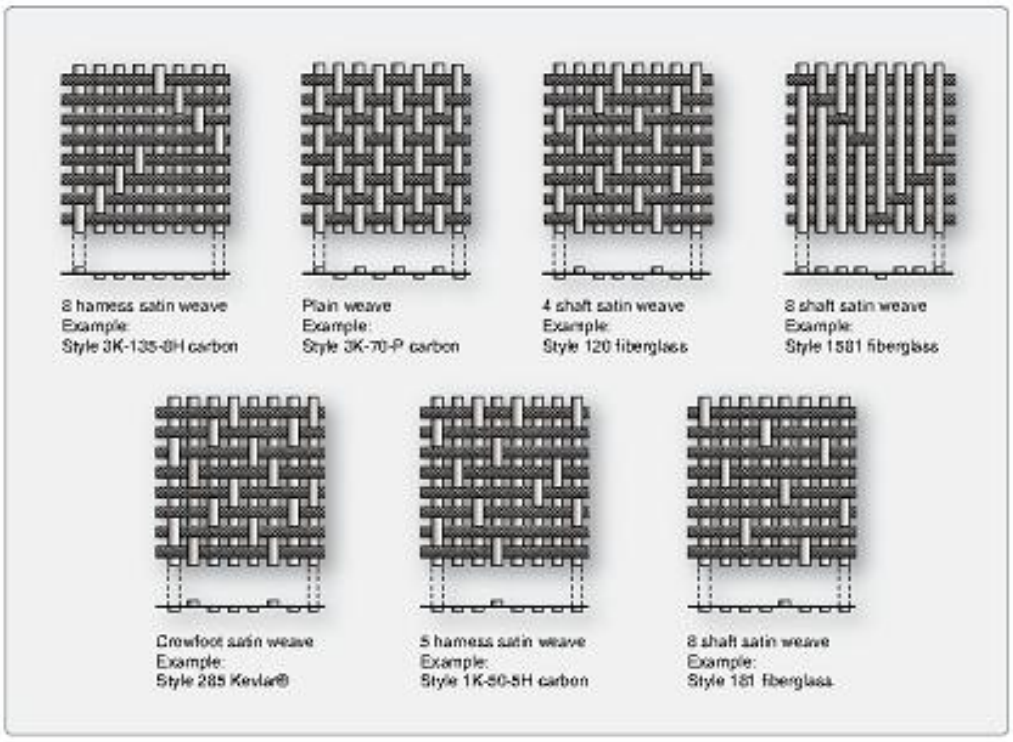

Fig. 10 Typical fabric weave styles [18]

Knitted or stitched fabrics can offer many of the mechanical advantages of unidirectional tapes. Fiber placement can be straight or unidirectional without the over/under turns of woven fabrics. The fibers are held in place by stitching with fine yarns or threads after preselected orientations of one or more layers of dry plies. These types of fabrics offer a wide range of multi-ply orientations. Although there may be some added weight penalties or loss of some ultimate reinforcement fiber properties, some gain of interlaminar shear and toughness properties may be realized. Some common stitching yarns are polyester, aramid or thermoplastics. (Fig. 11) [18].

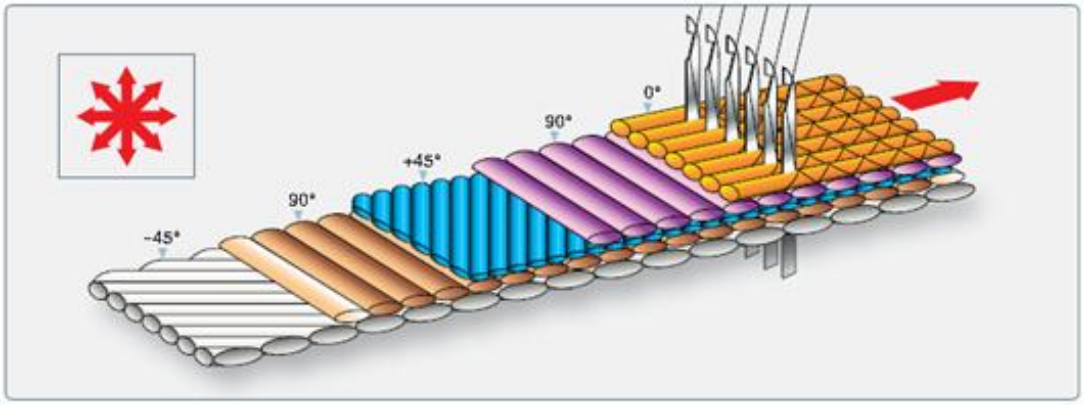

Fig. 11 Nonwoven material (stitched) [18]

B. Types of Fiber

Glass, carbon, boron or aramid fibers are the most common choices for advanced composite parts. The best fiber for a particular application depends on the required strength, stiffness, corrosion resistance and budget. Glass fiber is the most common reinforcing material used in polymer matrix composites. These have high tensile strength but low modulus compared with other fibers. Typical variants are:

- E-glass
- ECR-glass

- S-glass, R-glass and Te-glass
- Silica/quartz
- D-glass

The different types of glass are supplied in several different configurations, including:

- Fiberglass rovings
- Sheet moulding compound
- Woven rovings
- Chopped strand mat

Carbon fiber is the reinforcement material of choice for “advanced” composites, Carbon fiber exhibits excellent fatigue resistance which does not suffer from stress rupture compared with glass or aramid fibers. Carbon fibers are supplied in tows and may vary from 1000 fibers per tow to hundreds of thousands per tow. Untreated carbon fibers do not wet easily, so adhesion to the matrix must be achieved by mechanical interference coupled with surface treatment and chemical bonding between the fiber and the matrix. Typically they are defined as standard, intermediate and high modulus fibers. Carbon fiber properties are given in Table 1 [17].

Table 1 Carbon fiber properties [17]

	Standard modulus	Intermediate modulus	High modulus
Tensile Strength	3450-4830 MPa	3450-6200 MPa	3450-5520 MPa
Young's Modulus	220-241 GPa	290-297 GPa	345-448 GPa
Elongation at break	1.5-2.2%	1.3-2.0%	0.7-1.0%

Aramid fibers have the highest strength to weight ratio compared to other commercially available fibers. Kevlar manufactured by DuPont is a familiar brand name. Aramid fiber exhibits similar tensile strength to glass fiber, but can have modulus at least two times as great. Aramid is very tough allowing significant energy absorption but, compared to carbon, it is lower in compressive strength and has poorer adhesion to the matrix. It is also susceptible to moisture absorption. Aramid fiber properties depend on the structure used and can be tailored for high toughness or high modulus. Aramid (Kevlar) fiber properties are given in Table 2 [17].

Table 2 Aramid (Kevlar) fiber properties [17]

	Kevlar 29 High toughness	**Kevlar 49 High modulus**	**Kevlar 149 Ultrahigh modulus**
Tensile Strength	3.6 GPa	3.6-4.1 GPa	3.4 GPa
Young's Modulus	83 GPa	131 GPa	179 GPa
Elongation at break	4%	2.80%	2.0%

Boron fiber actually predates carbon fiber as a high-modulus reinforcement material. The cost of boron, however, has seen its demise, with its replacement with carbon fiber. They do not differ greatly from glass fiber in tensile strength, but can have modulus five times that of glass. Since the objective of reinforcement is to stiffen, this is a significant advantage. Their use is confined to niche markets, where the modulus advantage over carbon fiber is critical [17].

Fiber reinforcement materials are added to the resin system to provide strength to the finished part. The selection of reinforcement material is based on the properties desired in the finished product. These materials do not react with the resin but are an integral part of the advanced composite system. Potential worker exposure is typically higher in facilities that manufacture the fibers or use them to produce prepreg material. Most of the fibers in use are considered to be in the nonrespirable range. However, they do have the potential to cause eye, skin, and upper respiratory tract irritation as a result of the mechanical properties of the fibers [17].The three basic types of fiber reinforcement materials in use in the advanced composite industry are:

- carbon/graphite
- aramid
- glass fibers

Fibers used in advanced composite manufacture come in various forms, including:

- yarns
- rovings
- chopped strands
- woven fabric
- mats

Each of these has its own special application. When prepreg materials are used in parts manufacture, woven fabric or mats are required. In processes such as filament wet winding or pultrusion, yarns and rovings are used [12]. The most commonly used reinforcement materials are carbon/graphite fibers (the terms graphite and carbon are often used interchangeably). This is due to the fact that many of the desired performance characteristics require the use of carbon/graphite fibers. Currently, these fibers are produced from three types of materials known as precursor fibers:

- polyacrylonitrile (PAN)
- rayon
- petroleum pitch

The carbon/graphite fibers are produced by the controlled burning off of the oxygen, nitrogen and other noncarbon parts of the precursor fiber, leaving only carbon in the fiber. Following this burning off (or oxidizing) step, the fibers are run through a furnace to produce either carbon or graphite fibers. Carbon fibers are produced at furnace temperatures of 1 000-2 000 ℃, while graphite fibers require temperatures of 2 000-3 000 ℃. At these temperatures the carbon atoms in the fibers are rearranged to impart the required characteristics to the finished fiber. The PAN-based fiber is the more commonly used precursor in the advanced composite industry today [17]. Aramid fibers are another human-made product. These fibers are produced by manufacturing the basic polymer, then spinning it into either a paper-like configuration or into fiber. Aramid fibers have several useful characteristics:

- high strength and modulus;
- temperature stability;
- flex performance;
- dimensional stability;
- chemical resistance; and
- textile process ability.

Textile (continuous filament) glass fibers are the type used in composite reinforcement. These fibers differ from the wool type in that they are die-drawn rather than spun. A number of solvents are used in the advanced composites industry. These may be introduced into the workplace in three basic ways:

- as part of the resin or curing agent;
- during the manufacturing process; or
- as part of the clean-up process.

Most of the solvents used may be introduced in any or all of the three ways above. For this reason it would be difficult, if not impossible, to separate the solvents into the categories of use. The solvents discussed in this section are grouped by chemical class:

- ketones
- alcohols
- chlorinated hydrocarbons
- others

Several solvents may be used in any one composite process. One or more may be introduced as part of the resin or curing agent, while another may be a part of the manufacturing process. Still another may be used for clean-up. Thus, the hazard

information for all products used in the process must be considered when evaluating potential exposures. The supplier's Material Safety Data Sheet (MSDS) should be consulted for more specific hazard information [17].

C. Resins

The resin systems used to manufacture advanced composites are of two basic types: thermosetting and thermoplastic. Thermosetting resins predominate today, while thermoplastics have only a minor role in manufacturing advanced composites. Thermoset resins require addition of a curing agent or hardener and impregnation onto a reinforcing material, followed by a curing step to produce a cured or finished part. Once cured, the part cannot be changed or reformed, except for finishing [21]. Some of the more common thermosets include:

- epoxies
- polyurethanes
- phenolic and amino resins
- bismaleimides (BMI, polyimides)
- polyamides

Of these, epoxies are the most commonly used in today's PMC industry. Epoxy resins have been in use in U.S. industry for over 40 years. The basic epoxy compounds most commonly used in industry are the reaction product of epichlorohydrin and bisphenol-A. Epoxy compounds are also referred to as glycidyl compounds. There are several types of epoxy compounds including glycidyl ethers (or diglycidyl ethers), glycidyl esters and glycidyl amines. Several of these compounds are reactive diluents and are sometimes added to the basic resin to modify performance characteristics. The epoxy molecule can also be expanded or cross-linked with other molecules to form a wide variety of resin products, each with distinct performance characteristics. These resins range from low-viscosity liquids to high-molecular weight solids. Typically they are high-viscosity liquids [17].

Since epoxies are relatively high molecular-weight compounds, the potential for respiratory exposure is fairly low. The potential for respiratory exposure is increased when the resin mixture is applied by spraying or when curing temperatures are high enough to volatilize the resin mixture. The potential for dermal exposure is typically much greater than respiratory exposure when working with epoxies. Several advanced composite processes involve some worker contact with the resin mixture. The second of the essential ingredients of an advanced composite system is the curing agent or hardener. These compounds are very important because they control the reaction rate and determine the performance characteristics of the finished part. Since these compounds act as catalysts for the reaction, they must contain active sites on their molecules. Some of the most commonly used curing agents in the advanced composite industry are the aromatic amines. Two of the most common are 4,4’-methylene-dianiline (MDA) and 4,4’-sulfonyldianiline (DDS). Like the epoxies, these compounds have a very low vapor pressure and usually do not present an airborne hazard unless in a mixture that is sprayed or cured at high temperatures. However, potential for dermal exposure is frequently high. The aromatic amines may permeate many of the commonly used protective gloves and thus may be particularly difficult to protect against [17, 18].

Several other types of curing agents are also used in the advanced composite industry. These include aliphatic and cycloaliphatic amines, polyaminoamides, amides, and anhydrides. Again, the choice of curing agent depends on the cure and performance characteristics desired for the finished part. Polyurethanes are another group of resins used in advanced composite processes. These compounds are formed by reacting the polyol component with an isocyanate compound, typically toluene diisocyanate (TDI); methylene diisocyanate (MDI) and hexamethylene diisocyanate (HDI) are also widely used. While the polyols are relatively innocuous, the isocyanates can represent a significant respiratory hazard as well as a dermal hazard. Phenolic and amino resins are another group of PMC resins. With respect to the phenol-formaldehyde resins, the well-known hazards of both phenol and formaldehyde must be protected against. In addition to traces of free formaldehyde, they may also contain free phenol, and contact with these resins in the uncured state is to be avoided. The urea- and melamine-formaldehyde resins present similar hazards. Free formaldehyde, which is present in trace amounts and may be liberated when their resins are processed, can irritate the mucous membranes. The bismaleimides and polyamides are relative newcomers to the advanced composite industry and have not been studied to the extent of the other resins [17]. Thermoplastics currently represent a relatively small part of the PMC industry. They are typically supplied as nonreactive solids (no chemical reaction occurs during processing) and require only heat and pressure to form the finished part. Unlike the thermosets, the thermoplastics can usually be reheated and reformed into another shape, if desired.

IV. MANUFACTURING TECHNOLOGY OF ADVANCED COMPOSITES

The industry can be generally divided into two basic segments, industrial composites and advanced composites. Several of the composites manufacturing processes are common to both segments. The industrial composites industry has been in place for over many years in the world. This large industry utilizes various resin systems including polyester, epoxy and other specialty resins. These materials, along with a catalyst or curing agent and some type of fiber reinforcement (typically glass fibers) are used in the production of a wide spectrum of industrial components and consumer goods and a variety of other parts and components. This sector of the composites industry is characterized by the use of expensive, high-performance resin

systems and high-strength, high-stiffness fiber reinforcement. The aerospace industry, including military and commercial aircraft of all types and also wind turbine blades industry, is the major customer for advanced composites [17].

The feature common to all composite processes is the combining of a resin, a curing agent, some type of reinforcing fiber, and in some cases a solvent. Typically, heat and pressure are used to shape and "cure" the mixture into a finished part. In composites, the resin acts to hold the fibers together and protect them, and to transfer the load to the fibers in the fabricated composite part. The curing agent, also known as hardener, acts as a catalyst and helps in curing the resin to a hard plastic. The technology used in manufacturing wind turbine blades has evolved over the past 20-plus years (Fig. 12).

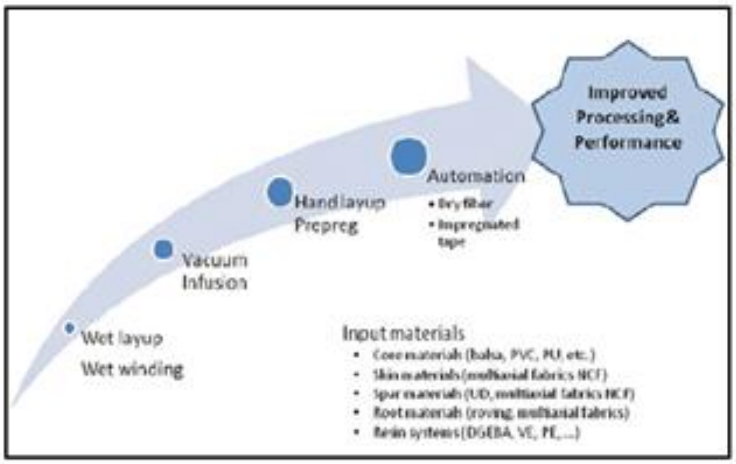

Fig. 12 Evolution of wind turbine production [22]

Blade making has migrated toward processes that minimize cycle time and reduce both cost and the probability of defects. Early blade building techniques grew out of the boat building industry, using processes that were high in labor and prone to inconsistencies and defects. Vacuum infusion took blade manufacturing technology to a higher level, with improvements in consistency and performance of a blade. Prepreg - or “pre-impregnated” - technology further enhanced blade performance by combining resins and reinforcements in a more rigorously controlled manner before placement in the blade mold. Today the trend is toward Automated Tape Layup (ATL) or Automated Fiber Placement (AFP) to reduce labor and improve quality, whether one uses dry fiber or prepreg tape (Fig. 12) [22].

The basic advanced composite manufacturing which is using wind turbine blades process types are described below.

A. Resin formulation consists of mixing epoxy or other resins with other ingredients to achieve desired performance parameters. These ingredients may be curing agents, accelerators, reactive diluents, pigments, etc.
B. Prepregging involves the application of formulated resin products, in solution or molten form, to a reinforcement such as carbon, fiberglass or aramid fiber or cloth. The reinforcement is saturated by dipping through the liquid resin (solution form, see Fig. 13) or by being impregnated through heat and pressure (hot melt form, see Fig. 14).

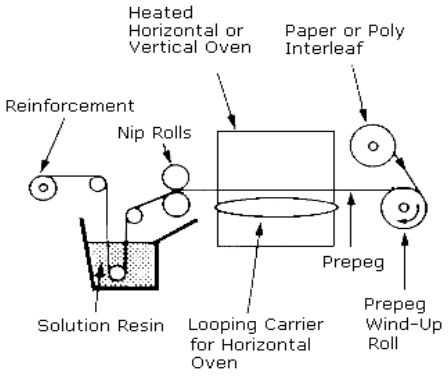

Fig. 13 Solution prepegging [17]

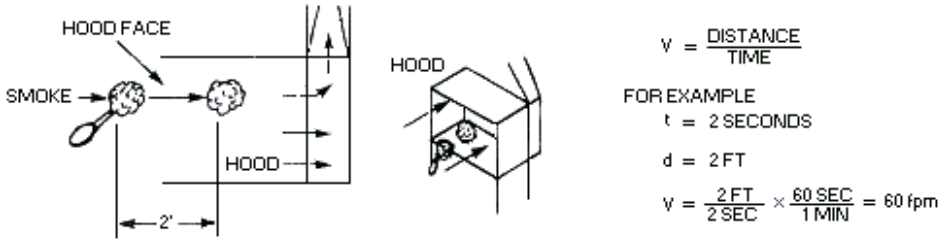

Fig. 14 Hot melt prepegging [17]

In the filament wet winding process, continuous fiber reinforcement materials are drawn through a container of resin mixture (Fig. 15) and formed onto a rotating mandrel to achieve the desired shape. After winding, the part is cured in an oven [23].

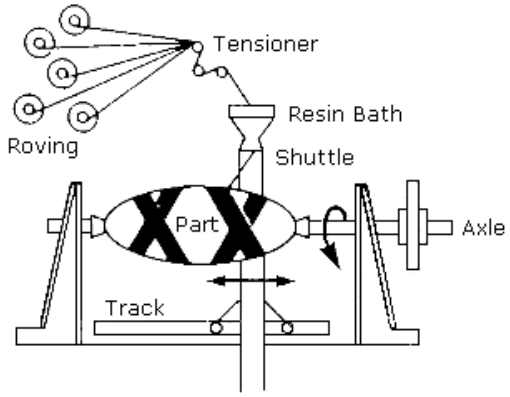

Fig. 15 Wet filament winding [17]

A prepreg product is laid down and formed to the desired shape (Fig. 16). Several layers may be required. After forming, the lay-up assembly is moved to an autoclave for cure under heat, vacuum and pressure.

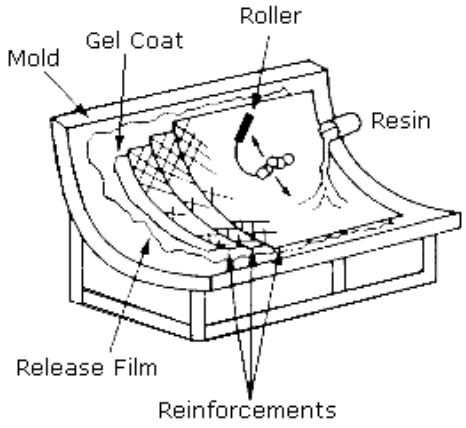

Fig. 16 Hand lay-up of prepreg [17]

In automated tape lay-up process, the prepreg tape material is fed through an automated tape application machine (robot). The tape is applied across the surface of a mold in multiple layers by the pre-programmed robot (Fig. 17).

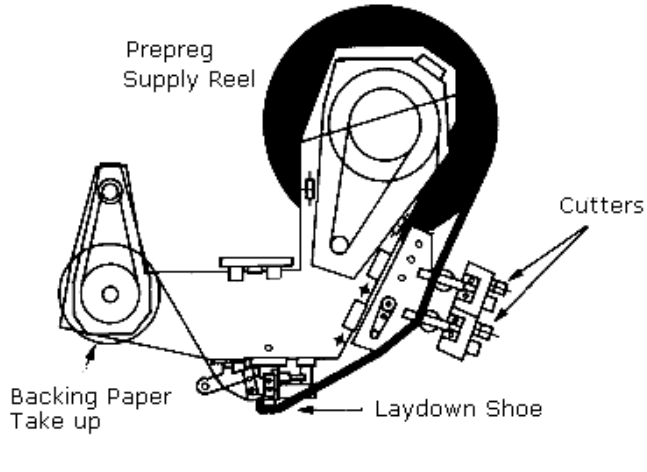

Fig. 17 Automated lay-up [17]

Most parts made by hand lay-up or automated tape lay-up must be cured by a combination of heat, pressure, vacuum and inert atmosphere. To achieve proper cure, the part is placed into a plastic bag inside an autoclave (Fig. 18). A vacuum is applied to the bag to remove air and volatile products. Heat and pressure are applied for curing. Usually an inert atmosphere is provided inside the autoclave through the introduction of nitrogen or carbon dioxide. Exotherms may occur if the curing step is not done properly.

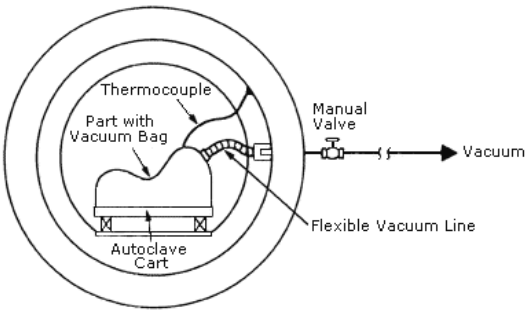

Fig. 18 Vacuum bagging and autoclave [17]

Many of the parts made in advanced composite processes require some machining and/or finishing work. This may involve drilling, sanding, grinding or other manual touch-up work. These processes vary widely, depending on the size of the finished part and the amount of finishing work required. Repair of damaged advanced parts is frequently required. The process may consist of several steps including cutting out of the damaged material, depainting of the surface to be repaired, patching and sanding of the damaged area, and repainting of the repaired area [17, 23].

V. ECONOMIC ASPECT OF ADVANCED COMPOSITE MATERIALS

According to market experts, the global industry for composites materials is estimated to grow in the mid-single digits in the next five years. The two sectors that will drive this growth are anticipated to be aerospace and wind energy, expected to grow by 15.6% and 13.3% each year respectively (Fig. 19) [24].

A June 2012 report from AMI Consulting values the global composite wind turbine blade market at an estimated €4 billion in 2011, of which approximately €1.5 billion was raw materials. AMI calculates that the global demand for materials for the production of wind turbine blades grew by over 20% per annum in the last five years [25, 26].

Materials used to manufacture rotor blades for wind turbines are subject to special requirements. The number of load cycles and the load variability are far beyond what is encountered by other structures in aviation, shipbuilding and bridge building. The development of new materials is also driven by the economics of wind turbine design. To maximise return on investment, the average blade size is growing longer and heavier requiring greater quantities of raw materials. As blade length approaches 90 m, increased sophistication in blade design, materials and manufacture are required. A larger surface area of the blade effectively increases the tip-speed ratio of a turbine at a given wind speed, increasing the amount of energy that can be produced. An important goal of larger blade systems is to control blade weight. Since blade mass scales as the cube of the turbine radius, loading due to gravity constrains the systems with larger blades [25].

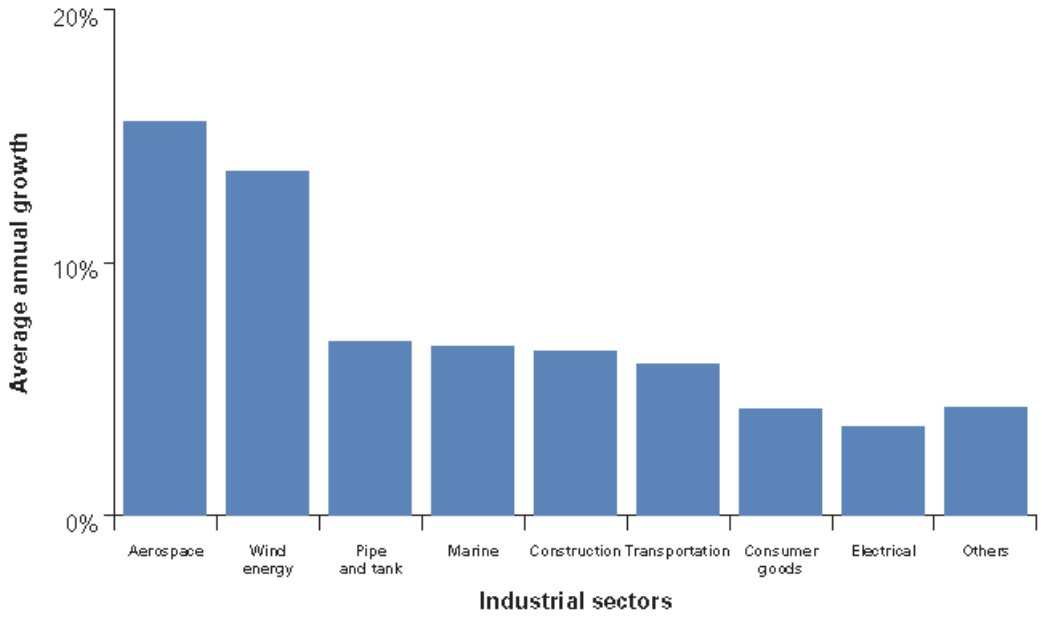

Fig. 19 Average annual global growth composite material forecasts by market segment, 2009-2014 [24]

Prepreg is a glass or carbon fiber reinforcement that is impregnated with resins such as epoxies. They are supplied in roll form and cured with the application of heat and pressure to produce high quality laminates with superior stiffness and strength – at low weights. Prepreg is an ideal cost-effective technology for the manufacture of large composite parts as the process is readily automated and the materials are easy to handle. Carbon fiber prepregs are a cost effective option for very large diameter blades, as less material is required to achieve the strength and stiffness of glass structures. Hybrid reinforcements of glass and carbon are also a potential option [19].

The global composite industry is becoming increasingly competitive. Market barriers exist that may hinder further commercial investment in composites and technological development. Economical focus is on advanced composites where it is believed that a competitive advantage can be built, there will be an increase in wind turbine blades market share of existing sectors and the use of composites in new industries is ensured [27].

Polymer matrix composites (commonly known as PMCs or fibre reinforced polymer/plastic – FRPs) have a wide range of properties depending on the fiber or matrix used. Most provide improved strength-to-weight ratios, stiffness-to-weight ratios, fatigue properties and corrosion resistance, in comparison to other commonly used engineering materials such as aluminium alloys. Their manufacture often depends on the formulation and combination of component materials including chemicals from a highly-skilled and technically-advanced composites industry [19].

Manufacturing blades in the 40-50 m range involves proven fiberglass composite fabrication techniques. For larger blades – currently limited to about 73.5 m – advanced composite materials pioneered in the aerospace industry are being specified. Carbon fiber reinforced laminates offer the greatest stiffness and strength to weight ratio. Carbon fiber reinforced load-bearing spars can reduce weight and increase stiffness. These benefits increase as blade size increase. The use of carbon fibers in 60 m turbine blades is estimated to reduce total blade mass by 38% and decrease cost by 14% compared to 100% fiberglass. One example of an advanced composite is carbon fiber reinforced plastic (CFRP). This has long been used in technology-intensive applications such as wind turbine blades due to its significant strength, stiffness and weight advantages over other engineering materials. Solutions focused on reducing the cost and time to manufacture CFRP components could make composites a more viable substitute for other materials. Carbon fibers have the added benefit of reducing the thickness of fiberglass laminate sections, further addressing the problems associated with resin wetting of thick lay-up sections. Wind turbines also benefit from the general trend of increasing use and decreasing cost of carbon fiber materials [25].

As we move towards a low carbon economy, it will become critical to consider the whole life impacts of innovative materials, from feedstock and manufacture to end-of life options. While composites in general possess many attributes that contribute favourably to a low carbon agenda, through the reduction of energy consumption in transport due to light weighting and the elimination of electrochemical corrosion, their role in developing sustainable products requires further work. Most resin systems are currently oil based, while both carbon and glass fibers are produced using energy intensive processes.

VI. CONCLUSIONS

The economics and the benefits of renewable sources of energy and in particular wind power are becoming increasingly convincing across the globe. Wind has the advantages of stable generation costs, low operating costs, renewable, short energy

payback, less time-to-market, abundant resource and environmentally preferable. Latest technological developments taking place in the area of reliability of wind turbines and improvements in the properties of the materials used will make wind energy more competitive in the next decade.

Wind turbine blades must be strong enough to withstand the applied loads without failure; thus, the ultimate strength must be sufficient to with sustain extreme loads, and the fatigue strength must be sufficient to withstand the time-varying loads throughout the intended life of the blade. The blades must also be stiff enough to prevent collision with the tower under extreme conditions. Stiffness is also important locally for preventing buckling of those parts of the blade that experience compressive stresses. To minimize the cost of the power generated, the blade construction needs to be as light as possible; this has to be achieved through optimization of the structural arrangement and dimensions in accordance with the materials selection. The production processes used for manufacturing the blades must be sufficiently consistent and reliable to ensure that the end product is always compatible with the design assumptions and calculations.

Composites offer many advantages in wind turbine blade construction. Composites are also unique in their ability to be tailored for different properties using various reinforcement configurations, matrix materials and manufacturing processes. Wind turbine design has improved substantially due to composites technology, and as composite use becomes more common place there exists the need to minimize the time required to fabricate blades while tightening dimensional tolerances and repeatability. Many institutions are investigating and addressing these concerns in an attempt to improve the manufacturability of wind turbine blades.

Advanced composites like fiber-reinforced composites of the type used in wind turbine blades are laminates composed of several layers of reinforcing fabric impregnated with and held together by an adhesive resin. Such laminates can be very strong and stiff when loaded in their own plane, but are much weaker when loaded out-of-plane because the layers, or plies, can more readily be pulled apart. The in-plane properties are largely determined by the fibers, whereas the out-of-plane properties depend heavily on the strength and adhesive capability of the resin matrix [23, 26]. Increasingly enabled by the introduction of newer polymer resin matrix materials and high performance reinforcement fibers of glass, carbon and aramid, the penetration of these advanced materials has witnessed a steady expansion in uses and volume. The increased volume has resulted in an expected reduction in costs.

To improve materials for wind turbine blades, one should do things a little differently.

REFERENCES

[1] Vardar, A and Bülent Eker, "Design of a Wind Turbine Working with the Continuity Principal," *Energy, Exploration &Exploitation*, vol. 24, no. 4 - 5 / Aug., 2006.

[2] Dan Ancona and Jim McVeigh, "Wind Turbine –*Materials and Manufacturing Fact Sheet*" 2001, Princeton Energy Resources International, LLC.

[3] Hogg, P., "*Wind Turbine Blade Materials, Supergen wind Phase 1 Final Assembly*," University of Loughborough, 25th Mar. 2010.

[4] Department of Energy, *"Wind Power Today,"* DOE/GO-102001-1325, May. 2001.

[5] Eker, B., Ayşegül Akdoğan, Ali Vardar., "Using of Composite Material in Wind Turbine Blades," *Journal of Applied Science*, vol. 6, Issue 14, p. 2917-2921.

[6] Hyla I., Śleziona J., Composite Materials, Basis of Mechanics and Designing, *Publishers of Silesian University of Technology*, Gliwice, 2004.

[7] Boczkowska A., Kapuściński J., Lindemann Z., Witemberg-Perzyk D., Wojciechowski S: "Composites," *Oficyna Wydawnicza Politechniki Warszawskiej*,Warszawa, 2003.

[8] Żółkiewski, S., "Selection and Impact of Parameters in Composite Materials Designing," *13th World Congress in Mechanism and Machine Science*, Guanajuato, México, 19-25 Jun., 2011.

[9] http://www.gurit.com/.

[10] Hayman, B. and Jakob Wedel-Heine, "*Materials Challenges in Present*," http://www.mrs.org/bulletin/, vol. 33, 2008.

[11] Babu, K. Suresh, N. V. Subba Raju, M. Srinivasa Redd and D. Nageswara, "The Material Selection For Typıcal Wind Turbine Balades Using A. MADM Approach & Analysis of Blades," *MCDM 2006*, Chania, Greece, Jun. 19-23, 2006.

[12] Eker B., Akdoğan A., Vardar A., "Choosing Suitable Material for Wind Turbine Construction," *Agricultural Engineering Semposium*, Leuven, Belgium, 2004.

[13] Brondsted, P., Hans Lilholt, Aege Lystrup., "*Composite Materials for Wind Power Turbine Blades*,"Annv. Rev. Mater. Res 2005, 35: 505-38.

[14] http://www.diim.unict.it/users/fgiudice/pdfs/SM_2.1.pdf.

[15] Brondsted, P., "*Composite Materials for Wind Turbine Blades*," Riso National Laboratory for Sustainable Energy.

[16] Samir, A., Izhar-ul Haq., *Wind Blade Material Optimization, Advances in Mechanical Engineering*, ISSN: 2160-0619, vol. 2, no. 4, Dec., 2012.

[17] OSHA Polymer Matrix Materials: Advanced Composites, *U.S. Department of Labor*. Archived from the original on 28 May 2010. Retrieved 2010-06-05.

[18] http://www.faa.gov/regulations_policies/handbooks_manuals/aircraft/amt_airframe_handbook/media/ama_Ch07.pdf.

[19] ACG (Copyright 2006). "Introduction to Advanced Composites and Prepreg Technology" (free PDF download). *Advanced Composites Group*. Retrieved 2010-06-05.

[20] http://en.wikipedia.org/wiki/Advanced_composite_materials_(engineering).

[21] Pilato, L.; and Michno, Michael J. (Jan. 1994). "Advanced Composite Materials (Chapter 1 Introduction, and Chapter 2 "Matrix Resins")", *Springer-Verlag* New York. ISBN 978-3-540-57563-4.

[22] Watson, J. C and Juan C. Serrano, "*Composite Materials for Wind Blades*," September, 2010, http://www.ppg.com/en/Pages/home.aspx.

[23] http://abdmatrix.com/ATM/files/Introduction%20to%20Composite%20Materials.pdf.

[24] Anonymous, "Global Composite Market 2009–2014; *Materials, Markets and Technologies*," Lucintel, 2009.

[25] H. G. Willett, "*Characterisation of Composites Used in Wind Turbine Blade Manufacture*" http://www.reinforcedplastics.com/.

[26] Day, Dwayne A. (2003). "Composites and Advanced Materials" (Centennial of Flight Commemoration Act Public Law 105-389 105th Congress (Nov. 13, 1998)). *NASA. U.S. Centennial of Flight Commission.* Archived from the original on 28 May 2010. Retrieved 2010-06-05.

[27] www.onlyalpha.com.

Ayşegül AKDOĞAN EKER is Professor in the Mechanical Engineering Department at the University of Yıldız Technical of Turkey. She is also the chair of Mechanical Engineering Department in her university since 2010. She earned her Sc. Dr degree in 1987 from İstanbul Technical University. She has edited and published seven books and more than 150 papers in referred journals and conference proceedings, and served on editorial boards of various technical journals. She was given many national and international awards for her research on materials. Her current research focuses on advanced composite materials and applications of nano and smart materials.

Bülent EKER is Professor in the Biosystems Engineering Department at the University of Namık Kemal of Turkey. He is also the general director of Technology Development District in Tekirdağ since 2010. He earned his Sc. Dr degree in 1983 from Ankara University. He has edited and published seven books and more than 350 papers in referred journals and conference proceedings, and served on editorial boards of various technical journals. He was given many national and international awards for his research on materials and structures. His current research focuses on advanced composite materials and structures for wind turbine blades and innovative large wind energy production control systems.

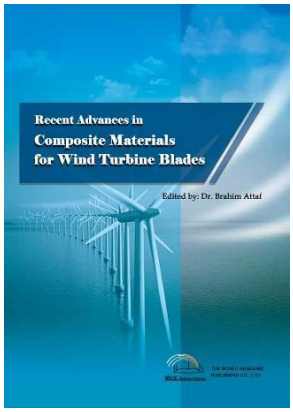

Recent Advances in Composite Materials for Wind Turbine Blades
Edited by Dr. Brahim Attaf

ISBN 978-0-9889190-0-6

Hard cover, 232 pages

Publisher: The World Academic Publishing Co. Ltd.

Published in printed edition: 20, December 2013

Published online: 20, December 2013

This book of science and technology provides an overview of recent research activities on the application of fibre-reinforced composite materials used in wind turbine blades. Great emphasis was given to the work of scientists, researchers and industrialists who are active in the field and to the latest developments achieved in new materials, manufacturing processes, architectures, aerodynamics, optimum design, testing techniques, etc.. These innovative topics will open up great perspectives for the development of large scale blades for on- and off-shore applications. In addition, the variety of the presented chapters will offer readers access to global studies of research & innovation, technology transfer and dissemination of results and will respond effectively to issues related to improving the energy efficiency strategy for 2020 and the longer term.

How to cite this book chapter

Eker A. A. and Eker B. (2013). General Assessment of Fıber - Reınforced Composıtes Selectıon in Wınd Turbıne Blades, *Recent Advances in Composite Materials for Wind Turbines Blades*, Dr. Brahim Attaf (Ed.), ISBN 978-0-9889190-0-6, WAP-AMSA, Available from: http://www.academicpub.org/amsa/chapterInfo.aspx

World Academic Publishing - Advances in Materials Science and Applications

Chapter 5

On the Fluid-Structure Interaction of a Composite Wind Turbine Blade

Roham Rafiee

Composites Research Laboratory, Faculty of New Sciences & Technologies,
University of Tehran, Tehran, 1439955941, Iran

Roham.Rafiee@ut.ac.ir

I. INTRODUCTION

Global warming of the earth and lack of fossil fuels from one hand and the increasing demand for electricity from other hand have turned the global attentions toward pollution free electricity generation from clean and renewable energy resources. Among different renewable energy resources, wind energy is of growing importance which can be inferred from the installed capacity of the wind turbines during the past decades. As a frontier element in capturing wind energy, the blade plays a key role in the efficient performance of a wind turbine dictated by economical power generation indicators. The importance of blade is a twofold issue: it is required not only to get as much wind energy as possible in a limited period of time that wind flows; but also to present a structure capable of operating for about 20 years without any severe defect. Consequently, the wind turbine blade has to incorporate both proper aerodynamic performance and appropriate structural stiffness at the same time exposing to different working conditions.

A wind turbine blade is required to provide a strong and light structure in order to accommodate different loading conditions during different experienced events by the wind turbine and also start operating at low wind speed regime. These should be accomplished while the aerodynamic performance is maintained in optimum condition during the lifetime. Moreover, random nature of wind flow, long and flexible structure of wind turbine blades and their continuous operation under different circumstances render them as fatigue critical components. From structural point of view, the composite materials are the only solution addressing all aforementioned structural design constraints. The blades of the modern horizontal axis wind turbines (HAWT) are full composite structures which are generally made of Glass/Epoxy while in a very long blade a hybrid configuration of Carbon/Epoxy and Glass/Epoxy in critical areas is used [1]. Fig. 1 shows a production process of a 23-meter composite wind turbine blade using hand lay-up process utilizing Prepreg materials while the longer wind turbine blades are manufactured using vacuum infusion process (VIP) method for better and more uniform impregnation of dry fabrics and more rapid mass production [2].

Fig. 1 A production process of a composite wind turbine blade using hand lay-up method (Courtesy of Sabaniroo Co., Iran)

Converting kinematic energy of wind inflow to electricity, the generated power by wind turbines is proportional to the swept area by the rotor [3]. Thus, it would be reasonable to increase the cost efficiency of a wind turbine by increasing the rotor diameter. Nowadays, the modern HAWTs with the capacity of 500 kW up to 5 MW are equipped with the blade length ranging from 15 to 75 meters. An increasing trend in the length of a wind turbine blade demands more clarified understanding

of its structural behaviour from different viewpoints. The investigation of the interaction between aerodynamics and structure which falls into aeroelasticity study has to be taken into account during the design process of wind turbine. The lack of control regarding this interaction may lead to a reduction in power production capability of a wind turbine. A wind turbine blade is subjected to aerodynamic loadings which will induce some variations to the primary geometry of the blade. The variation in the geometrical shape is not negligible due to the flexible structure of blades; and this will, however, cause some variations in imposed aerodynamic forces. Increasing the level of the blade deflection engenders significant changes in the elastic and aerodynamics forces, thus affecting the overall performance of a wind turbine. This phenomenon will also cause some uncertainties in induced stress components in the critical region of the blade.

II. STATE OF THE ART

The main objective of this chapter is (i) to study the fluid-structure interaction on a commercial wind turbine blade under various operational conditions and (ii) to evaluate the degree to which this phenomenon will change the stress components in composite layers of the investigated blade structure. A semi-coupled method as an iterative approach is employed in this context to perform aeroelastic analysis on a specific wind turbine blade. A semi-coupled technique implies on dividing the problem into fluid and structural spaces which are solved sequentially and the output of each space is fed into the other space as input.

The wind turbine blade under consideration in this study belongs to 660 kW wind turbine, manufactured in Iran after technology transfer from Vestas Wind System A/S [4]. The rotor of the investigated wind turbine consists of three blades and a nose cone. The rotor drives the main shaft of the wind turbine which is connected to the three-stage planetary gearbox with 1:52 ratio. The output of the gearbox is transmitted to an asynchronized generator which produces 660 kW electricity. The whole components for transmitting kinematic energy of the wind flow and power generation are placed inside the nacelle on the top of 42 meter tower. Installed in Iran, the whole wind turbine structure is shown in Fig. 2. The investigated wind turbine is categorized under the constant speed type by maintaining the rotating speed of rotor at 28.5 rpm using pitch power regulation system. The power regulating mechanism makes blades rotate about 89 degree along their longitudinal axis dependently. Thus, the angle of attack in different cross sections of a blade is changed in accordance with wind speed variation. Moreover the wind turbine is equipped with active yaw control system keeping turbine in wind flow direction by rotating the whole nacelle around the tower.

Fig. 2 Investigated 660 kW wind turbine (Courtesy of Sabaniroo Co., Iran)

The length of the blade investigated within this chapter is 23 meters and its mass is about 1250 kg. The structure of the blade consists of two main structural parts (shell and spar). The spar is located inside the shell, it is mainly responsible to support different load cases and its cross section has a box shape. The shell of the blade provides pressure distribution required for blade rotation and thus its cross section is in the form of specific airfoils due to aerodynamic considerations associated with efficiency of the blade in capturing wind energy. It can be understood that while the spar contributes considerably to the structural aspects of the blade, the shell is responsible for aerodynamic performance of the blade. This wind turbine blade has a twist angle about 15 degrees from root to tip to keep the angles of attack all along the blade compatible with relative wind velocity and the blade has also a tapered shape.

III. MODELLING

Model preparation includes constructing geometrical and finite element models for both aerodynamic and structural analyses. Firstly, a fundamental geometrical model of the blade is constructed as a wireframe model on the basis of available cross section profiles of the shell and spar in different stations from the root to the tip of the blade. The Loft method is used to draw surface in the spaces between these cross sections converting the wireframe to surface model. Both wireframe and surface models are shown in Fig. 3.

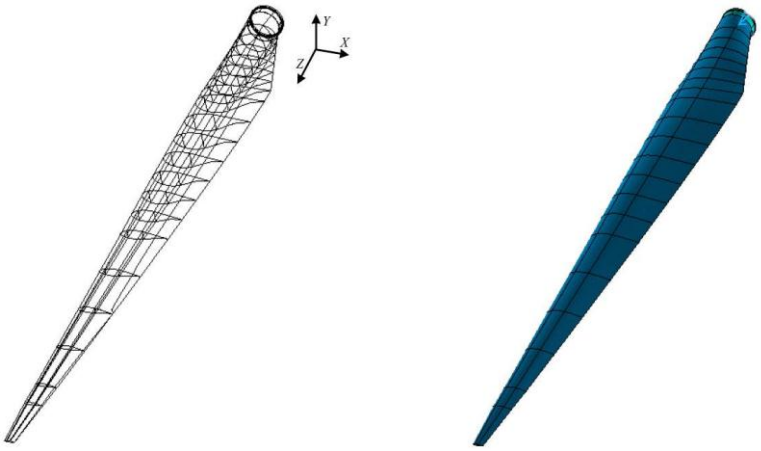

Fig. 3 Wireframe (left) and surface (right) models of the wind turbine blade

For constructing structural finite element model, second order shell elements were selected from element library of ANSYS [5]. The selected element is powered with a feature to analyse layered shells which is compatible with composite plies of the structure. Thanks to manual meshing method, the whole model contains quadratic elements with appropriate aspect ratio avoiding any triangular element. From structural convergence study on the mesh density of the model, it is inferred that 8505 elements are sufficient for the finite element analysis. The whole nodes placed on the root region of the model are restricted from any movement as the boundary conditions used in the case of static analysis. The procedure of obtaining mechanical properties of composite layers is comprehensively explained in the next section.

The aerodynamic finite element model is constructed on the same geometry platform used for structural analysis. Following the same pattern of the blade outer elements, fluid elements which are in direct contact with blade surface are constructed using FLOTRAN142 and free mesh method [5]. Wind velocity along X-direction on the side planes are constantly taken as free wind flow speed. Multiplying angular velocity of the blade by the radius of blade at each station, the linear velocity of the blade due to rotation is obtained and applied to each corresponding station in Y-direction. The applied pressure on the trailing edge of the wind blade is taken equal to zero. Due to no-slip condition, velocity is taken equal to zero in all directions on the shell.

IV. MATERIAL PROPERTIES

Three different types of Prepreg Glass/Epoxy fabrics are used in the manufacture of structural blades. Tri-axial and bi-axial fabrics are used in the shell structure in the form of [0/±45] and [±45], respectively. Bi-axial and Uni-directional (U-D) fabrics are used in the spar structure. It is worth mentioning that tri-axial and bi-axial fabrics utilized for manufacturing the investigated wind turbine blade are not woven fabrics and U-D plies with mentioned orientations are stitched together. Two kinds of foams are also used in the shell and spar structure to provide sandwich panels. Prepregs have had a considerable impact on the evolution of composite industries in the late 20th century. Used in all aerospace programs worldwide, they are also enabling a new generation of high speed trains and fast ships and long wind turbine blades to become reality rather than designer's dream. A Prepreg consists of a combination of a matrix (e.g., resin) and fibre reinforcement. It is ready to use in the component manufacturing process. In this technology, reinforcing fibres are impregnated with resin before manufacturing process and this makes the process easier and more economic [6]. Furthermore, control of fibre volume fraction is handled better. The fabrics consist of at least two threads that are weaved together and called "warp" and "weft" or are stitched together in non-woven form. The weave style can be varied according to crimp and drapeability. Low crimp gives better mechanical performance because straighter fabrics carry greater loads [6]. It has been proven that crimp will negatively affect fatigue life of structure [7]. Geometric of woven fabric produces out of plane curvature in plies and consequently stress concentration appears. Compressive strength of fibres in woven fabrics is approximately half of straight fibres in stitched form [8]. In order to overcome this problem using stitched form instead of woven fabrics is recommended [8]. The main criteria that influence the selection of Prepregs for particular application are performance and cost and the main advantages of using them can be summarized as lower fabrication cost, reduced energy consumption, optimized weight and better mechanical properties under cyclic loading, tensile, stiffness and corrosion.

For structural FE analysis, complete sets of mechanical properties are required. Mechanical properties of U-D are available experimentally, while limited data are available for bi-axial and tri-axial laminates. Namely, elastic moduli in 0° and 45° directions are experimentally available for these laminates [9] as depicted in Fig. 4. Bi-axial and tri-axial laminates can be both taken into account sometimes as [±45] and [0/±45] when 0° in Fig. 4 is considered and sometimes they can be considered as [0/90] and [0/90/-45], respectively, when 45° direction in Fig. 4 is considered. The available and non-available mechanical properties of all aforementioned layers are presented in Table 1.

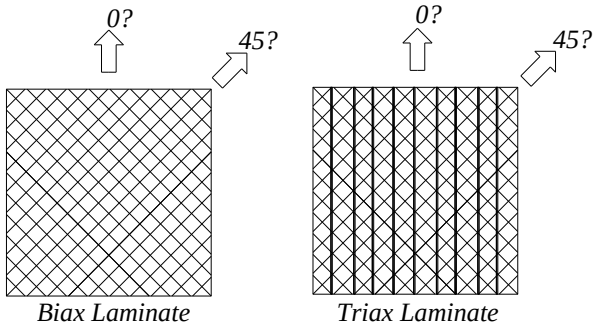

Fig. 4 Directions of Bi-axial and Tri-axial Laminates

As it can be seen from Table 1, elastic moduli E_1 and E_2 are equal in [±45], [0/90] and [0/90/-45] due to symmetry. Since both tri-axial and bi-axial laminates consist of the same U-D fibres stitched together, the non-available properties of these laminates can be obtained.

TABLE 1 AVAILABLE AND NOT-AVAILABLE MECHANICAL PROPERTIES [9]

Laminate Name	Configuration	E_1 (GPa)	E_2 (GPa)	ν_{12}	E_6 (GPa)
U-D	[0]	43	9.77	0.32	3.31
Bi-axial	[±45]	6.8	6.8	N/A	N/A
Bi-axial	[0/90]	16.7	16.7	N/A	N/A
Tri-axial	[0/±45]	20.7±3.1	N/A	N/A	N/A
Tri-axial	[0/90/-45]	15.1±2.3	15.1±2.3	N/A	N/A

A. General governing equations

Stiffness matrix of a U-D ply is written as [10]:

$$\begin{bmatrix} Q_{XX} & Q_{XY} & 0 \\ Q_{XY} & Q_{YY} & 0 \\ 0 & 0 & Q_{SS} \end{bmatrix} \tag{1}$$

where,

$$Q_{XX} = \frac{E_X}{1-\nu_{XY}\nu_{YX}} \quad , \quad Q_{YY} = \frac{E_Y}{1-\nu_{XY}\nu_{YX}} \quad , \quad Q_{XY} = \frac{\nu_{YX}E_X}{1-\nu_{XY}\nu_{YX}} \quad , \quad Q_{SS} = G \tag{2}$$

Involved parameters in set of Eq. (2) are in the space of on-axis coordinate system and "*x*" devotes to longitudinal fibre direction and "*y*" devoted to transverse direction. ν_{XY} is major Poisson's ratio and ν_{YX} is minor Poisson's ratio. If one needs stiffness matrix in any desired direction, transformation from on-axis coordinate system to off-axis has to be performed using following relation [11]:

$$\begin{bmatrix} Q_{11} \\ Q_{22} \\ Q_{12} \\ Q_{66} \\ Q_{16} \\ Q_{26} \end{bmatrix} = \begin{bmatrix} m^4 & n^4 & 2m^2n^2 & 4m^2n^2 \\ n^4 & m^4 & 2m^2n^2 & 4m^2n^2 \\ m^2n^2 & m^2n^2 & m^4+n^4 & -4m^2n^2 \\ m^2n^2 & m^2n^2 & -2m^2n^2 & (m^2-n^2)^2 \\ m^3n & -mn^3 & mn^3-m^3n & 2(mn^3-m^3n) \\ mn^3 & -m^3n & mn^3-m^3n & 2(mn^3-m^3n) \end{bmatrix} \begin{bmatrix} Q_{XX} \\ Q_{YY} \\ Q_{XY} \\ Q_{SS} \end{bmatrix} \tag{3}$$

$$m = Cos\theta \quad , \quad n = Sin\theta$$

For the ply where fibres are oriented in the direction of 0 °, we have:

$$\begin{aligned} Q^0_{11} &= Q_{XX} \\ Q^0_{22} &= Q_{YY} \\ Q^0_{12} &= Q^0_{21} = Q_{XY} \\ Q^0_{66} &= Q_{SS} \\ Q^0_{16} &= Q^0_{26} = 0 \end{aligned} \tag{4}$$

Similarity, for ply with fibres at 90 °:

$$\begin{aligned} Q_{11}^{90} &= Q_{22}^{0} \\ Q_{22}^{90} &= Q_{11}^{0} \\ Q_{12}^{90} &= Q_{21}^{90} = Q_{12}^{0} \\ Q_{66}^{90} &= Q_{66}^{0} \\ Q_{16}^{90} &= Q_{26}^{90} = Q_{16}^{0} \end{aligned} \tag{5}$$

For a 45 °ply and a -45 °ply, we have:

$$\begin{aligned} Q_{11}^{45} &= Q_{11}^{-45} \\ Q_{22}^{45} &= Q_{22}^{-45} \\ Q_{12}^{45} &= Q_{21}^{45} = Q_{12}^{-45} = Q_{21}^{-45} \\ Q_{66}^{45} &= Q_{66}^{-45} \\ Q_{16}^{45} &= Q_{26}^{45} = -Q_{16}^{-45} = -Q_{26}^{-45} \end{aligned} \tag{6}$$

Equivalent stiffness matrix of a composite composed of two plies can be calculated using the following relation:

$$\frac{1}{h}A_{ij} = Q_{ij}^{\alpha}p^{\alpha} + Q_{ij}^{\beta}p^{\beta} \tag{7}$$

where, "*h*" is the laminate thickness, α is the angle of first ply in accordance of selected coordinate system, β is the angle of second ply and "*p*" is the ply fraction. Based on technical data from supplier of investigated bi-axial laminate [9], both ply fractions are considered to be the same. Therefore, we have:

$$p^{0} = p^{90} = p^{45} = p^{-45} = 0.5 \tag{8}$$

Using Eqs. (7) and (8), we have:

$$\frac{1}{h}A_{ij}^{[0/90]} = 0.5(Q_{ij}^{0} + Q_{ij}^{90}) \qquad \frac{1}{h}A_{ij}^{[45/-45]} = 0.5(Q_{ij}^{45} + Q_{ij}^{-45}) \tag{9}$$

By calculating the inverse of matrix [*A*], we have:

$$\left[\frac{1}{h}[A]\right]^{-1} = h[A]^{-1} = h[a] \tag{10}$$

Where, [*a*] is the compliance matrix and its terms are as follows [11]:

$$[a] = h\begin{bmatrix} 1/E_1 & -\nu_{12}/E_2 & \nu_{16}/E_6 \\ -\nu_{12}/E_2 & 1/E_2 & \nu_{26}/E_6 \\ \nu_{16}/E_6 & \nu_{26}/E_6 & 1/E_6 \end{bmatrix} \tag{11}$$

It can be seen that in Eq. (11), all "*x*" and "*y*" superscripts have been changed to numerical superscripts which representing properties of a laminated composite instead of single ply. Now, the same calculation has to be performed for other aforementioned configurations.

B. Bi-axial Laminate with [±45] Configuration

Stiffness matrix of this composite is calculated using Eqs. (3), (6) and (9):

$$\frac{1}{h}[A^{[\pm 45]}] = \frac{1}{h}\begin{bmatrix} A_{11}^{[\pm 45]} & A_{11}^{[\pm 45]} & 0 \\ A_{11}^{[\pm 45]} & A_{11}^{[\pm 45]} & 0 \\ 0 & 0 & A_{11}^{[\pm 45]} \end{bmatrix}$$

$$\begin{aligned} [A_{11}^{[\pm 45]}] &= 0.25Q_{XX} + 0.5Q_{XY} + 0.25Q_{YY} + Q_{SS} \\ [A_{22}^{[\pm 45]}] &= 0.25Q_{XX} + 0.5Q_{XY} + 0.25Q_{YY} + Q_{SS} \\ [A_{12}^{[\pm 45]}] &= [A_{21}^{[\pm 45]}] = 0.25Q_{XX} + 0.5Q_{XY} + 0.25Q_{YY} - Q_{SS} \\ [A_{66}^{[\pm 45]}] &= 0.25Q_{XX} - 0.5Q_{XY} + 0.25Q_{YY} \end{aligned} \tag{12}$$

Compliance matrix is calculated using Eq. (11), after replacing known parameters by their values given in Table 1:

$$[a] = h\begin{bmatrix} 1/6.8 & -\alpha/6.8 & 0 \\ -\alpha/6.8 & 1/6.8 & 0 \\ 0 & 0 & 1/G_{[\pm 45]} \end{bmatrix} \tag{13}$$

where, α is the major Poisson's ratio of bi-axial laminates.

After inversing matrix [*a*] expressed by Eq. (13), equalizing them to their corresponding members in Eq. (12) and omitting repeated equations, we get:

$$\begin{aligned} 0.25Q_{XX} + 0.5Q_{XY} + 0.25Q_{YY} + Q_{SS} &= \frac{0.147059}{0.0216263 - 0.0216263\alpha^2} \\ 0.25Q_{XX} + 0.5Q_{XY} + 0.25Q_{YY} - Q_{SS} &= \frac{0.147059\alpha}{0.0216263 - 0.0216263\alpha^2} \\ 0.25Q_{XX} - 0.5Q_{XY} + 0.25Q_{YY} &= G_{[\pm 45]} \end{aligned} \tag{14}$$

C. Bi-axial Laminates with [0/90] Configuration

Stiffness matrix of this configuration is derived using Eqs. (3), (5) and (9):

$$\frac{1}{h}[A^{0/90}] = \frac{1}{h}\begin{bmatrix} 0.5Q_{XX} + 0.5Q_{YY} & Q_{XY} & 0 \\ Q_{XY} & 0.5Q_{XX} + 0.5Q_{YY} & 0 \\ 0 & 0 & Q_{SS} \end{bmatrix} \tag{15}$$

Compliance matrix is calculated using Eq. (11), after replacing known parameters by their values given in Table 1:

$$[a] = h\begin{bmatrix} 1/16.7 & -\beta/16.7 & 0 \\ -\beta/16.7 & 1/16.7 & 0 \\ 0 & 0 & 1/G_{[0/90]} \end{bmatrix} \tag{16}$$

where, β is major Poisson's ratio of composites.

After inversing the matrix expressed by Eq. (16), equalizing them to their corresponding members in Eq. (15) and omitting repeated equations, we have:

$$\begin{aligned} 0.5Q_{XX} + 0.5Q_{YY} &= \frac{0.0598802}{0.00358564 - 0.00358564\beta^2} \\ Q_{XY} &= \frac{0.0598802\beta}{0.00358564 - 0.00358564\beta^2} \\ Q_{SS} &= G_{[0/90]} \end{aligned} \tag{17}$$

D. Tri-axial Laminate with [0/±45] Configuration

In order to calculate matrices related to tri-axial composites, the same method of bi-axial laminate is employed. The only difference is referred to ply fractions. According to information from supplier [9], the amount of fibres in 0 °direction is equal to 254 kg/m^2 and the amount of fibres in 45 °direction and -45 °direction is equal to 230 kg/m^2. Therefore, we have:

$$\begin{aligned} p^0 &= \frac{425}{425 + 230 + 230} = 0.48 \\ p^{45} = p^{-45} &= \frac{230}{425 + 230 + 230} = 0.26 \end{aligned} \tag{18}$$

Stiffness matrix of this configuration is can be written in the following form using Eqs. (4), (6), (7) and (18):

$$\frac{1}{h}[A^{[0/\pm 45]}] = \frac{1}{h}\begin{bmatrix} 0.61Q_{XX} + 0.26Q_{XY} + 0.13Q_{YY} + 0.52Q_{SS} & 0.13Q_{XX} + 0.74Q_{XY} + 0.13Q_{YY} - 0.52Q_{SS} & 0 \\ 0.13Q_{XX} + 0.74Q_{XY} + 0.13Q_{YY} - 0.52Q_{SS} & 0.13Q_{XX} + 0.26Q_{XY} + 0.61Q_{YY} + 0.52Q_{SS} & 0 \\ 0 & 0 & 0.13Q_{XX} - 0.26Q_{XY} + 0.13Q_{YY} + 0.48Q_{SS} \end{bmatrix} \tag{19}$$

Compliance matrix is calculated using Eq. (11) and known parameters given in Table 1:

$$[a]=h\begin{bmatrix} 1/(20.7\pm3.1) & -\varphi/(20.7\pm3.1) & 0 \\ -\varphi/(20.7\pm3.1) & 1/E_2 & 0 \\ 0 & 0 & 1/G_{[0/\pm45]} \end{bmatrix} \tag{20}$$

Where, φ is the major Poisson's ratio of the tri-axial composites with [0/±45] configuration.

After inversing the matrix expressed by Eq. (20), equalizing them to their corresponding members in Eq. (19) and omitting repeated equations, we have:

$$\begin{aligned} 0.61Q_{XX}+0.26Q_{XY}+0.13Q_{YY}+0.52Q_{SS} &= \frac{1}{0.0483092-0.00233378E_2\varphi^2} \\ 0.13Q_{XX}+0.26Q_{XY}+0.61Q_{YY}+0.52Q_{SS} &= \frac{0.0483092E_2}{0.0483092-0.00233378E_2\varphi^2} \\ 0.13Q_{XX}+0.74Q_{XY}+0.13Q_{YY}-0.52Q_{SS} &= \frac{0.0483092E_2\varphi}{0.0483092-0.00233378E_2\varphi^2} \\ 0.13Q_{XX}-0.26Q_{XY}+0.13Q_{YY}+0.48Q_{SS} &= G_{[0/\pm45]} \end{aligned} \tag{21}$$

E. Tri-axial Laminate with [0/90/-45] Configuration

Extraction method of stiffness matrix of this configuration is the same as the method employed for the case of tri-axial laminates with [0/±45] configuration. The only difference can be found in ply fraction due to new distribution of fibres as below:

$$\begin{aligned} p^{-45} &= \frac{425}{425+230+230}=0.48 \\ p^{0}=p^{90} &= \frac{230}{425+230+230}=0.26 \end{aligned} \tag{22}$$

Stiffness matrix of this configuration can be written in the following form using Eqs. (4)- (7) and (22):

$$\frac{1}{h}[A^{[0/90/-45]}]=\frac{1}{h}\begin{bmatrix} 0.38Q_{XX}+0.24Q_{XY}+0.38Q_{YY}+0.48Q_{SS} & 0.12Q_{XX}+0.76Q_{XY}+0.12Q_{YY}-0.48Q_{SS} & -0.12Q_{xx}+0.12Q_{YY} \\ 0.12Q_{XX}+0.76Q_{XY}+0.12Q_{YY}-0.48Q_{SS} & 0.38Q_{XX}+0.24Q_{XY}+0.38Q_{YY}+0.48Q_{SS} & -0.12Q_{xx}+0.12Q_{YY} \\ -0.12Q_{xx}+0.12Q_{YY} & -0.12Q_{xx}+0.12Q_{YY} & 0.12Q_{XX}-0.24Q_{XY}+0.12Q_{YY}+0.52Q_{SS} \end{bmatrix} \tag{23}$$

Compliance matrix is calculated using Eq. (11) and the known parameters given in Table 1:

$$[a]=h\begin{bmatrix} 1/(15\pm2.3) & -\xi/(15\pm2.3) & \mu/G_{[0/90/-45]} \\ -\xi/(15\pm2.3) & 1/(15\pm2.3) & \mu/G_{[0/90/-45]} \\ \mu/G_{[0/90/-45]} & \mu/G_{[0/90/-45]} & 1/G_{[0/90/-45]} \end{bmatrix} \tag{24}$$

where, ξ is the minor Poisson's ratio of tri-axial laminate with [0/90/-45] configuration and μ is the coupling Poisson's ratio in "16" plan. In general case, Q_{16} is not equal to Q_{26}. But in this particular case, it can be seen that these two parameters are equal and it has to be considered in compliance matrix too.

After inversing the matrix expressed by Eq. (24), equalizing them to their corresponding members in Eq. (23) and omitting repeated equations, we have:

$$
\begin{aligned}
0.38Q_{XX} + 0.24Q_{XY} + 0.38Q_{YY} + 0.48Q_{SS} &= \frac{0.066G_{[0/90/-45]} - \eta^2}{G_{[0/90/-45]}(0.004356 - 0.004356\xi^2) - 0.132(1+\xi)\eta^2} \\
0.12Q_{XX} + 0.76Q_{XY} + 0.12Q_{YY} - 0.48Q_{SS} &= \frac{0.066G_{[0/90/-45]} + \eta^2}{G_{[0/90/-45]}(0.004356 - 0.004356\xi^2) - 0.132(1+\xi)\eta^2} \\
0.13Q_{XX} + 0.74Q_{XY} + 0.13Q_{YY} - 0.52Q_{SS} &= \frac{0.066G_{[0/90/-45]}(1+\xi)\eta}{G_{[0/90/-45]}(0.004356 - 0.004356\xi^2) - 0.132(1+\xi)\eta^2} \\
0.12Q_{XX} - 0.24Q_{XY} + 0.12Q_{YY} + 0.52Q_{SS} &= \frac{G^2_{[0/90/-45]}(0.004356 - 0.004356\xi^2)}{G_{[0/90/-45]}(0.004356 - 0.004356\xi^2) - 0.132(1+\xi)\eta^2}
\end{aligned}
\tag{25}
$$

F. Direct Method

In this method, mechanical properties of U-D fibre presented in Table 1 are inserted into Eqs. (12), (15), (19) and (23) to obtain properties of bi-axial and tri-axial laminates. Using this approach, significantly higher values for Young's moduli along "1" and "2" directions than experimentally reported values in Table 1 are obtained. This is originated from the fact that the volume fraction of glass fibre in U-D ply is reported as 44%; whereas it is reported as 38% for bi-axial and tri-axial laminates. Therefore, this approach cannot be applicable as the reported experimentally values for U-D ply in Table 1 cannot be extended to the U-D plies in bi-axial and tri-axial fabrics.

G. Inverse Method

In this method, we assume that mechanical properties of U-D fibres in bi-axial and tri-axial laminates are unknown. Thus, considering sets of Eqs. (14), (17), (21) and (25), we have 14 equations with 14 unknown parameters. Namely all Q_{XX}, Q_{XY}, Q_{YY} and Q_{SS}, which are also unknown. It should be noted that in this approach, properties of U-D fabrics (reported in Table 1) are totally different from properties of U-D fabrics constructing bi-axial and tri-axial laminates due to different volume fractions.

At a glance, it can be seen that solving this set of equations due to its non-linear nature is not simple. Since some of these equations are highly dependent on other equations, ordinary and classical solutions are not possible. In order to simplify the solution, it should be known that the major Poisson's ratio of a [0/90] composites has to have an amount between 0.05 and 0.1; this point is chosen as a start point of solution. And by considering β as a known parameter will reduce the number of unknowns. Furthermore, in such situation, there is no need to use complex equations of tri-axial composite with [0/90/-45] configuration. The equations of [0/90/-45] will be used just to verify the results. Using trial and error approach, it was realized that when considering β as a value of 0.06 will result in acceptable values for mechanical properties of U-D fabrics.

According to Table 1, elastic modulus of tri-axial laminates is placed between the upper and lower values. However, using upper and middle values as the first guess in inverse method will not lead to acceptable results; therefore lower magnitude for elastic modulus is the value selected. Now, using obtained results and available equations, E_2 of tri-axial composite with [0/±45] configuration and its Poisson's ratio can be calculated. Therefore, full mechanical properties of bi-axial and tri-axial laminates are extracted. These values are inserted in Table 2.

TABLE 2 CALCULATED MECHANICAL PROPERTIES FOR BI-AXIAL AND TRI-AXIAL LAMINATES

Laminate Name	Configuration	E_1 (GPa)	E_2 (GPa)	ν_{12}	E_6 (GPa)
Bi-axial	[0/90]	16.7*	16.7*	0.06	2.01
Tri-axial	[0/±45]	17.6*	7.01	0.52	5.075

*: experimental observation (See Table 1)

In order to verify the results, elastic modulus of tri-axial composite with [0/90/-45] configuration is also calculated and compared with its original amount which has been obtained from experiment and reported by its supplier [9]. According to aforementioned calculation, amount of this elastic modulus is equal to 13.6 GPa and it is located in the reported interval in Table 1 (15±2.3 GPa). The obtained values in Table 2 (for bi-axial and tri-axial) laminates and experimentally obtained values for U-D fabrics (the first row of Table 1) are used as required mechanical properties in FE model. The lay-up sequence of the both shell and spar structures of the blade are entered into ANSYS very carefully in complete accordance with technical drawings of the blade. A cut section of a real finite element model considering thickness of different parts is depicted in Fig. 5.

The final check is carried out on the whole structure of the blade. The first natural frequencies of the blade associated with flap-wise and edge-wise are obtained using modal analysis of ANSYS and compared with available experimental data [12]. A good agreement between these results is reported in Table 3, which has established our confidence toward proper FE modelling of the blade.

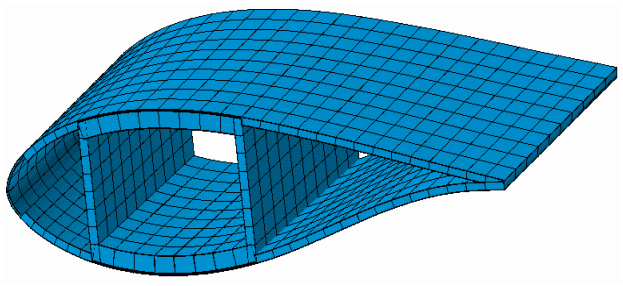

Fig. 5 A cut section of the FE model of the investigated blade

TABLE 3 FREE VIBRATIONS ANALYSIS OF INVESTIGATED WIND TURBINE BLADE

	Flap-wise frequency (Hz)	**Edge-wise frequency (Hz)**
FEA	1.089	1.953
Experimental data [12]	1.09	1.97
Error estimation %	0.09	0.8

V. LOADINGS

A wind turbine blade experiences different load cases during its mission arising from various resources. The load cases are defined as a combination of specific operating and external conditions [13] as illustrated in Fig. 6.

Due to the very rare occurrence of extreme external condition and fault operation conditions and as a result of insignificant influence of the events after the occurrence of the fault and transport, erection and maintenance on aeroelasticity, normal operating conditions and normal external conditions are taken into account in this research chapter.

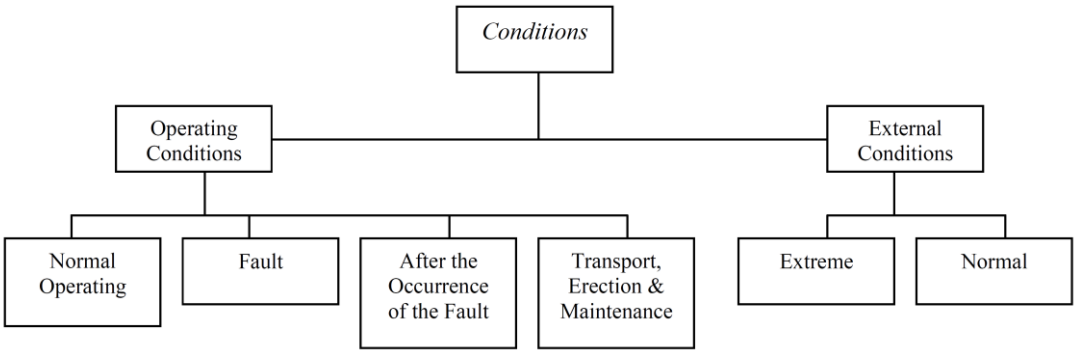

Fig. 6 Operating and external conditions on a wind turbine

Normal operating conditions are divided into four events: (i) stand-by, (ii) start-up, (iii) power production and (iv) normal shut-down events.

(i) Stand-by condition is defined as the situation that there is neither a fault/shut-down condition nor wind speed is outside the range of power production interval.

(ii) Start-up event takes place when the turbine is experiencing transient event either from stand-by to power production situation or from lower wind speed to higher value during power production.

(iii) In power production condition, a turbine generates power within cut-in and cut-out wind speeds.

(iv) Normal shut down implies on transient situation from power production to stand-by conditions or from a higher wind speed to a lower one.

The associated wind speeds with different events of normal operating conditions are presented in Table 4 accompanied with comprising load cases.

Among all load cases, aerodynamic loading on the blade is of a great importance for aeroelasticity analysis. The wind turbine blade is also subjected to other load cases consisting of blade, changes in wind direction, annual gust, centrifugal force, gyroscopic forces due to yaw movements of the turbine, force arisen from start/stop angular acceleration and activation of mechanical brake during different events. The aforementioned load cases were evaluated and it was found out that gyroscopic forces and the force arising from mechanical brake activation can be neglected in comparison with the other load cases. Aerodynamic loading is obtained using aerodynamical FEM which has been already constructed in section III. Germanschier Lloyd rules have provided a clear insight to calculate other mentioned load cases [13].

TABLE 4 CLASSIFICATION OF NORMAL OPERATING CONDITIONS AND INVOLVED LOAD CASES

Wind Speed V (m/s)	$V < 4$	$V = 4$	$4<V<25$	$V = 25$
Event / Load case	**Stand-by**	**Start-up**	**Power production**	**Shut-down**
Aerodynamic load	☑	☑	☑	☑
Weight of blade	☑	☑	☑	☑
Annual gust	☑	☑	☑	☑
Changes in wind direction	☑	☒	☑	☒
Centrifugal force	☒	☒	☑	☒
Gyroscopic forces	☒	☒	☑	☒
Start/stop angular acceleration	☒	☑	☒	☑
Activation of mechanical brake	☒	☒	☒	☑

VI. ANALYSIS OF FLUID-STRUCTURE INTERACTION (FSI)

A comprehensive aeroelastic analysis was performed on normal operating conditions of the turbine covering all stand-by, start-up, power production and shut-down events. For stand-by and start up events, wind speed is assumed equal to 4 m/s according to Table 4. For the event of shut-down, 25 m/s is chosen as the wind flow speed. For the interval of 4 to 25 m/s which is representative of power production event, once 15 m/s is selected as the rated wind speed and also another simulation is carried out on the most frequent wind speed in the mentioned interval. Statistical study on the governing wind pattern of the wind farm provides the probability density function of the wind regime in the form of the Weibull distribution [14]. Weibull function of the wind farm for the investigated turbine was expressed as [15]:

$$h(V) = \left(\frac{1.425}{9.3206}\right)\left(\frac{V}{9.3206}\right)^{(0.425)} e^{-\left(\frac{V}{9.3206}\right)^{1.425}} \tag{26}$$

where, V is a wind speed and $h(V)$ is the corresponding probability of occurrence. The mode wind speed as the most frequent happening wind speed is obtained as 5 m/s. The Weibull graph corresponding to Eq. (26) is drawn in Fig. 7.

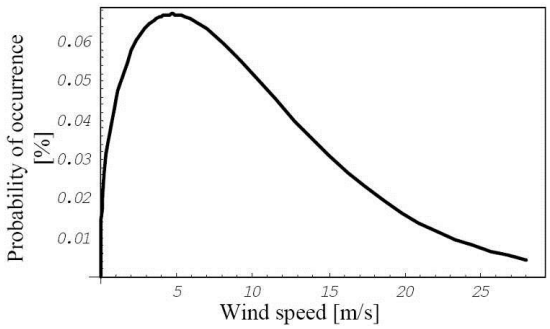

Fig. 7 Probability density function of the wind flow [15]

The global flowchart of semi-couple method for studying the fluid-structure interaction (FSI) of the blade is presented in Fig. 8. In this method an iterative approach is employed to investigate the aeroelastic behaviour of the wind turbine blade. The modelling procedure contains three different phases: aerodynamic analysis, structural analysis and convergence study.

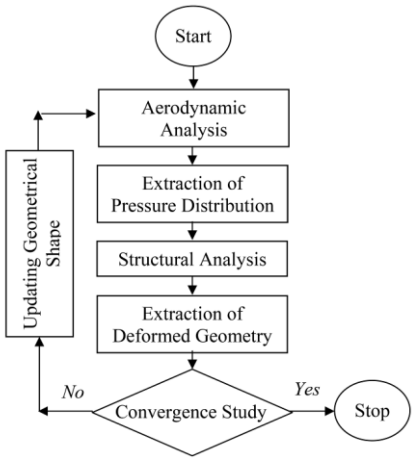

Fig. 8 Flowchart of semi-coupled approach for aeroelasticity study

The modelling starts by an aerodynamic analysis on the primary and undeformed geometry of the blade. The aerodynamic analysis is performed on constructed aerodynamic FE model (section III) using fluid solver of ANSYS software. The output of the aerodynamic analysis which is obtained in the form of pressure distribution on each node is converted to the structural loading for the preceding step of aeroelastic analysis. Obtained aerodynamic loadings and specific combinations of other load cases, summarized in Table 4, are applied to the structural FE model. A non-linear static analysis is executed on structural FE model to obtain deformed shape of the blade. The main reason of conducting non-linear analysis is placed behind the fact that the long and flexible structure of the blade experiences the nonlinearly in the form of large rotation. The deformed shape of the blade is considered as the updated geometrical shape for aerodynamic analysis in the next iteration and the whole procedure is repeated till the convergence is met. The solution is converged when the deflection of the blade experiences stationary status. If the convergence is met, the iteration stops and the final results are reported.

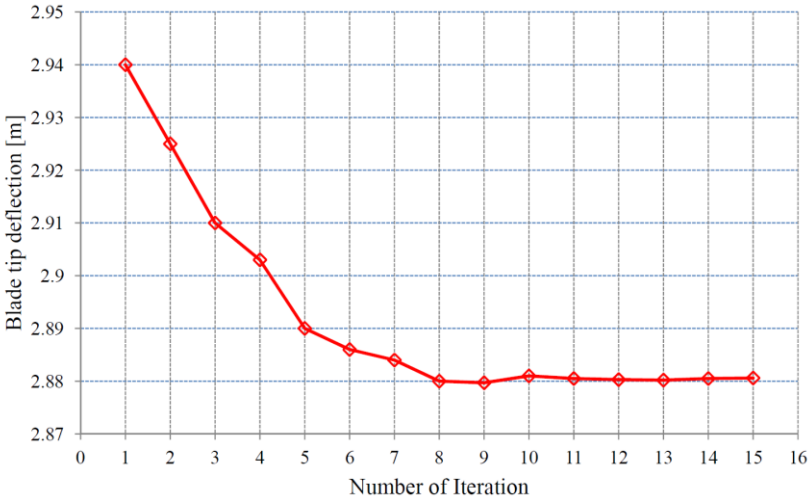

Fig. 9 Convergence of iterative aeroelastic solution

A sample convergence study for iterative aeroelastic simulation is shown in Fig. 9 for the event of power production wherein wind flow speed is taken equal to 5 m/s. It can be seen from Fig. 9 that the solution is converged after eight iterations.

VII. RESULTS AND DISCUSSION

The variation in aerodynamic loading arisen from aeroelasticity phenomenon is reported in Fig. 10 for different events in comparison with corresponding events without aeroelastic coupling consideration. It can be inferred from presented results in Fig. 10 that the most influenced case is attributed to the power production event at rated wind speed which will significantly affect the power production efficiency of the wind turbine. Although the maximum wind speed is used in the aeroelastic simulation for the event of normal shut-down, the variation is less pronounced comparing to power production and start-up. This is originated from the fact that in this event the blade is rotated using pitch mechanism, thus total deflection of the blade will be reduced. So it can be understood that pitch power regulating mechanism does not only regulate the power production of the turbine by adjusting aerodynamic performance of the blade but also has a positive influence on structural behaviour of the blade by exposing stiffer cross sections of the blade to the experienced loadings.

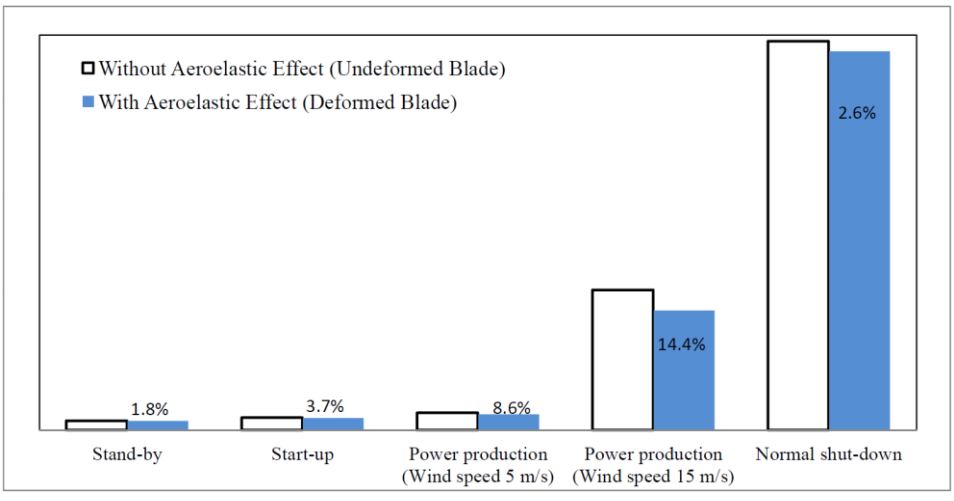

Fig. 10 Variations in aerodynamic loading due to aeroelastic coupling [16]

As a matter of fact, the results imply that the blade deformation has a considerable influence on aerodynamic loadings. For better understanding of this correlation, the distribution of aerodynamic forces along the blade length is presented in Fig. 11 for the event of power production at rated wind power speed (V=15 m/s). The results reveal significant reduction in aerodynamic forces which stems from variations in the effective angle of attack of blade cross sections at different stations.

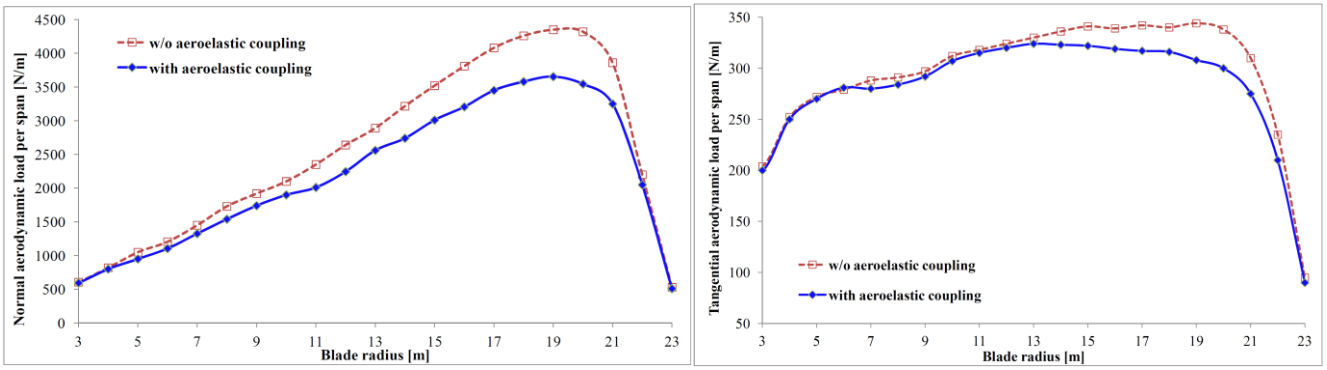

Fig. 11 Distribution of aerodynamic forces at rated wind speed

As a consequence of the variation in aerodynamic loadings, it is expected that induced stress components in critical regions of the blade structure vary too. A comparison between maximum stress components with both aeroelastic coupling and without aeroelastic coupling is presented in Table 5. It is worth mentioning that due to the pitch control system, the location of critical regions wherein maximum stress components are experienced varies for each event in accordance with global status of the blade. Due to unsymmetrical lay-up sequence of composite laminates in the blade structure, it can be seen that induced stress components in some cases are increased.

TABLE 5 MAXIMUM STRESS COMPONENTS AND TIP DEFLECTION OF THE BLADE [16]

Event	Tip Deflection (m)		Longitudinal Stress (MPa)		Transverse Stress (MPa)		In-plane Shear Stress (MPa)	
	A*	B**	A	B	A	B	A	B
Standby	1.22	1.23	503.2	520.1	12.2	13.6	19.7	21.3
Start-up	1.64	1.67	602.4	650.3	9.3	12.9	30.1	32.5
Power production (5 m/s)	2.88	2.94	693.2	705.3	14.6	15.8	28.1	29.2
Power production (15 m/s)	4.07	4.21	762.6	725.0	17.3	15.5	20.4	18.1
Shut-down	4.28	4.33	747.6	764.0	27.41	19.0	17.6	21.3

*A: results with aeroelastic coupling, **B: results without aeroelastic coupling [17]

VIII. CONCLUSIONS

Subjected to different load cases arisen from variety of experiencing events, the blades of modern HAWTs are fully made of composite materials to provide a strong and light structure. The very large and flexible structure of the wind turbine blade necessitates the investigation of aeroelasticity phenomenon for better understanding of the aerodynamic performance of the blade in capturing the wind energy. The interaction between elastic and aerodynamics forces, i.e. static aeroelasticity, is studied for a composite wind turbine blade. A 3D finite element model of the blade is built. A proper aerodynamic model is constructed for extracting aerodynamic forces due to the considerable contribution of this load case in mechanical behaviour of the blade. Another finite element model for application of structural analysis is also built on the same geometry platform of the aerodynamic model while all detailed structural aspects are taken into account. The mechanical properties of all comprising composite laminates are extracted using available limited experimental data and the model is verified to raise the confidence toward employment of proper FE model. In addition to the aerodynamic forces, other load cases, occurred during the normal operating conditions of the blade, are identified and evaluated.

A semi-couple approach is utilized for studying fluid-structural interactions. At the very first stage, the preliminary geometry of the blade (unreformed shape) is analyzed and aerodynamic forces are extracted. All load cases are applied to the structural FE model and non-linear static analysis is carried out to obtain the deflected shape of the blade. The deformed shape of the blade is used to extract updated aerodynamic forces in accordance with updated geometry of the blade and then the results of aerodynamic forces are inserted into structural solver as the input. This approach is repeated until the stationary deflected shape of the blade is obtained. Four different normal operating conditions as stand-by, start-up, power production and normal shut-down are analyzed. For the event of power production, two different wind inflow speed associated with rated wind power and also the mode wind speed value obtained from statistical analysis of governing wind pattern are studied. The results demonstrate that generally efficiency of wind turbine blade is reduced due to the variations imposed to the effective angle of attack along the length of the blade. Since the investigated wind turbine blade is equipped with pitch power regulating mechanism, which can rotate blade along its length with wind inflow speed variation, the total deflection of the blade does not

necessarily increase in higher wind speeds. The results imply on variations of the induced stress levels in critical regions which is important from structural point of view.

REFERENCES

[1] Y. Golfman, *Hybrid Anisotropic Materials for Wind Power Turbine Blades*, CRC Press, Taylor & Francis Group, 2012.

[2] A. Brent Strong, *Fundamental of Composites Manufacturing Material, Methods, and Applications*, 2nd ed., Society of manufacturing engineers, 2008.

[3] D. A. Spera, *Wind Turbine Technology*, ASME Press, New York, 1994.

[4] http://www.vestas.com/.

[5] Ansys Ver 5.4, User Manual, Element Manual, SAS IP Inc., 2003.

[6] "Prepreg technology," Hexcel Composites, Duxford, 1997.

[7] H. J. Sutherland, "On the fatigue analysis of wind turbines," Sandia National Laboratories, Albuquerque, New Mexico, Jun. 1999, SAND99-0089.

[8] J. F. Mandel, D. D. Samborsky, D. S. Cairns, "Fatigue of composite materials and substructures for wind turbine blades," Sandia National Laboratories, Albuquerque, New Mexico, March 2002, SAND2002-0771.

[9] "HexPly Data Sheets, M9.6 Series for Wind Turbine Blade Application, Hexcel Composites Co., 2002.

[10] Data Sheets, M9.6 Series for Wind Turbine Blade Application, Hexcel Composites Co., France Branch, 2002.

[11] S. W. Tsai, S. V. Hoa, D. Gay, Composite Materials, Design and Applications, CRC Press, 2003.

[12] "Technical Description: SSN47-660," Sabaniroo Co., Iran, 200.

[13] Germanischer Lloyd, *Rules and Regulations, IV – Non-Marine Technology*, Regulation for the certification of Wind Energy Conversion System, Germany: Germanischer Lloyd, 1993.

[14] R. Gasch, J. Twele, *Wind Power Plants, Fundamental, Design, Construction & Operation*, James & James, 2002.

[15] M. M. Shokrieh, R. Rafiee *Fatigue life prediction of wind turbine rotor blades manufactured from composites*, In: Vassilopoulos, A. P., Editor, *Fatigue Life Prediction of Composites and Composite Structures*, Woodhead Publishing Limited, Oxford Cambridge New Delhi, 2010.

[16] R. Rafiee, M. Fakoor, "Aeroelastic investigation of a composite wind turbine blade," Wind and Structures, In Press, 2013.

[17] M. M. Shokrieh, R. Rafiee, "Simulation of fatigue failure in a full composite wind turbine blade," Composite Structures, vol. 74, pp. 332-342, 2006.

Dr. Roham RAFIEE has received his PhD in 2010 from mechanical engineering Dept. of Iran University of Science and Technology focusing on nanocomposites. He has done his MSc and BSc theses in the field of composite materials and structures. He has published 20 ISI papers, 30 international conference papers and two chapters of two different books in Woodhead publishing and Springer. He has also registered three patents in the field of nanocomposites and composite structures. He has 11 years of experience in different industrial sections including wind turbines, composite pipes, strategic planning and technology transfer projects. His research interests can be summarized as carbon nanotube reinforced polymers, mechanics of composite materials, design and analysis of composite structures, fatigue modelling of composite structures, finite element modelling and analysis. He is currently an assistant professor of the Faculty of New Sciences and Technologies in University of Tehran. He is already the vice president of a company producing composite pipes and also member of the board of a company producing wind turbines. He is also senior consultant of different companies and industrial group. He is currently cooperating with University of Weimar (Germany) as a member of PhD community and also UPM (Malaysia) as an advisor of PhD thesis.

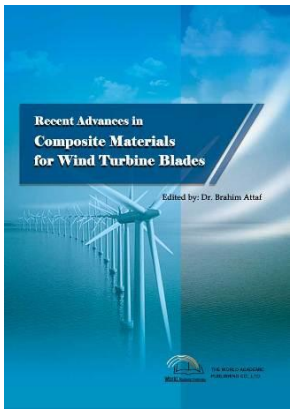

Recent Advances in Composite Materials for Wind Turbine Blades
Edited by Dr. Brahim Attaf

ISBN 978-0-9889190-0-6

Hard cover, 232 pages

Publisher: The World Academic Publishing Co. Ltd.

Published in printed edition: 20, December 2013

Published online: 20, December 2013

This book of science and technology provides an overview of recent research activities on the application of fibre-reinforced composite materials used in wind turbine blades. Great emphasis was given to the work of scientists, researchers and

industrialists who are active in the field and to the latest developments achieved in new materials, manufacturing processes, architectures, aerodynamics, optimum design, testing techniques, etc.. These innovative topics will open up great perspectives for the development of large scale blades for on- and off-shore applications. In addition, the variety of the presented chapters will offer readers access to global studies of research & innovation, technology transfer and dissemination of results and will respond effectively to issues related to improving the energy efficiency strategy for 2020 and the longer term.

How to cite this book chapter

Rafiee R. (2013). On the Fluid-Structure Interaction of a Composite Wind Turbine Blade, *Recent Advances in Composite Materials for Wind Turbines Blades*, Dr. Brahim Attaf (Ed.), ISBN 978-0-9889190-0-6, WAP-AMSA, Available from: http://www.academicpub.org/amsa/chapterInfo.aspx

World Academic Publishing - Advances in Materials Science and Applications

Chapter 6

Spar Shape Optimization of a Multi Megawatt Composite Wind Turbine Blade: Modal Analysis

Mostapha Tarfaoui[*1], Owaisur Rahman Shah[1]

[1]ENSTA-Bretagne, MSN/LBMS/DFMS
2 rue François Verny, 29806 Brest Cedex – France
[*1]mostapha.tarfaoui@ensta-bretagne.fr

I. INTRODUCTION

The problem of energy that we face today revolves around two main factors: energy generation/transmission and greenhouse gas emissions. Renewable energy sources are an inevitable part of the solution, and wind energy is, at the moment, the fastest growing installed production technology.

We are currently witnessing a substantial growth in the wind energy sector worldwide. This growth is expected to accelerate even more in the foreseeable future. This means that a massive number of wind turbine blades will be produced in the forthcoming years. There is a large potential for economizing material in these blades. Commercial wind turbines have increased consistently in size during the past thirty years, largely for the economic reasons in an attempt to reduce the cost of electricity generation. This is due to the fact that the wind speed – and hence the wind power captured – increases with altitude and that reducing the number of individual turbine units helps reduce the overall cost of a wind farm, especially in the case of offshore farms. Currently the largest machine; has a rated output of 5MW and a rotor diameter of 124m and so the question arises as to what the ultimate limits on size might be? The increase in diameter also makes the requirements related to rotor and blade mass more severe. For a complete discussion of design requirements, interested readers can refer to Burton et al. [1].

As part of the certification procedure, all wind turbine blade prototypes are subjected to an experimental test procedure in order to ensure that the produced wind turbine blade fulfils the actual design and safety requirements. In addition to experimental tests of load carrying capacity under extreme loading, and tests of its fatigue resistance, it is common practice to compliment with these the tests related to basic dynamic properties of the blades, such as natural frequencies and damping properties, as these are essential for the structural integrity of the entire wind turbine. Usually, these dynamic characteristics are determined for the first 3 - 4 flexural bending modes and for the first torsional mode.

However, detailed knowledge of natural frequencies and structural damping characteristics does not in itself guarantee/ensure an optimal dynamic behaviour of the wind turbine, when subjected to aerodynamic forces arising from the applied wind field. In recent years, stability problems in wind turbine structures have obtained increased attention due to the trend towards larger and more flexible structures. A well-known example of a stability problem, that eventually might lead to failure of the whole structure, is the occurrence of dynamically unstable edgewise vibrations (flutter). For aerodynamic loading in general, and for dynamic stability problems in particular, the deflection patterns of the wind turbine blades are of vital importance. For a wind turbine blade, the deflections of interest include; lateral translations (flapwise, edgewise) and cord rotation (about the blades longitudinal axis).

For reasons of simplicity the wind turbine blades are usually modelled as beam structures for running aeroelastic computations. Warping is usually neglected, justified by the fact that the main components are structures with closed cross sections, whereas the structural couplings between flexural bending in the two principal directions and structural couplings between torsion and flexural bending are usually included, as such structural couplings may significantly affect the aerodynamic load characteristics of a wind turbine blade. Although, in principle, included in the traditional Euler or Timoshenko beam modelling of wind turbine blades, the correct specification of such structural couplings is a delicate matter.

Modal analysis is by far the most common method used to characterize the dynamics of mechanical systems, and it produces very illustrative and easily interpretable results. Modal analysis has also been used to identify approximate mode shapes, associated with the dominating deflection direction only (i.e. mode shapes excluding structural coupling between torsion, flapwise and edgewise deformations), of medium size wind turbine blades [2].

Large wind turbine blades are typically manufactured with thin skins made of composite materials. Glass fibre/epoxy and wood laminates/epoxy are the most commonly used materials, but carbon fibre composites are also finding their way in

recently. Wind turbine blades are usually constructed from several parts glued together: compressive side, tensile side and shear webs. Their external geometry is fairly complex, made of 3D surfaces resulting from the aerofoil sections put together with varying twist angles, chord lengths and pitch axis locations. With regard to of the internal structure, the manufacturing methods often result in thick adhesive joints in key structural locations and this can be represented in numeric/computer models by 3D adhesive mesh elements.

The design of a wind turbine structure involves many considerations such as strength, stability, cost and vibration. Reduction of vibration is a good measure for a successful, safe design of the blade structure. It may foster other important design goals, such as low cost and high stability level. A good design philosophy for reducing vibration is to separate the natural frequencies of the structure from the harmonics of rotor speed. This would avoid resonance where large amplitudes of vibration could severely damage the structure. Frequency placement is one of the techniques used for separating frequencies. An objective function is formulated for minimizing the discrepancies between the desired frequencies and the actual ones [3]. The chosen design variables were the values of a set of lumped masses located at specified points along the blade span as well as the distribution of the wall thickness of the main box-beam cross section. The resulting optimum solutions were strongly dependent on the values of the desired (target) frequencies, which are chosen fairly arbitrarily. Pritchard and Adelman [4] formulated a mathematical programming optimization model by considering minimization of the induced shearing forces at rotor hub as a measure of vibration reduction. Design variables were taken to be the sizes and locations of the tuning masses along blade span, which has the disadvantages of increasing structural mass. Other techniques, sometimes referred to as "modal shaping" or "modal tailoring", alter the vibration mode shapes of the blades through mass and stiffness modification to make them less responsive to the air-loads [5, 6].

This chapter describes the creation of a numerical model which parametrically describes the geometry of the blade with composite materials for wind turbines of 5MW. Full FE models of the blades are constructed and solved in the time or frequency domain to capture all relevant behavioural aspects and stability issues. Two different issues are discussed here. First, being the choice of three degrees of freedom in each cross-section to describe the motion of the blade. Whereas the second is the extraction of mode shapes and natural frequencies of the blade.

II. BLADE GEOMETRY

The main objective in the design of wind turbines is to find a rotor that meets the basic conditions required. The most important condition is to get a rotor to deliver the required power output at a particular wind speed. It is necessary to take into account the importance of the geometry of the rotor, first and foremost taking into consideration the aerodynamic performance, strength and stiffness conditions and most importantly, the costs.

The turbine has an intended power rating 5MW with a blade length of 48m, aerodynamic characteristics were obtained through a study of commercially available examples, where we had the distribution curves of chord, the twist, the pre-bend, thickness, and the distance between the pitch axis and the trailing edge of several blades used at our disposal. A numerical model was created by averaging all the above mentioned data.

Once all the values have been determined, we selected the airfoil profiles. The chosen standard was that of DUWind (Research on wind energy at the Delft University of Technology). Then, we searched the published data, the original coordinates of each of these airfoils (raw sections), and both the extrados and the intrados. Four different types of airfoils were selected, excluding the circle and transitions, as illustrated in Fig. 1.

The blade that we will study is assembled on a three-bladed offshore wind turbine which generates a maximum power of 5MW. The general specifications of the studied blade are given in Table 1.

- *Circle*
- *CircleTrans172*
- *CircleTrans144*
- *CircleTrans71*
- *DU-00-W2-401*
- *DU-00-W2-350*
- *DU-91-W2-250*
- *DU-93-W-210*

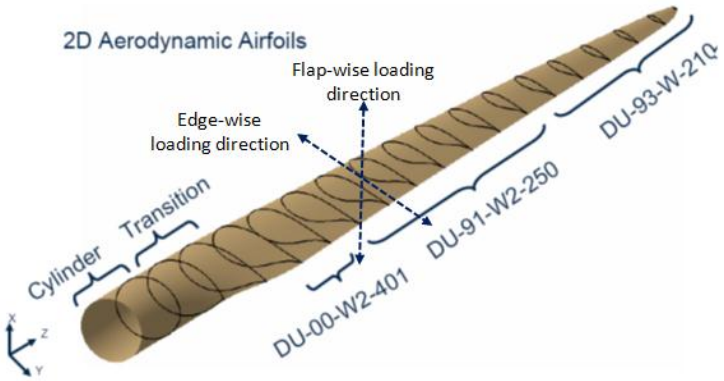

Fig. 1 Different Airfoils along the blade

TABLE 1 GENERAL SPECIFICATIONS OF THE BLADE

Length (mm)	48000
Maximum cord (mm)	3932
Position twists maximum (mm)	R9000
Fluid speed upstream of blade (m/s)	25
Angular velocity (rpm)	15,7
Frequency of solicitation: Fr (Hz)	0,26
Power (MW)	5

A. Choice of the Profile

Fig. 2 shows the variation of the optimum power coefficient (C_p) with the designed tip-speed ratio (TSR) for a blade made of NACA 4-digit airfoil families. It is seen that C_p increases rapidly with TSR up to its optimum value after which it decreases gradually. The optimum range of the TSR is observed to lie between 6 and 11, depending on the type of airfoil. The effect of wind shear and tower shadow result in a reduction of the power coefficient by about 16%. The value of the designed TSR at which $C_{p,max}$ occurs is also reduced by about 9%. It is also observed that blades with NACA 1412 and 4412 produce higher power output as compared with other airfoil types. Fig. 3 gives a schematic representation of initial profile NACA 4412 selected with the blade representation. The results of the optimal distribution of the cord for a blade of 48m in diameter and having various profiles are summarized in Fig. 4.

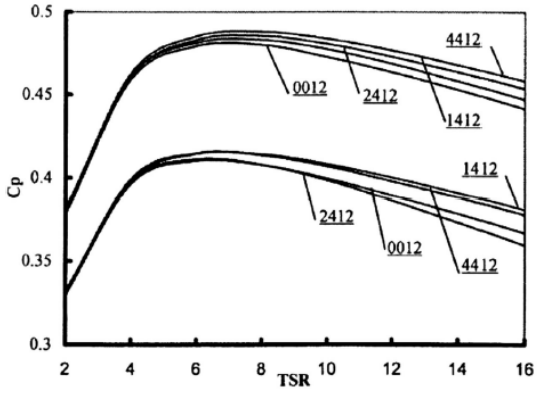

Fig. 2 Variation of the optimum power coefficient with TSR for a three bladed rotor of NACA 4-digit airfoil [1]

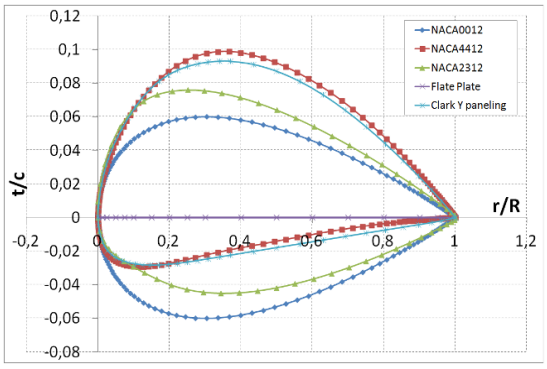

Fig. 3 Section profiles, NACA 4412

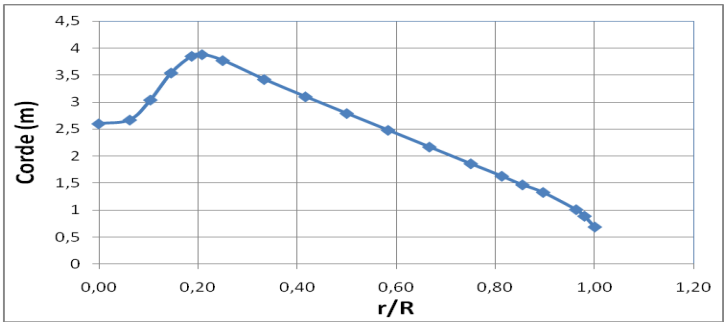

Fig. 4 Evolution of the blade chord; profile NACA 4412

B. Extrados, Intrados and Spar

The design of the aerofoil profile of a wind turbine blade is a compromise between aerodynamic and structural (stiffness) considerations. Aerodynamic considerations dominate the design of the outer two thirds of the blade while structural considerations are more important for the design of the inner one third of the blade. Structurally the blade is typically hollow, with the outer geometry formed by two shells: one on the suction and one on the pressure side. To transfer shear loads, one or more structural webs perpendicular to the airfoil cord, are fitted to join the two outer shells together, as shown in Fig. 5.

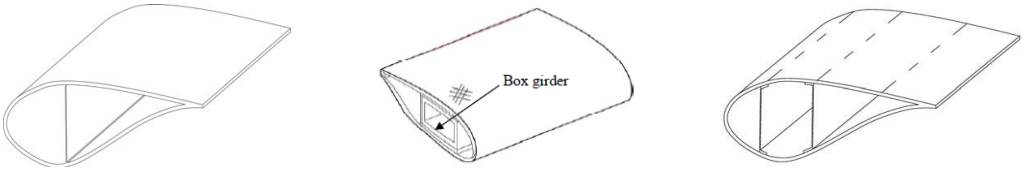

(a) *(b)* *(c)*

Fig. 5 Sketches of different blade concepts

III. FINITE ELEMENT MODELLING AND STRUCTURAL DESIGN OPTIMIZATION

The finite element method (FEM) is very useful and has traditionally been used in the development of wind turbine blades in order to investigate the overall behaviour in terms of, for example, eigen-frequencies, tip deflections, and global stress/strain levels.

Only a limited number of publications on Finite Element (FE) modelling and structural analysis of wind turbine blades are available in the current literature [7-13]. This research field is becoming increasingly important as the blades gradually are becoming sufficiently large enough to cause flutter instability.

A. Shear Web Transverse Placement

The transverse placement of the shear webs within the aerofoil sections naturally influences the structural properties of the assembly. Due to the twist angle variations along the blade length, a bending loading state always induces torsion in some sections of the blade. This torsion modifies the angle of attack of the aerodynamic surfaces; in turn causing a modification in loading: such a phenomenon is generally described as aero-elastic.

The finite element method has traditionally been used in the development of wind turbine blades, mainly to investigate the general behaviour in terms of, for example, its eigen-frequencies, tip deflections, and global stress/strain levels. This type of FE-simulation usually predicts the global stiffness and stresses with a good accuracy. Another factor is that a relatively simple shell model can be used for representing the global behaviour, while a computationally more expensive 3D-solid model may be necessary to predict this localized behaviour.

The influence of the shear-web placement on the blade mass, bending stiffness and bending-torsion coupling is studied in this chapter. Five different geometries are examined as shown in Fig. 6. In each one, the shear-webs are moved in opposite directions further from one another, from being very close to one another to being near the leading and trailing edges.

(1) Blade with web of form T (39% length of the cord)
(2) Blade with one shear web (39% length of the cord)
(3) Blade with two shear webs (between 49% and 29% length of the cord)
(4) Blade with three shear webs (between 49% and 29% length of the cord)
(5) Blade with web of form H (between 49% and 29% length of the cord)

In a concern of being most precise and of formulating the most adequate model, we chose to carry out two types of modelling:

- The first one uses shell elements for the modelling of the blade formulated in only one part.
- The second models the components of the blade with separate part:
  - The blade alone (modelling with shell elements).
  - The spar (with a 1 or 2 shear webs, modelling with shell elements).
  - The adhesive (modelled by 3D elements)).

For an optimization study of the blades, Fig. 6 shows the finite element models associated with different geometrical shapes of webs. In the next section of this work one will consider that:

✓ Model 1: blade with spar with only one web (created with only one part).
✓ Model 2: blade with spar with two webs (created with only one part).

- ✓ Model 3: blade with spar forms H (created with only one part).
- ✓ Model 4: all (created with 4 independent parts): blade, spar with only one web and adhesive, Fig. 7.
- ✓ Model 5: all (created with 4 independent parts): blade, spar with two webs and adhesive, Fig. 7.

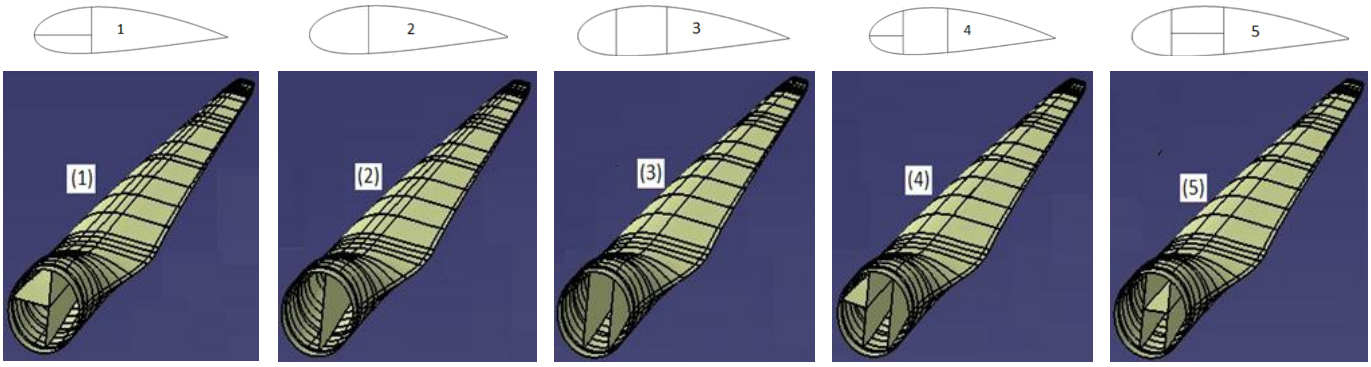

Model (1) *Model (2)* *Model (3)* *Model (4)* *Model (5)*

Fig. 6 Blades with different shear-web transverse placement

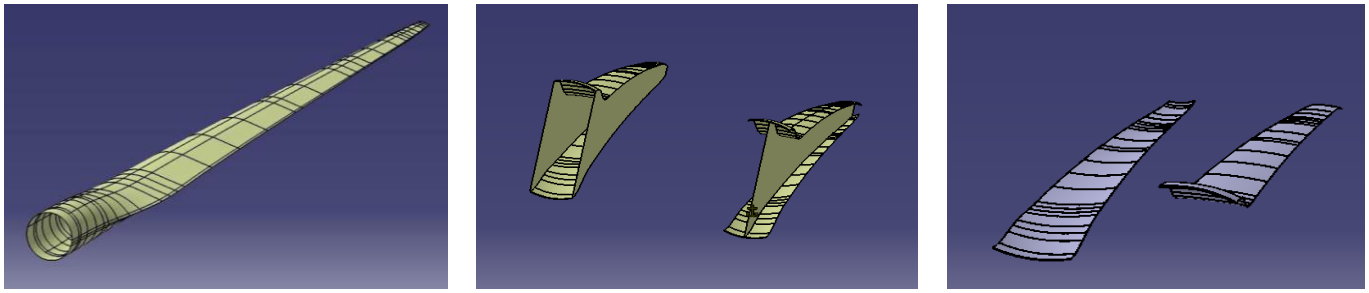

(a) Blade, intrados/extrados, shell elements *(b) Spar, shell elements* *(c) Adhesive, 3D elements*

Fig. 7 Blade FE model with 4 independent parts

B. Materials and Lamination Strategy

A wide range of materials and manufacturing techniques are utilized in the wind turbine industry. The material combinations used are predominantly composite laminates with embedded threaded steel rods in the root section connecting the blade to the turbine hub. In bolted connection polyester, vinylester and epoxy resins are common, matched with reinforcing wood, glass and carbon fibres. Some designs integrate carbon and glass fibre as well as birch and balsa wood [14-15].

Both the materials and the lamination strategy are selected through the UpWind data. UpWind is a European project funded under the Sixth EU Framework Program. Its task is to design powerful wind turbines (8-10 MW) for both onshore and offshore installation. The materials used were of 5 different types: UD, Triax, R4545, Foam and Webs, whose properties are shown below in Table 2a. The mechanical properties of composite materials are given in Table 2b. The laminates used, consist of plies with various orientations. Here, the UD, the Triax and the R4545 are composite materials (orthotropic) while the rest are isotropic materials, in order to achieve the best cost and weight saving. The materials and lamination strategy chosen for blade of 48m long was: a triax stack with adhesive to decrease the natural frequency of the blade. Also, within the UpWind strategy, the Shear Webs will be changed to Foam, because it has higher density and a lower natural frequency. To better understand, Table 3 shows the lamination which we will consider, section by section. Fig. 8 shows the lamination zones of the blade. The distribution thickness over the blade length is given in Table 4.

TABLE 2 MATERIAL SPECIFICATIONS

Materials		**E_{11} (MPa)**	**E_{22} (MPa)**	**G_{12} (MPa)**	**ν_{12}**	**ρ (kg/m³)**
Orthotropic Composites	UD	38887	9000	3600	0,249	1869
	TRIAX	24800	11500	4861	0,416	1826
	R4545	11700	11700	9770	0,501	1782
Isotropic Composites	SKINFOAM	256	256	22	0,3	200
	ADHESIVE	3000	3000	1150	0,3	1200

(a) Mechanical properties of materials used

Laminates	Plies (°)
UD	0
TRIAX	[-45/0/45]
R4545	[-45/45]

(b) Orientation of the layers of the laminates

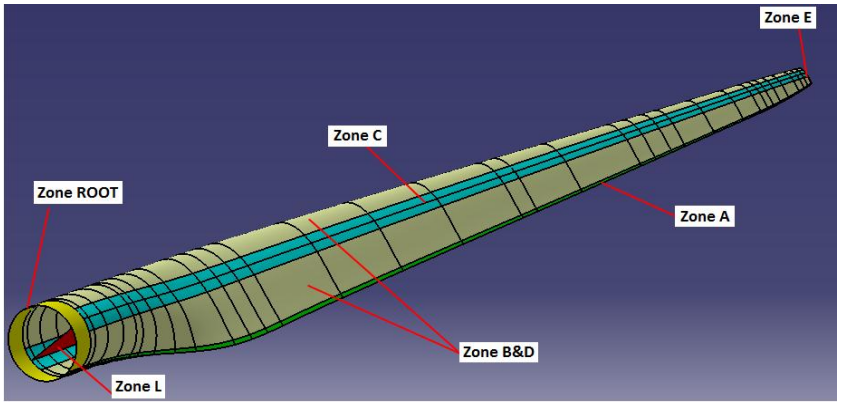

Fig. 8 Lamination zones of the blade

TABLE 3 PARTITION ZONES

Zone	Localization
L	Shear webs
ROOT	Zone fixing of the blade
A	Zone joining of the blade
B&D	Zone leading and trailing edge
C	Contact blade/Shear webs
E	Blade tip

TABLE 4 DISTRIBUTION THICKNESS ALONG THE BLADE ON THE CONTACT ZONE: BLADE/SPAR

r (m)	e (mm)
0 - 0.9	90.24
0.9 - 1.2	32.2
1.2 - 3	34.2
3 - 5	19.16
5 - 7	53.88
7 - 9	94.36
9 - 12	93.42
12 - 16	91.54
16 - 20	85.9
20 - 24	80.26
24 - 29	72.74
29 - 32	60.99
32 - 36	51.12
36 - 37	33.73
37 - 41	20.1
41 - 47.97	12.11
47.97 à48	12.11

C. Mesh Part

For the 5 developed models, shell elements of type S4R were used. Below, are the characteristics of the 5 models with a 200 mm mesh element size. Solid elements C3D8R were used to mesh the adhesive (models 4 and 5). Fig. 9 shows an example of the mesh carried out for model 3. The difference between the two cases of materials assignment affects the mass of the intrados/extrados face and webs (see Table 5). The overall assets of the blade are almost the same for the two types of modelling.

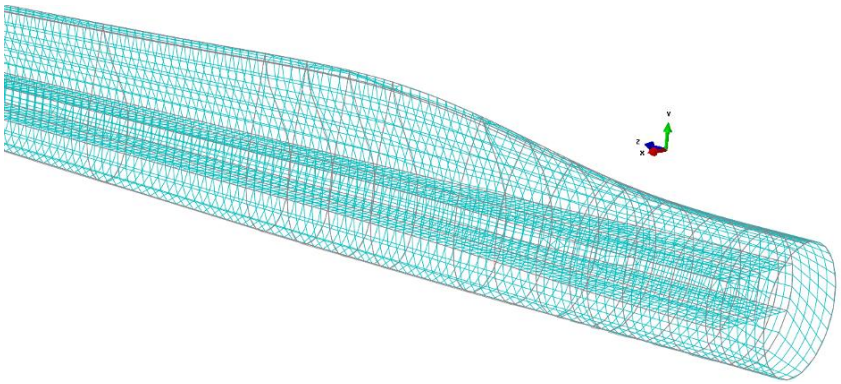

Fig. 9 High fidelity finite element model of a wind turbine blade, mesh of model 3

TABLE 5 CHARACTERISTICS OF THE MODELS

	Model	Masse (T)	Number of elements	Number of nodes	Element type	Element size (mm)
case 1	Blade without spar	11.19685	14336	14307	S4R	200
	1	12.91847	10200	9926	S4R	200
	2	13.78327	11636	11086	S4R	200
	3	14.25972	12480	11703	S4R	200
case 2	Blade without spar	6.31685	24344	24582	S4R	200
	4	12.91637	21993	26088	S4R+C3D8R	200
	5	13.77408	24336	28108	S4R+C3D8R	200

The mass of the various components of the blade enables us to target the optimizable zones of to save on the materials used. One can see the distribution of the mass of the blade for each portion in Table 6. It is clear that the heaviest part of the blade is in its first 10 meters. It is the critical zone where the damage and the failure of the blade are, in general, localized. It is always necessary to reinforce the structure at this location. It also shows that the sensitivity of this zone is related to the variation thickness of the blade, therefore there is an abrupt fall in the mass and thickness.

Note that, as the shear-web spacing increases, the blade mass grows significantly. This is because in the particular layup used, the composite stack applied in the outer skin in-between the two shear-webs is significantly heavier than that applied near the leading and trailing edges. In terms of blade stiffness, one can see that the increase in shear-web spacing also brings higher stiffness values, both in terms of linear and angular displacements. Although the analysis results presented here are valid, they raise the question of cross-coupling between the various design parameters, and it emerges that parameter that sweeps with cross coupling of several independent parameters would be necessary. Alternatively, and perhaps more comprehensively, optimization graphs could be produced from the script where iso-parameter contours can be interpolated, improving the understanding of the interdependency between various design parameters.

TABLE 6 EXAMPLE OF THE BLADE MASS DISTRIBUTION FOR MODEL 1, 2 AND 3

	Model 1	Model 2	Model 3
r(m)	**m_1**	**m_2**	**m_3**
0 - 10	4.98625	5.28053	5.41147
10 - 15	1.99579	2.11253	2.17563
15 - 20	1.73363	1.83743	1.89523
20 - 25	1.45289	1.54405	1.59631
25 - 30	1.14438	1.22373	1.26947
30 - 35	0.78333	0.85035	0.89086
35 - 40	0.45732	0.51200	0.54795
40 - 45	0.26461	0.30575	0.33611
45 - 48	0.10027	0.11690	0.13669
Total mass	12.91847	13.78327	14.25972

IV. MODAL ANALYSIS

To estimate the mode shapes and natural frequencies, a modal analysis is performed by using Abaqus computational code. The blade structure properties are approached by neglecting the elasticity (but not the weight) of the tip brake mechanism and by assuming the root part to be fully clamped (Fig. 10). Furthermore, the material damping properties are not taken into account. Basically, the blade model is a shell model. The defined surface area is subsequently subdivided into 8-nodes quadrangular and 6-nodes triangular shell elements with quadratic interpolation functions. The performed modal analysis gives estimates of all natural frequencies and mode shapes, for the investigated blade up to, and including, the first torsional natural

frequency. The estimated natural frequencies and mode shapes for the five models obtained from a FE model of the investigated blade have been compared. The natural frequencies, obtained from modal analysis, are presented in Table 7. This study is done in order to evaluate the state-of-the-art blade modelling capacity and in addition to gain inspiration for further improvements.

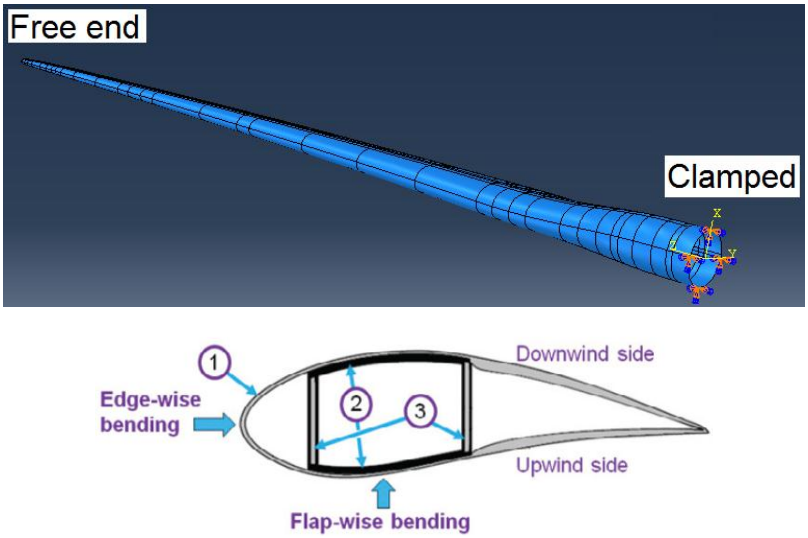

Fig. 10 Boundary conditions of the modal study

TABLE 7 MODES AND DEFLECTIONS

Model	1st mode (flap-wise)	2nd mode (edge-wise)	3rd mode (flap-wise)
1	0.76632	0.88886	2.2711
2	0.68936	0.82776	2.1051
3	0.66633	0.80179	2.0397
4	0.71308	0.8521	2.1566
5	0.69261	0.83065	2.1157
Model	**Deflection (mm)**		
1	1.338	1.239	1.124
2	1.205	1.259	1.101
3	1.202	1.253	1.102
4	1.217	1.274	1.107
5	1.198	1.249	1.101

A. Mode Shapes

The mode shape results, associated with the lowest 2 blade natural frequencies, are illustrated in Fig. 11. For each particular mode, the modal deflection has been resolved in a flapwise, an edgewise and a torsional deflection. For each deflection component, an example of the eigenforms obtained from the FE-modelling of model 3 is done for illustration. In order to facilitate the interpretation, the cross section displacement and rotation, associated with the FE-modelling, is defined as displacement and rotation of a line connecting the leading edge with the tailing edge for a given cross section. In analogy, the bending deflection is defined as the deflection of a radial spline, along which the longitudinal web is attached to the blade surface. A mode shape is uniquely determined apart from amplitude.

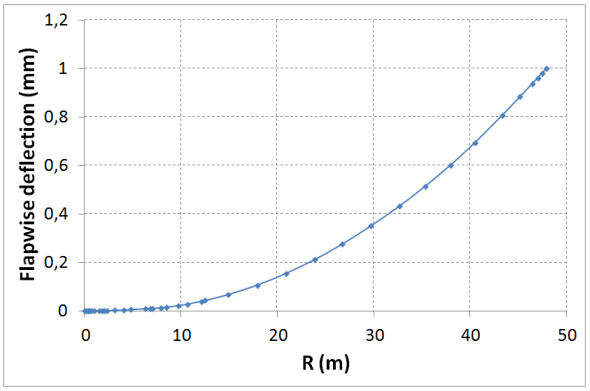

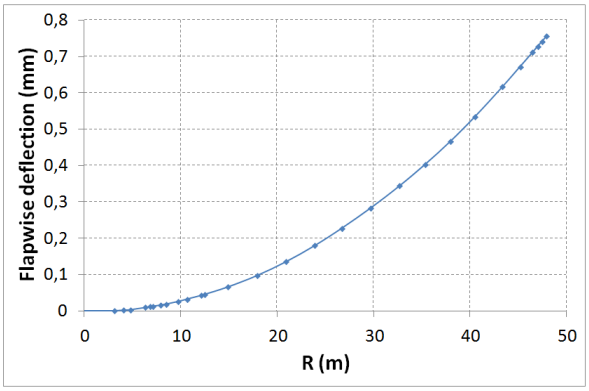

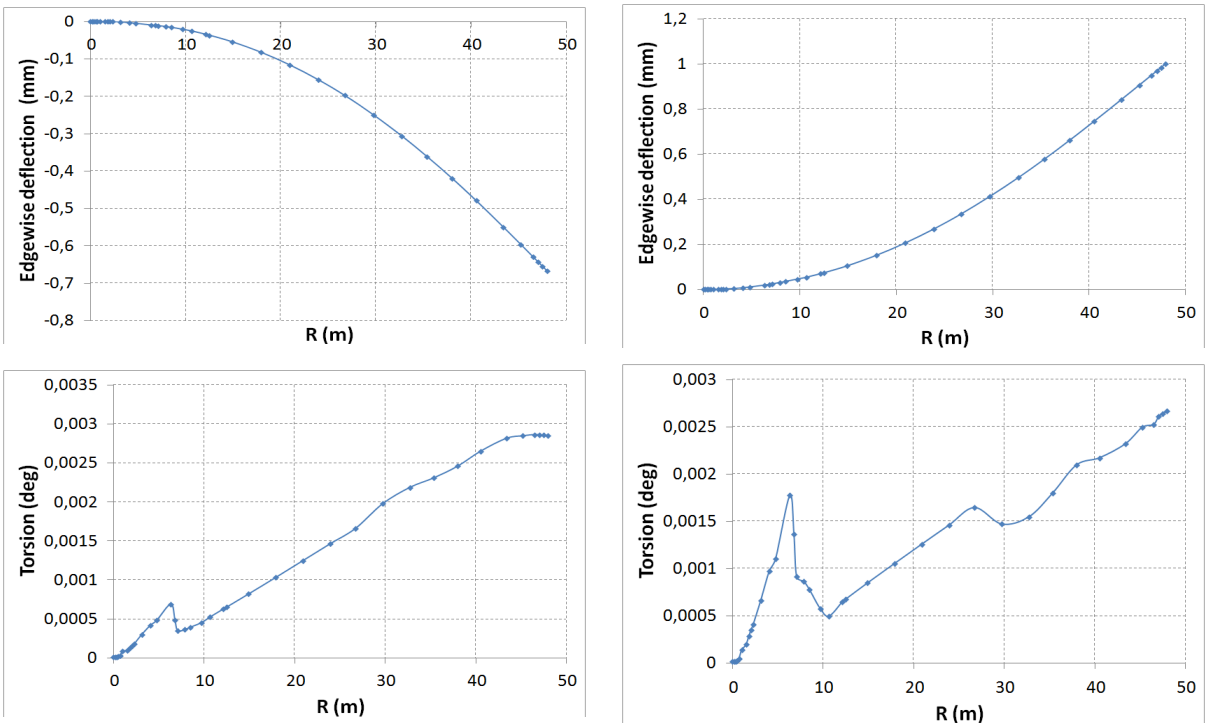

(a) Mode 1 *(b) Mode 2*

Fig. 11 First and second blade mode, model 3

B. *Discussion*

The structural coupling, between the dominating deflection and the two remaining (secondary) deflection components, is identified for all the analysed mode shapes. The coupling between bending deflection and torsion requires special attention due to the direct implications for the aerodynamic loading. This coupling is of course especially important for the mode shapes associated with the lower and most important natural frequencies.

Aeroelastic calculations are traditionally based on a Timoshenko beam modelling of the wind turbine blade. Although the bending torsion couplings usually are included in the beam representation, the correct specification of these structural couplings is a delicate matter. The magnitude of the observed bending/torsion coupling effects suggests that these may significantly affect the aerodynamic load characteristics of the wind turbine blade. This emphasizes the need for careful specification of such coupling effects in the aeroelastic computations. In addition, the structural coupling between the two bending components is essential for the correct modelling of aerodynamic damping [17]. For illustration, the mode shape results, associated with the lowest 3 blade natural frequencies are illustrated in Fig. 12.

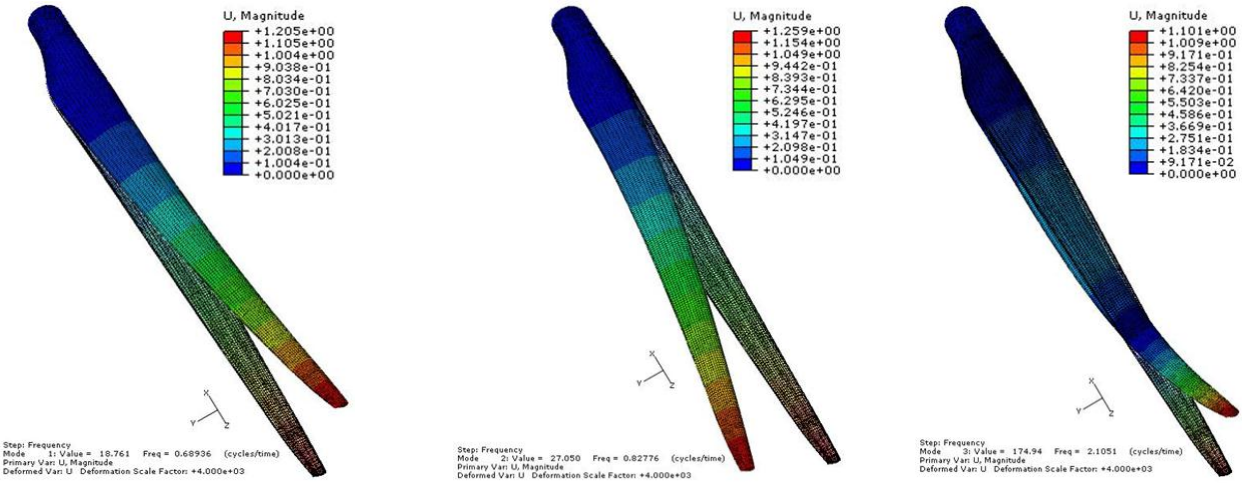

(a) 1st Mode *(b) 2nd Mode* *(c) 3rd Mode*

Fig. 12 Eigen-frequencies, model 2

V. PHENOMENON OF RESONANCE

According to standard GL Wind2003 (Germanischer Lloyd Wind Energy GMBH, 2005), the condition below must be checked to avoid the phenomenon of resonance:

$$F_r / F_{0,n} \leq 0.95 \quad (1)$$

where:

$F_{0,n}$ is the *n-th* natural frequency of the structure

F_r is the loading frequency, F_r =0.26*Hz*.

One applying this condition for the first two modes, one concluded that the effect of resonance does not occur for the 5 models, Table 8.

TABLE 8 COMPUTATION RESULTS OF THE RESONANCE EFFECT

Effect of resonance for the 1st mode (Flapwise) & 2nd mode (Edgewise)		
Model	**$F_r/F_{0,1}$**	**$F_r/F_{0,2}$**
1	0.339	0.292
2	0.377	0.314
3	0.390	0.324
4	0.364	0.305
5	0.375	0.313

VI. CONCLUSIONS

Composite laminated plate structure has been widely used in wind turbine blade. In this chapter, combining composite laminated plate blade's characteristics of hierarchical structure, based on finite element analysis software ABAQUS, laminated shell and solid element are used to create finite element model, and the finite element modal analysis is made to obtain modal parameters and the natural frequency spectrum of blade.

A fibreglass blade was designed for the 48m wind turbine blade through the use of finite element analysis techniques with special consideration given to the minimisation of manufacturing complexity and cost. The modal analysis performed in this study gives estimates of 3 lower natural frequencies and mode shapes, for the 48m blade investigated. The results are based on a finite element method performed in different cross sections along the blade. The estimated natural frequencies and mode shapes have subsequently been compared to check that the resonance mode of the system is not reached. Natural frequencies and mode shapes, obtained from a FE model of the investigated blade, are performed in order to evaluate the state-of-the-art blade modelling capacity and in addition, to gain inspiration for further improvements.

The present investigation has demonstrated that essential dynamic properties of wind turbine blades, like natural frequencies and mode shapes, can be numerically determined by use of the modal analysis technique. Blades with different spar geometry have been considered and the most appropriate of these has been selected. Although the comparison is based only on FE results on a 48m blade, the recommendations given are believed to be valid also for other types (sizes, designs ...) of wind turbine blades. The results have laid a foundation for further study of the wind turbine blade's vibration, structural dynamics and other issues.

ACKNOWLEDGMENTS

The work, presented in this report, has been funded by the WinFlo consortium. NASS & WIN, DCNS, IFREMER and VERGNET are gratefully acknowledged for assisting in performing this PhD work.

REFERENCES

[1] K. Malawi, Special issues on design optimization of wind turbine structures. In: Al-Bahadly.2, I. (Ed.) Wind Turbines. Intech. I, 2010.

[2] G. C. Larsen and A. Kretz, Experimental Determination of Stiffness Distributions and Mode Shapes of Wind Turbine Blades. Risø-R-773(EN), 1995.

[3] D. A. Peter, M. P. Rossow, K. Timothy, Design of helicopter rotor blades for optimum dynamic characteristics, J. Comput. Math. Appl. 12A (1) 85–109, 1986.

[4] J. I. Pritchard, H. M. Adelman, Optimal placement of tuning masses for vibration reduction in helicopter rotor blades, AIAA J. 28 (2) 309–315, 1990.

[5] R. B. Taylor, Helicopter vibration reduction by rotor blade modal shaping, 38th Annual Forum of the American Helicopter Society, Paper A-82-38-09-3000, Anaheim, CA, pp. 90–101, 1982.

[6] M. W. Davis, Optimization of helicopter rotor blade design for minimum vibration, NASA CP-2327, 609–625, 1984.

[7] T. Burton, D. Sharpe, N. Jenkins, E. Bossanyi, "Wind Energy Handbook," John Wiley & Sons, Chichester, England, 2001.

[8] A. Maheri, S. Noroozi, J. Vinney, "Combined analytical/FEA-based coupled aero structure simulation of a wind turbine with bend–twist adaptive blades" Original Research Article Renewable Energy, vol. 32, iss. 6, pp. 916-930, 2007.

[9] A. Maheri, S. Noroozi, J. Vinney, "Application of combined analytical/FEA coupled-aero-structure simulation in design of wind turbine adaptive blades." J Renew Energy, doi:10.1016/j.renene.2006.10.012, 2006.

[10] A. Maheri, S. Noroozi, J. Vinney, "Combined analytical/FEA-based coupled-aero-structure simulation of wind turbines with bend-twist adaptive blades." J Renew Energy; 32 (6): 916–30, 2007.

[11] H. J. Lin, W. M. Lai, Y. M. Kuo, "Combined analytical and finite element beam model for wind turbine blades." J Reinf Plast Comp; 29 (16): 2422–37, 2010.

[12] Y. J. Lee, Y. T Jhan, C. H Chung, "Fluid–structure interaction of FRP wind turbine blades under aerodynamic effect" Composites Part B: Engineering, vol. 43, iss. 5, pp. 2180-2191, 2012.

[13] G. Li, S. S. Pang, Y. Zhao, S. I. Ibekwe, "Local buckling analysis of composite laminate with large delaminations induced by low velocity impact." Polym Composite; 20 (5): 634–42, 2009.

[14] Dayton A. Griffin, "Evaluation of design concepts for adaptive wind turbine blades," SANDIA report 2002 (SAND2002-2424).

[15] B. Yang, D. Sun, "Testing, inspecting and monitoring technologies for wind turbine blades" Renewable and Sustainable Energy Reviews, vol. 22, pp. 515-526, 2013.

[16] Jinshui Yang, Chaoyi Peng, Jiayu Xiao, Jingcheng Zeng, Suli Xing, Jiaotong Jin, Hang Deng, "Structural investigation of composite wind turbine blade considering structural collapse in full-scale static tests." Composite Structures, vol. 97, pp. 15-29, 2013.

[17] J. T. Petersen, H. A. Madsen, A. Bjӧrk, P. Enevoldsen, S. Øye, H. Ganander and D. Winkelaar. "Prediction of dynamic loads and induces vibrations in stall." Risø-R-1045(EN), 1998.

Mostapha TARFAOUI was born in BenSlimane, Morocco in December, 18 1967. Ph.D. Engineering Science: Mechanics and Materials, 1999. Professor: Mechanics and Materials at ENSTA Bretagne, Brest, France, 2010. Main research topics: Naval and Offshore structures - composite materials - mechanical behaviour - static and dynamic response - finite element analysis - residual strength - damage modelling - fracture behaviour - interlaminar fracture toughness - correlation of structure & properties, computer modelling and data bases - Renewable Marine Energies.

M. TARFAOUI is professor specialized in structural mechanics. His main expertise is focused on the composite materials behaviour. This includes the static and dynamic responses involved in the shipbuilding structures to finite element analysis. He has expertise in Dialogue test/calculation in the heterogeneous structures relationships and numerical modelling. He obtained his Ph.D. of Engineering Science (Faculty of Science, University Haute Alsace, France) in 1999 (dissertation: "Finite element analysis of mechanical behaviour of plain and twill fabrics") and M.S. Physics and Applications (Faculty of Science, University Haute Alsace, France) in 1993. He participated in many congresses (CanCOM, HIPER, ICCM, CFM, IMAC, ESMC, CST, JNC…). He is member of Organization committee and Scientific committee of the international Congress (ACMA, JET…), he was chairman and co-chairman of different congress sessions for example: "Impact and Dynamic Response I and II" session in ICCM 14. Some references:

- M. TARFAOUI, S. CHOUKRI and A. NEME, Dynamic Response of Symmetric and Asymmetric E-glass /epoxy Laminates at High Strain Rates. Key Engineering Materials vol. 446, pp. 73-82, 2010.
- G. MOHAMED, M. TARFAOUI and V. BERTRAM. FEA of dynamic behaviour of Top hat bonded stiffened composite panel. Key Engineering Materials vol. 446, pp. 137-145, 2010.
- M. TARFAOUI. Experimental Investigation of Dynamic Compression and Damage Kinetics of Glass/Epoxy Laminated Composites under High Strain Rate Compression. Book: Advances in Composite Materials. Chapter 16, pp. 359-382, 2011.

Professor TARFAOUI is a membership of AFM (French Association of Mechanics), AMAC (Association for Composite Materials) and AF3M (Association Franco-Maghrebian of Mechanics and Materials). He is reviewer of international scientific journals: Journal of Composite Materials, Advanced Materials Research, Computational Materials Science, Applied Mechanics and Materials, Journal of Reinforced Plastics and Composites, Mechanics of Advanced Materials and Structures, Mécanique & Industries, Matériaux et Techniques…

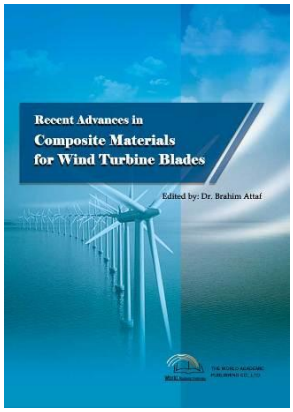

Recent Advances in Composite Materials for Wind Turbine Blades
Edited by Dr. Brahim Attaf

ISBN 978-0-9889190-0-*6

Hard cover, 232 pages

Publisher: The World Academic Publishing Co. Ltd.

Published in printed edition: 20, December 2013

Published online: 20, December 2013

This book of science and technology provides an overview of recent research activities on the application of fibre-reinforced composite materials used in wind turbine blades. Great emphasis was given to the work of scientists, researchers and industrialists who are active in the field and to the latest developments achieved in new materials, manufacturing processes, architectures, aerodynamics, optimum design, testing techniques, etc.. These innovative topics will open up great perspectives for the development of large scale blades for on- and off-shore applications. In addition, the variety of the presented chapters will offer readers access to global studies of research & innovation, technology transfer and dissemination of results and will respond effectively to issues related to improving the energy efficiency strategy for 2020 and the longer term.

How to cite this book chapter

Tarfaoui M. and Rahman Shah O. (2013). Spar Shape Optimization of a Multi-megawatt Composite Wind Turbine Blade: Modal Analysis, *Recent Advances in Composite Materials for Wind Turbines Blades*, Dr. Brahim Attaf (Ed.), ISBN 978-0-9889190-0-6, WAP-AMSA, Available from: http://www.academicpub.org/amsa/chapterInfo.aspx

World Academic Publishing - Advances in Materials Science and Applications

Chapter 7

Finite Element Modeling of Composite Wind Turbine Blades

Ajaya K. Nayak

Civil Engineering Department, Veer Surendra Sai University of Technology, Burla 768018
Sambalpur, Odisha, India

ajayanayak07@gmail.com

I. INTRODUCTION

This chapter involves the finite element modelling of composite wind turbine blades. The two dimensional formulations for plates and shells are based on displacement based methods as opposed to force based methods. A brief background of the finite element procedures is discussed. The governing equations of motion for plate problems are covered. The two dimensional shell analyses are based on flat-facetted, doubly-curved and three dimensional degenerated concepts. Exact three dimensional solutions for plates and shells are included. Finally plane stress, plane strain and generalised plane strain finite element formulations for composite material parts in a composite wind turbine blade are discussed.

II. BACKGROUND TO THE MODELLING CONCEPT

Composite materials possess certain inherent characteristics, which give rise to many challenging issues in wind turbine blades. The advantages of fibre-reinforced polymer (FRP) composites is that the interaction of the polymer matrix with reinforced fibres of high strength and stiffness governs the structural integrity of composites in wind turbine blades and therefore helps in achieving the desired performance. Since mechanical performance and structural integrity of FRP composite material depend on the effectiveness of the bond between resin and fibre in transferring stress across the interface, the selectivity of resin systems for improved fibre-matrix interfacial strength assumes paramount significance. Although the incorporation of fibres dominates the wear and friction processes of FRP composites, the role of the resin matrices is almost equally important. Firstly because matrix characteristics greatly control the interfacial phenomena and secondly because the matrix serves as a medium that transfers the load to the fibres and separates the individual fibres thereby preventing any brittle crack. Hence, studies of variability of materials and defects have been an intense field of research in most practical wind turbine applications. The finite element method due to its versatility is a proven tool to deal with various issues in wind turbine blades.

The finite element method [1-2] simulates the behaviour of a real structure by approximating it with that of a model composed of sub-regions or ‘elements’ in which the displacement field is restricted to a linear combination of pre-selected displacement patterns or ‘shape functions’. The configuration of the model is therefore specified by the magnitudes of the generalised coordinates associated with the shape functions. The configuration which minimizes the potential energy is determined and this configuration is then interpreted as an approximation to the configuration of the structure. The success or failure of the model to represent the conditions in the structure depends primarily on the set of shape functions selected and the compatibility conditions imposed along the boundaries of the elements.

Certain minimum conditions may be set down in an attempt to ensure that the behaviour of the model is a close approximation to the behaviour of the structure. These are summarized as:

1) Completeness requirements [3-7]. The shape function should include rigid body displacements and the constant-strain states associated with the problem under investigation.

2) Continuity requirements [3-7]. The configuration produced by the shape functions should satisfy the minimum internal and external compatibility conditions which are associated with the problem under investigation. Boundary compatibility should be maintained along the total perimeter of the element.

A systematic method for selecting a set of shape functions satisfying the minimum conditions has been successfully introduced based on the utilization of natural coordinates [3-7], interpolating functions [3-7] and complete polynomials [3-7]. The generalized coordinates are identified as the physical displacement quantities at the nodes and the formulation is simplified relating generalised coordinates and nodal displacements.

The finite elements commonly used in structural mechanics are based assumed displacement fields [3-7] and assumed stress fields [3-7]. In the assumed displacement based finite element formulation, the displacements within an element are adequately described by a simple polynomial that satisfies the potential energy principle [3-7]. In the assumed stress finite element formulation [3-7], the stress field must satisfy the equilibrium equation so that it is convenient to begin with a stress function. Hence generalised force degrees of freedom (dof) are primary variables as opposed to displacement degrees of freedom in displacement based FE formulations. In the mixed finite element formulations [3-7], both force and displacement dof are primary unknowns. Hybrid finite element formulations [3-7] maintain an assumed stress field within the element and assumed displacement patterns on their boundaries. In the subsequent sections, finite elements for plates and shells based on the assumed displacement fields in two and three dimensional theories are discussed.

III. TWO DIMENSIONAL FE FORMULATIONS FOR SANDWICH PLATES

Sandwich plates [8-10] in thick and thin regimes develop both membrane, bending and shear stresses under static and dynamic environments. Hence transverse shear deformations [11-17] are to be included in the development of the resulting two dimensional finite element formulations.

The displacement field based on a first order shear deformation theory [7] is expressed (see Fig. 1) as

$$u_1 = \sum_{i=1}^{4}\left(u_{oi}N_i + z\psi_{xi}N_i\right) + \left(y_{14}N_8 - y_{21}N_5\right)\theta_{z1} + \left(y21N_5 - y_{32}N_6\right)\theta_{z2} + \left(y_{32}N_6 - y_{43}N_7\right)\theta_{z3} + \left(y_{43}N_7 - y_{14}N_8\right)\theta_{z4}$$

$$u_2 = \sum_{i=1}^{4}\left(v_{oi}N_i + z\psi_{yi}N_i\right) + \left(x_{41}N_8 - x_{12}N_5\right)\theta_{z1} + \left(x_{12}N_5 - x_{32}N_6\right)\theta_{z2} + \left(x_{23}N_6 - x_{34}N_7\right)\theta_{z3} + \left(x_{34}N_7 - x_{41}N_8\right)\theta_{z4}$$

$$u_3 = w_o \tag{1}$$

where u_1, u_2 and u_3 are the displacement components in the *x*, *y* and *z* directions respectively, of a generic point in the laminate space; u_o, v_o and w_o are the in-plane and transverse displacements of a point (*x*,*y*) on the mid-plane respectively; ψ_x and ψ_y are the rotations of normal to the mid-plane about *y* and *x* axes respectively; θ_{zi} (*i*=1, 4) are the drilling rotations; N_i (*i*=1,4) are the shape functions; $x_{ij} = x_i - x_j$ and $y_{ij} = y_i - y_j$ are corner coordinate differences.

The shape functions N_i (*i*=5, 8) associated with drilling rotations [18] are expressed as:

$$N_5 = \frac{1}{16}\left(1-\xi^2\right)\left(1-\eta\right) \qquad N_6 = \frac{1}{16}\left(1+\xi\right)\left(1-\eta^2\right) \qquad N_7 = \frac{1}{16}\left(1-\xi^2\right)\left(1+\eta\right) \qquad N_8 = \frac{1}{16}\left(1-\xi\right)\left(1-\eta^2\right)$$

where, ξ and η are the usual iso-parametric coordinates.

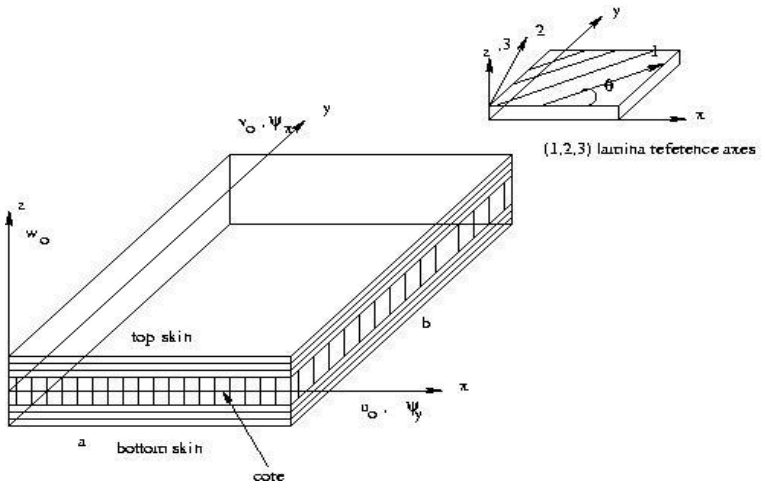

Fig. 1 Sandwich plate geometry with laminate reference axes, and fibre orientation

The strains in small deflection linear domain associated with the displacement field in Eq. (1) are

$$\varepsilon_1 = \varepsilon_1^o + z\kappa_1^o \qquad \varepsilon_2 = \varepsilon_2^o + z\kappa_2^o \qquad \varepsilon_3 = 0 \qquad \varepsilon_4 = \varepsilon_4^o \qquad \varepsilon_5 = \varepsilon_5^o \qquad \varepsilon_6 = \varepsilon_6^o + z\kappa_6^o \tag{2}$$

where

$$\varepsilon^o = \left(\varepsilon_1^o, \varepsilon_2^o, \varepsilon_6^o\right)^T = \left(\frac{\partial u_{do}}{\partial x}, \frac{\partial v_{do}}{\partial y}, \frac{\partial u_{do}}{\partial y} + \frac{\partial v_{do}}{\partial x}\right)^T$$

$$u_{do}=\sum_{i=1}^{4}\left(u_{oi}N_i\right)+\left(y_{14}N_8-y_{21}N_5\right)\theta_{z1}+\left(y_{21}N_5-y_{32}N_6\right)\theta_{z2}+\left(y_{32}N_6-y_{43}N_7\right)\theta_{z3}+\left(y_{43}N_7-y_{14}N_8\right)\theta_{z4}$$

$$v_{do}=\sum_{i=1}^{4}\left(v_{oi}N_i\right)+\left(x_{41}N_8-x_{12}N_5\right)\theta_{z1}+\left(x_{12}N_5-x_{23}N_6\right)\theta_{z2}+\left(x_{23}N_6-x_{34}N_7\right)\theta_{z3}+\left(x_{34}N_7-x_{41}N_8\right)\theta_{z4}$$

$$\kappa^o=\left(\kappa_1^o,\kappa_2^o,\kappa_6^o\right)^T=\left(\frac{\partial\psi_x}{\partial x},\frac{\partial\psi_y}{\partial y},\frac{\partial\psi_x}{\partial y}+\frac{\partial\psi_y}{\partial x}\right)^T\quad \varepsilon^s=\left(\varepsilon_5^o,\varepsilon_4^o\right)^T=\left(\frac{\partial w_o}{\partial x}+\psi_x,\frac{\partial w_o}{\partial y}+\psi_y\right)^T \tag{3}$$

As seen from Eqs. (2) and (3), the transverse shear strains are constant through the laminate thickness as a result of which there is need for the shear correction factors [10-15].

The generalized mid-surface strains at any point given by Eq. (3) can be expressed in terms of nodal displacements $\{\delta\}_{(e)}$ as follows:

$$\varepsilon^{o(e)}=\left[B_\varepsilon^o\right]^{(e)}\{\delta\}_{(e)}\ ,\ \kappa^{o(e)}=\left[B_\kappa^o\right]^{(e)}\{\delta\}_{(e)}\ \text{and}\ \varepsilon^{s(e)}=\left[B_\varepsilon^s\right]^{(e)}\{\delta\}_{(e)} \tag{4}$$

where $\left[B_\varepsilon^o\right]$, $\left[B_\kappa^o\right]$ and $\left[B_\varepsilon^s\right]$ are generated strain-displacement matrices. One basic problem inherent in the use of standard interpolation of the strains for the transverse shear components is that the element locks when it is thin. The reason for this locking is that the element, when loaded in pure bending, will exhibit spurious transverse shear energy. In order to overcome the shear locking, Dvorkin and Bathe [19] proposed assumed interpolations for the shear strain to develop a four node assumed strain degenerated plate element [20].

The substitute shear strain fields are chosen as follows:

$$\bar{\varepsilon}_{\xi\varsigma}^s=\sum_{i=1}^{1}\sum_{j=1}^{2}P_i(\xi)Q_j(\eta)\bar{\varepsilon}_{\xi\varsigma}^{sij} \tag{5}$$

$$\bar{\varepsilon}_{\eta\varsigma}^s=\sum_{i=1}^{21}\sum_{j=1}^{1}Q_i(\xi)P_j(\eta)\bar{\varepsilon}_{\mu\varsigma}^{sji} \tag{6}$$

where, $Q_1(z)=(1+z)/2$, $Q_2(z)=(1-z)/2$ and $P_1(z)=1(z=\xi,\eta)$ in which $\bar{\varepsilon}_{\xi\varsigma}^{sij}$ and $\bar{\varepsilon}_{\eta\varsigma}^{sij}$ are the $m\times n$ unknown substitute shear strain parameters associated with two sets of $m\times n$ sampling points $\left(\hat{\xi}_i,\hat{\eta}_j\right)$ and $\left(\breve{\xi}_j,\breve{\eta}_i\right)$.

In order to eliminate locking, the following equations are obtained:

$$\bar{\varepsilon}_{\xi\varsigma}^s\left(\hat{\xi}_i,\hat{\eta}_j\right)=\varepsilon_{\xi\varsigma}^s\left(\hat{\xi}_i,\hat{\eta}_j\right)(i=1,\ldots,m;\ j=1,\ldots..n) \tag{7}$$

$$\bar{\varepsilon}_{\eta\varsigma}^s\left(\breve{\xi}_j,\breve{\eta}_i\right)=\varepsilon_{\eta\varsigma}^s\left(\breve{\xi}_j,\breve{\eta}_i\right)(i=1,\ldots,n;\ j=1,\ldots..m) \tag{8}$$

It is possible to write

$$\bar{\varepsilon}^s=\begin{Bmatrix}\bar{\varepsilon}_5^o\\ \bar{\varepsilon}_4^o\end{Bmatrix} \tag{9}$$

where, $\bar{\varepsilon}_5^o$ and $\bar{\varepsilon}_4^o$ are obtained from $\bar{\varepsilon}_{\xi\varsigma}^s$ and $\bar{\varepsilon}_{\eta\varsigma}^s$ given by Eqs. (5) and (6) by tensor transformation. The transformation of the strain tensor in curvilinear coordinates may be written as

$$e_{\alpha\beta}=\frac{\delta x^i}{\delta\varepsilon_\alpha}\frac{\delta x^j}{\delta\varepsilon_\beta}\varepsilon_{ij} \tag{10}$$

where, it is assumed that $e_{\alpha\beta}$ is the strain tensor in the (ξ,η) coordinate system and ε_{ij} is the strain tensor in the (x,y) system [19]. For implementation purpose, ε^s in Eq. (4) is replaced by $\bar{\varepsilon}^s$ where $\bar{\varepsilon}^s$ is the substitute shear strains to remove spurious zero energy modes. Hence the substitute shear strain $\bar{\varepsilon}^s$ is given by

$$\bar{\varepsilon}^{s(e)}=\left[\bar{B}_\varepsilon^s\right]^{(e)}\{\delta\}_{(e)} \tag{11}$$

where, $\left[\overline{B}_{\varepsilon}^{s}\right]^{(e)}$ is generated strain displacement matrix.

For arbitrary values of virtual displacements, the following assembled equation for transient analysis is stated as:

$$[M]\{\ddot{\Delta}\}+[K]\{\Delta\}=\{F\} \tag{12}$$

Here the unknown vector $\{\Delta\}$ is generated by the assemblage of element degrees of freedom $\{d\}_e^T$, e=1, 2,… total degrees of freedom in the region **R**. The assembled stiffness and mass for transient analysis are

$$[K]=\sum_e \int_{A_e}\left[B_{\varepsilon}^{o^T} AB_{\varepsilon}^{o}+B_{\varepsilon}^{o^T} BB_{\kappa}^{o}+B_{\kappa}^{o^T} BB_{\varepsilon}^{o}+B_{\kappa}^{o^T} DB_{\kappa}^{o}+\overline{B}_{\varepsilon}^{s^T} A^{s}\overline{B}_{\varepsilon}^{s}\right]dA \tag{13}$$

where, A_{ij}, B_{ij}, D_{ij} are the plate stiffness, defined by

$$\begin{aligned}\left(A_{ij}, B_{ij}, D_{ij}\right)&=\int_{-h/2}^{h/2}\overline{Q}_{ij}\left(1, z, z^2\right)dz(i, j=1,2,6)\\ \left(A_{ij}^{s}\right)&=\int_{-h/2}^{h/2}\overline{Q}_{ij}K_1^2K_2^2(1)dz(i, j=5,4)\end{aligned} \tag{14}$$

where, K_1^2 and K_2^2 are the shear correction factors [16-17] calculated from the shear strain energy formulation.
$\overline{Q}_{ij}$ are the transformed plane stress reduced elastic stiffness coefficients, which are given as

$$\begin{aligned}\overline{Q}_{11}&=Q_{11}c^4+2(Q_{12}+2Q_{66})c^2s^2+Q_{22}s^4\\ \overline{Q}_{12}&=(Q_{11}+Q_{22}-4Q_{66})c^2s^2+Q_{12}\left(c^4+s^4\right)\\ \overline{Q}_{16}&=\left(Q_{11}c^2+(Q_{12}+2Q_{66})\left(s^2-c^2\right)-Q_{22}s^2\right)cs\\ \overline{Q}_{22}&=Q_{11}s^4+2(Q_{12}+2Q_{66})c^2s^2+Q_{22}c^4\\ \overline{Q}_{26}&=\left(Q_{11}s^2+(Q_{12}+2Q_{66})\left(c^2-s^2\right)-Q_{22}c^2\right)cs\\ \overline{Q}_{66}&=(Q_{11}+Q_{22}-2Q_{12})c^2s^2+Q_{66}\left(c^2-s^2\right)^2\\ \overline{Q}_{55}&=\left(c^2Q_{55}+s^2Q_{44}\right)\quad \overline{Q}_{44}=\left(c^2Q_{44}+s^2Q_{55}\right)\\ \overline{Q}_{45}&=cs(Q_{44}-Q_{45})\quad \overline{Q}_{54}=cs(Q_{55}-Q_{44})\end{aligned} \tag{15}$$

where, $\left\lfloor Q_{ij}\right\rfloor_k$ is constitutive matrix at lamina level; $c=\cos\theta$; $s=\sin\theta$; θ is the angle between the lamina *x* axis and lamina principal x_i axis; with $Q_{11}=E_1/(1-\nu_{12}\nu_{21})$, $Q_{12}=\nu_{12}E_2/(1-\nu_{12}\nu_{21})$, $Q_{22}=E_2/(1-\nu_{12}\nu_{21})$, $Q_{66}=G_{12}$, $Q_{55}=G_{13}$, $Q_{44}=G_{23}$, $E_i(i=1,2)$ are the Young's moduli, G_{12}, G_{13} and G_{23} are the shear moduli, ν_{12} and ν_{21} are the Poisson's ratios.

The consistent mass matrix $[M]$ in Eq. [12] can be obtained from the kinetic energy of the system

$$\left(\int_V \rho(\ddot{u}_1\delta u_1+\ddot{u}_2\delta u_2+\ddot{u}_3\delta u_3)dV\right) \tag{16}$$

where $\rho(x, y, z)$ and V are the density of the shell at (x, y, z) and volume of the shell respectively.

A 2x2 Gauss-Legendre rule (i.e., full integration scheme) is employed to integrate bending, membrane, shear and inertia terms in the energy expressions for the four node drilling degrees of freedom plate element. The developed finite element should pass the pathological tests [21, 22] so that these could be used with confidence.

Numerical results are presented to assess the behaviour of a family of plate bending elements (FSDTC4, FSDTV4 and ECPT4) based on a unified first order shear deformation theory. FSDTC4, FSDTV4 and ECPT4 denote 4-node plate bending elements based on a first-order shear deformation theory with the shear correction factor of 5/6 (FSDTC) [13, 14], first order shear deformation theory with the shear correction factor from strain energy [15] formulation (FSDTV) and equivalent classical plate theory (ECPT) with the use of empirical shear correction factor derived from patch test considerations respectively. It is well known that the CPT under-predicts the deflection than shear deformable plate theories for thick laminates [13, 14]. It is found that the deflection and frequency results [13-14] from FSDT are functions of shear correction factors and width to thickness ratios of laminates and CPT results. Hence in the present analysis, equivalent classical plate theory (ECPT) results are obtained with the use of empirical shear correction factors which are found to be functions of

Reissner's homogeneous shear correction factors (5/6) and side to thickness ratio (a/h).

In order to confirm the convergence characteristics of FSDTC4, FSDTV4 and ECPT4, a patch test is performed on plates with various mesh patterns which can represent constant moment in plates. Note that for isotropic plates, FSDTC4 and FSDTV4 give identical results. The rectangular plate in consideration is simply supported at three corners (i:e w = 0) and loaded with a concentrated load of 2 at the fourth corner and moments applied at the boundary as shown in Fig. 2.

The geometrical and material properties with consistent units are: a = 20:0, b = 10:0, h = variable, E =2:1x10^6, Poisson ratio=0.30. In order to establish the benchmark for comparison, widely used DKT plate bending element [23] is implemented presently. The mesh patterns employed for rectangular and triangular plate bending elements are shown in Fig. 2. The results from HSDT4, FSDTC4 and ECPT4 are compared with DKT in Table 1. From the results, it is observed that all the plate models compare well with each other for width to thickness ratio of 10^4 which is also reported in [19].

From numerical experiments, it is found that a value of shear correction factor

$$K_{thin} = \frac{K_c^2}{thinparameter} 10^{\left(6K_c^2 - \log 10(thinparameter)\right)}$$

where, $K_c^2 = 5/6$, thin parameter = length/thickness ratio with FSDT4 gives close results with respect to DKT results which we will denote as ECPT4 (Equivalent classical four node plate element). The comparative results from ECPT4 are also shown in Table 1. As seen from the results, ECPT4 compares very well with DKT results for a wide range of width to thickness ratios.

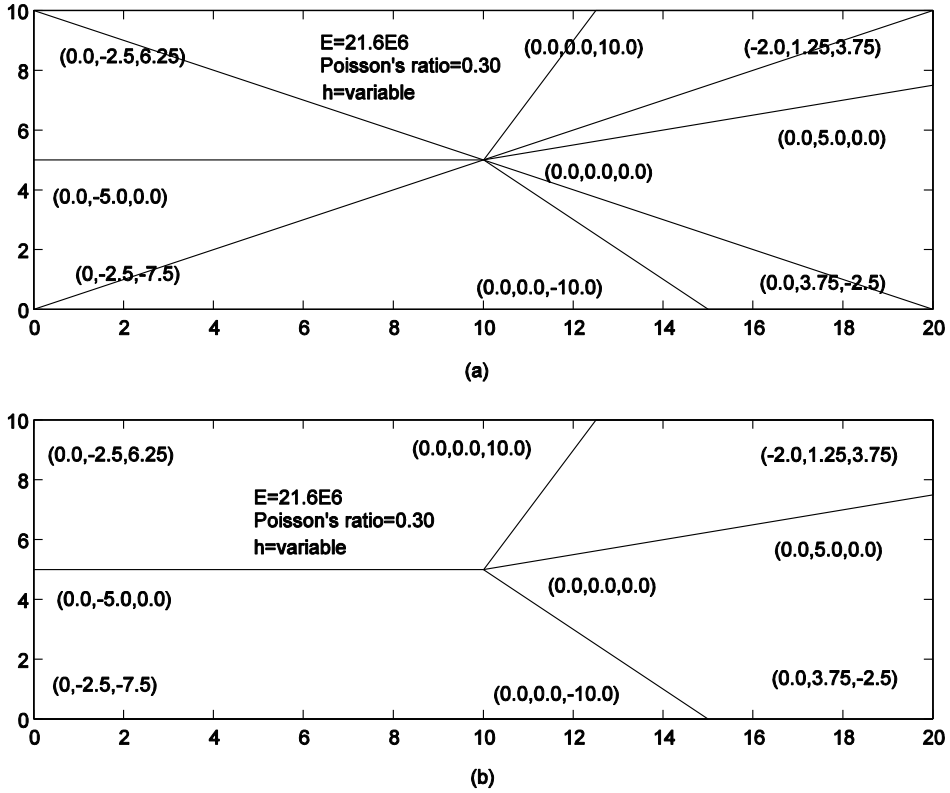

Fig. 2 Mesh patterns for (a) triangular and (b) rectangular elements, the boundary loads (*Pz; Mx; My*) are indicated in the brackets [24]

TABLE 1 VERTICAL CORNER DISPLACEMENT OF A RECTANGULAR PLATE UNDER CONSTANT MOMENT PATCH TEST [24]

b/h	DKT	ECPT4	FSDT4
5 0.	0.185714*	0.185717	0.196634
10	0.00148571	0.00148574	0.00150764
20	0.0118857	0.0118859	0.0119296
30	0.0401143	0.0401149	0.0401801
40	0.0950857	0.0950871	0.0951735
50	0.185714	0.185717	0.185824
10^2	1.48571	1.48574	1.48593
10^3	1485.71	1485.74	1485.72
10^4	0.148571**	0.148589	0.148571

*Multiplied by 10^{-2} ** multiplied by 10^7

Again the static and free vibration analysis of simply supported laminated composite (0/90) plates with the following

material and geometric properties: $E_1/E_2=25$, $G_{12}/E_2=G_{13}/E_2=0.5$, $G_{23}/E_2=0.20$, a/b=1; a mesh density of 9 nodes per quarter of the plate is employed to obtain present FEM results. The results for the central deflection $100wE_2h^3/\left(b^4q_o\right)$ under sinusoidal loading and the fundamental frequencies $\omega\frac{a^2}{h}\sqrt{\frac{\rho}{E_2}}$ from FSDTC, FSDTV, CPT, ECPT, FSDTC4, FSDTV4 and ECPT4 are shown in Table 2. As seen from the results, there is close agreement among analytical and numerical results.

IV. TWO DIMENSIONAL FE FORMULATIONS FOR SANDWICH SHELLS BASED ON FLAT-FACETTED SHELL FORMULATION

The procedures of deriving the shell equations based on flat-facetted formulations are the same as that of the previous section. Only the transformation matrix [1] will be used to convert stiffness, mass matrices and force vectors from local to global coordinates.

By the rules of orthogonal transformation the stiffness, mass and buckling matrices of an element in global co-ordinate become

$$[K]^g = T_g{}^T[K]T_g \tag{17}$$

$$[M]^g = T_g{}^T[M]T_g \tag{18}$$

where, T_g is the transformation matrix from local to global axes as given below

$$T_g=\begin{bmatrix} T_{gtop} & 0 \\ 0 & T_{gbot} \end{bmatrix} \quad T_{gtop}=\begin{bmatrix} \cos(X,x) & \cos(X,y) & \cos(X,z) \\ \cos(Y,x) & \cos(Y,y) & \cos(Y,z) \\ \cos(Z,x) & \cos(Z,y) & \cos(Z,z) \end{bmatrix} \quad T_{gbot}=\begin{bmatrix} \cos(Y,y) & -\cos(Y,x) & \cos(Y,z) \\ -\cos(X,y) & \cos(X,x) & -\cos(X,z) \\ \cos(Z,y) & -\cos(Z,x) & \cos(Z,z) \end{bmatrix}$$

$$0=\begin{bmatrix} 0 & 0 & 0 \\ 0 & 0 & 0 \\ 0 & 0 & 0 \end{bmatrix} \tag{19}$$

and (X,x) denotes the angle between the positive X (global) and *x* (local) axes.

V. TWO DIMENSIONAL FE FORMULATIONS FOR SANDWICH SHELLS BASED ON FLAT-FACETTED SHELL FORMULATION

A composite doubly curved composite sandwich shell as shown in Fig. 3 is represented by the curvilinear dimensional coordinates *x* and *y* that coincides with the mid-surface of the shell and *z*-axis is oriented in the thickness direction. The displacement components of a generic point in the shell are assumed as given by Eq. (1).

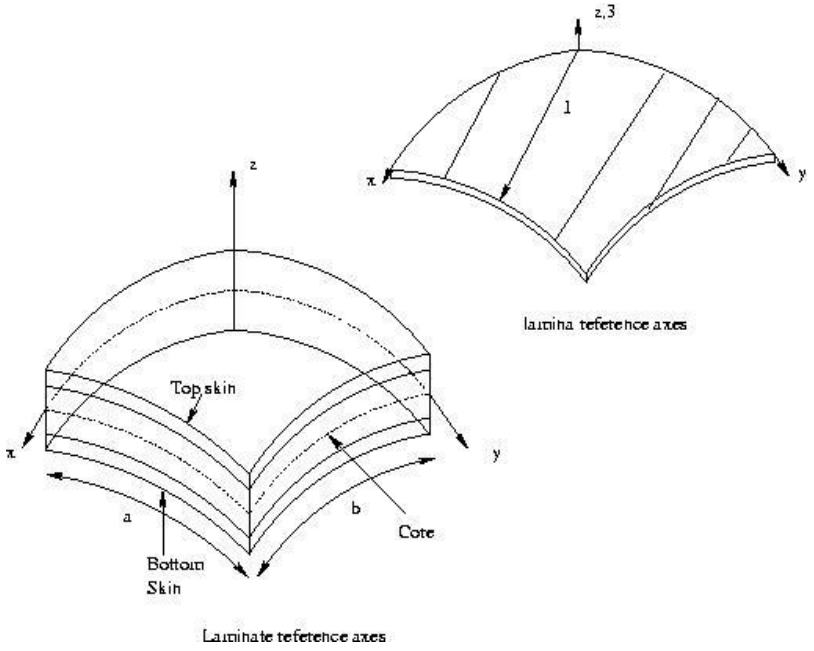

Fig. 3 Doubly curved Laminate geometry with positive set of lamina/laminate reference axes, displacement components and fibre orientation

TABLE 2 THE CENTRAL DISPLACEMENT $100wE_2h^3/\left(b^4q_o\right)$ AND FUNDAMENTAL FREQUENCY $\omega\frac{a^2}{h}\sqrt{\frac{\rho}{E_2}}$ OF LAMINATED COMPOSITE (0/90) PLATES [24]

b/h	FSDTC	FSDTV	CPT	ECPT	FSDTC4	FSDTV4	ECPT4
$100wE_2h^3/\left(b^4q_o\right)$							
10	1.2373	1.2398	1.0636	1.0637	1.2346	1.2372	1.0605
20	1.1070	1.1076	1.0636	1.0637	1.1039	1.1045	1.0605
100	1.0653	1.0653	1.0636	1.0637	1.0621	1.0621	1.0605
$\omega\frac{a^2}{h}\sqrt{\frac{\rho}{E_2}}$							
10	8.9001	8.8912	9.5661	9.5653	8.9380	8.9291	9.6098
20	9.4745	9.4718	9.6635	9.6627	9.5182	9.5155	9.7092
100	9.6873	9.6872	9.6952	9.6944	9.7335	9.7331	9.7403

The strains in small deflection linear domain associated with the displacement field in Eq. (1) in the doubly curved shell formulation are

$$\begin{aligned}
\varepsilon_{xx} &= \varepsilon_{xx}^o + z\kappa_{xx}^o + \frac{w_o}{R_1} \\
\varepsilon_{yy} &= \varepsilon_{yy}^o + z\kappa_{yy}^o + \frac{w_o}{R_2} \\
\varepsilon_{zz} &= 0 \\
\varepsilon_{yz} &= \varepsilon_{yz}^o - \frac{v_o}{R_2} - z\frac{\psi_y}{R_2} \\
\varepsilon_{xz} &= \varepsilon_{xz}^o - \frac{u_o}{R_1} - z\frac{\psi_x}{R_1} \\
\varepsilon_{xy} &= \varepsilon_{xy}^o + z\kappa_{xy}^o
\end{aligned} \tag{20}$$

where, R_1 and R_2 are the principal radii of curvature of the middle surface [7]. For plates, both radii of curvature have a very high value close to infinity ($1/R_1=0$ and $1/R_2=0$). The other notations used in Eq. (20) are defined by Eq. (3). As usual, Hamilton's principle [5] is used to derive the equations of motion appropriate for the displacement field in Eq. (1), the strain displacement Eq. (20) and the constitutive relations in Eqs. (4) to (8) to represent Eq. (9). The membrane, bending and shear strains for doubly curved shell formulation are represented by

$$\varepsilon_m = \begin{Bmatrix} \frac{\partial u_o}{\partial x} + \frac{w_o}{R_1} \\ \frac{\partial v_o}{\partial y} + \frac{w_o}{R_2} \\ \frac{\partial v_o}{\partial x} + \frac{\partial u_o}{\partial y} \end{Bmatrix} \quad \varepsilon_b = \begin{Bmatrix} \frac{\partial \psi_x}{\partial x} \\ \frac{\partial \psi_y}{\partial y} \\ \frac{\partial \psi_y}{\partial x} + \frac{\partial \psi_x}{\partial y} \end{Bmatrix} \quad \varepsilon_s = \begin{Bmatrix} \psi_x + \frac{\partial w_o}{\partial x} - \frac{u_o}{R_1} \\ \psi_y + \frac{\partial w_o}{\partial y} - \frac{v_o}{R_2} \\ -\frac{\psi_x}{R_1} \\ -\frac{\psi_2}{R_2} \end{Bmatrix} \tag{21}$$

The stress resultant vector $\left(N_{xx}, N_{yy}, N_{xy}, M_{xx}, M_{yy}, M_{xy}, Q_{xz}, Q_{yz}, S_{xz}, S_{yz}\right)$ are given by the following equations

$$\begin{Bmatrix} N_{xx} & M_{xx} \\ N_{yy} & M_{yy} \\ N_{xy} & M_{xy} \end{Bmatrix} = \int_{\frac{-h}{2}}^{\frac{h}{2}} \begin{Bmatrix} \sigma_{xx} \\ \sigma_{yy} \\ \sigma_{xy} \end{Bmatrix} (1 \quad z) dz \quad [Q] = \begin{Bmatrix} Q_{xz} & S_{xz} \\ Q_{yz} & S_{yz} \end{Bmatrix} = \int_{\frac{-h}{2}}^{\frac{h}{2}} \begin{Bmatrix} \sigma_{xz} \\ \sigma_{yz} \end{Bmatrix} (1, z) dz \tag{22}$$

The laminate constitutive relations are obtained as

$$\begin{Bmatrix} N \\ M \\ Q \end{Bmatrix} = \begin{bmatrix} A & B & 0 \\ B & D & 0 \\ 0 & 0 & A^s \end{bmatrix} \begin{Bmatrix} \varepsilon_m \\ \varepsilon_b \\ \varepsilon_s \end{Bmatrix} \tag{23}$$

The virtual work equation can be written in compact form as

$$\begin{aligned} &\int_o^t \int_A \left(\delta\varepsilon_m{}^T A\varepsilon_m + \delta\varepsilon_m{}^T B\varepsilon_b + \delta\varepsilon_b{}^T B\varepsilon_m + \delta\varepsilon_b{}^T D\varepsilon_b + \delta\varepsilon_s{}^T A^s \varepsilon_s \right) dA dt + \\ &\int_o^t \int_A qdwdAdt \\ &= \int_o^t \int_A \begin{bmatrix} I_1\left(\ddot{u}_o\delta u_o + \ddot{v}_o\delta v_o + \ddot{w}_o\delta w_o\right) + I_2\left(\ddot{\psi}_x\delta u_o + \ddot{\psi}_y\delta v_o + \ddot{u}_o\delta\psi_x + \ddot{v}_o\delta\psi_y\right) + \\ I_3\left(\ddot{\psi}_x\delta\psi_x + \ddot{\psi}_y\delta\psi_y\right) \end{bmatrix} dA dt \end{aligned} \tag{24}$$

Once the virtual work equation is known, the finite element models that pass the benchmark tests [21, 22] can be readily obtained by following the steps as mentioned earlier by Eqs. (15) to (19).

VI. TWO DIMENSIONAL FE FORMULATIONS FOR SANDWICH SHELLS BASED ON THREE DIMENSION DEGENERATED SHELL FORMULATION

In this approach, the three dimensional stress and strain conditions are degenerated to shell behaviour. The definition of independent rotational and displacement degrees of freedom permits transverse shear deformation to be taken into account, since rotations are not tied to the slope of the mid-surface. This approach is equivalent to using a general shell theory and reduces to the Eq. (1) when applied to the plates. A typical quadrilateral degenerated shell element is shown in Fig. 4. Also, triangular degenerated shell elements can be represented similar to Fig. 4. The displacement components of the mid-point of the normals, the nodal coordinates, global stiffness matrices, applied force vectors etc. are referred the global coordinate system *(x, y, z).* At k^{th} node, $\vec{V}_{3k}$ is constructed as a vector joining the top and bottom of the node in nodal coordinate system $\left(\vec{V}_{1k}, \vec{V}_{2k}, \vec{V}_{3k}\right)$. $\vec{V}_{1k}$ is constructed parallel to the global *xz* plane or is assumed parallel to *x* axis when $\vec{V}_{3k}$ is in y direction. And consequently $\vec{V}_{2k}$ is derived as cross products of $\vec{V}_{3k}$ and $\vec{V}_{1k}$. $\xi - \eta - \zeta$ is a natural coordinate system; ξ and η are the curvilinear coordinates at the middle surface. ζ is linear coordinate in thickness direction with ζ =+1 and –1 at top and bottom surfaces, respectively.

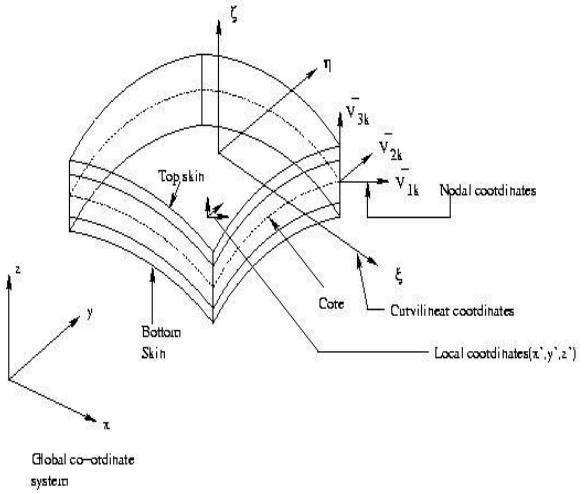

Fig. 4 Degenerated quadrilateral shell element with various co-ordinate systems

The position of an arbitrary point of the shell [1] is obtained as

$$\begin{Bmatrix} x \\ y \\ z \end{Bmatrix} = \sum_{k=1}^{n} N_k \begin{Bmatrix} x_o^k \\ y_o^k \\ z_o^k \end{Bmatrix} + \frac{\zeta}{2} \sum_{k=1}^{n} N_k h_k \begin{Bmatrix} \hat{V}_{3k}^x \\ \hat{V}_{3k}^y \\ \hat{V}_{3k}^z \end{Bmatrix} \tag{25}$$

where, $\hat{V}_{ik}^{j}$ (i=1,2,3) is the j^{th} component of unit vector along nodal vector $\vec{V}_{ik}$ at node k and h_k is the thickness of shell at node k and n is the number of nodes. x_o^k , y_o^k and z_o^k are the Cartesian coordinates of the mid-point of the shell at k^{th} node. The global displacement components of any point in the shell global coordinate system in terms of thickness coordinate z is given by

$$u_i = u_{oi}^k + \hat{V}_{1k}^i \delta_1 + \hat{V}_{2k}^i \delta_2 \quad (i=1,2,3) \tag{26}$$

where u_i (i=1,2,3) are the displacements u, v and w in global coordinate x, y and z directions respectively. u_{oi}^k (i=1, 2, 3) are the displacements in the midpoint of the normal in global coordinate system.

$$\delta_1 = z\beta_1 \quad \delta_2 = -z\beta_2 \tag{27}$$

Expanding the Eq. [26], the element displacement field is expressed as

$$\begin{Bmatrix} u \\ v \\ w \end{Bmatrix} = \sum_{k=1}^{n} N_k \begin{Bmatrix} u_o^k \\ v_o^k \\ w_o^k \end{Bmatrix} + \sum_{k=1}^{n} N_k \zeta \frac{h_k}{2} \begin{bmatrix} \tilde{V}_{1k}^x & -\hat{V}_{2k}^x \\ \hat{V}_{1k}^y & -\hat{V}_{2k}^y \\ \hat{V}_{1k}^z & -\hat{V}_{2k}^z \end{bmatrix} \tag{28}$$

where, u_o^k , v_o^k and w_o^k are the displacement components of the midpoint of the normal in global coordinate system.

The normal strain component in the thickness direction is neglected. Owing to this assumption, the five strain components in local coordinate system are given by

$$\begin{Bmatrix} \varepsilon_{x'} \\ \varepsilon_{y'} \\ \varepsilon_{xy'} \\ \varepsilon_{xz'} \\ \varepsilon_{yz'} \end{Bmatrix} = \begin{Bmatrix} \dfrac{\partial u'}{\partial x'} \\ \dfrac{\partial v'}{\partial y'} \\ \dfrac{\partial u'}{\partial y'} + \dfrac{\partial v'}{\partial x'} \\ \dfrac{\partial u'}{\partial z'} + \dfrac{\partial w'}{\partial x'} \\ \dfrac{\partial v'}{\partial z'} + \dfrac{\partial w'}{\partial y'} \end{Bmatrix} \tag{29}$$

where, ε with subscripts x' and y' are the normal strains in the respective directions and with subscripts $x'y'$, $x'z'$ and $y'z'$ are the shear strains on $x'y'$, $x'z'$ and $y'z'$ planes respectively; u', v' and w' are the displacement components in the local coordinate system.

The relation between the displacements derivatives in local and global coordinates is given by

$$\begin{bmatrix} \dfrac{\partial u'}{\partial x'} & \dfrac{\partial v'}{\partial x'} & \dfrac{\partial w'}{\partial x'} \\ \dfrac{\partial u'}{\partial y'} & \dfrac{\partial v'}{\partial y'} & \dfrac{\partial w'}{\partial y'} \\ \dfrac{\partial u'}{\partial z'} & \dfrac{\partial v'}{\partial z'} & \dfrac{\partial w'}{\partial z'} \end{bmatrix} = \begin{bmatrix} l_1 & l_2 & l_3 \\ m_1 & m_2 & m_3 \\ n_1 & n_2 & n_3 \end{bmatrix}^T \begin{bmatrix} \dfrac{\partial u}{\partial x} & \dfrac{\partial v}{\partial x} & \dfrac{\partial w}{\partial x} \\ \dfrac{\partial u}{\partial y} & \dfrac{\partial v}{\partial y} & \dfrac{\partial w}{\partial y} \\ \dfrac{\partial u}{\partial z} & \dfrac{\partial v}{\partial z} & \dfrac{\partial w}{\partial z} \end{bmatrix} \begin{bmatrix} l_1 & l_2 & l_3 \\ m_1 & m_2 & m_3 \\ n_1 & n_2 & n_3 \end{bmatrix} \tag{30}$$

where l_i , m_i and n_i (i=1,2,3) are the components of unit vectors.

The relation between the derivatives in global coordinates and natural coordinates is expressed as

$$\begin{bmatrix} \frac{\partial u}{\partial x} & \frac{\partial v}{\partial x} & \frac{\partial w}{\partial x} \\ \frac{\partial u}{\partial y} & \frac{\partial v}{\partial y} & \frac{\partial w}{\partial y} \\ \frac{\partial u}{\partial z} & \frac{\partial v}{\partial z} & \frac{\partial w}{\partial z} \end{bmatrix} = \begin{bmatrix} \frac{\partial x}{\partial \xi} & \frac{\partial y}{\partial \xi} & \frac{\partial z}{\partial \xi} \\ \frac{\partial x}{\partial \eta} & \frac{\partial y}{\partial \eta} & \frac{\partial z}{\partial \eta} \\ \frac{\partial x}{\partial \zeta} & \frac{\partial y}{\partial \zeta} & \frac{\partial z}{\partial \zeta} \end{bmatrix}^{-1} \begin{bmatrix} \frac{\partial u}{\partial \xi} & \frac{\partial v}{\partial \xi} & \frac{\partial w}{\partial \xi} \\ \frac{\partial u}{\partial \eta} & \frac{\partial v}{\partial \eta} & \frac{\partial w}{\partial \eta} \\ \frac{\partial u}{\partial \zeta} & \frac{\partial v}{\partial \zeta} & \frac{\partial w}{\partial \zeta} \end{bmatrix} \tag{31}$$

The displacement derivatives with respect to ξ are given by

$$\begin{Bmatrix} u_{,\xi} \\ v_{,\xi} \\ w_{,\xi} \end{Bmatrix} = \sum_{k=1}^{n} N_{k,\xi} \begin{Bmatrix} u_o^k \\ v_o^k \\ w_o^k \end{Bmatrix} + \sum_{k=1}^{n} N_{k,\xi} \zeta \frac{h_k}{2} \begin{bmatrix} \tilde{V}_{1k}^x & -\hat{V}_{2k}^x \\ \hat{V}_{1k}^y & -\hat{V}_{2k}^y \\ \hat{V}_{1k}^z & -\hat{V}_{2k}^z \end{bmatrix} \begin{Bmatrix} \beta_{1k} \\ \beta_{2k} \end{Bmatrix} \tag{32}$$

Similarly the displacement derivatives with respect to η and ζ can be obtained. The strain displacement equation relating strain components in Eq. (2) in global coordinate system to the nodal variables can be obtained. The stress components can be obtained by utilising Eqs. (4) and (5). Again Hamilton's equation Eq. (9)) and Virtual work principles (Eq. (14)) as described previously are applied to get the system stiffness, mass matrices and force vectors.

VII. THREE DIMENSIONAL FE FORMULATIONS FOR SANDWICH SHELLS BASED ON SOLID SHELL FORMULATION

The various coordinate systems as described in Fig. 4 are also used to derive solid shell finite elements. In the global coordinate, the position vector X of a point inside the element can be described as:

$$X = \overline{X} + \zeta P \tag{33}$$

where $\overline{X}$ is the position vector for the mid-surface and P is half of the vector pointing from the lower face to the upper face.

Let X_i^U and X_i^L (i=1,2,3,4) be the nodal position vectors for nodes in the upper face and lower face of the element respectively, and

$$\overline{X}_i = \frac{1}{2}\left(X_i^U + X_i^L\right) \qquad P_i = \frac{1}{2}\left(X_i^U - X_i^L\right) \tag{34}$$

where $\overline{X}_i$ is the position vector at the node on the mid-surface and P_i is half of the nodal vectors pointing from the lower nodes to the upper ones.

The position vector X and the displacement vector u in the form of isoparametric mapping can be expressed as

$$X = \sum_{k=1}^{n} N_k (\overline{X}_k + \zeta P_k) \tag{35}$$

$$u = \sum_{k=1}^{n} N_k (\overline{u}_k + \zeta p_k) \tag{36}$$

where

$$\overline{u}_i = \frac{1}{2}\left(u_i^U + u_i^L\right) \tag{37}$$

$$p_i = \frac{1}{2}\left(p_i^U + p_i^L\right) \tag{38}$$

Here u_i^U and u_i^L are nodal displacement vectors (in the local coordinate) for the upper and the lower faces, respectively.

With the definitions in Eqs. (35) and (36), the solid shell element formulations are similar to the shell elements as described previously. Hence following the usual finite element formulations, the system stiffness, mass matrices and force vectors can be obtained. It should be noted that solid finite elements contain degrees of freedom at the upper and lower faces of the laminae. Hence the laminate analysis is carried out by assembling the matrices layer by layer as opposed to two dimensional formulations described previously.

VIII. PLANE STRESS ANALYSIS FOR COMPRESSIVE STRENGTH OF THICK COMPOSITE STRUCTURES

The composite material usage in primary load bearing structures has led to increasing thickness of the fabricated composite parts. The manufacturing of thicker composite parts can lead to the introduction of defects during the resin infusion and curing process. Typical defects like fiber waviness, voids and delaminations are observed in such components. Understanding the compressive strength limits of UD composites and their dependency on the defect size is critical from a structural design perspective [21]. Micromechanical modeling of composite parts to predict compressive strength of a thick UD composite material is challenging due to the computational cost of modelling individual fibers and matrix layers.

Waviness can be induced in the fiber during the layup and resin infusion process or during the curing process due to thermal mismatch between laminate and the mold surface. Typically, fiber waviness will lead to local shear yielding of the matrix layers adjacent to the wavy fibers, which causes fiber microbuckling and kink-band type of failure. Another mode of failure observed under compression is by splitting at the fiber-matrix interface.

The number of experimental studies [21] on the thickness effects on compressive strength is rather limited. This is primarily due to the fact that problems related with testing, such as increased chances of premature failure due to end crushing, are exacerbated with thicker composites. In spite of such difficulties, test results have revealed the tendency that the failure strength decreases with increasing thickness of composite laminates. Hence, there is a definite need to develop reliable models that capture this thickness scaling trend while incorporating fiber waviness as the sole failure mode. This can lead to computational as well as experimental benefits in predicting compressive response of thick composites using scaled, thin coupon finite element and test geometries.

To enable a controlled study on fiber wave induced compressive failure in this work, the fiber wave has been characterized by the fiber wave length (L) and height (a), along with the coupon thickness (tc) (Fig. 5), with the fiber waves present all through the coupon thickness.

The overall coupon length was chosen appropriately - short enough that global Euler buckling would be avoided and long enough that the ends did not affect the stress state near the wavy region. In all analyses and testing carried out, it was verified that the Euler critical buckling load was much higher than the peak stress obtained for the corresponding case thus eliminating global buckling as a failure mode.

In this approach, a scaled down model of the composite with alternating layers of fiber and resin was created. The resin layers were epoxy (Fig. 6) and modeled with elastic-plastic material properties and the glass fiber was modelled using linearly elastic properties [25].

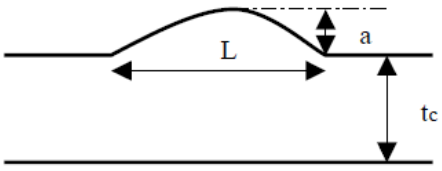

Fig. 5 Schematic of a Coupon with a Fiber Wave

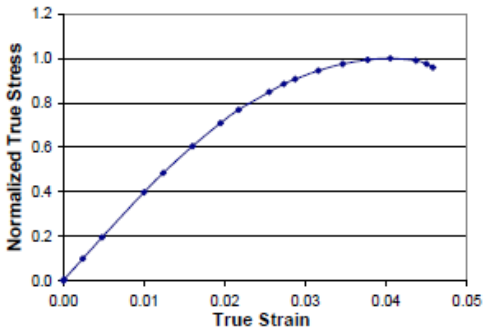

Fig. 6 Normalised stress-strain curve for resin

A parametric FE micromechanical model (Figs. 7 and 8) was developed in ANSYS® to model compression on a two-dimensional coupon with a given surface defect and coupon thickness. The required geometric inputs and material parameters are read in to generate the model through ANSYS® scripts.

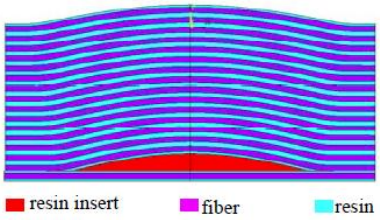

Fig. 7 Micromechanical model geometry

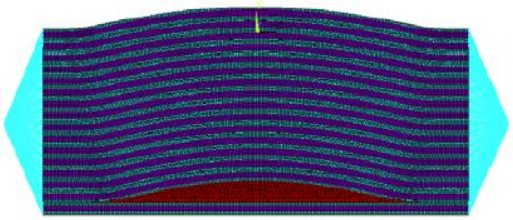

Fig. 8 FE Micromechanical model with coupled end face constraints

The surface and interior defect waves are generated using a combination of a cosine function and a circular fillet that smoothly transitions the cosine curve to the straight portion of the coupon. Propagating the surface wave towards the root defect along directions obtained using the surface and root defect waves generates the intermediate layers. It is worth noting

that the intermediate layers will be of uniform thickness only for the case when this propagation direction coincides with the normal at each point on the cosine curves (of the surface and root defects). For any other direction of propagation, the layers will have non-uniform thicknesses. In order to address issue, the intermediate layers are generated as follows: (i), the centroidal line of a fictitious tow comprised of one fiber layer with half a layer of resin on either side is propagated by the aforementioned approach; (ii), fiber areas of uniform thickness are generated about each centroidal line; and (iii), the remaining areas surrounding the fibers are filled with resin. This approach ensures that the fiber layers are of uniform thickness and all non-uniformity is distributed in the resin layers, thus mimicking a practical fabrication process.

Here, a practical issue resulting from the use of fillets in the geometry is addressed. The user input wave heights (of surface and interior waves) are lowered because of fillet insertion at ends of the wave geometries. Further, the defect locations through the thickness as well as the coupon thickness are modified because of the discreteness of the number of fiber and matrix layers. The input wavelengths (of surface and interior waves) remain unchanged. In order to correct for these modifications to the desired inputs, an inverse geometry calculation is performed over a design space to find the right required input geometry values that will generate the desired user-input geometries. The user-input geometry is set as the target with respect to which the cost of deviating is minimized. This results in generating a model whose dimensions best match the user-input geometry.

A nonlinear, large deformation analysis is carried out using displacement controlled axial compressive loading applied to the end faces, each of which is coupled to a multi-point constraint (MPC) node. The peak load is captured as a nodal reaction load at the point of unloading, representing a fiber microbuckling instability. The post peak analysis is not continued, as the interest is to capture the first point of failure.

The tow-level model is one in which the fiber and resin properties are homogenized to generate effective properties of a tow layer (Fig. 9).

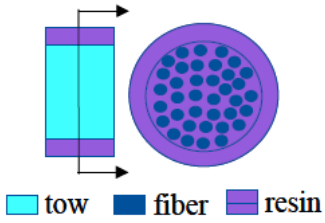

Fig. 9 Schematic cross section of a tow layer embedded in resin.

Comparing identical coupon and wave geometries modeled with a tow model vs. a micromechanics model as described previously leads to the following modifications:

(i) The tow has linearly elastic properties obtained from homogenizing the linearly elastic moduli of the fiber and resin.

(ii) The thickness of the tow, which is several times the fiber thickness, is computed by ensuring that the overall fiber volume fraction remains the same between both modeling approaches. One important consequence of this modification is that the effective resin thickness that can be plastically deformed reduces when compared to the micromechanics model. In general, this results in higher coupon peak compressive response than a micromechanics model of identical coupon and wave geometries.

(iii) The material properties for the tow have to be specified using local element coordinates because the homogenization creates a material directionality to the tow layer.

Thus, the tow model enables a reduced computational cost arising from discretization, model size and analysis time. However, this computational advantage also results in the loss of some stress state detail within the tow (i.e., in the individual fibers and resin comprising the tow) as well as the overhead of maintaining local element coordinates to specify material properties for the tow. The material properties of the tow layer as well as the creation of the FE model including the local element coordinates are shown in Figs. 10 and 11.

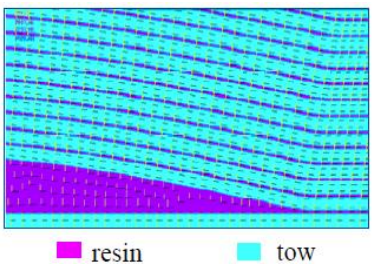

Fig. 10 FE Tow level model of the coupon

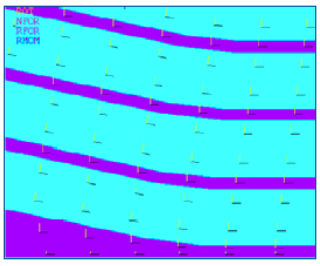

Fig. 11 View of elemental coordinate systems in the FE Tow level model of the Coupon

The micromechanical model was evaluated against a physical coupon test and the tow model for peak compressive coupon response. The parameterized micromechanical model was run for different coupon thicknesses while maintaining the other non-dimensional geometric parameters, i.e., the wave aspect ratio (aR = L/a) and the wave height as a percentage of the thickness (wH = a/tc), constant. The peak compressive response is compared between the micromechanics analyses and the physical test in Fig. 12. A tapering plateau effect of the compressive response with respect to coupon thickness is immediately apparent from the micromechanical analysis. The fluctuations in micromechanical peak stress with respect to thicknesses less than 4 mm are not considered to be significant. However, the overall trend of peak stress tapering to a plateau with increasing coupon thickness still remains. Further, beyond around 6 mm of coupon thickness, the micromechanics results are in excellent agreement with the tests (performed on a coupon 20 mm thick). The test coupons were made from a panel and the wave defect height and other parameters were measured at five different locations for each panel. The variability in the various defect geometric parameters leads to variability in the failure strength of the composites. Another component adding to variability in the failure strength of tested coupons is the material property variation of the resin. The good agreement between the micromechanical kink-band model and the experimental test indicates that the first peak stress is largely governed by kink-band formation as the failure mechanism.

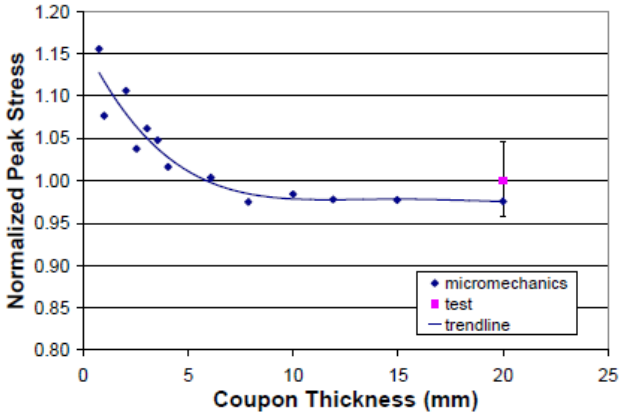

Fig. 12 Comparison of micromechanics with physical test for a defect geometry with a_R=37,
Stresses are normalised with respect to the test average peak stress

Next, the micromechanical model was evaluated against the tow model for a specific wave geometry. The peak compressive response for increasing coupon thicknesses in the micromechanics model was compared (Fig. 13) with the tow model results for a 20 mm thick coupon. As discussed previously, the peak compressive response from the tow model upper-bounds the converged (with respect to coupon thickness) micromechanics response. This brings to attention that the strain levels in the resin within the tow reach yield values, which are not captured by the homogenized, linearly elastic tow material properties. It provides further support to the fact that the micromechanics model affords a level of detail that is both necessary and sufficient - necessary because of the results in Fig. 13, and sufficient because of the good agreement with the coupon test in Fig. 12.

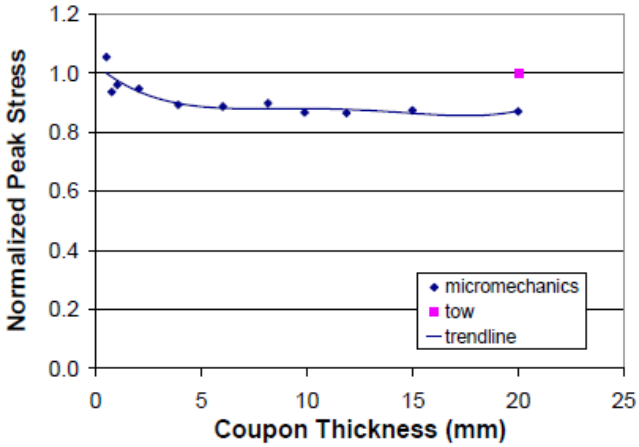

Fig. 13 Comparison of micromechanics with tow level for a defect geometry with a_R=17.46.
Stresses are normalised with respect to the tow peak stress

Further, the micromechanical model was compared with the tow model for different wave geometries for a fixed wave height (Fig. 14). It is evident that a 6 mm thick micromechanics model sufficiently captures the compressive peak response as provided by a 20 mm thick tow model for a variety of wave geometries.

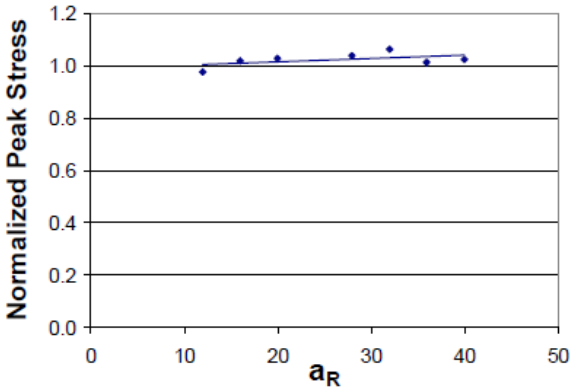

Fig. 14 Comparison of micromechanics with tow model for varying fiber wave geometries. Each entry is the ratio of the peak stress in a 6 mm thick micromechanics coupon model to that in a 20 mm thick tow coupon model

Finally, the thickness variation in the micromechanics model is explored in the case of severe defect geometry with steep fiber waves (Fig. 15). The conclusions from Figs. 12 and 13 on the thickness variation of the compressive response remain applicable to this case too, and a tapering trend of the compressive response with respect to coupon thickness is observed once again.

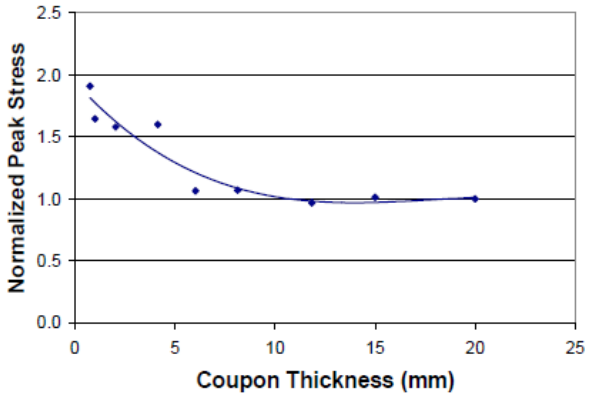

Fig. 15 Micromechanics thickness scaling results for a severe defect geometry with a_R =8. Stresses are normalized with respect to the peak stress corresponding to tc=20 mm

IX. PLANE STRAIN ANALYSIS FOR TENSILE STRENGTH OF T-COMPOSITE JOINTS

T joints form parts of composite wind turbine blades. Hence MSC/PATRAN 2005 was used as the pre-processor for the T joint analysis [26] as shown in Fig. 16.

Fig. 16 Test set up for a T-Joint

For the simulations and post-processing steps, ABAQUS 6.7 was used. The details of a 3D model was prepared in PATRAN as shown in Fig. 17.

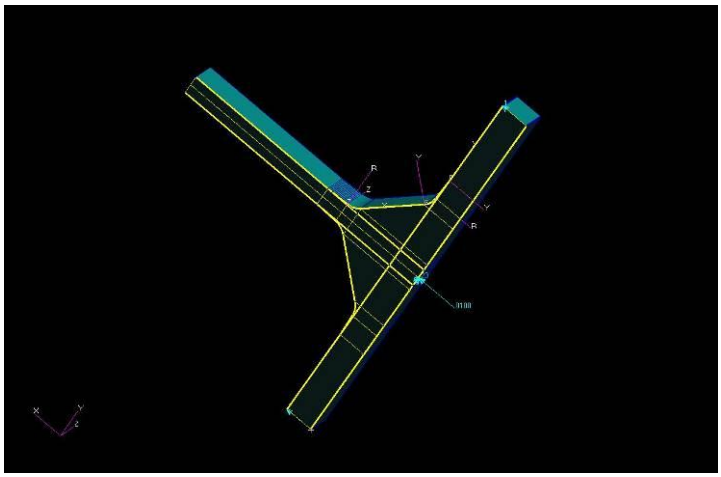

Fig. 17 Three dimensional model of a Tee Joint with load and material coordinate systems

The T joint was reduced to a 2D model in the *x-y* plane under plane strain for initial analysis. Local rectangular coordinate systems were implemented in the structural parts so as to assign material properties accordingly. A cylindrical coordinate system was applied for the materials in the curved region of the T-Joint. For initial analysis, three nodded triangular elements are used. The coordinates of all points as shown in Fig. 17 were calculated by implementing sub-elements of T Joint in ABAQUS/CAE. The numerical values are then used in PATRAN to create 3D and 2D models. It was decided to assume plane stress conditions followed by plane strain conditions to understand the behaviour of T-Joint qualitatively. The following material properties are used for the materials used in the T-Joint.

- For 0/90 Woven Roving Lamina:

$E_{11} = 23.47$ GPa, $E_{22} = 23.56$ GPa, $E_{33} = 10.45$ GPa, $G_{12} = 3.41$ GPa, $G_{13} = 3.25$ GPa, $G_{23} = 3.25$ GPa, $\nu_{12} = 0.128$, $\nu_{13} = 0.406$, $\nu_{23} = 0.406$.

- For +/- 45 ST Lamina:

$E_{11} = 16.96$ GPa, $E_{22} = 23.56$ GPa, $E_{33} = 16.96$ GPa, $G_{12} = 3.33$ GPa, $G_{13} = 3.25$ GPa, $G_{23} = 3.33$ GPa, $\nu_{12} = 0.154$, $\nu_{13} = 0.293$, $\nu_{23} = 0.267$.

- For Balsa:

$E_{11} = 1.355$ GPa, $E_{22} = 0.054$ GPa, $E_{33} = 0.054$ GPa, $G_{12} = 0.201$ GPa, $G_{13} = 0.201$ GPa, $G_{23} = 0.059$ GPa, $\nu_{12} = 0.351$, $\nu_{13} = 0.351$, $\nu_{23} = 0.360$.

The details of the behaviour of the T-joint under 0.01 inch displacement at the center are shown in Figs. 18 and 19 for plane strain conditions.

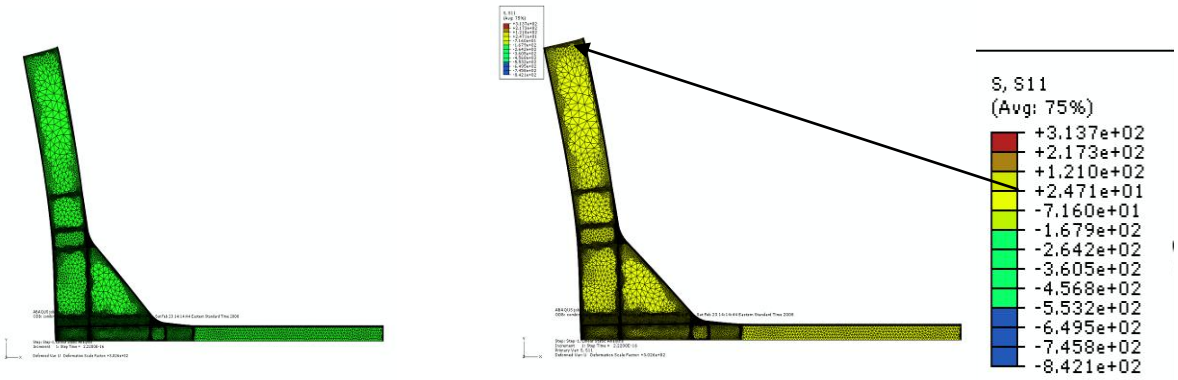

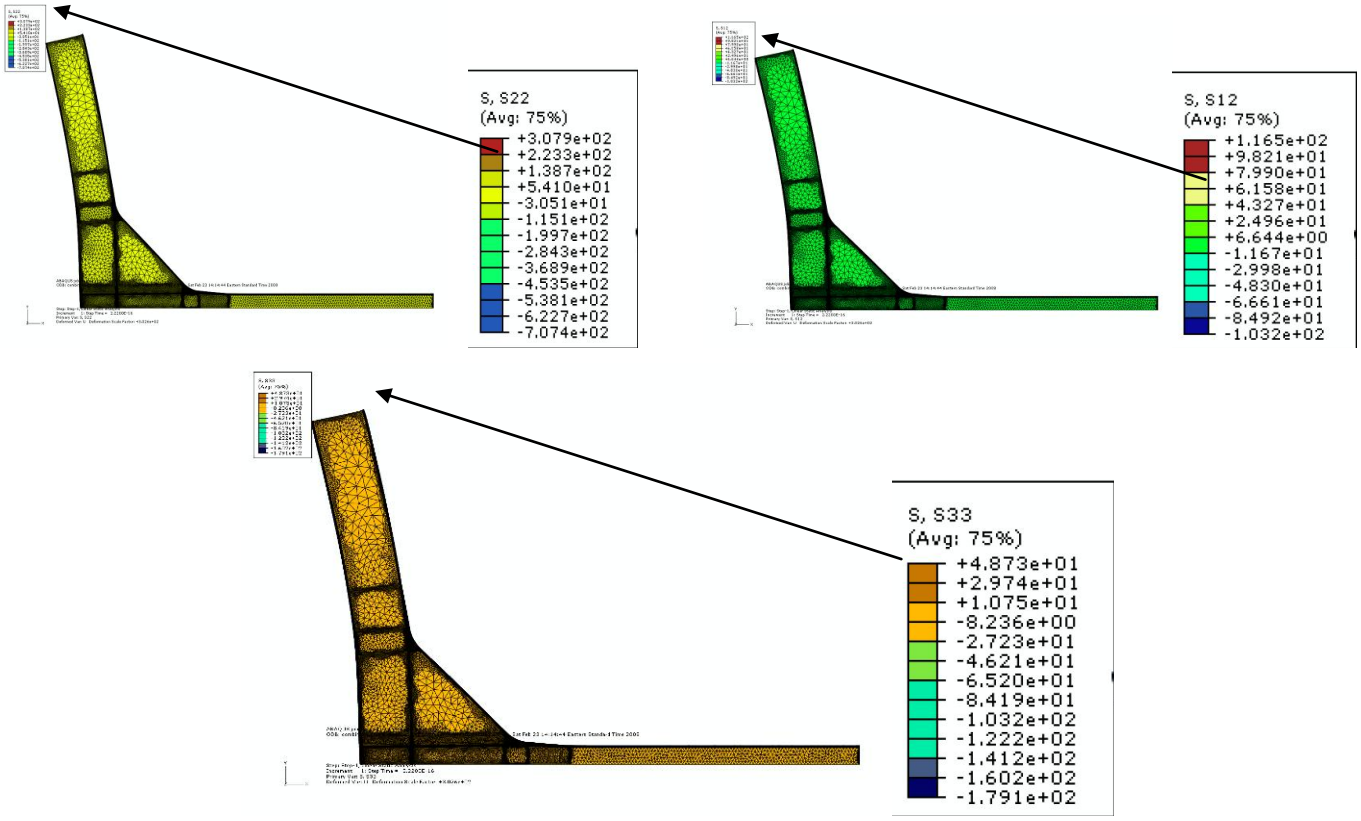

Fig. 18 Deformed shape and stress distributions of the T-joint under 0.01 inch loading under plane strain condition

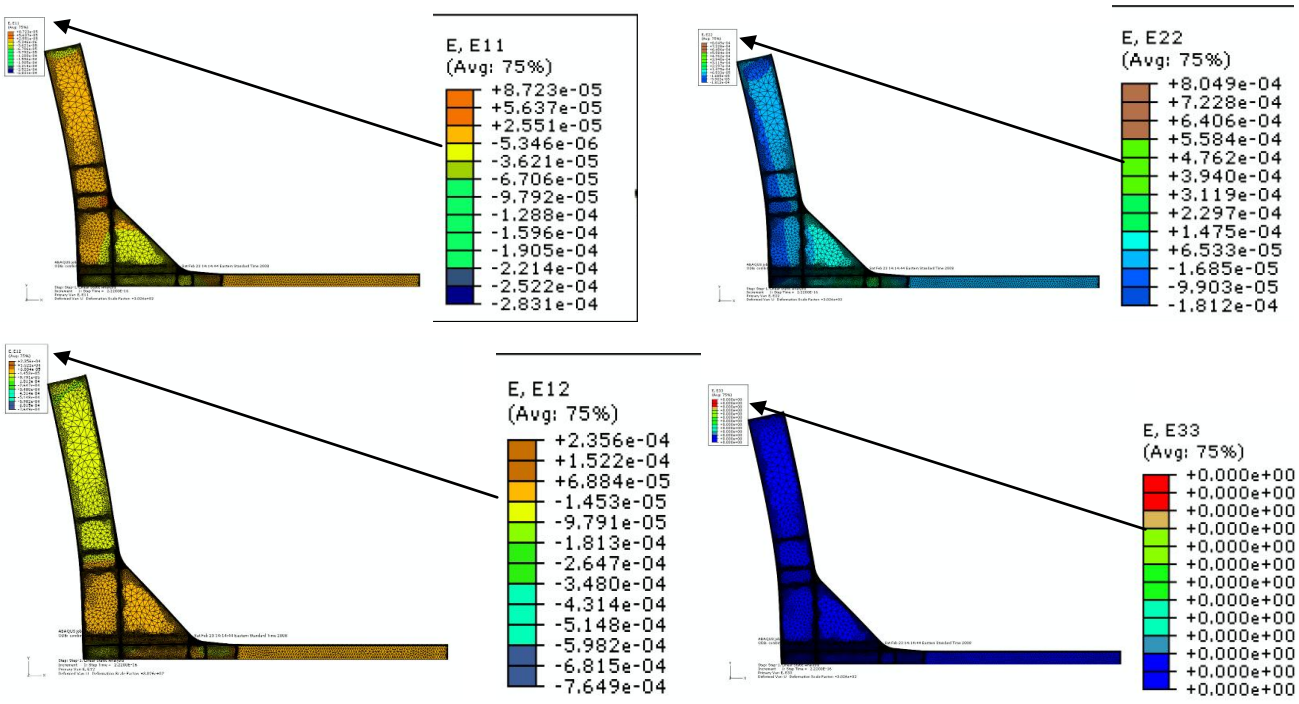

Fig. 19 Strain distributions of the T-joint under 0.01 inch loading under plane strain condition

X. GENERALIZED PLANE STRAIN ELEMENTS

Though plane stress and plane strain elements give stress distributions in Joints, it is not possible to obtain all the components of strain and stress distributions in a joint using plane stress and plane strain elements. Hence generalized plane strain analysis is carried out to get the results for three dimensional stress and strain distributions in a laminate. In order to test the accuracy of generalized plane strain elements, two patch tests are performed on isotropic and anisotropic materials. The patch size is a=1mm, b=1mm, h=1mm as shown in Fig. 20.

The following material properties are selected: For isotropic cases: $E = 210.0\,\text{GPa}$ and $\nu = 0.30$ IM7/8552 unidirectional graphite/epoxy prepeg [27] $E_{11} = 161.0$ GPa, $E_{22} = E_{33} = 11.38$ GPa, $G_{12} = G_{13} = 5.17$ GPa, $\nu_{12} = \nu_{13} = 0.32$, $G_{23} = 3.92\,\text{GPa}$, $\nu_{23} = 0.45$ Analysis is performed on CMAP [26] (composite material application program based on closed form solution) to get the information about the strains to be applied to the considered problem. A load of 2100 MPa is applied in x-direction which generates a strain of 0.01 in x-direction and -0.0030 in y-direction. As expected the strain in z-direction is $\varepsilon_{zz} = -\nu_{xz}\varepsilon_{xx}$. A generalized plane strain element (CPEG3N) [28] is implemented to generate the test problem for ABAQUS element CPEG3. Details of the generalised plane strain finite element formulation can be found in [28]. It was found that ABAQUS CPEG3 element does not pass the required test for anisotropic cases. A problem is under taken for a laminated $(0/45/-45/90)_s$ plate under tension in x-direction. a=1mm, b=267.2mm, h=10.688mm, b/h=25, $h_{ply} = 1.336$mm. The model is created in ABAQUS as shown in Fig. 21 to generate the input file for CPEG3N.

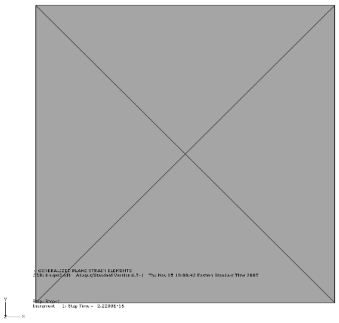

Fig. 20 Patch test problem for isotropic and anisotropic cases

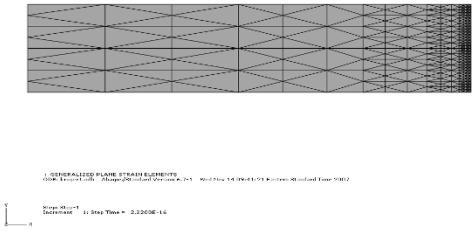

Fig. 21 Test problem for free edge problem

The results for stresses and strain are compared with CMAP developed by UD-CCM. Details are shown in Figs. 22-34.

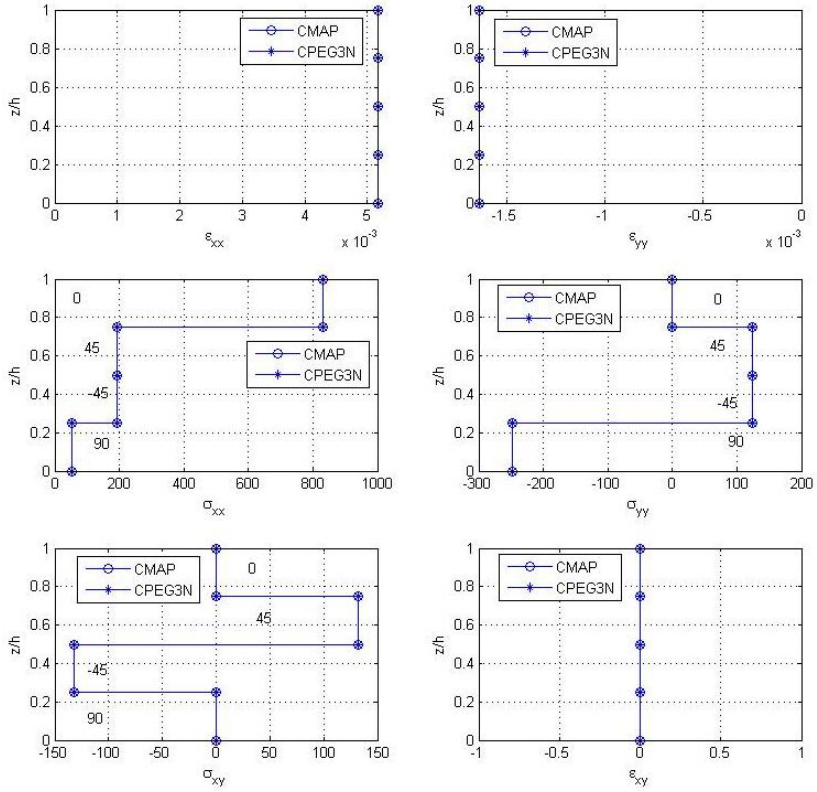

Fig. 22 Test problem for laminate $[0/45/-45/90]_S$ free edge problem, Variation of stresses and strains through the thickness

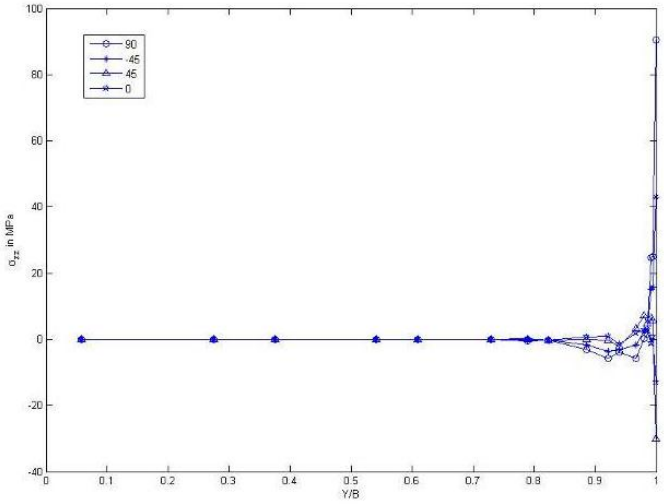

Fig. 23 Test problem for laminate $[0/45/-45/90]_S$ free edge problem, Variation of σ_{zz} stress through the width

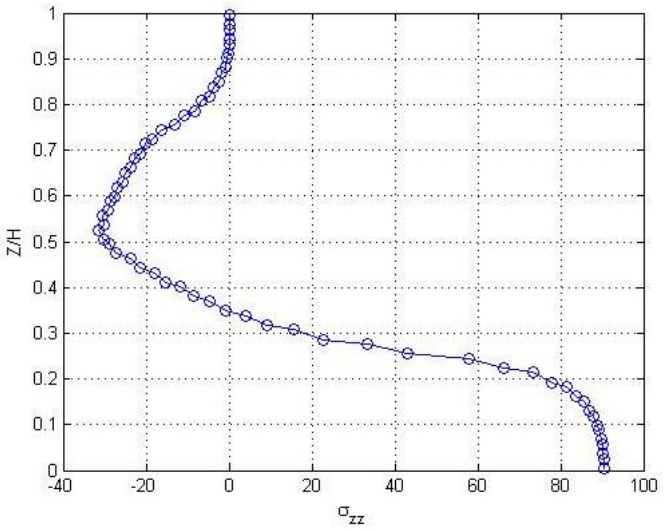

Fig. 24 Test problem for laminate $[0/45/-45/90]_S$ free edge problem, Variation of σ_{zz} stress through the thickness

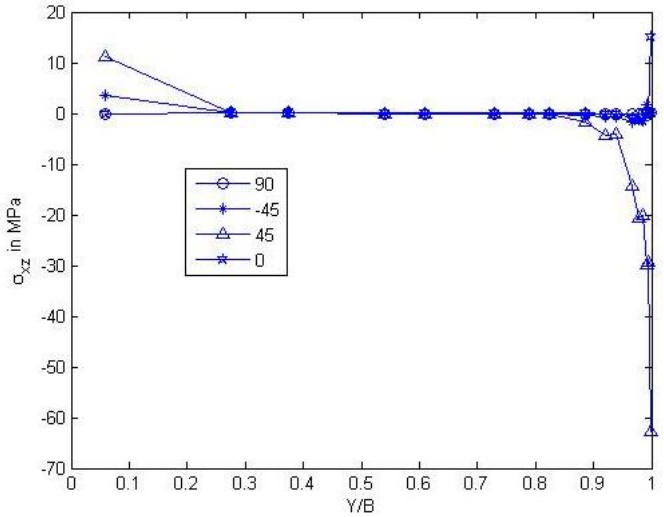

Fig. 25 Test problem for laminate $[0/45/-45/90]_S$ free edge problem, Variation of σ_{xz} stress through the width

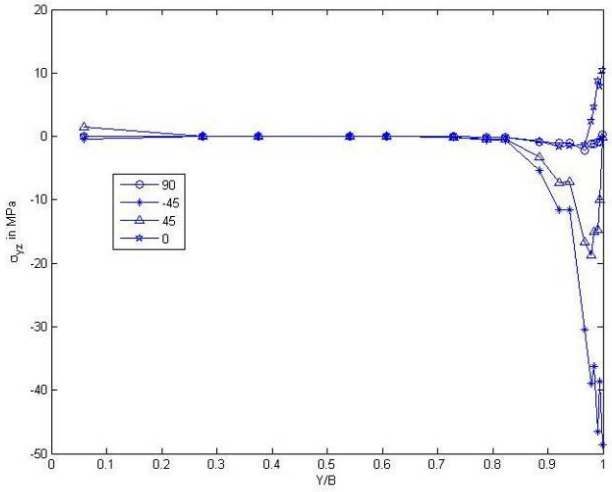

Fig. 26 Test problem for laminate $[0/45/-45/90]_S$ free edge problem, Variation of σ_{yz} stress through the width

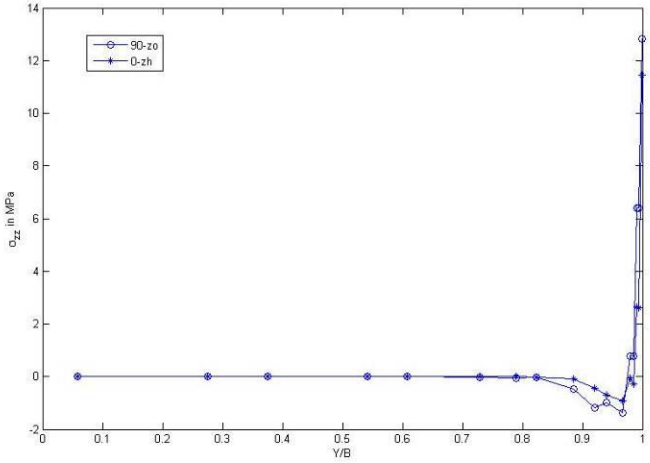

Fig. 27 Test problem for laminate $[0/90]_S$ free edge problem, Variation of σ_{zz} stress through the width

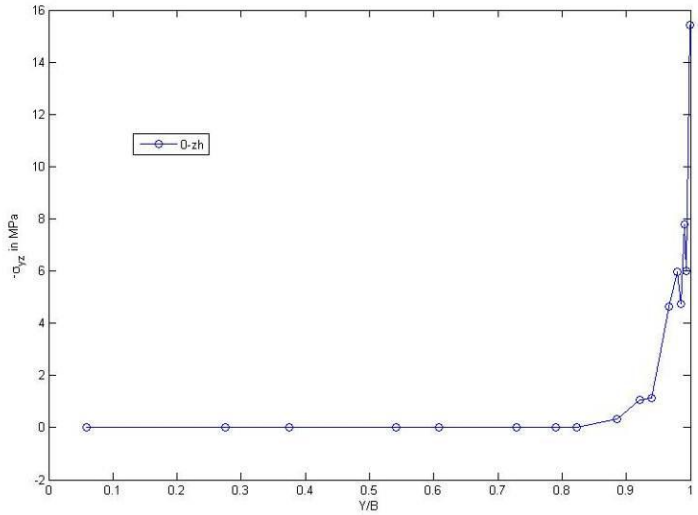

Fig. 28 Test problem for laminate $[0/90]_S$ free edge problem, Variation of σ_{yz} stress through the width

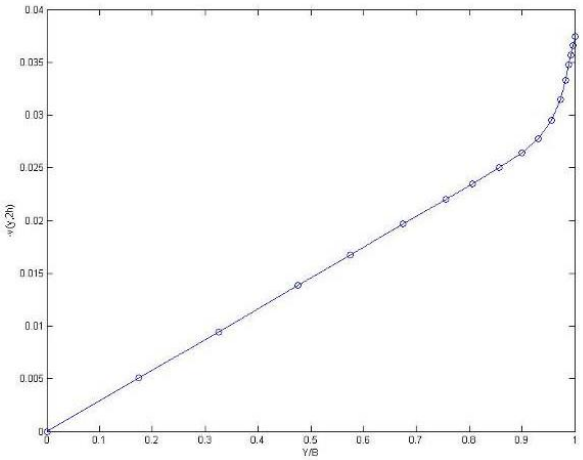

Fig. 29 Test problem for laminate $[0/90]_S$ free edge problem, Variation of v(y,2h) through the width Y/B

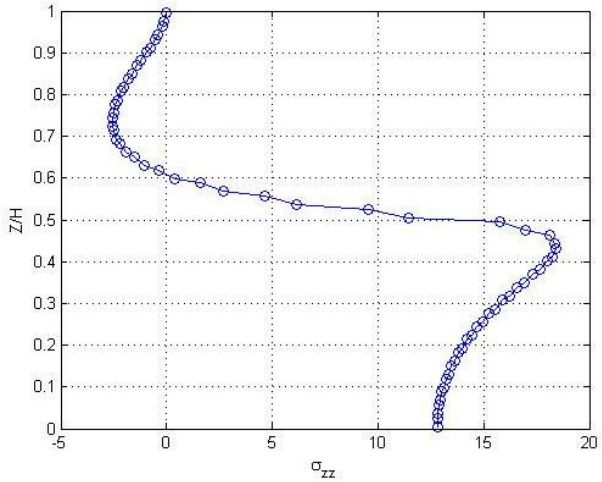

Fig. 30 Test problem for laminate $[0/90]_S$ free edge problem, Variation of σ_{zz} stress through the thickness Z/H

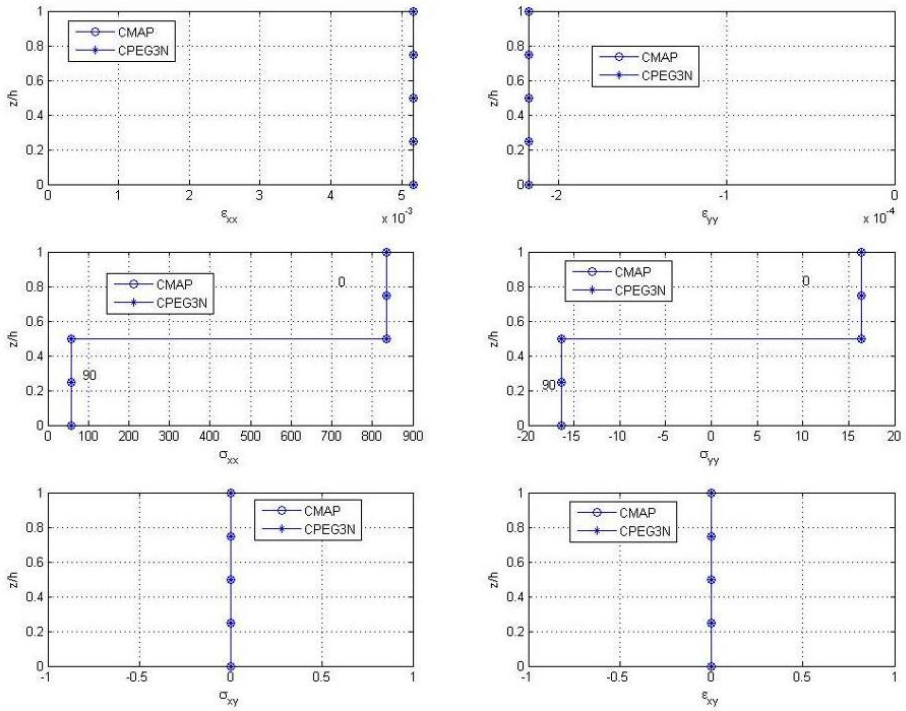

Fig. 31 Test problem for laminate $[0/90]_S$ free edge problem, Variation of stresses and strains through the thickness z/h

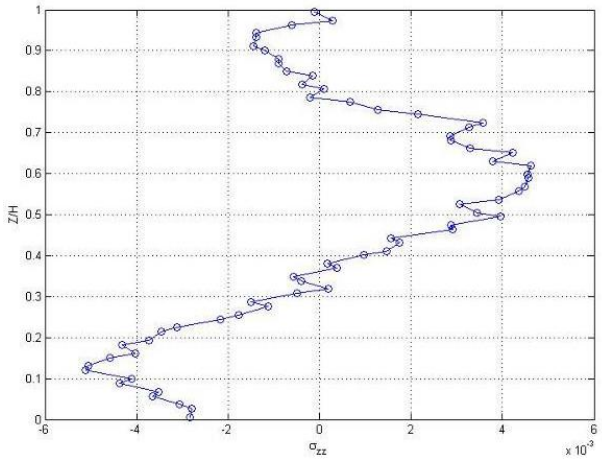

Fig. 32 Test problem for laminate $[0]_8$ free edge problem, Variation of σ_{zz} stress through the thickness Z/H

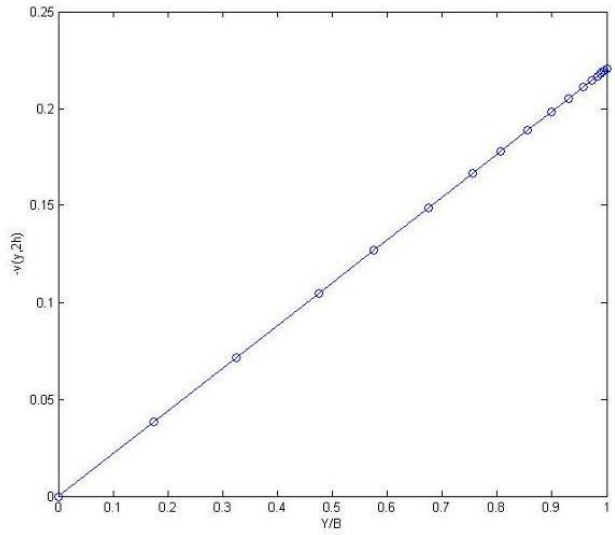

Fig. 33 Test problem for laminate $[0]_8$ free edge problem, Variation of v(y, 2h) through the width Y/B

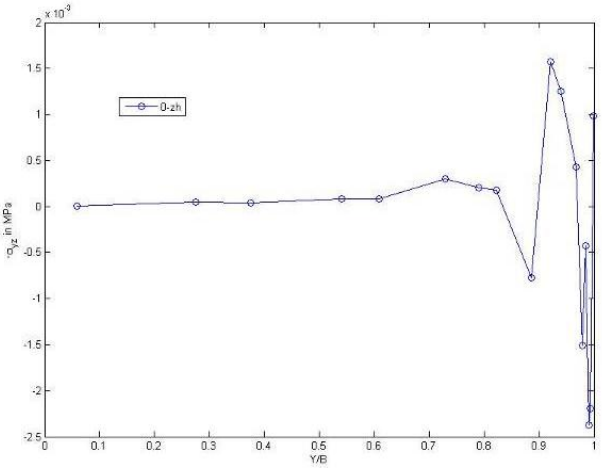

Fig. 34 Test problem for laminate $[0]_8$ free edge problem, Variation of σ_{yz} stress through the width Y/B

The details of other finite elements for composite panels which find applications in composite wind turbine blades under varying loading conditions can be found in [29-38].

XI. CONCLUSIONS

In this chapter, various formulations in the analysis of composite plates and shells are described. Plane stress, plane strain and generalised plane strain finite element approaches to deal with composite materials which found applications in composite

wind turbine applications are discussed. The following specific conclusions can be made:

- Two dimensional finite element formulations for composite sandwich plates are presented. A plate bending element based on first order shear deformation theory (FSDT) is developed. A drilling rotational degree of freedom is implemented within the plate finite element formulation. Assumed strain concept is adopted for a defect free finite element. Widely used discrete Kirchhoff theory (DKT) plate bending element based on classical laminate plate theory (CLPT) is implemented for a patch test problem. An empirical shear correction factor which is a function of Reissner's classic shear correction factor of 5/6 and thin parameter involving length to thickness ratios is proposed. It is found that the results from FSDT with the use of empirical shear correction factor gives close results with respect to CLPT. Hence it could be stated that the CLPT is a subset of FSDT with the use of appropriate shear correction factor.
- Two dimensional assumed strain finite element formulations for sandwich shells based on flat facetted shell formulation are developed. Transformation matrix from local to global axes is used for obtaining stiffness and consistent mass matrices. It is found that the shell finite element with incorporation of drilling rotational degree of freedom passes the obstacle tests and gives satisfactory results on a wide range of static and dynamic field problems.
- Two dimensional finite element formulation based on doubly curved shell formulation is presented. Two dimensional finite element formulations for sandwich shells based on three dimensional degenerated shell formulation is discussed. Since for very thick plates and shells, two dimensional formulations give unsatisfactory results, a three dimensional FE formulations for sandwich shells based on solid shell formulation is given.
- The compressive peak response of a coupon with fiber waviness is studied for different wave geometries and coupon thicknesses. Two modelling approaches are explored - (i) a micromechanics approach in which individual fiber and resin layers are explicitly modelled, and (ii) a tow-level approach in which the fiber and resin properties are homogenized to generate effective properties of a tow which is comprised of a fibers and resin. The following points are in order. a) The micromechanics model is in excellent agreement with the coupon test confirming that first failure is kink-band dominated. b) The tow model provides an upper-bound to the peak compressive response generated from the micromechanics model. It is hypothesized that this is caused by the tow properties being elastic whereas the micromechanics includes the complete elastic-plastic detail of the resin within the tow thereby capturing the material behaviour more accurately. c) In both the above comparisons, the peak compressive response from the micromechanics model is studied for increasing coupon thicknesses and a tapering trend converging to a plateau value was observed. d) A 6 mm thick micromechanics model is able to capture the peak compressive response of a 20 mm thick tow model for a variety of fiber wave geometries, thereby lending support to the fact that an appropriately scaled micromechanics model is capable of capturing bulk response for thick geometries accurately, while simultaneously including individual fiber and resin detail.
- A plane strain finite element formulation for tensile strength of T composite joints has been discussed. Different coordinate systems have been used to carry out the analysis. Though it is possible to get two dimensional stress and strain parameters within a plane strain formulation, it is not possible to get all three dimensional quantities required for complete study. Hence a generalised plane strain formulation is discussed where it is possible to get all the three dimensional quantities.

It is hoped that all finite element formulations discussed above are essential to model the composite wind turbine blades for complex design issues.

REFERENCES

[1] R. A. Shenoi, A. Groves and Y. D. S. Rajapakse, "*Theory and Applications of Sandwich Structures*," Dorset Press, Dorchester, Dorset, UK. 2005.

[2] A. K. Nayak and R. A. Shenoi, "The finite element analysis of sandwich plates and shells" in *Theory and Applications of Sandwich Structures edited by* R. A. Shenoi, A. Groves and Y. D. S. Rajapakse pp. 267–286, 2005.

[3] O. C. Zienkiewicz, "*The finite element method*," 1977, 3rd Edition, Mc-Grawhill, London.

[4] R. D. Cook, "*Concepts and applications of finite element analysis*," 1981, 2nd Edition, John Wiley and Sons, New York.

[5] K. J. Bathe, "*Finite element procedures in engineering analysis*," 1982, Printice-Hall, Englewood Cliffs, New Jersey.

[6] J. N. Reddy, "*An introduction to the finite element method*," 1993, McGraw-Hill, Inc, New York.

[7] J. N. Reddy, "*Mechanics of laminated composite plates and shells, Theory and Analysis*," 2004, 2nd Edition, CRC Press, Boca Raton.

[8] J. R. Vinson, "*The behaviour of sandwich structures of isotropic and composite materials*," 1999, Technomic Publishing Co, Inc, Lancaster.

[9] J. R. Vinson, "*Sandwich Structures*," Applied Mechanics Reviews, ASME, 2001, vol. 54, 201-214.

[10] A. K. Noor, W. S. Burton and C. W. Bert, "*Computational models for sandwich panels and shells*," Applied Mechanics Reviews, ASME, 1996, vol. 49, pp. 155-199.

[11] T. Kaneko, "*On Timoshenko's correction for shear in vibrating beams*," Journal of Physics D, Applied Physics, 1975, vol. 8, pp. 1927-1936.

[12] T. S. Chow, "*On the propagation of flexural waves in an orthotropic laminated plates and its response to an impulsive load*," Journal of Composite Materials, 1971, vol. 5, pp. 306-319.

[13] J. M. Whitney, "*Stress analysis of thick laminated composite and sandwich plates*," Journal of Composite Materials, 1972, pp. 426-440.

[14] J. M. Whitney, "*Shear correction factors for orthotropic laminates under static load*," Journal of Applied Mechanics, 1973, pp. 302-304.

[15] T. S. Chow, "*Theory of unsymmetric laminated plates*," Journal of Applied Physics, 1975, vol. 46, 219-221.

[16] P. MadabhusiRaman and J.F. Davalos, "*Static shear correction factor for laminated rectangular beams*," Composites Part B-Engineering, 1996, vol. 27, pp. 285-293.

[17] V. Birman and C. W. Bert, "*On the choice of shear correction factor in sandwich structures*," Journal of Sandwich Materials and Structures, 2002, pp. 83-95.

[18] R. D. Cook, "*Four node flat shell element-Drilling Degrees of Freedom, Membrane Bending Coupling, Warped Geometry and Behavior*," Computers and Structures, 1994, pp. 549-555.

[19] E. N. Dvorkin and K. J. Bathe, "*A Continuum Mechanics Based Four-Node Shell Element for General Non-linear Analysis*," Engineering Computations, 1984, pp. 77-88.

[20] A. K. Nayak, R. A. Shenoi and J. I. R. Blake, "*A study of transient response of initially stressed composite sandwich folded plates*," Composites Part B, 2013, pp. 1-15.

[21] K. M. Rao and U. Srinivas, "*A set of pathological tests to validate new finite elements*," Sadhana-Academy Proceedings in Engineering Sciences, 2001, pp. 549-590.

[22] R. H. MacNeal and R. L. Harder, "*A proposed standard set of problems to test finite element accuracy*," Finite Elements in Analysis and Design, 1985, pp. 3-20.

[23] J. L. Batoz, "*An explicit formulation for an efficient triangular plate bending element*" International Journal for Numerical Methods in Engineering, 1982, pp. 1077-1089.

[24] A. K. Nayak, R. A. Shenoi and J. I. R. Blake, "*A computer aided FEM Based numerical solution for transient response of laminated composite plates with cutouts*," Accepted for publication in International Conference on Structural Engineering and Mechanics, Dec. 2013, NIT Rourkela, India.

[25] K. Chadrasekere, D. Patro, A. K. Nayak, S. C. Quek and C. Yerramalli, "*Scaling studies in modelling for compressive strength of thick composite structures*," Proceedings of the ASME International Mechanical Engineering Congress and Exposition, Vancouver, Canada, 2010, pp. 1-7.

[26] A. K. Nayak, J. W. Gillespie Jr and D. Heider, "*Testing and analysis of T-joint under tensile loading*," Internal Report, Center for Composite Materials, University of Delaware, USA, 2008, pp. 1-30.

[27] R Krueger, I. L. Paris, T. K. O'Brien and P. J. Minguet, "*Comparison of 2D finite element modelling assumptions with results from 3D analysis for composite skin stiffner debonding*," Composite Structures, 2002, pp. 161-168.

[28] R. D. Kriz, "*Influence of Ply Cracks on Fracture strength of graphite-epoxy laminates at 76K*," Effects of defects in composite materials, ASTM STP836, American Society for Testing and Materials, 1984, pp. 250-265.

[29] A. K. Nayak, R. A. Shenoi and S. S. J. Moy "*Dynamic response of composite sandwich plates subjected to initial stresses*," Composites Part A- Applied Science and manufacturing, 2006, 37, pp. 1189-1205.

[30] A. K. Nayak, R. A. Shenoi and S. S. J. Moy, "*Transient response of composite sandwich plates*," Composite structures, 2004, vol. 64, pp. 249-267.

[31] A.K. Nayak, R.A, Shenoi and J.I.R. Blake, "*Transient response of initially stressed composite sandwich plates*," finite Elements in Analysis and Design, 2006, vol. 42, pp. 821-836.

[32] A.K. Nayak, S.S.J. Moy and R.A. Shenoi, "*Quadrilateral finite elements for multilayer sandwich plates*," Journal of strain analysis, IMech E, 2003, 38, pp. 1-18.

[33] A. K. Nayak and R. A. Shenoi, "*Assumed strain finite elements for buckling and vibration analysis of initially stressed damped composite sandwich plates*," Journal of Sandwich Structures and Materials, 2005, pp. 307-334.

[34] A. K. Nayak, S. S. J. Moy and R. A. Shenoi, "*A higher order finite element theory for buckling and vibration analysis of initially stressed composite sandwich plates*," Journal of Sound and Vibration, 2005, pp. 763-780.

[35] A. K. Nayak, S. S. J. Moy and R. A. Shenoi, "*Free vibration analysis of composite sandwich plates based on Reddy's higher order theory*," Composites Part B: Engineering, 2002, vol. 33, pp. 505-519.

[36] A. K. Nayak, R. A. Shenoi and J. I. R. Blake, "*Analysis of damped composite sandwich plates using plate bending elements with substitute shear strain fields based on Reddy's higher order theory*," Journal of Mechanical Engineering Sciences, IMechE, Part C, 2002, pp. 591-606.

[37] M. Jureczko, M. Pawlak, A Mezyk, "*Optimisation of wind turbine blades*," Journal of Materials Processing Technology, 2005, 167, pp. 463-471.

[38] A. Ghoshal, M. J. Sundaresan, M. J. Schulz, P. F. Pai, "*Structural health monitoring techniques for wind turbine blades*," 2000, vol. 85, pp. 309-324.

Dr Ajaya Nayak is currently a Reader within the Civil Engineering Department, Veer Surendra Sai University of Technology, Burla, Odisha, India. He was an Associate Professor in Civil Engineering, Kalinga Institute of Industrial Technology University, Bhubaneswar for two and half months. He was a Lead Engineer, Material Mechanics Laboratory, Material System Technologies, General Electric Global Research, Bangalore, India for two and half years after working as a Research Associate in Center for Composite Materials, University of Delaware, USA for Six Months. Previously He worked as a Research Fellow, Ship Science Department, University of Southampton, UK for five and half years.

Dr Nayak received a Bachelor of Engineering Degree with Honors (Civil Engineering) from the National Institute of Technology, Rourkela, India, 1994, Master of Engineering Degree (Structural Engineering) from the Indian Institute of

Science, Bangalore, India, 1999 and a Ph.D. in sandwich structures (School of Civil Engineering and the Environment and School of Engineering Sciences) from the University of Southampton, UK in 2002. He has about two years civil engineering industry experience in India prior to joining Master of Engineering degree program. He has more than 50 publications including 9 peer reviewed journal papers and one book chapter. He has about seven years Teaching experience during the time at VSSUT, Burla, KIIT University, Bhubaneswar, General Electric Global Research, Bangalore, India and University of Southampton, UK.

His current research interests are in the Composites, Structural health monitoring, Processing, Reliability and safety, Mechanics, Fracture and fatigue, Design. His teaching interests are in the Structural Integrity, Marine safety and environmental engineering, Finite element analysis, Failure of materials, Mechanics, Numerical methods, Structures and materials, Theory of plate structures, Structural analysis, Materials and structural engineering. He has guided two MTech Students in Structural Engineering at VSSUT, Burla and acted as MS and PhD external examiners in Sambalpur University and Indian Institute of Science, Bangalore respectively. He is a reviewer for a number of Journals. He organised a National Conference in Recent Advances in Mechanics and Materials RAMM-2012 in VSSUT, Burla in 2012.

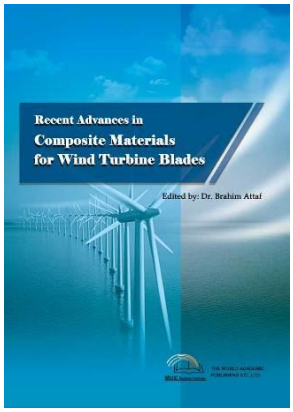

Recent Advances in Composite Materials for Wind Turbine Blades
Edited by Dr. Brahim Attaf

ISBN 978-0-9889190-0-6

Hard cover, 232 pages

Publisher: The World Academic Publishing Co. Ltd.

Published in printed edition: 20, December 2013

Published online: 20, December 2013

This book of science and technology provides an overview of recent research activities on the application of fibre-reinforced composite materials used in wind turbine blades. Great emphasis was given to the work of scientists, researchers and industrialists who are active in the field and to the latest developments achieved in new materials, manufacturing processes, architectures, aerodynamics, optimum design, testing techniques, etc.. These innovative topics will open up great perspectives for the development of large scale blades for on- and off-shore applications. In addition, the variety of the presented chapters will offer readers access to global studies of research & innovation, technology transfer and dissemination of results and will respond effectively to issues related to improving the energy efficiency strategy for 2020 and the longer term.

How to cite this book chapter

Nayak A. K. (2013). Finite Element Modeling of Composite Wind Turbine Blades, *Recent Advances in Composite Materials for Wind Turbines Blades*, Dr. Brahim Attaf (Ed.), ISBN 978-0-9889190-0-6, WAP-AMSA, Available from: http://www.academicpub.org/amsa/chapterInfo.aspx

World Academic Publishing - Advances in Materials Science and Applications

Chapter 8

Multidisciplinary Optimization of Wind Turbine Blades with Respect to Minimize Vibrations

Mariola Jureczko

Department of Theoretical and Applied Mechanics, Silesian University of Technology
Konarskiego 16 A Street, 44-190 Gliwice, Poland
Mariola.Jureczko@polsl.pl

I. INTRODUCTION

The main objectives of the research related to the development of wind energy are focused on increasing wind turbine power output and decreasing cost of obtained energy. Although wind turbine power output depends on blades shape and their dimensions (i.e., the power output increases three times with respect to the blade length), it is profitable to produce light and long blades, but this requires necessity of proper selection of materials and structures. However, it is important to note that increasing blade length means changing wind turbine dynamic properties. Another reason to design blades that ensure a maximum possible power output and functioning properly and trouble-free for many years, is the fact that they only cost about 10% of the total manufacturing cost of a wind turbine. From a technical point of view, the design of wind turbine consists of looking for solutions that allow the wind turbine to produce as much as possible electrical power per year. On the other hand, the aerodynamic efficiency of the wind turbine depends on the shape of the blade profile. Therefore, the choice of the optimal shape of the wind turbine blade is a primary task in the design process of wind turbine.

The design process of wind turbine blades places strong emphasis on reducing its mass, ensuring adequate load transfer, which often means a reduced stiffness. According to the rules based on experience, the mass of the blade should increase three times depending on its length. Such dependence may be softened by the use of certain techniques, such as modification in blades construction or development of methods for their production. Goeij et al [1] have described some different concepts of production, taking into account the fatigue of composites loaded eccentrically with respect to the fiber orientation. The publication contains also a description of the construction of the blades, manufacturing techniques, materials used. Naturally, modifications in the materials used is another technique - modifications of composite material used as sheathing material may lead to an increase in the thickness and density of balsa layer, or increase of reinforcement layers or changes in the type of fibers and their orientation. The composite materials used in the spars may be modified in a similar manner.

However, while designing wind turbine blades, it is important that the shape of the blade must ensure adequate aerodynamic properties, proper shape and stiffness to avoid collisions with the tower when wind blowing at high speed. Lifetime of wind turbines is at least 20 years. In addition, the wind turbine must provide the possibility of a low noise generation. The outer layer of the sheathing (gel-coat) must be resistant to dirt and temperature variations, which means providing a high aerodynamic efficiency under different weather conditions.

The necessity for consideration of various aspects of design process of wind turbine blades makes the optimization a very complex task, which requires applications supporting multi-criteria optimization methods. The main goal of the optimization process of wind turbine blades, due to the dynamic changes in the operating conditions of wind turbine, is to provide adequate dynamic characteristics for the whole system. The dynamic characteristics of wind turbines depend on the natural frequencies and spectral functions. The model presented in this chapter does not include aerodynamic damping, thus the dynamic properties of wind turbine depends only on the form and values of stiffness matrix and mass matrix. The aim of the research presented in this chapter is to minimize vibration amplitudes of wind turbine blades which are loaded with mass and aerodynamic forces. Loads are determined on the basis of modified BEM method. Calculations are performed for horizontal axis wind turbines (HAWTs). According to IEC classification of turbines, the weather conditions correspond to a wind turbine of Class I.

II. DETERMINATION OF BLADE GEOMETRY

The process of designing wind turbine blades is based on a certain type of optimization process during which the optimal geometry of the blade is determined. This will ensure the production of wind power less than or equal to the rated power of the generator. The determination of optimal shape of wind turbine blades is a compromise between adequate mechanical and

aerodynamic properties. Thus, the optimization of geometric properties of wind turbine blade involves the determination of:

- the distribution of the pitch angle along the blade span;
- the distribution of the twist angle along the blade span;
- the distribution of the inflow angle along the blade span;
- the distribution of the chord width along the blade span.

Optimal values of geometric properties of wind turbine blade are developed based on the dependencies described in Blade Element Momentum Theory [2, 3], the values are presented in the graphs shown in Figs. 1-4.

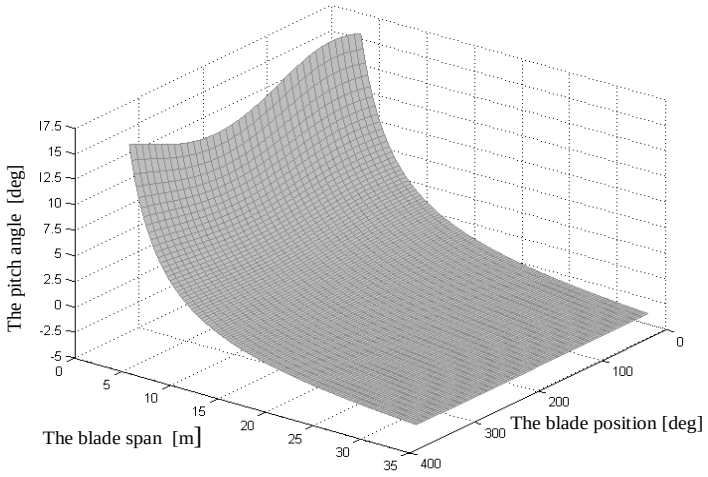

Fig. 1 Distribution of the pitch angle along the blade span depending on the blade position

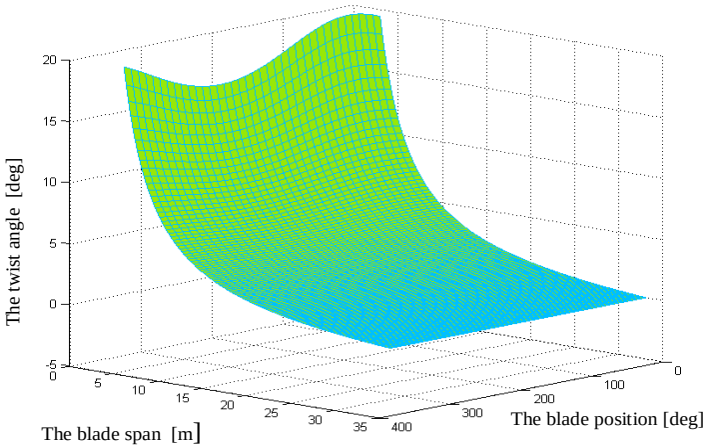

Fig. 2 Distribution of the twist angle along the blade span depending on the blade position

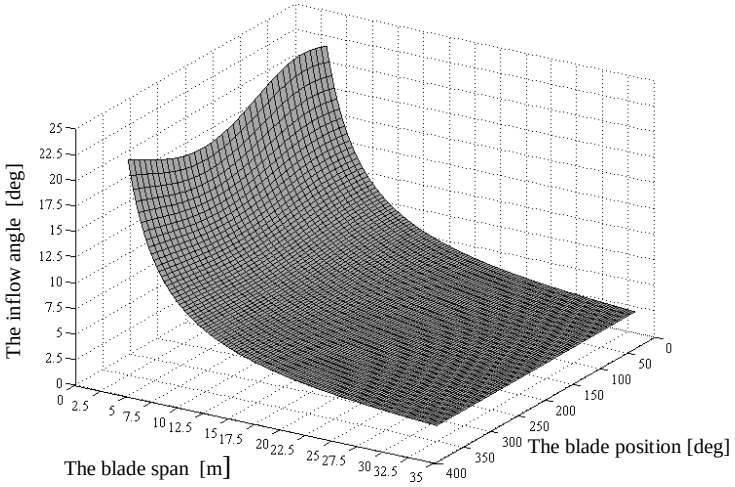

Fig. 3 Distribution of the inflow angle along the blade span depending on the blade position

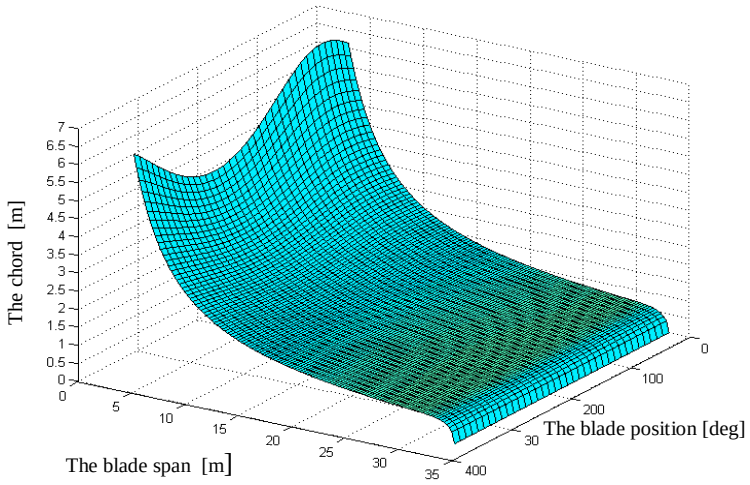

Fig. 4 Distribution of the chord along the blade span depending on the blade position

With the increase of the normal component of induced velocity, which increases proportionally with the distance between rotor axis and aerodynamic cross-section, the value of lift force will also increase. Reducing the width of the blade between the leading edge and trailing edge, namely the reduction of the chord in direction of the blade tip, makes it possible to counteract this phenomenon. But having a significant load at the blade tip makes it necessary to increase the chord at the tip. Aerodynamic cross-sections near hub transfer significant loads and stresses from other parts; therefore the blade profile near the hub has a larger size with respect to the rest of the blade construction. Whereas, along the blade span, it becomes thinner to maintain proper aerodynamic properties. In order to ensure better fit the end of the blade to the hub it has a rim shape [4, 5].

III. NUMERICAL MODEL OF THE WIND TURBINE BLADE

The work presented in this chapter was performed on a three-bladed horizontal axis wind turbine. The turbine under investigation is a turbine rotor which uses asynchronous motor-driven, upwind type with pitch regulation system. The blade was divided into 23 aerodynamic cross-sections, selecting for each one a different airfoil. The numerical model uses airfoil series FFAW3-xxx and RISØ procedures, characterized by further relations between the profile width, the chord length and the aerodynamic properties. The thickness-to-chord ratio depends on the selected aerodynamic profiles. Near the root of the blade, circular profiles are used with a thickness-to-chord ratio equal to 100%, which decreases smoothly to 14% on the tip of the blade.

Additionally, in order to increase the longitudinal stiffness of the blade made of composite, either longitudinal spars or transversal spars are bonded into the half-shells. With this solution the blade internal structure is more stiff and resistant to wind loads [6]. To enable the blade to respond to change in wind velocity vector, which experiences along its span during the rotation, the cross-section of the blade must be twisted along the shear axis along the blade span (Fig. 5) [7]. According to literature data it appears that gravity center of aircraft wing is located between the center of elasticity and the center of aerodynamic forces (center of pressure). In aircraft the position and the order of centers are different than in wind turbine blades. According to [4], the blade is to be twisted around the shear axis. In modern wind turbines, the center of elasticity is placed between the gravity center and the center of aerodynamic forces. The position of the spars can be determined with respect to the position of the shear axis. However, twisting the wind turbine blade along the shear axis must be controlled at the same time as the positioning of the centers of gravity and aerodynamic. These positions and the shear axis can be adjusted by changing the location of the spars and the possible modification of their shape [8].

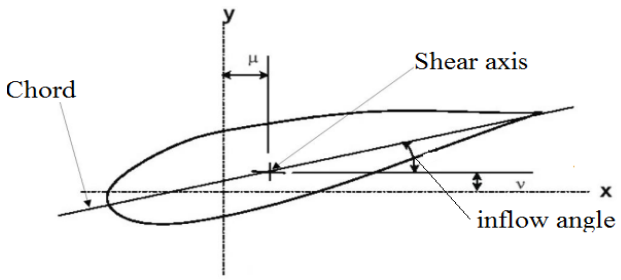

Fig. 5 Location of the shear axis and the main axes of the coordinate system [7]

The longitudinal spars are not twisted in the similar way as airfoils. When twisting the longitudinal spars, the blade would have the form shown in Fig. 6.

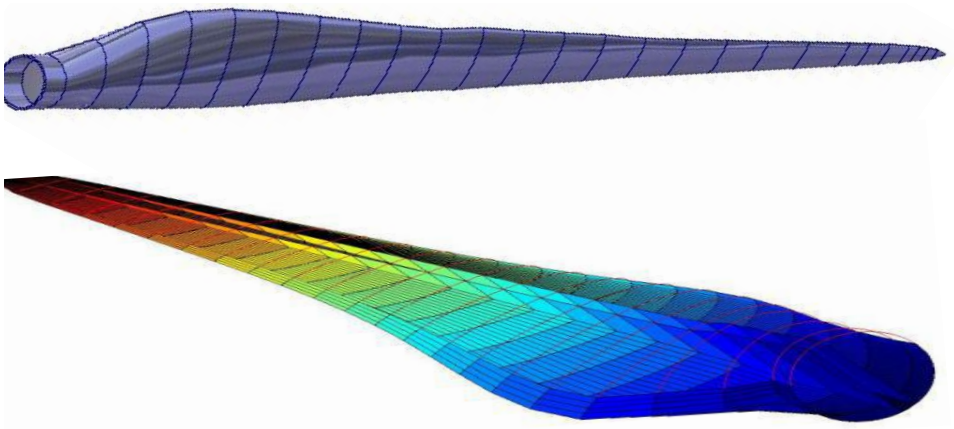

Fig. 6 The model of the blade in CAD software and Ansys

The aerodynamic profiles of wind turbine blade are decided about the aerodynamic characteristic of the blade. In [8] is mentioned that the location of the main longitudinal spars (also called supporting webs) together with the location of the transversal spars (also called stiffening ribs) will have the biggest influence on the bending modes of the blade. Twist of the blade is decided about value of aerodynamic loads, but also the direction in which the blade will vibrates. The twist of the longitudinal spars decides about pitch of principal bending axes. According to [4], the blade has to be twisted around the shear axis.

In addition, it should be pointed out that aerodynamic damping is a very important dynamic aspect. The negative value of aerodynamic damping means that some additional energy is added to the blade during vibration and the amplitude of vibration is increased. Aerodynamic damping has in-plane and out-of-plane components. Damping in in-plane direction will have the negative value if the blade section produces the power. If the damping in out-of-plane direction is positive, by twisting the blade the value of out-of-plane damping will decrease (but must be still positive) and the in-plane damping will receive positive values. Due to the twist of the spar, the blade will vibrate either edgewise or flapwise.

The developed structural model of the blade, which was created with Ansys® in the convention of finite element method, was used to analyse and minimize the amplitude of vibrations. Three groups of components, presented in Fig. 7, were selected for this model; these are: (i) the sheathing, (ii) the longitudinal spars (also called supporting webs) and (iii) the transversal spars (also called stiffening ribs). Selection of these components had enabled specification of various thicknesses, material data and defining various types of components.

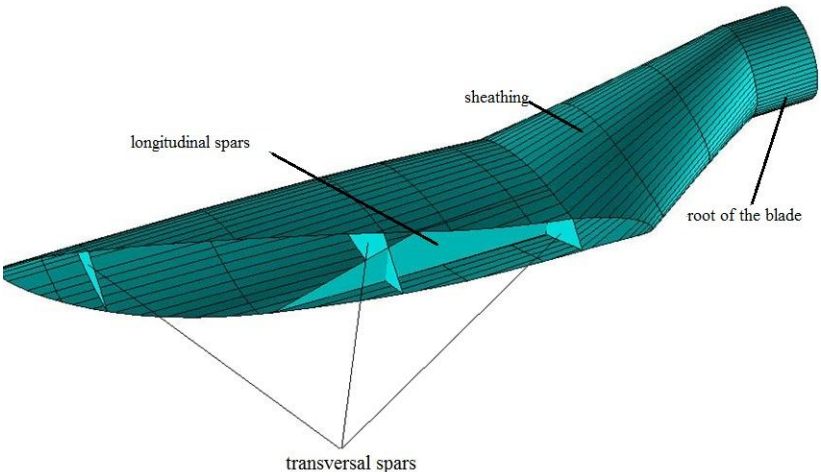

Fig. 7 The numerical model of a wind turbine blade

IV. STATE OF LOAD OF THE BLADE

The analysis of the state of load of wind turbine blade was based on the modified Blade Element Momentum theory [2, 3]. Both mass and aerodynamic loads were investigated. The determined values of mass and aerodynamic forces were used to analyse the blade stresses and strains under defined flow parameters during optimization processes. According to the presented results if only aerodynamic loads are considered the deflection of the blades is happening in the direction of the tower. Consequently, collision and damage of the wind turbine may occur. The rotor of the wind turbine rotates with constant angular velocity and the influence of centrifugal forces is significant. When the gravity and centrifugal forces are included in the load, the deflections of the blades are in opposite direction.

The analysis of the state of load on the wind turbine blade is intended to verify whether the turbine will withstand the action of load within an appropriate range of safety. Various cases of load on the blade, resulting from the action of various external factors on the turbine, have to be considered. The following types of states of load on a wind turbine blade can be defined as:

- Aerodynamic loads;
- Mass loads.

Aerodynamic loads of wind turbine blade are derived from the flow of air across the windwheel. An incoming stream of air with a velocity V_{inf} flows across the wind turbine rotor, parallel to its axis, and creates an aerodynamic force dR. The component parallel to the rotation plane of the rotor dF_{τ}^{w} causes the blade to turn, while the perpendicular component dF_{n}^{w} of the force creates an axial pressure which is transferred onto bearings. The aerodynamic force is the resultant of drag force dD acting along the velocity vector (but in the opposite sense) and is created due to the pressure of the air stream on the blade, and of lift force dL, acting perpendicularly to the direction of the velocity vector. The generation of the lift force can be explained on the basis of Bernoulli's law and theory of circulation. The upper surface of the blade is longer; therefore the air particles have to travel a longer distance above the blade than those under the blade. This phenomenon creates higher pressure above the upper part and lower pressure under the lower part. This pressure difference generates the lift force.

Aerodynamic loads applied on a wind turbine blade are shown in Fig. 8. The symbols used in Figs. 8 and 11 and Eqs. (1), (2), (4) and (6) are defined as follows:

$V_{rel}(r)$: relative velocity over the aerofoil at radius,
V_{inf}: velocity at infinity (see Fig. 11),
ω : angular velocity of rotor,
r : current radius of windwheel, i.e. position of the cross section under consideration in relation to the rotor,
α: : angle of attack,
θ : local twist angle of the blade, i.e. angle between chord line and plane of the rotor.

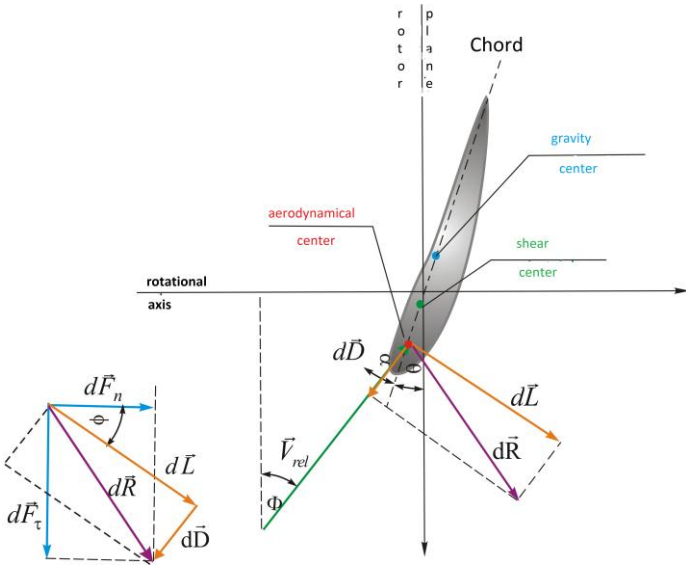

Fig. 8 Aerodynamic loads on aerofoil of a wind turbine blade

The lift and drag expressed per unit length are derived from the following relationships [2, 3]:

$$dL = \frac{1}{2} \cdot \rho \cdot V_{rel}^2(r) \cdot C_L(\alpha) \cdot c(r), \tag{1}$$

$$dD = \frac{1}{2} \cdot \rho \cdot V_{rel}^2(r) \cdot C_D(\alpha) \cdot c(r), \tag{2}$$

where, ρ is the density of air, $C_L(\alpha)$ is the lift coefficient at optimum angle of attack, $C_D(\alpha)$ is the drag coefficient at optimum angle of attack and $C(r)$ is the blade chord length at radius.

The projections of the resultant aerodynamic force on the coordinate axes of the rotor can be expressed in matrix form by the following equation:

$$\begin{Bmatrix} dF_{\tau}^{w} \\ dF_{n}^{w} \end{Bmatrix} = \begin{bmatrix} \sin\phi & -\cos\phi \\ \cos\phi & \sin\phi \end{bmatrix} \begin{Bmatrix} dL \\ dD \end{Bmatrix}, \tag{3}$$

where, pitch angle of the wind flow ϕ is determined from the relation discussed in [5], which takes account of the deviation of the wind turbine rotor both vertically and horizontally, and the inclination of the blade relative to the rotor plane. Thus, the distribution of aerodynamic forces along the blade span will vary depending on the angle position of the blade in a rotor plane. The trigonometric relationships were derived from Fig. 8:

$$\phi = \alpha_{opt} + \theta; \ \cos\phi = \frac{\omega \cdot r \cdot (1+a')}{V_{rel}}; \ \sin\phi = \frac{V_{\inf} \cdot (1-a)}{V_{rel}}, \tag{4}$$

where, *a* is the axial induction factor and *a'* is the tangential induction factor.

During the analysis of the state of loads of wind turbine blade, the assumption that was made is that the elastic axis is created by shear centers for each cross-section. The grid points are created along the centers of aerodynamic. The aerodynamic forces are applied directly to the grid point and act at the centers of aerodynamic. The force tangential to the rotor plane depends on wind velocity and angular position of the blade. At lowest wind velocities, it is easy to see a visible increase of these forces along the blade span. At higher wind velocities and by adjusting blade angle against wind velocity, the maximal force will move towards the rotor center and the power obtained in rotor will not change. This occurrence is called regulation through axis change against wind velocity.

The designated distributions of axial and tangential components of the aerodynamic forces are presented in the form of graphs as shown in Figs. 9 and 10, respectively.

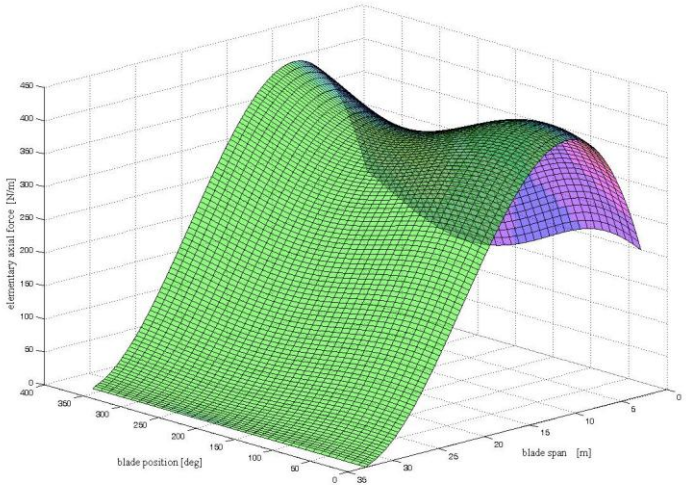

Fig. 9 Distribution of the elementary axial force along the blade span depending on the blade position

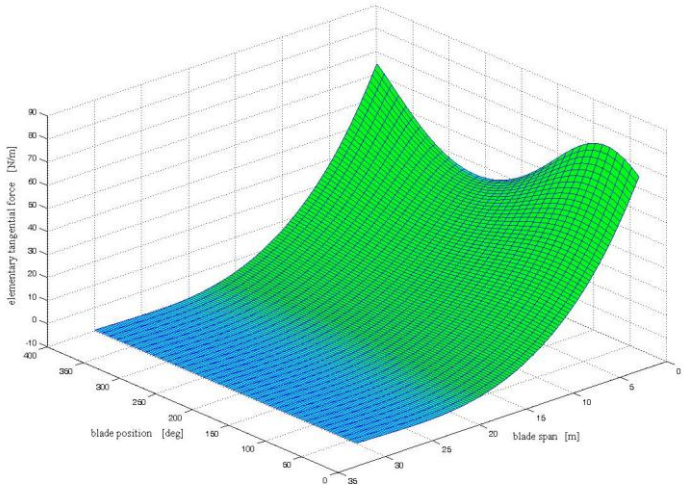

Fig. 10 Distribution of the elementary tangential force along the blade span depending on the blade position

As the wind turbine blade is slender, the loads associated with its inertia are limited to the loads generated by its weight, which causes sinusoidal loads whose frequency corresponds to the rotor rotation. Mass load of the blade is illustrated in Fig. 11.

Gravity forces are applied at the gravity centers. When the wind turbine rotor deflects vertically, then the gyroscopic forces on the blade are generated perpendicular to the rotor plane. Rapid rotor deflection causes an occurrence of large gyroscopic force in the rotor. In real control systems, the deflection of the rotor is programmed to occur slowly, so gyroscopic moments do not play a significant role.

The force of gravity is derived from the following relationship:

$$F_g = m_c \cdot g, \tag{5}$$

where, g is the acceleration of gravity and m_c is the total mass of the blade.

When the wind is blowing on wind turbine blade, this causes its retroversion. To ensure balanced loads that are generated from the wind velocity, the blades are retroversed with an angle β. This causes that tangential and axial components of the centrifugal force will occur along the blade span. The axial component, which acts in the direction opposite to the wind velocity, causes bending moment in the opposite direction of the torque that is created by the wind loads [2]. This effect is called centrifugal relief and its associated force is derived from the following formula:

$$dF_o = \int_r^R dF_o = \int_r^R r \cdot \omega^2 \cdot m dr, \tag{6}$$

where, r is the current radius of windwheel (i.e. position of the cross section under consideration in relation to the rotor); ω is the angular velocity of the rotor and m_i is the mass of the i-th segment of the blade.

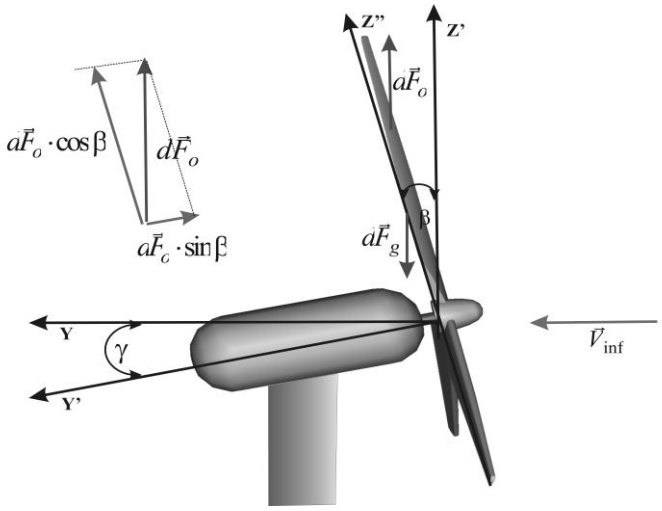

Fig. 11 Gravity and inertial loads on the wind turbine

V. REDUCTION OF THE NUMBER OF DEGREES OF FREEDOM IN THE NUMERICAL MODEL OF THE BLADE

The created simplified model of the real physical system was realized in order to enable the dynamic analysis of the real system to be performed [9].

One of the well-known methods of condensing complex models, which is used in many finite element software packages such as MSC/Nastran and Ansys, is the Guyana condensation method. This method is based on the assumption of energy conservation, kinetic and potential systems under the assumption that the relationship between the master and slave nodes is based on static analysis. To reduce the number of degrees of freedom the Guyana condensation method was applied [10].

According to the Guyana condensation method in the numerical model of complex model of wind turbine blade calculated vector of eigenvalues ϑ with *dofs x 1* dimension (where *dofs* – degrees of freedom) is decomposed as two vectors: subvector ϑ_{mdofs} composed of overrideing degrees of freedom (called master degrees of freedom, i.e., *mdofs*) and subvector ϑ_{sdofs} composed of secondary degrees of freedom (called slave degrees of freedom, i.e., *sdofs*).

By considering the mode condensation technique, only master-type degrees of freedom are saved, therefore self-issue of the structure may be solved using the following equation [11]:

$$\left(\mathbf{K}_K - \mathbf{M}_K \omega^2\right)\vartheta_{mdofs} = 0, \tag{7}$$

where, matrices of mass and stiffness, and eigenvalue vector decrease in sizes to *mdofs x mdofs* and *mdofs x 1*, respectively.

In the reduction of degrees of freedom in the discrete model, very important is appropriate selection of parent nodes called

master. Thus decision which nodes becomes master and which will be eliminated is difficult, also very important. Although we can give a hint that says that nodes to eliminate are these which influence on kinetic and potential energy is minimal, it requires a lot of intuition gained earlier, while condensing other models.

In this work the nodes which best reflects the first five mode shapes of wind turbine blade structure were selected as master nodes. The technique of selection of numerical model of master nodes is described in [9].

Comparison of dynamic properties of the numerical models of the blade before and after condensation was based on the criteria specified in the MAC according to the relation expressed by the following equation [12]:

$$MAC(t,k) = \frac{\left|\sum_{i=1}^{n} (\vartheta_t)_i \cdot (\vartheta_k)_i\right|^2}{\left\{\left(\sum_{i-1}^{n} (\vartheta_t)_i^2\right) \cdot \left(\sum_{i=1}^{n} (\vartheta_k)_i^2\right)\right\}} \tag{8}$$

where:

ϑ_t vector of eigenvalues of the complex numerical model,

ϑ_k vector of eigenvalues of the simplified numerical model.

Condensation of model can be considered as correct if the determined values of MAC criterion are in the range of 0.6-1.0. However, it would be better if this value is close to one [10].

The individual error of eigenvalues was determined using the following formula:

$$\delta f_i = \frac{\left|f_c^i - f_k^i\right|}{f_c^i}, \tag{9}$$

where:

f_c^i – i-th natural frequency of the system without condensation,

f_k^i – i-th natural frequency of the system with condensation.

The determined first five free vibration modes (i.e., natural frequencies and mode shapes) using MAC criterion and the individual error of eigenvalues are shown in Table 1.

TABLE 1 COMPARISON OF DYNAMIC PHENOMENA OF NUMERICAL MODEL OF THE BLADE WITHOUT AND WITH CONDENSATION

No mode shape	Model without condensation [natural frequencies Hz]	Model with condensation [natural frequencies Hz]	MAC criterion	δf [%]
1	 0.27666 Hz	 0.27839 Hz	1	0.6
2	 1.016254 Hz	 1.07095 Hz	0.9972	5
3	 1.1331 Hz	 1.1562 Hz	0.9996	2
4	 2.5354 Hz	 2.58234 Hz	0.9997	1.9
5	 3.7642 Hz	 3.782734 Hz	0.9989	0.5

Analysing obtained values of the MAC criterion (obtained values are close to one) and individual error of eigenvalues, it can be concluded that condensation process has been properly carried out. The simplified numerical model of wind turbine blade was applied to the analysis of the results obtained, i.e. comparison of the dynamic properties of numerical model of the wind turbine blade before and after optimization.

The structure of the numerical model reflecting the real system is described with the available data regarding the stiffness, inertia and damping matrices. The sizes of these matrices depend on the number of finite elements used for the discretization of the numerical model. So, to create a numerical model with large number of degrees of freedom necessities a long time numerical calculations, this can be realized to solve the dynamic problem of such model. The complex numerical model of the blade was applied to optimization calculations. This was ensured by the high accuracy of determining strength and modal properties of the blade model [9].

VI. SELECTION OF COMPOSITE MATERIALS

In the developed numerical model of wind turbine blade, three groups of components were selected; each one with a different material properties. Usually longitudinal spars responsible for the stiffness are made of carbon fibers. Calculations also assume that longitudinal and transversal spars are made of laminate with multiple layers of glass-epoxy, and orthotropic mechanical properties, and adjancted layers are oriented at $\pm 45°$. Calculations are performed using material properties values undertaken from [13]. It is important to note that the number of composite layers used for longitudinal and transversal spars may vary between locations along the blade span. Both longitudinal and transversal spars thickness are design variables. Thus, the number of composite layers is design variable also. Their number may be ranged from 10 to 30, so that the total thickness of the spars corresponds to the value obtained from the optimization.

The main role of the sheathing of wind turbine blade is to achieve best aerodynamically properties, it is usually made of glass fibers and represents a compromise between mechanical parameters and price. Using this criterion the sheathing is finally taken to be a 7-layer composite that contains: gel coat, laminate glass fibers randomly distributed in a matrix epoxy, the triaxial fabric is denoted CDB340 (it has a 25%, 25% and 50% distribution of $+45°$, $-45°$, and $0°$ fibers, respectively), balsa, the uniaxial fabric denoted A260, balsa, the triaxial fabric is denoted CDB340. The mass and stiffness properties for each material for calculations are taken from [14, 15]. Thickness of layers consisting of gel coat, laminate glass fibers randomly distributed in the matrix epoxy are taken from factory data. Balsa thickness is 0,75% and 1,5% of chord in selected aerodynamic part. Thickness of layer made of uniaxial fabric denoted A260 is calculated as 2% quotient of blades length and width. Using this assumptions, sheathing thickness changes proportionally along blade span, it is thick near the base (where the greatest load is applied) and thin at the tip. This construction corresponds well to the real constructions. The triaxial fabric (denoted as CDB340) layer thickness is taken from numerical calculations.

VII. FORMULATION OF OPTIMIZATION PROBLEM

The design of wind turbine blades requires a number of optimization criteria to be taken into account. In general these criteria are mutually uncountable, incomparable and in some cases even contradictory. In such cases the optimization process comes down to finding an optimum compromise by way of implementing preferences among the criteria or using additional information. It is not possible to formulate the problem of optimum design of wind turbine blades as a single-criterion optimization task. The problem of optimum design of the wind turbine blade was formulated as a multicriteria discrete – continuous problem, which enables simultaneous investigation of several criteria. The values of individual criteria depends both on parameters of continuous nature (thickness of chosen elements) and discrete nature (number of transversal spars, their arrangement along blade span). The important aspect of efficiency of scientific researches was to develop suitable way for the exchange of data and cooperation between commercial software Ansys® and author's proprietary program. The aim of this study was to develop a computer program package that would enable optimization of wind turbine blades with regard to a number of criteria.

Representation of the optimization criterion in the form of an explicit continuous function is difficult in practice; therefore optimization methods inspired by genetics and evolution are often applied. Such algorithms, called genetic algorithms, do not require an explicit objective function, and consequently this does not have to be a continuous and differentiable mathematical function. Another valuable advantage of genetic algorithms is that it readily enables combining the tasks of continuous and discrete optimization. Genetic algorithms were described by [16].

The authors have taken into account the following criteria in the process of wind turbine blades design [17-20]:

- minimization of generated blade vibrations;
- maximization of output generated;
- separation of the natural frequency of the blade from harmonic vibration associated with rotor rotation;
- separation of the natural frequencies of the blade and frequencies that comes from Karman vortices detachment;
- minimization of blade material cost;

- ensuring local and global stability of blade structure;
- ensure the durability and reliability of the blade;
- fulfillment of appropriate strength requirements by the blade structure.

The values of maximal displacements during blade vibration depend on its stiffness, which is a function of material density, thickness of separated structural elements of wind turbine blade, number of transversal spars and their arrangement along blade span. Therefore, when the stability of the blade structure criterion was considered, these parameters should be taken into account. Such a formulation of optimization problem also satisfies the criterion of generated output maximization, as the output of a wind turbine depends also on the optimum shape of blades, i.e. on their optimum geometrical features. These parameters also influence the weight of the blade and the cost of its production [1].

The mass and fabrication cost of a blade depend on the same parameters as the amplitude of blade vibrations. If the cost minimization criterion were considered, then the optimization task would have to be formulated as a weight minimization task. However, in order to ensure stability of the structure, the weight should be maximized. The side effect of such approach is possibility that eigenfrequencies of designed blade will be the same as resonance frequencies.

Furthermore, to meet the strength requirements of the structure, optimization of maximum displacements of the blade in transverse direction would have to be carried out with a limiting condition that permissible stresses be not exceeded. Therefore, it is necessary to optimize the blade maximal displacement, having strain constraints.

Minimization of vibrations is a good way to successfully design the blade structure and at the same time it contributes to other benefits, such as lower cost or high stability. However, when minimizing vibrations of the blade, the natural frequency of the blade must be separated from the harmonic vibration associated with rotor rotation. Such an approach prevents the occurrence of resonance, which under high amplitude of vibration could lead to destruction of the structure. Frequency spacing is one of the methods of isolating frequencies.

The main aim of the optimal – constructional process of wind turbine blade, from the point of dynamic phenomena is to ensure the suitable dynamic characteristics of the system. The dynamic characteristics of the system are defined by eigenfrequencies and frequency response functions, where the eigenfrequencies and frequency response functions were determined respectively from the following formulae:

$$\det\left(\mathbf{K}-\mathbf{M}\omega^2\right)=0\,, \tag{10}$$

$$\mathbf{H}(j\omega)=\left(-\mathbf{M}\omega^2+\mathbf{C}j\omega+\mathbf{K}\right)^{-1}, \tag{11}$$

where:

M – mass matrix,

K – stiffness matrix,

C – damping matrix,

ω – eigenfrequency.

The dynamic characteristics of the system, excluding damping, depend on forms and elements values of stiffness matrix **K** and mass matrix **M**, what follow from Eq.(9) and Eq.(10). In view of the above considerations, the optimization problem should be formulated as objective function, which allowing to the modifications of these matrices.

The stiffness matrix we can modify using, e.g. dependence on deflection:

$$\mathbf{F}=\mathbf{K}\cdot\mathbf{x}\Rightarrow\mathbf{x}=\mathbf{K}^{-1}\cdot\mathbf{F}\,, \tag{12}$$

where:

F –matrix of generalized forces,

x –matrix of generalized displacements.

Then the optimization task we can formulate as the minimization of the tip blade displacement task. Modifying the stiffness matrix **K**, the mass matrix **M** also undergoes a modification, for example, reducing the mass of the system causes a simultaneous decrease in the stiffness of this system.

As the next variant of optimization we can chose the criterion of the minimization of the mass of the blade as objective function and formulating other criteria as limitations. The minimization of the mass of the system is classic variant of the optimization problem applied in optimization of design features of the engineering system.

The separate investigation of above – mentioned criteria can lead to conflicting solutions, i.e. improvement of one can

result in deterioration the other. So, taking as the optimization criterion the minimization of the tip blade displacement criterion and the minimization of the mass of the blade criterion simultaneous, all above requirements will be satisfied.

In order to indicate of the most effective approach to shown problem of the minimization of the wind turbine blade vibration, three variants of optimization calculations were conducted:

- Variant I—chosen the criterion of the minimization of the mass of the blade as objective function and formulating other criteria as limitations;
- Variant II—chosen the criterion of the minimization of the tip blade displacement as objective function and formulating other criteria as limitations;
- Variant III—formulating objective function as a weighted sum of the most important criteria, i.e. the minimization of the mass of the blade and the minimization of the tip blade displacement and expression other criteria as limitations.

The column matrix of design variables can be represented in the following form:

$$\mathbf{X}^T = \left[X1, X2, X3, X4\right] \tag{13}$$

where:

X1 – the transversal spars thickness,

X2 – the longitudinal spars thickness,

X3 – number of transversal spars,

X4 – arrangement of transversal spars.

The other criteria were expressed in the form of inequality limitations $h_j(\mathbf{X})$:

- stresses generated in the blade cannot exceed permissible stresses - compliance with appropriate strength requirements of the structure:

$$\sigma(X) \le \sigma_{dop}, \tag{14}$$

- deformation of the blade must be less than the value of the permissible strain - fulfillment of the relevant conditions for the local stability of the structure:

$$\varepsilon(\mathbf{x}) \le \varepsilon_{dop}, \tag{15}$$

- displacement of individual nodes in the numerical model of the blade cannot exceed the set value - global stability must be ensured:

$$u_i(\mathbf{x}) \le u_{dop}, \tag{16}$$

- displacement of the numerical model of the tip blade cannot exceed the set value - local stability must be ensured. This displacement should not exceed 20% of the radius of the windwheel [14,15]:

$$u_{TIP}(\mathbf{x}) \le 0.2 \cdot R, \tag{17}$$

- separation of natural frequency of the blade f_b from harmonic vibration associated with rotor rotation. It is recommended that the natural frequency of the blade were located outside the scope of the harmonic vibration associated with rotor rotation at $\pm 12\%$ [4]:

$$f_b \notin \left\langle 0.8 \cdot f_w \ , \ 1.2 \cdot f_w \right\rangle, \tag{18}$$

- the natural frequency of the blade must be separated from the frequency of the Karman's vortex:

$$f_b \notin \left\langle 0.1 \cdot \frac{V_{\inf}}{c} \ , \ 0.3 \cdot \frac{V_{\inf}}{c} \right\rangle, \tag{19}$$

where, $V_{\inf}$ is the velocity at infinity and *c* is the length of chord.

- wind turbine blade weight must not exceed weight limit. According to [21] mass 1m2 blade should be from 1 kg to 1.5 kg:

$$m_{BLADE} \le m_{DOP}, \tag{20}$$

Further limitations apply to the values of design variables. These can be expressed by means of the following matrix

formula:

$$\mathbf{X}_{\min} \le \mathbf{X} \le \mathbf{X}_{\max}, \tag{21}$$

where:

$\mathbf{X}_{\mathbf{min}}$ – column matrix of minimum values of design variables (lower bound variables),

$\mathbf{X}_{\max}$ – column matrix of maximum values of design variables (upper bound variables).

A. Optimization Calculation – Variant III

Multi-criteria optimization problem was solved using the method of weighted sum [22-24]. Formulating objective function $F(\mathbf{X})$ as a weighted sum of most important criteria i.e. mass reduction and minimizing of the tip blade displacement [17]:

$$\begin{aligned} &\min_{\mathbf{X}\in\Omega} \; F(\mathbf{X}) = w_i \cdot M + w_k \cdot U \\ &h_j(\mathbf{X}) \le 0 \quad \text{dla} \quad j = 1,\ldots,n \end{aligned} \tag{22}$$

where:

Ω – domain of possible solutions within the space of objects,

$\mathbf{X}$ – column matrix of design variables,

$F(\mathbf{X})$ – objective function,

$h_j(\mathbf{X})$ – inequality constraints functions are submitted by dependencies from 14 to 20,

$\mathbf{w}$ – column array weights of the respective criterion functions, $w_{i,k} \in [0,1]$ and $(w_i + w_k)=1$,

$M = \dfrac{m}{m_{dop}}$ – standardized criterion function representing the weight of the blade,

$U = \dfrac{u}{u_{dop}}$ – standardized criterion function representing the displacement of the blade tip,

m_{dop} – permissible mass of blades,

u_{dop} – permissible displacement of the blade tip.

B. Optimization Calculation – Variant I and Variant II

The next variants of optimization calculations consisted of chosen the one criterion as objective function and formulating other criteria as limitations. Chosen objective function is:

- the minimization of the mass of the blade – variant I:

$$\begin{aligned} &\min_{\mathbf{X}\in\Omega} \; F(\mathbf{X}) = m(\mathbf{X}) \\ &h_j(\mathbf{X}) \le 0 \quad \text{dla} \quad j = 1,\ldots,n \end{aligned}, \tag{23}$$

where:

Ω –domain of possible solutions within the space of objects,

$\mathbf{X}$ – column matrix of design variables,

$F(\mathbf{X})$ – objective function,

$h_j(\mathbf{X})$ – inequality constraints functions are submitted by dependencies from 14 to 20.

- the minimization of the tip blade displacement – variant II:

$$\begin{aligned} &\min_{X\in\Omega} \; F(\mathbf{X}) = u_{TIP}(\mathbf{X}) \\ &h_j(\mathbf{X}) \le 0 \quad \text{dla} \quad j = 1,\ldots,n \end{aligned}, \tag{24}$$

where:

Ω – domain of possible solutions within the space of objects,

$\mathbf{X}$ – column matrix of design variables,

$F(\mathbf{X})$ – objective function,

$h_j(\mathbf{X})$ – inequality constraints functions are submitted by dependencies from 14 to 20.

VIII. CHOICE OF OPTIMIZATION METHODS

Because the optimization task is solved is a discrete-continuous task, where criterion does not occur in explicit function, the classical methods cannot be used. Simultaneously due to the presence of variables both discrete and continuous, the simple genetic algorithm had to be modified in order to adapt solving the given optimization problem.

Modification mainly applies to one-point crossover operation. Shift is made in this algorithm by 7 bits. Cross point is selected from first to last bit of shorter chromosome (individual with less number of transversal spars). This modification to genetic algorithm is described in detail in [9]. Block diagram presenting the operating of modification genetic algorithm is presented in Fig. 12.

Optimization calculations were done with the use of the authors' proprietary program that implemented a modified genetic algorithm, for which the following assumptions were made:

- number of individuals 20
- number of populations (STOP criterion) 50
- probability of crossing 0.7
- probability of mutation 0.03

In the optimization process design, the variables were: thickness of transversal spars (denoted by tsr), thickness of longitudinal spars (denoted by tsw), number of transversal spars (denoted by nsr) and their arrangement along the blade span (i.e. numbers of assigned transversal spars – denoted by srN).

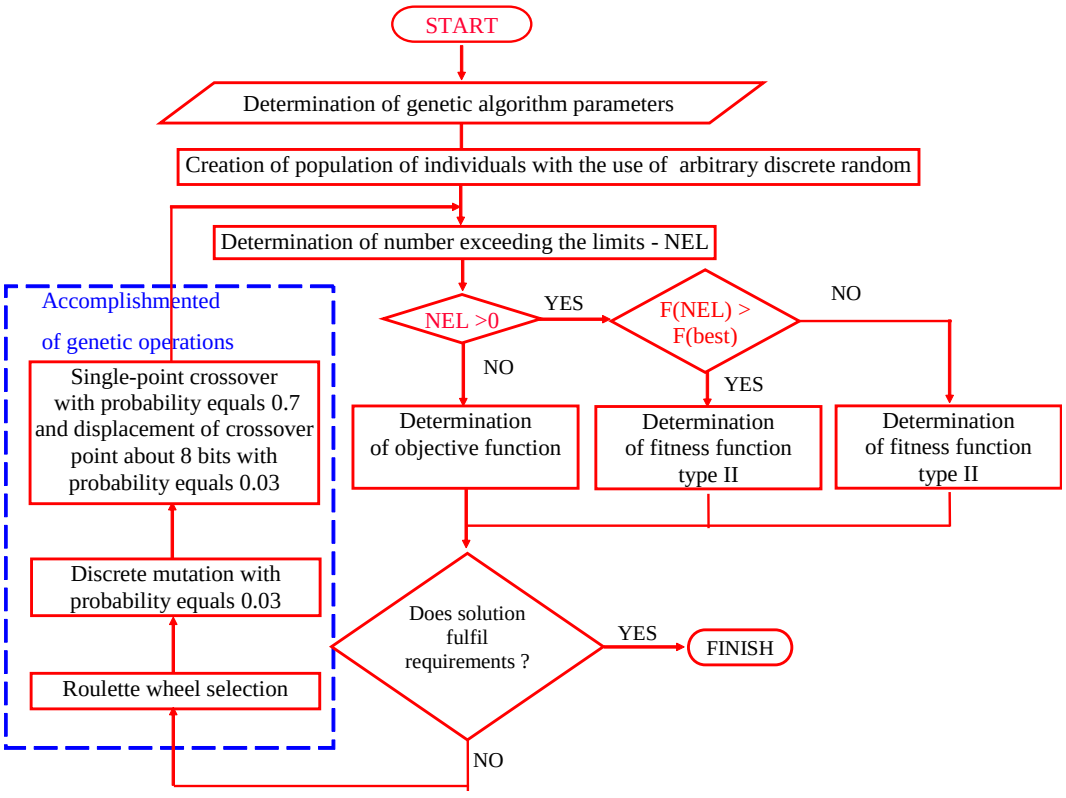

Fig. 12 Block diagram presenting the operating of modification genetic algorithm

IX. ANALYSIS OF OPTIMIZATION PROCESS EFFICIENCY

The comparison of mechanical and modal properties of wind turbine blade with constructional features obtained from literature (before optimization) and obtained as a result of optimization process, for conducted variants of optimization calculations, is shown in Table 2.

TABLE 2 COMPARISON OF MECHANICAL AND MODAL PROPERTIES OF THE WIND TURBINE BLADE BEFORE AND AFTER OPTIMIZATION PROCESS

Objective function		Theoretical model	Variant I	Variant II	Variant III
Design variables	tsr	0.06	0.02	0.0956	0.0960
	tsw	0.06	0.0331	0.0966	0.0702
	nsr	27	4	17	14
	srN	from 4 what 4 to 108	3; 42; 84; 90	2; 14; 21; 32; 35; 36; 58; 60; 75; 76; 84; 94; 101; 103; 106; 108; 109	5; 8; 9; 11; 14; 15; 16; 33; 34; 36; 45; 69; 78; 82
Mass of the blade [kg]		1119.3	831.786	1487.2	1240.7
Maximal stress [MPa]		227	322	164	204
Maximal strain [%]		0.4842	0.5876	0.3376	0.4438
Displacement of the tip blade [m]		6.244	5.987	4.401	5.493
Eigenfrequencies values [Hz]	1	0.27666	0.25953	0.29001	0.28109
	2	0.9804	0.91616	1.1142	1.0566
	3	1.1331	1.0543	1.2687	1.1721
	4	2.5354	2.3819	2.6546	2.5736
	5	3.7642	3.5295	4.1414	3.8928

Obtained amplitude-frequency characteristics of displacement signal determined for chosen nodes of the blade model before optimization process and after the minimization of objective function expressed as a weighted sum of the most important criteria, i.e. the minimization of the mass of the blade and the minimization of the tip blade displacement are shown in Fig. 13.

In addition, the results of simulation of displacement vibration signals determined for chosen nodes of the blade model before optimization process and after objective function as a weighted sum expressed of the most important criteria, i.e. the minimization of the mass of the blade and the minimization of the tip blade displacement are shown in Fig. 14. Models of reduced number of degrees of freedom were used. The solution was chosen from Pareto's set.

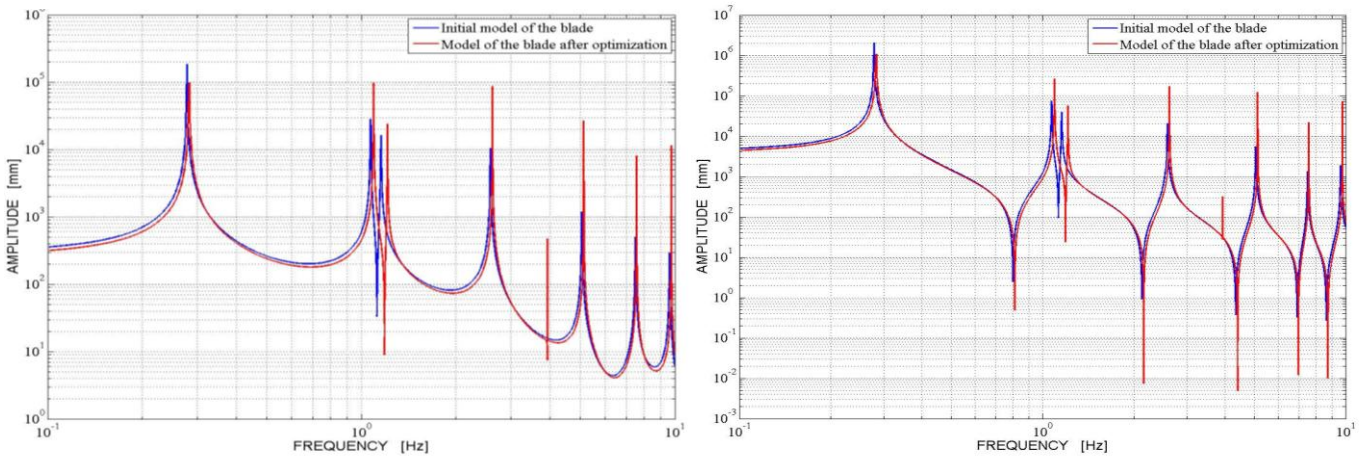

(a) (b)

Fig. 13 Amplitude-frequency characteristics of displacement signals using the logarithmic amplitude axis determined for: (a) the node in the middle of the blade span, (b) the node at the tip blade

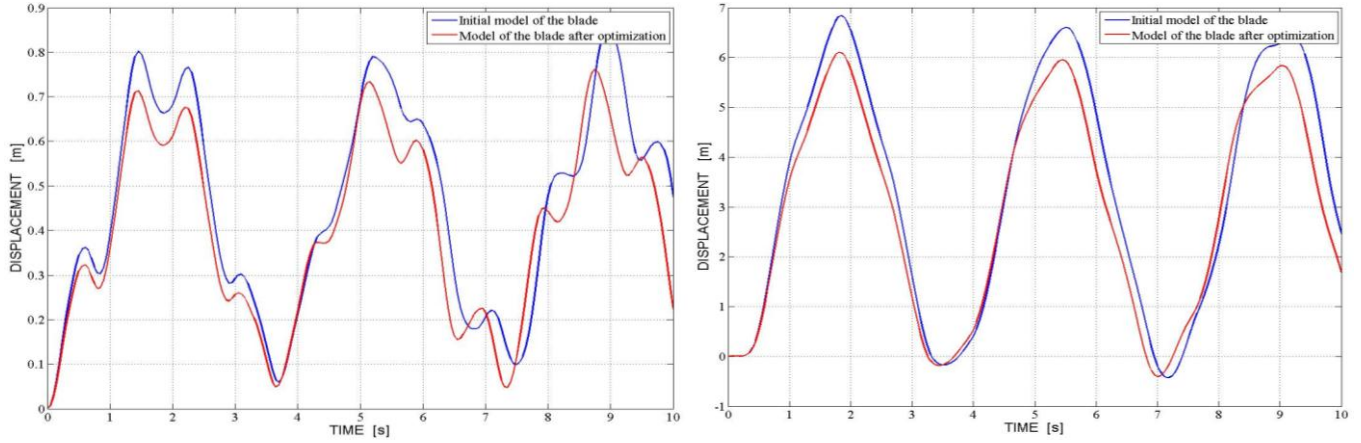

(a) (b)

Fig. 14 Results of simulation of displacement vibration signals determined for: (a) the node in the middle of the blade span, (b) the node at the tip blade

Obtained amplitude-frequency characteristics of displacement signal determined for chosen nodes of the blade model before optimization process and after the minimization of the mass of the blade are shown in Fig. 15.

Furthermore, the results of simulation of displacement vibration signals determined for chosen nodes of the blade model before optimization process and after the minimization of the mass of the blade are shown in Fig. 16. Models of reduced number of degrees of freedom were used.

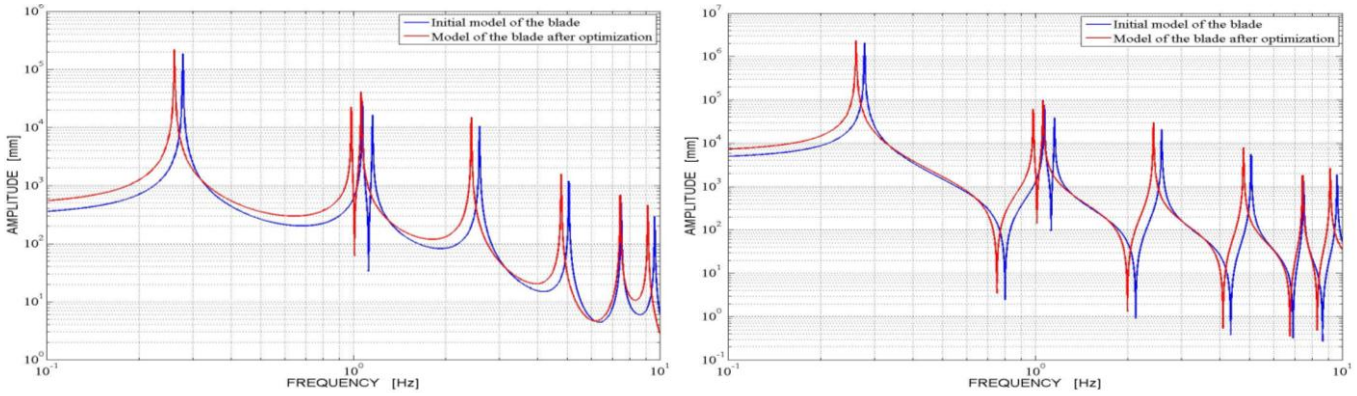

(a) (b)

Fig. 15 Amplitude-frequency characteristics of displacement signals using the logarithmic amplitude axis determined for: (a) the node in the middle of the blade span, (b) the node at the tip blade

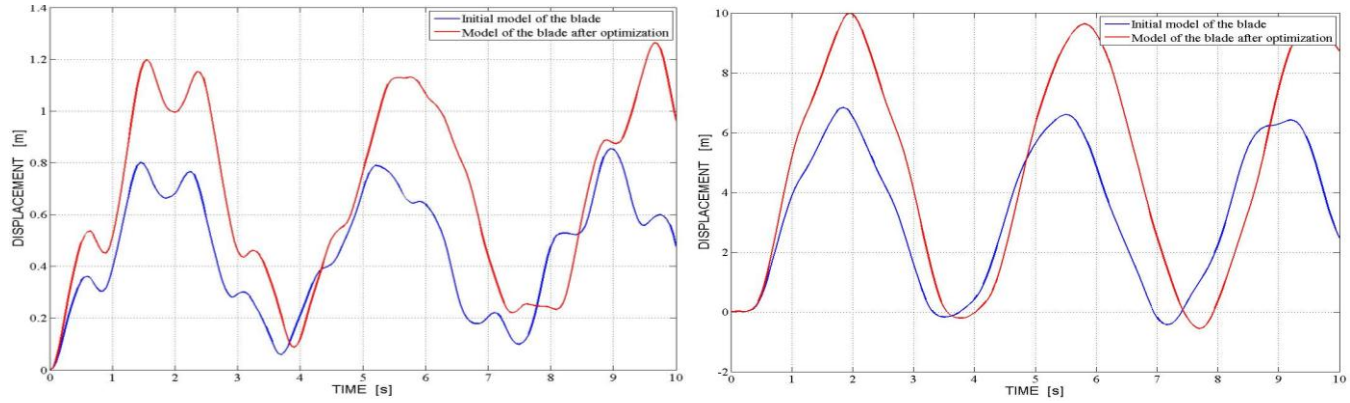

(a) (b)

Fig. 16 Results of simulation of displacement vibration signals determined for: (a) the node in the middle of the blade span, (b) the node at the tip blade

Obtained amplitude-frequency characteristics of displacement signal determined for chosen nodes of the blade model before optimization process and after the minimization of the tip blade displacement are shown in Fig. 17.

In addition, the results of simulation of displacement vibration signals determined for chosen nodes of the blade model before optimization process and after the minimization of the tip blade displacement are shown in Fig. 18. Models of reduced number of degrees of freedom were used.

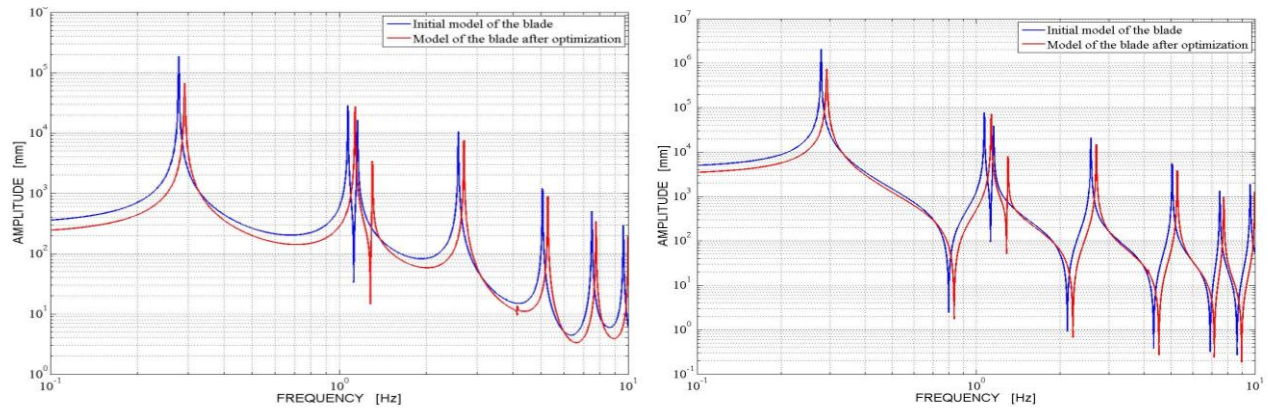

(a) (b)

Fig. 17 Amplitude-frequency characteristics of displacement signals using the logarithmic amplitude axis determined for: (a) the node in the middle of the blade span, (b) the node at the tip blade

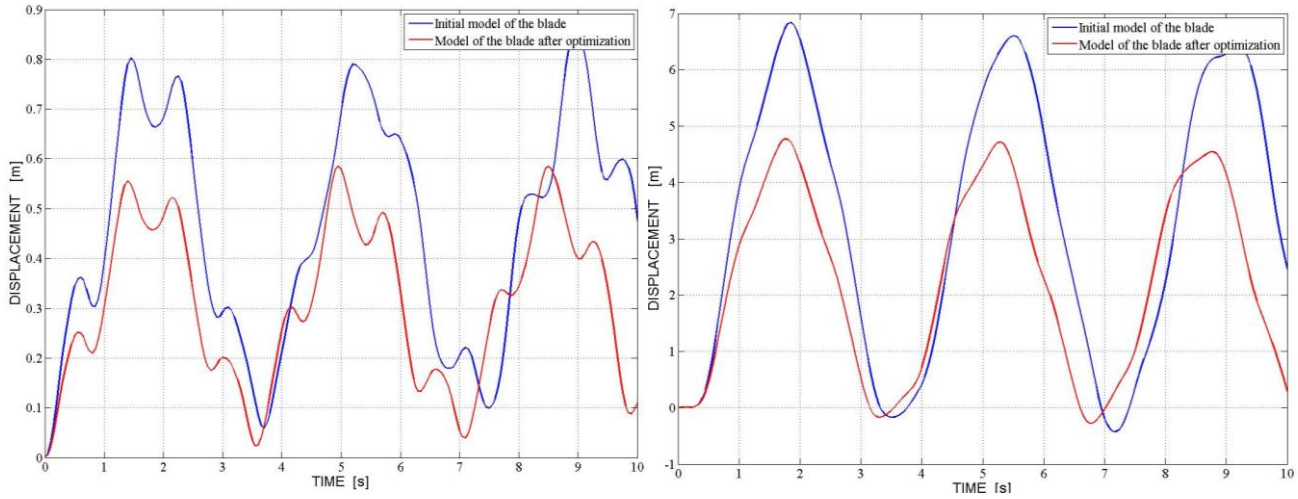

(a) (b)

Fig. 18 Results of simulation of displacement vibration signals determined for: (a) the node in the middle of the blade span, (b) the node at the tip blade

For the three variants of optimization processes, numerical calculations make it possible to conclude that:

- The model of the blade with constructional features obtained as a result of the minimization of the tip blade displacement is characterized by the best stiffness for the sake of the minimization of the blade vibration;
- The model of the blade with constructional features obtained as a result of the minimization of the mass of the blade is characterized by the tip blade displacement with values near the permissible value. This can cause the damage of the wind turbine;
- The considered Pareto's solution is characterized by the value of the tip blade displacement, which is contained in permissible limit;
- The total mass of the blade with constructional features obtained as a result of the minimization of the mass is about 26 % smaller than before the optimization, which reduces the material cost;
- The total mass of the blade with constructional features obtained as a result of the minimization of the tip blade displacement is about 32 % larger than before the optimization, which is the reason for increase in material cost;
- The total mass of the blade with constructional features which are result of the minimization of the weighted function (the considered Pareto's solution) is about 11 % larger than before the optimization, which is the reason for negligible increase in material cost;
- The eigenfrequency range of the blade model for all three variants does not agree with the resonance frequencies range.

The analysis of the results of numerical simulations of displacement vibration signals and the obtained amplitude-frequency characteristics determined for chosen nodes of the blade allow us to put forward the following conclusions:

- the use of minimization of the blade mass as the optimization criterion increased the value of the amplitude vibrations of the numerical model of wind turbine blade comparing to values for the blade model before optimization;
- the use of the minimization of the tip blade displacement as the optimization criterion reduces significantly the value of the amplitude vibrations of the numerical model of wind turbine blade;
- the use in optimization process objective function as a weighted sum of the most important criteria (the considered Pareto's solution) increase values of the amplitude vibrations of the numerical model of wind turbine blade in comparison with values for the blade model before optimization.

Therefore, the use of the minimization of the tip blade displacement as the optimization criterion allowed getting the best solution, which fulfils all guidelines for the wind turbine design. The model of the blade with constructional features acquired in the result of this optimization task is characterized by the best stiffness, the smallest blade tip displacement, the smallest values of the amplitude vibrations of the numerical model of wind turbine blade and a small increase of the blade mass.

In order to fulfill all applied criteria, it is difficult to discern the optimum solution. The best solution in terms of minimizing material cost does not ensure suitable stiffness of the blade and vice versa. The use of the weighted sum as objective function is the best approach to be considered within this task, which allows determining Pareto's set. On this basis, the solution can be determined, which satisfies the required conditions of the task. In the considered case, the chosen solution from obtained Pareto's set [9] provides decrease of blade vibration about of approximately 13 % with a negligible increase of 10 % of the blade mass.

X. CONCLUSIONS

The work presented in this chapter shows that use of the genetic algorithm enables effective forming of dynamic properties of the wind turbine blades, causing considerable reduction of the blade amplitude vibrations. The obtained results of numerical calculations prove the applicability of the developed models and investigation methods used for the determination of dynamic properties of systems.

The choice of a genetic algorithm as an optimization method enables effectively solving problems connected with multidisciplinary discrete-continuous optimization of a complex dynamic system.

The current work demonstrates that the presented computation algorithm is an effective aid in determining optimum structural features at the stage of design and it ensures proper dynamic properties of the system to be designed. This enables considerable time savings in the design process and a reduction in costs of manufacturing of product. However, it should be underlined that the application of the genetic algorithm can provide results with some inaccuracies, which are actually resulting from the stochastic character of calculations.

The main advantage of the approach proposed in this work is to investigate the structural dynamics problem of the complex mechanical systems via the connection of the author's proprietary program that implements multidisciplinary discrete-continuous method with the commercial software Ansys®, which creates a numerical model of the blade using the finite element approach. In the calculations, the use of the algorithm of the optimization method, which was based only on the values of objective function, has expanded the class of systems and problems to which the proposed methodology of investigations can be used to solve these problems. The developed methods for modeling and optimization can be used to solve a large number of problems dealing with structural dynamics.

REFERENCES

[1] W. C. Goeij, M. J. L. Tooren and A. Beukers, "Implementation of bending torsion coupling in the design of a wind turbine rotor – blade," *Applied Energy*, vol. 63, 1997.

[2] O. L. Martin Hansen, *Aerodynamics of wind turbines*, 2nd ed., published by Earthscan in the UK and USA, 2008.

[3] David A. Spera, "Wind turbine technology, fundamental concepts in wind turbine engineering," *ASME Press*, New York 1998.

[4] *Guidelines for design of wind turbines.* 2nd ed. DNV/Risø. Denmark 2002.

[5] K. Y. Maalawi and H. M. Negm, "Optimal frequency design of wind turbine blades," *Journal of Wind Engineering and Industrial Aerodynamics*, 90, pp. 961-986, 2002.

[6] B. Attaf and L. Hollaway, "Vibrational analyses of glass reinforced polyester composite plate reinforced by a minimum mass central stiffener," *Composities*, vol. 21 no. 5, pp. 425-430, 1990.

[7] D. J. Malcolm and D. L. Laird, "Modelling of blades as equivalent beams for aeroelastic analysis," *AIAA* Reno Jan. 2003.

[8] *One-dimensional variations: Blades*, Dutch Offshore Wind Energy Converter project, LM Glasfiber Holland BV, 2003.

[9] A. Mężyk and M. Jureczko, "Optymalizacja wielokryterialna łopat elektrowni wiatrowej ze względu na minimalizację drgań," *Wydawnictwo Politechniki Śląskiej*, Gliwice 2006. Monograph "Multidisciplinary optimization of the wind turbine blade with respect to minimize vibrations," *Publishers of the Silesian University of Technology*, Gliwice 2006. ISBN 83-7335-334-8.

[10] R. J. Guyan, "Reduction of stiffness and mass matrices," *AIAA Journal*, vol.3, no. 2, 1965.

[11] W. Heylen, S. Lammens and P. Sas, *Modal analysis theory and testing*. KU Leuven, Belgia 1997.

[12] D. J. Ewins, *Model validation: correlation for updating*, Sadhana, vol. 25, Part 3, pp. 221-234, Jun. 2000.

[13] V. Tita, J. Carvalho and J. Lirani, "A procedure to estimate the dynamic behaviour of fiber reinforced composite beams submitted to flexural vibration," *Journal of Mat. Res*. vol. 4 no. 4, 2001.

[14] D. A. Griffin, *Blade system design studies. Volume I: Composite technologies for large wind turbine blades*, SAND2002-1879, Unlimited Release. Printed Jul. 2002.

[15] D. A. Griffin, "Turbine design. Scaling studies technical. Area 1. Composite blades for 80 - 120 meter rotor," *National Renewable Energy Laboratory*, 2001.

[16] David E. Goldberg, "Genetic algorithms in search, optimization, and machine learning," *Addison-Wesley Publishing Company*, Inc. 1989.

[17] M. Jureczko, "Optymalizacja własności dynamicznych łopaty elektrowni wiatrowej," *Acta Mechanica et Automatica*. Quarterly, vol. 2 no. 1, pp. 37-44, Poland, 2008.

[18] M. Jureczko, "Formulation of optimization problem of the horizontal axis wind turbine blade," *23rd IFIP TC 7 Conference on System Modelling and Optimization*, Jul. 23-27, Book of Abstracts pp. 406-408, Cracow 2007.

[19] M. Jureczko and A. Mężyk, *Multidisciplinary optimization of wind turbine blades with respect to minimize vibrations*, International Society for Structural and Multidisciplinary Optimization, 21-25 May, Book of Abstracts pp. 67, Full paper on CD, 7th World Congress on Structural and Multidisciplinary Optimization. Seoul, Korea Płd. 2007.

[20] M. Jureczko, M. Pawlak and A. Mężyk A, "Optimisation of Wind Turbine Blades," *Elsevier. Journal of Materials Processing Technology*, vol. 167, iss 2-3, pp. 463-471, Glasgow 2005.

[21] R. Scherer, "Blade design aspect," *Renewable Energy*, vol. 16, pp. 1272-1277, 1999.

[22] I. Y. Kim and O. L. Wek, "Adaptive weighted-sum method for bi-objective optimization: Pareto front generation," *Structural Multidisciplinary Optimization*, vol. 29, pp. 149-158, 2005.

[23] R. T. Marler and J. S. Arora, "Survey of multi–objective optimization methods for engineering," *Structural Multidisciplinary Optimization*, vol. 26, pp. 369-395, 2004.

[24] L. Pavlovčič, A. Krajnc and D. Beg, "Cost function analysis in the structural optimization of steel frames," *Structural Multidisciplinary Optimization*, vol. 28, pp. 286-295, 2004.

Mariola Jureczko was born in Poland. She obtained her Master of Engineering degree from the Silesian University of Technology, Gliwice (Poland) in 1998. Then she received her Ph.D. degree in technical sciences from the same university in 2006.

Since 2001, she has been working at the Faculty of Mechanical Engineering in the Silesian University of Technology. Currently, she serves as Assistant Professor in the Silesian University of Technology within the Department of Theoretical and Applied Mechanics in Poland.

Dr Jureczko is a member of the Polish Society for Theoretical and Applied Mechanics in Poland. Her research interests include multidisciplinary design optimization (e.g. wind turbine, mining machinery), renewable energy sources and computational fluid mechanics. Dr Jureczko has published many scientific papers (more than 30 publications and presentations) and she is the author of one monograph and one academic textbook. She has successfully supervised many engineers and students.

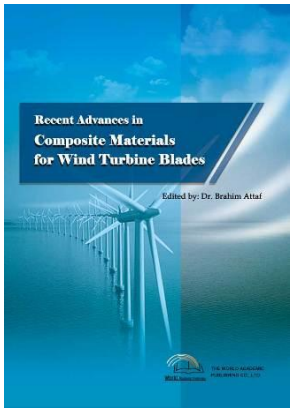

Recent Advances in Composite Materials for Wind Turbine Blades
Edited by Dr. Brahim Attaf

ISBN 978-0-9889190-0-6

Hard cover, 232 pages

Publisher: The World Academic Publishing Co. Ltd.

Published in printed edition: 20, December 2013

Published online: 20, December 2013

This book of science and technology provides an overview of recent research activities on the application of fibre-reinforced composite materials used in wind turbine blades. Great emphasis was given to the work of scientists, researchers and industrialists who are active in the field and to the latest developments achieved in new materials, manufacturing processes, architectures, aerodynamics, optimum design, testing techniques, etc.. These innovative topics will open up great perspectives for the development of large scale blades for on- and off-shore applications. In addition, the variety of the presented chapters will offer readers access to global studies of research & innovation, technology transfer and dissemination of results and will respond effectively to issues related to improving the energy efficiency strategy for 2020 and the longer term.

How to cite this book chapter

Jureczko M. (2013). Multidisciplinary Optimization of Wind Turbine Blades With Respect to Minimize Vibrations, *Recent Advances in Composite Materials for Wind Turbines Blades*, Dr. Brahim Attaf (Ed.), ISBN 978-0-9889190-0-6, WAP-AMSA, Available from: http://www.academicpub.org/amsa/chapterInfo.aspx

Chapter 9

Testing and Condition Monitoring of Composite Wind Turbine Blades

Wenxian Yang

School of Marine Science and Technology, Newcastle University
Newcastle upon Tyne NE1 7RU, United Kingdom
wenxian.yang@ncl.ac.uk

I. INTRODUCTION

In a wind turbine system, blades are one of the most critical components. They capture energy from wind and convert it to a mechanical energy for electricity power generation. However, once the blades are defective, the power generation efficiency of the turbine will be significantly affected. In worse case when the blade is seriously damaged, the turbine will have to be shut down completely for the sake of safety. Furthermore, they are exposed in direct harsh environment, suffering constantly varying wind loads, experiencing temperature and humidity changes, erosion and corrosion, as well as the cyclic fatigue loads arising from their self-weights in operation. As a consequence, blades are also the most vulnerable component in the entire wind turbine system. The long-term onshore wind farm practice has shown that blade failures account for about 10% of all wind turbine failures reported [1, 2], and result in over 15% of total downtime of the turbines [3, 4], which means a significant revenue loss to operators. Therefore, blade failures have a profound impact on the cost of energy from wind. To improve the reliability of wind turbine blade is of great significance to increase the availability of the wind turbines and economic return from them.

At present, two tendencies are being exhibited in the wind industry; these are: (i) more and more wind turbines are being deployed offshore and in remote lands, where expensive operation and maintenance costs (e.g., blade inspection and repair) are always associated with due to the limited accessibility of site; (ii) wind turbine, more precisely wind turbine blade, is continually growing in size, which requests the blades to be more reliable and stronger than ever before to sustain higher static and cyclic loads that are randomly applied to the turbines. Both tendencies request researchers and designers to further improve the long-term reliability of wind turbine blades, so that to reduce their failure rate and downtime. Today, many measures can be taken to reach such a purpose; for example adopting a more conservative design of the blade by using a larger factor of safety, enhancing the quality control in the manufacturing process, taking an innovative manufacturing method to reducing the potential failure risks emerging in conventional ‘sandwich’ blade structures, using more reliable light-weight materials to replace the glass fibre that is being popularly used in turbine blades, etc. However, every improvement needs to be fully validated in advance before extensive application. Therefore, various subcomponent and full scale blade testings are often conducted in laboratory. In contrast to testing in field, laboratory testing is regarded as one of the most feasible and cost-effective approach to obtaining a comprehensive understanding of the quality and reliability issues of a new blade design within constrain of time and expenses. However, it is aware that laboratory testing of a wind turbine blade, especially the fatigue testing of the blade, is still time consuming and costly.

Laboratory testing can help to quickly prove the new design and/or improvement, and predict the long-term reliability of blade in its 20 to 30 years life time. But laboratory testing cannot fully guarantee the actual energy capture efficiency of a wind turbine blade in operation. In practice, the blades will operate in harsh environments and experience various severe loading conditions that can be distinctly different from those simulated in laboratory testing. In order to ensure the reliability of wind turbine blades and their high energy capture efficiency over a long service period, it is essential to have an instant understanding of the actual health condition of the blades and their energy capture efficiency, particularly under extreme weather and loading conditions (e.g. raining and snowing storms, lightning strike, typhoon, etc.). Thereby, remote online condition monitoring is strongly recommended to the operator. Today, condition monitoring has been widely recognised as a key measure to protect blades and the entire wind turbine system from being damaged under extreme conditions and guarantee their high energy capture efficiency under normal conditions [5].

In view of the great significance of laboratory testing and condition monitoring in achieving the long-term reliability of wind turbine blades and ensuring their high energy capture efficiency in practical operation, an overview of the knowledge, practices and relevant lessons learnt in laboratory testing and condition monitoring of full scale wind turbine blades are introduced in the following sections.

II. FAILURE MODES OF WIND TURBINE BLADES

The typical structure of a blade used for large Megawatt-scale wind turbines is shown in Fig. 1. The spar structure of the blade varies considerably with manufacturers, but it is typically in the form of a box beam or one or more webs, which may be adhesively bonded to form an integral part of the aero-shell structure. In most structural designs, adhesive joints are present along the leading and trailing edges for sustaining the core bonding on sandwich panels.

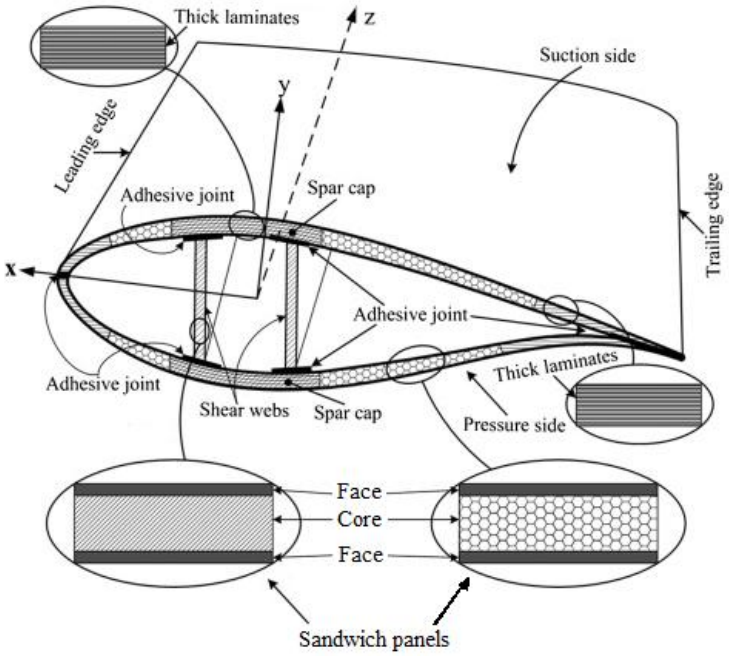

Fig. 1 Typical structure of a blade for large Megawatt-scale wind turbine

The spar beam is made of unidirectional fibres aligned with the blade axis. As the primary load-bearing component, it will provide both bending stiffness and torsional rigidity to the blade. The aero-shell defines the blade profile. It is typically constructed using fibre-reinforced polymeric composites and sandwich structures with lightweight PVC (polyvinyl chloride) foam or balsa wood cores bonded to the spar beam through high-toughness adhesives. These high-toughness adhesives are also used to bond the laminates at leading and trailing edges of the blade. In the design of long blades for Megawatt-scale wind turbines, carbon fibres and fiberglass/carbon hybrids are often adopted by taking advantage of their higher stiffness to reduce the static and cyclic blade deflections and also to improve the blade buckling resistance. Similar to the manufacturing process of aircraft wings and composite boat hulls, wind turbine blades are manufactured also using the popular hand lay-up technique, pre-preg technology and vacuum assisted resin transfer moulding [6].

Fig. 2 shows the schematic of the flapwise and edgewise loads that would be suffered by wind turbine blades in operation. Herein, it should be aware that in reality, the actual loading condition experienced by the blade is much severer than this due to wind turbulences.

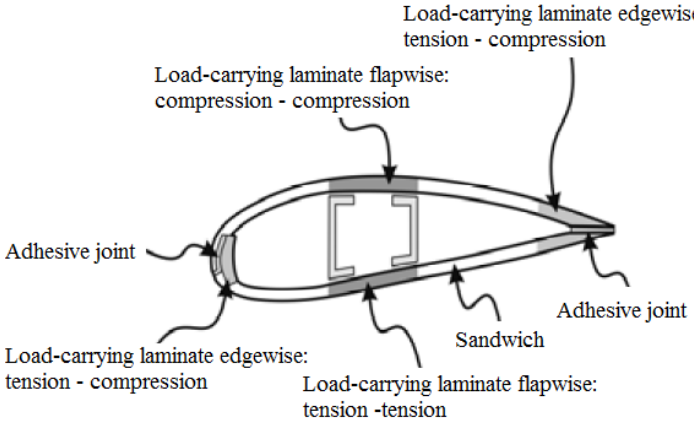

Fig. 2 Schematic of the flapwise and edgewise loads suffered by wind turbine blade

Owing to the aforementioned specialities of wind turbine blade in design, material, structure, and complex loads being subjected, the blade is often damaged by various means, as shown in Fig. 3.

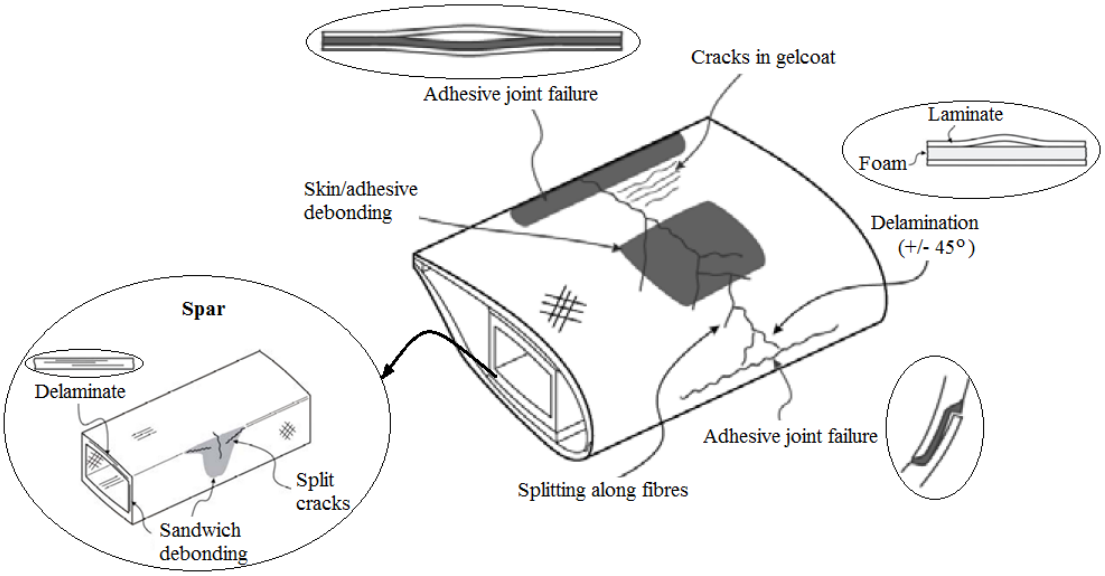

Fig. 3 Failure modes of wind turbine blades

During rotation, the wind turbine blade is subjected to large edgewise and flapwise bending moments, which, together with the self-weight of blade, introduce cyclic stresses in the aeroshell, in adhesive joints and in spar beam. Over a long period, splitting cracks (along fibres), delamination (between composite plies), and debonding (along adhesive joints) will initiate inevitably. But if these micro-defects cannot be detected and repaired instantly, a catastrophic failure of the blade could be resulted in the end, even the entire machine could be lost in storm.

In addition to the random fatigue loads, the thermal expansion induces dimensional mismatches between blade aeroshell and spar beam, and blade sandwich structures can cause blade damage as well, although a well-designed composite joint allows for a certain amount of elastic modulus mismatch. But in any case, defects or cracking between composite plies and the vicinities of geometry changes are inevitable even through in normal operating conditions of the blade.

Since wind turbine blades are made of composite materials, the most common failure mechanisms related to composite materials are listed in Table 1 for information.

TABLE 1 FAILURE MODES OF COMPOSITE MATERIALS [7]

Failure mechanism	Comments
Global buckling	○ Global buckling of laminate
Fibre failure	○ Fibre failure with dominant strain parallel to the fibre direction exceeding the tensile or compressive strength capacity of the individual fibres. ○ Fibres can buckle at a micro and macro levels. Buckling will reduce the compression strength drastically, with imperfections further increasing the effect of buckling. ○ Fibres generally do not yield experiencing brittle fracture.
Matrix failure	○ Matrix failure can occur due to longitudinal/transverse tensile and compressive or in-plane shear stresses. ○ Matrix failure results in degraded strength and stiffness of the laminate, and can lead to further delamination. ○ Can be critical for transverse loaded UD laminates, and in 0 ⁄90 ° laminate loaded in in-plane shear, as well as at joint details. ○ Yielding of the matrix material is also to be evaluated. ○ Matrix failure analyses shall consider both the matrix and the interface to the fibre. Seizing of the fibre may have a significant impact on the interface strength.
Inter-laminar failure	○ Inter-laminar shear failure occurs in the matrix between adjacent plies/laminate due to shear stresses. ○ Inter-laminar tension failure occurs in the matrix between adjacent plies/laminate due to tensile stresses. ○ These failure modes can lead to delamination and sub-laminate buckling.
Sandwich failure	○ Ultimate failure of the sandwich core material due to tensile, compressive and shear loading. ○ Local yielding of the sandwich core due to tensile, compressive and shear loading. ○ The sandwich interface with the laminate. ○ Additional potential buckling failure modes for the sandwich structure of wrinkling, shear crimpling and face dimpling.
Fatigue failure	○ Cyclic loading leads to the accumulation of fatigue damage, with the fatigue damage phases characterised by matrix cracking, delamination, progressive fibre breaking, and final fracture. ○ If it can be demonstrated that the structure can withstand the degradations inherent in the fatigue damage phases, then the fatigue failure mode can be selected as final fracture.

Herein, it is worth noting that fracture resistance of blade adhesive joints varies with different types of load modes. For instance, the adhesive joints of a rotating blade are usually subjected to mixed mode loads (i.e., Mode I and Mode II). An interface flaw along an adhesive joint in one region could be harmless, but the same size of adhesive joint flaw located in other region could propagate quickly due to different mode mixities or higher stresses. In view of this, the technique used for evaluating blade cracking behaviour should be applicable to a wide range of mode mixities. This point of view, to certain extent, highlights the necessity and importance of both static and fatigue blade tests, in which the blade can suffer from different types of loadings.

To capture more energy from wind, wind turbines are preferred to be deployed in remote open locations, where wind has high speed and less turbulence. However, the open field makes the turbine easy to be the tallest structure in the vicinity. As a consequence, the turbine has high probability of being struck by lightning in harsh weather environment. Statistics have shown that more than 90% of lightning strikes to a wind turbine connect with the blades. As lightning can produce very brief but extraordinary high temperatures (often more than 30 000^{o}C), the blade composites could catch fire once the built-in lightning current conductor of the blade are not perfect in either design or performance.

III. BLADE TESTING METHODS AND ASSOCIATED FACILITIES

An increase in blade length indicates a corresponding increase in load levels. As being subjected to higher level of loads, the blades for large Megawatt-scale wind turbines require more extensively laboratory testing to ensure that the new design is able to continually provide long-term reliability. In other words, the blade should not fail before the end of its expected service life. Survey shows that 90% of the uncertainty concerning fatigue life predictions for wind turbine blades can be attributed to uncertainties related to material properties [8]. Thus, the aim of testing the blade is to demonstrate whether the structural parts and materials of the blade are able to withstand the ultimate loads probably occurring in extreme climates, and whether they can show high reliability when suffering long-term fatigue loads experienced in normal service conditions. To reach such objective, the testing of full scale blades generally consists of static testing and fatigue testing.

A. Static Testing Methods and Systems

The purpose of the static testing is to predict the blade capability of withstanding ultimate loads as those caused by storm, hurricane, typhoon or others happening in extreme weather. The objective of this type of testing is to determine and/or verify the ultimate strength of the blade through analysis of the testing results, which could be the distribution of strains along blade length under different static loading conditions or other related information.

In static testing, distributed loads are applied to the blade statically in one direction to establish the required ultimate strength. Such a test can be performed in a number of ways. In the very early days of the wind industry, static testing of wind turbine blade was conducted by placing sandbags along the blade length to mimic the bending moment distribution, as shown in Fig. 4.

Fig. 4 The early experience of static blade testing using sandbags

Later on, ballast weights were hung at specific locations of the blade to create the expected static loads. In the case of testing long blade, the blade under investigation will usually be attached to the test stand at a specific angle in order to prevent the tip of the blade from touching the ground, as shown in Fig. 5.

Fig. 5 Static testing of a long blade using ballast weights

In the past, hydraulic actuators were also experienced for creating the expected bending moment loads along the blade length. But the large deflections resulting from long wind turbine blades under static testing make them an expensive option. For this reason, today hydraulic actuators are rarely used in the static testing of large wind turbine blades. However, they are often adopted in the static testing of marine turbine blades attributed to their short length, as seen in Fig. 6.

Fig. 6 Static testing of a marine turbine blade using hydraulic actuators

Nowadays, the most popular force application method used in static testing of full scale wind turbine blade is resorting electric winches attributed to their ease of control, as shown in Fig. 7.

(a) Horizontal arrangement

(b) Vertical arrangement

Fig. 7 Static testing of a long blade using electric winches

As shown in Fig. 7, the static testing is generally performed by attaching wooden saddles to the blade at the prescribed locations along blade length. These saddles are carefully shaped (see Fig. 8a), so that they can fit snugly around the blade profile in order to minimize the risk of damaging the local blade skin due to stress concentration at load application locations. Winches (see Fig. 8b) attached to the saddles are then used to load the blade such that the bending moment distribution along blade length can match as closely as possible the ultimate loads that the blade exercises in service.

(a) Wooden saddle (b) Winches

Fig. 8 Saddle and winches used in static testing of blade

B. Single-axis Fatigue Testing Method and Systems

Fatigue testing of a wind turbine blade is performed mainly in order to identify structural defects inherent in either the design or manufacturing process and verify durability of the blade withstanding long-term fatigue loads during the course of its design life of 20 years or more. A modern multi-Megawatt wind turbine can undergo more than 100 million revolutions, which indicates that its blades will undergo at least 100 million cycles of fatigue loads. In each cycle, the loads applied to the blade will oscillate and regularly cause the maximum deflections in both flapwise and edgewise directions, as illustrated in Fig. 9. However, it is impractical to take the blade through so many cycles in laboratory testing because that would take several years to complete. Hence, in laboratory testing an increased load is usually adopted to achieve an equivalent amount of damage [9] accumulated after approximate 1 million cycles, allowing the testing to be completed in just a few weeks.

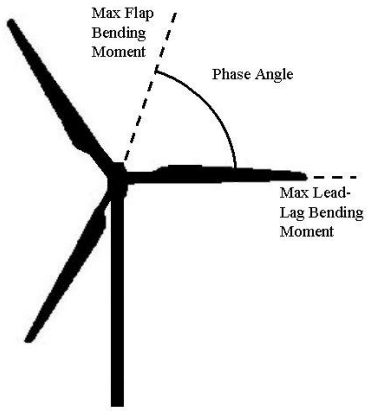

Fig. 9 Positions where the maximum flapwise and edgewise deflections occur

Fatigue testing of wind turbine blades provides extremely valuable data for blade manufacturers and turbine end-users, in terms of design validation and certification for in-service requirements [10]. Fatigue testing at present tends to use only one loading direction at a time, with flapwise and edgewise testing done separately. Such a testing procedure is called single-axis fatigue testing. It is a gross simplification of the fatigue loads experienced by the blade in service, but is seen as the best that can be reasonably achieved within time and cost constrains.

Fatigue testing of blade is conducted using either forced displacement or resonant methods. Both methods will be introduced below. Moreover, various practical means for introducing the loads into blade have been devised, including the use of hydraulic actuators for forced actuation and the use of rotating eccentric masses or oscillating masses to induce resonant loading. All these load application devices will be graphically illustrated as well.

1) Forced Displacement Testing:

Forced displacement testing is a method of performing fatigue testing by displacing the blade using mechanical means. The forcing mechanism can be a hydraulic cylinder, or some other mechanical mechanisms such as a rotating cam and rod or lever. An example of a forced displacement system using a hydraulic cylinder actuator is shown in Fig. 10. In this example, the fatigue load is applied to a single load application point. However, multiple load application points are possible. In a similar way as mentioned in static testing, in principle the simultaneous use of multiple load application systems in fatigue testing will enable the distribution of bending moments along the blade length to be as close as possible to the designed distribution curve, therefore a more reliable prediction to the durability of the blade is obtained. However, this will increase the complexity of the control. To certain extent, it can be said that using an advanced control method or algorithm to ensure all load application systems be able to move in synchronisation and work correctly is always a challenging issue in practical testing.

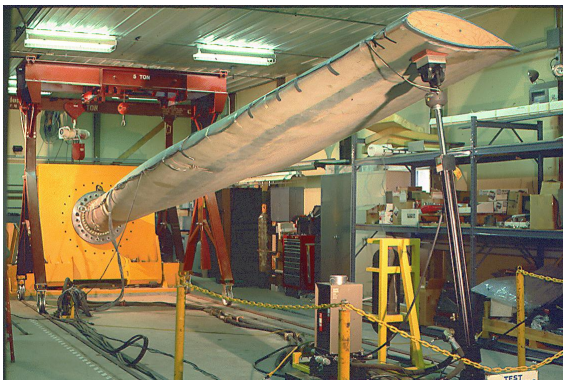

Fig. 10 Example of a forced displacement testing using a hydraulic actuator

In such a test, a known force is applied at each specific location on the blade, delivering the required root bending moment for the fatigue testing. The forcing mechanism needs to be able to displace the blade at a sufficient distance to generate the required tension and compression forces to the blade. Attributed to the controllable nature of forced displacement testing, the generated loading can be either constant or variable, depending on the concrete requirement of testing. To control the testing accurately, feedback information of loads and displacements is essential in the testing procedure. Sometimes, the measurements of strains and accelerations are also required.

2) Resonant Testing:

The resonant testing exploits the resonant natural frequency of the blade. By exciting the blade at its first natural frequency the blade can be displaced and loaded in a cyclic manner. Excitation of the blade can be achieved in several ways, but whichever method is used, the function of the exciter is to maintain energy input into the oscillation and to balance out the losses that occur through material and aerodynamic damping, which would otherwise cause the blade resonance to decay with time. At present, two main methods are being popularly adopted in achieving resonant excitation for fatigue testing. They are accomplished through either a rotating eccentric mass (see Fig. 11a) or oscillating masses (see Fig. 11b).

(a) Rotating eccentric mass (b) Oscillating mass

Fig. 11 Resonant excitation for fatigue testing

Rotating eccentric masses, powered by an electric motor, can provide fixed-amplitude fatigue testing. Once the location and size of mass have been chosen, the frequency of rotation becomes the only variable that could be controlled when the test is underway. However, since the frequency is actually fixed by the natural frequency of the blade and the test equipment, it is in effect not actually a controllable variable and the testing must be performed at this frequency. In actual testing, minor changes in natural frequency of the blade do arise due to changes in stiffness of the blade (for example resulted by the changes in temperature and thus material modulus). But these changes can be accommodated by adjusting the rotational speed of the mass. If variable-amplitude fatigue testing is required, it is necessary to stop the testing and change the mass, which then requires the test frequency to be re-determined.

Oscillating masses, powered by hydraulics, move linearly and are able to perform both constant- and variable-amplitude fatigue testing more easily than rotating eccentric masses. This is because the amplitude of mass movement can be altered without changing the test set-up and this allows for changes in the strain levels to be introduced if variable-amplitude fatigue testing is required. But they are also constrained to operate at the natural frequency of the blade and test system.

Other methods for inducing resonant fatigue loads could be used, dependent on the ingenuity of the test designer. But any resonant fatigue system needs to provide a means of introducing energy into the blade, whilst not retaining a fixed connection between the blade and the floor, or other similar sturdy reaction point.

In the long-term practice of fatigue testing, the blade testing technology and operating system are also improved gradually

in order to achieve more accurate control of loads, higher reliability of testing systems and a more efficient and cost-effective testing. Take the blade testing technology evolution at National Renewable Energy Centre (Narec, UK) as an example. Narec's first fatigue testing method was developed through a Cooperative Research & Development Agreement (CRADA) with National Renewable Energy Laboratory (NREL, USA). This technology used a moving mass, powered by hydraulics, resonating at the natural frequency of the blade, as illustrated in Fig. 12.

Fig. 12 Narec's first fatigue testing equipment – a resonant mass system powered by hydraulics

This first system required two support saddles to be mounted on the blade, with the moving mass system mounted at the top of these two saddles. As can be seen in Fig. 12, the moving mass is mounted well above the blade. The entire testing set-up is simple. However, the testing on blades of around 40m length revealed that there were limitations to using this test set-up. This is due to the "toppling" effects of the mass mounted above the blade. The forces generated by the oscillating movement of the resonant mass system create an over-turning moment on the saddles, which leads to high point stresses at the edges of the saddles acting on the skins of the blades. The option of reinforcing the saddles to make them more rigid was considered, but the added mass required made the solution impractical. Moreover, the testing equipment was originally set up in order to perform a flapwise fatigue testing. It did not lend itself to easily perform an edgewise fatigue testing, which would require a large resonant mass system to be balanced on the edge of the blade at some height above the blade edge that would be very unstable position.

To overcome the difficulties of applying the first generation of resonant mass system to performing the fatigue testing in edge direction and the limitations in performing flapwise testing, the second generation of resonant mass system, called as 'saddlebag', was developed, as shown in Fig. 13. In essence, it is a resonant mass driven by a through-rod hydraulic cylinder. Herein, it is worth noting that in Fig. 13 only one 'saddlebag' resonant mass system is illustrated. But in practical prototype test, a pair of hydraulic systems was used in order to reduce torsion loads and generate larger excitation force with smaller individual resonant mass. The second system was mounted on the opposite of the blade. The results obtained from trial tests with the saddlebag system were positive and fully demonstrated the advantage of positioning the moving masses close to the blade neutral axis. The through-rod hydraulic cylinders were suitable for proving the concept, but were not optimum, since the seals on the hydraulic cylinders were subjected to loads from the moving masses and wear rates on the seals were too high to be used in commercial tests.

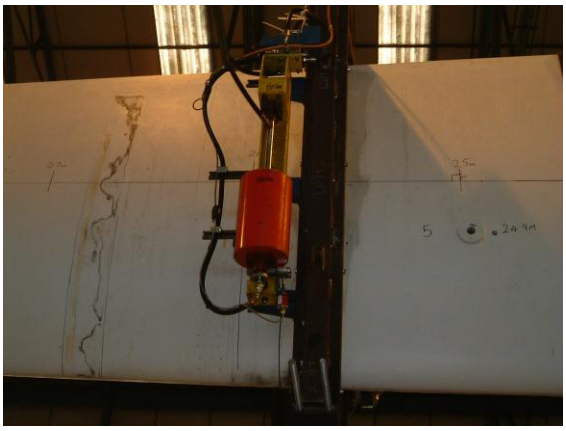

Fig. 13 Narec's 'saddlebag' resonant mass system

The third generation and also the final development of Narec's fatigue testing system was to keep the same concept of moving masses located near to the blade neutral axis, but the moving masses are mounted on rails to prevent loading onto the hydraulic seals. This third generation of system is Narec's Compact Resonant Mass (CRM) system, as illustrated in Fig. 14.

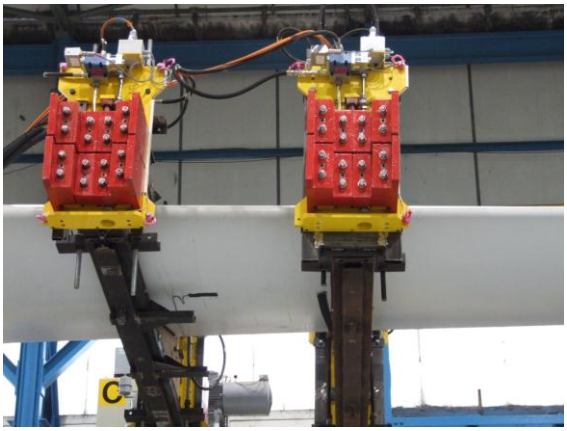

Fig. 14 Narec's compact resonant mass (CRM) system

Within Narec's CRM system the variables are:

- position of CRM along the blade length;
- size of moving mass;
- frequency of moving mass;
- amplitude of mass movement.

Some of these variables are linked together, for instance altering the mass of CRM will change the natural frequency as well. So, although frequency is a variable, the natural frequency is in fact fixed for a particular blade and mass combination. Hence for maximizing efficiency of energy transfer, the CRM system needs to be controlled so that its frequency of movement matches the natural frequency of the blade-mass system.

The control of a fatigue testing usually resorts strain gauge signals that provide feed-back to ensure that the blade is being tested at the correct strain level. If the strain level alters outside of pre-set limits then the CRM control system can change either the natural frequency and/or amplitude of mass movement to bring the strain back to the correct level. Several other signals are also monitored to provide emergent shut-down capability, e.g. accelerations, overall blade deflection and strain levels.

The latest progress of Narec on developing the advanced blade fatigue testing technology is that Narec has mastered the technique of utilizing multiple sets of CRM units to accomplish the resonant testing of a long wind turbine blade. The CRM units move in synchronisation at the resonant frequency of the blade-mass system. It can be said that this is a major move forward in technology, since it allows the energy input system to be distributed over the length of the blade. Undoubtedly, this significantly improves the bending moment distribution of the blade being tested in comparison with a single load introduction point method and also reduces the loads into the blade at any given point.

C. Dual-axis Fatigue Testing Method and Systems

The single-axis flapwise and edgewise fatigue testings of a full scale wind turbine blade are usually performed sequentially, e.g. first testing in edgewise followed by testing in flapwise direction. To shorten the testing duration, dual-axis fatigue testing of blade is now discussed with great interest in both industrial and academic communities. In dual-axis fatigue testing, both flapwise and edgewise loads are applied simultaneously to the blade, not only allowing to accomplish the fatigue testings in both directions in parallel in a shorter overall duration but better simulating the loads that are actually experienced by a blade in service. In addition, it is found that the phase angle between the flapwise and edgewise loads also have a significant effect on the amount of damage that accumulates around the blade [11]. This finding further highlights the significance of dual-axis fatigue testing. But at present, dual-axis testing is still an area of research under investigation in several countries [10, 12]. It is not an industry standard, nor are there many requests from blade manufactures for this type of testing.

A dual-axis fatigue testing could be delivered potentially by using several methods. The conceptually simplest method is to use forced actuation as illustrated in Fig. 15, which is used in the Stevin lab at Delft University of Technology in Netherlands. In the forced actuation test set-up, the hydraulic actuators react from frames to load the blade in flap- and edge-directions, and any combination of flapwise and edgewise loads can be applied to the blade.

A second possible technique was developed by NREL in USA, as illustrated in Fig. 16. It is a test set-up using hydraulic actuator and side-mounted push-rod. In the testing operation, forced actuation is used for the flap-direction and a second cam mounted push-rod provides edge loading. The edge loading is applied in synchronisation with the flap loading so that the phase angle between flapwise and edgewise loadings is maintained within the required limits.

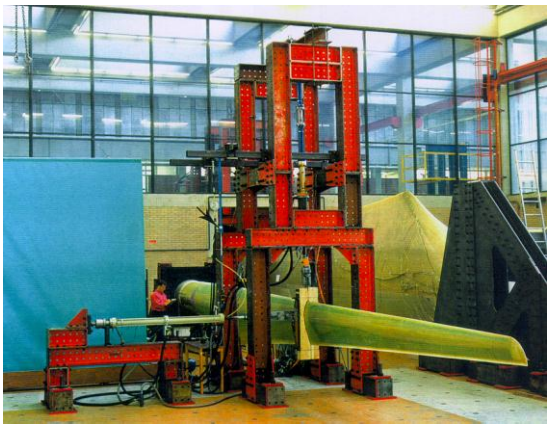

Fig. 15 Dual-axis test set-up using hydraulic actuators

Fig. 16 Dual-axis test set-up using hydraulic actuator and side-mounted push-rod

The main limitation with the aforementioned two test set-ups respectively developed by Delft University of Technology and NREL is that for long blades it becomes extremely difficult to apply the large deflections required. Long-stroke actuators will be needed to create the large deflection of the blade. These require heavy reaction frames and large hydraulic flow capacities, which will significantly increase the testing cost. In view of this, a third dual-axis fatigue testing method was recently developed by Narec in the UK, as illustrated in Fig. 17 [13]. This method uses resonant excitation simultaneously in both flap- and edge-directions.

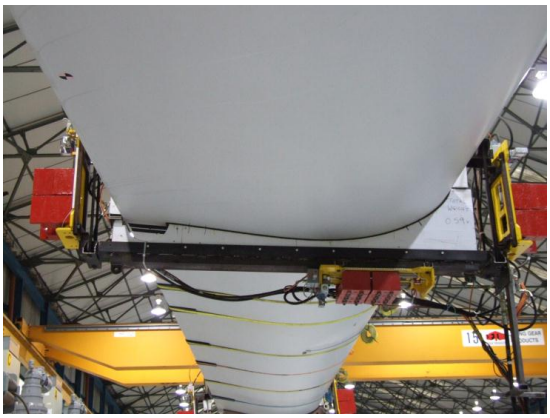

Fig. 17 Narec's CRM set-up for dual-axis testing

Prototype testing of this new method has been conducted by Narec. In the testing, a full-size blade of around 40 m length was excited in flap- and edge-directions simultaneously [13], and the testing results were promising. In this new achievement, Narec used its CRM system mounted in two orthogonal directions. The CRM system consists of a few sliding masses mounted on rails. The sliding masses moved by hydraulic rams as seen in Fig. 17. Since the flap- and edge-direction first natural frequencies are not the same, two separate CRM systems are respectively controlled to oscillate at the required flapwise or edgewise frequencies.

Experimental investigations have shown that in dual-axis testing, the resultant motion of the blade and the induced strain levels follow a complex pattern, which appears to be chaotic, but is in fact not, it being a pre-determined if sensitive

combination of flapwise and edgewise loadings. The normalised path of the tip of a blade undergoing a dual-axis testing is shown in Fig. 18. It indicates how the blade experiences a full range of loadings, rather than the constant amplitude loading undergone in single-axis testing.

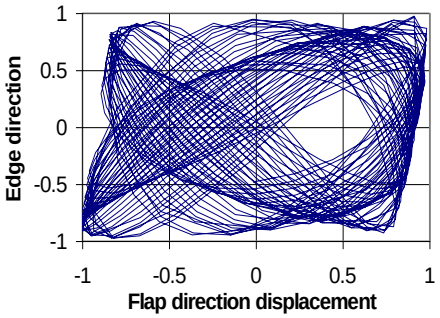

Fig. 18 The normalised movement orbit of a blade tip during dual-axis testing

D. Lightning Strike Testing

Blade represents a special lightning protection challenge unique to wind turbines. The wind turbine blades are complex in geometry and construction, and up to more than 60 m long, made from fibre reinforced composite materials, placed on more than 100 m high tower, and rotate in a vertical plane (for horizontal-axis wind turbines), while exposed to direct lightning attachment. Moreover, wind turbines are usually deployed in open field, making their blades be the most exposed structural elements in vicinities. In lightning strike, the blade will experience the full electromagnetic and mechanical (pressure wave) impact and energy content from the lightning current, the electric field, and the magnetic field associated with the lightning strike. For these reasons, the wind turbine blades have to be safely protected once they are struck by lightning strikes. In fact, this risk is always inevitable in wind turbine operation. To date, the lightning protection of blades fabricated from composite materials has been addressed in different ways by blade manufacturers, firstly on a trial and error basis, and over the last decade on the use of more dedicated research and development programs including field and laboratory testings. The lightning protection concepts that are popularly used in large modern composite material wind turbine blades are shown in Fig. 19, which shows the basic structure and composition of the blade lightning protection systems.

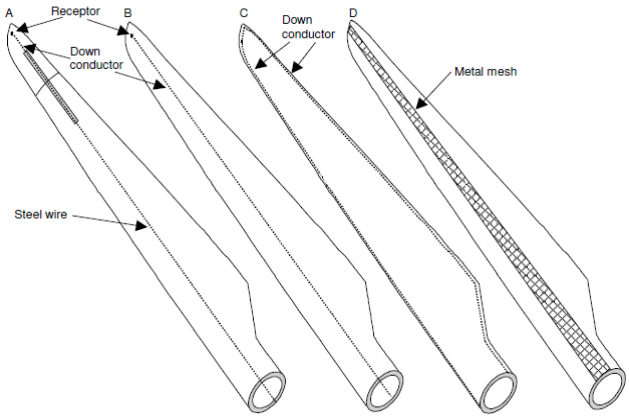

Fig. 19 Lightning protection concepts for large modern composite wind turbine blades

The Part 24 of IEC 61400 standard has explained how to apply the existing technologies to the lightning protection of wind turbine and its critical substructures, especially the blades. In this standard, an effort has also been made to describe a range of high voltage and high current tests, which were originally developed and used successfully for qualification of aircraft structure. In recent years, the similar tests have been adapted to the lightning strike testing of wind turbine blades.

The criteria for adequacy of protection for blades are to show that the design and positioning of the lightning air termination system on the blade ensure efficient lightning interception, and that the down conductor system can sustain the effects of lightning current corresponding to the lightning protection level I (unless shown by risk analysis that LPL-II or LPL-III is sufficient) as shown in Table 2.

TABLE 2 LIGHTNING PROTECTION LEVELS

Protection level	Peak current (kA)	Specific energy content (kJ/Ohm)	Average rate of current rise (kA/μs)	Total charge transfer (C)
I	200	10 000	200	300
II	150	5 600	150	225
III/IV	100	2 500	100	150

Although lightning may attach anywhere on most of the blade surfaces, the long-term field experience shows that the majority of lightning attachments are located at blade tip, and that only a minority attaches elsewhere on the blade. It is therefore concluded that the air termination system positioning tools in IEC 62305-3 [14] do not apply to wind turbine blades. In view of this, in wind turbine blade lightning strike testing it requires to verify the ability of the air termination system and down conductor system to intercept lightning strikes and conduct lightning currents by either of the following methods:

- High voltage and high current tests;
- Demonstration of similarity of the newly designed blade type with a previously certified blade type, or a blade type with documented successful lightning protection in service for a long period under lightning strike conditions;
- By using analysis tools previously verified by comparison with test results or with blade protection designs that have had successful service experience.

At the moment, the laboratory testing of the lightning protection system of wind turbine blades has not been widely performed due to the high costs of professional equipment and facilities. But some testing organizations have either partially or completely possessed this capability. For example, the lightning impulse generator at Narec can generate both lightning (1.2/50μs) and switching impulse (250/2500μs) voltage waveforms with positive and negative magnitudes up to 3.2MV and 2MV, respectively. This enables Narec to conduct both swept-channel and leader-attachment tests on wind turbine blades. The overview of equipment for lightning strike testing and an illustrative lightning strike testing example are shown in Fig. 20.

(a) Equipment (b) Illustrative example

Fig. 20 Overview of equipment for blade lightning strike testing and an illustrative example

The items to be tested would usually be specimens of the blade, including the tip and sufficient portions of the blade inboard of the tip to represent the complete lightning protection design including down conductor systems, connecting components and other components of the lightning protection design.

The tests include both high voltage strike attachment tests and high current physical damage tests:

- The high voltage strike attachment tests are intended for wind turbine blades. The tests can be used to assess location of possible leader attachment points and flashover or puncture paths on blades, optimization of the location of protection devices (e.g. air terminals, receptors, etc.), flashover or puncture paths along or through dielectric surfaces, and performance of protection devices.
- The high current physical damage tests are used to assess actual damage from lightning currents, for example arc attachment damage, hot spot formation, metal erosion at receptors, adequacy of protection materials and devices, magnetic force effects, blast and shock wave effects, behaviour of joints and hardware assemblies, and voltages and currents at points of interest throughout a lightning protection system. The testing methods depicted in the standard are applicable to both complete tip designs and to smaller sections of the down conductor.

The test specifications will include discussion of purpose of test, detailed instructions of each test set-up, test specimen selection, test impulse waveforms, measurements and data recordings, data interpretation and step-by-step test procedures.

IV. STANDARDS FOR WIND TURBINE BLADE TESTING

Today, blade testing has been required as part of turbine certification to meet international design standards, such as IEC and DNV, benefiting developers in mitigating the technical and financial risk of deploying mass-produced wind turbines. To perform the static and fatigue testing of full-scale wind turbine blades, there are already a number of blade testing facilities that have been established across the world, for example Risø National Laboratories in Denmark, National Renewable Energy Laboratory (NREL) in USA, National Renewable Energy Centre (Narec) in the UK, the Centre for Renewable Energy and Sources (CRES) in Greece, the wind turbine Materials and Constructions Knowledge Centre (WMC) in Netherlands, National Renewable Energy Centre (CENER) in Spain, LM glass fibre in-house testing facility in Denmark, the Blade Test Centre Gujarat (BTCG) in India, SGS's blade testing facilities around the world and so on. All these testing organizations are required to run the testing laboratory in accordance with the standard ISO 17025, which provides general requirements for the competence of calibration and testing laboratories.

The requirements to the structural safety and design loads of wind turbine blade have been specified in the Part 1 of IEC 61400 standard. Static and fatigue testing is an essential element of wind turbine certification. In order to provide valid static and fatigue type testing, there are three key areas that need to be addressed, i.e. right loads, right test specimen, and right documentation. The right loads are addressed through the correct development of extreme and fatigue loads, the selection of the correct safety factors, and the correct set-up and execution of test program. Although there will always be one particularly fatigue area on the blade, it is still desirable to obtain the correct bending moment distribution over as much of the length of the blade as possible; the right test specimen is addressed through the selection of a representative test blade, and the inclusion of critical structural elements during the test; and finally the testing program must be thoroughly documented, capturing the key information required to provide confidence in the test results, the design, and ultimately to achieve certification. The detailed requirements for full scale blade testing are already specified in the standard IEC 61400 Part 23. The major manufacturers, laboratories, research institutions and certificating bodies have participated in developing these standards. However, the detailed qualification of blade materials, design, and manufacturing procedures are yet to be included. For this reason, DNV issued a new standard DNV-DS-J102: Design and manufacture of wind turbine blades, offshore and onshore wind turbines in October 2010, replacing its previous version DNV-OS-J101 issued in 2004 and providing a more comprehensive and detailed guideline to the development of new wind turbine blades. The contents widely cover the blade material qualification, design analysis, blade manufacturing, blade testing, and documentation requirements. At present, DNV-DS-J102 standard serves as detailed guidance to achieve IEC WT-01 certification for wind turbine blades.

As mentioned above, the lightening protection of wind turbines, particularly the lightning protection of wind turbine blade, as well as the known lightning protection technologies have been specified in the standard IEC 61400 Part 24, which is however limited to horizontal axis wind turbines. The standard uses the lightning current parameters defined in the standard IEC 62305-1 for wind turbine lightning protection system design, and for lightning protection component dimensioning, selection and testing. The lightning current parameter values defined in IEC 62305-1 standard are generally considered adequate for lightning protection of wind turbines.

In wind turbine blade engineering, the qualification of materials, design and manufacturing procedures is dependent on the individual blade manufacturers. They utilise unique and individual materials, design approaches, and manufacturing processes, the details of which are often confidential. This is one of the major differences when compared to other industries, such as civil engineering and ship building, where the materials, design solutions and manufacturing methods are more or less common for all manufacturers.

In addition to the IEC and DNV standards mentioned above, some other industry standards are in connection with the qualification, design analysis and testing of composite materials. Some of them are listed in Table 3 [7].

TABLE 3 GUIDELINES AND STANDARDS IN CONNECTION WITH COMPOSITE DESIGN AND TESTING

Reference	Title
ASTM C297	Determination of the core flat wise tension strength of sandwich structures
ASTM C613	Standard test method for constituent content of composite prepreg by soxhlet Extraction
ASTM D 5379	Standard test method for shear properties of composite materials by the V-notched beam method
ASTM D1781	Standard test method for climbing drum peel for adhesives
ASTM D2344	Standard test method for short-beam strength of polymer matrix composite materials and their laminates
ASTM D2584	Standard test method for ignition loss of cured reinforced resins
ASTM D3167	Standard test method for floating roller peel resistance of adhesives
ASTM D3171	Standard test methods for constituent content of composite materials
ASTM D3479	Standard test method for tension-tension fatigue of polymer matrix composite materials
ASTM D3529	Standard test method for matrix solids content and matrix content of composite prepreg
ASTM D3530	Standard test method for volatiles content of composite material prepreg
ASTM D3531	Standard test method for resin flow of carbon fibre-epoxy prepreg
ASTM D3532	Standard test method for gel time of carbon fibre-epoxy prepreg
ASTM D5528	Standard test method for mode I inter-laminar fracture toughness of unidirectional fibre-reinforced polymer matrix composites
ASTM D5868	Standard test method for lap shear adhesion for fibre reinforced plastic (FRP) bonding
ASTM D695	Standard test method for compressive properties of rigid plastics
Danish Energy Agency	Recommendation for design, documentation and test of wind turbine blades
ISO 14129	Fibre-reinforced plastic composites – determination of the in-plane shear stress/strain response, including the in-plane shear modulus and strength, by the ±45 °tension test method.
MIL-HDBK-17-1F	Volume 1. Polymer matrix composites guidelines for characterization of structural materials
MIL-HDBK-17-3F	Volume 3. Polymer matrix composites materials usage, design, and analysis

V. STRUCTURAL HEALTH AND PERFORMANCE MONITORING OF WIND TURBINE BLADES

Blades are crucial and expensive components of a wind turbine. However, they are one of the components that are most likely to fail [4] due to their exposure to high loads even in normal operation. Moreover, failure of a blade can cause significant

downtime or even machine loss, as well as negative publicity. Particularly with present large megawatt wind turbines and the highly competitive electricity generation market, the loss of revenue from one machine due to component failure can cause considerable financial stress to operators. So, to understand the actual health condition of the blades and detect their structural failure as early as possible is of significance not only to the revenue of an individual wind farm operator but to the competitiveness of the whole wind industry. For this reason, condition monitoring is regarded as one of the most efficient and cost-effective approaches to minimizing the risk of blade failure and the downtime.

In the standard IEC 61400 Part 23, the failures of a wind turbine blade are categorized into three levels according to their severity, effects and consequences, as listed in Table 4 [10].

TABLE 4 FAILURES OF A WIND TURBINE BLADE

Damage levels	Presentation of the failures
Catastrophic failure	o Breaking of primary blade structure o Complete failure of structural elements, internal and external bond lines, skins, shear webs, root fasteners o Major parts become separated from the main structure
Functional failure	o Reduction in stiffness by 5-10% o Permanent deformation o Substantial permanent change of cross-sectional shape o After unloading the blade, a mechanism is no longer capable of performing its designed objective
Superficial failure	o Small cracks not causing significant strength degradation or bond line weakening o Gel coat cracking o Paint flaking o Surface bubbles o Minor elastic panel buckling o Small delamination

However, the failures mentioned in the standard are all characterized by the physical damages of material and structure of the blade. In condition monitoring practice, some blade-related rotor failures are also need to monitor. They could be not harmful to the structural health of the blade, but could result in significant degeneration in energy capture efficiency. This kind of failures could be characterized by [15]:

- increase in the blade surface roughness due to pollution, icing, blowholes, exfoliation, remains of insects, etc.
- mass imbalance due to icing, water penetrating through cracks, loose material (e.g. remaining material from production processes) moving inside the blades, etc.
- aerodynamic asymmetry due to blade pitch angle failures, aerodynamic profile production tolerances, profile deformation during operation, etc.

Accordingly, the existing blade condition monitoring techniques can be roughly classified into two categories, i.e. (1) structural health condition monitoring, and (2) energy capture efficiency monitoring. The former is for detecting the structural failures occurring in blade, and the latter is for detecting the change in performance due to failures or defects of the blades or associated systems (e.g. pitch control system).

As depicted in [15], up to now condition monitoring of wind turbine blade is accomplished mainly by visual inspections onsite at regular intervals (usually once every 2 years) to provide ‘snapshots’ of the actual rotor condition, as shown in Fig. 21. Obviously, it is unlikely to perform such kind of work in unfavourable weather conditions. For this reason, the suitable time for carrying out onsite inspection of wind turbine blades is limited, as wind turbines are intended to be deployed in remote windy and cold areas. Moreover, onsite inspection of blade requires specialized equipment (cranes, working platforms, etc.) and expert personnel, consuming a lot of time and money. For offshore wind turbines, onsite blade inspections will become even more problematic and cost intensive due to the limited access to rough sea site and additional costs on vessels, cranes and other tools specially required in the work on sea. For these reasons, online condition monitoring is strongly recommended, especially for those wind turbines deployed offshore and in remote lands. The benefits of having a blade condition monitoring system can be summarized as:

- avoidance of premature breakdown: prevent catastrophic blade failures and secondary damages;
- reduction in time for blade inspection and maintenance cost: inspection interval can be increased with online inspection, prolong the service life of a blade, and schedule the replacement of defective blades at right time;
- supervision at remote sides and remote diagnosis: reduce the times of visual inspection at remote sites;
- improvement of capacity factor: with early warning of impending failures of blades, maintenance action can be taken during low wind season and hence will not lower the capacity factor very much;
- support for the improvement of blade design: the condition monitoring data obtained can be used to improve designs for the next generation of turbine blades with higher reliability.

(a) Before inspection

(b) In inspection

Fig. 21 Visual inspection of wind turbine blades

In the past decades, lots of efforts have been expended to develop the condition monitoring techniques for wind turbine blades [5, 16, 17, 18]. A brief overview of existing techniques is given below, although a truly effective and reliable online monitoring technique has not been fully achieved today.

A. Structural Health Monitoring

Although structural damage can happen to any structural component of a highly loaded wind turbine, the most common type of structural damages stem from blade or tower failures [19]. Accordingly, extensive attention has been given to detecting the structural failures of blade by using various non-destructive testing techniques. The major of them include [16, 20]:

1) Vibration Analysis:

Vibration analysis is the most known technology applied for condition monitoring. The types of sensors used depend on the frequency range, i.e. displacement transducers are used for low-frequency range, velocity transducers for middle-frequency range, and accelerometers for high frequency range. In the current condition monitoring practice, research people rarely use vibration sensors to measure the vibration response directly from the blade. But the cases of successful application of vibration analysis in blade condition monitoring are often reported. For example, it was reported in [15] that a rotor mass imbalance fault was successfully detected with the aid of two accelerometers. Both accelerometers were installed in the nacelle of a constant speed 600 kW wind turbine. One was in front of the tower vertical axis (i.e. close to the rotor when looking from the hub), and the other was located at the rear of the vertical tower axis. The rotor mass imbalance fault was resulted from an asymmetric icing condition of the blades. An illustrative example of this situation is shown in Fig. 22.

Fig. 22 Ice on wind turbine blade

2) Acoustic Emission:

Acoustic emission is now a popular idea used for monitoring the structural health condition of wind turbine blades, although this technique has not been fully validated in wind industry. Acoustic emission monitoring is realized through a piezoelectric acoustic sensor, which is attached to the blade by flexible glue with low attenuation, as shown in Fig. 23.

The sensor is able to detect the high frequency component of the elastic waves (or stress release waves) generated by the energy loss processes due to cracking, deformation, debonding, and delamination failures occurring in the blades. It has been reported that acoustic emission event will cluster around a certain point where damage occurs [21]. So, acoustic emission monitoring is potentially an effective method for locating the blade failure or damage locations. In addition, acoustic emission signals are characterized in terms of amplitude and energy, and inferences can be made about the kinds of damage processes taking place in the blade. However, acoustic emission is less capable in damage characterization and further damage evaluation if a suitable algorithm is not available. The varying wind loads applied to the blade makes such kind of testings further

challenging.

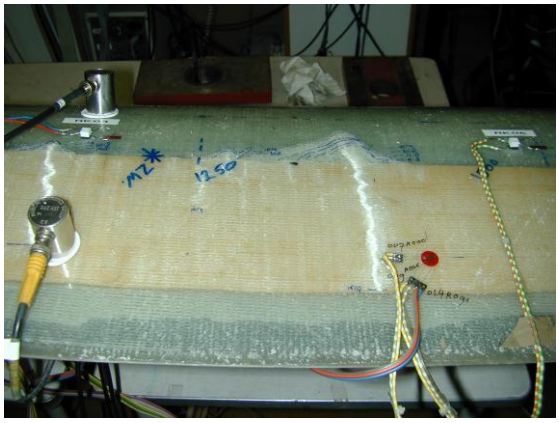

Fig. 23 Acoustic sensors attached to blade

3) Thermography:

Thermography is often applied to monitoring and failure detection of electronic and electric components. For example, hot spots, due to degeneration of electric or electronic components or bad contact, can be readily identified by the approach of thermography. In recent years, thermography has been further applied to wind industry. The successful detection of blade failures by thermography in the lab has been reported [20], as shown in Fig. 24. It is especially effective in detecting subsurface defects or anomalies that can cause temperature differences on surface of the blade. The advantage of thermography is that it is able to produce a full-field measurement in image form, which allows a fast evaluation even for a non-professional user. The main problem of thermography monitoring technique lies in the thermal excitation method. Passive excitation can be used but is limited to those composite materials that produce excessive heat during operation of the blade. In addition, environmental temperature is also a factor that cannot be ignored in thermography testing.

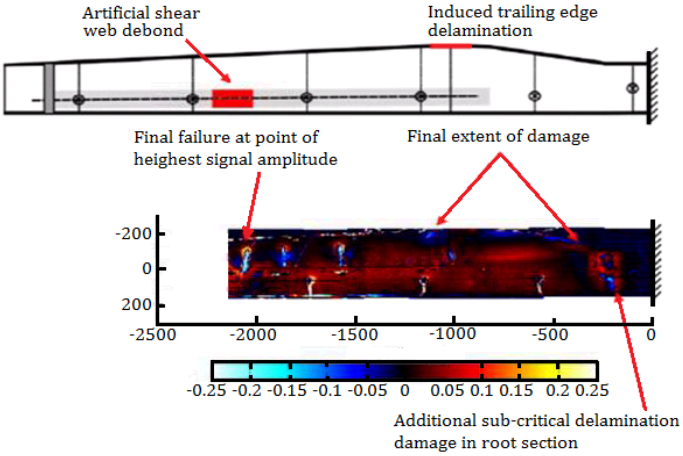

Fig. 24 Detecting defects in blade by thermography

4) Ultrasonic Detection:

Ultrasound is a well-established method for investigating the inner defects of composite structures, such as wind turbine blades. The basic principle of the technique is that an ultrasonic wave is passed through the material and is then reflected and/or mode converted by a defect. Ultrasound probing will typically reveal planar cracks (e.g. delamination) oriented perpendicular to the direction of sound wave propagation. The transmit time and/or amplitude of the feedback ultrasonic signals will be monitored. The transmit time can be used to determine the position of the defect relative to the position of the transducer, while the amplitude can be used to assess the severity (or size) of the defect. At present, the ultrasound-based blade monitoring techniques have been commercialized. Fig. 25 shows a blade ultrasonic detection system developed by a Danish company named Force Technology.

In the system, four ultrasonic transducers are used. A special control system was designed to ensure that transducers can properly touch the varying blade profile at different positions. A camera was installed in the front of the system, avoiding the system goes over the blade. The defects (e.g. cracks, delamination, etc.) can be successfully detected and easily observable from a 3D testing image. However, like other ultrasonic detection systems, this system also requires special couplant with low attenuation to enhance the detecting capability of the ultrasonic transducers. This constrain significantly limits the onsite application of ultrasonic techniques in wind farms.

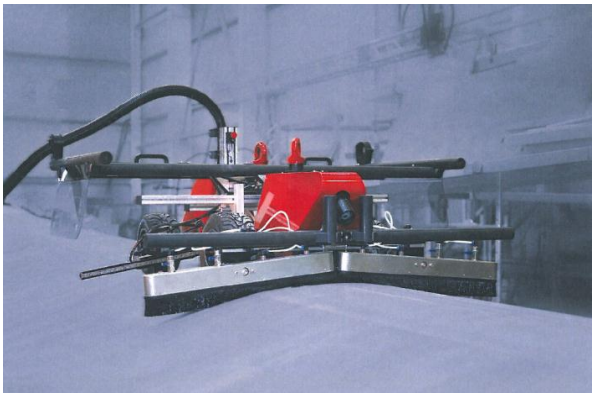

Fig. 25 Ultrasonic detection system for wind turbine blade

5) Fibre Optics:

An optical fibre is a glass or plastic fibre designed to guide light along its length. Optical fibres are widely used in fibre-optic communication, which permits transmission over longer distance with less loss and at higher data rates than other forms of wired and wireless communications. Moreover, they are immune to electromagnetic interference. In application, the optical fibre will be attached to the test specimen. The optical power of a light source will reduce when it goes through the optical fibre. The reduction depends on the strain of the fibre. This principle is adopted to sense the strain in the structure being tested. In wind industry, this technique was developed for evaluating the structural health condition of wind turbine blades through measuring the strains and therefore bending moments in root sections of the blades. Currently, many companies across the world are developing such kind of techniques and systems for application in wind farms. One of the proven systems is the Rotor Monitoring System (RMS) developed by Moog Insensys, as shown in Fig. 26. Up to date, RMS has been utilized for accomplishing multiple health detection items of wind turbine blades, such as ice detection, rotor imbalance detection, lightning strike detection, and blade damage detection.

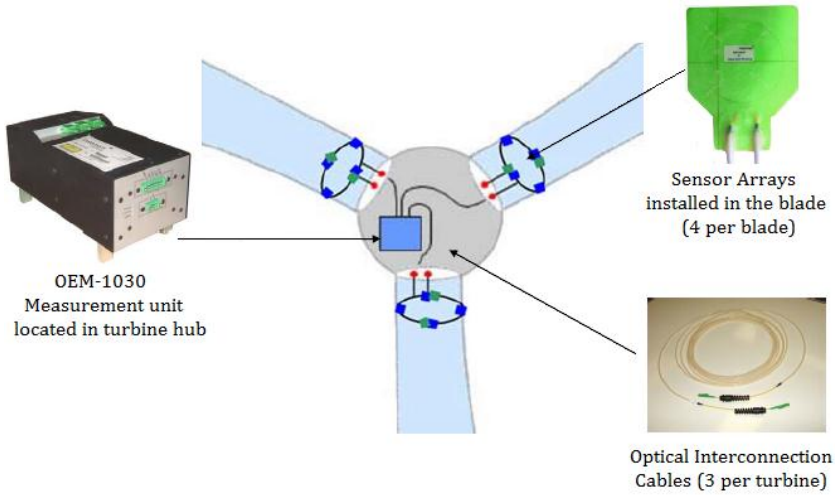

Fig. 26 Typical configuration of Insensys RMS system

6) Laser Doppler Vibrometer:

The laser Doppler vibrometers are a type of non-contact velocity transducers based on analysing the Doppler effect on a laser beam emerging from a solid surface. Previously, laser Doppler vibrometers have been widely used for monitoring the vibration of rotating machinery. Such technique was further applied to monitoring the variation in the relative distance between wind turbine blades and tower [22]. This is because that approximately 63.4% of the structural damages in wind turbines leading to catastrophic accidents are due to the sudden deformity or displacement change between the blades and the tower [19]. The LDS system developed in [22] consists of a sensor head and controller. It employs triangulation measurement principles, whereby the laser emitter projects an infrared laser beam that creates a spot on the rotating blade surface. Reflected light from the surface is detected by the light receiver inside the sensor head. Therefore, LDS system does not need any special surface preparation to detect the reflected light. The displacement values of the blades are acquired through use of a DAQ system (NI, Terminal block 2120 and Digitizer PCI 6221) in real time to monitor abnormal blade deflection. The displacement is continuously monitored by impinging the laser beam of the non-contact LDS at the rotating blades in an operating condition of a wind turbine. Damage such as nacelle tilt, bolt loosening, or blade mass loss causes measurement irregularities or changes, indicating the detection of any possible damage. The installation of the LDS system on a wind turbine is illustrated in Fig. 27.

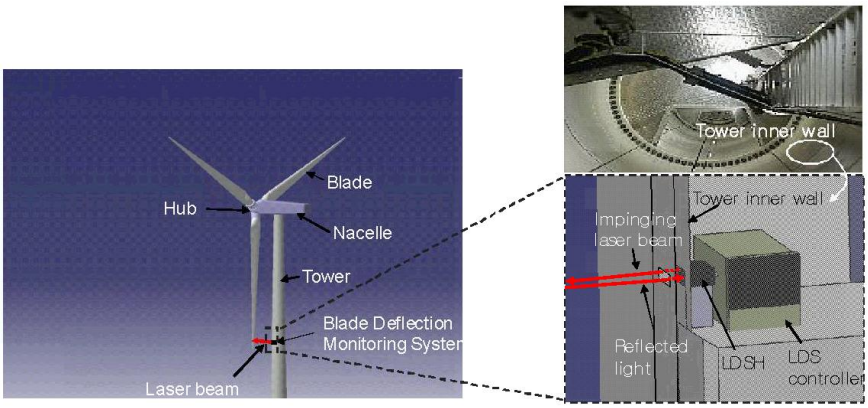

Fig. 27 The blade deflection monitoring system installed on a wind turbine

7) Electrical Resistance-based Damage Detection:

Carbon fibres used in wind turbine blades have high electric conductivity while the polymer matrix of a carbon-fibre-reinforced plastic (CFRP) is an insulating resistor. In practice, CFRP laminates have finite electrical resistance in every direction. The electrical resistance in the transverse direction is much larger than in the direction of the fibre orientation. If a delamination crack propagates in the resin-rich interlaminate, the crack breaks the fibre-contact-network between the plies. The breakage of the contact network causes an increase in the electrical resistance of the carbon/epoxy-laminated composites, which enables delamination crack detection by measuring the electrical resistance change in a CFRP composite laminate. A delamination crack is detected using the electrical resistance change between the two mounted electrodes, as shown in Fig. 28.

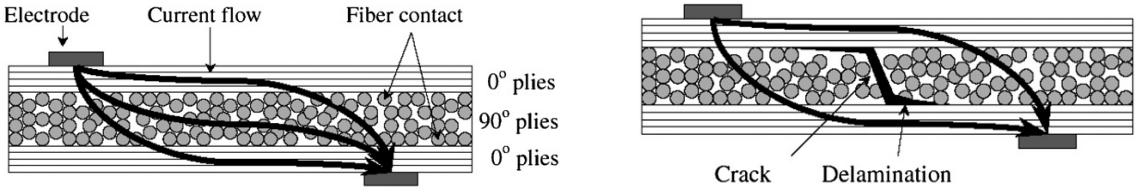

(a) Electrical network structure of the fibre in a CFRP laminate

(b) The electrical network is broken with delamination and matrix cracking

Fig. 28 Schema of a practical structure of a carbon/epoxy composite when an electrical current is applied [16]

A wireless delamination detection system is composed of a sensor module that has a ceramic oscillator connected to the electrodes mounted on the composite surface and its receiver. The ceramic oscillator of the sensor module is used for wirelessly transmitting the electrical resistance change data as the oscillating frequency changes to its receiver. The oscillating frequency of the sensor circuit increases with the increase of electrical resistance of CFRP laminates, indicating the occurrence of delamination in the CFRP laminates.

8) Mechanical Strain Gauge:

Mechanical strain gauges are popularly used in static and fatigue testing of full scale wind turbine blades. As shown in Fig. 29, they are glued to the surface of the blade being tested to provide accurate measurement of the bending and stretching loads of the blade. At present, mechanical strain gauge might be the cheapest and the most reliable approach for fault detection, lifetime forecasting and protecting against high stress levels of wind turbine blades. However, owing to the inherent reliability issues of the material mechanical strain gauges can be used in laboratory testing but unsuited to onsite applications.

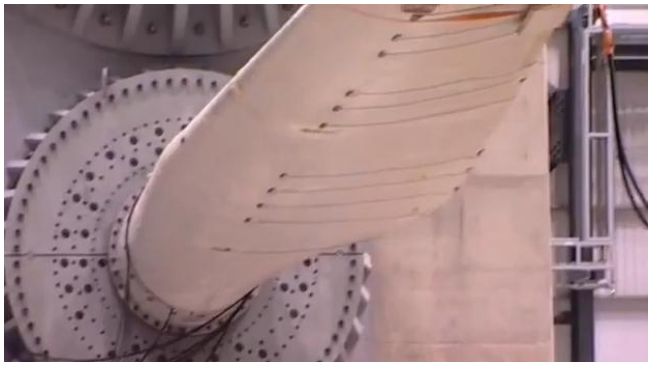

Fig. 29 The array of mechanical strain gauges in fatigue testing of a wind turbine blade

B. Performance Monitoring

In spite of the great effort already done, the majority of the aforementioned Non-destructive testing techniques are still not ideal for performing the online monitoring of wind turbine blades in operation. In addition, some blade defects, e.g. rough surface of the blade caused by ice/snow, insect remains or dusts, are not actually the structural damage of blades. They however do significantly degenerate the energy capture efficiency of the blade. For these reasons, instead of spending lots of money and attention to conduct the structural damage detection, the operator would rather to make more effort on improving the capacity factor of wind turbines by taking advantage of available resources in wind farm. The data collected by the wind farm Supervisory Control and Data Acquisition (SCADA) system is one of the most valuable resources available to utilize. The SCADA system is originally designed for operating wind turbines, ensuring they are conforming to the designed power curve and protecting the turbines in extreme weather and loading conditions. It measures the operating and performance parameters from those key subassemblies or components of the turbines regularly (usually at 10 minutes intervals). Through analysing these SCADA data, the operator can count the electric power generated by the turbines and understand their operating/health conditions approximately. Owing to being collected by using a low sampling rate, the SCADA data can hardly be applied to performing condition monitoring using conventional spectral analysis approaches. They however may be used to carry out some simple condition monitoring tasks of those key components of the turbines if a suitable algorithm is available [23, 24, 25]. Researches have shown that many correlation relations among wind turbine operating/performance parameters can be used for assessing blade conditions or early detecting the faults in blades. For instance, a total of 6 parameters, i.e. wind speed, rotor speed, generator power, generator speed, gearbox vibration and gearbox oil level, are proposed for condition monitoring a wind turbine blade in operation [23]. The judging procedures are:

Step 1: Check the correlation between generator speed and generator power to assess the health condition of generator;

Step 2: If generator is fine, check the correlation between rotor speed and generator speed, the correlation between rotor speed and gearbox vibration and temperature, as well as the gearbox lube oil level against time, to assess the health condition of gearbox and coupling;

Step 3: If above correlations are well maintained, the miscorrelation between wind speed and rotor speed, and the miscorrelation between wind speed and shaft torque would indicate something wrong with one or more blades of the turbine.

Owing to the shortage of wind turbine SCADA data, the kinds of blade performance/condition monitoring techniques have not been fully demonstrated, although their preliminary application results are promising [23]. To facilitating understanding, the wind speed - rotor torque correlation curves obtained before and after the presence of a blade defect are shown in Fig. 30. From this figure, it can be clearly seen that the torque-speed curve gradually sinks over time. And from this phenomenon, it can be inferred that the energy capture efficiency of the blade is degenerating gradually with the growth of defect.

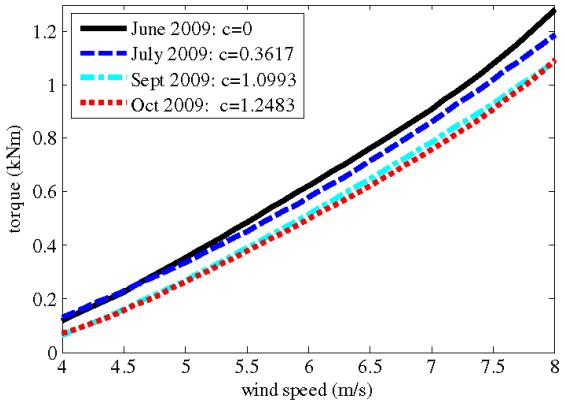

Fig. 30 The correlation between wind speed and shaft torque [23]

The influences of ice, snow, dust and insect remains on the energy capture efficiency of wind turbine blade are often reported. They are characterized by either gradual or sudden change of wind speed – power curves. All these environmental factors take negative effect on blade's performance mainly through changing the surface roughness of the blade. A successful surface roughness assessment technique or device is still sought for today. At the moment, the assessment of the blade surface roughness is still accomplished by the means of visual inspection.

VI. GENERAL SUMMARY

A. Single-axis Fatigue Testing

Fatigue testing of wind turbine blades has developed to its present capabilities of testing over 60 m long blades, and delivers an important part of the proving process for wind turbine performance. Several different fatigue testing methods are possible, which can broadly be classified as either forced displacement or resonant testing. Both testing methods are currently

used in performing fatigue testing of wind turbine blades. Each of them has both advantages and disadvantages. To benefit the future R&D work, their major limitations are summarized as follows:

1) Forced Displacement Testing:

Forced displacement as a testing method requires equipment that is able to physically move the blade through the required deflections. As blades get longer the deflections required also rise and the demands made on testing equipment, particularly hydraulic cylinders, become much higher. With hydraulic cylinders the key factors to consider are the stroke length to achieve the required deflection, and the hydraulic fluid flow rates needed. Stroke lengths may rise to several metres, and the hydraulic fluid flow rates required, to support these stroke lengths, can rise to thousands litres per minute (1000L/min). Long stroke length, high load hydraulic cylinders are expensive and the cylinders themselves are subjected to fatigue wear due to the testing.

The cost of pumping large amounts of hydraulic fluid is a major consideration for a forced displacement testing. This cost is mainly the cost of energy for moving the hydraulic fluid and for providing cooling for the fluid. There is a direct relationship between the amount of deflection needed and the quantity of energy required, and with a forced actuation system there are very limited means of reducing this energy cost.

For a forced displacement system the blade needs to be able to take the loads that are input from the actuation equipment. These loads can rise to high levels if only one or two load points are used, which requires the blade to be reinforced at these loading points. Blade reinforcement will alter the blade performance and behaviour, and whilst this should not be an issue for the fatigue test, if further static testing is required after the fatigue test, then this reinforcement may interfere with obtaining valid static test results.

A forced displacement system using hydraulic actuators requires robust and fail-safe control systems, since the very nature of hydraulic systems means that they have the potential to move very rapidly with high forces, with the possibility of severely overloading the blade. Hence, once the hydraulic cylinder is connected to the blade, there is the risk that any control system malfunction or operator error could damage the blade.

2) Resonant Testing:

The main limitation of resonant testing methods is that they can only be performed at the first natural frequency of the blade plus test equipment system. This means that it is not possible to alter the duration of testing time, and as blades get longer, natural frequencies become lower and testing times increase and become longer. In addition, for a resonant testing method the testing equipment is normally mounted on the blade, which introduces an amount of static mass as well as the dynamic moving mass that excites the blade. This added mass also reduces the natural frequency.

The equipment that is mounted on the blade is subjected to the movement of the blade and in particular the accelerations as the blade cyclically oscillates, reversing direction through each cycle. On longer blades these accelerations can reach high levels and exciter equipment needs to be designed to accommodate these accelerations and induced forces.

With resonant testing the damping forces due to aerodynamic resistance, particularly in the flap orientation, become very significant for long blades. These aerodynamic damping forces arise because of the large deflections that blades are subjected to, and the resultant large volumes of air that are displaced by each sweep of the blade. The energy input to sustain resonance on long blades needs to be carefully considered, and the test apparatus designed appropriately to ensure effective transfer of energy from the exciter system to the blade under test.

For rotating mass excitation the only significant variable is the amount of dynamic mass and just adding more can lead to a case of diminishing returns. With oscillating mass it is possible to vary both mass and amplitude of mass movement, giving greater flexibility, but also creating other interactions between moving mass and the accelerations that can be sustained by the test equipment.

B. Dual-axis Fatigue Testing

In contrast to single-axis fatigue testing, dual-axis testing shows the following advantages:

- provide a better test of the blade by combining load cases;
- reduce the time of testing by combining the flapwise and edgewise testings to run in parallel rather than sequentially.

However, despite the quick progress and innovations in developing new dual-axis testing methods and facilities, many issues still remain to solve in this field, namely:

- flapwise and edgewise loads are not applied in a predictable order;
- the number of load cycles applied in flap and edge develop at different rates;
- loads onto the non-major blade axes are difficult to define prior to the start of the test;
- the number of load cycles applied to non-major blade axes only becomes known as the testing proceeds;

- blade manufacturers at present have procedures for developing damage equivalent loads (DEL) for a single-axis fatigue testing, and these DELs are used to define the load level for the single-axis fatigue testing. These procedures are not easily adaptable to the resonant dual-axis testing method;
- the material property data requirements for the DEL analysis on a dual-axis testing are not the same as those for a single-axis fatigue testing, and blade manufacturers will need to invest in more material testing if they wish to exploit resonant dual-axis testing.

At present, both testing organizations and universities are performing research activities aiming to investigate the various points detailed above. Once these issues are solved successfully, it is believed that dual-axis testing will be popularly adopted in the full-scale testing of wind turbine blades attributed to its superiorities to single-axis testing.

C. Blade Lightning Strike Testing

It is well-known that wind turbines are frequently struck by direct lightning strikes. The risk of suffering struck has proved to increase with the increasing size of wind turbines. This fact cannot only be explained by the increase in collection area, but apparently the amount of upward initiated flashes from these relatively high structures has increased drastically as well. Fortunately, both research and experience accumulated over the last decades have shown that wind turbine can be effectively protected against lightning strike by applying the well-known and proven lightning protection techniques. This is the case for the electrical and control systems, and also for most of the wind turbine structures. The exceptions are the blades for which new protection systems have had to be developed and tested.

At present, many testing bodies have either partially or fully possessing the capability of performing the lightning strike testing of wind turbine blades. Moreover, lightning strike accidents of wind turbines are often reported [19]. However, there are still not many requests from blade manufacturers for this type of testing. So, it can be said that today static and fatigue testings are still the mainstream items of blade testing, because most blade failures stem from the damages resulted by ultimate loads in severe weather conditions or long-term fatigue loads in a normal operating condition.

D. Blade Condition Monitoring

Many techniques for non-destructive testing were performed in assessing the health condition of wind turbine blades. These techniques are either simple or complicated, either cheap or costly. Most of them have shown promising testing results in laboratory and some of them have been commercialized and adopted for monitoring blade during static and/or fatigue testing. However, few of them are really suited to onsite application in wind farm. Among these techniques, fibre optic strain gauge measurement is a best proven technique in wind industry. It was originally designed for controlling the bending moment loads of the blades and protecting them from being damaged when overloaded. Now, its application has been further extended to detecting the failures of turbine rotor. Despite these achievements, to fulfil a successful structural health monitoring of a long blade (> 60 m length) by the approach of fibre optic strain gauge measurement is still a challenging issue, especially under constantly varying loading and operating conditions of wind turbines.

Performance monitoring of blades by taking advantage of wind turbine SCADA data is a cost-effective and therefore promising technique. The IEC 61400 standard has specified the parameters that are essential to be collected by wind turbine SCADA system. If the additional values of these SCADA parameters and the knowledge behind them can be fully explored, many critical wind turbine failures, including blade failures, can be early detected in advance. Unfortunately, the wind industry today has not been fully standardized. The wind turbine design, the manufacturing process and the SCADA systems equipped in the turbines are different from manufacturer to manufacturer. Moreover, the SCADA data collected from wind turbines are currently being regarded as highly confidential properties of turbine suppliers. Access to these data cannot be made open to the public. Undoubtedly, all these restrictions have significantly delayed the progress in R&D for condition monitoring techniques.

ACKNOWLEDGMENTS

The author would like to thank National Renewable Energy Centre (Narec) in the UK, National Renewable Energy Laboratory (NREL) in the USA, and Risø National Laboratories in Denmark for their kind supports, discussions and helpful suggestions. This work was also supported by the National Natural Science Foundation of China with project reference number 51075331 and European FP7 project OPTIMUS with reference number 322430.

REFERENCES

[1] P. J. Tavner, J. Xiang, and F. Spinato, "Reliability analysis for wind turbines," *Wind Energy*, vol. 10, pp. 1-18, 2007.

[2] J. Ribrant, and L. Bertling, "Survey of failures in wind power systems with focus on Swedish wind power plants during 1997-2005," *IEEE Transactions on Energy Conversion*, EC22 (1), pp. 167-173, 2007.

[3] Winstats Newsletter, vol. 17, no. 2, Forlaget Vistoft, Spring 2004.

[4] P. J. Tavner, Offshore wind turbines: Reliability, availability & maintenance, ISBN: 978-1-84919-229-3, IET Press, 2012.

[5] Wenxian Yang, P. J. Tavner, C. J. Crabtree, Y. Feng, and Y. Qiu, "Wind turbine condition monitoring: Technical and commercial challenges," *Wind Energy*, Aug. 2012, DOI: 10.1002/we.1508.

[6] P. Brøndsted, H. Lilholt, and A. Lystrup, "Composite materials for wind power turbine blades," *Annual Review of Materials Research*, vol. 35, pp. 505-538, 2005.

[7] DNV Standard DNV-DS-J102, "Design and manufacture of wind turbine blades, offshore and onshore wind turbines," Oct. 2010.

[8] C. J. Christensen, K. O. Ronold, and M. T. Thøgersen (Det Norske veritas), "Calibration of partial safety factors for design of wind turbine rotor blades against fatigue failure in flapwise bending," Risø-R-1204(DA), Risø National Laboratory, Roskilde, Denmark, Aug. 2000.

[9] G. Freebury, W. Musial, "Determining equivalent damage loading for full-scale wind turbine blade fatigue tests," NREL/CP-500-27510, National Renewable Energy Laboratory, USA, Feb. 2000.

[10] Technical Specification, IET TS 61400-23 Wind turbine generator systems – part 23: Full-scale structural testing of rotor blades.

[11] S. Hughes, W. Musial, T. Stensland, "Implementation of two axis servo-hydraulic system for full-scaletesting of wind turbine blades," Windpower'99, NREL: Burlington, Vermont, 1999.

[12] R. Court, A. Waggott, P. Hope, I. Williamson, "Blade testing – Narec's innovations in full scale dual axis fatigue testing," EWEC08, Brussels, Mar. 31 – Apr. 3, 2008.

[13] R. Court, S. Ridley, H. Jones, P. A. Bonnet, A.G. Dutton, "Fatigue testing of wind turbine blades with computational verification," ICCM17, Edinburgh, 27-31 Jul., 2009.

[14] Technical Specification, IEC 62305: Lightning protection, 2006.

[15] P. Caselitz, J. Giebhardt, "Rotor condition monitoring for improved operational safety of offshore wind energy converters," *ASME Journal of Solar Energy Engineering*, vol. 127, pp. 253-261, 2005.

[16] C. C. Ciang, J. R. Lee, H. J. Bang, "Structural health monitoring for a wind turbine system: a review of damage detection methods," *Measurement Science and Technology*, vol. 19, pp. 1-20, 2008.

[17] Y. Amirat, M. E. H. Benbouzid, E. Al-Ahmar, B. Bensaker, S. Turri, "A brief status on condition monitoring and fault diagnosis in wind energy conversion systems," *Renewable and Sustainable Energy Reviews*, vol. 13, pp. 2629-2636, 2009.

[18] W. Q. Jeffries, J. A. Chambers, D. G. Infield, "Experience with bicoherence of electrical power for condition monitoring of wind turbine blades," *IEE Proceedings Vision, Image and Signal Processing*, vol. 45, pp. 141-148, 1998.

[19] Caithness windfarm information forum, Wind turbine accident data to Jun. 30th, 2013. http://www.caithnesswindfarms.co.uk/page4.htm (Accessed 18th Jul., 2013).

[20] Z. Hameed, Y. S. Hong, Y. M. Cho, S. H. Ahm, C. K. Song, "Condition monitoring and fault detection of wind turbines and related algorithms: A review," *Renewable & Sustainable Energy Review*, vol. 13, pp. 1-39, 2009.

[21] E. R. Jørgensen, K. K. Borum, M. McGugan, C. L. Thomsen, F. M. Jensen, C. P. Debel, and B. F. Sørensen, "Full scale testing of wind turbine blade to failure – flapwise loading," *Risø-R-1392 (EN) Report*, Risø National Laboratory, Denmark, 2004.

[22] H. C. Kim, P. Giri, and J. R. Lee, "A real-time deflection monitoring system for wind turbine blades using a built-in laser displacement sensor," *The 6th European Workshop on Structural Health Monitoring*, Dresden, Germany, Jul. 3-6, 2012.

[23] Wenxian Yang, R. Court, and J. S. Jiang, "Wind turbine condition monitoring by the approach of SCADA data analysis," *Renewable Energy*, vol. 53, pp. 365-376, 2013.

[24] M. Schlechtingen, I. F. Santos, and S. Achiche, "Wind turbine condition monitoring based on SCADA data using normal behavior models. Part 1: system description," *Applied Soft Computing*, vol. 13, pp. 259–270, 2013.

[25] Y. Wang, D. Infield, "Supervisory control and data acquisition data-based non-linear state estimation technique for wind turbine gearbox condition monitoring," *IET Renewable Power Generation*, vol. 7, pp. 350-358, 2013.

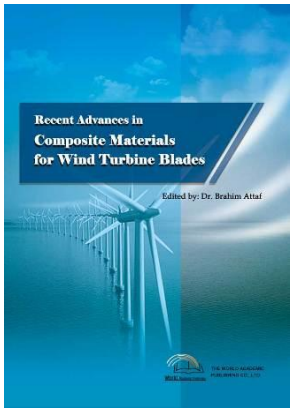

Recent Advances in Composite Materials for Wind Turbine Blades
Edited by Dr. Brahim Attaf

ISBN 978-0-9889190-0-6

Hard cover, 232 pages

Publisher: The World Academic Publishing Co. Ltd.

Published in printed edition: 20, December 2013

Published online: 20, December 2013

This book of science and technology provides an overview of recent research activities on the application of fibre-reinforced composite materials used in wind turbine blades. Great emphasis was given to the work of scientists, researchers and industrialists who are active in the field and to the latest developments achieved in new materials, manufacturing processes,

architectures, aerodynamics, optimum design, testing techniques, etc.. These innovative topics will open up great perspectives for the development of large scale blades for on- and off-shore applications. In addition, the variety of the presented chapters will offer readers access to global studies of research & innovation, technology transfer and dissemination of results and will respond effectively to issues related to improving the energy efficiency strategy for 2020 and the longer term.

How to cite this book chapter

Wenxian Yang (2013). Testing and Condition Monitoring of Composite Wind Turbine Blades, *Recent Advances in Composite Materials for Wind Turbines Blades*, Dr. Brahim Attaf (Ed.), ISBN 978-0-9889190-0-6, WAP-AMSA, Available from: http://www.academicpub.org/amsa/chapterInfo.aspx

World Academic Publishing - Advances in Materials Science and Applications

Chapter 10

Mechanical Characterization of Rigid PUR Foams Used for Wind Turbine Blades Construction

Emanoil Linul[*1], Liviu Marsavina[2]

[1,2]Mechanics and Strength of Materials Department, Politehnica University of Timisoara
1 Mihai Viteazu Avenue, Romania

[*1]linul_emanoil@yahoo.com; [2]lmarsavina@yahoo.com

I. INTRODUCTION

The design and structural reliability of advanced materials like composites and sandwich materials require a better understanding of how the fracture process initiates and progresses to final failure. The sandwich structural concept consists of two (or more) thin, stiff, strong and relatively dense faces sheets which are bonded to a thick and low density core. This structural assembly offers superior specific flexural stiffness and strength. To this end, advanced composite sandwich structures have been widely used in aerospace structures, marine industry, automobiles, wind turbine blades, pipelines, bridge decks, etc. due to their superior structural capacity in carrying transverse loads with minimal weight penalty [1-3].

Most wind turbines have the same basic parts: blades, shafts, gears, generator and a cable (some turbines do not have gearboxes). These components work together to convert the wind energy into electricity. As we know wind turbines capture most of energy depending on the size of their propellers (i.e., blades). So, the blades are the most important critical parts of wind turbine [4]. The thin sheets (glass fiber reinforced composites – GFRP, carbon fiber reinforced composites – CFRP, etc.) which forms the shell of the wind blade, although may be mechanically strong enough to endure the loads but as a whole structure it is not stiff enough and would undergo large deflection under wind loads. In order to obtain a deflection as small as possible and adequate stiffness of composite sandwich structure requires the correct choice of the core material, so the blade can effectively endure the loads. Types of foams that can be suitably used as cores for wind blades structures are as follows: polyvinyl chloride (PVC) foam, polystyrene (PS) foam and polyurethane (PUR) foam [5].

In order to obtain a greater efficiency of energy capture, there has been a dramatic increase in the size and power output of wind turbines during the past 20 – 30 years, from a rated power of 50 kW to multi – megawatt (≈ 5 – 7 MW) power plants of today (see Fig. 1). The wind industry is focused on developing longer blades that take advantage of recent developments in the field of composite technology to increase wind turbine energy output without adding excessive weight or sacrificing essential strength. It is anticipated that wind turbines with a rated power output in the range of 8 – 10 MW and a rotor diameter from 180 – 200 m will be developed and installed within the next 10 – 15 years [4].

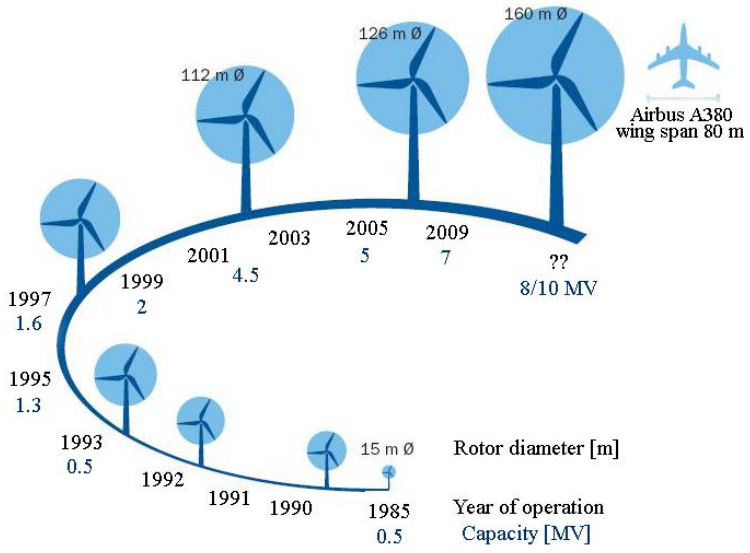

Fig. 1 Size evolution of wind turbine blades

This trend to perform longer blades brings with it a new engineering challenge, notably: creating blades that are both strong and light in weight. While weight increases with the sheer size of the blade, structural modifications necessary to increase the blade strength – to stand up to the added forces generated by rotation of the larger blades – can add even more weight. With the lack of proper attention to weight savings in the design and fabrication of large blades, raw material costs and fabrication cycle times can increase excessively. But heavy blades are also a problem in the field where greater stress concentrations may be developed on wind turbine bearing sets. In addition, most importantly, extra weight imposes a much higher fatigue penalty during wind turbine operation, which shortens the blade lifetime. One approach to reduce the blade mass and the resulting weight is to use more carbon fiber in composite lay-ups, but this can increase material expense considerably. Another potentially more promising route to reducing mass and controlling blade weight are improvements in foam core properties, resin systems and skin/core bonding. Advances achieved in these areas can reduce the blade mass, extend its entire life and lower the fabrication cycle time and the associated cost.

Several studies have been carried out and many analytical/numerical models have been performed in order to investigate the mechanical behavior of the wind turbine blades [6-10]. The aerodynamic properties of a wind turbine airfoil were investigated by Sicot et al. [6], focusing particularly on stall mechanisms. Also, a method to determine the position of the separation point and the value of the chordwise pressure gradient in the separated area has been proposed. They have shown that, for the same angle of attack, the separation point is nearer to the trailing edge when the inflow turbulence level increases (a stall delay). Likewise, the fatigue life for operating more than 20 years was estimated by Kong et al. [7] using (i) the well – known S-N linear damage equation, (ii) the load spectrum and (iii) Spera's empirical formulae. Furthermore, a study with a discussion concerned with an actual collapse testing under the flap – wise loading for a large full – scale composite wind turbine blade was conducted by Yang et al. [8] to assess and evaluate the structural response of the blade during loading and after collapse by correlating experimental results with numerical model predictions. A technique of videometrics was adopted to measure the integral deformation and the local deformation of the wind turbine blade under the flap – wise loading. Another study of prismatic composite I-beams, designed within the UpWind – project to examine the mechanical behavior of adhesive bond lines, were numerically and experimentally investigated by Zarouchas et al. [9]. The results of the simulation were directly compared with the experimental observations coming from Digital Image Correlation Technique (DICT) and conventional techniques (Linear Variable Differential Transformers – LVDT and strain gages). On the other hand, Yang and Sun [4] have undertaken studies on the testing, inspecting and monitoring technologies for wind turbine blades, including mechanical property testing, non – destructive testing/inspecting, full – scale testing, structural health monitoring and condition monitoring. And then, the development trends and some suggestions of testing, inspecting and monitoring technologies for wind turbine blades were fully discussed. In addition, the progressive failure process of composite sandwich wind turbine blades subjected to wind load was studied via both theoretical and experimental approaches by Chen and Kam [10]. In the theoretical study, the wind pressure acting on the wind blade surface was estimated on the basis of an aerodynamic analysis. Whereas, in the experimental investigation, a composite sandwich wind blade was fabricated for the purpose of strength testing.

In this context, a variety of synthetic polymer foams and different wood sorts are used as core materials in the sandwich blade structures. Fig. 2 presents a cross section through a wind turbine blade after Yang et al. [8].

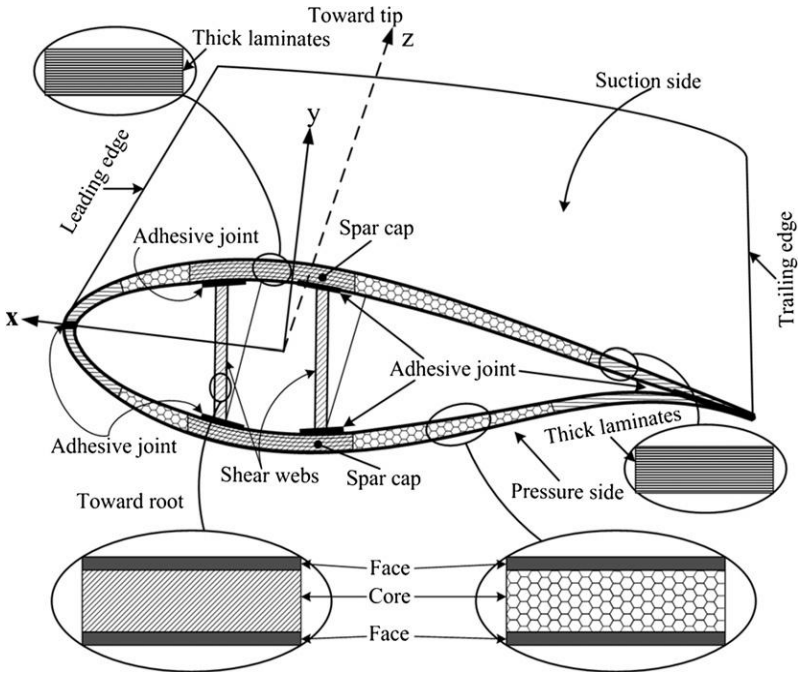

Fig. 2 Cross-section through a wind turbine blade after Yang et al. [8]

Since sandwich structures are manufactured by different methods such as: (i) resin transfer moulding, (ii) compression moulding and (iii) autoclave vacuum bag moulding, two important factors are frequently overlooked [11]: (1) the bonding between the face and core of sandwich structures is assumed to be perfect bonding and (2) in many cases the manufacturing parameters of the sandwich structures are selected as the same as those of the composite faces [12].

Mechanical property testing is usually carried out on coupons and subcomponents with a representative lay – up and a similar processing way to that of the blade in question. Mechanical properties are measured under tensile, compressive and shear loads, or combinations thereof, which mainly include static testing, fatigue testing and modal testing. The purpose of static testing is to verify the capacity of sustaining limit load [4]. The prediction of this type of damage has attracted much interest since such an attainment would increase the confidence on the design of sandwich structures and subsequently expand their field of application. There is a high demand for these materials to withstand both static and dynamic loads without the risk of brittle fracture.

This work aims to provide a better understanding of the failure mechanisms in wind turbine blade with the focus on the core materials (rigid polyurethane foams). In this respect we will make a mechanical characterization of rigid PUR foams under different loading conditions. This characterization of selected cores will be done through static and dynamic tests using different densities, loading speed, temperature and different loading plans according to the core forming plan. This investigation has to be done because as it can be seen from Fig. 3 that faces/core material of a sandwich beam/panel can fail in several ways: (i) it may fail by the yielding or fracture of the faces (as shown in Fig. 3b); (ii) the compression face may "wrinkle" or "dimple" (as shown in Fig. 3c); (iii) the core can fail, usually in shear (as shown in Fig. 3d). However, compression and tensile failures or local crushing can also occur. Further to that, the bond between the face and the core can also fail; and since resin adhesives are usually brittle, debonding may occur by brittle fracture (as shown in Fig. 3e). As a final point, the sandwich can fail by indentation of the faces and core at the loading point [1, 2]. These material properties are critical in the structural performance of the foam core of wind turbine blade.

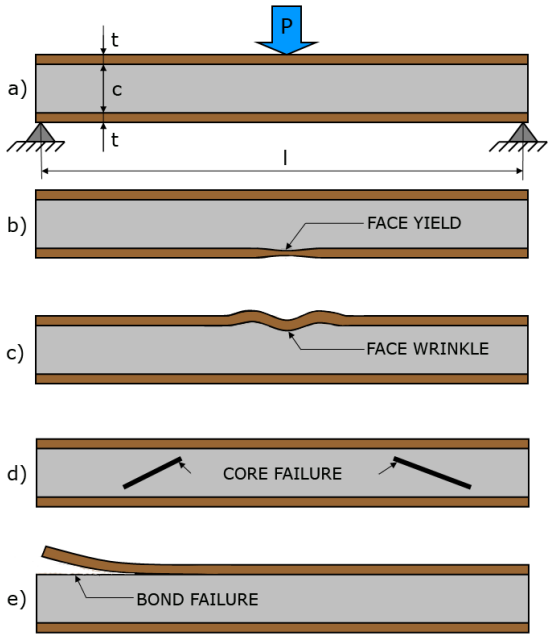

Fig. 3 Failure modes of sandwich beams or panels

The initiation, propagation and interaction of failure modes depend on the type of loading, constituent of material properties and geometrical dimensions. The experimental program was specifically designed according to the aim of the work. Considering the types of loading and types of foam, the following aspects have been analyzed: determination of mechanical characteristics in static and dynamic compression tests and determination of fracture toughness both under static and dynamic regime on notched specimens. Finally, at the end of the section, a microstructural analysis was presented for specimens both before and after deformation.

II. STATIC AND DYNAMIC COMPRESSION TESTS

Research on characterization of cellular materials under compressive loading conditions has been widely reported as in [13–16]. The various properties and attributes investigated include energy absorption, density, cell structure, yield criteria, strain rate, energy efficiency, etc. Avalle at al. [13] have presented an optimization procedure in order to identify the micromechanical parameters from uniaxial compression test of different types of foams. The effect of the density and filler size was also investigated in [14]. Ramsteiner et al. [17] have analyzed the parameters influencing the mechanical properties of foam. The parameters that were identified and studied are the following: the structure of the foam, the matrix material of the

foam, the density of the foam, cell orientation and testing temperature. Linul et al. [18] have presented a comparison, of stress-strain response in compression, between experimental results and micromechanical modeling for PUR foams. The crush behavior of Rohacell structural foam was investigated by Li et al. [19]. Tu et al. [20] presented the plastic deformations of PUR foam under static compressive loading and proposed a theoretical approach to describe the deformation localization.

The mechanical behavior of rigid polyurethane foams under compressive loading is probably the primary property that distinguishes it from non-cellular solids. The use of foams in kinetic energy absorption and structural applications, whereby they are subjected to static and dynamic loading, motivates the need to study their mechanical properties [21].

A. Static Compression Tests of Rigid PUR Foam

This study presents the determination of the main mechanical properties of polyurethane foam in static compression. The influence of density, loading speed effect and forming plane on mechanical properties were investigated. The main parameters studied in compression include: Young's modulus, yield stress, plateau stress and densification strain; defined as follows (see Fig. 4):

- Young's modulus, E [MPa] – the ratio of stress (nominal) to corresponding strain below the proportional limit of a material expressed in force per unit area based on the minimum initial cross-sectional area [22].
- Compressive yield point, σ_y [MPa] – the first point on the stress-strain diagram at which an increase in strain occurs without an increase in stress [22].
- Plateau stress, σ_{pl} [MPa] – constant stress when strain increases [1, 20]. For many types of rigid PU foams, the plateau regime starts from the crush strain, ε_y, or crush stress, σ_y, representing the initiation of the new deformation mechanism of the cell wall or the cell wall failure, and ends at a critical strain, ε_D, representing the onset of densification [19].

The onset strain of densification can be determinates by several methods [19]:

- Method I – The onset strain of densification is defined by the intersection of the tangents to the stress plateau regime and the densification regime [23-25].

- Method II – The onset of densification is defined as the strain at the local minimum before the stress rises steeply [26].

- Method III – The onset strain of densification is defined as the strain at which the slope of the tangent is equal to that of the elastic regime [25].

- Method IV – Li et al. [19], suggest using the energy efficiency expressed by Eq. (1). The onset strain of densification is defined as the strain at which the slope of the curve in a plot of energy efficiency (η) versus strain (ε) is zero, Eq. (2) [27].

$$\eta(\varepsilon) = \frac{1}{\sigma(\varepsilon)} \cdot \int_0^{\varepsilon} \sigma(\varepsilon) \cdot d\varepsilon \tag{1}$$

$$\left. \frac{d\eta(\varepsilon)}{d\varepsilon} \right|_{\varepsilon=\varepsilon_D} = 0 \tag{2}$$

Based on the experimental data the energy efficiency (according to Eq. (1)) is plotted in Fig. 5 for rigid polyurethane foams with densities of 40, 80 and 200 kg/m3, and the onset strain of densification is determined according to Eq. (2).

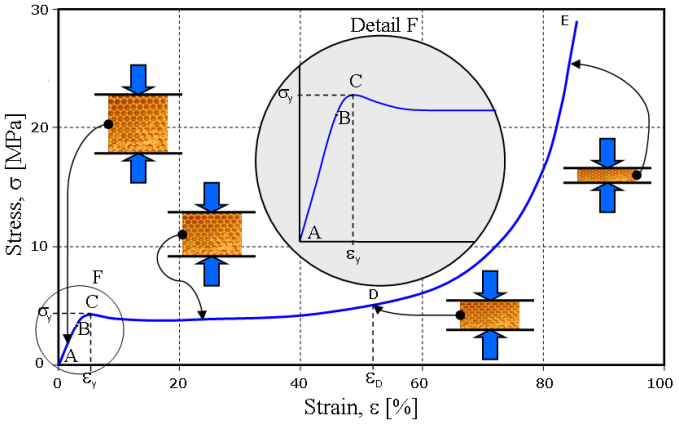

Fig. 4 Typical stress – strain curve for rigid polyurethane foam

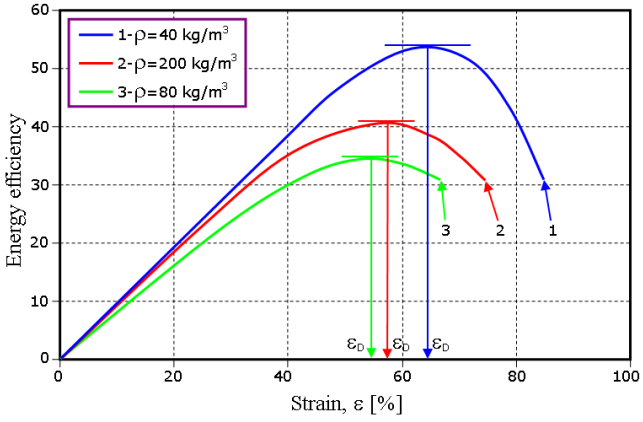

Fig. 5 Energy efficiency-strain curves for three different densities

The specimens used for experimental tests were in the form of cubes [14, 28]. Shapes of used specimens are shown in Fig. 6, in the same figure are presented: comparisons between the initial shapes (before test) and final shapes (after test) of the specimen [18].

Experimental tests were performed on a Walter Bay 10 kN testing machine (Fig. 7a) at room temperature. The samples were subjected to a uniaxial compressive loading at a speed of 2 mm/min, except for samples that are used for determining the effect of loading speed, where 1; 5; 10 and 20 mm/min were used. Figure 7b shows the positioning of the specimen. For each type of test, 5 specimens were used and the tests were performed in accordance with ASTM D1621 – 00 Standard Test Method for Compressive Properties of Rigid Cellular Plastics [22]. Also, it should be pointed out that specimens have to be placed on the centre of the plates.

Fig. 6 Compression specimens used in the experimental program

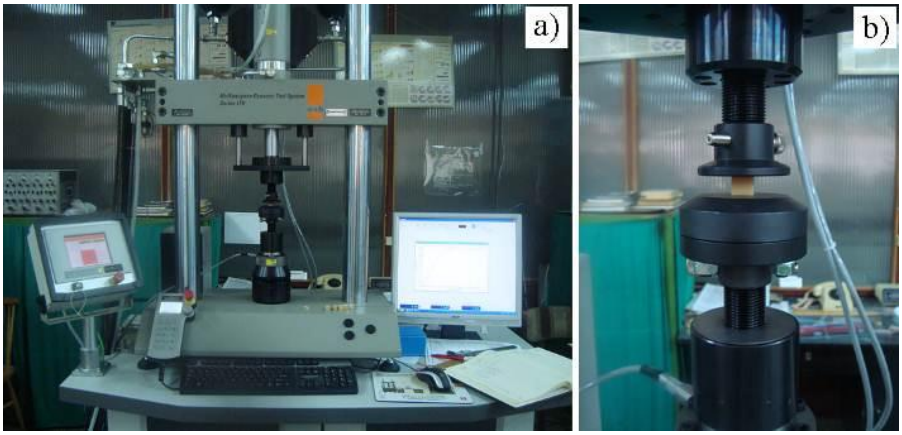

Fig. 7 A Walter Bay 10 kN testing machine

Fig. 8 presents typical stress – strain curves for different densities, showing an increase of mechanical properties with increasing density. Mean values of these properties as a function of density and loading speed are listed in Table 1 and 2.

Figs. 9 and 10 presents the influence of loading speed and effect of loading direction, respectively on compressive behavior of 140 kg/m3 closed – cell PUR foams. For the in – plane loading direction a constant plateau was obtained, while for out – of – plane load the plateau has a linear hardening for the same foam density.

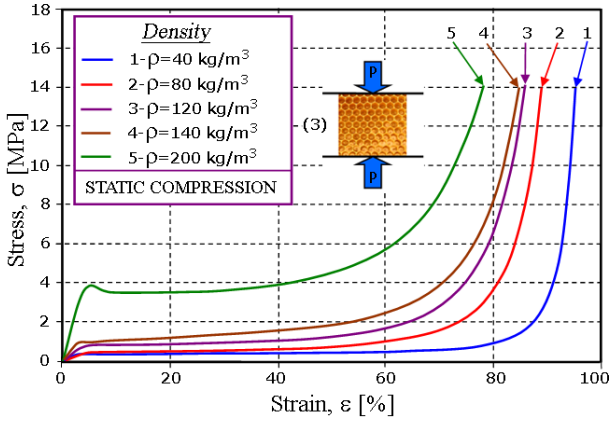

Fig. 8 Typical stress-strain curves in compression. Effect of density

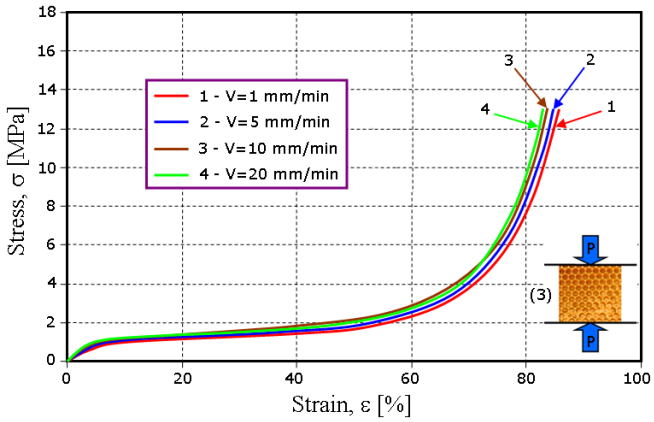

Fig. 9 As Fig. 8 in compression. Effect of loading speed

TABLE 1 MEAN VALUES OF MECHANICAL PROPERTIES FOR STATIC COMPRESSION AS A FUNCTION OF DENSITY

Density [kg/m^3]	Geometrical parameters			Loading direction	Young's Modulus [MPa]	Yield Stress [MPa]	Plateau Stress [MPa]	Densification [%]
	h [mm]	b_1 [mm]	b_2 [mm]					
40	12.78	12.78	12.66	(3)	4.20	0.38	0.39	65.53
80	15.08	14.90	14.84		7.90	0.48	0.51	54.57
120	15.42	15.28	15.22		18.37	0.89	0.93	54.31
140	14.02	12.06	12.04		34.11	1.05	1.21	54.47
200	11.76	11.72	11.72		121.99	4.14	3.86	55.75

TABLE 2 MEAN VALUES OF MECHANICAL PROPERTIES FOR STATIC COMPRESSION AS A FUNCTION OF LOADING SPEED

Density [kg/m^3]	Geometrical parameters			Loading speed [mm/min]	Young's Modulus [MPa]	Yield Stress [MPa]	Plateau Stress [MPa]	Densification [%]
	h [mm]	b_1 [mm]	b_2 [mm]					
140	13.2	13.6	13.6	1	18.94	1.01	1.16	50.71
	13.6	13.6	13.8	5	21.67	1.07	1.22	52.17
	13.2	13.4	13.6	10	22.48	1.17	1.30	50.56
	13.4	13.2	13.6	20	25.57	1.22	1.40	53.87

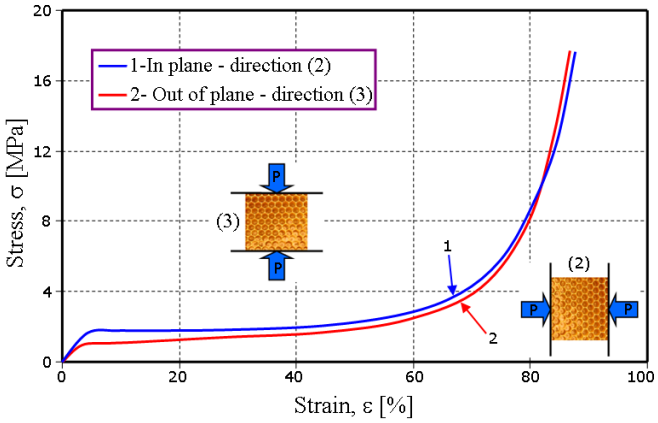

Fig 10 Typical stress-strain curves in compression. Effect of loading direction

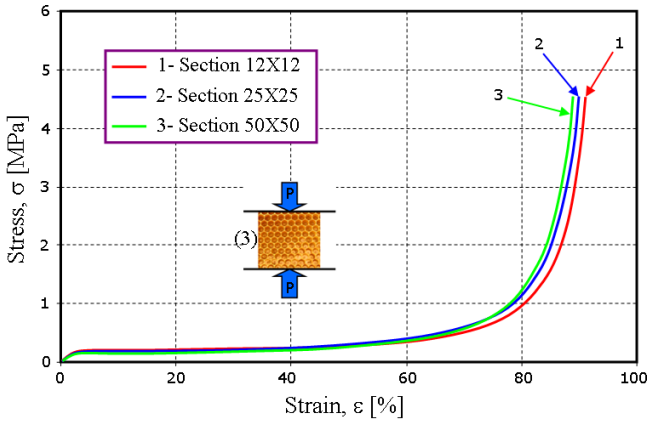

Fig. 11 As Fig. 10 in compression. Effect of cross-section

In Fig. 12 are shown the sampling of the compression specimens extracted from a rectangular SF plate and the two loading directions that were used in the compression tests. In this respect, all tested specimens were cut from the same plate.

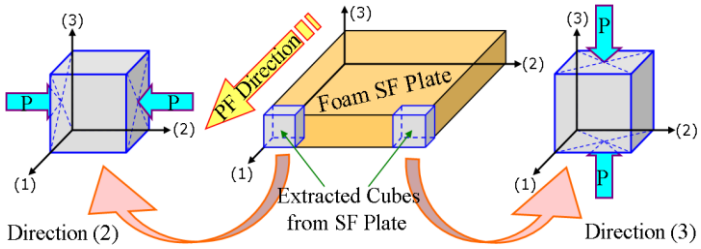

Fig. 12 The sampling of the cube specimens from a rectangular plate

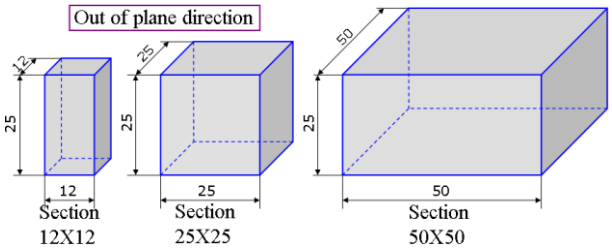

Fig. 13 Shapes used as specimens for cross section study

The shapes and geometrical parameters of specimens for cross section study are shown in Fig. 13; whereas Fig. 11 illustrates typical stress – strain curves. In this case the samples had the same height (h=25 mm), but different values for b_1 and b_2, (12×12, 25×25, 50×50 mm^2, respectively). It is observed from Fig. 11 that the cross – section shows a relatively small influence on the mechanical properties in compression.

As a result of cross – section influence, Table 3 presents the mean values of the mechanical characteristics in static compression for 140 kg/m^3 foam density.

TABLE 3 MEAN VALUES OF MECHANICAL PROPERTIES FOR STATIC COMPRESSION AS A FUNCTION OF CROSS – SECTION

Density [Kg/m^3]	Geometrical parameters			Cross section	Young's Modulus [MPa]	Yield Stress [MPa]	Plateau Stress [MPa]	Densification [%]
	h [mm]	b_1 [mm]	b_2 [mm]					
40	25.0	12.2	12.2	12X12	4.91	0.23	0.24	53.82
	25.2	25.2	25.4	25X25	5.17	0.20	0.21	53.68
	24.8	49.8	50.0	50X50	5.32	0.16	0.18	53.63

B. Dynamic Compression Tests of Rigid PUR Foam

For the characterization of mechanical behavior on dynamic compression loading, rigid PUR foams used in the experimental program correspond to the static compression tests. The specimens used in this case are identical to those used for static compression tests and are shown in Fig. 6. The specimens were subjected to uniaxial dynamic compression with loading speed ranging from 0.62 – 6 m/s, using different temperature scales (i.e., 20, 60 and 100 ℃).

Experimental tests were made in the Strength of Materials Laboratory at Lublin University of Technology, Poland. Tests were carried on a 40 kN Instron – Dynatup impact testing machine as shown in Fig. 14.

Fig. 14 A Instron – Dynatup 40 kN impact testing machine

Mechanical behavior of rigid foams under compression tests was determined in accordance with the ASTM D1621 – 00, Standard Test Method for Compressive Properties of Rigid Cellular Plastics [22].

The following subsection will study in detail the influence of density, loading speed, material orientation and temperature on the mechanical properties of rigid PUR foams that are subjected to dynamic compression loads. Parameters such as Young's modulus, yield stress, plateau stress and densification have a very important role in the real applications of these materials and for this reason the foam behavior will be presented under different loading and temperature conditions.

1) Influence of density

From the data provided by the test machine, the conventional characteristic curves for the tested specimens were plotted. Fig. 15 shows a comparison of typical stress – strain curves for the four densities of rigid PUR foams (i.e., 40; 80; 120 and 140 kg/m^3) that are subjected to dynamic compression. Presented curves are obtained from out – of – plane loading direction at room temperature. Variations of Young's modulus with density for out-of-plane loading direction (direction (3)) are presented in Fig. 16.

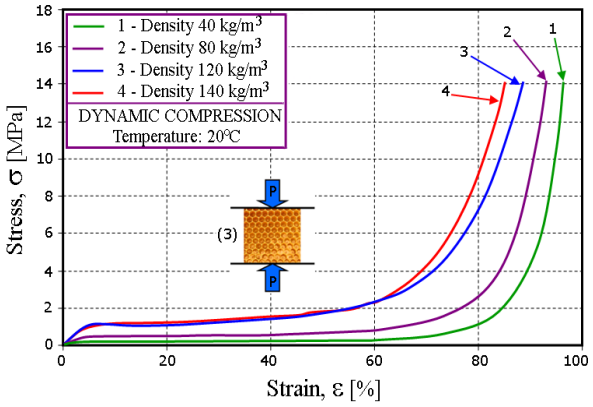

Fig. 15 Typical stress-strain curves. Effect of density

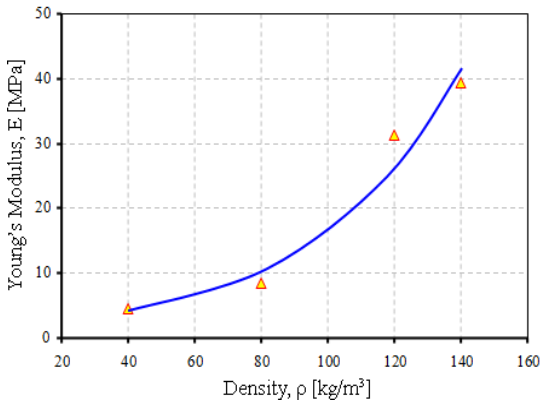

Fig. 16 Young's modulus variation with density. Effect of density

From the recorded stress – strain diagrams, the following regions can be identified: the first part of the curve shows a linear – elastic behavior up to material yield point (up to a strain of 5% approximately), a small softening in stress after yield, a plateau after yield (between 10 – 50%) and in the end there is an increase in stress without a significant increase in strain, commonly known as densification (above 50% strain).

Both Figs. 15 and 16 show a significant increase of mechanical properties (Young's modulus, yield stress and plateau stress) with increasing of density. This means that the density has a major role in determining the mechanical properties in compression. On the other hand, it was found that only densification decreases with increasing of foams density from a value of about 67% to a value of about 57%.

Mean values of mechanical properties for both in-plane (direction (2)) and out-of-plane loading direction (direction (3)), respectively are presented in Table 4 and Table 5.

TABLE 4 MEAN VALUES OF MECHANICAL PROPERTIES ON DYNAMIC COMPRESSION FOR DIRECTION (2)

Density [kg/m^3]	Loading Speed [m/s]	Young's Modulus [MPa]	Yield Stress [MPa]	Plateau Stress [MPa]	Densification [%]
40	0.62	3.89	0.39	0.39	66.02
	0.78	4.12	0.37	0.37	62.86
	0.94	4.50	0.37	0.38	64.89
80	0.78	5.37	0.49	0.48	59.71
	1.09	6.40	0.42	0.42	53.98
	1.28	5.98	0.42	0.43	58.93
120	1.28	33.90	1.53	1.48	58.80
	1.67	31.30	1.72	1.47	54.13
	1.98	32.16	1.73	1.60	57.34
140	0.94	33.10	1.72	1.62	56.88
	1.28	39.43	1.83	1.71	57.60
	1.67	33.47	1.84	1.55	57.12

TABLE 5 MEAN VALUES OF MECHANICAL PROPERTIES ON DYNAMIC COMPRESSION FOR DIRECTION (3)

Density [kg/m^3]	Loading Speed [m/s]	Young's Modulus [MPa]	Yield Stress [MPa]	Plateau Stress [MPa]	Densification [%]
40	0.62	4.49	0.39	0.39	66.77
	0.78	4.04	0.38	0.38	66.07
	0.94	4.49	0.37	0.37	65.13
80	0.78	7.74	0.54	0.54	62.97
	1.09	8.41	0.55	0.53	57.05
	1.28	8.42	0.47	0.49	55.02
120	1.28	24.57	1.17	1.15	59.79
	1.67	26.98	1.12	1.07	57.29
	1.98	26.89	1.10	1.15	58.09
140	0.94	22.37	0.98	1.04	56.98
	1.28	24.82	1.10	1.20	56.91
	1.67	25.62	1.05	1.01	52.89

2) Influence of loading speed

Considering the wide range of applications of cellular materials, it is very important to know how these materials behave in different dynamic loads that can be applied at different speeds. Thus, another important parameter is studied in this chapter, it concerns the influence of loading speed on the mechanical behavior of rigid foams. Fig. 17 shows the influence of the mentioned parameter on the compressive behavior of three different densities 80, 93 and 200 kg/m^3. The specimens were subjected to uniaxial dynamic compression with loading speed within the range of 0.62 – 6 m/s at room temperature of (20 ℃). Figure 18 shows the variation of Young's modulus with loading speed for two different densities (93 and 200 kg/m^3).

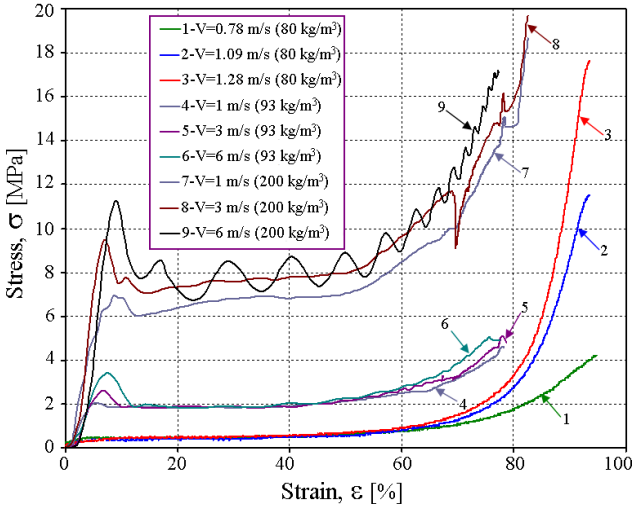

Fig. 17 Stress-strain curves. Effect of loading speed

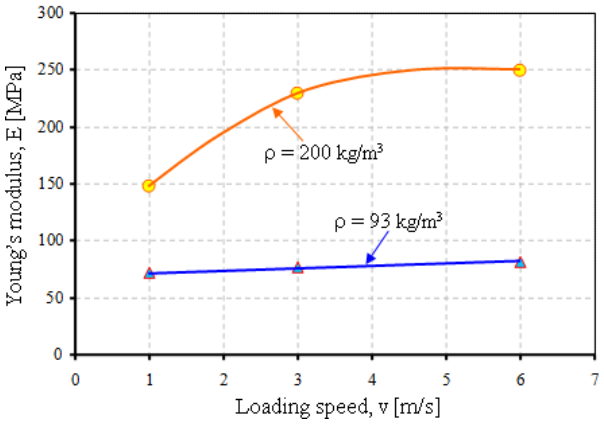

Fig. 18 Young's modulus variation with density. Effect of loading speed

From Figs. 17 and 18 it can easily be seen that the loading speed has a little influence on the mechanical properties in dynamic compression for low density PUR foams (80 and 93 kg/m^3), while for foam with high density (200 kg/m^3), loading speed has a major influence. Also, it can be observed that the biggest influence is obtained for linear-elastic region, yield stress and densification region, while plateau region almost coincide. The yield stress difference between the highest and lowest loading speed is about 1.8 times.

3) Influence of temperature

Considering sudden temperature changes (from one region/country to another) is very important to carrying out a study of the influence of temperature on mechanical behavior of core wind turbine blade. This study was performed for four different rigid PUR foams at three different temperatures: 20, 60 and 100°C and two loading directions (in – plane and out – of – plane). Table 6 recapitulates the mean values of the mechanical characteristics on dynamic compression behavior depending on temperature for the two loading directions.

TABLE 6 MECHANICAL PROPERTIES DEPENDING ON TEMPERATURE

Denity [kg/m^3]	Loading direction	Temperature [℃]	Young Modulus [MPa]	Yield Stress [MPa]	Plateau Stress [MPa]	Densification [%]
40	(2)	60	4.46	0.37	0.37	65.35
		100	21.52	0.24	0.20	62.02
	(3)	60	4.04	0.37	0.37	64.40
		100	16.62	0.39	0.31	64.41
80	(2)	60	8.80	0.50	0.48	54.16
		100	46.50	0.58	0.44	52.10
	(3)	60	55.40	0.62	0.57	53.59
		100	64.72	0.51	0.40	53.51
120	(2)	60	69.80	1.93	1.57	59.09
		100	120.74	1.66	1.30	56.20
	(3)	60	80.48	1.46	1.33	59.43
		100	63.57	1.18	1.10	56.26
140	(2)	60	40.62	1.94	1.71	55.73
		100	50.73	0.78	0.72	56.18
	(3)	60	52.66	1.35	1.35	53.69
		100	12.99	0.58	0.67	54.21

For this purpose and for easier understanding of the behavior, Fig. 19 shows the effect of temperature on the stress-strain curves only for 140 kg/m^3 foam density at 1.67 m/s loading speed; the load has been applied in – plane.

According to the results shown in Fig. 19, it can be seen that at room temperature (20 ℃) and a temperature of 60 ℃, the foam behavior is approximately the same for both cases, while at higher temperatures (100 ℃), the foam behaves differently and changes in its properties are discerned. It should be noted that, for polyurethane foams, the temperature of 100 ℃ is considered to be high because their melting temperature is around 150 ℃.

1) Influence of forming plane

Foam anisotropy is a very important parameter and this should be considered in both practical applications and modeling of the mechanical properties. Thus, choosing the properly of this parameter, we can obtain the desired characteristics for practical applications. Fig. 20 presents the influence of forming plane and loading direction on dynamic compression. In this case, a foam with a density of 140 kg/m^3 at room temperature (20 ℃) and a loading speed v=1.67 m/s was investigated.

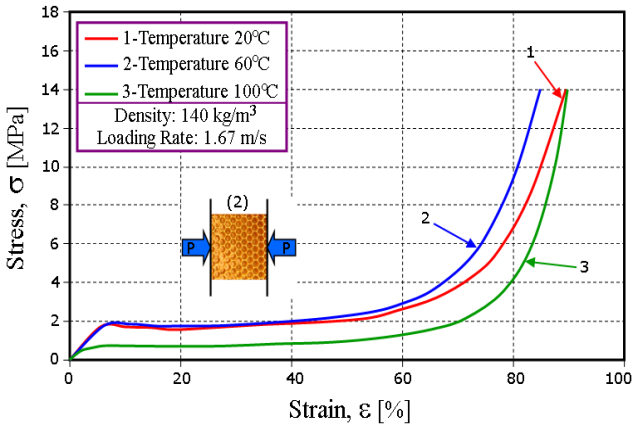

Fig. 19 Stress-strain curves. Effect of temperature

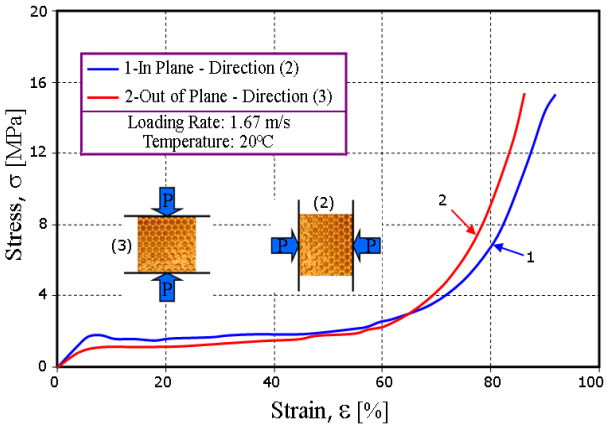

Fig. 20 Stress-strain curves. Effect of forming plane

Loading direction has a significant contribution to the compressive mechanical properties; this aspect highlights the anisotropic behavior of foam. Anisotropy aspect is particularly strong for high – density foam (140 kg/m^3), while in the case of low – density foam (40 kg/m^3) is poor and almost unobservable. In the case of 140 kg/m^3, the material is highly anisotropic, much higher in – plane than out – of – plane, for which the Young's modulus increases from 24.82 MPa to 39.43 MPa, the yield stress increases from 1.10 MPa to 1.83 MPa and the plateau stress increases from 1.20 MPa to 1.71 MPa, while the densification remains the same (approximately 57%) – see Table 4 and 5.

C. Comparison between Static and Dynamic Parameters in Compression

Fig. 21 presents a comparison between stress – strain curves for compressive tests, both in static and dynamic regime. The tests were carried out for several densities, and in Fig. 21 are shown only the results for 140 kg/m^3 density in two loading planes (in – plane and out – of – plane). In this case, the temperature used was 20 ℃ and the loading speed was 2 mm/min ($3.3 \cdot 10^{-5}$ m/s) in static conditions and 1.67 m/s under dynamic conditions.

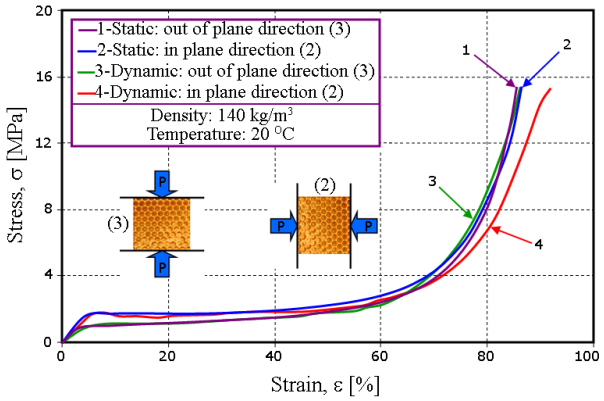

Fig. 21 Stress – strain curves showing a comparison between static and dynamic behavior

As it can be seen from Fig. 21, the behavior under static and dynamic regime of rigid polyurethane foams is almost identical for the applied conditions; the major difference is only between forming planes. According to the results presented in Tables 1, 4, 5 and Figs. 22-25 Young's modulus, yield stress, plateau stress and densification are seen to be dependent on the density. In addition, these diagrams show a comparison between static and dynamic parameters at room temperature [18, 29].

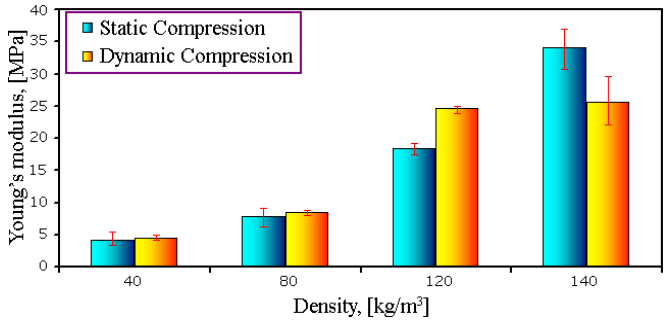

Fig. 22 Young's modulus results versus density. Static – dynamic comparison

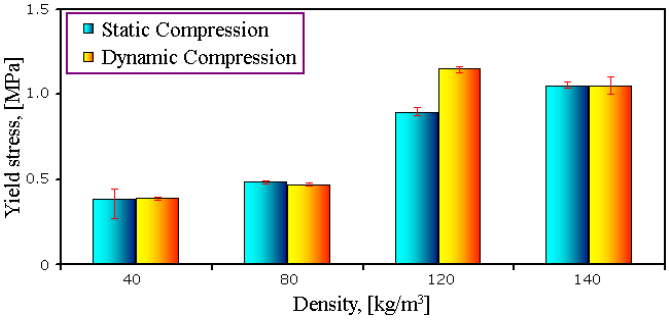

Fig. 23 Yield stress results versus density. Static – dynamic comparison

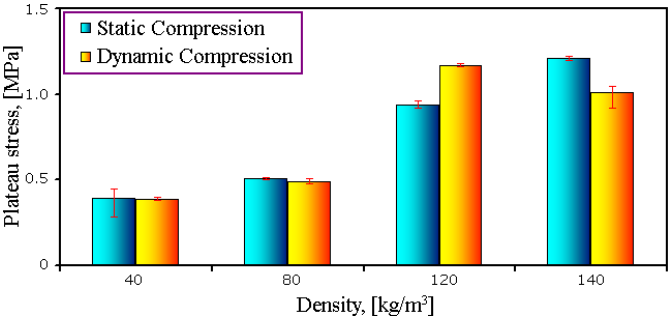

Fig. 24 Plateau stress results versus density. Static – dynamic comparison

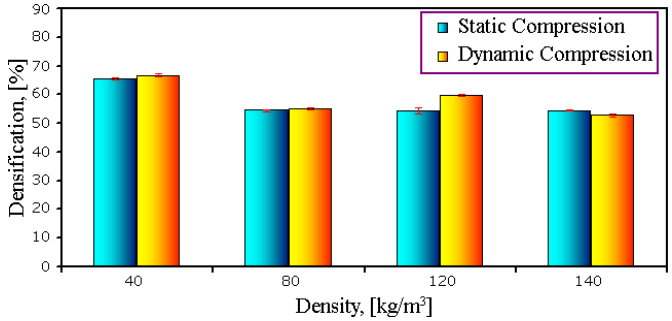

Fig. 25 Densification results versus density. Static – dynamic comparison

III. FRACTURE TOUGHNESS TESTS

Many efforts have been made in recent years to determine the fracture toughness of such foams under static and dynamic loading conditions [30-37]. McIntyre and Anderson [31], have measured the K_{IC} for different densities, using single edge notch specimen, made of rigid closed – cell PU foams for different densities. They found that the fracture toughness is independent of crack length and deduced a linear correlation of K_{IC} with density for foams with densities less than 200 kg/m^3. At higher densities the correlation becomes non – linear. Linear relationship between K_{IC} and density (90-235 kg/m^3), was also obtained by Danielsson [32] for PVC Divinicel HD using three point bending test specimen. Burman [33] presented fracture toughness results for two commercial foams Rohacell WF51 (density 52 kg/m^3) and Dyvinicell H100 (density 100 kg/m^3) using SENB specimens. Vianna and Carlsson [34] presented results of fracture toughness for PVC foams of different densities (36, 80, 100, 200 AND 400 kg/m^3). Kabir and Sasha [35] using 3PB tests have determined fracture toughness for polyvinyl chloride (PVC) and polyurethane (PU) foams. Also, fracture toughness was investigated by Marsavina and Linul [36], and Linul et al. [37] for three different densities of rigid polyurethane (PUR) foams (40, 140 and 200 kg/m^3).

In order to verify that a valid K_{IC} has been determined, it is necessary to first calculate a conditional result, K_Q, which involves a construction on the test record, and then determine whether this result is consistent with the size of the specimen. Fig. 26 presents the force – displacement curve, where the critical load P_Q can be determined.

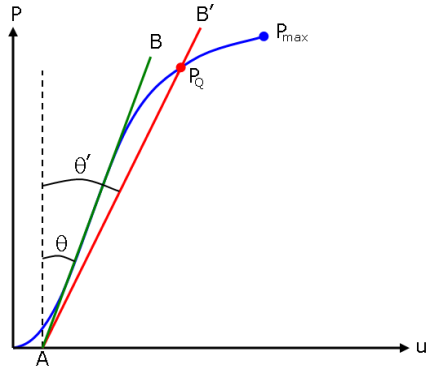

Fig. 26 Force – displacement curve for determining the critical load P_Q

The procedure to determine the critical load is as follows: (i) draw a best straight line (AB) to determine the initial compliance, C ($C=\tan\theta$; $1.05C=\tan\theta'$). C is given by the reciprocal of the slope of line (AB); (ii) draw a second line (AB') with a compliance of 5 % greater than that of line (AB). If the maximum load that the specimen was able to sustain, P_{max}, falls within lines (AB) and (AB'), use P_{max} to calculate K_Q. If P_{max} falls outside line (AB) and line (AB'), then use the intersection of line (AB') and the load curve as P_Q. Furthermore, if $P_{max}/P_Q < 1.1$, use P_Q in the calculation of K_Q. However, if $P_{max}/P_Q > 1.1$, the test is invalid [38].

For a specimen that meets the condition $L/W=4$, K_Q can be determined by the following relation:

$$K_Q = \left(\frac{P_Q}{BW^{1/2}}\right) f\left(\frac{a}{W}\right), \text{ with: } 0 < \frac{a}{W} < 1 \tag{3}$$

where f(a/W) is a non – dimensional function, given by:

$$f\left(\frac{a}{W}\right) = 6\sqrt{\frac{a}{W}}\,\frac{\left[1.99 - \frac{a}{W}\left(1-\frac{a}{W}\right)\left(2.15 - 3.93\frac{a}{W} + 2.7\left(\frac{a}{W}\right)^2\right)\right]}{\left(1+2\frac{a}{W}\right)\left(1-\frac{a}{W}\right)^{3/2}} \tag{4}$$

Where, P_Q is the force acting on the specimen; B is the specimen thickness; W is the specimen height; A is the crack length and S is the span length.

In order to validate the result obtained according to these test methods, the following size criteria must be satisfied:

$$a, B, (W - a) \geq 2.5\left(\frac{K_Q}{\sigma_{ys}}\right)^2 \tag{5}$$

where, σ_{ys} is the yield stress of the material for the temperature and loading speed of the test.

If condition (5) is satisfied, the critical stress intensity factor, K_{IC}, is considered to be equal to the calculated stress intensity factor, K_Q, so:

$$K_{IC} = K_Q \tag{6}$$

A. Static Fracture Toughness Tests of Rigid PUR Foam

Experimental tests for determining the static fracture toughness were made in the Strenght of Materials Laboratory, Faculty of Mechanical Engineering from Timisoara using a tension – compression Zwick/Roell 005 testing machine of 5 kN, (Fig. 27). Tests were performed at room temperature, 20±2 ℃, using specimens with the shape and dimensions shown in Fig. 28. For determining the fracture toughness of materials under investigation, notched specimens loaded in three – point bending were experienced. In the experimental program, rigid PU foams with 40 and 140 kg/m^3 were used. Fig. 29 presents the shape of the specimens tested. Both specimens and notches were cut from the same rectangular plate with a blade thickness of 0.6 mm.

Fig. 27 The 5 kN Zwick Roell 005 testing machine used for 3PB tests

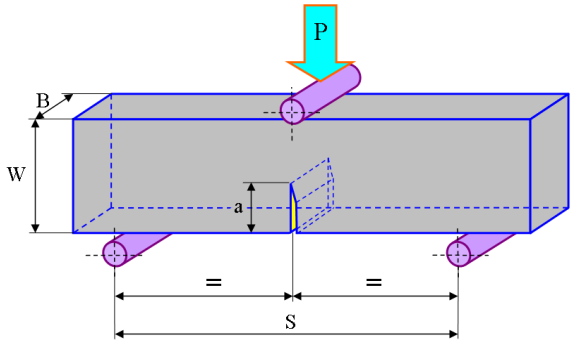

Fig. 28 Shape and dimensions of specimens used in the 3PB tests

Fig. 29 Specimens used in the three – point bending tests

The specimens were subjected to static three – point bending (3PB). The loading speed was 2 mm/min for determining the influence of loading direction, and a speed of 2, 20, 200 and 400 mm/min for determining the influence of loading speed. For each type of test, 5 specimens were used, and the tests were performed according to ASTM D 5045 – 99 (*Standard Test Methods for Plane – Strain Fracture Toughness and Strain Energy Release Rate of Plastic Materials*) [38] and in fact, it was taken into account that the load must act exactly on the notch direction.

1) Influence of loading speed

According to the influence of loading speed, the mean values of the fracture toughness obtained from the experimental tests for rigid polyurethane foam with 140 kg/m^3 density are listed in Table 7.

TABLE 7 MEAN VALUE OF THE MECHANICAL CHARACTERISTICS FOR ANALYSED FOAMS AFTER 3PB TESTS

Density [Kg/m^3]	Samples dimensions				Loading speed [mm/min]	Critical load [N]	Fracture toughness [MPa m$^{0.5}$]	$2.5\left(\frac{K_Q}{\sigma_{ys}}\right)^2$
	Width [mm]	High [mm]	Span length [mm]	Crack length [mm]				
140	13.9	24.9	100	12.5	2	34.70	0.156	7.9
	13.1	25.0			20	30.64	0.149	6.9
	14.6	25.1			200	28.50	0.137	4.7
	12.8	24.9			400	25.06	0.130	4.9

Fig. 30 presents the load – displacement curves for the studied foam and Fig. 31 shows the variation of fracture toughness versus loading speed.

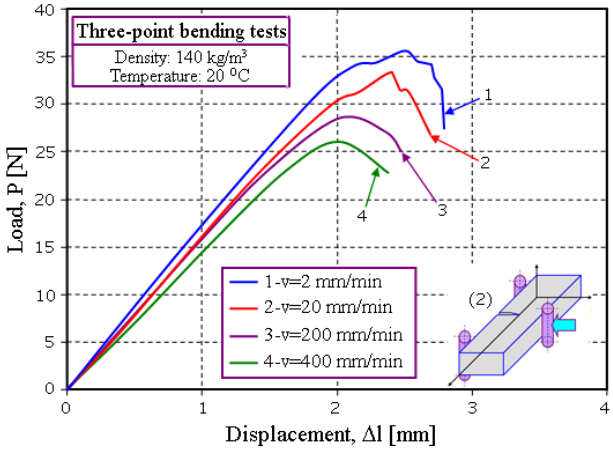

Fig. 30 Load-displacement curves for effect of loading speed

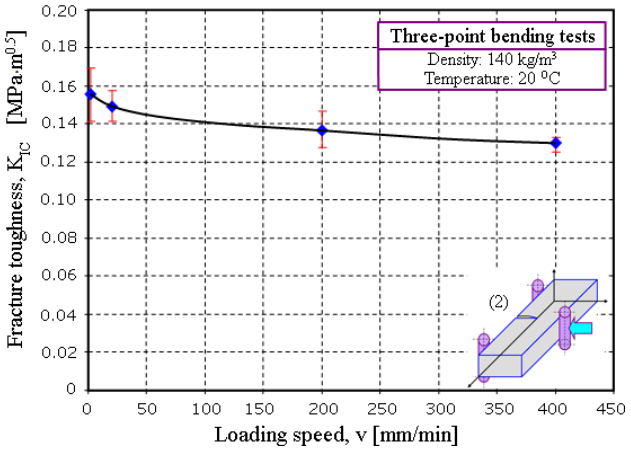

Fig. 31 Variation of fracture toughness versus loading speed

2) Influence of loading direction

The fracture toughness of anisotropic foams depends on the direction in which the crack propagates. This is the best defined with two subscripts, the first indicating the normal to the crack plane, the second the direction of crack propagation [1]. Fig. 32 is shows the sampling of the 3PB specimens extracted from a rectangular SF plate, and Fig. 33 shows the influence of loading direction on the mechanical characteristics at 3PB.

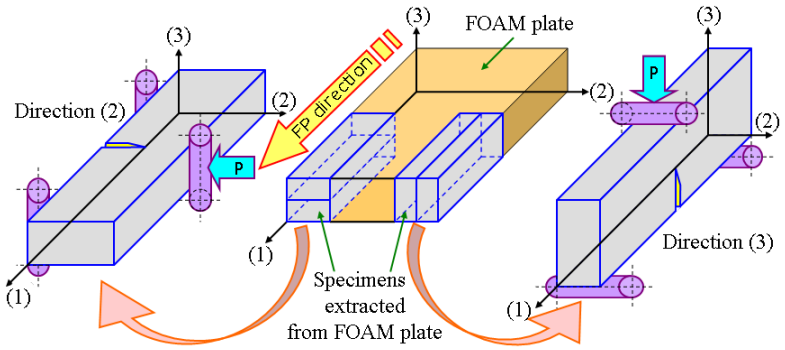

Fig. 32 The sampling of the 3PB specimens extracted from a rectangular SF plate

Loading direction emphasizes anisotropic behavior of the foam. The obtained mean values of fracture toughness are listed in Table 8. For all tested specimens, plane strain condition (3) was fulfilled and it can be observed from Table 8 that the variation of fracture toughness with load direction is insignificant (for this type of foam). It should be noted that brittle fracture was observed for all tested specimens. The linear – elastic behavior was confirmed during the tests when no cushioning occurs and no plastic deformations remain after the test [13].

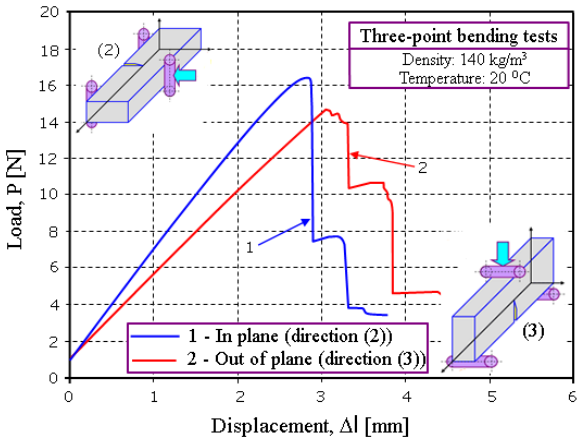

Fig. 33 Load-displacement curves for 3PB tests. Effect of loading direction

TABLE 8 MEAN VALUES OF FRACTURE TOUGHNESS VERSUS LOADING DIRECTION

Density [Kg/m^3]	Samples dimensions				Loading direction	Critical load [N]	Fracture toughness [MPa m$^{0.5}$]	$2.5\left(\frac{K_Q}{\sigma_{ys}}\right)^2$
	Width [mm]	High [mm]	Span length [mm]	Crack length [mm]				
40	25.5	49.4	180	25.0	(2)	16.4	0.0279	20.1
	25.1	50.2			(3)	14.2	0.0276	15.1

3) Size effect

Of particular interest is the fracture toughness of such foams because foam cracking weakens the structure's capacity for carrying load and absorbing energy [39]. In such case, the failure of the foam may be brittle, as revealed most clearly by the notched specimen tests of Zenkert [40] and Zenkert and Bäcklund [41], (and partly also suggested by holed panel tests of Olurin et al. [42] and Fleck et al. [43]). The brittle failure must generally be expected to exhibit a pronounced size effect [44, 45]. A size effect was revealed already in 1989 by Zenkert and Bäcklund's tests of notched foam beams. However, the size effect is important for extrapolating laboratory test data to very large structure. One of the most conclusive analytical descriptions of the size effect is presented by Zdenek et al. [46]. They presented simple formulae which would be easily usable in design and which could be exploited for conventional identification of material fracture properties from the measured size effect on the load capacities of notched foam specimens. They explored whether the energetic size effect law for quasi – brittle structures with large cracks, proposed by Bažant [47], extended by Bažant and Kazemi [48] and verified for concrete rocks, sea ice, ceramics, fiber composites and other quasi-brittle materials [44, 45], can be applied to rigid polyurethane foam and used for material parameter identification.

In this subsection the size effect was carried out on samples of polyurethane foam with a density of 40 kg/m3, with closed cells which are widely used as cores in sandwich panels. The static three point tests were performed in Laboratory from the Faculty of Building and Architecture at Lublin University of Technology. A 2 kN MTS static testing machine was used for bending tests, as shown in Fig. 34. In Fig. 35 are presented the sizes of specimens used in the experimental program. High dimensions samples were cut with a blade, and small dimensions samples were performed using a Secotom 10 cutting machine. All the specimens were cut from the same plate and had the same thickness B = 20 mm.

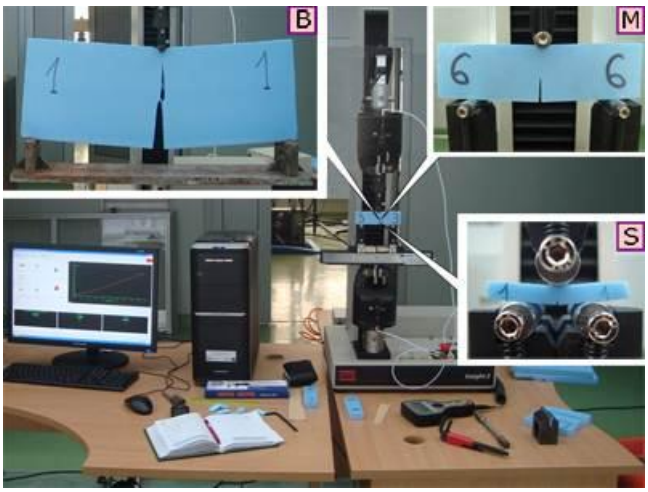

Fig. 34 A 2 kN MTS testing machine – seze effect

Fig. 35 Size effect samples

To determine the size effect of Mode I fracture toughness, specimens geometrically similar in two dimensions with length-to-width ratio 5:2 were selected. Their widths were W = 5.33; 36.89 and 256 mm, with a variation of span length S=13.33; 92.22 and 640 mm. Also, the notches having a length of 0.4W were cut with the two devices. Fig. 36 shown typical load – displacement curves obtained for different size specimens during the 3PB test. In this case, all the specimens have the same width B (20 mm), with different value of high, W, span length, S and crack length, a.

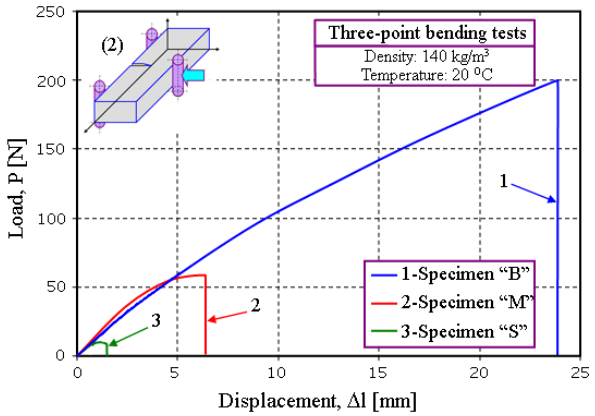

Fig. 36 Load – displacement curves. Size effect

In Table 9 are listed the main values of fracture toughness for foam with 40 kg/m^3 density, obtained from size effect tests.

TABLE 9 FRACTURE TOUGHNESS AND NOMINAL STRENGTH VALUES OBTAINED FROM THE SIZE EFFECT TESTS

Specimen Type	Density ρ [kg/m^3]	Specimen Dimensions				Loading Direction	Critical Load P [N]	Fracture Toughness K_{IC} [MPa m$^{0.5}$]	Nominal Strength σ_N [MPa]
		Width B [mm]	High W[mm]	Span Length S [mm]	Crack Length a [mm]				
"S"	40	20	5.33	13.33	2.13	(2)	8.71	0.047	0.323
							8.78	0.048	0.366
							9.12	0.049	0.345
							8.70	0.047	0.378
							8.64	0.047	0.362
"M"			36.89	92.22	14.76		43.54	0.090	0.221
							40.02	0.083	0.203
							43.60	0.090	0.221
							46.35	0.096	0.235
							50.85	0.105	0.258
"B"			256.00	640.00	102.40		217.11	0.170	0.091
							200.16	0.157	0.086
							212.51	0.166	0.090
							205.12	0.161	0.087
							215.95	0.169	0.091

Fig. 37 presents the variation of fracture toughness with crack length, a. It can be observed that the size effect has an influence on fracture toughness, which increases with increasing crack length.

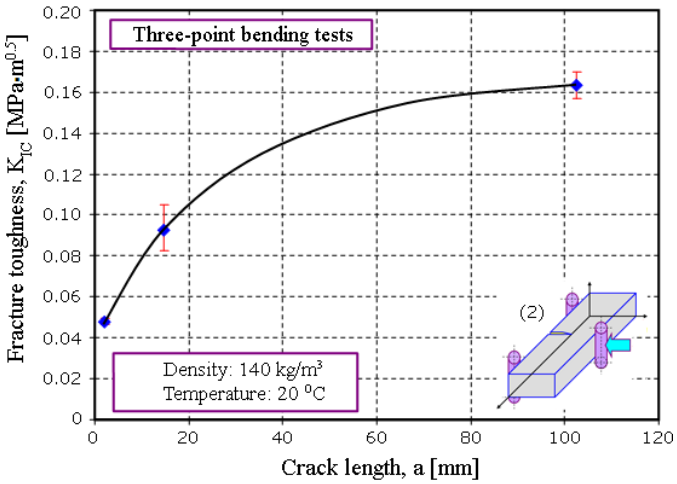

Fig. 37 Variation of K_{IC} with crack length

The size effect is defined as the dependence of the nominal strength, $\sigma_N = 3P_{max}S/(2BW^2)$, as a function of the characteristic specimen size W (here taken as the specimen width). Thus, the nominal strength is a parameter of the maximum load, having the dimension of stress. The size effect is best highlighted in a plot of Log (σ_N) versus log (W), presented in Fig. 38. If the failure of the foam obeyed linear elastic fracture mechanics (LEFM), the logarithmic size effect plot would have to be a straight line with the slope equal to –1/2 [46], shown by a dotted line in Fig. 38. A ductile behavior following the strength of material with no size effect would be a horizontal line $\sigma_N = \sigma_f$, where σ_f is the failure or plastic stress. The obtained experimental results are asymptotic to these approaches and they have the following form:

$$\sigma_N \propto \sigma_f (1+W/Wo)^{-1/2} \tag{6}$$

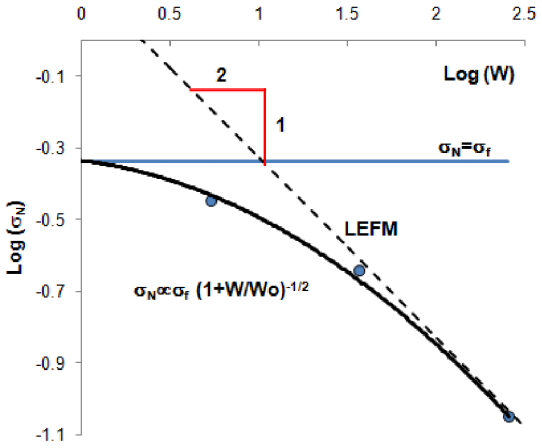

Fig. 38 Results of size effect tests of nominal strength of geometrically similar prismatic foam specimens with similar one-sided notch subjected to 3PB tests

Where, Wo represents the transitional size, which can be obtained by the intersection point of LEFM asymptote and the strength of materials horizontal line. For the investigated polyurethane foam $Wo \approx 10$ mm. This value was obtained using a failure stress $\sigma_f = 0.46$ MPa, determined experimentally on tensile tests.

For $Wo > 10$ mm the foam behavior is brittle, and the results are very close to the asymptotic line from LEFM approach, which means that, on the scale of the tests and of course on larger scales corresponding to structures, the material behaves in an almost brittle manner. For small specimens, a slight deviation occurs and the scaling should be done according with strength of plasticity approaches. Bazant [45] introduces also the brittleness number $\beta = W/Wo$ which allow to distinguish a brittle material $\beta \to \infty$ to a ductile (non – brittle) material $\beta \to 0$.

B. Dynamic Fracture Toughness Tests of Rigid PUR Foam

The principle of impact and instrumented impact tests of plastic materials are given in EN ISO 179 – 2:2000 [49] and Katthoff [50]. A KB Pruftechnik pendulum (Germany) was used for the instrumented impact tests (Fig. 39) with the following main characteristics: pendulum mass 2.04 kg, pendulum length 0.386 m, drop height 0.742 m, drop angle 157.32 º, pendulum energy 7.5 J, impact velocity 3.815 m/s. A four – channel data acquisition A/D card (AdLink NuDAQ PCI – 9812) was used for recording the load in time, and then the load – displacement curve was determined. A check for energy loses due to friction was performed prior to testing and it was found that the frictional loss was 0.059 J which represents 0.4% of the nominal energy of the pendulum 14.847 J. This fulfils the standard [49] condition that the energy loss due to friction should be less than 1%. Tests were performed at room temperature.

Fig. 39 Impact pendulum

Fig. 40 Specimens for impact tests

Three-point bending rigid polyurethane foam (40, 80, 120 and 140 kg/m^3 density) notched specimens shown in Fig. 40 were experimentally tested. Fig. 41 presents load – displacement curves for the above mentioned densities.

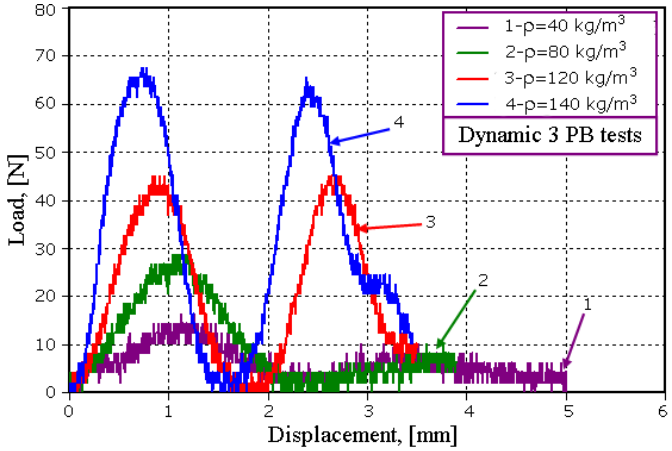

Fig. 41 Typical load- displacement curve from instrumented impact tests.

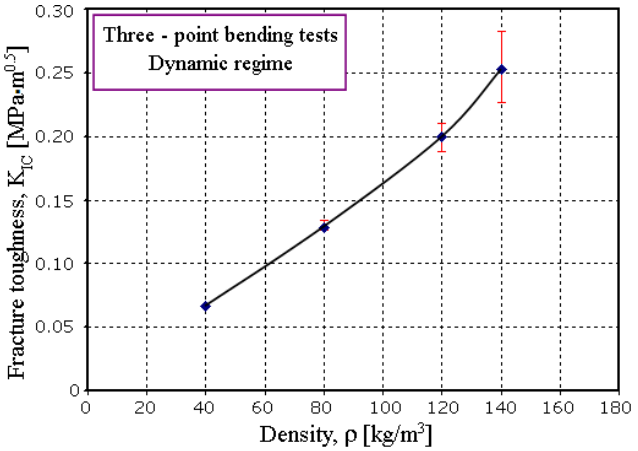

Fig. 42 Fracture toughness variation versus density

The dynamic fracture toughness was determined following the same procedure as in the case of static tests using relations (1) and (2). The mean values obtained in this case are presented in Table 10. These results were obtained in – plane loading direction – the direction (2) – at room temperature.

TABLE 10 MEAN VALUES OF DYNAMIC FRACTURE TOUGHNESS DEPENDING ON FOAM DENSITY

Density [kg/m^3]	Geometrical parameters				Critical load [N]	Fracture toughness [MPa m$^{0.5}$]	Energy [J]
	Width [mm]	High [mm]	Span length [mm]	Crack length [mm]			
40	13.48	25.39	100	12	14.360	0.066	0.084
80	13.91	25.54			29.120	0.129	0.110
120	13.04	25.00			40.606	0.200	0.140
140	13.02	25.70			54.600	0.253	0.196

According to the results presented in Table 10, Fig. 42 shows the fracture toughness variation depending on density. From this figure it can be seen that with increasing of density a significant increase of the fracture toughness is obtained, which means that the density plays a major role in determining the fracture parameters. Rigid polyurethane foams have a brittle fracture without plastic deformation as was mentioned above.

Fig. 43 presents the energy-time variation. In this case, also, the energy values increases with increasing of density.

C. Comparison between Static and Dynamic Fracture Toughness for 3PB Tests

Fig. 44 presents a comparison of the fracture toughness values obtained from both static and dynamic test. Experimental tests were performed on PUR foams with different densities using notched specimens loaded in 3-point bending at a 2 mm/min ($3.3 \cdot 10^{-5}$ m/s) loading speed for static tests, respectively 3.815 m/s for dynamic tests. Both in static and in dynamic regime the used temperature was 20 ℃.

As it can be seen from Fig. 44, rigid PUR foams behaves differently in the two regimes. The dynamic fracture toughness is about two times higher than static one.

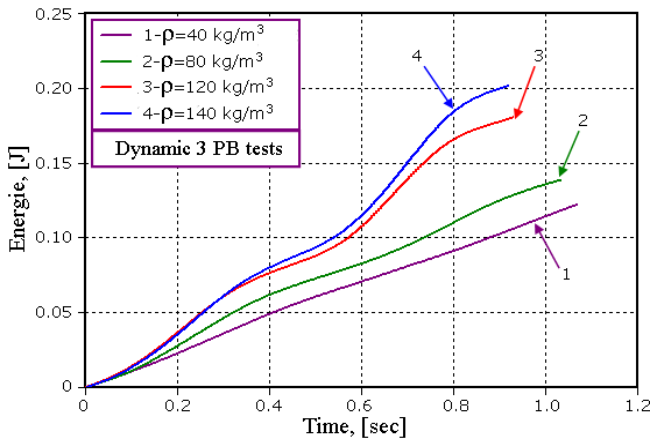

Fig. 43 Energy – time variation depending density

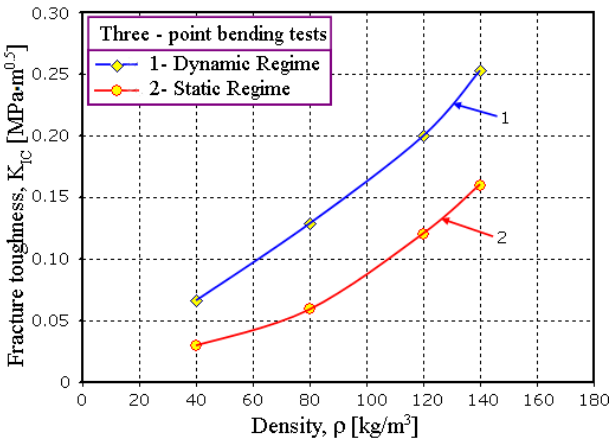

Fig. 44 Static and dynamic fracture toughness comparison

IV. MICROSTRUCTURAL ANALYSIS OF USED FOAMS

For analyzed foams, a microstructural analysis was made. The equipment used for microstructural characterization consists of Scanning Electron Microscope which is presented in Fig. 45. The analysis was done for both before (initial surface) and after (broken surface) compression and 3PB tests in the Strength of Materials Laboratory from the Lublin University of Technology, Poland.

Fig. 45 Scanning Electron Microscope used for microstructural analysis

Fig. 46 shows cell shapes before and after dynamic compression tests for foam with 140 kg/m^3 density. After compression tests the foam shows a total destruction of cells, which increases the stress delivered to an almost constant strain (known as densification). In the moment of densification, due to the filling of the gaps in the foam, this one acts almost like a solid material.

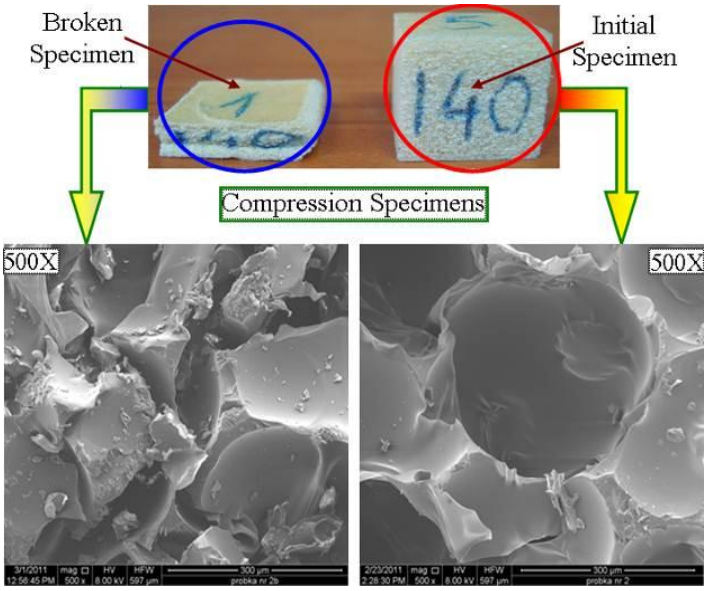

(a) fractured surface (b) initial surface

Fig. 46 SEM images of used PUR Foams

Initial and broken surfaces of rigid PUR foam used in 3PB experimental programs are presented in Fig. 47. Also, in the same figure is shown the cellular structure of foam having closed cell with ρ=40 and140 kg/m^3 density.

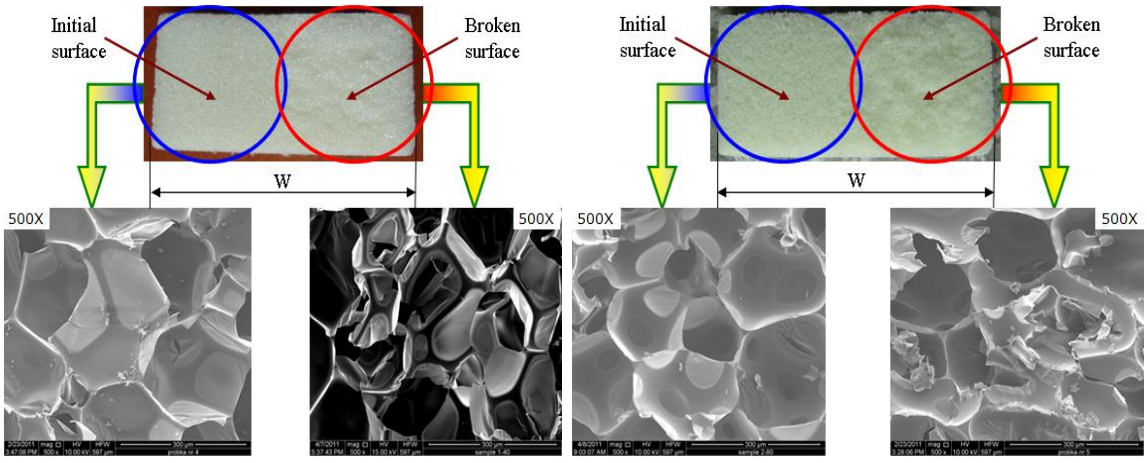

(a) 40 kg/m^3 density (b) 80 kg/m^3 density

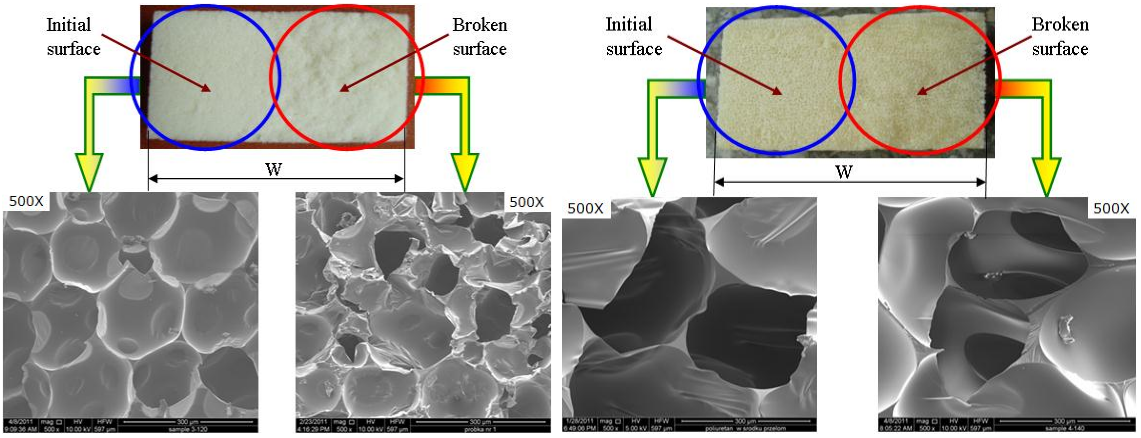

(c) 120 kg/m^3 density (d) 140 kg/m^3 density

Fig. 47 The microstructure of rigid polyurethane foams used for 3-point bending tests

All 3PB tested specimens show a quasi-brittle fracture without plastic deformations and cushioning.

V. CONCLUSIONS

Besides many other applications, polymeric cellular materials are used in the construction of wind turbine blade parts or entire sections. This book chapter presents the failure mechanisms in wind turbine blade with the focus on the core materials (rigid PUR foams). In this respect we made a mechanical characterization of rigid PUR foams under different loading conditions. This characterization of cores was done through static and dynamic tests with a focus on the influence of density (in the range of 40-200 kg/m^3), influence of loading speed (from $1.67.10^{-4}$ m/s – static tests to 6 m/s – impact tests), influence of forming plane (in-plane and out-of-plane loading direction), influence of temperature (from 20 ℃ to 100 ℃) and size effect on the mechanical properties. The most important mechanical properties which was studied are Young's modulus, yield stress, plateau stress, densification and fracture toughness.

After the experimental investigations, the following conclusions can be drawn:

D. For static and dynamic compression tests

- The experimental study presents a comparison of the stress-strain response in dynamic compression. It can easily be seen that with increasing of density we obtain a significant increase of mechanical properties, which means that the density has an important role in determining the dynamic compressive behavior.

- Loading speed has a little influence on mechanical properties in dynamic compression for low density of PUR foams (80 and 93 kg/m^3), while for high densities loading speed it has a major influence (200 kg/m^3). It can be observed that the biggest influence is obtained for linear – elastic region, yield stress and densification region.

- The loading direction has a major influence on the compressive mechanical properties in dynamic conditions, this parameter clearly showing the anisotropic aspect of foam. For an in – plane loading direction a constant plateau was obtained, while for out – of – plane load the plateau has a linear hardening (for the same foam density).

- From Fig. 11 it can be observed that cross-section shows a relatively small influence on the mechanical properties.

- According to the results presented in Fig. 19, it can be seen that at lowest temperatures (20 and 60°C) the behavior of foam is approximately the same, while at high temperature (100 ℃), foams show a major change in their properties.

- Also, the calculation of densification strain for rigid polyurethane foams was presented. The onset strain of densification is an important parameter in the design and modeling of cellular materials.

E. For static and dynamic fracture toughness tests

- This section presents influence of few parameters on fracture toughness of rigid PUR foams: influence of density, influence of loading speed, influence of forming plane and size effect.

- The values of fracture toughness for PUR foams are in the range of $10^{-3} – 10^{-1}$ MPa·m$^{0.5}$. Fracture toughness increase with increasing of density and decrease with increasing of loading speed.

- Loading direction emphasizes anisotropic behavior of the foam. For this type of PUR foam with 40 kg/m^3 density, the same fracture toughness was approximately obtained.

- Experimental investigations on size effect of closed-cell PUR foam of density 40 kg/m^3 were carried on 3-point bending specimens of different sizes, keeping constant the specimen thickness B=20 mm and ratio between crack length a and specimen width W: a/W = 0.4. A strong size effect in the closed – cell PUR foam (PUR 40) is experimentally demonstrated, representing the transition between strength of materials approach (with no size effect) and asymptotic case of linear elastic fracture mechanics. The size effect is also highlighted by the fracture toughness results, which increased with increasing specimen width and accordingly crack length. From the practical point of view and in order to determine the fracture toughness of this PUR foam, a minimum width size W_o=10 mm should be used, which represents approximately 33 cells (mean cell size for investigated foam was 0.3 mm). The size effect in foam is important for extrapolating laboratory tests data to very large structures, such as wind turbine blades. To summarize, the size effect presented in Fig. 38, demonstrates that the current design practice, in which the tensile failure of foam is generally predicted on the basis of strength criteria or plasticity, is acceptable only for small structural parts. In the case of large structural parts, the size effect must be taken into account, and linear elastic fracture mechanics concepts must be applied, especially in the presence of long cracks or large damage zones.

F. For Microstructural Analysis

Also at the end of this book chapter is shown a microstructural analysis for both before (initial surface) and after (broken surface) compression and three – point bending tests.

- After compression tests the foam shows a total destruction of cells, which increases the stress delivered to an almost constant strain (known as densification). In the moment of densification, due to the filling of the gaps in the foam, this one acts almost like a solid material, see Fig. 46.

- All 3PB tested specimens show a quasi – brittle fracture without plastic deformations and cushioning.

As a final conclusion we can say that one of the most significant parameter on the mechanical properties for cellular materials is the density. Hence, the mechanical properties of foams can be controlled, making them attractive in structural application requiring particular strength or stiffness to weight ratios. Cellular materials have plastic plateau and densification in compression, while in tensile they are quasi-brittle.

ACKNOWLEDGMENTS

This work was supported by the strategic grant POSDRU 6/1.5/S/13 (2008) of the Ministry of Labour, Family and Social Protection, Romania, co–financed by the European Social Fund – Investing in People and by a grant of the Romanian National Authority for Scientific Research, CNCS – UEFISCDI, project PN-II-ID-PCE-2011-3-0456, contract number 172/2011.

REFERENCES

[1] L.J Gibson, M.F Ashby, Cellular solids. Structure and properties, Second edition, published by the Press Syndicate of Cambridge, 1997.

[2] E. Linul, L. Marşavina, A. Cernescu, Assessment of sandwich beams using failure mode maps, 16th International Conference on Composite Structures, Porto, Portugal, Jun. 2011.

[3] G. Ji, Z. Ouyang and G. Li, Debonding and impact tolerant sandwich panel with hybrid foam core, Comp. Struct. 103, 2013, 143-150.

[4] B. Yang and D. Sun, Testing, inspecting and monitoring technologies for wind turbine blades: A survey, Renewable and Sustainable Energy Reviews 22, 2013, 515-526.

[5] S. Ahmed and D. Izhar-ul-Haq, Wind Blade Material Optimization, Advances in Mechanical Engineering, vol. 2, no. 4, Dec., 2012.

[6] C. Sicot, P. Devinant, S. Loyer and J. Hureau, Rotational and turbulence effects on a wind turbine blade. Investigation of the stall mechanisms, Journal of Wind Engineering and Industrial Aerodynamics 96, 2008, 1320-1331.

[7] C. Kong, T. Kim, D. Han and Y. Sugiyama, Investigation of fatigue life for a medium scale composite wind turbine blade, International Journal of Fatigue 28, 2006, 1382-1388.

[8] J. Yang, C. Peng, J. Xiao, J. Zeng, S. Xing, J. Jin and H. Deng, Structural investigation of composite wind turbine blade considering

structural collapse in full-scale static tests, Composite Structures 97, 2013, 15-29.

[9] D. S. Zarouchas, A. A. Makris, F. Sayer, D. Van Hemelrijck and A. M. Van Wingerde, Investigations on the mechanical behavior of a wind rotor blade subcomponent, Composites: Part B 43, 2012, 647-654.

[10] C. P. Chen and T. Y. Kam, Failure Analysis of Small Composite Sandwich Turbine Blade Subjected to Extreme Wind Load, Procedia Engineering 14, 2011, 1973-1981.

[11] A. Mirzapour, M. H. Beheshty and M. Vafayan, The response of sandwich panels with rigid polyurethane foam cores under flexural loading, Iranian Polymer Journal, 14 (12), 2005, 1082-1088.

[12] C.S. Lee and D.G. Lee, Co-cure method for foam sandwich composite manufacture, Comp. Struc., 66, 2004, 231-238.

[13] M. Avalle, G. Belingardi and R. Montanini, Characterization of polymeric structural foams under compressive impact loading by means of energy-absorption, International Journal of Impact Engineering 25, 2001, 455-472.

[14] M. Avalle, G. Belingardi and G. Ibba, Mechanical models of cellular solids: Parameters identification from experimental tests, International Journal of Impact Engineering 34, 2007, 3-27.

[15] M. C. Saha, H. Mahfuz, U. K. Charavarthy, M. Uddin, M. E. Kabir and S. Jeelani, Effect of Density, Microstructure, and Strain Rate on Compression Behavior of Polymeric Foams, Materials Science and Engineering, A406, 2005, 328-336.

[16] S. Ouellet, D. Cronin and M. Worswick, Compressive Response of Polymeric Foams Under Quasi-static, Medium, and High Strain Rate Conditions, Polymer Testing, 25, 2006, 731-743.

[17] F. Ramsteiner, N. Fell and S. Forster, Testing the deformation behaviour of polymer foams, Pol. Test., 20, 2001, 661-670.

[18] E. Linul, L. Marsavina and A. V. Cernescu, Effect of loading speed, the direction of formation and density of rigid polyurethane foams subjected to compression, Acta Tehnica Napocensis, Series: Mech. Eng. Mat. Sci. 53, 2010, 311-316.

[19] Q. M. Li, I. Magkiriadis, J. Harrigan, Compressive strain at the onset of densification of cellular solids, J of Cell Plastics, 42, 2006, 371.

[20] Z. H. Tu, V. P. W. Shim, and C. T. Lim, Plastic deformation modes in rigide polyurethane foam under static loading, International Journal of Solids and Structures 38, 2001, 9267-9279.

[21] A. Ajdari, Mechanical behaviour of cellular structures a finite element study, Master on Science in Mechanical Engineering, Northeastern Universty, boston, Massachusetts, Apr., 2008.

[22] ASTM D1621 – 00, Standard Test Method for Compressive Properties of Rigid Cellular Plastics.

[23] T.G. Nieh, K. Higashi and J. Wadsworth, Effect of Cell Morphology on the Compressive Properties of Open-cell Aluminum Foam. Material Science and Engineering, A283 (1-2), 2000, 105-110.

[24] A. Paul and U. Ramamurthy, Strain rate Sensitivity of a Closed-cell Aluminum Foam, Mat. Sci. and Eng., A281 (1), 2000, 1-7.

[25] K. C. Chan, L. S. Xie, Dependency of Densification Properties on Cell Topology of Metal Foams. Scripta Mat., 48 (8), 2003, 1147-1152.

[26] M. Vural and A. G. Ravich, Microstructural Aspects and Modeling of Failure in Naturally Occurring Porous Composites. Mechanics of Materials, 35 (3-6), 2003, 523-536.

[27] N. Tuncer, G. Arslon, Designing Compressive properties of titanium foams. J. of Material Science, 2009, 1477-1484.

[28] L. Marsavina, T. Sadowski, D. M. Constantinescu and R. Negru, Polyurethane Foams Behaviour. Experiments versus Modeling. Key Engineering Materials, vol. 399, 2008, 123-130.

[29] T. Wiydia, C. W. Macosko, Nanoclay-Modified Rigid Polyurethane Foams, J. of Macromolecular Sci., Part B: 44, 2005, pp. 897-908.

[30] H. Altenbach and A. Ochsner, Cellular and Porous Materials in Structures and Proceses, CISM Courses and Lectures, vol. 521. Ed. Springer Wien New York, Udine, 2010.

[31] A. McIntyre, G. Anderson, Fracture properties of rigid PU foam over a range of densities, Polymer, 20, 1979, pp. 247-253.

[32] M. Danielsson, Toughened rigid foam core material for use in sandwich construction, Cell. Pol., 15, 1996, pp. 417-435.

[33] M. Burman, Fatigue crack initiation and propagation in sandwich structures, Report no. 98-29, Stockholm, 1998.

[34] G.M. Viana and L. A. Carlsson, Mechanical Properties and Fracture Characterization of Cross-Linked PVC Foams, J. Sandw Struct Mater, 4, 2002, pp. 91-113.

[35] Md.E. Kabir, M. C. Saha and S. Jeelani, Tensile and fracture behavior of polymer foams, Mat. Sci. and Eng. A, 429, 2006, pp. 225-235.

[36] L. Marsavina, E. Linul, Fracture toughness of polyurethane foams, Experimental versus micromechanical models, Fracture of Materials and Structures from Micro to Macro Scale. 18th European Conf. on Fracture, Dresden, Germany, Aug. 30-Sep. 03, 2010.

[37] E. Linul, L. Marsavina and A. Cernescu, Determination of fracture toughness for cellular materials such as polyurethane foams, Fracture Mechanics. 15th National Symposium National on Fracture Mechanics, Ed. Universitatii Petrol-Gaze Ploiesti and Ed. Universitatii "Lucian Blaga" from Sibiu, 6-7 Nov, 2009, Sibiu, pp. 15-22.

[38] ASTM D 5045-99 Standard Test Methods for Plane-Strain Fracture Toughness and Strain Energy Release Rate of Plastic Materials.

[39] L. Marsavina, Fracture mechanics of cellular solids, in Cellular and porous materials in structures and processes, Springer, 2010, 1-33.

[40] D. Zenkert, PVC sandwich core materials: fracture behaviour under mode II and mixed mode loading, Mat Sci Eng. 108, 1989, 233-240.

[41] D. Zenkert, J. Bäcklund, PVC sandwich core materials: mode I fracture toughness. Comp. Sci. Tech. 34, 1989, 225-242.

[42] O. B. Olurin, N. A. Fleck, M. F. Ashby, Tensile and compressive failure of notched cellular foams, Adv Eng Mat 3 (1–2), 2001, 55-58.

[43] N. A. Fleck, O. B. Olurin, C. Chen, M. F. Ashby, The effect of hole size upon the strength of metallic and polymeric foams, J. of the Mech. and Phys. of Sol. 49, 2001, 2015-2030.

[44] Z. P. Bažant, J. Planas, Fracture and size effect in concrete and other quasi-brittle materials, CRC Press, Boca Raton and London (Sections 9.2 and 9.3), 1998.

[45] Z. P. Bažant, Scaling of Structural Strength, Hermes-Penton, London, 2002.

[46] P. Zdenek, Z. P. Bažant, Z. Yong, Z. Goangseup, M. D. Isaac, Size effect and asymptotic matching analysis of fracture of closed-cell polymeric foam, Int. J. of Sol. and Struc. 40, 2003, 7197-7217.

[47] Z. P. Bažant, Size effect in blunt fracture: Concrete, rock, metal, J. of Eng. Mech. ASCE 110, 1984, 518-535.

[48] Z. P. Bažant, M. T. Kazemi, Determination of fracture energy, process zone length and brittleness number from size effect, with application to rock and concrete, Int. J. of Fract. 44, 1990, 111-131.

[49] EN ISO 179–2:2000. Plastics – Determination of Charpy impact properties. Part 2: instrumented impact test.

[50] J. F. Kalthoff, Characterization of the dynamic failure behaviour of a glass – fiber / vinyl – seter at different temperatures by means of instrumented Charpy impact testing, Comp. Part. B 35, 2004, 657–663.

Emanoil LINUL was born in Năsăud, Romania on November 12, 1984. He is an Assistant Lecturer in the Department of Mechanics and Strength of Materials at POLITEHNICA University of Timisoara, Romania. Dr. Linul obtained his Ph.D. Degree in the Engineering Science field under the supervision of Prof. Liviu Marşavina – Thesis Title: "Study of the Influence Factors Affecting the Mechanical Properties of Rigid Polyurethane Foams", September 9, 2011. Throughout the last year of his Ph.D. Thesis he worked with experienced researchers, i.e. Prof. Tomasz Sadowski and his team from Lublin University of Technology, Poland.

In addition to teaching activities, Dr. Linul is a member of Romanian Society for Experimental Stress Analysis (ARTENS) and of Romanian Association for Fracture Mechanics (ARMR), since 2009. Currently, he is a Research Assistant and working as a scientist in the National Grant "Micro-mechanical modeling of cellular materials with refinements on fracture and damage", where he is investigating cellular materials (rigid PU foams) behavior.

His main research interests include: (i) experimental characterization of cellular materials (compression, tensile, shear, bending and fracture tests); (ii) development of micro-mechanical models to estimate mechanical properties of cellular materials; (iii) implementation of constitutive material models in Finite Element Analysis; (iv) investigation of the size and notch effects on cellular materials using Theory of Critical Distance; (v) evaluation of the behavior of cellular materials under dynamic (impact, fatigue and energy absorption) loading; (vi) investigation of the effect of micro-structural damage on the mechanical properties of cellular materials using Digital Image Correlation (DIC) and thermography systems.

Also, he recently collaborated with Dr. Jaroslav Kovacik from Slovak Academy of Science, Bratislava, Slovakia on mechanical behavior of aluminum foams field. As a result of research work, since 2010 he has published more than 25 papers in journals, publications and book conferences of which 15 in the ISI circuit (7 papers in ISI Journals and 8 papers in ISI Proceedings).

Liviu MARŞAVINA was born in Anina, Romania on September 23, 1963. He is a Professor in the Department of Mechanics and Strength of Materials at POLITEHNICA University of Timisoara (UPT), Romania, since 2006 and was Head of Strength of Materials Department of UPT (2008-2011). With a Ph.D. Thesis entitled "Numerical Methods Used in Fracture Mechanics" and with an experience in this field, he has published more than 80 scientific/technical papers.

Professor Marsavina attended several specialized courses of which the most important are: (i) Course "Optical Methods in Solid Mechanics", Loughborough University, UK, March-June 2000; (ii) PECO Workshop IE-W03 "Best Practice of Advanced Fracture Assessment", Petten, NEDERLAND, April 2003 and (iii) Advanced course: "Multi-scale Modelling of Damage and Fracture Processes in Composite Materials" at International Centre for Mechanical Sciences, CISM Udine, ITALY, May 2004.

Dr. Marsavina has different positions in international research environment: (i) Postdoctoral researcher at Loughborough University, UK in 2000; (ii) Research Associate at the University of Sheffield, UK from 2001-2002; (iii) Marie Curie Experienced Researcher at Lublin University of Technology, Poland from 2007-2008.

Besides teacher position he has the following positions: (i) member of the CSUD (Council of Doctoral Studies); (ii) Ph.D. supervisor from 2007; (iii) member in the committee for Ph.D. examination/defence at UPT, Politehnica University of Bucharest, Lille University (France), Loughborough University (UK); (iv) member in the CNTDCU (National Council for Titles, Diplomas and University Certificates) of Romanian Ministry of Education; (v) member in the CNCS (National Council of Scientific Research) of Romanian Ministry of Education; (vi) member of ARTENS (Romanian Society for Experimental Stress Analysis); (vii) member of SIAC (Romanian Society for Computer – Aided Engineering); (viii) member and vice-president of ARMR (Romanian Association for Fracture Mechanics); (ix) member of AGIR (Romanian Engineering General Association); (x) member of EU – RA (European Research Associates) and (xi) member of ESIS (European Structural Integrity Society).

Dr. Marsavina is co-editor of Bulletin of Romanian Association of Fracture Mechanics and member in Advisory Board of International Journal of Structural Integrity. Also, he is reviewer for the following journals: Fatigue and Fracture of Engineering Materials and Structures (Blackwell Ltd.) from 2001; Journal of Sound and Vibration (Elsevier) from 2006; Computational Material Science (Elsevier) from 2006; Construction and Building Materials (Elsevier) from 2007; International Journal of Solids and Structures (Elsevier) from 2009; Mechanical Research Communications (Elsevier) from 2009; Mechanics of Advanced Materials and Structures (Taylor and Francis) from 2009; Journal of Mechanical Science and Technology (Springer) from 2010; Engineering Fracture Mechanics (Elsevier) from 2010 and Frattura ed Integrità Strutturale (Gruppo Italiano Frattura) from 2012.

Research interests of Dr. Marsavina are: (i) Fracture mechanics and structural integrity; (ii) mechanical testing; (iii) fatigue of materials; (iv) composite materials including cellular materials; (v) experimental stress analysis (photoelasticity, thermoelasticity, Digital Image Correlation) and (vi) numerical stress analysis for evaluating the fracture parameters.

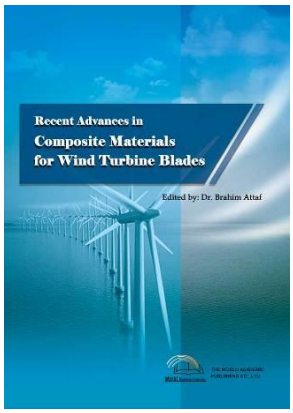

Recent Advances in Composite Materials for Wind Turbine Blades
Edited by Dr. Brahim Attaf

ISBN 978-0-9889190-0-6

Hard cover, 232 pages

Publisher: The World Academic Publishing Co. Ltd.

Published in printed edition: 20, December 2013

Published online: 20, December 2013

This book of science and technology provides an overview of recent research activities on the application of fibre-reinforced composite materials used in wind turbine blades. Great emphasis was given to the work of scientists, researchers and industrialists who are active in the field and to the latest developments achieved in new materials, manufacturing processes, architectures, aerodynamics, optimum design, testing techniques, etc.. These innovative topics will open up great perspectives for the development of large scale blades for on- and off-shore applications. In addition, the variety of the presented chapters will offer readers access to global studies of research & innovation, technology transfer and dissemination of results and will respond effectively to issues related to improving the energy efficiency strategy for 2020 and the longer term.

How to cite this book chapter

Linul E. and Marsavina L. (2013). Mechanical Characterization of Rigid PUR Foams Used for Wind Turbine Blades Construction, *Recent Advances in Composite Materials for Wind Turbines Blades*, Dr. Brahim Attaf (Ed.), ISBN 978-0-9889190-0-6, WAP-AMSA, Available from: http://www.academicpub.org/amsa/chapterInfo.aspx

World Academic Publishing - Advances in Materials Science and Applications

Chapter 11

Investigation of Polymer Composites for Wind Turbines Blades

N. Chikhradze*, G. Abashidze

Mining Institute
7, Mindeli str., Tbilisi, Georgia
*g.pkhaladze@mail.ru

I. INTRODUCTION

For the recent years, considerable attention has been dedicated to renewal power sources, such as wind power. This work was carried out in order to develop a small wind turbine of 1-10kW power generation capacity. This wind turbine is designed to be energetically more efficient by 30-50% having a lower specific cost (by 25-30%). In this chapter, an issue concerns the development of a new type of composite materials for potential application within the wind turbine blades structural design. We present the results of research work undertaken on the development of flexible technology for fabrication of hybrid composites reinforced with carbon, basalt and glass fibers. The new composites were fabricated using strengthened epoxy matrices. Basalt fibers for composite were produced from raw materials with chemical composition: SiO_2 – 49%; Al_2O_3 – 16%; CaO – 9%; FeO – 6.5%; MgO – 6%; Fe_2O_3 – 5%; Na_2O – 3%, K_2O – 1.5%; TiO_2 – 1.3%; H_2O – 1.6%.

The wind-power engineering is a priority area of energy generation due to its resource-saving and ecological safety. The power cost primary is determined substantially by basic power element-blades. At present, hybrid fibers (carbon and glass) are mainly used for fabrication of the blades [1], however, there are some works dedicated to reinforce epoxy matrices with basalt and other fibers [2]. The task of cost reduction may be solved through application of the less expensive materials in comparison with carbon fibers. For blade development, an application of new composite hybrid material is suggested on combinations of high-strength and high-modulus carbon and basalt fibers. Basalt reinforcing element of composite was prepared on basis of Georgian raw materials. The problem consists in partial substitution of expensive carbon fiber in the material.

Basalt fibers are practically highly competitive with glass ones by main mechanical characteristics and surpasses them by some of them, in particular, by water-resistance and chemical stability. But in the form of twisted and non-twisted threads, roving, roving cloth and discrete fibers, basalt fibers represent an alternative and promising reinforcing element for composites. In addition, at solving of a series of specific problems, for example, for preparation of materials with predetermined strength and deformation characteristics in different directions of load application, the combination of glass, high-strength basalt, high-strength and high-modulus carbon fibers were used, that is to say, the production of composites, reinforced by hybrid fibers (HFRC) was organized.

In parallel with the advantages, HFRC, undoubtedly, are characterized by some disadvantages, which must be taken into account at the preparation and operation of blades with the use of HFRC. These disadvantages involve:

- Structural non-uniformity and inadequate stability of the technology of preparation, which leads to considerable dissipation of mechanical and other indices that may attain to 15-20% in relation to average values even at standard short-term testing. At long-term, testing the dissipation increased.
- Polymeric nature of a matrix determines an enhanced sensitivity of materials to the prehistory of preparation and to temperature-time regime of further operation, which is responsible for determining strength and deformation properties of HFRC. At moderate temperatures, for traditional structural materials, a temperature-time dependence of mechanical and other properties appears only slightly, whereas the presence of polymeric matrix in the considered materials predetermines an impossibility to evaluate strength or deformability even at room temperature without time indication in the course of which the materials are in the stressed state.
- Directional locating of reinforcing fibers in the plane of reinforcement as well as a lamination of the structure in the direction perpendicular to the mentioned plane, causes an anisotropy of mechanical and other properties. As a rule, a number of characteristics, necessary for the determination of one or other properties of reinforced plastics, is considerably more important than for isotropic materials. Moreover, the regularities of the behavior of reinforced plastics at mechanical testing depend on the direction of load application. In instance for oriented composites, a tension diagram in the direction of

reinforcement is governed by Hooke's law. At loading at an angle to the direction of reinforcement, this diagram is getting considerably nonlinear.

- A lamination of the structure of polymeric composites predetermines their low resistance to interlayer shear and to transverse breaking off. Therefore, at bending, these materials may be destroyed because of the fact that tangential stresses will be higher than material's resistance to interlayer shear instead of the fact that normal stresses (extending or compressing) may attain the limiting values.

- Deformations, generated perpendicularly to reinforcing fibers, are mainly realized in matrix interlayers because of low rigidity of the latter in comparison with glass, basalt or carbon fibers; this leads in fact to the formation of the cracks in the interlayers of a binder between the fibers or at phase boundaries. Low crack resistance is particularly characteristic of oriented plastics. The cracks have little or no effect on the values of characteristics, obtained as a result of short-term testing. However, such characteristics of a material as hermeticity, resistance to corrosive media, mechanical and electrotechnical properties in the conditions of long-term operation at the appearance and intergrowth of the track are significantly impaired.

- Relatively low value of modulus of elasticity of reinforced plastics and composites leads to the fact that load-carrying ability of thin-wall structures is limited by deformability and stability instead of the strength. For complete use of high strength characteristics of the composites, it is profitable to design the item and structure as three-layered or to provide the stiffening ribs. Designing must be carried out in such a way that the material will operate in tension instead of compression, whenever possible.

Considered peculiarities of reinforced polymers, in general, and of HFRC, in particular, must be taken into account the considered peculiarities of reinforced polymers, in general and HFRC, in particular, must be taken into account at designing of blades of the wind turbine.

Appearance of new generation of reinforced polymers (i.e., HFRC) is due to the quest for preparation of the materials, characterized by higher initial mechanical and other indices and by higher stability of these indices at the action of various operating factors.

At the present time, the volumes of the production and the use of composites reinforced by high-strength and high-modulus fibers are not big. The main barrier to the extension of fields of use of such materials, in wind power engineering, is their high cost.

In regard to the cost of HFRC, it should be noted that the ways for their cost reduction, probably, are linked not with increase of output rate, but with reduction in price of raw materials and mechanization of the production. In this regard, a problem of the cost reduction for composites seems to be very topical through even partial replacement of expense and deficit carbon fiber by incomparably cheap basalt fiber without considerable loss of main operating properties of the material. Moreover, the share of reinforcing fibers as well as of a binder in the expenses of raw materials is distinct for the composites of various types. For the composites, in which the nonwoven reinforcing elements are used in the form of threads and mats, the expenses of reinforcing materials attain 30-35% of all material expenses. At the same time, the expenses of reinforcing materials in the form of cloths may attain 50-70% at the preparation of basalt plastics. Therefore, an essential method in the reduction of composite's cost may be achieved by replacing the cloths from twisted threads by nonwoven reinforcing materials and roving cloths.

Price cost reduction for HFRC is also possible at the expense of introducing efficient fillers-reinforcers into the matrix composition. This method allows a considerable decrease of fiber content without an essential reduction of characteristics of the resulting material.

One more way to enhance the efficiency of HFRC use in practice, is a rational design and application of products with regard to the influence of real environment on the material. Below the primary attention is given to more or less detailed consideration of these problems.

II. APPROACH TO THE ESTIMATION OF DURABILITY OF COMPOSITES FOR WIND TURBINE BLADES

In the design of wind turbine blades from composite materials, primarily the values of their calculated resistances are necessary. The long-term resistance (R_{cl}) of the material in normal conditions is calculated by the product of (i) the normative resistance of the material, (ii) the coefficient of long-term resistance and (iii) the coefficient of the uniformity of its mechanical characteristics. In other words, this may be given by the following relation: $R_{cl}=R_{nor}K_{\ell\text{-}t}K_u$

The normative resistance (R_{nor}) was determined from a strength limit of the materials under study by the results of short-term testing of small samples, carried out in accordance with acting standards. The coefficient of long-term resistance ($K_{\ell\text{-}t}$) was determined by testing to failure of the series of the samples of the materials at long-term loading at the stresses comprising a definite part from a strength limit of the material. Uniformity coefficient (K_u) was determined by well-known three sigma rule by calculation of arithmetic mean and by root-mean-square deviation of the strength, which are defined on the basis of statistical analysis of the results of mass testing of strength properties of HFRC.

Calculated resistances of the materials, operating at the joint action of static load and regimes, different from normal ones (elevated temperature, high humidity, corrosive medium and etc.) were determined by multiplying the long-term calculated resistances into corresponding coefficients of operating conditions:

$$R_{c\ell}^{T} = R_{c\ell} \cdot K_T, \qquad R_{c\ell}^{w} = R_{c\ell} \cdot K_w, \qquad R_{c\ell}^{cor} = R_{c\ell} \cdot K_{cor}, \qquad R_{c\ell}^{atm} = R_{c\ell} \cdot K_{atm}$$

where: K_T, K_w, K_{cor}, K_{atm} are coefficients of operating conditions of composites, service of which is provided, respectively, at elevated temperature, in water or at high humidity at the action of corrosive media, in atmospheric conditions, as well as at synchronous long-term action of load as well as of external factors. In some cases the coefficients of operating conditions can be determined at the joint action of various factors, for example, of temperature, water /humidity ($K_{T,w}$).

The results of determination of normative resistances at various types of stressed state (tension, bending, compression, shear: R_{nor}^{t}, R_{nor}^{b}, R_{nor}^{c}, R_{nor}^{sh}, respectively) as well as of short-term modulus of elasticity in tension, bending and compression (e.g., E_{s-t}^{t}, E_{s-t}^{b}, E_{s-t}^{c}, respectively) and coefficients of uniformity of strength properties of the materials under study, are all given in Table 1.

Concerning the problem on uniformity coefficient of material, it should be noted that tests carried out for its determination were performed at room temperature – humid conditions. Incidentally, in the course of operating of the structures by the use of plastic materials, they may undergo various temperature- humid effects and it may be suggested that these effects may exert some influence not only to the variation of absolute values of mechanical properties of HFRC, but, to some extent, they may reflect on the indices of uniformity of strength properties of the materials. To check this suggestion, the investigations were carried out in order to reveal the influence of preliminary action on the indices of uniformity of strength properties of HFRC-2 and HFRC-4 at tension. The results of these testings are given in Table 2. They involve the data necessary to calculate the uniformity coefficient (number of testing – n, arithmetic – mean value for strength - σ_{av}, mean square deviation - σ' as well as variation coefficient – V). The regimes of preliminary action on the samples of the material were: №1 – holding in laboratory room; №2 – heating at 353K over 10 days; №3 – steeping over 1 day; №4 – steeping over 10 days; №5 – steeping over 10 days by further drying over 10 days; №6 – steeping over 10 days at 353K.

TABLE 1 NORMAL RESISTANCE, SHORT-TERM MODULUS OF ELASTICITY AND UNIFORMITY COEFFICIENTS FOR HFRC

Material	R_{nor}^{t} **(MPa)**	R_{nor}^{b} **(MPa)**	R_{nor}^{c} **(MPa)**	R_{nor}^{sh} **(MPa)**	E_{s-t}^{t} **(GPa)**	E_{s-t}^{b} **(GPa)**	E_{s-t}^{c} **(GPa)**	K_u
HFRC-1	195.6 / 163.1	480.2 / 270.3	261.1 / 219.1	10.2 / 8.1	9.4 / 3.9	14.5 / 3.4	10.6 / 4.2	0.72
HFRC-2	292.5 / 228.2	567.2 / 351.4	410.2 / 319.9	12.2 / 10.2	15.0 / 5.4	23.4 / 5.4	14.6 / 5.8	0.68
HFRC-3	455.4 / 6.9	718.1 / 19.9	420.8 / 8.0	24.8 / 1.2	96.9 / 5.8	78.6 / 5.2	78.1 / 4.1	0.74
HFRC-4	132.2 / 85.6	415.7 / 95.9	160.2 / 107.7	8.8 / 2.4	49.7 / 19.8	58.8 / 16.4	51.0 / 16.7	0.70

Remark: HFRC-1, HFRC-2, HFRC-3, HFRC-4 – composites of different composition and fiber orientation.
The values given in numerator and denominator are along and transversely to X axis (Figs. 3, 6).

TABLE 2 STATISTICAL PROCESSING OF THE RESULT OF TESTING TO REVEAL THE INFLUENCE OF PRELIMINARY ACTION OF VARIOUS FACTORS ON UNIFORMITY INDICES

Material	**Act. reg.**	**n**	σ_{av}, **(MPa)**	σ' **(MPa)**	**V (%)**	K_u
HFRC-2 (δ=1.5mm)	№1	92	292	29	9.9	0.70
	№2	95	262	25	9.5	0.71
	№3	99	277	29	10.5	0.69
	№4	100	295	30	10.2	0.69
	№5	93	290	31	10.7	0.68
	№6	95	277	30	10.8	0.68
HFRC-4 (δ=0.8mm)	№1	100	155	10	6.5	0.80
	№2	100	166	18	10.8	0.67
	№3	95	125	12	9.6	0.71
	№4	96	115	12	10.4	0.69
	№5	99	140	14	10.0	0.70
	№6	91	111	12	10.8	0.68

As it can be seen from Table 2 that the variation of K_u is relatively small and the maximum reduction of K_u comprises 6 % for HFRC. Hence, the value of K_u, obtained by testing in normal temperature- humid conditions, may be used by confidence at

practical calculations.

Under prolonged (long-term) strength of the solid the dependence of time duration up to its failure on the stress and temperature is meant. The coefficient of long-term resistance is a value, determined by testing of a series of the materials samples under prolonged loading to failure at the stresses, constituent a definite part from material strength limit. Thus, in the terms "long-term resistance" and "durability" an equal meaning is assigned.

III. EXPERIMENTS ON COMPOSITE MATRIX STRENGTHENING

Investigation was concerned with epoxy Diane resin with passive diluents – didutylphtalate (15m.f. per 100m.f. of resin). Resin had a density of 1.168 $g.cm^{-3}$, viscosity at 20°C – 120 P, involved epoxy groups – 17 mass %, total chlorine – 0.85 mass %, chlorine ions – 0.007 mass %, volatiles – 0.85 mass %, time of gelation of resin at 100°C comprised 3.0 hours.

As ingredients, reinforcing a resin, were used: powders of boron carbide (100 μm) and silicon carbide (80 μm), of zirconium diboride (100 μm), as well as mullitelike oxide crystals $3Al_2O_3 \cdot 2SiO_2$ (diameter 2-8 μm, length 80-200 μm), basalt powder (100 μm) and diluvium powder (60 μm). Diluvium had the following chemical composition, respectively: SiO_2 – 57.5; Al_2O_3 – 19; Fe_2O_3 – 7.4; CaO – 1.1; MgO – 3.0; R_2O – 5.2. Above are listed powders that were prepared by technology elaborated by the authors. For the production of boron carbide, amorphous boron and technical carbon were used as ingredients. Prepared mixture was briquetted in graphite mould. Boron carbide was synthesized in vacuum electric furnace. Synthesis was performed at the temperature of 1850±25°C, endurance – 2.5 hours. Cooling proceeds was performed in vacuum over 10 hours. Zirconium diboride was produced by method of boron carbide reduction. Zirconium dioxide and carbide were preliminary processed in vacuum for charge production. Mullites like crystals were prepared using the method of oxide solution crystallization in melt bed. Basalt powder preparation includes the following operations: crushing of basalt stones at the hydraulic press; melting; crushing and grinding of ingot; fractionation of the grinded powder at horizontal screen.

An amount powders, added to epoxy resin, was 7% from resin mass. Hardener of the compositions was polyethylene polymine (12% from resin mass), containing 36% of total nitrogen (in terms of dry substance).

The following series were prepared: "a" – pure epoxy resin; compositions: "b" – with diluvium, "c" – with boron carbide; "d" – with silicon carbide; "e" – with $3Al_2O \cdot 2SiO_2$; "f" – with ZrB_2; "g" – with basalt. Moulding of samples on tension in the form of mortar briquettes of (50X4X2) mm size were prepared in the castings. Samples – strips, dedicated from fatigue test, were prepared, too and measured: (170x15x3) mm.

Short-term mechanical testing's of the mouldings with an automatic recording of deformation were carried out on the machine FPZ-100 of German production. Strength and deformation characteristics of compositions were determined and based on a comparison of these data with characteristics of pure epoxy, degree of resin reinforcement was concluded.

For material testing on fatigue bending the device shown in Fig. 1 has been used. The main parameters of the device: simultaneous testing of 3 sheets or samples; bending angle from 20° to 180°; samples clamp width up to 30 mm; weights for preliminary load from 0.2 to 5 kgf; number of bends per minute – 100; counters (3 pieces) with an automatic turn-off at sample breakage.

The sample was fixed in the clamp, which is swung about its axis of rotation. The clamp is designed so that the bend axis is coincident with the axis of rotation at the swinging the clamped sample is repeatedly bended by weights, which impart to the sample the definite preliminary tension. Bending angle was selected as 20°, load – 2 kgf, number of the bends per minute – 100.

An endurance coefficient was determined from appropriate compositions (series "d'', "g''), from the viewpoint of reinforcement. Under an endurance coefficient a ratio between residual strength of composition after cyclic testing and its short-term statically strength is meant. The level of this ratio, whereby it reduces slightly regardless of a number of cycles, was taken as an endurance coefficient.

Fig. 1 Device for testing bending fatigue

The results of testing of composition samples (σ) and deformability (*E*) are given in Table 3. The amount of tested samples in each series is n=6; and the coefficient of variation of obtained data is variable from 5 to 8%.

TABLE 3 RESULTS OF SHORT-TERM STATICALLY TESTING OF COMPOSITION SAMPLES

Series of composition	σ (MPa)	Reinforcement coefficient	$E \times 10^{-3}$ (MPa)	Coefficient of rigidity's elevation
"a"	56.6	-	25.0	-
"b"	21.8	No reinforcement	11.2	No elevation
"c"	37.6	The same	24.4	The same
"d"	62.7	1.11	31.0	1.24
"e"	33.0	No reinforcement	21.1	No elevation
"f"	53.1	The same	26.1	1.04
"g"	64.9	1.15	32.2	1.29

Effect of resin reinforcement has been obtained as a result of the addition of silicon carbide to it as well as of basalt powder. Increase of the value of the modulus of elasticity was also noted for compositions containing these ingredients. An addition of zirconium carbide to resin gives an insignificant increase of its conventional coefficient of rigidity. An attention must be given to the fact that basalt powder of a given fraction of grinding, by its efficiency, is just as good as such reinforcers as boron and silicon carbides and zirconium diboride and in some cases outperform them. Considerable increase of longitudinal strains was noted for composition containing diluvium, which has a layered structure. This composition is close to elastomer by its characteristics.

Diagram of fatigue strength for compositions "g" and "d" is presented in Fig. 2. It was shown that a considerable drop of strength of composition, containing silicon carbide and basalt powder, practically does not take place at the threshold of 10^6 cycles. Endurance coefficient of compositions "d" and "g" comprises 0.21 and 0.24, respectively.

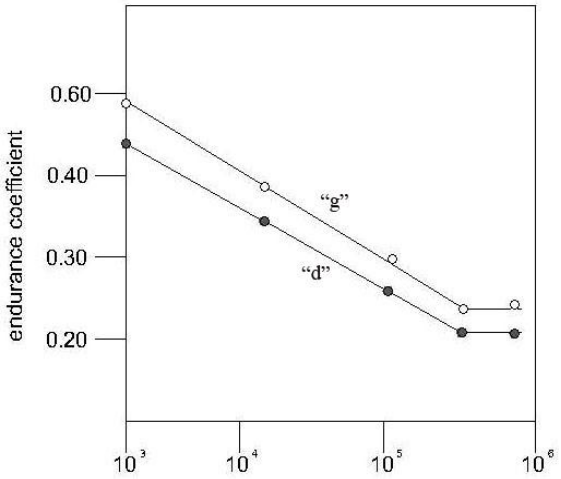

Fig. 2 Diagram of fatigue strength for compositions "d" and "g"

IV. COEFFICIENT OF OPERATING CONDITION OF HFRC AT ELEVATED TEMPERATURE

The aim of the work involves determination of the coefficients of operating conditions (COC) of a composite for predetermined service life and temperature (K_τ^T). The COC represents a ratio between a breaking stress after an interval, corresponding to service life of wind turbine blades that is long-term breaking stress and a breaking stress obtained by standard short-term testing of the material at room temperature (σ_{sh-t}):

$$K_\tau = \frac{\sigma_{l-t}}{\sigma_{sh-t}} \tag{1}$$

Direct experimental determination of σ_{l-t} is connected with difficulties, namely, with necessity for the maintenance of constant outer conditions and predetermined stress over a long time. Extrapolation of experimental date and predetermined time of stress action is carried out by use of S. N. Zhurkov' s equation based on the kinetic nature of the strength of solids:

$$\tau = \tau_0 \exp\left(\frac{U_0 - \gamma\sigma}{kT}\right) \tag{2}$$

where, τ is the time before material destruction; τ_0 is a constant, approximately equal to 10^{-13} sec, which in order of a value is near to the period of thermal oscillations of atoms; U_0 is the initial activation energy of the process of material destruction; γ is

the average coefficient of overstresses; T is the absolute temperature; k is the Boltzmann's constant; σ is the stress applied on a material.

In this case, we have tried to realize a possibility of the account of joint effect of stress, time and temperature by accelerated method for the determination of $\sigma_{l\text{-}t}$ by use of the well-known parametric method of S. Goldfein. The method is based on a combination of temperature (T_i) and time to material failure (τ_f) in one parameter whereby a long-term strength is determined using the following equation:

$$P = \frac{T_0 T_i}{T_0 - T_i}\left(c + \lg\tau_f\right) \tag{3}$$

where, T_0 is a temperature at which an infinitely small stress causes the materials failure; c =20 for solid materials, including the present research, since a binder is in glass state.

The sense of Eq. (3) includes possibility to construct dependence $\sigma = f$ (p) by short-term testing at elevated temperatures and by varying T and τ_f and to calculate a long-term strength at various temperatures. According to the work undertaken in [3], it was shown that from Eq. (2) a linear relationship between the parameter P and the long-term strength ($\sigma_{l\text{-}t}$) is evident:

$$\sigma_{l-t} = a - bP \tag{4}$$

Where, $a = \frac{U_0}{\gamma}$ and $b = \frac{2.3k}{\gamma}$

According to the recommendations of investigators of wind turbines, at manufacturing of blade shells, the carbon fibers should be arranged at an angle of -20° relative to the blade axis (i.e., X-axis) and the glass fibers should be perpendicular to the carbon fibers [4-6]. At manufacturing of spar reinforcing, fibers were arranged parallel and at +45° angle to X-axis. The structure of composites destined accordingly for shell and spar of blade is shown in Fig. 3.

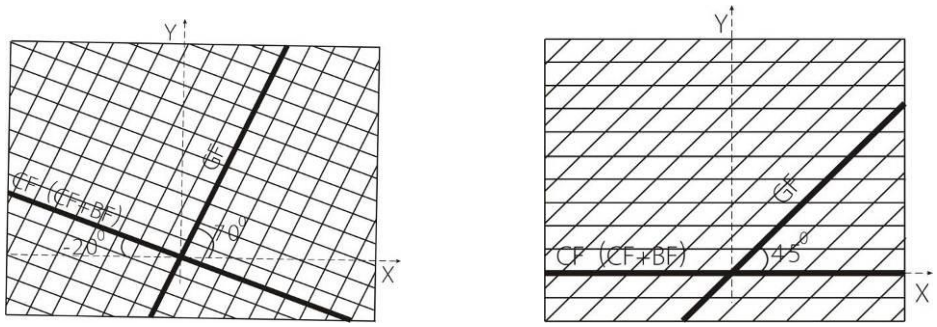

(a) (b)

Fig. 3 Scheme of arrangement of reinforcing elements in composite destined for (a) shell and (b) spar

Six types of composites were selected as research objects representing monolithic layered reinforced materials. In the composites 1, 2 and 3 destined for a shell, carbon fibers (CF) and glass fibers (GF) are used. The relation between these two types of fibers is GF: CF=0.3:0.7 (according to mass). In a midpoint of cross-section of composite 1, CF were interchanged with GF. The number of layers is 7 for CF and 4 for GF. In composite 2, CF partially (up to 20% of their mass) are replaced by basalt fibers (BF) by way of fabric. In composite 3, number of replaced BF is 30%. Composites 4, 5 and 6 are intended for spar. Composite 4 is made of used CF by way of roving. In composites 5 and 6, CF partially (accordingly, by 20 and 30%) are replaced by BF, again by way of rovings. In all cases, the fabrics manufactured from non-twisted rovings were used.

Fabric from polyacrylonitrile carbon roving has thickness of 0.7 mm; surface density 200-800 g.m^{-2}; density in warp 2.1-3.8 th/cm; density in weft 3.2-4.0 th/cm. The fabric from basalt roving of a thickness of 0.4-0.9 mm has surface density 300-700 g.m^{-2}; density in warp 1.7-3.5 th/cm; density in weft 2.9-4.0 th/cm.

The mode of preparation of composite - prepreg technology (PrT): layer-by-layer lining and forming of prepregs in thermal chamber. The thickness of the composite sheet was 6-8 mm with a density of 1.5g.cm^{-3}.

Short- and long term tests of monolithic samples cut-out from sheets were carried out on bending. Size of samples-scantlings was (150x55x2) mm. Speed of movement of machine's head was 30mm/min. Heating regime of samples was 50 ℃ per hour.

The procedure for determination of the values of the COC for the investigated composites involves the following:

- Determination of the values of breaking stress by standard short-term static testing at room temperature ($\sigma_{sh\text{-}t}$).
- Determination of the values breaking stress at the temperature 293, 310, 330, 360 K.
- Justification of selection of T_0, involving in Eq. (3).

- Calculation of the values of a parameter P for testing temperatures.
- Construction of dependence: "strength-parameter P" with coefficients $\boldsymbol{a}$ and b as illustrated in Eq. (4).
- Calculation of $\sigma_{l\text{-}t}$ for predetermined service life and temperature 330 K.
- Determination of $K_\tau = \sigma_{l-t} / \sigma_{sh-t}$.

To select the values of T_0, that is to say zero strength, the indexes of sharp increase of composites deformation were used. Such approach to determine T_0, in relation to glass plastics, has been previously used in the work published in [7].

Thermo-mechanical curves at various stresses were constructed and the temperature was determined at which a sharp increase of deformation takes place by application to the material the stress tending to zero. As it can be evidently seen from Fig. 4, 510 K can be admitted for T_0.

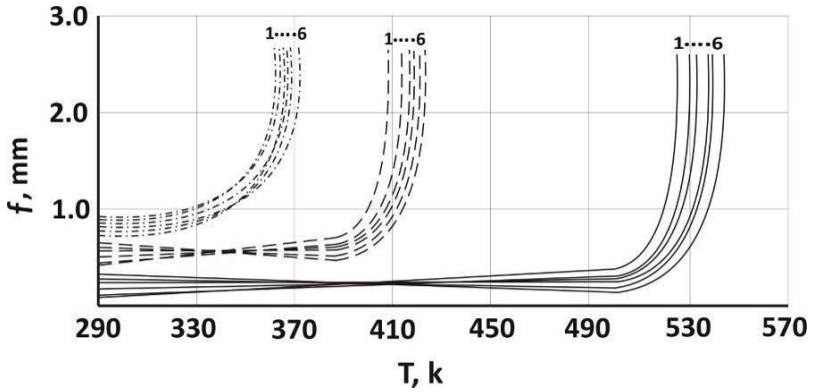

Fig. 4 Thermo-mechanical curves of 1-6 composites at various stresses: ——1 MPa; - - - 60 MPa; — . — . 120 MPa

Table 4 shows the values of short term strength (MPa) and logarithm of time before fracture (sec) of samples of the composites 1-6 at temperatures 293, 310, 330, 360 K. At each temperature, at least 10 samples have been tested. The coefficient of experimental data variation has been changed over the range 9-16%.

TABLE 4 VALUES OF SHORT TERM STRENGTH AND LOGARITHM OF TIME BEFORE FRACTURE OF COMPOSITES

T, k	Composites											
	1		2		3		4		5		6	
	σ_{sh-t}	$\lg\tau_f$	σ_{sh-t}	$\lg\tau_f$	σ_{sh-t}	$\lg\tau_f$	σ_{sh-t}	$\lg\tau_f$	σ_{sh-t}	$\lg\tau_f$	σ_{sh-t}	$\lg\tau_f$
293	770	2.11	700	1.82	660	1.76	911	1.86	801	1.76	755	1.66
310	690	1.86	660	1.79	600	1.71	818	1.34	750	1.05	665	1.11
330	620	1.33	580	1.26	555	1.20	746	1.00	680	1.07	601	0.99
360	590	0.91	565	0.85	503	0.76	650	0.96	580	0.85	532	0.76

Based on these data, by using of found value of T_0, parametric curves are built and shown in Fig. 5.

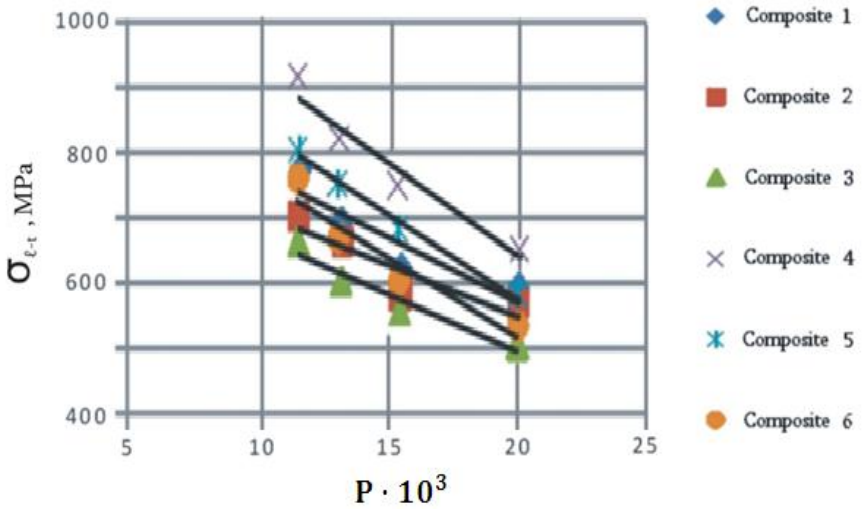

Fig. 5 Parametric straight line for composites 1-6

Table 5 shows the values of coefficients a and b expressed by Eq. (4) resulted from statistical treatment of experimental data.

TABLE 5 VALUES OF COEFFICIENT A AND B

Coefficients	Composites					
	1	**2**	**3**	**4**	**5**	**6**
a	981.4	936.0	936.6	1115.0	1132.0	1111.0
b	-0.014	-0.018	-0.021	-0.018	-0.024	-0.025

Coefficients of correlation characterizing level of linear connections $\sigma_{\ell-t}$ and *P* for the composites 1-6, accordingly are as follows: 0.980; 0.828; 0.933; 0.980; 0.989 and 0.910.

At expected operation life of turbine blades 300 000 hours, in conditions of temperature influence 330K, calculated acc. to Eq (3) P=23800. Required blades of COC materials, identified acc. to Eq. (1) are recapitulated in Table 6:

TABLE 6 THE COC OF COMPOSITES 1-6

COC	Composites					
	1	**2**	**3**	**4**	**5**	**6**
K_t^T	0.80	0.68	0.62	0.75	0.66	0.62

Thus, according to these calculations, sufficiently long-term time of exploitation of a wind turbine's blade at possible elevated temperature, can reduce COC up to certain level, however, such reduction is not significantly enough to lose operating capacity of the blades working on bending.

V. TESTING OF COMPOSITES UNDER DYNAMIC LOADS

At Prepreg Technology (PrT), the layers of preliminary impregnated belts prepared from the fibers of given orientation were collected into package and pressed in thermal chamber.

In the composite of series 1, only high-strength and high-modulus carbon fibers are located in parallel and at an angle of 45^0 to X-axis (Fig. 6). In the composite of series 2, the carbon fiber of the same location of the fibers – 20% is replaced by high-strength basalt fiber. In the composite of series 3, the content of basalt fiber is increased to 40%.

Composites have the following characteristics: density 1.49-1.55 g.cm^{-2}; porosity 9.2-9.7%; phase concentrations: of matrix 61.1-67.0%, of fibers 38.9-43.0%. The samples dedicated for testing on cyclic twisting followed by their testing on tension represent the right-angled strips of (160x15x2) mm size, cut from the composite plates in parallel to X-axis.

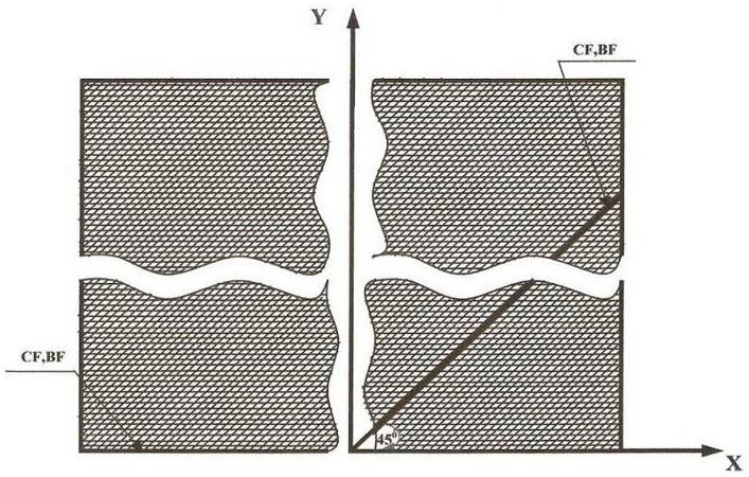

Fig. 6 Scheme of arrangement of reinforcing elements in composite

For composite testing on twisting, the machine equipped by exciter of cyclic displacements was used (Fig. 7). Range of amplitude variation of the displacements: 0-16 mm, the limit of permissible error ± 0.02 mm at maximum amplitude of the displacements. Excitation frequency in this case comprised 90 min^{-1}. The angle of alternating twisting of the samples comprised 20 °at the testing.

Essence of the method involves the determination of the endurance factor of the material operating alternately on twisting. Under the endurance factor, the ratio between composite residual strength after cyclic testing and its short-term static strength is meant. The level of this ratio, at which it slightly reduces regardless of the number of cycles, is taken as the endurance factor.

The results of the testing of the composites on endurance at twisting are presented in Fig. 8. Experimental points are obtained as the samples pass the definite number of the cycles on twisting (10^3, 10^4, 10^5 and etc.) and after the determination of residual strength of these samples at short-term tension.

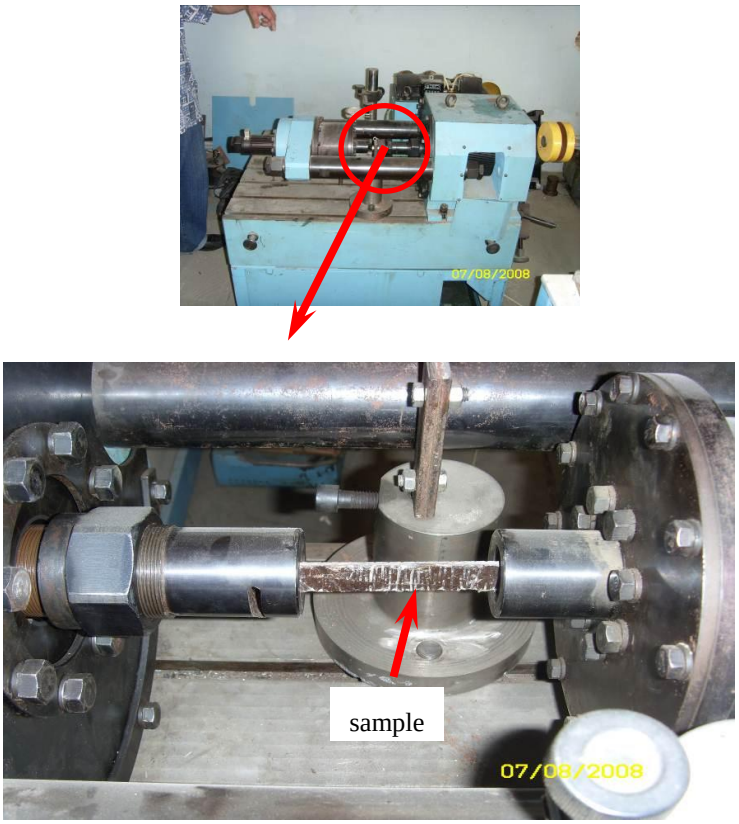

Fig. 7 The Machine for testing on twisting

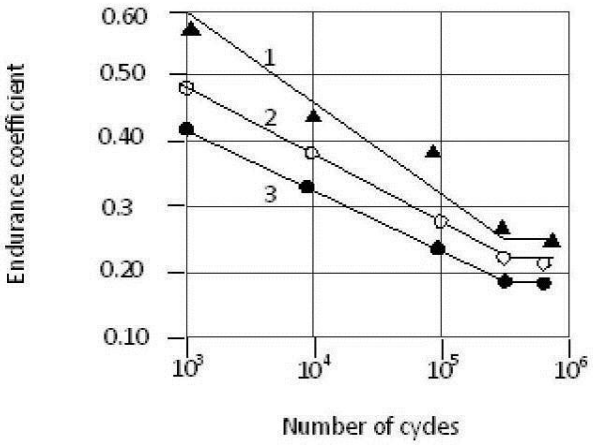

Fig. 8 Endurance of composites 1, 2 and 3

From the plot illustrated by Fig. 8, it should be concluded that after about 5.10^5 cycles twisting the further decrease of material strength is not observed. Endurance coefficients for the composites 1, 2, 3 are 0.25; 0.22; 0.18, respectively. It should be added that endurance coefficient of the composites depends on a type of matrix and technological regimes of their production. Under PrT, maximum values of endurance coefficient are observed in the composites on more plastic matrix.

VI. CONCLUSIONS

1. At present a sufficient experience is accumulated in world practice in the field of the technology of preparation of basalt plastics and composite materials with reinforcing structures from hybrid fibers. In parallel with it, it should be noted that at present the data for physical-mechanical properties of basalt plastics and composites on the basis of hybrid fibers as well as for variation of these properties in expected operating conditions are extremely limited, which retards their use as structural materials.

2. By addition of silicon carbide to epoxy resin in amount of 7% from a resin mass, an increase of static strength and modulus of elasticity may be attained by 11 and 24%, respectively. An addition of basalt powder to a resin in same amount leads to the increase of a strength and modulus of elasticity by 15 and 25%, respectively. From these data, an effect of the

reinforcement of epoxy resin by basalt powder deserves an attention, since basalt is a most non-scarce and cheap reinforcer for resin.

As a result of cyclic alternating loading (by frequency 100 min^{-1}) of composition samples, containing silicon carbide and basalt powder, on bending at an angles of 20^{o}, their endurance coefficient is in the range of 0.21 - 0.24.

3. Endurance coefficient on twisting of composites based on epoxy matrix and high-strength, high-modulus carbon fiber is 0.25. In the composite, partial substitution of basalt fiber (20%, 30%) for carbon fiber causes reduction of endurance coefficient up to 0.22 and 0.18, accordingly. Thus, at partial substitution of basalt fiber for carbon fiber, the composites retain operability at alternating cyclic twisting.

4. The proposed exploitation time of a wind turbine at elevated temperature (up to 330 K) estimated of for 35 years, causes reduction of COC on bending of composites based on epoxy matrix, carbon and glass fibers being considered in present work of structures up to 0.75.....0.80.

At the same conditions, it is expected reduction of COC of composites with hybrid reinforcement (carbon, glass, basalt). However, at the above mentioned significant duration of materials' exploitation, such reduction of COC is quite acceptable. It can be recommended partial substitution (up to 20-30%) of basalt fibers for expensive and deficit high-strength and high-module carbon fiber at manufacturing of wind turbine blades. Herewith, COC of material is not decreased below 0.62.

The obtained values of COC of composites based on epoxy matrix and hybrid fibers can be recommended for estimation on strength of constructions of wind turbine blades, as well as constructions with other functions working at the same conditions.

REFERENCES

[1] P. Bronds, H. Lilhopt, A. Lystrup: *Annual Review of Materials Research*, vol. 35, pp.505-538, 2005.

[2] J. M. Park, W. G. Shin, D. J. Yoon: *Composites Science and Technology*, v. 59, 1.3, pp. 355-370, Feb. 1999.

[3] Yu. M. Tarnopolski, A. M. Skudra. Structural strength and deformability of glass reinforced plastics. Zinatne, Riga, 1966 (Конструкционная прочность и деформативность стеклопластиков, Зинатне, Рига, 1966).

[4] D. A. Griffin: SAND 2002-1879, vol. I, Albuquerque, NM: Sandia National Laboratories, 2002.

[5] D. A. Griffin, T. D. Aswill: *Proceedings of the 48 International SAMPE Symposium and Exhibition*. Long Beach, CA, 2003.

[6] D. A. Griffin: SAND 2004-0073, vol. II, Sandia National Laboratories, 2004.

[7] V. I. Alperin. Constructional glass reinforced plastics. Publisher "Khimia", M, 1979 (Конструкционные стеклопластики. Изд-во «Химия», М. 1979).

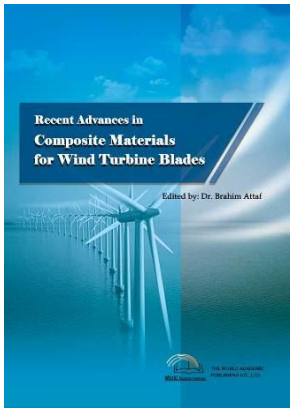

Recent Advances in Composite Materials for Wind Turbine Blades
Edited by Dr. Brahim Attaf

ISBN 978-0-9889190-0-6

Hard cover, 232 pages

Publisher: The World Academic Publishing Co. Ltd.

Published in printed edition: 20, December 2013

Published online: 20, December 2013

This book of science and technology provides an overview of recent research activities on the application of fibre-reinforced composite materials used in wind turbine blades. Great emphasis was given to the work of scientists, researchers and industrialists who are active in the field and to the latest developments achieved in new materials, manufacturing processes, architectures, aerodynamics, optimum design, testing techniques, etc.. These innovative topics will open up great perspectives for the development of large scale blades for on- and off-shore applications. In addition, the variety of the presented chapters will offer readers access to global studies of research & innovation, technology transfer and dissemination of results and will respond effectively to issues related to improving the energy efficiency strategy for 2020 and the longer term.

How to cite this book chapter

Chikhradze N. and Abashidze G. (2013). Investigation of Polymer Composites for Wind Turbine Blades, *Recent Advances in Composite Materials for Wind Turbines Blades*, Dr. Brahim Attaf (Ed.), ISBN 978-0-9889190-0-6, WAP-AMSA, Available from: http://www.academicpub.org/amsa/chapterInfo.aspx

World Academic Publishing - Advances in Materials Science and Applications

Chapter 12

Study of Composite and Sandwich Plates Extracted from Wind Turbine Blade Structures under Harsh Environmental Conditions

Bong Taek Oh

Mechanical Design Engineering, ChungNam National University/Adjunct Professor
CEO, TOMS Co., LTD. /Center for Composite Materials
296-3 Seonjin-li Sachun-si Gyeonsangnam-do Rm.317 Seoul, Korea
btoh@tomskorea.kr

I. INTRODUCTION

For current reliability and safety standards, the efficiency of a wind turbine plant depends mainly on the capacity of the rotor blades to extract energy from the incoming wind. Because of strong competition from other energy sources, wind turbines must be cost-effective. In determining their cost, material selection and manufacturing processes are crucial. Modern wind turbine blades are constructed with fiber-reinforced plastics (FRP) owing to their superior strength-to-weight ratio. Most wind turbines, both large and small, have the same basic parts: blades, shafts, gears, generator, and a cable. These components work together to convert the wind energy into electricity. As we know wind turbines detain the most energy using the propeller-like blades. So the blades are the most important parts of a wind turbine. The cost to manufacture a wind turbine blade is about 15–20% of the turbine's total production cost. In order to increase their energy conversion efficiency, the size of blades have becomes larger, blade diameters ranging from 20 to 100 meters or more [1]. However, these lager blades are encountering harsher and more complex service environments, which have led to several safety problems. The blades can be damaged by moisture absorption, sleet, ultraviolet radiation, atmospheric corrosion, fatigue, wind gusts, or lightning strikes, to name a few hazards. Wind turbine blade failure is very costly because it can damage other blades, the turbine itself, and other turbines located in neighborhood [1]. Clearly, it is important to detect any damage before it leads to catastrophic blade failure.

II. TRANSIENT THERMAL STRESS ANALYSIS OF LAMINATED COMPOSITE

Because wind speed generally increases by 0.1m/s per 100m of altitude for the first 1000m, high altitudes are often the best sites for wind farms. However, wind farms located at high altitudes in cold regions often face icing conditions during the winter. Icing happens when supercooled water droplets hit a surface colder than 0 ℃ and freeze upon impact. To understand the behaviour of wind turbine blades under these conditions, transient analysis for composite structure under low temperature is needed [2-3].

A. Transient Thermal Analysis Model

Transient thermal stress analysis was performed using finite element analysis to analyze the thermal stress distribution of a cryogenic composite immersed in liquid nitrogen (LN_2, -196 °C). The representative volume elements and configuration of cryogenic composite are shown in Fig. 1(a) and (b). Fig. 1(a) shows the global and material coordinate systems of composite laminate. The x-y-z axis will designate the global coordinate of a composite piece. Each layer in that composite may have different fiber orientation that will require a separate coordinate system. The direction along the fiber is designated by 1-direction while the direction transverse to it is designated by 2-direction or the matrix direction. The x-y-z and 1-2-3 coordinate systems coincide in the case of uniaxial composite [4].

The temperature distribution can be obtained by solving the transient heat transfer equation for each material point in the laminate for each ply. Eq. (1) can be obtained by considering the uncoupled theory (neglecting the effect of linear thermal expansion coefficient) and no internal heat generation in the heat equation [5].

$$\rho c_p \frac{\partial T}{\partial t} - k_{ij} T_{,ji} = 0 \qquad \text{where } i, j = x, y, z \tag{1}$$

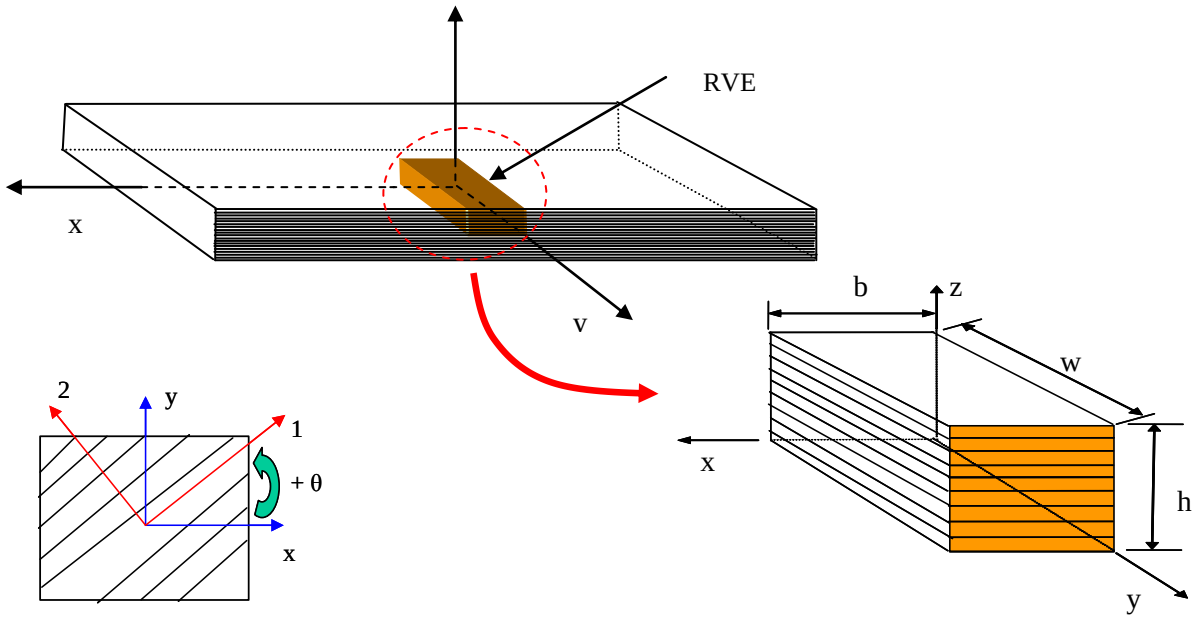

(a) Representative volume element (b) Specimen configuration

Fig. 1 Representative volume element and configuration of a symmetric composite laminate

where k_{ij}, T, ρ and C_p are second-order thermal conductivity tensor, temperature, density and specific heat, respectively. The planes $x = 0$, $x = b$, $y = 0$ and $z = 0$ are assumed to be fully insulated:

$$\frac{\partial T}{\partial n} = 0 \qquad \text{at } x = 0,\ x = b,\ y = 0,\ \text{and } z = 0 \tag{2}$$

where n is the unit normal vector to the respective plane.

The planes $y = w$ and $z = h$ are maintained at -196 °C, that is:

$$T(x, w, z) = T(x, y, h) = -196°C \tag{3}$$

Based on the temperature distribution at every time step of the analysis, the static stress can be calculated using the balance of linear momentum. The dynamic effects are neglected since the time scale is much smaller than the characteristic time for transient heat transfer.

$$\sigma_{ij,j} = 0 \qquad \text{where } i, j = x, y, z \tag{4}$$

where σ_{ij} is the second-order stress tensor. The one-way coupling with the thermal field enters through the constitutive equation for a linear thermoelastic solid:

$$\sigma_{ij} = C_{ijmn}\{\varepsilon_{mn} - \alpha_{mn}\Delta T\} \qquad \text{where } i, j, m, n = x, y, z \tag{5}$$

where $\varepsilon_{mn} = \frac{1}{2}(u_{i,j} + u_{j,i})$; C_{ijmn}, α_{mn}, and u_i are fourth-order elastic stiffness tensor, second-order thermal expansion coefficient tensor, and displacement vector, respectively. Substituting Eq. (5) into Eq. (4), one obtains the following field equation:

$$C_{ijmn}\, u_{m,nj} = C_{ijmn}\, \alpha_{mn}\, T_{,j} \qquad \text{where } i, j, m, n = x, y, z \tag{6}$$

Because of symmetries in the geometric domain shown in Fig. 2, only half of the total numbers of plies were modeled through the thickness, also half of width was modeled through the x-direction. The boundary conditions on the plane $y = 0$ and $z = 0$ can be expressed as follows

$$u_y(x, 0, z) = 0,\ u_z(x, y, 0) = 0 \tag{7}$$

where u_x and u_z are the displacement in the x and z directions, respectively. Due to the periodicity in the *y*-direction, periodic boundary conditions were applied on the planes $x = 0$ and $x = b$ as follows:

$$u_x(0, y, z) = u_x(b, y, z) + < \frac{\partial u_x}{\partial x} > b$$
$$u_y(0, y, z) = u_y(b, y, z) + < \frac{\partial u_y}{\partial x} > b \quad (8)$$
$$u_z(0, y, z) = u_z(b, y, z) + < \frac{\partial u_z}{\partial x} > b$$

where u_x, u_y, and u_z are the displacements in the x, y, and z directions, respectively. The volume averaged displacement gradients, $< \frac{\partial u_x}{\partial x} >$, $< \frac{\partial u_y}{\partial x} >$, and $< \frac{\partial u_z}{\partial x} >$, were treated as unknowns in the finite element analysis, and determined while solving. The planes $y = w$ and $z = h$ have zero traction boundary conditions.

B. Effect of Laminate Thickness

To study the effect of total laminate thickness, symmetric laminates with stacking sequences $[0/-45/90/45/0/45/90/-45/0]_s$ and $[0/-45/90/45/0]_s$ have been adapted for transient analysis of IM7/977-2. As it can be seen from Figs. 2 and 3 that the thicker laminate has higher stress pattern than thinner laminate has.

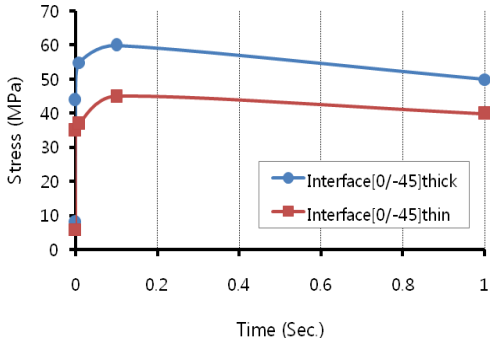

Fig. 2 Out-of-plane stress on surface ply under thermal loading for a $[0/-45/90/45/0/45/90/-45/0]_s$ and $[0/-45/90/45/0]_s$ laminates of IM7/977-2 as a function of time

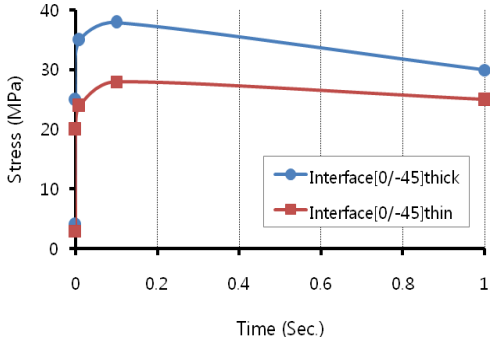

Fig. 3 Out-of-plane stress on surface ply under thermal loading for a $[0/-45/90/45/0/45/90/-45/0]_s$ with 250 μm and 125 μm ply thickness of IM7/5250-4 as a function of time

C. Effect of Ply Thickness

The effect of ply thickness on the free-edge under thermal loading as a function of time was inspected. The thicker ply has higher in-plane stress σ_{22} at the peak point in the stress curve in a very short time. Even higher ply level stress at the peak point in the stress curve was observed for out-of-plane stress σ_{33}, which may cause the delamination on the free-edge. The ply with 250 μm thickness has twice higher out-of-plane stress in a very short time than the ply with 62.5 μm thickness. To reduce the effect of thermal shock, which may cause the delamination, the high peak point stress should be suppressed. The methodology for suppressing the free-edge delamination was investigated in the next section.

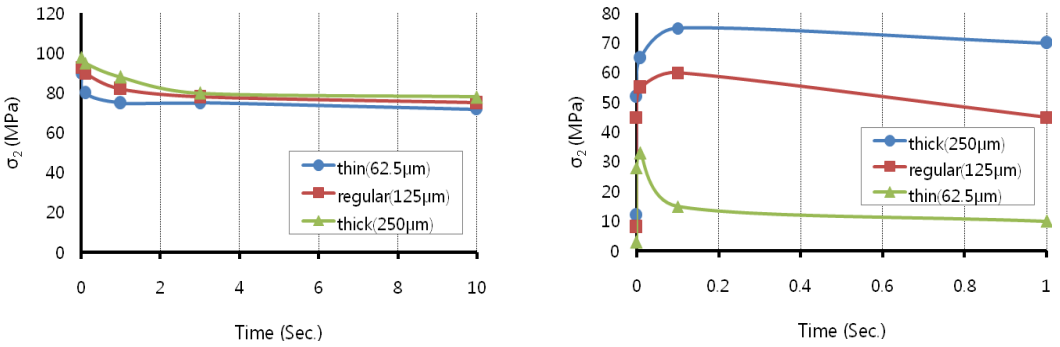

(a) In-plane stress (b) Out-of-plane stress

Fig. 4 Effect of ply thickness on the free-edge under thermal loading for a $[0/-45/90/45/0/45/90/-45/0]_s$ of an IM7/977-2 laminate as a function of time

D. Effect of Insulation Layer

A further investigation of the sudden exposure to cryogenic temperatures was conducted numerically. A lay-up, $[90_2/0_2]_S$, of IM7/5250-4 with and without insulating layer was used for the study of insulation layer on thermal shock. The transient thermomechanical analysis with and without insulation layer was performed using FEA model. In order to reduce the thermal shock, an insulating layer was added to the surface of IM7/5250-4 composite laminate with $[90_2/0_2]_S$. The thermal conductivity of the insulating layer was taken to be about 3 times less than the thermal transverse conductivity of the IM7/5250-4 laminate. Fig. 5 shows the out-of-plane stress distributions without insulation after 0.1, 1, and 20 seconds. Stress distributions with insulation layer after 0.1, 1, 120, and 1800 seconds are shown in Fig. 6. Thickness of the insulating layer was 3mm. Ply level stresses in the laminate without the insulation decreased and saturated after 20 seconds. However, the stresses in the laminate with the insulation increased and saturated after 1800 seconds. Both with and without insulation cases converged to 10 MPa of maximum stress σ_{33} in 90 °ply (Ply 2) as expected.

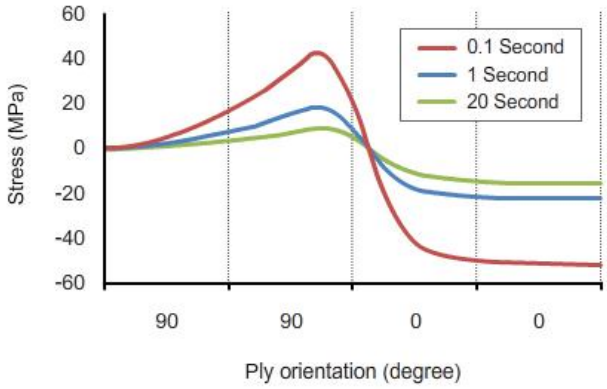

Fig. 5 Stress σ_{33} distributions under thermal loading after 0.1; 1 and 20 seconds without insulation for a $[90_2/0_2]_S$ of an IM7/5250-4 composite laminate

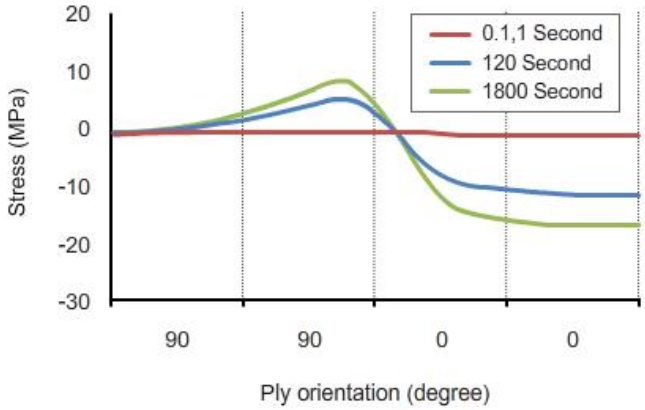

Fig. 6 Stress σ_{33} distributions under thermal loading after 0.1; 1; 120 and 1800 seconds with insulation (3mm) for a $[90_2/0_2]s$ of an IM7/5250-4 composite laminate.

A plot of the maximum value of σ_{33} in 90 °ply (ply 2) as a function of time is shown in Fig. 7 to identify the effect of time and insulation layer.

The peak point in the stress curve (Fig. 7a) was observed for the model without insulation in a very short time. Maximum stress σ_{33} without insulation goes up to 40 MPa, which is 4 times higher than saturated maximum stress (10 MPa), in a very short time. However, there is no peak point in the stress curve for the model with insulation layer (Fig. 7b). The maximum stress in the z-direction, σ_{33}, increased gradually. The peak point in stress curve for the model without insulating layer may have caused edge delaminations in cryogenic composite laminates. Hence, ply-level stress σ_{33} on the free-edges due to thermal shock can be reduced by introducing the insulation layer. Experimental work is needed to compare and verify numerical results for the effect of thermal shock in cryogenic composite laminates. Future study will be focused on the damage characterization on the edge of cryogenic composite laminates with and without insulation layer.

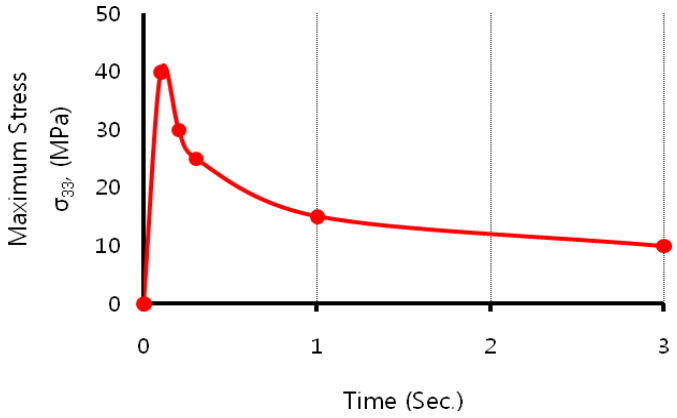

(a) without insulation

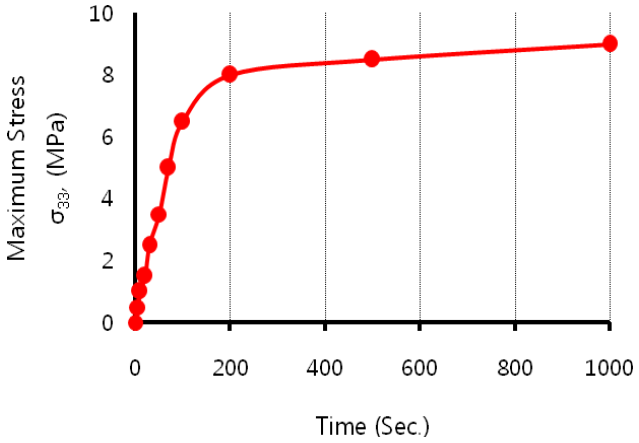

(b) with insulation

Fig. 7 Maximum stresses σ_{33} on 90 °ply as a function of time of an IM7/5250-4 composite laminate

III. DAMAGE CHARACTERIZATION IN COMPOSITES FOR WIND TURBINE BLADES UNDER HARSH ENVIRONMENT

A. Experimental Apparatus and Materials

Pictures of the thermomechanical test system for thermal cycling, uniaxial tension and four-point bending test are shown in Fig. 8(a)-(c), respectively. A high density polyethylene cryogenic dewar shown in Fig. 8(a) was used for the thermal cycles and an MTS 880 Materials Test System was used for the mechanical loading of the composite laminates tested at both room and cryogenic temperatures. Fig. 8(b) shows the custom designed cryogenic chamber for uniaxial tension test, which was mounted on the MTS 880 frame. Since steel has a relatively low thermal conductivity at cryogenic temperatures, the chamber was built of stainless steel. An aluminum foil insulator was added around the chamber in order to improve insulation. A four-point bending test fixture, as shown in Fig. 8(c), for cryogenic environment was developed for small specimens (15 cm in length, 2.54 cm in width). This test was designed to facilitate the study of damage development under variable stress states as is often the case in cryogenic tanks and permeability experiments under load.

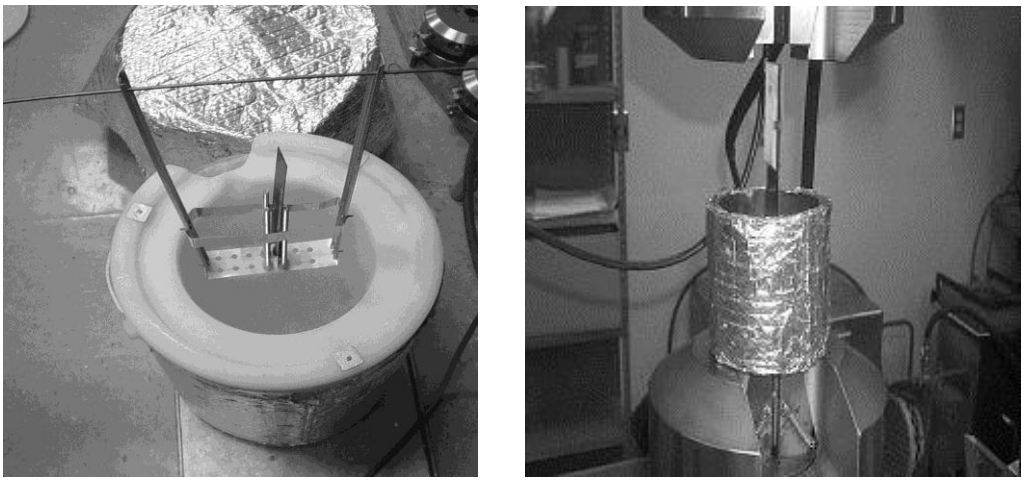

(a) (b)

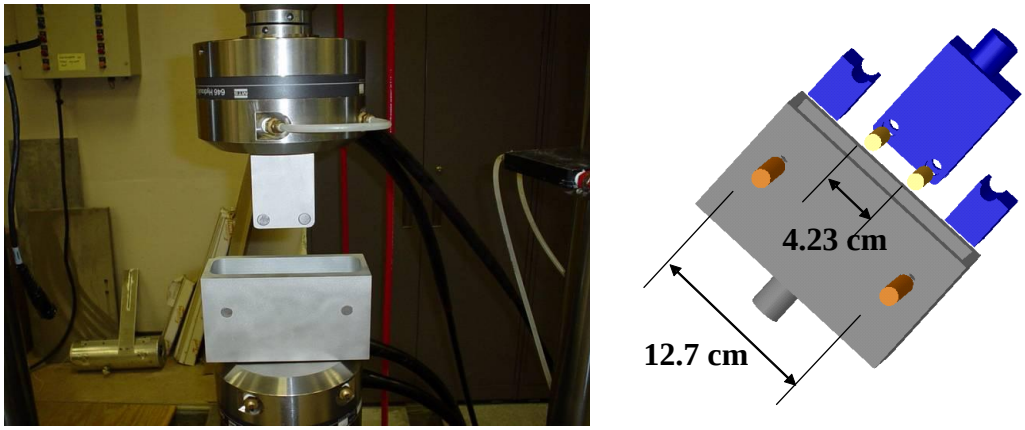

(c)

Fig. 8 Experimental apparatus: (a) cryogenic dewar, (b) cryostat system mounted on an MTS 880 frame and (c) four-point bending test apparatus.

The specimens for both uniaxial tension and four-point bending test were provided by Lockheed Martin and Air Force Research Laboratory (AFRL), respectively. The specimens for uniaxial tension test as shown in Fig. 9(a) were 18-ply graphite epoxy IM7/977-2 laminates with $[0/-45/90/45/0/-45/90/45/0]_S$ stacking sequence, and with dimensions of 15.24 cm [6”] (gage length) x 9.144 cm [3.6”] (width) x 0.225 cm [0.088”] (thickness). The specimens had undergone prior thermomechanical testing, including thermal cycles from room temperature to liquid nitrogen (-196°C) and mechanical cycles at cryogenic temperatures (-196°C). From the specimens received, they were tested under additional thermomechanical loading. For the thermomechanical loading tests, the original specimens were cut into three pieces (A, B and C), as illustrated in Fig. 9(a). The specimens for four-point bending test and thermal shock test as shown in Figs. 9(b) and (c) were 8-ply graphite epoxy IM7/5250-4 laminates with $[90_2/0_2]_S$ stacking sequence. Thermomechanical effective properties for both material systems were found in the literature [6-8].

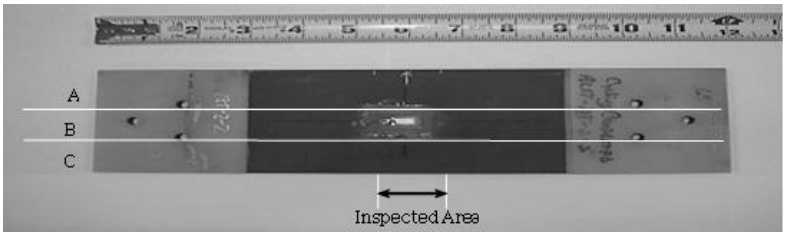

(a)

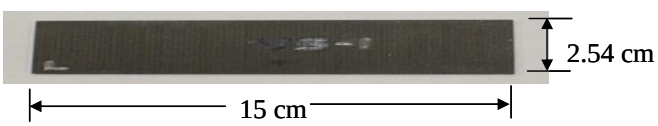

(b)

(c)

Fig. 9 Cryogenic composite laminates: (a) IM7/977-2, (b) IM7/5250-4, (c) IM7/5250-4 without insulation (left) and with insulation (right).

B. Thermomechanical Cycles

Thermal loading usually consists of cycling between room or a higher temperature and a cryogenic temperature (most often liquid nitrogen, i.e. –196°C). Mechanical loading typically takes place at cryogenic temperatures, with an applied maximum stress level being a portion of the ultimate strength. Combined thermal cyclic loading (room temperature to -196°C) and mechanical loading at -196°C and room temperature are performed on cryogenic composite laminates for the uniaxial tension test. More specifically, thermal cycling (room temperature to -196°C) in the absence of mechanical load, thermal cycling followed by mechanical cycling at room temperature, and mechanical cycling at cryogenic temperatures as well as mechanical loading at room temperature are the loading paths that have been investigated as shown in Fig. 10 for 18-ply graphite epoxy IM7/977-2 laminates with $[0/-45/90/45/0/-45/90/45/0]_S$ stacking sequence. First, a laminate specimen was mechanically tested at room temperature in uniaxial tension to failure in order to determine the Young's modulus and ultimate tensile strength.

During the mechanical loading, the stress and strain values were obtained. The strain values were calculated by using the cross-head displacement, while the stress values were determined from a load cell attached on the cross-head. The Young's modulus and ultimate tensile strength were determined to be 61.2 GPa and 787.02 MPa, respectively. Then, a second laminate was cut into three pieces from the original specimen shown in Fig. 9(a), and machined with a dimension of 25.4 cm x 2.54 cm (10" x 1") according to ASTM standards, D3039/3039M-00 recommendation. Three specimens were tested with three loading paths as shown in Fig. 3.

IM7/5250-4 laminates with $[90_2/0_2]_S$ stacking sequence was cycled using four-point bending test system. The first and second specimens underwent four-point bending test at room temperature (RT), and the third specimen was subjected four-point bending test at -196 ℃. However, higher bending moment was applied to the second specimen at RT. A bending moment of 0.573 $N{\cdot}m$ was applied to first and third specimens, which results to a maximum tensile stress equal to 40% of the ultimate tensile strength on the outer 90 ° ply. For the second specimen, a bending moment of 1.21 $N{\cdot}m$ was applied so that the maximum tensile stress on the 90 ° ply is the same with the maximum tensile stress used by a combined mechanical and thermal loading.

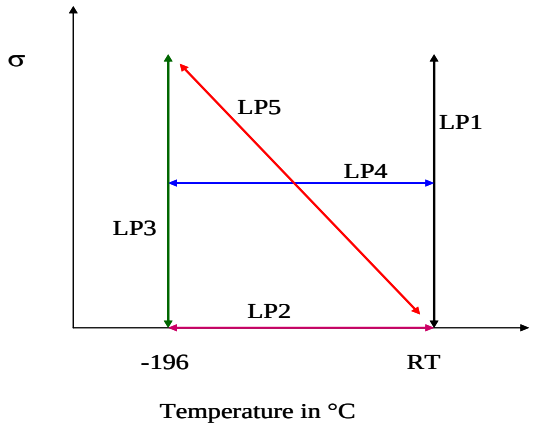

Fig. 10 Various thermomechanical loading paths

C. Damage Analysis (Microcrack Density)

In this section, the experimental work on characterization of damage developed during thermomechanical cycling of cryogenic composite laminates will be discussed. Some researchers [9-12] have studied the damage evolution of cryogenic composites by applying different types of thermomechanical loading. This section is focused on damage analysis of cryogenic composite laminates subjected to thermomechanical load. The attention is given to the local multiaxial stress field (along the fibers direction) which is generated in the material and that is due to the orthotropic behavior. In composite materials, especially under fatigue loading, the presence of a multiple cracking condition is common; for this reason in order to evaluate the damage evolution it is very useful to consider the crack density as controlling parameter. In this section, only the transverse matrix crack was counted for crack density. The crack density is parameterized by summing over all plies the number of cracks in each ply per unit length on free-edge.

The three specimens for uniaxial tension test, indicated as A, B, and C in Fig. 9(a), were characterized for damage before any loading cycle was applied. Cracks were counted in each non-zero degree ply along a 32 mm (1.26") span centered lengthwise on each specimen. Specimen A underwent a total of 20 thermal cycles. Specimen B was subjected to two thermal cycles followed by two mechanical cycles at 60% of the ultimate tensile strength at room temperature. The four cycles were repeated three times, and the specimen was inspected after each mechanical and thermal loading cycle. Mechanical loading at cryogenic temperatures was applied to specimen C. More specifically, specimen C was immersed for 30 minutes in liquid nitrogen to guarantee that it had reached the same temperature as liquid nitrogen. Subsequently, the specimen was mechanically loaded while still being held in the liquid nitrogen, but the test was terminated early due to delamination reaching the grips. The specimen was examined using an optical microscope to collect damage state information, such as crack density for each ply and delamination length occurring at interfaces between plies. Fig. 11 shows the crack densities of the second ply from the outer surface [-45 °], and their increase with the number of loading cycles for specimens A, B, and C, respectively.

Similar trend in the rate of crack density growth has been observed in the third ply [90 °] of the specimens tested. The zero in the horizontal axis describes the initial state of each specimen, while each cycle on the graph corresponds to two physical cycles, either mechanical or thermal. When thermal cycles (specimen A) alone were applied, there were no additional cracks in the material up to 20 cycles. However, thermal cycling, followed by mechanical cycling at room temperature (specimen B), resulted in a rapid increase of microcracking induced damage, which saturated after it reached a level of about eight times the initial damage. Even higher rate of increase of damage densities was observed in specimen C, which was mechanically cycled at cryogenic temperatures, but delamination at the grips resulted in termination of the experiment.

The three specimens for four-point bending test, indicated as LP-A, B, and C in Fig. 12, were characterized for damage before any loading cycle was applied. Cracks were counted in each 90 degree ply along a 25.4 mm (1.0") span centered lengthwise on each specimen. Specimen LP-A underwent a total of 840 four-point bending test at room temperature. Specimen LP-B was subjected to higher bending moment at room temperature. The bending moment was applied to specimen LP-C at cryogenic temperature. The damage information was collected using the optical microscope for every 5 cycle.

Fig. 12 shows the crack density on the first ply from the outer 90 °ply, and their increase with the number of loading cycles for mechanical loadings at RT and -196 ℃, respectively. No cracking occurred up to 500 cycles for four-point bending test with the bending moment of 0.573 N·m at RT. However, four-point bending test at -196 ℃ resulted in TMC after 10 cycles. Higher bending moment was applied to verify if the cracks resulted due to the difference of ply level stress. After 10 cycles, the second specimen had almost the same crack densities with four-point bending test at -196 ℃. However it had about half the crack density after 30 cycles. The brittle nature of the specimen under cryogenic temperatures could be the cause for this difference. Results presented in [13-14] show the influence of cryogenic service temperatures on the strength, modulus, and fracture of IM7/977-3, a toughened graphite/epoxy. It was reported that the material becomes very brittle and the strength and modulus change at cryogenic temperature.

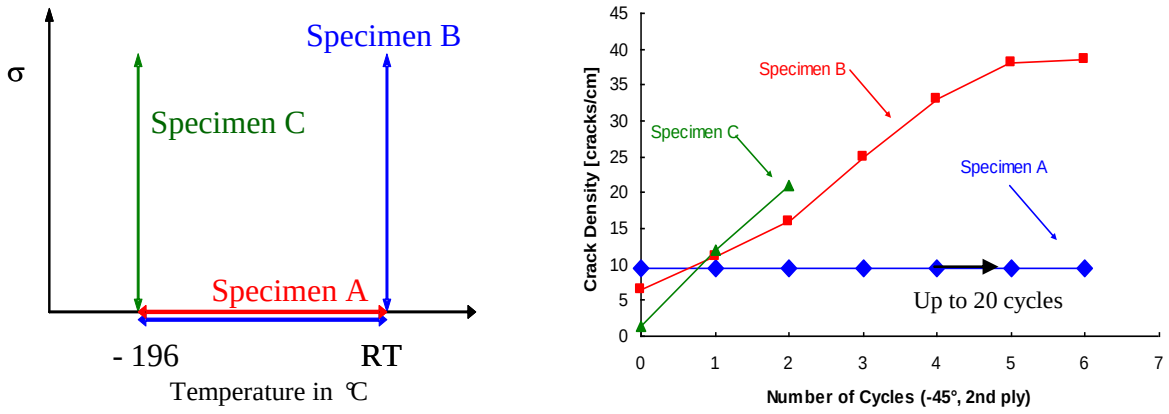

Fig. 11 Micro-crack density versus number of cycles for the [–45 °] ply (second from outer surface) of IM7/977-2 laminates with $[0/-45/90/45/0/-45/90/45/0]_S$ under uniaxial tension loading

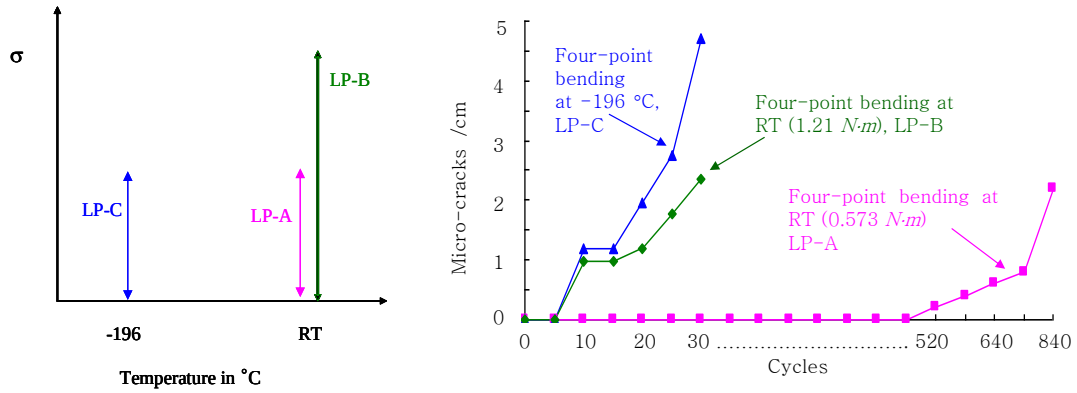

Fig. 12 Micro-crack density versus number of cycles for the [90 ¶ ply of IM7/5250-4 laminates with $[90_2/0_2]_S$ under four-point bending

Fig. 13 shows typical optical micrographs taken in the middle of the specimen edge at the end of the loading cycles. The initial damage state, which is the damage of specimen A, is shown in Fig. 13(a). The damage state after twelve loading cycles for specimen B and four mechanical cycles at cryogenic temperature for specimen C are shown in Figs. 13(b) and 13(c), respectively. Cracks were found only in plies 2, 3, and 4 in the $[0/-45/90/45/0/-45/90/45/0]_S$ laminate. No cracks were found in plies 15, 16 and 17. This is an unusual case (considering symmetric lay-up of the laminate) and a possible cause can be due to the presence of residual stresses resulting from manufacturing process or stress concentrations at micro cracks in the plies 2, 3 and 4. Delaminations were observed between plies 2-3, and 3-4. The majority of the interface cracks were observed between plies 2-3, as shown in Fig. 13(c).

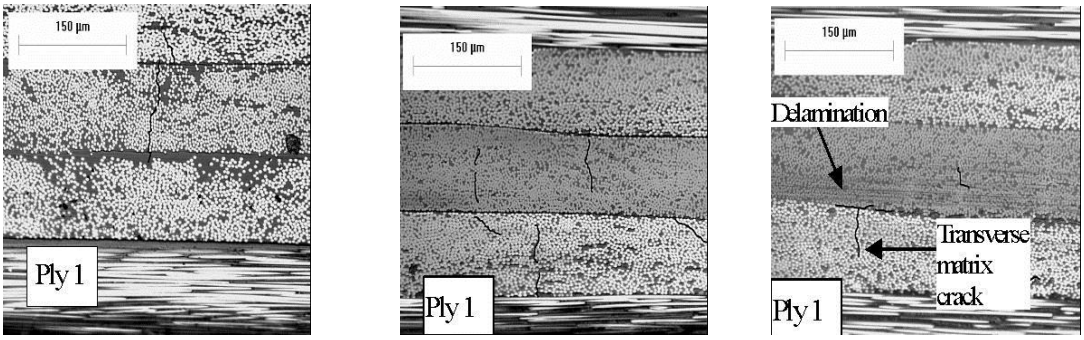

(a) (b) (c)

Fig. 13 Micrographs showing damage under uniaxial tension test: (a) specimen A, (b) specimen B, and (c) specimen C

From the above results, one can conclude that for simultaneous mechanical loading in a cryogenic environment, the chances of delamination and hence leakage is higher than thermal testing followed by mechanical loading at room temperature. Delaminations at transverse crack tips were also observed, which could be more critical for the permeability and leakage problem.

Figs. 14 and 15 show the optical micrographs for the four-point bending tests conducted under different loading paths. The initial state (damage free state), is shown in Fig. 14(a). The damage states after 50 and 520 loading cycles are shown in Fig. 14(b) and 14(c), respectively. Under cryogenic testing, the damage states before and after 10 loading cycles are shown in Fig. 15(a) and 15(b), respectively.

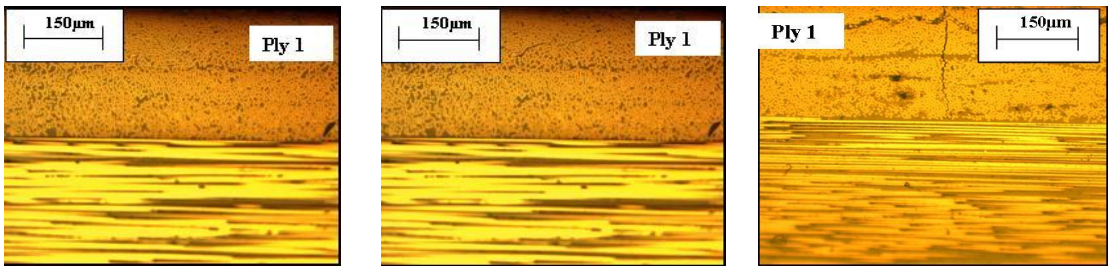

(a) (b) (c)

Fig. 14 Micrographs showing damage under four-point bending test at room temperature:
(a) before testing, (b) after 50 cycles, and (c) after 520 cycles

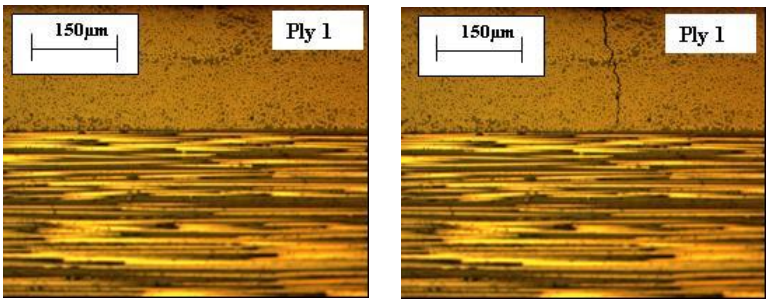

(a) (b)

Fig. 15 Micrographs showing damage under four-point bending test at -196 ℃: (a) before testing and (b) after 10 cycles

After thermomechanical loading cycles, delaminations were observed along the interface on the free-edges. The sudden exposure to cryogenic temperatures may have caused the delaminations and transverse matrix crack (TMC) on the free-edges, due to large temperature variation through the thickness and the resulting thermal stresses. Fig. 16 shows the experimental set-up and surface temperature results for wax insulation. Paraffin wax was used as an insulation material under cryogenic environment. A thermocouple was placed between wax and specimen surface. The surface of the specimen reaches LN2 temperature immediately without insulation, but with 3.5mm paraffin wax insulation it took 60 seconds to reach near LN2 temperature, which substantially reduces the thermal gradient in the laminate.

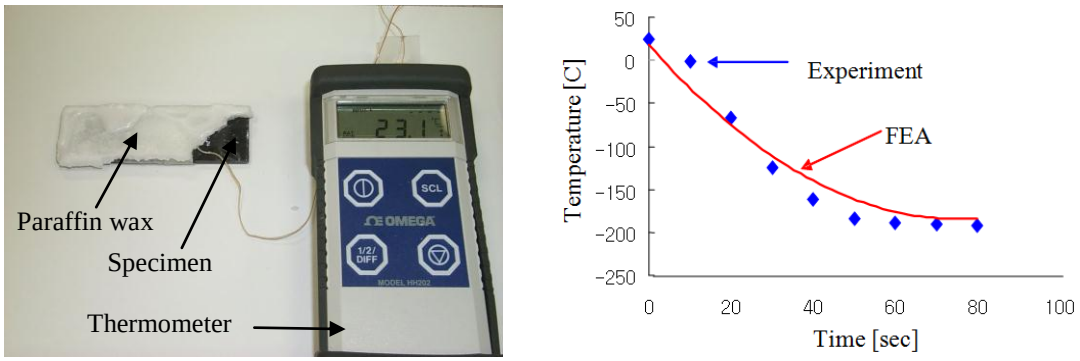

Fig. 16 Experimental set-up and surface temperature result for wax insulation

Thermal cycling was experimentally performed to verify the effect of thermal shock on damage in cryogenic composite laminates. The specimens tested were provided by AFRL, and they were 8-ply graphite epoxy IM7/5250-4 laminates with $[90_2/0_2]_S$ stacking sequence. The two specimens were characterized for the damage state before any loading cycle was applied. The TMC were counted in each 90 degree ply along a 30 mm span centered lengthwise on each specimen. The first specimen without wax insulation underwent a total of 45 thermal cycles, and characterized after every thermal cycle. The second specimen with wax insulation was subjected to a total of 40 thermal cycles. Fig. 17 shows the transverse crack densities of the 90 degree ply, and their increase with the number of loading cycles for the first and second specimens, respectively. When thermal cycles were applied to the second specimen, there were no TMC on the free-edges for 40 cycles. However, the TMC were initiated for the first specimen after 33 thermal cycles. Therefore, TMC observed in the first specimen are from thermal shock but not from thermal cycles. It is possible to remove the thermal shock effect on the edge during cryogenic test using wax insulation.

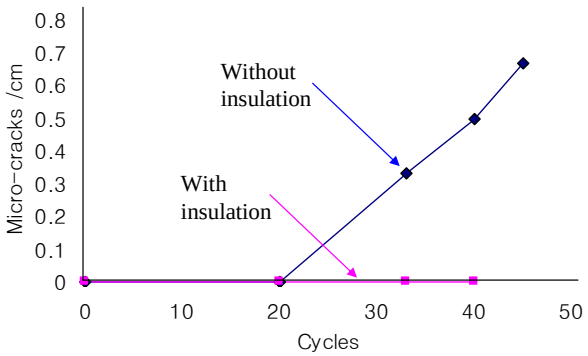

Fig. 17 Crack density vs. number of thermal cycles without and with wax

IV. PREDICTION OF MICROCRACKING

A. *Building RVE (Representative Volume Element) using FE Model*

Most of the analytical work for formation of damage was on transverse matrix cracks. However, initial studies were conducted and are continuing to determine the interaction of transverse matrix cracks and delaminations

In order to simulate cracks occurring in laminates a finite element model for a representative volume element (RVE) was built. The RVE (or unit cell) is defined herein as the smallest region that represents the behavior of the entire region without any mirroring or rotation transformations. Fig. 18(a) shows a laminate with matrix cracks, which are idealized based on the assumptions that the cracks are parallel to the *x1x3*-plane and extend through the entire length and thickness of the ply. The cracks are also assumed to be periodically distributed. Due to the assumptions, periodic boundary conditions are applied to the RVE. The RVE with one crack is extracted from the laminate. A finite element mesh was built for this RVE as shown in Fig. 18(b). The degree of degradation of a cracked laminate is directly related to the crack opening displacements.

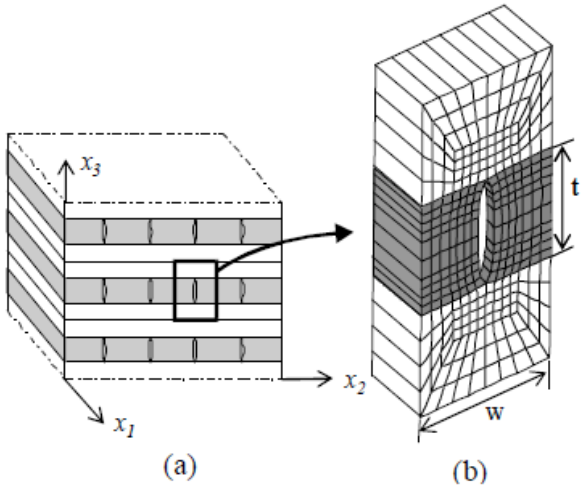

Fig. 18 Modeling a laminate with transeverse matrix cracks (TMC)

B. *Calculating COV (Crack Opening Volume) for a Laminate*

Since the damage level will increase with crack opening volume (COV), it is essential that we understand crack opening and factors that affect the crack opening. One of objectives in the current work is to show that the crack opening volume can be directly related to the degradation behavior of the effective moduli of a cracked ply. A simple expression for the COV will be derived based on the modulus reduction and the volume averaged strain or stress of a cracked ply for a given crack density. The study on the opening will extend to consider the delamination and matrix cracking together.

C. *Modeling of Delamination at the Intersection of Cracks*

Microcracking can lead to other forms of damage such as delamination. Laminate design may have a significant effect on the delamination initiation. A study is also being performed for delaminations that can form near the matrix crack tip.

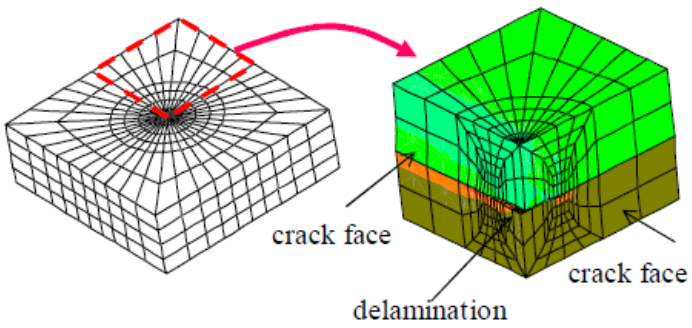

Fig. 19 Modeling of delamination at the intersection of cracks

The strain energy release rate for a delamination at the intersection of matrix cracks (Fig. 19) was calculated. Fig. 19 shows a finite element model with a circular delamination at the crossing matrix cracks. The strain energy release rate has been calculated for various stacking sequences for circular delaminations. Other delamination shapes, which are more realistic, will

be also studied in future work. The opening due to matrix cracks and the delamination at the crossing matrix cracks is currently being investigated. Finite element models were developed and analyzed under axial and biaxial loadings.

V. CONCLUSIONS

Optimal design of composite wind turbine blades requires an analysis that can predict microcracking under harsh environmental conditions. The current work is focused on laying the foundation for such an analysis. This requires experimental techniques to simulate the operating environment for the wind turbine, because this latter undergoes severe loading conditions. The high stress level can be reduced using insulating technique under low temperature, and the design method for lamina and laminate thickness should be considered.

In this chapter, transient thermomechanical finite element analysis was performed to study the effect of thermal shock for composite laminates with different material systems and lay-ups. Higher out-of-plane stresses on the free-edge were found in lay-up 1 for both material systems (IM7/977-2, IM7/5250-4). The IM7/5250-4 has higher out-of-plane stresses on the free-edge under thermal loading than the IM7/977-2 has. Both IM7/977-2 and IM7/5250-4 composite laminates have a peak point in the stress curve in a very short time; however, IM7/977-2 has higher out-of-plane stress at the peak point in the stress curve. The out-of-plane stress on surface ply is considered to be similar for both lay-ups. However, the stress pattern is quite different at very short time. The stress pattern is dramatically changed according to the stacking sequences for both materials, and this is the reason why study for lay-ups should be performed. The stacks starting with 0 ° fibre orientation have better stress pattern than stacks starting with other degrees, and the angle ply laminates have lower stress level than cross play laminates. Optimal design of composite blades requires an analysis that can predict microcracking induced permeability. The current work is focused on laying the foundation for such analysis. This requires the development of experimental techniques to simulate the operating environment for blades. Also, the study of thermal shock effect due to harsh environment needs to be investigated. Actual wind turbine composite blades do not have edges. However, coupon specimens, which are usually used for material testing due to the difficulty of full size testing, have edges. These free-edges could be the reason of edge delaminations during testing of composite laminates. This study examined the ply-level damage accumulated due to cycling IM7/977-2 and IM7/5250-4 cross-ply and angle-ply composite laminates under thermomechanical loadings.

No crack occurred up to 20 thermal cycles for 18-ply graphite epoxy IM7/977-2 laminates with $[0/-45/90/45/0/-45/90/45/0]_S$ stacking sequence. However, thermal cycling followed by the mechanical cycling (uniaxial tension loads) at room temperature, resulted in a rapid increase of microcracking induced damage. The highest rate of increase of damage densities was observed, when the specimen was mechanically cycled (uniaxial tension loads) at low temperatures. After uniaxial tension test at low temperature, delaminations were observed between the -45 ° and 90 ° plies (2nd and 3rd plies from outer surface) as well as 90 ° and 45 ° plies (3rd and 4th plies from outer surface). Delaminations at transverse crack tips were also observed, which could be more critical for the permeability and leakage problem.

No cracks occurred up to 500 cycles for four-point bending test at room temperature for 8-ply graphite epoxy IM7/5250-4 laminates with $[90_2/0_2]_S$ stacking sequence. However, four-point bending test at -196 ℃ resulted in transverse matrix cracks after 10 cycles on 90 degree ply (1st ply from outer surface). The parallel cracks to the specimen length direction for four-point bending test at room temperature were observed after 30 cycles on 90 ° ply. However, transverse matrix cracks were observed after four-point bending test at -196 ℃ on 90 ° ply. The length of cracks for four-point bending test at room temperature was between 12 μm and 50 μm after 30 cycles and increased up to 100 μm after 50 cycles. After 10 cycles for four-point bending test at -196 ℃, 250 μm of crack length was observed.

On applying thermal cycling to the specimen of 8-ply graphite epoxy IM7/5250-4 laminates with $[90_2/0_2]_S$ stacking sequence with wax insulation, the material showed no sign of crack development up to 40 cycles. However, cracks were initiated in the specimen without wax insulation after 33 thermal cycles on 90 ° ply (1st ply from outer surface).

REFERENCES

[1] B. Yang. and D. Sun, “Testing, inspecting and monitoring technologies for wind turbine blades: A survey,” Renewable and Sustainable Energy Reviews 22 (2013) 515-526.

[2] O. Parent and A. Ilinca, “Anti-icing and de-icing techniques for wind turbines: Critical review,” Cold Regions Science and Technology 65 (2011) 88-96.

[3] B. Natarajan et. al., Structural Analysis of Composite Wind Turbine Blade using Advanced Beam Model Approach, International Journal of Precision Engineering and Manufacturing, vol. 13, no. 12, 2245-2250, 2012.

[4] Bong Taek Oh, J. Noh, D. Lagoudas, and J. Whitcomb, Effect of Thermal Shock on Damage in Cryogenic Composite Laminates, 18th Annual Technical Conference American Society for Composites, Gainesville, Florida, Oct. 19-22 (2003).

[5] B. A. Boley and J. H. Weiner, “Theory of Thermal Stress” Dover Pub. Inc.

[6] Mohamed Elseifi, “A New Scheme for the Optimum Design of Stiffed Composite Panels with Geometric Imperfections,” Ph.D. Dissertation, College of Engineering, Virginia Polytechnic Institute and State University, 1998.

[7] Q. Li, L. Minnetyan, C. C. Chamis, “Structural Durability and Fatigue of Composites in Acoustic Environment,” Society for the Advancement of Materials and Process Engineering, Long Beach, CA, May 2002.

[8] S. Venkataraman, "Modeling, Analysis and Optimization of Cylindrical Stiffened Panels for Reusable Launch Vehicles Structures," Ph.D. Dissertation, College of Engineering, University of Florida, 1999.

[9] Robinson MJ et al. "Hydrogen permeability requirements and testing for reusable launch vehicle tanks," Proceedings of the 43rd AIAA/ASME/ASCE/AHS/ASC Structures, Structural Dynamics, and Materials Conference, Denver, CO; 2002. AIAA-2002-1418.

[10] S.S. Kessler, T. Matuszeski and H. McManus. "Cryocycling and Mechanical Testing of CFRP for the X-33 Liquid H_2 Fuel Tank Structure," Proceedings of the American Society for Composites (ASC), Sep. 9-12, 2001, Virginia Tech, Blacksburg.

[11] R. Y. Kim and S. L. Donaldson, Experimental Observation of Microcracking of Composite Laminates under Cryogenic Temperature, AIAA, Aug., 28-30 (2001).

[12] V. T. Bechel, M. B. Fredin, and S. L. Donaldson. "Combined Cryogenic and Elevated Temperature Cycling of Carbon/Polymer Composites," Society for the Advancement of Materials and Process Engineering, Long Beach, CA, May 2002.

[13] Bong Taek Oh, D. C. Lagoudas and S. Moon, Mechanical Characterization in laminated composite for cryogenic application, Polymer Composites, vol. 34, iss. 5, 607-615, May 2013.

[14] Bong Taek Oh, D. C. Lagoudas and S. Moon, Effect of insulation layer for thermal shock in cryogenic composite laminates, Polymer Composites, vol. 34, iss. 4, 531-536, Apr. 2013.

Oh Bong Taek is the CEO of TOMS (Technology of Material Science) Co., LTD. and the adjunct professor of Mechanical Design Engineering at Chung Nam National University. The primary research areas of interest include structural stress analysis, composite design/analysis/test/repairing, and also CNT composites.

Dr. Oh received the Bachelor and M.S. of mechanical engineering degree from SoongSil University, Korea, and Doctorate degree (D.En.) in aerospace engineering from Texas A&M University in U.S.A.

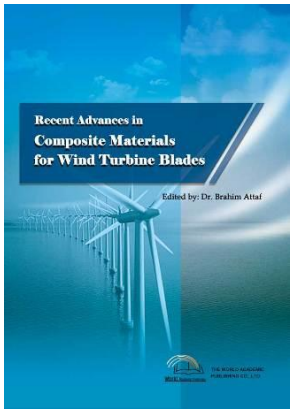

Recent Advances in Composite Materials for Wind Turbine Blades
Edited by Dr. Brahim Attaf

ISBN 978-0-9889190-0-6

Hard cover, 232 pages

Publisher: The World Academic Publishing Co. Ltd.

Published in printed edition: 20, December 2013

Published online: 20, December 2013

This book of science and technology provides an overview of recent research activities on the application of fibre-reinforced composite materials used in wind turbine blades. Great emphasis was given to the work of scientists, researchers and industrialists who are active in the field and to the latest developments achieved in new materials, manufacturing processes, architectures, aerodynamics, optimum design, testing techniques, etc.. These innovative topics will open up great perspectives for the development of large scale blades for on- and off-shore applications. In addition, the variety of the presented chapters will offer readers access to global studies of research & innovation, technology transfer and dissemination of results and will respond effectively to issues related to improving the energy efficiency strategy for 2020 and the longer term.

How to cite this book chapter

Bong Taek Oh (2013). Study of Composite and Sandwich Plates Extracted from Wind Turbine Blade Structures under Harsh Environmental Conditions, *Recent Advances in Composite Materials for Wind Turbines Blades*, Dr. Brahim Attaf (Ed.), ISBN 978-0-9889190-0-6, WAP-AMSA, Available from: http://www.academicpub.org/amsa/chapterInfo.aspx

World Academic Publishing - Advances in Materials Science and Applications

Chapter 13

Fatigue Life Prediction for Adhesively Bonded Root Joint of Composite Wind Turbine Blade Using Cohesive Zone Approach

Vahid Azimzadeh Kalkhoran[1], Davood Salimi-majd[2], Bijan Mohammadi[*3]

School of Mechanical Engineering, Iran University of Science and Technology
Narmak, Tehran, Iran

[1]V_Azimzadeh@mecheng.iust.ac.ir; [2]Salimi_Majd@mecheng.iust.ac.ir; [*3]Bijan_Mohammadi@iust.ac.ir

I. INTRODUCTION

In order to estimate the cost effectiveness of a wind turbine system, the fatigue life of wind turbine blades is an essential step in the design process. The blades of a wind turbine are considered to be the most basic and the most critical component of the wind turbine system. In general the major cause of wind turbine blade failure is fatigue phenomenon, where wind turbine blades are subjected during working conditions to different loads such as aerodynamics, gyroscopic and gravitational forces. These loading conditions will cause fatigue failure of the blade mainly at root joint, where the most critical zone of the blade is located.

Fatigue in the particular application of wind turbine rotor blades is discussed by Kensche [1]. Joosse and van Delft [2] expressed their concern on excluding fatigue as a research subject and reviewed research performed in the Netherlands between 1984 and 1996. Further to that, Sutherland [3] and Mandell [4] have a long record of rotor blade material fatigue research. Veers et al [5] used a computer code called FAROW to probabilistic analysis of the Fatigue and Reliability of Wind turbine component. Kong et al [6] investigated the fatigue life of a medium scale horizontal axis wind turbine system by using the S–N damage equation, the load spectrum and Spera's empirical formulae.

In aeronautical composite fatigue research, strength degradation models have been extensively formulated. These models take into account the order of load cycles, by quantifying the strength degradation in a cycle-by-cycle analysis. Comparing the instantaneous strength to the instantaneous load, these models are used as life prediction methods. Incorporating the static and fatigue scatter in the analysis creates a probabilistic life prediction estimate. Wahl [7] proposed to use residual strength analysis for composite wind turbine, and a validated non-linear model using repeated block tests and single R-value modifications of Wisper spectrum. Shokrieh and Rafiee [8] used a progressive damage model for lifetime prediction of a horizontal axis wind turbine composite blade; they employed accumulated fatigue damage modelling as a damage estimation rule and investigated fatigue of composite wind turbine blade by using developed stiffness degradation method. Jin et al [9] studied the life prediction of a composite wind turbine blade subjected to creep and fatigue loading using Micromechanics of failure (MMF) and accelerated test methods (ATM); they predicted the life of a wind blade using the master curves and load distribution that are calculated from finite element analysis of wind turbine blades. Jang et al [10] presented a methodology to predict the fatigue life of a small wind turbine composite blade using a wind speed history and the interaction between flapwise and edgewise bending moments.

Movaghghar [11] proposed an energy based model for predicting fatigue life and evaluation of progressive damage in a full composite wind turbine blade. His assumption was based on that the damage growth rate in composite material depends on the maximum value of elastic strain energy per cycle; he obtained critical stresses from ANSYS analysis and estimated fatigue life of the blade. Veers [12] described the method to produce an estimate of blade life based upon descriptions of the cyclic stresses and wind speeds in terms of probability density functions by using Miner's cumulative damage rule.

Blades of horizontal axis wind turbines (HAWT) are now completely made of composite materials due to lower weight and proper stiffness, while providing good resistance to the static and fatigue loading. Wind turbine blade root consists of several parts of composite and metal elements, these parts joint together by adhesive bonding. The most likely places for fatigue weakness are at joints and the main failure mechanism at the root joint may be debonding at the layers of composite to composite or composite to metal bonded area. The goal of this fatigue analysis is to investigate the initiation and growth of debonding in root joint and predict the fatigue life of root joint.

II. STATE OF THE ART

As a case study, a 23 m blade of a V47-660 wind turbine, manufactured by Vestas Company, was selected. Electric power that can be obtained from the wind by this model of wind turbine is 660 kW. The V47-660 blades use basic NACA-63-xxx airfoil series [13]. In the first step, wind turbine blade was modelled in full scale using Ansys 14.5 commercial finite element software [14], then forces that causing cyclic loading at the blade are calculated and in the next step fatigue analysis is performed using cohesive zone model. The main advantage of this method is that there is no need to determine initial crack before analysis. By using developed model and performing its material constants, initiation and growth of debonding is investigated and the life of the root joint is obtained.

III. MODELLING

A wind turbine blade is typically made up of an outer shell, a main spar and root joint. The outer shell gives the blade its aerodynamic profile and carries the edgewise loads; near the root the blade cross section changes from a wing profile to a circular profile. The main spar carries the flapwise loads; the current blade uses a box spar internal to the blade which can accept loads in all directions (Fig. 1).

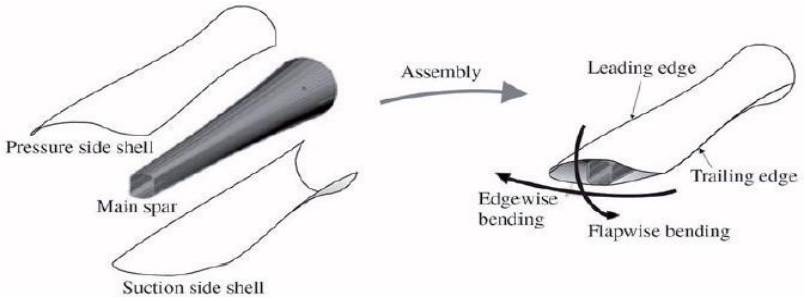

Fig. 1 Components of a wind turbine blade and their load carrying functions [15]

Cross section of the current blade is substantially rectangular, in other words first side of spar is in contact with a first inner surface of the skin and a second side is in contact with a second inner surface of the skin; Noted that the spar and shell are bonded together by adhesive. Fig. 2 shows the cross section of spar. As it can be seen from this figure the blade uses a box spar internal to the blade. In a main spar a rectangular beam containing the flanges and shear webs that are made as one piece (Fig. 3).

Fig. 2 Cross section view of blade spar

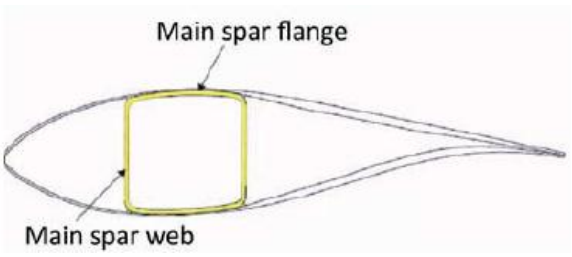

Fig. 3 Section of wind turbine blade with internal main spar

The root joint consists of several parts of composite and metal elements. These parts are joined together by adhesive bonding. The root joint is the only metallic part in the current blade that connects the whole blade structure to the hub by screws. The cross section view of the root joint is shown in Fig. 4 and the whole root joint is shown in Fig. 5.

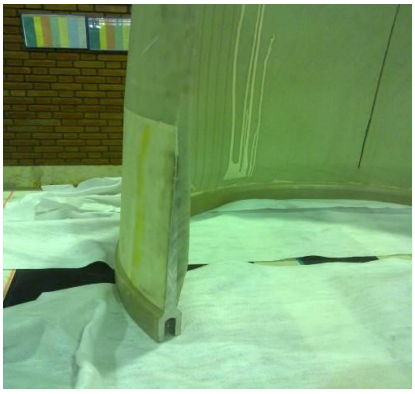

Fig. 4 Cross section view of root joint

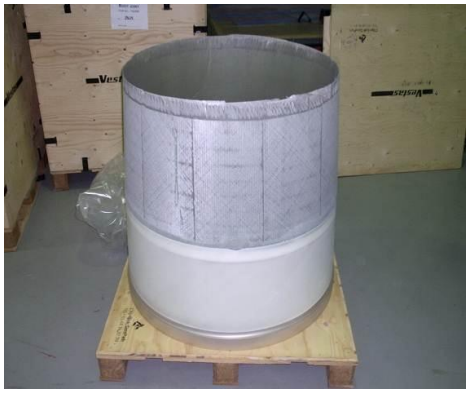

Fig. 5 Root joint of current blade

Profiles that provided shell shape changes from a circular tube to an airfoil section extending longitudinally from the root to tip of the blade. The trailing edge and the leading edge of the blade are both linear. Some physical characteristics data of the investigated blade are shown in Table 1 [8].

TABLE 1 PHYSICAL CHARACTERISTICS DATA OF THE BLADE [8]

Length	22900 mm
Twist	15.17^0
Maximum chord	2087 mm
Station of maximum chord	R4500
Minimum chord	282.5 mm
Weight of blade	1250 kg
Station of CG	R8100
Tip to tower distance	4.5 m
Surface area	28 m^2
Airfoil cross-section types	FFA-W3,NACA-63-xxx,MIX

The finite element program used for the structural analysis is well-known commercial software Ansys 14.5 [14]. To provide data for the finite element model, in the first step the root joint components must be fully model and then the spar and outer shell must be model. To model the root joint, cross section of whole root joint consists of metal and composite parts was created and by using extrude option in Ansys finite element Software, created area was extruded around canter line and the root joint was modelled. Second order cubic solid Elements SOLID185 with 8 node was used for meshing the root joint of the blade. Solid185 Structural Solid is suitable for modeling general 3-D solid structures particularly for composite structures. Fig. 6 shows the meshed model of the root joint consisting of metal part and composite parts.

To modelling spar and outer shell, a geometrical wire frame model was created based on cross section profiles of shell and spar which is the fundamental of geometrical model, geometrical modelling was completed by skinning surfaces among the cross section lines.

The 23 m blade spar and shell were meshed using shell elements. Ansys provides a wide range of different shell elements to choose from. For this reason the 4-node shell element SHELL181 was chosen for meshing the spar and shell. Using a shell element will reduce the amount of CPU (central processing unit) time necessary for analysis of the model.

Mesh density was increased near the root and a refinement study was conducted to show that the model mesh size was sufficient for convergence. Fig. 7 shows the finite element model of the turbine blade near the root.

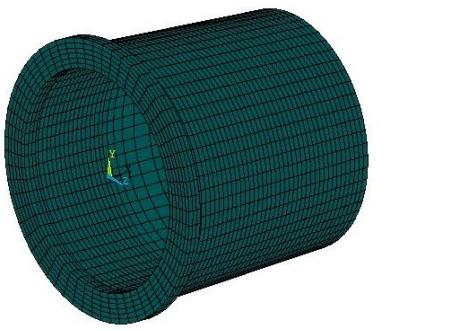

Fig. 6 Finite element model of root joint consist of metal and composite parts

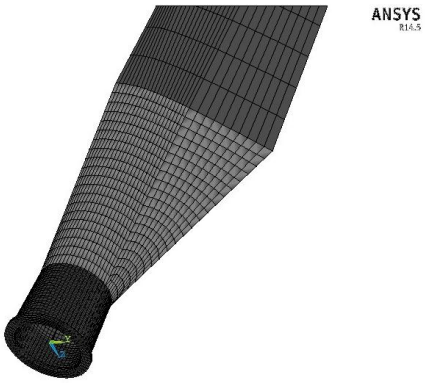

Fig. 7 Finite element model of turbine blade near the root

IV. LOADING

In general, fatigue loads are very important for the design and analysis of wind turbines. A wind turbine is subjected during its service life to a series of different loads both from the wind, gravity and during operation. In general, the loads that have significant effect on the fatigue of wind turbine are as follows:

- Flapwise and edgewise bending due to pressure load on the blade;
- Gravitational loads which change direction during the rotation and which mainly generate edgewise bending load;
- Inertia forces due to the rotation of the blade.

During operation, the blades on a wind turbine experience cyclic loading due to the Earth's gravitational field. During one rotation, the root of a blade, specifically the leading and trailing edges, will experience a tension-compression cycle due to the weight of the blade; this cyclic loading is significant and can influence the fatigue life of the blades. Because of the relatively low rotational speed, centrifugal forces are not very significant in wind turbines, and therefore these forces are neglected. The most obvious source of loading on the blades of a wind turbine is the wind itself. These loads are directly related to the power production of the wind turbine, when an airfoil is subjected to a relative wind velocity, a component of lift and drag are induced due to the aerodynamic properties of the profile. During the entire simulation and to simplify the analysis, the mean wind speed at hub is taken equal to 10 m/s.

The total lift and drag force can be expressed respectively as follows [16]:

$$F_{drag} = \frac{1}{2}\rho V_W^2 A C_D = 32KN \quad (1)$$

$$F_{Lift} = \frac{1}{2}\rho V_W^2 A C_L = 21KN \quad (2)$$

where A is the swept area of the blade, ρ is the density of surrounded air, C_D = 8/9 and C_L = 0.624 are the drag and lift coefficients, respectively (according to Betz theory) and V_W is wind mean speed [16].

Gravity force (F_g) and centrifugal force (F_r) are equal to:

$$F_g = m \times g = 1150 \times 9.8 = 11.27kN \quad (3)$$

$$F_r = m \cdot r \cdot \omega^2 = 1250 \times 7.5 \times (28.5 \times 2\pi/60)^2 = 83.5kN \quad (4)$$

V. MATERIAL PROPERTIES

Currently, the rotor blades are constructed from fibre reinforced polymers, where the E-glass is the most commonly used reinforcement material. The shell consists mainly of ±45 °plies, with unidirectional laminate at the trailing and leading edges to carry the edgewise forces and bending moments. The aerodynamic shells are made by prepreg technology. In the investigated blade tri-axial and bi-axial fabrics are used in the shell structure. The configuration of the bi-axial laminate is $[0/90]_T$ and the configuration of the tri-axial laminate is $[0/+45/-45]_T$. The shell of the blade is a sandwich structure with a PVC foam which is provided to separate the composite skins; this will indeed increase the panel's second moment of area and thus the resistance to buckling.

Flanges and webs of the blade are also made of glass fiber composites, where unidirectional and bi-axial fabrics are used in the spar structure. Unidirectional plies are used to provide stiffness for bending and some ±45 °plies are included to provide resistance for buckling. The flanges must take high tensile stresses on the pressure side and compressive stresses on the suction side, so they are predominantly composed of unidirectional fibres in order to withstand these forces.

The shear webs are typically made up of fibres orientated at ±45 to transfer the shear loads and keep the spar caps from moving relative to each other.

It should be noted that the composite parts of the root joint are mainly made up of bi-axial and unidirectional fabrics and the metal used at the root joint is aluminium alloy 5083. The mechanical properties of the material considered in the analysis are shown in Table 2 [9] and the mechanical properties of aluminium that require to analysis are listed in Table 3.

TABLE 2 MECHANICAL PROPERTIES OF FABRICS [8]

Composites	Configuration	E_1 (MPa)	E_2 (MPa)	ν_{12}	E_6 (MPa)
Unidirectional	-	43	9.77	0.32	3.31
Bi-axial	$[\pm 45]_T$	6.8	6.8	0.06	-
Bi-axial	$[0/90]_T$	16.7	16.7	0.06	2.01
Tri-axial	$[0/\pm 45]_T$	17.6	7.01	0.52	5.07

TABLE 3 MECHANICAL PROPERTIES OF ROOT JOINT METAL (ALUMINIUM ALLOY 5083)

Property	Value
Density	2650 Kg/m^3
Modulus of Elasticity	72 GPa

VI. FATIGUE DAMAGE MODELING

In this study, the adhesive debonding on the root joint of the wind turbine blade was investigated using a cohesive zone model. The use of cohesive zone models (CZM's) coupled to conventional FE analyses is the most widespread method of predicting static or fatigue damage uptake in structures [17]. The advantage of this method is the possibility of modeling the

debonding initiation and propagation without requirement to the presence of initial crack. Although in this method damage and delamination is modeled as the stiffness loss of the interface element, this approach does not require any remeshing for the analysis of debonding. The CZM's are based on the assumption that one or multiple fracture interfaces/regions can be artificially introduced in structures, in which damage growth is allowed by the introduction of a possible discontinuity in the displacement field. In other words, this model is based on a softening constitutive relation in the damaged area around the crack tip. The mechanism of this method for the bi-linear model is shown in Fig. 8.

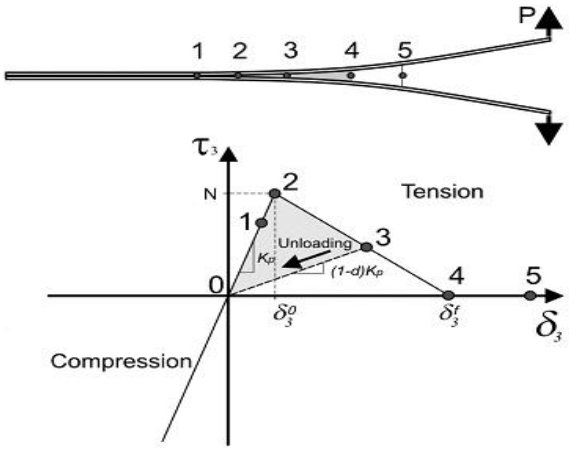

Fig. 8 The damaged area around the crack tip and the constitutive relation of cohesive zone model [18]

According to Fig. 8, the relationship between stress and strain (or displacement) in the interface element is initially linear elastic but when the stress reaches a maximum amount (that is the interlaminar strength), the stiffness degradation of the interface element starts to finally reach zero. In this state, the interface element is fully damaged. The ratio of lost stiffness to the initial stiffness in each state is called the damage variable. The technique consists of the establishment of traction-separation laws (addressed as CZM laws) to model interfaces or the finite regions. The CZM laws are established between paired nodes of cohesive elements, and they can be used to connect superimposed nodes of elements representing different materials or different plies in composites, to simulate a zero thickness interface or they can be applied directly between two non-contacting materials to simulate a thin strip of finite thickness between them, e.g. to simulate an adhesive bond.

It should be noted that in the modeling of debonding when using the cohesive zone concept, the area under the curve of constitutive equation in the stress-displacement space, is equal to the fracture toughness of corresponding loading mode. Balzani and Wagner [18] presented a robust solid like interface element based on the cohesive zone model for modeling delamination in laminated composites under mixed mode conditions. The cohesive interface element used in this study that has been implemented in the Ansys software, is based on the constitutive equations developed by the above mentioned researchers.

A. Constitutive Equations for Quasi-static Loading

The concept of cohesive zone was proposed to describe damage under static loads at the cohesive process zone ahead of the apparent crack tip, which can be understood as a phenomenon of micro voids formation that grows with the increase of the load, forming thin fibrils until the crack appears. The interface element used in this study is an 8-node solid continuum element with finite thickness called "the solid-like interface element". The formulation of this element is based on the isoparametric hexahedral solid element formulation but it is only comprised of three components of the stress instead of the six components. Since the task of interface element is to predict the initiation and propagation of delamination, therefore the stress tensor of this element only includes the normal stress in the thickness direction and the out of plane shear stresses. Fig. 9 illustrates the schematic of this interface element [18].

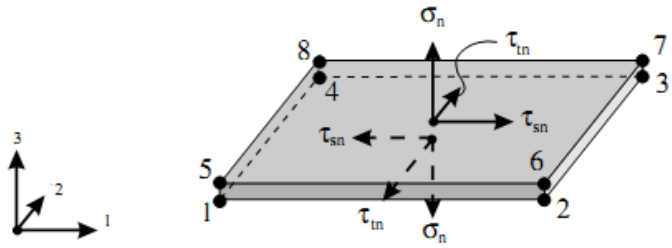

Fig. 9 A solid-like interface element [18]

In order to predict the delamination initiation considering the mixed mode condition, the summation of quadrature of stresses used in this research is as follows [19]:

$$\left(\frac{\langle \sigma_n \rangle}{\sigma_n^o}\right)^2 + \left(\frac{\tau_{sn}}{\tau_{sn}^0}\right)^2 + \left(\frac{\tau_{tn}}{\tau_{tn}^0}\right)^2 = 1 \tag{5}$$

where <> are the Macaulay brackets and given by:

$$\langle x \rangle = \begin{cases} 0 & x \le 0 \\ x & x > 0 \end{cases} \tag{6}$$

Since normal compressive stress does not have any effect on the delamination, so operator <> has been used in which if the applied normal stress is compressive, zero value is substituted instead of it.

In this study, the damage propagation is evaluated using B-K criterion which originally proposed by Kenane and Benzeggagh [20]. This criterion is based on the fracture toughness of modes I and II likewise, parameter η which is obtained from MMB test and is expressed as follows:

$$G_{IC} + (G_{IIC} - G_{IC})\left(\frac{G_{Shear}}{G_T}\right)^{\eta} = G_C, \quad G_T = G_I + G_{Shear} \tag{7}$$

The constitutive relation of cohesive zone model is expressed as follows:

$$\sigma = c\varepsilon,\ \sigma = \{\tau_{sn}, \tau_{tn}, \sigma_n\}^T,\ \varepsilon = \{\gamma_{sn}, \gamma_{tn}, \varepsilon_n\}^T \tag{8}$$

$$c = \begin{cases} KI & \varepsilon_m^* \le \varepsilon_m^0 \\ (1-d)KI + dKI_c & \varepsilon_m^0 \prec \varepsilon_m^* \prec \varepsilon_m^f \\ KI_c & \varepsilon_m^* \ge \varepsilon_m^f \end{cases} \tag{9}$$

$$I_c = \begin{bmatrix} 0 & 0 & 0 \\ 0 & 0 & 0 \\ 0 & 0 & \dfrac{\langle -\delta_n \rangle}{-\delta_n} \end{bmatrix} \tag{10}$$

In Eq. (7), ε_m^* is the maximum value of effective strain in every load step which has been used for considering the irreversibility condition of damage process. Also, indexes 0 and f corresponds to initiating the damage process and complete failure, respectively. Parameters d, k and c are damage variable, initial elastic rigidity as well as reduced stiffness matrix of the interface element, respectively. In addition, matrix I is the identity matrix ordered 3. Using the operator <> at the Eq. (6), absence of orthogonal rigidity reduction during the presence of compressive stress due to prevent from entering the cracked layers to each other for strains more than ε_m^f has been considered.

So, the explicit equation of the damage parameter for the bilinear constitutive relation is obtained in the most general form of mixed mode as follows:

$$d = \frac{\varepsilon_m^f(\varepsilon_m^* - \varepsilon_m^0)}{\varepsilon_m^*(\varepsilon_m^f - \varepsilon_m^0)} \tag{11}$$

B. Constitutive Equations for Fatigue Loading

Turon et al [21] proposed a damage model for simulating the interlaminar failure of stacked composites under high cycle fatigue loads. There model was based on providing a cohesive law that link fracture mechanics to damage mechanics in order to estimate the evolution of the damage variable during fatigue cycles. The model that was used in this study to predict debonding in adhesive joints of wind turbine blade root joint under fatigue loading is based on the research work presented in [21]; where the principle of this method will be described in the following section.

In order to evaluate the fatigue damage variable growth rate, researchers [21] stated that if the A_d is damaged area of

cohesive element, the rate of fatigue damage variable growth can be expressed as:

$$\frac{\partial d}{\partial N} = \frac{\partial d}{\partial A_d}\frac{\partial A_d}{\partial N} \tag{12}$$

Turon et al [21] used the concept of dissipating energy (irreversible) to define damaged area and according to Fig. 10 set the ratio of the damaged area, A_d , with respect to the area A_d associated with the area of the element equal to the ratio of dissipated energy to the critical energy release rate during the damage process in each state of damage variable [22], So:

$$\frac{A_d}{A_e} = \frac{E}{G_c} \tag{13}$$

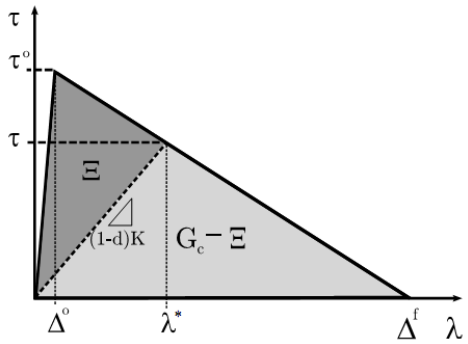

Fig. 10 The concept of dissipated energy in softening law [22]

Using Eq. (13) and Fig. 10, it can easily be shown that in the bilinear model the final equation for damaged area can be written as follows:

$$A_d = A_e\left[\frac{d\varepsilon_m^0}{(1-d)\varepsilon_m^f + d\varepsilon_m^0}\right] \tag{14}$$

Turon et al [21] defined the growth rate of the damaged area for cohesive element under fatigue loading similar to Paris law as follows:

$$\frac{\partial A_d}{\partial N} = A_e\left[\frac{C}{L_{cz}}\left(\frac{\Delta G}{G_C}\right)^m\right] \tag{15}$$

where A_e is the area of a cohesive element in the plane that delamination accrued and L_{cz} is the cohesive zone length perpendicular to the crack front. Also m and c are material constants in Paris law for crack growth rate and ΔG is equal to strain energy release rate at current fatigue cycle. It should be noted that ΔG is also defined as the area under the curve of constitute equation in the stress-displacement space.

By using Eqs. (12)-(15), the evolution of the damage variable as a function of the number of cycles can be written as:

$$\frac{\partial d}{\partial N} = \begin{cases} \dfrac{\left[(1-d)\varepsilon_m^f + d\varepsilon_m^0\right]^2}{\varepsilon_m^f \varepsilon_m^0}\left[\dfrac{C}{L_{cz}}\left(\dfrac{\Delta G}{G_c}\right)^m\right] & G_{max} \geq G_{th} \\ 0 & \text{otherwise} \end{cases} \tag{16}$$

where G_{max} is the maximum energy release rate and G_{th} is the energy release rate threshold.

VII. DETERMINATION OF COHESIVE PARAMETERS

Finite element analysis that include CZM techniques offer a powerful means to account for the largely nonlinear fracture behaviour of modern adhesively bonded joints, but the CZM parameters require careful calibrations by experimental data and respective validation in order to accurately simulate the failure process. In recent years, many works were published regarding the definition of the CZM parameters (G_c and σ_c in Mode I, II and mix mode) and a few data reduction techniques are currently available that enclose varying degrees of complexity and expected accuracy of the results. The most commonly used

experimental set-ups in order to measure Mode I, Mode II and Mix mode of cohesive laws is the Double Cantilever Beam (DCB) test, the End Notch Flexure (ENF) test and Mix Mode Bending (MMB) test, respectively which are standardized in standard associations (e.g. ASTM) for unidirectional polymeric composites. Fig. 11 shows the undeformed DCB specimen, where a_0 is the original crack length, b is the specimen width, h is the thickness of the specimen, L is total length and P is the applied load [23].

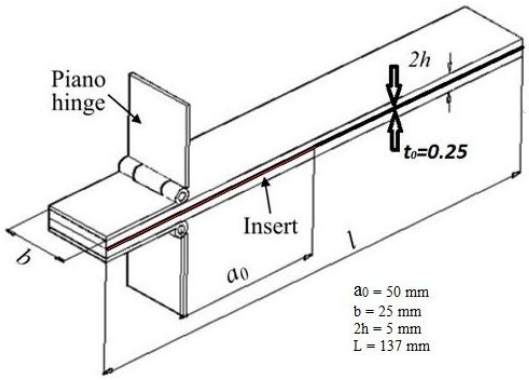

Fig. 11 Undeformed DCB specimen [23]

In order to obtain Mode I adhesive fracture toughness, tests were performed under static and fatigue loading in accordance with ASTM D5528 and D6115 [23], [24]. The adherent material selected for mechanical testing was the unidirectional fiberglass laminate and a thin film of Teflon was used as the insert. In all cases, HUNTSMAN Epoxy XB5047 / XB5067 was utilized as the adhesive material system. Before fatigue testing, static tests were conducted on the specimens to study their static failure behaviour and define the cohesive zone model. The static tests were executed in displacement control at a rate of 1 mm/min and the corresponding load level and back-face strain data were recorded. Fatigue testing was carried out at 5 Hz with a load ratio of 0.5.

In order to obtain required cohesive parameters associated with Mode II adhesive fracture toughness, ENF tests were performed under static and fatigue loading. Four series of static ENF tests were conducted on a type DP-5/3 machine with displacement control at a rate of 2mm/min and four series of fatigue tests were conducted under load control at 5 Hz with a load ratio of 0.5.

For the measurement of mixed mode cohesive parameters, different experimental set ups have been used. Efforts have been made to find a test set up that will allow testing under the full range of mode mixities. One of the most used experiment set ups is the Mixed Mode Bending (MMB) [25]. This method was standardized by ASTM standard [26]. Fig. 12 gives the MMB test base geometries.

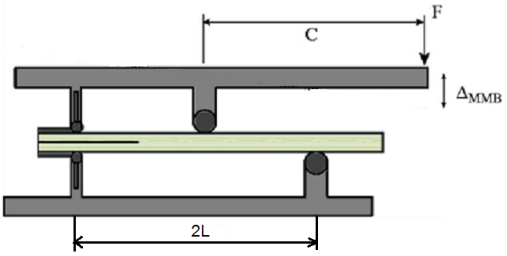

Fig. 12 Base geometry of MMB test [27]

The MMB test provides an easy variation of the mode ratio by just altering the lever length of the loading lever. Four series of static MMB tests were conducted with displacement control at a rate of 2mm/min and four series of fatigue tests were conducted under load control at 5 Hz with a load ratio of 0.5 with mode ratio of 0.5. Also, three series of SLJ tests were conducted to obtain the shear strength of the adhesive according to ASTM D5868 [28].

Two types of adhesive bonding are available at the root joint, one is composite to composite bonding and the other is composite to metal (aluminum) bonding; due to this reason all tests were repeated for composite to metal bonding. The results of performed tests are summarized in Tables 4-7.

TABLE 4 RESULTS OF STATIC TESTS FOR COMPOSITE-COMPOSITE BONDING

K(MPa)	τ_n^0(MPa)	τ_s^0(MPa)	G_{Ic}(N/mm)	G_{IIc}(N/mm)	η
5400	15.4	15.4	0.208	0.706	2.07

TABLE 5 RESULTS OF STATIC TESTS FOR COMPOSITE-ALUMINUM BONDING

K(MPa)	τ_n^0(MPa)	τ_s^0(MPa)	G_{Ic}(N/mm)	G_{IIc}(N/mm)	η
4600	13.1	13.1	0.203	0.57	2.04

TABLE 6 RESULTS OF FATIGUE TESTS FOR COMPOSITE-COMPOSITE BONDING

G_{Ith} (N/mm)	G_{IIth} (N/mm)	η_{th}	C_I (mm/Cycle)	C_{II} (mm/Cycle)	C_m (mm/Cycle)	m_I	m_{II}	m_m
0.025	0.135	5.77	0.00009	0.0054	3.41E14	3.21	6.72	7.48

TABLE 7 RESULTS OF FATIGUE TESTS FOR COMPOSITE-ALUMINUM BONDING

G_{Ith} (N/mm)	G_{IIth} (N/mm)	η_{th}	C_I (mm/Cycle)	C_{II} (mm/Cycle)	C_m (mm/Cycle)	m_I	m_{II}	m_m
0.018	0.126	5.79	0.00013	0.0061	3.49E14	3.15	6.67	7.52

It should be noted that to approximate Paris law constants in the mixed mode delamination, the method proposed by Blanco et al [29] was used.

VIII. FATIGUE INVESTIGATION OF THE BLADE

In order to evaluate the fatigue life of wind turbine blade, in the first step critical position of blade was determined. Probable critical position of the blade is horizontal position in which gravity force and lift force are codirectional and the other critical position is vertical in which gravity force and centrifugal force are codirectional. The gravity force and the centrifugal force were applied at the center of mass and the aerodynamic force was applied in the form of triangular distribution to the top surfaces of the blade. Boundary conditions corresponding to the root consisted of fixing all the six degrees of freedom of nodes.

By using cohesive zone model concept and parameters that was obtained from test results, a material called “usermat” was defined in Ansys material library. After performing static analysis on the two probable positions, results show that horizontal position is the most critical. Figs. 13 and 14 show the damage contour result for the horizontal position and vertical position respectively at the adhesive part of root joint. Fig. 15 shows x component of blade displacement under static load. As shown in Figs. 13-15, damaged area for horizontal position is more important than vertical position; which determines that horizontal position is critical.

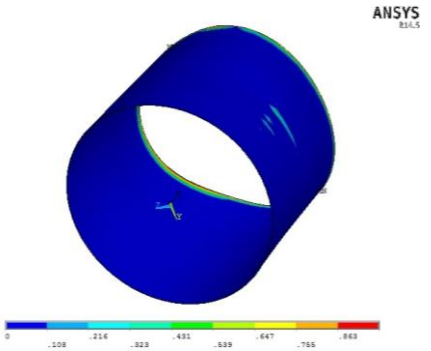

Fig. 13 Damage contour for horizontal position at the root joint adhesive

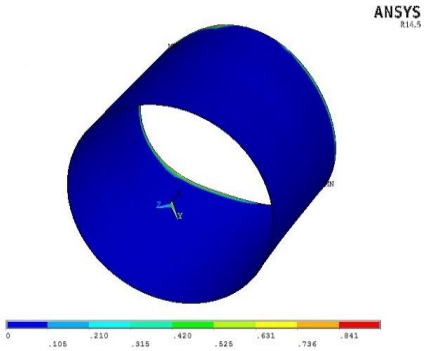

Fig. 14 Damage contour for vertical position at the root joint adhesive

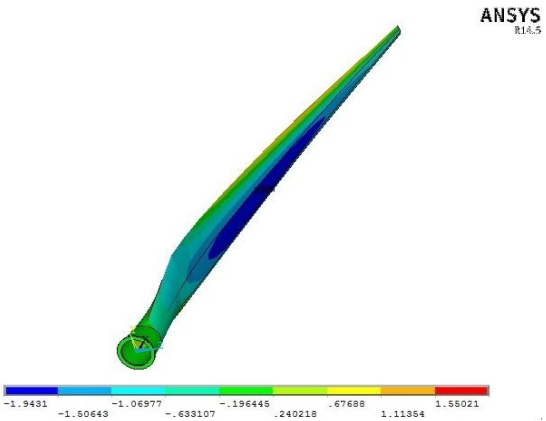

Fig. 15 X component of blade displacement under static load

By using cycle jumping strategy and executing code, debonding of adhesive joints at the root joint of the composite wind turbine blade was examined. At the end of the analysis the number of cycles to failure was obtained to be equal to 7.4×10^8 cycles. This value indicates that the blade satisfies the design requirements. Figs. 16-20 show damage variable contour at different cycles from first cycle to last cycle that failure occurs at the blade root joint. As shown in these figures, damaged area increase by increasing the number of cycles (N indicates cycle number).

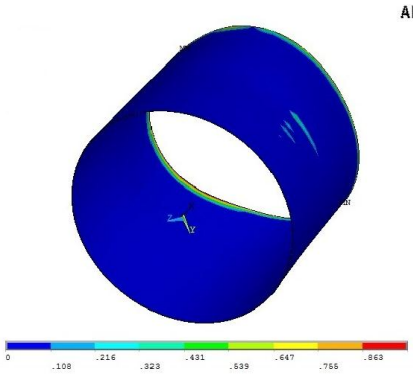

Fig. 16 Damage contour at the root joint adhesive when $N=10^2$

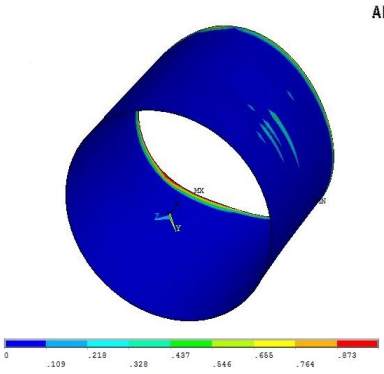

Fig. 17 Damage contour at the root joint adhesive when $N=10^5$

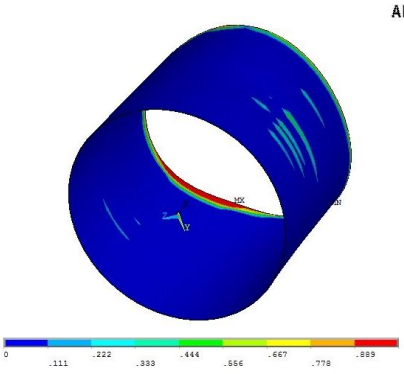

Fig. 18 Damage contour at the root joint adhesive when $N=10^6$

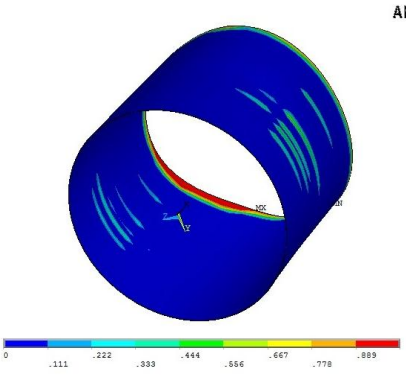

Fig. 19 Damage contour at the root joint adhesive when $N=10^8$

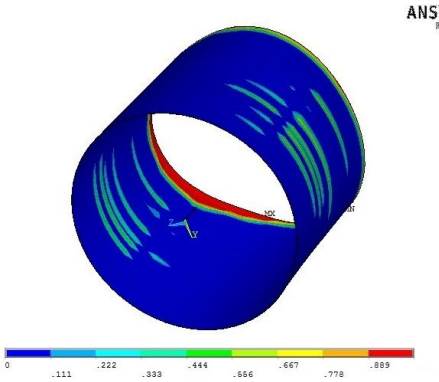

Fig. 20 Damage contour at the root joint adhesive when $N=7.4\times10^8$ (last cycle)

IX. CONCLUSIONS

In this study, initiation and growth of debonding at the root joint of composite wind turbine blade due to fatigue loading was investigated by using the cohesive zone model. It was estimated that 10^8 load cycles will happen in the prospected lifetime of 20 years of a wind turbine. During this lifetime, the rotor blades are exposed to various hostile conditions and loads, where structural components joined together by adhesive bonding must withstand such loading conditions. In order to predict damage due to fatigue loading in the horizontal axis of a wind turbine with 46 meter rotor diameter, a cohesive zone constitutes law based on dissipated energy was implemented and after performing a series of DCB, ENF, MMB and SLJ tests, using cohesive zone model concept and parameters that were obtained from test results, a material was defined in ANSYS material library. The static analysis was performed to determine the critical position of the wind turbine blade. Numerical results show that the horizontal position is the critical position for wind turbine blade under fatigue loading. After carrying out static analysis, the horizontal position was used to perform fatigue analysis. So, by using developed models and performing material constants, after model analysis, debonding of adhesive joints at the wind turbine blade was investigated and the fatigue life of the root joint was obtained. The estimated fatigue life obtained satisfies the design requirements.

REFERENCES

[1] C. W. Kensche, "Fatigue of composites for wind turbines," International Journal of Fatigue, 28: 1363–1374, 2006.

[2] P. A. Joosse, D. R. V Van Delft, "Has fatigue become a wearisome subject? Overview of 12 years of Materials Research in the Netherlands," Proc. European Union Wind Energy Conference, Belguim, pp. 902-906, 1996.

[3] H. J. Sutherland, "On the fatigue analysis of wind turbines," Sandia National Laboratories report: SAND99-0089, pp. 10-12, Albuquerque, New Mexico, Jun. 1999,

[4] H. J. Sutherland, J. F. Mandell, "Optimized Goodman diagram for the analysis of fiberglass composites used in wind turbine blades,"

proc. ASME/AIAA Wind Energy Symposium, paper AIAA-2005-0196, 2005.

[5] P. S. Veers, C. H. Lange and S. R. Winterstein "FAROW: A Tool for Fatigue and Reliability of Wind Turbines," Proceedings of Windpower 93, AWEA, p. 342, Washington, DC, 1993,

[6] C. Kong, Y. Sugiyama, C. Soutis, "Investigation of fatigue life for a medium scale composite wind turbine blade," International Journal of Fatigue 28 1382–138, 2006.

[7] N. K. Wahl, "Spectrum fatigue lifetime and residual strength for fiberglass laminates," Ph.D. Thesis, Montana State University, Bozeman, 2001.

[8] M. M. Shokrieh, R. Rafiee, "Simulation of fatigue failure in a full composite wind turbine blade," Journal of Composite Structures. 74–332–342, 2006.

[9] K. K. Jin, M. Ghulam, "Life prediction of wind turbine blades," Brain Korea 21 Project.

[10] Y. J. Jang, C. W. Choi, K. W. Kang, "Fatigue life prediction of small wind turbine composite blade using generated 1-Hz wind speed history and flapwise-edgewise moment interaction," 9th International Conference on Fracture & Strength of Solids Jun. 9-13, Korea, 2013.

[11] A. Movaghghar, "A method of estimating wind turbine blade fatigue life and damage using continuum damage mechanics," International Journal of Damage Mechanics, 810-821, Aug. 21, 2012.

[12] P, S. Veers, "Blade fatigue life assessment with application to VAWTS," ASME Journal of Solar Energy Engineering, vol. 104, May 1982.

[13] J. F. Johnston, W. A. Farone, A. Mikhail, "United States patent number 4976587," 1990.

[14] ANSYS Ver. 14.5 user manual.

[15] E. Lund and J. Stegmann. "On structural optimization of composite shell structures using a discrete constitutive parameterization." Wind Energy, 8(1):109–124, 2005.

[16] J. S. Rajadurai, T. Christopher, G. Thanigaiyarasu, B. N. Rao, "Finite element analysis with an improved failure criterion for composite wind turbine blades," Forsch Ingenieurwes, 72: 193–207, 2008.

[17] P. P. Camanho, C.G. Davila, M.F. Moura, "Numerical simulation of mixed mode progressive delamination in composite materials," Journal of Composite Materials, 37(16), pp. 1415-1438, 2003.

[18] C. Balzani, W. Wagner, "An interface element for the simulation of delamination in unidirectional fiber-reinforced composite laminates," Engineering Fracture Mechanics, 75, pp. 2597-2615, 2007.

[19] L. Ye, "Role of matrix resin in delamination onset and growth in composite laminates," Composites Science and Technology, 33, pp. 257-277, 1988.

[20] M. L. Benzeggagh, M. Kenane, "Measurement of mixed mode delamination fracture toughness of unidirectional glass/epoxy composites with mixed-mode bending apparatus," Composites Science and Technology, 49, pp. 439-449, 1996.

[21] A. Turon, J. Costa and C. G. Dávila, "Simulation of delamination in composites under high-cycle fatigue," Composites Part A: Applied Science and Manufacturing, 38(11), pp. 2270-2282, 2008.

[22] Mi, Y., M. A. Crisfield, G. A. Davies. "Progressive delamination using interface elements," J Composite Materials, 32(14), pp. 1246-1272, 2012.

[23] ASTM D55228-94a, "Standard test method for mode I interlaminar fracture toughness of unidirectional fiber reinforced polymer matrix composites," Annual book of ASTM standards vol. 15.06. USA: ASTM, 2002.

[24] ASTM D6115-97, "Standard test method for mode I fatigue delamination growth onset of unidirectional fiber reinforced polymer matrix composites," Annual book of ASTM standards vol. 15.03. USA: ASTM.

[25] J. R. Reeder, A. Crews, "A mixed mode bending method for delamination testing," AIAA J; 28: 1270-6, 1990.

[26] ASTM D6671, "Standard test method for mixed mode I, mode II Interlaminar fracture toughness of unidirectional fiber reinforced polymer matrix composites," Annual book of ASTM standards vol. 15.03. USA: ASTM.

[27] L. Lampani, "Finite element analysis of delamination of a composite component with the cohesive zone model technique," journal of Engineering Computations, vol. 28, iss. 1, pp. 30-46, 2011.

[28] ASTM D5868, "Standard test method for lap shear adhesion for fiber reinforced plastic (FRP) bonding," Annual book of ASTM standards vol. 15.03. USA: ASTM.

[29] N. Blanco, E. K. Gamstedt., and J. Costa, "Mixed-mode delamination growth in carbon fiber composite laminates under cyclic loading," International Journal of Solids and Structures, 41(15), pp. 4219-4235, 2004.

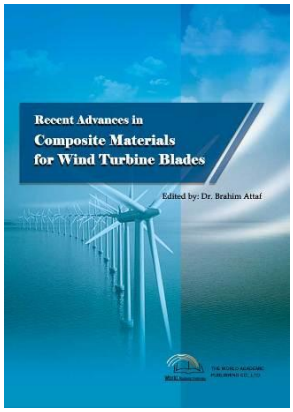

Recent Advances in Composite Materials for Wind Turbine Blades
Edited by Dr. Brahim Attaf

ISBN 978-0-9889190-0-6

Hard cover, 232 pages

Publisher: The World Academic Publishing Co. Ltd.

Published in printed edition: 20, December 2013

Published online: 20, December 2013

This book of science and technology provides an overview of recent research activities on the application of fibre-reinforced composite materials used in wind turbine blades. Great emphasis was given to the work of scientists, researchers and industrialists who are active in the field and to the latest developments achieved in new materials, manufacturing processes, architectures, aerodynamics, optimum design, testing techniques, etc.. These innovative topics will open up great perspectives for the development of large scale blades for on- and off-shore applications. In addition, the variety of the presented chapters will offer readers access to global studies of research & innovation, technology transfer and dissemination of results and will respond effectively to issues related to improving the energy efficiency strategy for 2020 and the longer term.

How to cite this book chapter

Azimzadeh Kalkhoran V., Salimi-majd D. and Mohammadi B. (2013). Fatigue Life Prediction for Adhesively Bonded Root Joint of Composite Wind Turbine Blade Using Cohesive Zone Approach, *Recent Advances in Composite Materials for Wind Turbines Blades*, Dr. Brahim Attaf (Ed.), ISBN 978-0-9889190-0-6, WAP-AMSA, Available from: http://www.academicpub.org/amsa/chapterInfo.aspx

World Academic Publishing - Advances in Materials Science and Applications